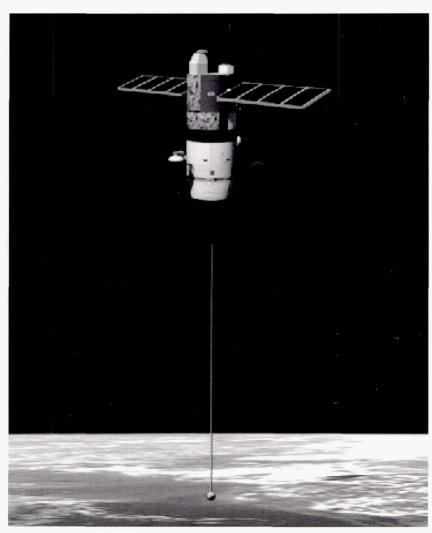


Tether Technology Interchange Meeting

J.K. Harrison, Compiler Marshall Space Flight Center, Marshall Space Flight Center, Alabama



Proceedings of a meeting sponsored by NASA Marshall Space Flight Center and held in Huntsville, Alabama September 9–10, 1997

The NASA STI Program Office...in Profile

Since its founding, NASA has been dedicated to the advancement of aeronautics and space science. The NASA Scientific and Technical Information (STI) Program Office plays a key part in helping NASA maintain this important role.

The NASA STI Program Office is operated by Langley Research Center, the lead center for NASA's scientific and technical information. The NASA STI Program Office provides access to the NASA STI Database, the largest collection of aeronautical and space science STI in the world. The Program Office is also NASA's institutional mechanism for disseminating the results of its research and development activities. These results are published by NASA in the NASA STI Report Series, which includes the following report types:

- TECHNICAL PUBLICATION. Reports of completed research or a major significant phase of research that present the results of NASA programs and include extensive data or theoretical analysis. Includes compilations of significant scientific and technical data and information deemed to be of continuing reference value. NASA's counterpart of peer-reviewed formal professional papers but has less stringent limitations on manuscript length and extent of graphic presentations.
- TECHNICAL MEMORANDUM. Scientific and technical findings that are preliminary or of specialized interest, e.g., quick release reports, working papers, and bibliographies that contain minimal annotation. Does not contain extensive analysis.
- CONTRACTOR REPORT. Scientific and technical findings by NASA-sponsored contractors and grantees.

- CONFERENCE PUBLICATION. Collected papers from scientific and technical conferences, symposia, seminars, or other meetings sponsored or cosponsored by NASA.
- SPECIAL PUBLICATION. Scientific, technical, or historical information from NASA programs, projects, and mission, often concerned with subjects having substantial public interest.
- TECHNICAL TRANSLATION.
 English-language translations of foreign scientific and technical material pertinent to NASA's mission.

Specialized services that complement the STI Program Office's diverse offerings include creating custom thesauri, building customized databases, organizing and publishing research results...even providing videos.

For more information about the NASA STI Program Office, see the following:

- Access the NASA STI Program Home Page at http://www.sti.nasa.gov
- E-mail your question via the Internet to help@sti.nasa.gov
- Fax your question to the NASA Access Help Desk at (301) 621–0134
- Telephone the NASA Access Help Desk at (301) 621–0390
- Write to: NASA Access Help Desk NASA Center for AeroSpace Information 800 Elkridge Landing Road Linthicum Heights, MD 21090–2934



Tether Technology Interchange Meeting

J.K. Harrison, Compiler Marshall Space Flight Center, Marshall Space Flight Center, Alabama

Proceedings of a meeting sponsored by NASA Marshall Space Flight Center and held in Huntsville, Alabama September 9–10, 1997

National Aeronautics and Space Administration

Marshall Space Flight Center

Available from:

NASA Center for AeroSpace Information 800 Elkridge Landing Road Linthicum Heights, MD 21090–2934 (301) 621-0390 National Technical Information Service 5285 Port Royal Road Springfield, VA 22161 (703) 487–4650

TABLE OF CONTENTS

SESSION I—RECENT MISSION RESULTS

Session Chair: J. Ballance, Marshall Space Flight Center

N.H. Stone (Marshall Space Flight Center); K.H. Wright and J.D. Winningham (Southwest Research Institute); K. Papadapolous (Science Applications International Corporation); T.X. Zhang, K.S. Hwang, and S.T. Wu (The University of Alabama in Huntsville); and U. Samir (Tel Aviv University)	1
TiPS: Results of a Tethered Satellite System J. Barnds (Swales Aerospace); B. Kelm, S. Coffey, and B. Purdy (Naval Research Lab); and M. Davis (Allied Signal Technical Services Corp.)	13
Tethered Satellite System Time Domain Observer Development for STS-75 Mission H. Biglari (Boeing Company)	31
STS-75/TSS-1R Tether Control & Dynamics Operations J.L. Williams, Jr. (United Space Alliance)	41
The Dynamics of the TiPS Tether Experiment J.R. Glaese (Control Dynamics Division of bd Systems)	51
SESSION II—PLANNED MISSIONS	
Session Chair: V. Keller, Marshall Space Flight Center	
The BOLAS Mission H.G. James (Communications Research Centre)	71
Propulsive Small Expendable Deployer System (ProSEDS) Space Demonstration L. Johnson and J. Ballance (Marshall Space Flight Center)	103
The "Terminator Tether™:" A Near-Term Commercial Application of the NASA/MSFC ProSEDS Experiment R.L. Forward and R.P. Hoyt (Tethers Unlimited); and C. Uphoff (ACTA Consulting Group)	109
The YES Satellite: A Tethered Momentum Transfer in the GTO Orbit M. Kruijff and E.J. van der Heide (ESA/ESTEC)	131
Experiments in Tether Dynamics Planned for ATEx's Flight M.F. Zedd (Naval Research Laboratory)	149

SESSION III—FUTURE MISSIONS

Session Chair: E. Lorenzini (SAO)

A Station Tethered Express Payload System (STEPS) J.A. Carroll (Tether Applications)	187
Multiple Tethered Satellites for Ionospheric Studies (MTSIS) B. Gilchrist (University of Michigan) and R.A. Heelis (University of Texas at Dallas)	191
Tethered Satellite Investigations of the Ionosphere and Lower Thermosphere R.A. Heelis (University of Texas at Dallas)	205
Space Tethers Design Criteria D.D. Tomlin, G.C. Faile, K.B. Hayashida, C.L. Frost, C.Y. Wagner, M.L. Mitchell, J.A. Vaughn, and M.J. Galuska (Marshall Space Flight Center)	223
GRADSAT: A Danish Geomagnetic Gradient Mission J. Merayo (Technical University of Denmark)	239
SESSION IV—TRANSPORTATION	
Session Chair: J. Glaese (Control Dynamics/bd Systems)	
Tether Transport System Study Summary D. Vonderwell, M. Bangham, H. Dionne, B. Fleming, B. Klus, K. Herring, E. Suggs, and L. Walker (Boeing); E. Lorenzini, M.L. Cosmo, and M. Kaiser (Smithsonian Astrophysical Observatory); L. Vestal, L. Johnson, and C. Carrington (Marshall Space Flight Center)	255
Tether System for Exchanging Payloads Between the International Space Station and the Lunar Surface R.P. Hoyt (Tethers Unlimited)	271
Orbiter-Towed Reboost for ISS C. Carrington and V. Keller (Marshall Space Flight Center)	286
Application of an Electrodynamic Tether System to Reboost the International Space Station I.E. Vas, T.J. Kelly, and E. Scarl (Boeing Company)	305
An Overview of Electrodynamic Tether Performance in the Jovian System D.L. Gallagher, (Marshall Space Flight Center); F. Bagenal (University of Colorado); J. Moore (SRS Technologies); and L. Johnson (Marshall Space Flight Center)	335

SESSION V—ADVANCED TETHER TECHNOLOGY

Session Chair: K.J. Welzyn (Marshall Space Flight Center)

Oedipus-C Mission Tether Dynamics Result A.M. Jablonski and F.R. Vigneron (Canadian Space Agency); G. Tyc (Bristol Aerospace Limited); and H.G. James (Communications Research Centre)	347
The Hoytether: A Failsafe Multiline Space Tether Structure R.P. Hoyt and R.L. Forward (Tethers Unlimited)	369
Technology of Bare Tether Current Collection R.D. Estes (Smithsonian Astrophysical Observatory); J.R. Sanmartin (Universidad Politecnica de Madrid); and M. Martinez-Sanchez (Massachusetts Institute of Technology)	379
Validity of the Orbital-Motion-Limited Regime of Cylindrical Probes J.R. Sanmartin (Universidad Politecnica de Madrid) and R.D. Estes (Harvard-Smithsonian Center for Astrophysics)	399
POSTER SESSION	
Response of Electrodynamic Tethers in Ionospheric Plasma Due to Step Changes	
in Voltage S.G. Bilen and B.E. Gilchrist (University of Michigan)	421
Ferromagnetically Screened Reverse Conductor (FSRC)-Tether: A New Tether Principle G. Liebscher (Electronic Components Consultants-Germany)	435
Past, Present, and Future Activity on Tethered Systems F. Angrilli, R. Basso, G. Bianchini, S. Bortolami, R. DaForno, S. Debei, G. Fanti, F. Reccanello, B. Saggin, and A. Zago (University of Padua-Italy)	439

Session I—Recent Mission Results

A Review of Scientific and Technological Results from the TSS-1R Mission

N. H. Stone¹, K. H. Wright², J. D. Winningham², K. Papadapolous³, T. X. Zhang⁴, K. S. Hwang⁴, S. T. Wu⁴, and U. Samir⁵

Abstract

The Tethered Satellite System (TSS) program was designed to provide a unique opportunity to explore certain space plasma-electrodynamic processes and the orbital mechanics of a gravity-gradient stabilized system of two satellites linked by a long conducting tether. A unique data set was obtained during deployment which has allowed significant science to be accomplished. This paper focuses on results from the TSS-1R mission that are most important to the future technological applications of electrodynamic tethers in space—in particular, the current collection process. Of particular significance is an apparent transition of the physics of current collection when the potential of the collecting body becomes greater than the ram energy of the ionospheric atomic oxygen ions. Previous theoretical models of current collection were electrostatic—assuming that the orbital motion of the system, which is highly subsonic with respect to electron thermal motion, was unimportant. This may still be acceptable for the case of relatively slow-moving sounding rockets. However, the TSS-1R results show that motion relative to the plasma must be accounted for in orbiting systems.

- ¹ Space Sciences Laboratory, NASA Marshall Space Flight Center, Huntsville, Alabama 35812.
- ² Southwest Research Institute, Department of Space Sciences, San Antonio, Texas 78228
- ³ Science Application International Corporation, McLean, Virginia 22012
- ⁴ Center for Space Plasma Aeronomy and Astrophysics, The University of Alabama in Huntsville, Huntsville, Alabama, 35899
- ⁵ Department of Geophysics and Planetary Science, Tel Aviv University, Tel Aviv Israel

1. Mission Background

The Tethered Satellite System (TSS) program is a binational collaboration between NASA and the Italian Space Agency (ASI) with NASA providing the Shuttle-based deployer and tether and ASI providing a satellite especially designed for tethered deployment. Twelve science investigations, given in Table 1, were supported by NASA, ASI, or the Air Force Philips Laboratory. The TSS-1R mission was the second flight of the TSS hardware. Its goals were to provide unique opportunities to explore (1) certain space plasma-electrodynamic processes—particularly those involved in the generation of ionospheric currents, and (2) the orbital mechanics of a gravity-gradient stabilized system of two satellites linked by a long conducting tether.

TSS-1R was launched February 22, 1996 on STS-75 into a 300-km, circular orbit at 28.5° inclination. Satellite flyaway occurred at MET 3/00:27 and a unique data set was obtained over the next 5 hours as the tether was deployed to a length of 19,695 m. At MET 3/05:11, during a day pass, the tether suddenly broke near the top of the deployer boom. The break resulted from a flaw in the tether insulation which allowed the ignition of a strong electrical discharge that melted the tether. The operations that had begun at satellite flyaway, however, resulted in the acquisition of a significant data set that is providing an understanding of tether dynamics and electrodynamics necessary for practical applications of tether technology in space.

2. Instrumentation and Measurements

The TSS converted mechanical energy into electrical energy in a classical demonstration of Faraday's law. The configuration was such that the satellite received a positive bias, as a result of the motional emf, and collected electrons from the ionosphere. This current was conducted through the tether to the orbiter where the circuit could be closed back to the ionosphere (see Fig. 1). There were four basic electrical configurations at the orbiter: (1) Open circuit with no current flow—in which case the full tether-generated emf existed across the open switch; (2) Passive current closure—in which current was controlled by adding a load resistance in series with the tether, and closure was through the collection of positive ions by conducting surfaces on the negatively charged orbiter; (3) Addition of SETS experiment's Fast-Pulse Electron Gun (FPEG) to the above circuit to discharge the orbiter; and (4) Use of the ASI Core electron gun—in which case tether current flowed directly to the gun cathode (the orbiter was not part of the electrical circuit) and was emitted back in to the ionosphere. An electrical schematic is shown in Figure 2.

The TSS was instrumented to control the tether current (as described above) and diagnose the environmental space plasma properties under highly nonequilibrium conditions. The investigations, shown in Table 1, provided the required ensemble of instruments which were mounted on either the orbiter or the satellite, as indicated in the table. Ground-based RF measurements were also made, and ionosound data, combined with several models, were used to predict the ambient ionospheric conditions (*Szuszczewicz et al.*, 1997). A functional schematic of the TSS and the location of its instrumentation is given in Figure 1. A detailed description of the instrumentation, which also flew on the TSS-1 mission, is provided in a special TSS-1 issue of *Il Nuovo Cimento* (1994). The interdependence of the TSS investigations resulted in an integrated approach to the science, with all the instrumentation and hardware being operated as a single experiment. Science

results are published in a special issue of Geophysical Research Letters (see Stone and Bonifazi, 1997 and papers following).

The data set obtained from TSS-1R, in one sense, falls far short of premission expectations. There was no opportunity to execute the detailed experiments that had evolved over several years of planning. In fact, operations were limited to calibration functions that were intended to provide a basis for the science experiment, to be conducted at station 1 (full deployment of 2,000 km). As a result, the data set obtained lacks a systematic approach and does not provide complete information. In another sense, however, the TSS-1R data set includes more than could have been hoped for under the circumstances as it became clear that the measurements differed significantly from pre-mission theoretical predictions. In fact, the tether break itself provided an especially intriguing and potentially valuable event in which large currents (>1 A) at high satellite potentials (>1 kV) began flowing ~10 s prior to the break and continued for ~90 s after separation (Gilchrist et al., 1997). The data obtained during deployment are also unique in that they have uncovered new and unexpected physical processes discussed below. Though limited, the data set is of high quality and includes 13 major operational sequences, covers a significant portion of the planned ranges of the tether current and voltage, and includes a variety of ionospheric conditions. Figure 2 provides the conditions under which data were obtained for the various operational sequences used in the papers that follow.

3. Technical and Results

The most fundamental scientific result from the mission to date is that the various theoretical current collection models developed over the past 70 years (e.g., Langmuir and Blodgett, 1923, 1924; Beard and Johnson, 1961; Parker and Murphy, 1967) do not include the full range of processes by which an electrically biased, mesosonic satellite (supersonic with respect to the ion sound speed but subsonic with respect to that of the electrons) interacts with its environmental space plasma. This manifests itself in three striking difference between the predictions of Theoretical Model and the actual physical observations:

- (1) the predicted relation between satellite potential and charge collection (the current-voltage characteristic) is, correspondingly, incorrect.
- (2) a variety of specific physical effects, including the creation of suprathermal charged particle populations, plasma waves, and magnetic perturbations were observed. These effects may be related to the unexpected nature of the current-voltage relationship.
- (3) a sharp transition in the interaction process was found to occur at the relatively low spacecraft potential of +5 V—the ram energy of the dominant atomic oxygen ions. The reflection of ionospheric ions by the satellite when its potential exceeded the ion ram energy was expected. However, a transition in the basic physical processes involved was a complete surprise.

The disagreement observed between the measured TSS-1R current-voltage characteristic and the predictions of the theoretical models may provide for the most significant improvement to our understanding of the physics of current collection in space since the Langmuir-Blodgett model was introduced in 1923 to explain how an electrostatic probe collects current from an unmagnetized, stationary laboratory plasma (*Papadopoulos*, 1996). The Langmuir-Blodgett theory was modified by Parker and Murphy in 1967 to account for the fact that the ionospheric plasma has an imbedded magnetic field which reduces cross-field charge mobility—limiting current collection approximately to a magnetic

flux tube. (A review of the theory is given in *Laframboise and Sonmor*, 1993.) The magnetically limited model seemed to explain observations made from several relatively slow-moving sounding rocket experiments and was accepted as authoritative for the past 30 years—until the TSS-1R mission. Immediately, even during the 5 hours of data acquisition, it became obvious that serious differences existed between theoretical models and the measured results. For example, Figure 3 shows that the attractive potential required on the satellite to collect a given current is typically an order of magnitude less than that predicted by the Parker-Murphy model (*Thompson et al.*, 1997). This shows that current collection is far more efficient than predicted and suggests the requirement for rather rigid adherence of electrons to magnetic field lines assumed in the magnetically limited models may be too severe.

The sharp transition observed in the satellite particle and field environment at a potential of +5 V seems to suggest an abrupt modification of the physical processes. Below +5 V, mostly accelerated ionospheric thermal electrons were observed. However, when the satellite potential increased beyond the +5 V level, a sudden onset of suprathermal (~200 eV) electrons, plasma waves, magnetic perturbations, and turbulence in the satellite sheath were observed (see Winningham et al., 1997; Iess et al., 1997; Mariani et al., 1997; and Wright et al., 1997, respectively). The suprathermal flux intensity grew rapidly with increasing satellite potential and quickly swamped the ionospheric thermals. Specifically, a 10 V increase in satellite potential resulted in as much as 6 orders of magnitude increase in suprathermal electron flux. (Winningham et al., 1997). In addition, relatively energetic ions were observed outflowing from the satellite's sheath. The ram energy of ionospheric atomic oxygen ions is ~5 eV, so that the critical voltage for the transition is the level at which oxygen ions would be reflected or strongly deflected out of the sheath. It appears possible that the outflowing ions, or possibly the expulsion of ions from the plasma sheath, may provide the free energy required to drive the energization of the suprathermal electrons.

These effects are important to all electrodynamic tether applications because their net effect is to increase the current available at any given value of the emf and ionospheric conditions. This increases the ability of the system to convert orbital kinetic energy into electrical power, or conversely, electrical power into an electrodynamic propulsion force.

Specifically, if we take a typical current-voltage profile from TSS-1R and plot the satellite potential required to collect a given current as a function of tether current, as shown in Figure 4a, we see that the potential requirements of the Parker-Murphy model far exceed the actual TSS-1R data. This means that much less work had to be done to collect electrons that predicted, and this, in turn, means that less of the available motional emf is used to collect the electrons that make up the tether current—leaving more useful power. In addition to the work required to collect electrons at the satellite, the work done to by the electron gun on the Orbiter to inject them back into the ionosphere must also be taken into account, along with the resistive potential drop in the tether. The usable power is, there given by:

$$P_{usable} = (I_{tether} \times \Phi_{e\,mf}) - (I_{tether} \times \Phi_{satellite}) - (I_{tether} \times \Phi_{e\text{-gun}}) - (I^2_{tether} \times R_{tether}).$$

If the usable power is plotted as a function of the tether current, as shown in Figure 4b, we see that the Parker-Murphy model predicts the usable power to increase with current up to about 250 mA and then decrease to zero at about 440 mA. For a given emf, the total power generated increases with increasing current. However, the Parker-Murphy model

predicts that the collection process becomes increasingly inefficient with increasing current so that eventually, all available energy is used to collect electrons, and none is left to do useful work. Note, however, that this is not what actually happened. The importance of the enhanced current collection discussed earlier is apparent here because, due to the ease of electron collection from the ionosphere, the usable power developed by the TSS did not peak, but continued to increase over the range of the measurements.

In addition to shedding new light on the basic current-voltage relationship, with all of its technical implications, the present TSS-1R data set may also provide scientists glimpses of important space plasma processes that occur naturally near Earth and throughout the solar system. For example:

(1) The reflection of ions by the potential barrier around the positively biased satellite created counterstreaming ion beams that, in turn, generated a spectrum of lower hybrid waves. Similar processes are seen in ionospheric double layers, at the magnetopause and at the Earth's bow shock, all of which involve the basic physics of how charged particle beams couple to, and dissipate, energy in plasmas (*Kindel and Kennel*, 1971).

(2) The modulation of electron beams during TSS-1R operations (*Gough et al.*, 1997) may be related to the cyclotron resonant maser effect. This effect is thought to be involved in the production of auroral kilometric radiation (*Wu et al.*, 1989).

(3) There is strong evidence of pickup ion processes occurring in the vicinity of the TSS satellite. Such processes are commonly associated with solar wind interactions with planets and comets (*Intriligator et al.*, 1996).

(4) The characteristics of a high voltage, negatively charged spacecraft and its effects on the ionospheric plasma are important because this study (made possible for the first time by TSS-1R) can lead to improved techniques for biasing antennas in space to enhance their coupling to the magnetospheric plasma—which has direct applications to the measurement of dc electric fields and the efficiency of VLF/ULF transmissions (*Gentile et al.*, 1997).

Satellite-ionospheric interactions under controlled conditions unique to the TSS-1R can also be used to study the collisionless expansion of plasma into the void region of the satellite's wake (*Stone et al.*, 1988). This process has many potential applications in space and was suggested as a mechanism for closure of the wake of the Moon in the solar wind plasma by *Samir et al.* (1983). Recent measurements from the WIND mission appear to confirm this closure process (*Ogilvie et al.*, 1996).

Electrodynamic tethers can also enable a number of other unique experiments in which specific scientific cause and effect mechanisms can be studied. For example, tethers can be used as long antennas to emit ULF (Alfvén lower hybrid) waves which, if our present understanding is correct, will induce pitch-angle scattering and the precipitation of electrons trapped in the radiation belts (*Kennel and Petschek*, 1966).

4. Summary

Although our understanding of the TSS-1R data set is incomplete at this point, it is apparent that (1) a sharp transition in the physics of the interaction between the TSS and the ionosphere occurs, when the satellite potential exceeds +5 V, in which electron flux to the satellite changes from being primarily accelerated ionospheric thermals to being dominated by a new suprathermal electron population; and (2) the current-voltage characteristic, possibly as a result of the above transition, is in disagreement with magnetically limited current-collection models, such as test of Parker-Murphy, which require an order-of-

magnitude higher satellite potential to collect a given current than actually observed in the TSS-1R experiment. Current extraction from the ionosphere was surprisingly efficient—to the extent, in fact, that the TSS never pushed the ionospheric plasma's limits of conductivity (i.e., there was always usable power above the overhead required to collect electrons at the satellite and inject them back into the ionosphere not the orbiter). This result is extremely encouraging for scientific and technological applications of electrodynamic tethers, such as the generation and study of current systems, electromagnetic waves, or plasma disturbances in the ionosphere, the generation of electrical power or electrodynamic thrust, and the use of tethers as VLF/ULF antennas. The complex of effects observed at the satellite are shown schematically in Figure 5.

The TSS-1R observations show that there is much concerning space plasma physics that we still do not understand—even the rather basic process of current collection that was assumed to be well in hand. As the physics contained in the TSS-1R observations become more clear, this mission may well serve to elucidate plasma-electrodynamic processes commonly found to operate in the Earth's near space environment.

Acknowledgments

The authors, on behalf of the TSS-1R PI's, wish to acknowledge their indebtedness to the many members of the TSS team at NASA-MSFC, ASI, Lockheed-Martin, Alenia, NASA-JSC, and the crew of STS-75, who made the TSS a reality. The TSS science team also owes special thanks to Tom Stuart, NASA Program Manager; Robert Carovillano, NASA Program Scientist; Gianfranco Manarini, ASI Program Manager, and Jim Sisson, John Price, Billy Nunley (deceased), and Robert McBrayer; who served as NASA-MSFC Project Manager. We are also indebted to Stan Shawhan (deceased), Robert Hudson, and Richard Diller for their leadership at NASA Headquarters early in the program.

References

- Beard, D. B., and Johnson, F. S., Ionospheric limitations on attainable satellite potential, *J. Geophys. Res.* 66, 4113, 1961.
- Dobrowolny, M. (Ed.), Il Nuovo Cimento 17C (1), Special TSS-1 Issue, 1994.
- Dobrowolny, M., and Stone N.H., A technical overview of TSS-1: The first tethered-satellite system mission, *Il Nuovo Cimento*, *17C* (1), 1, 1994.
- Gentile, L. C., Burke, W. J., Huang, C. Y., Machuzak, J. S., Hardy, D. A., Olson, D. G., Gilchrist, B. E., Lebreton, J. P., and Bonifazi, C., Negative shuttle charging during TSS-1R, *Geophys. Res. Lett.* (in press 1997).
- Gilchrist, B E., Bonifazi, C., Bilen, S. G., Raitt, W. J., Burke, W. J., Stone, N. H., and Lembreton, J. P., Enhanced electrodynamic tether currents due to electron emission from a neutral gas discharge: Results from the TSS-1R mission, *Geophys. Res. Lett.* (in press 1997).
- Gough, M. P., Burke, W. J., Hardy, D. A., Huang, C. Y., Gentile, L. C., Rubin, A. G., Oberhardt., M. R., Drobot, A. T., Thompson, D. C., and Raitt, W. J., Megahertz electron modulations observed during TSS-1R, *Geophys. Res. Lett.* (in press 1997).
- Iess, L., Harvey, C., Vannaroni, G., Lebreton, J. P., Dorowolny, M., Manning, R., Onelli, A., DeVenuto, F., Plasma waves in the sheath of the TSS-1R satellite, *Geophys. Res. Lett.* (in press 1997).
- Intriligator, D. S., Sisco, G. L., and Miller, W. D., Interstellar pickup H⁺ ions at 8.3 AU: Pioneer 10 plasma and magnetic field analyses, *Geophys. Res. Lett.* 23, 2781, 1996.

- Kennel, C. F., and Petschek H. E., Limit on stably trapped particle fluxes, *J. Geophys. Res.* 71, 1, 1966.
- Kindel, J. M., and Kennel, C. F., Topside current instabilities, *J. Geophys. Res.* 76, 3055, 1971.
- Laframboise, J. G., and Sonmor, L. J., Current collection by probes and electrodes in space magnetoplasmas; A review, *J. Geophys. Res.* 98, 337, 1993.
- Langmuir, I., and Blodgett, K. B., Current limited by space charge between coaxial cylinders, *Phys. Rev.* 22, 347, 1923.
- Langmuir, I., and Blodgett, K. B., Current limited by space charge between concentric spheres, *Phys. Rev.* 23, 49, 1924.
- Mariani F., Candidi, M., Orsini, S., Terenzi, R., Agresti, R., Musmann, G., Rahm, M., Ness, N. F., Acuna, M., Panetta, P., and Neubouer, F., Current flow through high-voltage sheaths observed by the TEMAG experiment during TSS-1R, *Geophys. Res. Lett.* (in press 1997).
- Ogilvie, K. W., Steinbert, J. T., Fitzenreiter, R. J., Owen, C. J., Lazarus, A. J., Farrell, W. M., and Torbert, R. B., Observations of the lunar plasma wake from the WIND spacecraft on December 27, 1994, *Geophys. Res. Lett.* 23, 1255, 1996.
- Papadopoulos, D., Current collection in space plasmas from Langmuir to TSS-1R, EOS Trans. AGU 77 (46), 549, 1996.
- Papadopoulos, K., Chang C. L., Drobot, A. P., Stone, N. H., Bonifazi, C., Gilchrist, E. B., Hardy, K. A., Burk, W. J., The tethered satellite mission: Surprises and puzzles, *Nature*, submitted 1997.
- Parker, L. W., and Murphy, B. L., Potential buildup on an electron emitting ionospheric satellite, *J. Geophys. Res.* 72, 1631, 1967.
- Samir, U., Wright, Jr., K. H., and Stone, N. H., The expansion of a plasma into a vacuum: Basic phenomena and processes and applications to space plasma physics, *Rev. of Geophys. and Space Sci. 21*, 1631, 1983.
- Stone, N. H., Wright, Jr., K. H., Samir, U., and Hwang, K. S., On the expansion of ionospheric plasma into the near-wake of the space shuttle orbiter, *Geophys. Res. Lett.* 15, 1169, 1988.
- Stone, N. H., and Bonifazi, C., The TSS-1R mission: Overview and scientific context, *Geophys. Res. Lett.* (*in press 1997*).
- Szuszczewicz, E. P., et al., The first realtime worldwide ionospheric predictions network: An advance in support of spaceborne experimentation, on-line model validation, and space weather, *Geophys. Res. Lett.* (in press 1997).
- Thompson, D. C., Bonifazi, C., Gilchrist, B. E., Williams, S. D., Raitt, W. J., Lebreton, J. P., Burke, W. J., Stone, N. H., and Wright, Jr., K. H., The current-voltage characteristics of a large probe in low earth orbit: TSS-1R results, *Geophys. Res. Lett.* (in press 1997).
- Winningham, J. D., N. H. Stone, C. A. Gurgiolo, K. H. Wright, R. A. Frahm, and C. A. Bonifazi, Suparthermal electrons observed on the TSS-1R satellite, *Geophys. Res. Lett.* (*in press 1997*).
- Wright, K. H., Jr., Stone, N. H., Sorensen, J., Winningham, J. D., and Gurgiolo, C., Observations of reflected ions and plasma turbulence for satellite potentials greater than the ion ram energy, *Geophys. Res. Lett.* (in press 1997).
- Wu, C. S., and Yoon, P. H., and Freund, H. P., A theory of electron cyclotron waves generated along auroral field lines observed by ground facilities, *Geophys. Res. Lett.* 16, 1461, 1989.

PI/Institution	Investigation/Primary Function		
Orbiter-Mounted			
C. Bonifazi/ASI	DCORE	(e-guns, tether current control, I and V measurements	
B.E. Gilchrist/University of Michigan	SETS	(e-guns, tether current control; I, V, and plasma meas.	
D.A. Hardy/USAF Phillips Lab	SPREE	(ion and electron distributions and orbiter potential)	
S. Mende/Lockheed (Now at U.C. Berkeley)	TOP	(low light-level TV)	
Satellite-Mounted			
M. Dobrowolny/CNR/IFIS (Now at ASI)	RETE	(ac and dc electric fields, ambient electrons, sat. pot.)	
F. Mariani/Second University of Rome	TEMAG	(ac and dc magnetic fields)	
N.H. Stone/NASA/MSFC	ROPE	(ion and electron distributions, satellite potential)	
Ground-Based/Theoretical			
S. Bergamaschi/Padua University	TEID	(theoretical: tether dynamics)	
A. Drobot/SAIC	TMST	(theoretical: plasma-electrodynamic models)	
R.E. Estes/SAO	EMET	(ground-based measurements: em waves)	
G. Gullahorn/SAO	IMDN	(theoretical: tether dynamics)	
G. Tacconi/University of Genoa	OESEE	(ground-based measurements: em waves)	

 Table 1. TSS-1R Science Investigations

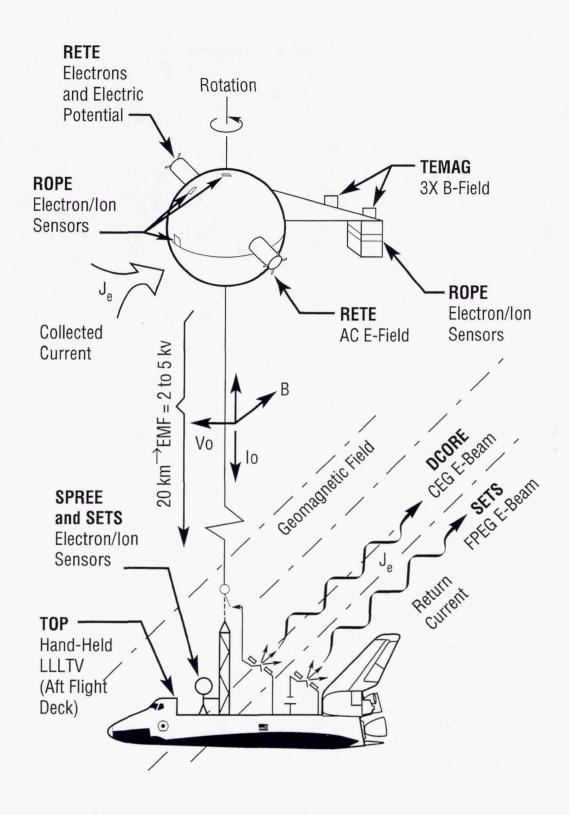


Figure 1. A functional schematic of the TSS-1R instrumentation and hardware.

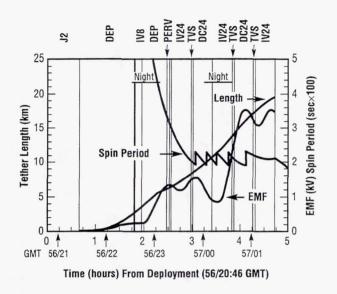


Figure 2. Conditions under which the TSS-1R data set was obtained. Occurrence of various science operating cycles listed across the top are denoted by vertical lines. (The definitions of these sequences are given in *Dobrowolny and Stone*, (1994).) Two night passes are shown by horizontal bars near the top. Time from flyaway is given across the bottom. Satellite spin (due to torque from the tether) was controlled at 0.25 rpm (period of ~200 s). Satellite flyaway occurred at GMT 56/20:46 (MET 3/00:27). (After Stone and Bonifazi, 1997).

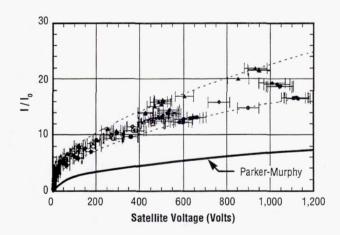


Figure 3. The TSS-1R current-voltage characteristics, obtained from the six Core electron gun controlled sweeps of the third IV24 cycle (beginning at 4:20 in Fig. 2), compared to the characteristic predicted by the Parker-Murphy model. (After Stone and Bonifazi, 1997).

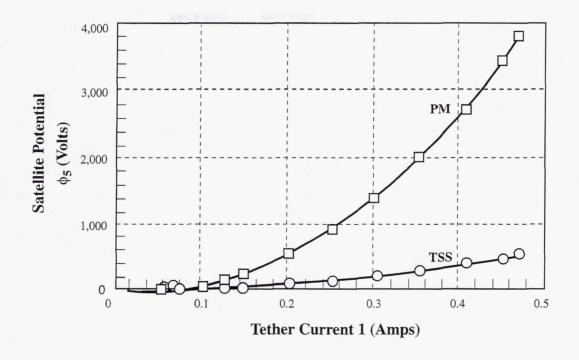


Figure 4a. Satellite voltage plotted as a function of tether current. (After Papadopoulos et al., 1997)

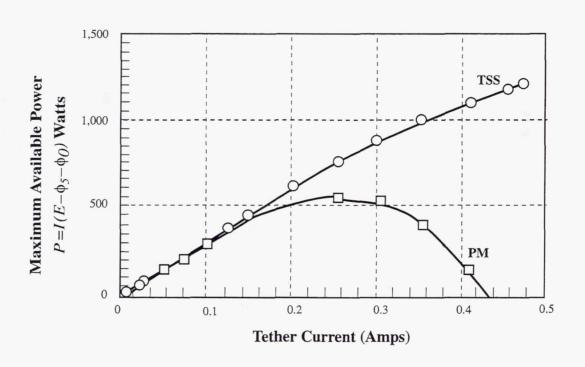


Figure 4b. Usable power plotted as a function of tether current (After Papadopoulos et al., 1997)

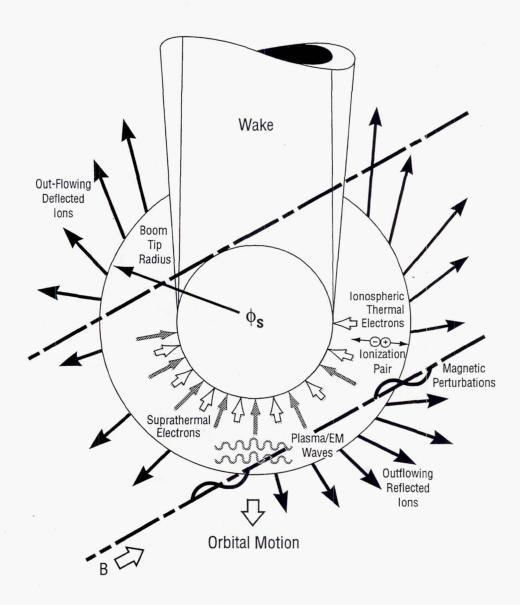


Figure 5. A composite schematic of the complex array of physical effects and characteristics observed in the near environment of the TSS satellite. (*After Stone and Bonifazi, 1997*).

TiPS: Results of a Tethered Satellite System

Jim Barnds (Swales Aerospace)

Bernard Kelm, Shannon Coffey, Bill Purdy (Naval Research Lab)

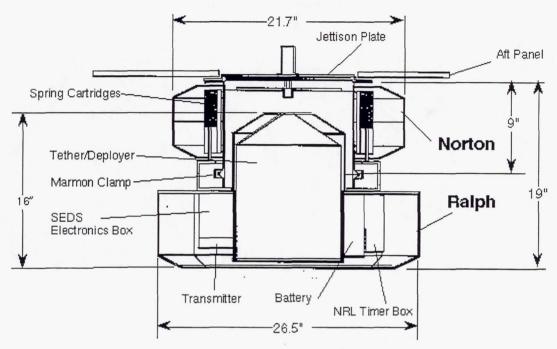
Mark Davis
(Allied Signal Technical Services Corp.)

TiPS: Tether Physics and Survivability Mission Goals and Objectives



- Study the dynamics of a tethered system
- Survivability
- Low cost secondary experiment
- Built on short schedule

System Description

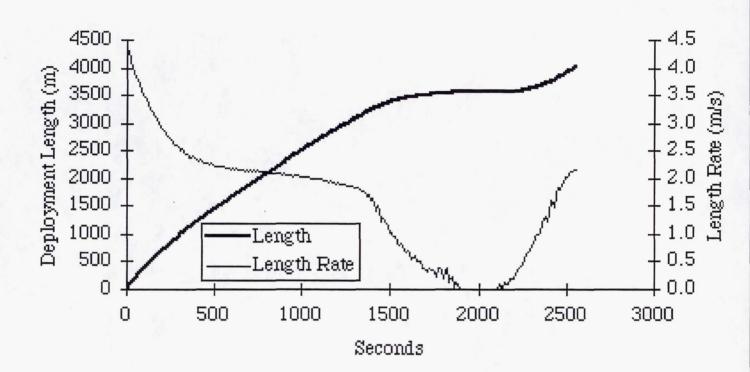


- Tether: Spectra 1000, 2-3 mm in diameter
- NASA supplied SEDS electronics
- NASA supplied canister
- No ACS, RCS, Solar Arrays
- Mass properties
 - Ralph: 95.3 lbs
 - Norton: 22.4 lbs
 - Tether: 12 lbs
- 18 Laser Retroreflectors on each endmass

Initial Mission Operations

- Deployed at 7:39 GMT, June 20, 1996
- Attitude at time of separation planned for 30 degrees from nadir
- Deployment was nominal
 - 42.5 minutes fully deploy
- Telemetry system operated nominally
- Received optical confirmation of deployment from SOR and Monument Peak Observatory

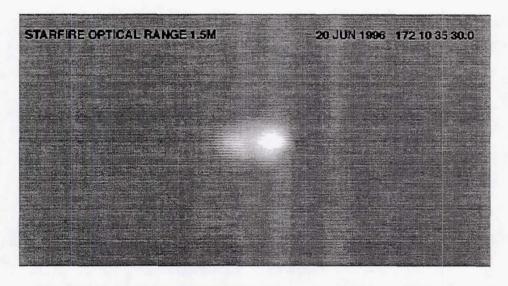
Deployment Profile

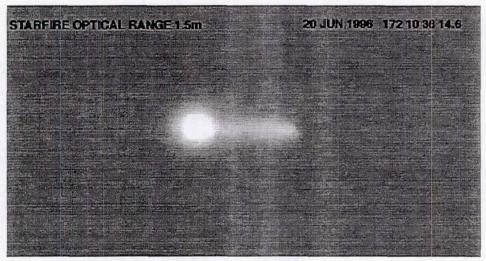


Nominal deployment

- Deployed to full length in 42.5 minutes
- Paused at 1900 seconds, restarted at 2100 seconds

Optical Confirmation of Deployment from STARFIRE Optical Range (SOR)





• Images produced by the SOR 1.5 meter telescope

Orbit and Attitude Determination

- Processing Laser and Radar Observations
 - GEODYN used to process all ranging data
 - GEODYN produced all state vectors (orbit and attitude) for tracking
 - Embedding of tether equations and partial derivatives into GEODYN

$$x - 2wy - wy - (1 + 2k-1) w^2 x = (T_x + F_x) / m$$

 $y + 2wx + wx - (1 - k-1) w^2 y = (T_y + F_y) / m$
 $z + k-1 w^2 z = (T_z + F_z) / m$

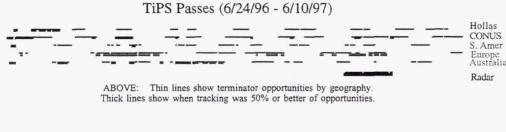
• Optical information used to empirically determine tether amplitudes and instantaneous orientations

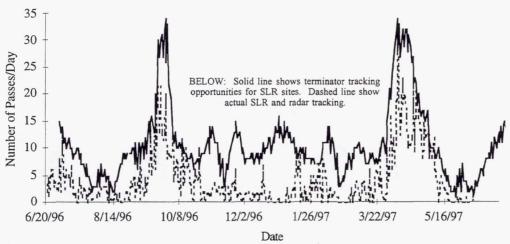
Tracking Network

- 27 Satellite Laser Ranging (SLR) sites
 - Provided laser ranging and video taping
 - Extreme accuracy thought necessary to estimate libration
- US Army ALTAIR Radar on Kwajalein Atoll
 - Coverage added to fill gaps in SLR data
- Maui Space Surveillance System
 - Provided optical images that enabled libration estimation
- Vandenberg AF Base
 - Received RF telemetry at time of deployment

Tracking Opportunities: Potential and Achieved

- SLR tracking generally limited by weather, elevation restrictions
- SLR tracking for TiPS also depended on terminator conditions
 - Normally received 2-3 passes per day
 - Two peaks with 10-20 passes per day
 - Except for peaks, unable to get sufficient data to determine tether motion
- RADAR data (2 tracks/day) from ALTAIR helped substantially during April and July, 1997





Range Data

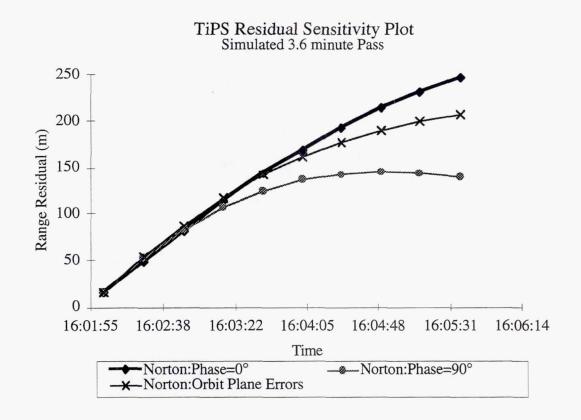
- Processing of SLR data difficult
 - Short passes
 - Orbit and libration periods are similar enough that long observation spans are necessary to separate the motions.
 - Majority of data on Ralph Few sites capable of dual ranging
 - Large coverage gaps
- Addition of RADAR data extremely helpful
 - Rapid switching between endmasses
 - Accuracy sufficient for libration determination
 - Reliable data source

Range Data Processing

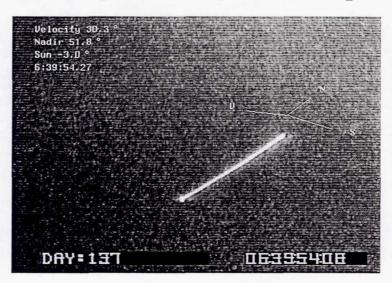
- Long-Arc Center of Mass Run
 - Tether held in alignment with nadir.
 - Endmasses offset from center of mass accounted for.
 - Assumed effects of tether motion would average out over many libration cycles.
 - Resulted in good center of mass ephemeris for TiPS
 - Allowed identification of errant or mistagged data.
- Single Pass Libration Determination Runs
 - All radar, multiple sites and dual ranged passes investigated
 - Orbit state tightly constrained
 - Good solutions fit to noise level of the data
 - <10 cm rms. for SLR data
 - <5 m for ALTAIR data
 - Resulting tether motion used as starting point for attempts at longer-arc libration runs.
- Multiple Pass Libration Determination Runs
 - Identified dense data sets in order to determine a coherent solution over multiple passes.
 - Longest fit obtained was 2.5 days (rms. error < 10 meters)

Libration Estimation Problem

- Orbit errors can look like tether errors
- Problem compounded for short arcs of data



TiPS Optical Analysis Technique



- Determine instantaneous tether orientation and libration amplitude
- Based on matching tether, nadir and velocity orientations in video frame to simulated telescope view of tether orientation
 - orbit propagated to the time of the observation to provide correct perspective
- Each frame gives indeterminate family of solutions
 - apparent length not used due to difficulties in determining fov & entire length not always in frame.
- With multiple frames from single pass and favorable pass geometry, we were often able to deduce amplitude information.

TiPS Optical Results

Amplitude Solutions

Date	In-Plane	Cross-Plane
21-Jun-96	40°±7°	25°±15°
24-Jun-96	35°±7°	21°±7°
21-Sep-96		5.2°±2°
23-Sep-96		6.6°±2°
25-Sep-96		8.5°±2°
26-Sep-96		6°±2°
29-Sep-96		5°±2°
11-Feb-97		7°±2°
6-Apr-97		5.5°±2°
20-Jul-97		5°±2°

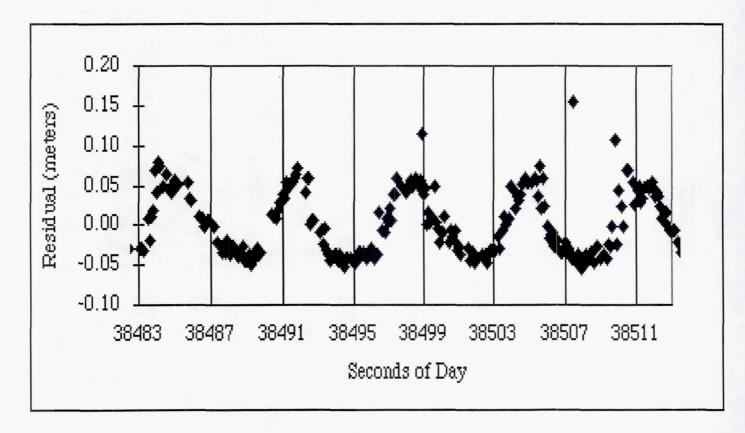
- Numerous point solutions were obtained and found to have excellent correlation with GEODYN predicts, particularly for in-plane angles
- Point solutions obtained during deployment indicate initial out-of-plane deployment angles between 30 and 37 degree's, ±10°

TiPS Optical Point Solutions

Observation Time	In-Plane	Cross-Plane	Observation Time	In-Plane	Cross-Plane
6/20/96 10:36:35	7 17 1	35°±10°	9/26/96 15:05:20	10.5°±2.5°	0°±2°
6/20/96 10:38:20	A LT	37°±10°	9/26/96 15:12:32	-10°±1°	100
6/20/96 10:42:43	9°±10°		9/26/96 15:18:03	-7°±1°	3°±1°
6/20/96 10:45:50		35°±10°	9/26/96 15:18:30	-10°±2°	737
6/20/96 10:48:35		30°±10°	9/27/96 13:59:40	3.5°±3.5°	
6/21/96 11:22:21	-4°±1°		9/27/96 14:03:16	3°±1°	
6/24/96 7:50:50	0°±5°		9/27/96 14:06:30	3°±3°	
6/24/96 7:55:49	14°±5°		9/28/96 5:11:50	-7°±2°	-3°±2°
6/24/96 7:58:00	14°±5°		9/28/96 5:18:13	-19°±1°	-5°±3°
6/24/96 9:51:00	8°±5°	-11°±5°	9/28/96 5:23:48	-12°±2°	-6°±2°
6/26/96 9:07:39		3°±9°	9/28/96 14:35:50		-6°±4°
8/19/96 7:56:00	2.5°±2.5°		9/28/96 14:43:22	2°±3°	
9/21/96 6:02:40	13°±2°	4° <u>+2</u> °	9/28/96 14:49:20		-12°±3°
9/21/96 6:05:39	13°±2°		9/29/96 15:23:06	1°±1°	
9/21/96 6:10:10	13°±2°	5°±2°	9/30/96 14:10:13	7	2°±2°
9/22/96 6:42:41	17.5°±2.5°	2.5°±2.5°	9/30/96 14:14:13	13°±1°	0°±2°
9/22/96 6:45:38	12.5°±2.5°	2.5°±2.5°	9/30/96 14:19:40	7	-3°±2°
9/22/96 6:49:28	5°±5°	2.5°±2.5°	10/1/96 14:52:25	7°±3°	0°±3°
9/23/96 5:31:44		-1°±1°	10/1/96 14:53:57	9°±2°	-3°±3°
9/23/96 5:36:31	-1°±1°		10/1/96 14:58:45	13°±3°	-4°±3°
9/23/96 5:42:44		6°±1°	2/11/97 6:07:44		0.5°±1.5°
9/24/96 6:11:53	7	5°±5°	2/11/97 6:13:30	-1°±2°	
9/24/96 6:16:30	4°±1°	5°±5°	2/11/97 6:18:35		-6.5°±1.5°
9/24/96 6:20:33		5°±5°	4/11/97 15:34:41		-3°±1.5°
9/25/96 5:01:52		-2°±1°	5/17/97 6:42:06	1.5°±1°	
9/25/96 5:07:23	-9°±2°	4°±1°	5/17/97 6:43:48		1°±1°
9/25/96 5:13:38		8°±1°	7/20/97 15:36:38	-1.5°±1°	
9/26/96 5:47:25	-10°±1°				

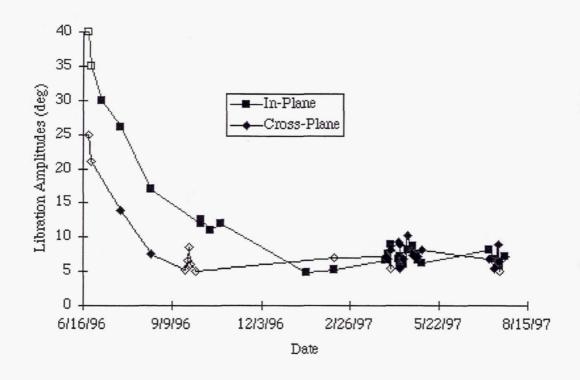
Rotation Rate Decreases

- SLR confirms rotation rate was 4.0 rpm at deployment
- Intermediate checks show a gradual decrease
- Latest data indicates rate is below 0.25 rpm
 - Unable to confirm exactly



Knowledge Gained About Librational Motion

- Observed a rapid decrease from the initially large libration amplitudes.
- Inplane and crossplane libations appeared to damp rapidly.
- Damping in good agreement with theoretical models.
 - Primary damping mechanism was internal friction
 - Tether expected to remain in current equilibrium state



Future Work

- Integrate data from Space Surveillance Network
- Many tools will be reused for ATEX (Advanced Tether Experiment)
- If funding available, will revise operations to determine TiPS motion in one year.

Tethered Satellite System Time Domain Observer Development for STS-75 Mission

Author: Haik Biglari, The Boeing Company McDonnell Douglas Aerospace haik.biglari@boeing.com

ABSTRACT

Under the influence of Earth's magnetic field the Tethered Satellite System (TSS) exhibits a special motion which resembles the motion of a child's skiprope. This motion known as SKIPROPE, only develops if the core of the tether is metallic. Active damping must be introduced to control the magnitude of this motion. Unfortunately, direct measurement of this motion is not technically feasible. Therefore, indirect measurements are needed to estimate the magnitude of this phenomenon. This paper presents a hybrid scheme in determining the magnitude and the phase of this motion for the STS075 mission. An adaptive Notch Prefilter was augmented with an Extended Kalman Filter operating at a sampling rate of 1 Hz. The resulting Observer was successfully used during the actual mission, until an unexpected fault broke the tether causing the observer to diverge.

NOMENCLATURE

x_i	Satellite quaternions $\forall i = \{1,2,3,4\}$	
$\begin{bmatrix} x_5 & x_6 \end{bmatrix}$	Skiprope motion in (U, V) plane.	
$\left[x_7 x_8 x_9 \right]$	Satellite rotational rates in rad/sec.	
$\begin{bmatrix} x_{10} & x_{11} \end{bmatrix}$	Skiprope velocity in (U, V) plane.	
x ₁₂	Tether density in kg/m.	
$\begin{bmatrix} x_{13} & x_{15} \end{bmatrix}$	Libration angle rates in rad/sec.	
$[x_{14} \ x_{16}]$	In-plane, out-of-plane libration angles.	
LVLH	Local Vertical Local Horizontal.	
TDSO	Time Domain Skiprope Observer.	
EKF	Extended Kalman Filter.	
I_{xx}	Satellite moment of inertia about x-axis.	
I_{n}	Satellite moment of inertia about y-axis.	

I_{zz}	Satellite moment of inertia about z-axis.
$\begin{bmatrix} t_x & t_y & t_z \end{bmatrix}$	Satellite torque due to tether motion.
$\left[N_x \; N_y \; N_z \right]$	Satellite torque due to thruster firings.
$\begin{bmatrix} a_U & a_V \end{bmatrix}$	Effective force due to magnetic field.
x	TSS state vector (16x1).
x	Estimate of TSS state vector (16x1).
и	TSS stochastic input (7x1) vector.
y	TSS measurement (15x1) vector.
m_o	Orbiter mass in SI units.
m_s	Satellite mass in SI units.
$P_{\mathbf{k}}$	State covariance matrix at time k.
K_k	Kalman gain at time k.
R	Measurement noise covariance matrix.
Q	Process noise covariance matrix (7x7).
B_{ϵ}	Earth's magnetic field (3x1) in LVLH.
I .	Tether current in SI units.
L	Tether length in SI units.
Ω	Shuttle orbit rate in rad/sec.

INTRODUCTION

In controlling Dynamical Systems, it is essential to have a knowledge of the controlled variable. This knowledge is sometimes available in the form of direct measurement. However, in most cases the controlled variable is not directly measurable. Kalman Filtering (KF), has been used since early 1960s to estimate the unmeasured system states which are observable. The method is based on the earlier work of Wiener's Least Squares Filtering in the mid 1940s [2] and is closely related to the Luenbeger Observer developed in the early 1960s. Application of the Kalman filter to Tethered Satellite technology

has been reported in [11, 13]. Other frequency domain approachs have been reported in [12,14].

In the Tethered Satellite System the variable to be controlled is the kinetic energy stored in the tether. This energy is in the form of skiprope motion as depicted in Fig. 1. This motion is initiated by a force induced from current flowing in the tether and the Earth's magnetic field. This force can be found from the following equation:

$$dF_r = I(dL \times B_s) \tag{1}$$

where; dF_T is the elemental force on the tether.

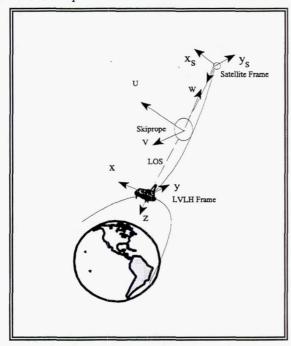


Figure 1. Tether skiprope motion

Assuming that only the first mode is present, Eq (1) can be expanded, resulting force will be:

$$dF_{T} = I |dL| [0 \ 0 \ -1]^{T} \times T_{2}^{T} T_{1}^{T} B_{LVLH}$$
 (2)

where; the T_1 and T_2 matrices are transformations from the libration frame to the LVLH frame. They are expressed as:

$$T_{1} = \begin{bmatrix} C(x_{14}) & 0 & -S(x_{14}) \\ 0 & 1 & 0 \\ S(x_{14}) & 0 & C(x_{14}) \end{bmatrix}$$

$$T_{2} = \begin{bmatrix} 1 & 0 & 0 \\ 0 & C(x_{16}) & S(x_{16}) \\ 0 & -S(x_{16}) & C(x_{16}) \end{bmatrix}$$

Simplifying Eq(2) we obtain:

$$dF_{T} = I |dL| [\hat{u} \hat{v}].$$

$$\begin{bmatrix} S(x_{16})S(x_{14}) & C(x_{16}) & -S(x_{16})C(x_{14}) \\ -C(x_{14}) & 0 & -S(x_{14}) \end{bmatrix} B_{LVLH}$$
(3)

Assuming that only the first mode is present, Eq (3) can be integrated in a closed form, then the U, V component of the resulting force per unit length will be:

$$a_{U} = \frac{4I}{\pi} [S(x_{16})S(x_{14}) \quad C(x_{16}) \quad -S(x_{16})C(x_{14})] \cdot B_{LVLH}$$

$$a_{V} = \frac{-4I}{\pi} [C(x_{14}) \quad 0 \quad S(x_{14})] \cdot B_{LVLH}$$
(4)

The induced force is only present during the time when current flows in the tether. Furthermore, during the first half of the skiprope period energy is pumped into the skiprope and during the second half of the skiprope period, energy is taken out of the skiprope. Therefore, by proper pulsing of the tether current the skiprope energy may be absorbed, and as a result the skiprope magnitude may be reduced.

A second method of reducing the skiprope magnitude is by performing a Shuttle yaw maneuver in the direction of the skiprope motion with the proper phase. Regardless of the damping method, it is important to correctly and reliably estimate both the magnitude and the phase of the skiprope motion. Since EKF is a model-based estimator, a simplified dynamical model of TSS becomes necessary.

TETHER DYNAMIC EQUATIONS

The dynamics of TSS is best described by a set of Partial Differential Equations (PDE). However, an approximation must be made for numerical implementation. One such approximation is to divide the tether into several sections, and lump the mass of each section into a bead. This technique converts a set of PDEs to a set of Ordinary Differential Equations (ODE). This method has become known as the TSS bead model. In our initial implementation a single bead model is used which is sufficient if only

the first mode is to be controlled. This formulation assumes an equivalent tether mass, rotating around the line-of-sight between the satellite and the Shuttle, which transfers it's energy to the satellite through a massless tether. A set of sixteen coupled non-linear differential equations describe this motion. The four equations describing the rigid body kinematics of the satellite are:

$$dx_{1}/dt = 0.5(x_{g}x_{2} - x_{g}x_{3} + x_{f}x_{4}) + 0.5\Omega x_{3} + u_{q}$$

$$dx_{2}/dt = 0.5(-x_{g}x_{1} + x_{f}x_{3} + x_{g}x_{4}) + 0.5\Omega x_{4} + u_{q}$$

$$dx_{3}/dt = 0.5(x_{g}x_{1} - x_{f}x_{2} + x_{g}x_{4}) - 0.5\Omega x_{1} + u_{q}$$

$$dx_{4}/dt = 0.5(-x_{f}x_{1} - x_{g}x_{2} - x_{g}x_{3}) - 0.5\Omega x_{2} + u_{q}$$

If we denote the instantaneous position of the tether at the mid node bead x_s, x_6 , (see

(U, V) plane in Figure 1.)

$$\frac{dx_5}{dt} = x_{10}$$

$$\frac{dx_6}{dt} = x_{11}$$
(6)

The rigid body dynamics for the satellite becomes:

$$\frac{dx_{7}}{dt} = \left[t_{x} + N_{x} + x_{g}x_{g}(I_{yy} - I_{zz})\right] / I_{zx} + u_{r}$$

$$\frac{dx_{g}}{dt} = \left[t_{y} + N_{y} + x_{f}x_{g}(I_{zz} - I_{xz})\right] / I_{yy} + u_{r}$$

$$\frac{dx_{g}}{dt} = \left[t_{z} + N_{z} + x_{f}x_{g}(I_{yy} - I_{zz})\right] / I_{zz} + u_{r}$$
(7)

Since the higher order modes are not modeled, and the thruster firing frequencies are much higher than one Hertz, the thruster firing terms $[N_x N_y N_z]$ can be neglected. However, to compensate, a higher process noise will be assumed. The set of equations describing the tether acceleration then becomes:

$$\frac{dx_{10}}{dt} / dt = \left[a_{U} - \pi^{2} F x_{J} L^{2} \right] / x_{12} + u_{u} dx_{11} / dt = \left[a_{V} - \pi^{2} F x_{J} L^{2} \right] / x_{12} + u_{v}$$
 (8)

The effective tether density is essentially constant and can be used as slack state variable. Therefore,

$$dx_{12}/dt = u_d ag{9}$$

The remaining four Equations describe the tether in-

plane and out-of-plane libration angles and their derivatives respectively are:

$$dx_{13}/dt = -3 \Omega^2 S(x_{14}) C(x_{14}) -$$

$$2(x_{13} + \Omega) [\dot{L}/L - x_{15} \tan(x_{16})] + u_{in}$$

$$dx_{14}/dt = x_{13}$$

$$dx_{15}/dt = -S(x_{16})C(x_{16})$$

$$[3\Omega^{2}C^{2}(x_{14}) + (x_{13} + \Omega)^{2}] - 2\dot{L}x_{15}/L + u_{out}$$

$$dx_{16}/dt = x_{15}$$
(10)

TETHER STATIC EQUATIONS

The following set of static equations are used to compute the forces and torques acting on the satellite.

$$\begin{bmatrix} t_x \\ t_y \\ t_z \end{bmatrix} = \begin{bmatrix} 0 & -r_z & r_y \\ r_z & 0 & -r_x \\ -r_y & r_x & 0 \end{bmatrix} \cdot A \cdot B \cdot C \cdot \begin{bmatrix} \pi x_s / L \\ -\pi x_6 / L \end{bmatrix} \cdot F \quad (11)$$

where A is the Direction Cosine matrix, which transforms vectors from LVLH to the satellite coordinate system. It is most conveniently expressed in terms of the elements of the quaternion vector:

$$A = \begin{bmatrix} x_1^2 - x_2^2 - x_3^2 + x_4^2 & 2(x_1x_2 + x_3x_4) & 2(x_1x_3 - x_2x_4) \\ 2(x_1x_2 - x_3x_4) & -x_1^2 + x_2^2 - x_3^2 + x_4^2 & 2(x_2x_3 + x_1x_4) \\ 2(x_1x_3 + x_2x_4) & 2(x_2x_3 - x_1x_4) & -x_1^2 - x_2^2 + x_3^2 + x_4^2 \end{bmatrix}$$

The tether tension F, can be approximated as:

$$F = 3 \Omega^2 L(m_0 - 0.5x_1L)(m_1 + 0.5x_1L) / (m_0 + m_1)$$

EXTENDED KALMAN FILTER

In the previous sections, we formulated the first mode equations of motion which govern the TSS. For the sake of simplicity, we shall refer to the resulting sixteen differential equations by the following state-space representation:

$$\dot{x} = f(x) + Gu
y = h(x) + Dv$$
(12)

where \boldsymbol{x} represents the state vector and \boldsymbol{u} , \boldsymbol{v} represent additive process noise and measurement noise, respectively and \boldsymbol{G} , \boldsymbol{D} are selection matrices. Therefore,

$$x = [x_1 \ x_2 \ x_3 \ \dots \ x_{16}]^T$$

$$\boldsymbol{u} = [u_q \ u_r \ u_u \ u_v \ u_d \ u_{in} \ u_{out}]^T$$

Where:

 $u_{o} = A$ 4-vector process noise for the satellite kinematics

u = A 3-vector process noise for the satellite dynamics

 u_5 = Process noise in the u direction

u = Process noise in the v direction

u = Process noise of the tether density

u 35 = Process noise of the in-plane libration angle

u ness = Process noise of the out-of-plane libration angle

Similarly the measurement noise ν may be expressed as:

$$\mathbf{v} = [\mathbf{v}_a \ \mathbf{v}_r \ \mathbf{v}_{ES} \ \mathbf{v}_B \ \mathbf{v}_p]^T$$

Where:

 $v_a = A$ 3-vector noise covariance of satellite attitude data $v_r = A$ 3-vector noise covariance of the satellite rate data

 v_{ES} = A 2-vector noise covariance of the Earth Sensor data

 $v_B = A$ 3-vector noise covariance of the magnetometer data

 v_p = A 6-vector noise covariance of the pseudo measurements

MEASUREMENTS

The measurement vector y, includes four distinct sets of measurements and a set of pseudo measurements:

$$y = [y_{attitude} \mid y_{rate} \mid y_{ES} \mid y_{B} \mid y_{Pseudo}]^T$$

where the first set of measurements are satellite attitude data with the following sequence.:

$$y_{attitude} = [y_p \ y_y \ y_r]$$

The second set of measurements are satellite rate data defined with the following sequence:

$$y_{rate} = [y_{\omega x} \ y_{\omega y} \ y_{\omega z}]$$

The next set of measurement data is the Earth Sensors, which are defined as:

$$y_{ES} = [y_{ES_p} \ y_{ES_p}]$$

This is followed by magnetometer measurements:

$$y_B = [B_x \ B_y \ B_z]$$

Each set of measurements is a function of system the state variable x. Therefore, the states may be computed from these measurements. Similarly, any measurement can be estimated using the estimated states. Thus, the residuals may be formed by finding the difference between the computed states from estimated states. This formulation naturally resolves the data drop out problem. If a particular measurement is not available then the corresponding computed state is replaced by estimated state. As a

result the corresponding residual becomes null, this in turn implies that the corresponding innovation equation will not update the state with new information, which is indeed true. The first set of computed states are the quaternions derived from the attitude measurements.

$$\begin{array}{l} \textit{Qmeas1} = \textit{C}(y_{y}/2)\textit{C}(y_{p}/2)\textit{S}(y_{f}/2) - \textit{S}(y_{y}/2)\textit{S}(y_{p}/2)\textit{C}(y_{f}/2) \\ \textit{Qmeas2} = \textit{C}(y_{y}/2)\textit{S}(y_{p}/2)\textit{C}(y_{f}/2) - \textit{S}(y_{y}/2)\textit{C}(y_{f}/2)\textit{S}(y_{f}/2) \\ \textit{Qmeas3} = \textit{S}(y_{y}/2)\textit{C}(y_{f}/2)\textit{C}(y_{f}/2) - \textit{C}(y_{y}/2)\textit{S}(y_{f}/2)\textit{S}(y_{f}/2) \\ \textit{Qmeas4} = \textit{C}(y_{y}/2)\textit{C}(y_{f}/2)\textit{C}(y_{f}/2) - \textit{S}(y_{y}/2)\textit{S}(y_{f}/2)\textit{S}(y_{f}/2) \\ \end{array}$$

For the Earth Sensor, the satellite roll and pitch angle are telemetered, which contain some information about the satellite quaternions. Therefore, to compute these quaternions a satellite yaw angle is also needed. This can be supplied from the estimated satellite yaw angle, which is derived from the estimated direction cosine matrix $A_{\rm ext}$. The

estimated satellite yaw Ψ , becomes:

$$\Psi = Atan \left[\frac{A_{est}(1,2)}{A_{est}(1,1)} \right]$$
 (13)

The computed quaternions found fromEarth Sensor data can be expressed as:

$$\begin{split} Qearth1 &= C(\Psi/2)C(y_{\it ep}/2)S(y_{\it ep}/2) - S(\Psi/2)S(y_{\it ep}/2)C(y_{\it ep}/2)\\ Qearth2 &= C(\Psi/2)S(y_{\it ep}/2)C(y_{\it ep}/2) - S(\Psi/2)C(y_{\it ep}/2)S(y_{\it ep}/2)\\ Qearth3 &= S(\Psi/2)C(y_{\it ep}/2)C(y_{\it ep}/2) - C(\Psi/2)S(y_{\it ep}/2)S(y_{\it ep}/2)\\ Qearth4 &= C(\Psi/2)C(y_{\it ep}/2)C(y_{\it ep}/2) - S(\Psi/2)S(y_{\it ep}/2)S(y_{\it ep}/2)\\ \end{split}$$

The magnetometer outputs are also a function of satellite quaternions:

$$y_B = A \cdot B_{LVLH} + v_B \tag{15}$$

where B_{LVLH} is computed from a Spherical Harmonic Expansion of Earth's magnetic field, based on the latitude and the longitude of LVLH origin.

PSEUDO MEASUREMENTS

The pseudo measurements are a set of computed quaternions from rates, the skiprope U component derived from the Adaptive Notch Filter (ANF) and the skiprope V component derived from the ANF. The computed quaternions from the rates are based on the discrete kinematic equation, where the previous angular rates and the previous set of quaternions are used to compute a new set of quaternions. The pseudo measurements provide complete observability with only gyro rate data when the satellite is not spinning. However, when the satellite spins the minimum required data is satellite rates, Earth sensor data, and magnetometer data. The set of equations

used for computation of the pseudo measurements

$$\begin{cases} V_{Preudo} = \\ [Cos(\omega_e T/2)I + \frac{1}{\omega_e} Sin(\omega_e T/2)\Omega_e][x_1 x_2 x_3 x_4]^T \\ U_{est} \\ V_{est} \end{cases}$$

Where ω_{a} , Ω_{a} may be computed from

$$\omega_{ex} = \omega_x + A(1,2) \Omega$$

$$\omega_{ey} = \omega_y + A(2,2) \Omega$$

$$\omega_{ez} = \omega_z + A(3,2) \Omega$$
(17)

$$\omega_e = \sqrt{\omega_{ex}^2 + \omega_{ey}^2 + \omega_{ez}^2} \tag{18}$$

$$\Omega_{e} = \begin{bmatrix}
0 & \omega_{ez} & -\omega_{ey} & \omega_{ex} \\
-\omega_{ez} & 0 & \omega_{ex} & \omega_{ey} \\
\omega_{ey} & -\omega_{ex} & 0 & \omega_{ez} \\
-\omega_{ex} & -\omega_{ey} & -\omega_{ez} & 0
\end{bmatrix}$$
(19)

THE ADAPTIVE NOTCH PREFILTER

This is a bandpass notch filter (complement of band reject notch filter) designed to provide a pseudo measurement for the skiprope. It is assumed that the satellite roll angle and the satellite pitch angles in (2,1,3) sequence are available. It is important to note that the telemetered data as received, is in (3,2,1) sequence which is not the proper sequence for this type of filter. This is due to the fact that the roll and pitch angle in this sequence are modulated by the yaw angle. The prefilter is adaptive because its center frequency is a function of the length of the tether. First, a sequence conversion is performed. Then the converted angles are fed to the prefilter. The prefilter processes the converted data by using a set of two second order notch filters. Each filter is centered around the natural frequency of the first mode of skiprope. The frequency domain representation of each notch filter becomes:

$$\frac{V_{est}(s)}{\Theta_{pitch}(s)} = \frac{s/\alpha}{(s/\alpha)^2 + s/\alpha + (\omega_s/\alpha)^2}$$
(20)

and similarly for the V component we have:

$$\frac{V_{est}(s)}{\Theta_{roll}(s)} = \frac{s/\alpha}{(s/\alpha)^2 + s/\alpha + (\omega_s/\alpha)^2}$$
(21)

 α is the bandwidth and ω_{r} is the Where, center frequency which is a function of tether tension, tether length, and tether density, as shown by the following equation:

$$\omega_s^2 = F \cdot \pi^2 / (L \cdot x(12)) \tag{22}$$

The bandwidth was set to .01 rad/sec which is about .5 deg/sec. Since the actual implementation requires Discrete Domain representation: The discrete Domain representation for the U component becomes:

$$\begin{bmatrix} x_1 \\ x_2 \\ n+1 \end{bmatrix} = \begin{bmatrix} -T\alpha + 1 & -T\omega_s^2 \\ T & 1 \end{bmatrix} \begin{bmatrix} x_1 \\ x_2 \\ n \end{bmatrix} + \begin{bmatrix} T \\ \theta \end{bmatrix} \theta_{pitch}(23)$$

And the skiprope estimate in the U direction becomes:

$$U_{est} = \begin{bmatrix} L\alpha & 0 \\ \pi & 0 \end{bmatrix} \begin{bmatrix} x_1 \\ x_2 \\ x_1 \end{bmatrix}$$
 (24)

Similarly, the roll data is processed by:

$$\begin{bmatrix} y_1 \\ y_2 \end{bmatrix}_{n=1} = \begin{bmatrix} -T\alpha + 1 & -T\omega_s^2 \\ T & 1 \end{bmatrix} \begin{bmatrix} y_1 \\ y_2 \end{bmatrix}_n + \begin{bmatrix} T \\ \theta \end{bmatrix} \theta_{roll} (25)$$

And the skiprope estimate in the V direction becomes:

$$V_{est} = \left[\frac{L\alpha}{\pi} \quad \boldsymbol{\theta}\right]_{y_2}^{y_1} \tag{26}$$

The Bode plot $\{\alpha = .01, \omega_s = (2\pi/600)\}\$ is shown in Figure

2. It should be noted that the above estimates must be adjusted to take into account the skiprope offset due to current flow, therefore the skiprope offset may be computed from:

$$\begin{bmatrix} \Delta U \\ \Delta V \end{bmatrix}_{n-1} = \begin{bmatrix} 1 - T \omega_s & 0 \\ 0 & 1 - T \omega_s \end{bmatrix} \begin{bmatrix} \Delta U \\ \Delta V \end{bmatrix}_n + \begin{bmatrix} Ta_U / (x_{12} \omega_s) \\ Ta_V / (x_{12} \omega_s) \end{bmatrix}$$
(27)

Correcting for the offset, we obtain:

$$U_{\text{est}} - U_{\text{est}} + \Delta U$$
 (28)

Similarly:

$$V_{est} - V_{est} + \Delta V$$
 (29)

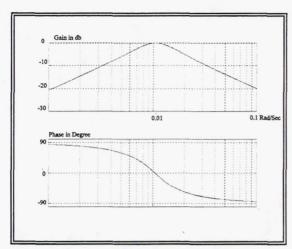


Figure 2. Frequency response of ANF.

THE EKF MEASUREMENT UPDATE

The EKF updates the skiprope estimates every second to reflect the effects of measurements. If no measurement is available then the state evolution is propagated by the model. Therefore, EKF time update takes the form of:

$$\dot{\hat{x}} = f(\hat{x}) \tag{30}$$

During the time update, the state covariances are also updated by first linearizing the state equations about the operating point:

$$F = \frac{\partial f}{\partial x} /$$

$$x = \hat{x}$$
(31)

$$H = \frac{\partial h}{\partial x} / x = \hat{x}$$
 (32)

which result in a linear system:

$$\begin{aligned}
\delta \dot{x} &= F \cdot \delta x + G u \\
\delta y &= H \cdot \delta x + D v
\end{aligned} \tag{33}$$

Then the above continuous system is converted to a discrete linear system by the exponential method:

Then the state covariance becomes:

$$x_{k} = \Phi_{k-1} \cdot x_{k-1} + \int_{t_{k,l}}^{t_{k}} \Phi_{k-1} \cdot G \cdot u_{k} d\tau$$

$$Then the state covariance becomes:
$$P_{k}^{T} = S_{k} P_{k}^{T} S_{k}^{T} + K_{k} R_{k} K_{k}^{T}$$$$

where Φ_{k} is the state transition matrix at time k, and is defined as:

$$\Phi_{k} = e^{F(x_{k})\Delta t} \tag{35}$$

Assuming that system dynamics and input do not change between the sampling interval ($\Delta t = 1 \text{ sec}$), Eq(20) then becomes:

$$x_k = \Phi_{k-1} \cdot x_{k-1} + w_k \tag{36}$$

Then, the corresponding discrete process noise

$$Q_{k} = [\Phi_{k} \cdot G \cdot Q \cdot G^{T} \Phi_{k}^{T}](\Delta t)$$
 (37)

where O is determined empirically using a high fidelity TSS simulation. Now the covariance P_{k} can be propagated during the time update (see section 5.3.3):

$$P_{k} = \Phi_{k-1} P_{k-1} \quad \Phi_{k-1}^{T} + Q_{k} \tag{38}$$

Measurement update is ideally performed once every second. Therefore, the system measurement equations must be linearized about the operating point after each measurement. Therefore, the variation in measurement becomes:

$$\delta y = H_k \cdot \delta x + D v \tag{39}$$

and corresponding measurement noise covariance becomes:

$$R_k = D \cdot R \cdot D^T \tag{40}$$

which results in a Kalman gain K_k , computed from:

$$K_{k}^{-} = P_{k}^{-} H_{k}^{T} [H_{k} P_{k}^{-} H_{k}^{T} + R_{k}]^{-1}$$
(41)

The measurement covariance matrix R_{k} diagonal matrix and it's diagonal elements may be increased to a large number if the corresponding measurement is not available or is not to be used. The next step is evaluation of the innovation equation:

$$\hat{x}_k = \hat{x}_k + K_k [y_k - h(\hat{x}_k)] \tag{42}$$

where the term in the bracket represents the residual of the estimation process, which has to be minimized in an optimal manner.

Finally, the state covariance matrix is updated with new information:

$$S_k = /I - K_k H_k / \tag{43}$$

$$P_k^* = S_k P_k^* S_k^T + K_k R_k K_k^T \tag{44}$$

EKF TIME UPDATE

Eq (2) thru Eq (11) are propagated in time until a new measurement becomes available. In normal operating conditions, approximately every second there should be a measurement. If no measurement becomes available by the end of any sample period, the filter goes into DEAD RECKONING mode until a new measurement becomes available. DEAD RECKONING can continue for approximately half of the orbit time. However, it is important to note that DEAD RECKONING is only meaningful when the TDSO has locked into an acceptable solution.

BAD DATA IDENTIFICATION & REJECTION

For robust operation of the EKF it is essential to identify and reject telemetry dropouts. A set of flags is needed to indicate whether data from the telemetry stream is to be used or rejected. If a measurement fails limit checking it's flag is set to zero, otherwise it is set to one. However, some measurement data may actually pass the limit checking process but still not contain valid data. Hence, these flags can also be set manually. An automatic bad data identification is also implemented where the residuals are normalized by their corresponding expected variations. If this quantity exceeds a predefined threshold then the corresponding measurement is declared bad.

THE PROBABILITY ELLIPSE

For every time step, the TDSO computes a 50% probability ellipse in the neighborhood of the estimated skiprope. The ellipse represents a region in space which is perpendicular to the tether at the mid node. The major and minor axis of ellipse are located in the U,V plane. If we designate this region by R then the problem is to find a region R such that the probability of finding the mid node at that region would be 50% or mathematically:

$$P\{(x,y \text{ of skiprope}) \in R\} = 0.5 \tag{45}$$

The joint probability density for this process is assumed to be Gaussion with a mean concentrated at the estimated value of the skiprope, therefore:

$$f(x, y) = \frac{e^{-0.5(x-u \ y-v)\Lambda^{-1}(x-u \ y-v)^{T}}}{2 \cdot \pi \cdot (det \Lambda)^{0.5}}$$
(46)

Where the covariance Λ , is updated every second from the

error covariance obtained from EKF:

$$\Lambda = \begin{bmatrix} P(5,5) & P(5,6) \\ P(6,5) & P(6,6) \end{bmatrix}$$
 (47)

For the ease of computation, we can remove the mean by sliding the coordinate system to u, v. We must keep in mind that the region R will be centered around u, v. Now, define a new moving coordinate system:

$$\begin{aligned}
x_1 &= x - u \\
x_2 &= x - v
\end{aligned} \tag{48}$$

Then the joint probability density becomes:

$$f(x_p, y_p) = \frac{e^{-0.5(x_1, y_p)\Lambda^{-1}(x_1, y_p)^T}}{2 \cdot \pi \cdot (det \Lambda)^{0.5}}$$
(49)

To find the region, we must double integrate Eq(49) and equate the result to 50%:

$$\int \int_{\{x_{I}, y_{I}\} \in \mathbb{R}_{I}} f(x_{I}, y_{I}) dx_{I} dy_{I} =$$

$$\int \int \int_{\{x_{I}, y_{I}\} \in \mathbb{R}_{I}} \frac{e^{-0.5(x_{I} y_{I})\Lambda^{-1}(x_{I} y_{I})^{T}} dx_{I} dy_{I} = 0.5$$

$$2 \cdot \pi \cdot (\det \Lambda)^{0.5} dx_{I} dy_{I} = 0.5$$

Now, change the coordinate system one more time to diagonalize the covariance matrix:

$$\begin{bmatrix} x_1 \\ y_1 \end{bmatrix} = A \cdot \begin{bmatrix} x_2 \\ y_2 \end{bmatrix} \tag{51}$$

Substituting Eq(4) in Eq(39)

$$\int_{\{x_2, y_2\} \in \mathbb{R}_2} \frac{e^{-0.5(x_2, y_2)A^T A^{-1} A(x_2, y_2)^T}}{2 \cdot \pi \cdot (\det \Lambda)^{0.5}} dx_2 dy_2$$
(52)

The exponent of Eq(41) has a covariance which is diagonal. Therefore Eq(41) can be rewritten as:

$$\int \int_{\{x_{2},y_{3}\}\in\mathbb{R}_{2}} \frac{e^{-0.5(x_{2},y_{3})[Diag(\sigma_{x}^{2},\sigma_{y}^{2})]^{-1}(x_{2},y_{3})^{T}}}{2\cdot\pi\cdot\sigma_{x}\cdot\sigma_{y}} dx_{2}dy_{2}$$

$$= 0.5$$

$$= 0.5$$

In order to integrate Eq(42) symbolically, we need to perform another change of variable:

$$\begin{bmatrix} x_3 \\ y_3 \end{bmatrix} = \begin{bmatrix} \sigma_x & \theta \\ \theta & \sigma_y \end{bmatrix} \begin{bmatrix} x_2 \\ y_2 \end{bmatrix}$$
 (54)

Eq(42) now becomes:

$$\int \int_{\{x_{y},y_{y}\}\in R_{3}} \frac{e^{-0.5(x_{3}^{2}\cdot y_{3}^{2})}}{2\cdot \pi} dx_{3} dy_{3}$$

$$= 0.5$$
(55)

To integrate Eq(44) we must express the integral in a cylindrical coordinate system:

$$\int_{r=0}^{r=c} \int_{\theta=0}^{\theta-2\pi} \frac{e^{-r^2/2}r}{2 \cdot \pi} dr d\theta$$

$$= 0.5$$
(56)

For Eq(45) to hold we must have:

$$c = \sqrt{\ln(4)} = 1.1774 \tag{57}$$

Which implies that the region is an ellipse, centered at (u, v), where the axis of the ellipse is rotated by the eigenvectors of Λ , and the semi-major and the semiminor axis are 1.1774 times the eigenvalues of Λ .

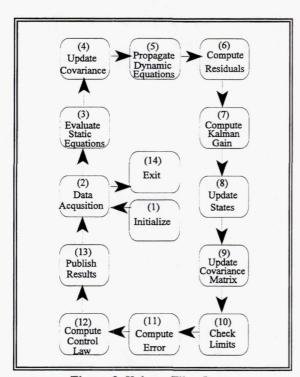


Figure 3. Kalman Filter Loop.

EKF LOOP

Figure 3. shows the sequence of execution of major TDSO functions. Blocks two through thirteen are executed every second. Block number one and block number fourteen are executed only once.

SUMMARY OF RESULTS

With proper choice of process noise, TDSO provides the satisfactory skiprope estimates. As

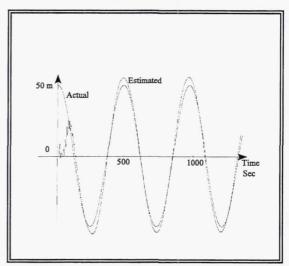


Figure 4. U Actual and U Estimated

evident, the convergence occurs in less than 250 seconds. The filter maintains a robust estimate, if system parameters_change within the expected range. Figure 4. compares a typical estimation of circular skiprope with This skiprope motion was actually observed with the estimator during STS-075 mission.

Since there is no direct skiprope measurement, the only reference is the ANF estimates. **Figure 5.** shows the comparison of the EKF estimates and the estimates obtained with the Adaptive Notch Filter.

CONCLUSION

An Adaptive Notch Filter (ANF) is augmented to an Extended Kalman Filter (EKF) for robust estimation of the motion of the tether in a Tethered Satellite System. The resulting hybrid filter is capable of estimating TSS skiprope throughout the mission. The accuracy of estimation is primarily a function of process noise specification. The filter operates in the presence of spin reversal and other disturbances and unmodeled dynamics. The filter was used successfully during the STS-075 mission.

ACKNOWLEDGMENT

The Author would like to thank NASA's support throughout all phases of this project. Specifically, my sincere appreciation goes to the following individuals: Mrs. Linda Brewster for superb software support, Mr. Jon Patterson for integration/testing and Mr. Geoffrey Hintze for the development of a preprocessor. My

gratitude goes to Dr. John Glaese and Mr. Don Tomlin for their comments on TSS dynamics. My special thanks goes to Mr. Zachary Galaboff for his dedicated efforts in making this project a success. My final thanks goes to my colleagues in Sverdrup for their encouragement, specifically I thank Mr. Mike Hannan for continued support.

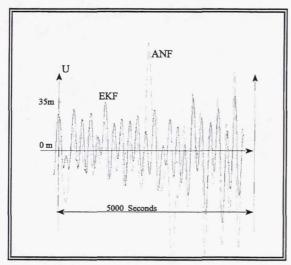


Figure 5. Estimated U component.

REFERENCES

- [1]] A. Gelb (Ed.), *Applied Optimal Estimation*, Cambrdge, Mass.: MIT Press, 1974.
- [2] R. G. Brown, P. Y.C. Hwang, Introduction to Random Signals and Applied Kalman Filtering, John Wiley & Sons, Inc. New York, 1992.
- [3] D. Graupe, *Identification of Systems*, Robert E. Krieger Publishing Co., Inc. New York, 1976.
- [4] J. R. Wertz (Ed), Spacecraft Attitude Determination and Control, Kluwer Academic Publishers, Boston Mass, 1990.
- [5] A. Papoulis, *Probability, Random Variables, and Stochastic Processes*, Mc Graw-Hill, New York 1984.
- [6] H. Biglari, "Preliminary TDSO Performance Analysis," Prepared for NASA by Sverdrup Technology Inc., Report No.: 611-019-94-05, Huntsville, Alabama, July, 1994.

- [7] H. Biglari, "TDSO Sensitivity Analysis," Prepared for NASA by Sverdrup Technology Inc., Report No.: 611-019-94-08, Huntsville, Alabama, September, 1994.
- [8] J.A. Lovingood, "A Technique for Including the Effects of Vehicle Parameter Variations in Wind Response Studies," NASA TM X-53042, May, 1964.
- [9] P.W. McBurney, "A Robust Approach to Reliable Real-Time Kalman Filtering," IEEE Position Location and Navigation Symposiu, San Diago, CA, pp 549-556, 1990.
- [10] J.V. Beck, K.J. Arnold, Parameter Estimation in Engineering and Science, John Wiley & Sons, New York, 1977.
- [11] J. Tietz, "Observer Engineering Notebook," MMAG, Denver, Colorado, Cont. NAS8-36000, 1992.
- [12] J. R. Glase, "A Complex Frequency Domain Skiprope Observer for Tethered Satellites ," Forth International Conference on Tethers in Speae, Smithsonian Institution, Washington D.C. Aprill 1995
- [13] H. Biglari, Z. J. Galabof, "An Extended Kalman Filter for Observing the Skiprope Phenomenan of Tether Satellite System," Forth International Conference on Tethers in Spcae, Smithsonian Institution, Washington D.C. Aprill 1995
- [14] A.M. Amini, G.E. Ioup, J.W. Ioup, "Constrained Itrative Spectral Deconvolution for Analysis of Closely Spaced Modal Peaks in the Fourier Transform of Tethered Satellite Dynamics Data, "Forth International Conference on Tethers in Speae, Smithsonian Institution, Washington D.C. Aprill 1995

Page intentionally left blank

STS-75/TSS-1R TETHER CONTROL & DYNAMICS OPERATIONS

Joseph L. Williams, Jr.*

The reflight of the tethered satellite system (TSS) onboard Space Shuttle Columbia during STS-75 provided many challenges to Mission Operations in preparation for and execution of the mission relating to deployment/retrieval of the tethered satellite and the control of tether dynamics. A new method of flight controller training was developed using the Internet as a backbone between the crew in the simulator, the Johnson Space Center (JSC) tether dynamics team on a set of workstations at JSC, and the Marshall Space Flight Center (MSFC) tether dynamics experts on a remote set of workstations at MSFC. This allowed the team to maximize use of the best available man-in-the-loop tether dynamics and Shuttle piloting system with the actual ground displays to be used in the Mission Control Center (MCC) in Houston, minimizing travel of the MSFC team to JSC. Finally, a clear operations concept was developed in the course of training in which a first-response team consisting of flight controllers at JSC was trained heavily in quick actions, and two teams of tether dynamics experts from MSFC, one hosted in the MCC Payload Operations Control Center (POCC) and the other in the Huntsville Operations Support Center (HOSC), were present to provide technical expertise in more long-range activities.

INTRODUCTION

The first flight of the Tethered Satellite System (TSS-1) on Space Shuttle Atlantis in August, 1992, was an extremely challenging mission. It pushed to the limits the flight crew, the supporting team on the ground, and the mission facilities. The job of my team was to control tether dynamics to ensure we met the TSS satellite deployment and retrieval profile, all of this under the auspices of the Houston Flight Director. Our primary responsibility was to oversee nominal delivery of the satellite to the onstation point, and to successfully retrieve the satellite. We produced the TSS DYNAMICS ¹ Flight Data File, which contained the procedures for nominal deployment/retrieval and the timeline defining their order of execution.

In an off-nominal situation, we were responsible for determining how to safe and recover the deployment/retrieval within the scope of our expertise and within the limits defined by the FLIGHT RULES², the document that defines the envelopes for mission success and crew safety. This involved managing tether dynamics to stop the system and

^{*} Rendezvous Guidance and Procedures Officer, United Space Alliance, 600 Gemini, Mail Code USH-423T, Houston, TX 77058, Joseph.L.Williams1@jsc.nasa.gov

¹ JSC-48087-75

² NSTS-18308

reconfiguring deployer guidance parameters to resume the mission. We also replanned activities and events relating to piloting the Orbiter and managing tether dynamics.

Pre-mission, our team served as consultants to the crew in the technical details of piloting the Orbiter in the presence of the attached TSS satellite. We provided familiarization and verification of the procedures with the crew to augment their mission preparation. We also assisted in the development of the FLIGHT RULES, drawing upon our expertise in shuttle operations and tether dynamics, to define rules governing the conduct of nominal and contingency tether operations. We also developed software for use by all parties to augment awareness of the state of the tethered system and to assist in decisions regarding actions to take.

We learned many lessons from that first experience. The Tether Control & Dynamics Operations Team (CDOT) was formed at the Johnson Space Center (JSC), Houston, in August, 1994, to address the challenges for the reflight of TSS-1 (TSS-1R), scheduled onboard Space Shuttle Columbia as part of STS-75 in February, 1996. Part of its charter was to address two specific areas relating to tether dynamics:

- How can we improve our readiness on the ground?
- How can we improve our realtime operations?

IMPROVING READINESS

Our first step was to make use of as many readily-available experts on tether dynamics as we could, tempered somewhat by concerns of economics. We identified personnel at both the Marshall Space Flight Center (MSFC) and JSC as candidates. MSFC had a team of tether dynamics experts in Huntsville who interfaced directly with the deployer hardware team pre-mission. They had great expertise in tether dynamics and ready access to key personnel on the deployer hardware side. Also, they had an interface to the TSS Mission Management structure in Huntsville. JSC also had developed tether dynamics expertise in Houston during the first tethered satellite mission. That expertise was augmented with personnel in Mission Operations who knew how to fly Shuttles and learned about tether dynamics and its ramifications to operations during the first mission. Finally, we had available a long-time tether expert as a consultant. This group of people formed the core of the operations team for managing tether dynamics. This will be discussed further later.

Another area we addressed early was that of how best to provide software support for tether dynamics training and realtime operations. It seemed clear to us that the best bang for taxpayers' dollars could be achieved if existing tools could be reshaped to meet the needs of tether dynamics operations. Furthermore, it had to fill the needs of both training and realtime operations for both flight controllers and the crew. This was an ambitious goal, but one we would not have undertaken without having the right pieces of the puzzle present already.

At JSC, we have the Rendezvous Operations Support Software (ROSS) as a basic telemetry acquisition, processing, and display system. This software was developed originally to support Shuttle rendezvous operations, but it is highly reconfigurable and could be easily tailored by the operators to display tether dynamics data as well as Shuttle-related data. Also, we have a standalone high-fidelity man-in-the-loop tether dynamics simulation called the Orbital Operations Simulator (OOS). This simulation was developed for tether analysis with a pilot in the loop. We felt it would be ideal if we could tie together

ROSS and OOS and use the integrated system for simultaneous crew and tether flight controller training.

To accomplish the link, we used a telemetry distribution system called the Information Sharing Protocol (ISP), developed at JSC. ISP is a system centered around a set of distributed, networked, TCP/IP (Transmission Control Protocol/Internet Protocol)compliant server applications communicating with client applications using ISP Application Programming Interface (API) function calls. In this case, we added a small layer of software to OOS to map internal variables into telemetry parameters and to publish this data to an ISP server. ROSS, in turn, acquired the OOS-generated "pseudo-telemetry" stream with its own acquisition module built from ISP API function calls, and supplied the data to ROSS shared memory for the ROSS display applications. For the realtime system in the Mission Control Center (MCC), the architecture could allow us to replace the pseudotelemetry source provided by OOS with a real telemetry source provided by the Orbiter without changing ROSS at all. Since our networking architecture was TCP/IP compliant, data could be routed over any network running that protocol -- such as the Internet. This offered great flexibility in development, testing, and operator training. For instance, the Skiprope Observer development team in Huntsville could tie into a telemetry stream we generated in Houston without requiring travel one way or the other.

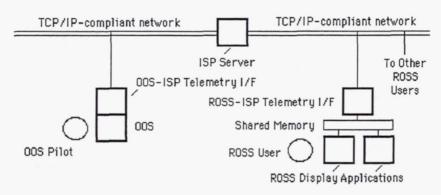


Figure 1. Tether Dynamics Simulation System Architecture

From this architecture the Tether Dynamics Simulation was born. This was completely workstation-based with OOS as a high-fidelity man-in-the-loop tether dynamics simulation piloted by the Shuttle crew. This pumped pseudo-telemetry data to an ISP server which was tied into by the users running ROSS. It was closed loop in that the ground would make appropriate calls to the crew, the crew would take the appropriate action, and the results could be seen by the ground. Two configurations of this system was used. One was where the crew was in one building at JSC, the JSC personnel were in another building at JSC, and the MSFC personnel were in Huntsville, all looking at the same data being served in realtime over the Internet. A second configuration was setup in the MCC. The crew was stationed on a Silicon Graphics workstation in the MCC, and this provided pseudo-telemetry data to an ISP server running in the control center. The tether dynamics team members were located on their respective consoles in the MCC, tied into the data with ROSS, and used the flight consoles to communicate with the crew. The Houston Flight Director and Capsule Communicator (CAPCOM) participated in each of the simulations, supported in some scenarios by the Houston Payloads Officer.

IMPROVING OPERATIONS

As we trained, we evolved our realtime operations into a two-pronged attack. First, we developed a Quick-Response Team. This team was trained in nominal TSS operations and in quick-response actions to off-nominal situations. The head of the team was the Rendezvous Guidance and Procedures Officer (RGPO) located in the Flight Control Room (FCR) of the MCC. The RGPO was responsible for the overall mission execution relative to deployment/retrieval of the satellite and management of tether dynamics. The RGPO also served as the direct point-of-contact between the tether dynamics team and the Houston Flight Director.

Supporting the RGPO was the rest of the quick-response team consisting of Tether Procedures Support, Tether Dynamics, Tether Dynamics Support, Profile, Skiprope Observer Support, and Rendezvous Operations Software Support.

- TETHER PROCEDURES SUPPORT was responsible for profile monitoring, performance gates GO/NOGO, deployment/retrieval procedures timeline execution, libration management, Orbiter Digital Autopilot (DAP) & Orbiter body pointing requirements for deployment/retrieval, and the relative motion trajectory during attached operations.
- TETHER DYNAMICS was responsible for tether lateral and longitudinal motion, skiprope management, tether twist, and satellite dynamics.
- PROFILE was responsible for deployment/retrieval profile monitoring and reconfiguration in contingency situations.
- TETHER DYNAMICS SUPPORT was responsible for managing tether motion.
- SKIPROPE OBSERVER SUPPORT was responsible for the operation of the Skiprope Observers.
- RENDEZVOUS OPERATIONS SOFTWARE SUPPORT was responsible for monitoring the distribution of tether dynamics data within the MCC and to the HOSC, and for the execution of ROSS (both onboard the Orbiter and on the ground).
- TETHER CONSULTANT provided guidance without being involved in the minute-to-minute details.

Second, we placed several of the MSFC tether dynamics experts in the Payload Operations Control Center (POCC) in the MCC. They served as liaisons to the deployer and satellite hardware communities co-located in the POCC. They were not required to travel to JSC for the Tether Dynamics simulations using the OOS-ROSS closed-loop system, but did travel to Houston for the Joint Integrated Simulations (JIS). DEPLOYER DYNAMICS, as the position was called, was staffed exclusively with personnel from MSFC.

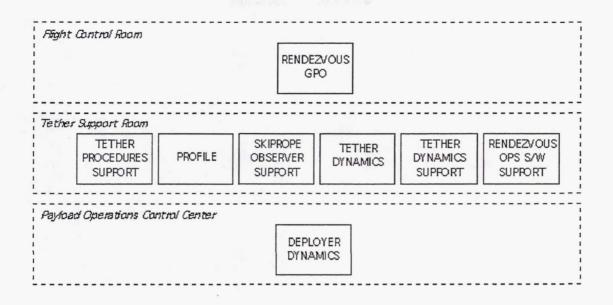


Figure 2. Tether Dynamics Realtime Operations Concept

This arrangement addressed the needs of supporting tether dynamics realtime operations in Houston. Several other tether dynamics experts served as consultants to the TSS Mission Management Team located in the Huntsville Operations Support Center (HOSC). We wished to address a need to send information from the MCC to the HOSC to augment the voice loops already in place. To do this, we extended the Internet-based architecture of our software system. The network in the MCC was also TCP/IP-compliant, so we could run ROSS and ISP in the control center as well. Furthermore, we shipped our tether computations, including the Skiprope Observer calculations, over a special TCP/IP line connecting the MCC with the HOSC. In Huntsville, the tether dynamics experts there used ROSS to acquire and display the results of our computations and thus could advise the TSS Mission Management team as to the status of the tether dynamics. This capability was available without requiring any changes to ROSS or ISP. It was simply an extension of the existing system, piggybacking on the JSC-to-MSFC line provided as part of the Remote Extension to Moscow (REM) gateway supporting Shuttle-Mir missions.

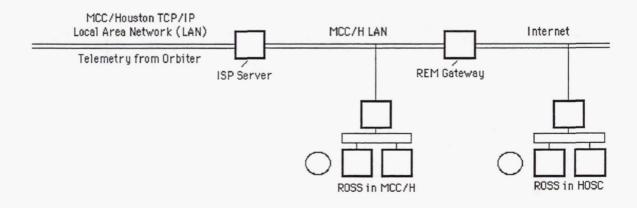


Figure 3. Software Architecture for Realtime Operations

One of the major crew requests from the first TSS mission was to have a suite of tools onboard to ease the burden of monitoring tether dynamics. Before, they had graphs and equations which required them to read numbers from a Shuttle display and either plot or compute numbers by hand. We chose to provide them with the same software we were running on the ground -- namely ROSS with ISP -- but running on an IBM ThinkPad laptop computer. For this, we ported a Unix variant called Linux to the ThinkPad and ported ROSS/ISP on top of that. Next, we tied this machine into a telemetry acquisition server onboard the Orbiter called PCDecom. PCDecom ran on another IBM ThinkPad and was tied directly into the Orbiter's telemetry processing hardware. This provided the crew with realtime tether dynamics data. Note that neither ROSS nor ISP source code had to be customized in any way to provide this capability to the crew. This approach provided the crew with a much requested capability with a minimal cost extension over that providing for critical support to the ground controller team.

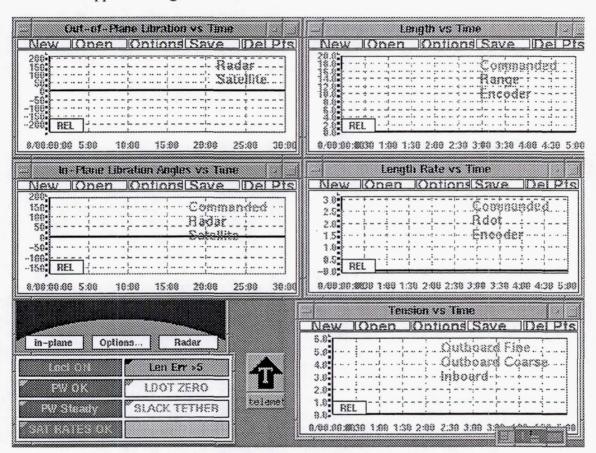


Figure 4. Sample ROSS Configuration for Onboard Use

The final area addressed for realtime operations was the TSS DYNAMICS Flight Data File (FDF). The TSS DYNAMICS FDF contained the crew procedures for the deployment/retrieval of the tether and the timeline defining the order of execution. It also addressed off-nominal scenarios. We created a "flipbook" describing quick 5-minute-orless actions to be taken by the crew to safe the system. The flipbook was referenced via a chart containing failure recognition cues.

In the tether break scenario that occured on STS-75, the confirming cue onorbit was visual. For ground controllers, not having the benefit of immediate visual confirmation,

the rest of the values clearly indicated a tether break: tether current=0, the SLK TETHER Fault Detection Annunciation (FDA), the SATZACCEL FDA and value=0 from the Z accelerometer, and high positive opening velocity from the Shuttle's rendezvous radar tracking system.

SIGNATURE \ FAILURE	TETHER BREAK	
LDOT		
TENSION	SLK TETHER	
PW		
MPC AMPS REEL		
REEL MOTOR VOLTS		
BRAKE	2 10	
SAT Z ACCEL	SAT Z ACCEL value=0	
TETHER CURRENT	0	
Θ, Φ		
RADAR	(HI +RDOT)	
VISUALS	TETHER ACCUM	

Legend: BOX = FDA message

BLANK = indication does not matter

(Parenthesis) = indication may or may not be present

Figure 5. TSS DYN Flipbook Matrix Example

The chart directed the crew to the appropriate quick-response procedure formatted in three columns: Orbiter actions, Satellite actions, and Deployer actions. Immediately following the tether break on STS-75, the crew proceeded to the TETHER BREAK section of the flipbook and performed the procedures indicated.

ORBITER	SATELLITE	DEPLOYER
1. CONTROL TETHER SLACK If slack tether exists in vicinity of orbiter: DAP: A/AUTO/PRI DAP TRANS: PULSE/PULSE/NORM(HI) FLT CNTLR PWR - ON Perform SLACK MANAGEMENT, FB 5-20 If slack continues in vicinity of orbiter: Go to CUT AND RUN, FB 5-24	1. TURN OFF INLINE THRUSTERS SM 214 TSS DEPLOY THRUSTERS IN2(IN1) OFF - ITEM 25(23) +9 9 EXEC (OFF)	(no actions)

Figure 6. TSS DYN Flipbook Procedure Example

CONCLUSIONS

How did we improve our readiness on the ground?

- We maximized our use of existing experts on-hand, both at JSC and MSFC.
- Closed-loop tether dynamics simulations provided a superior system for training the CDOT in tether dynamics operations. We suggest that this system should serve as model for similar future systems.
- The distributed networking architecture based upon ROSS and ISP proved to be an incredibly robust, reliable, and capable system. Architecture and approach used in all software phases should serve as model for similar future systems.

How did we improve our realtime operations?

- The use of JSC personnel as a quick-response team, and MSFC personnel as part of the TSS hardware team, proved to be an effective arrangement, considering both realtime execution and training costs.
- We hosted the same software on a laptop for crew use as that used for ground controller support. This reduced the cost of creating two separate systems.
- The TSS DYNAMICS Flight Data File, and especially the Flipbook, worked quite well, both for ground controllers and the crew onboard Space Shuttle Columbia.

APPENDIX

Table 1 STS-75 TETHER CONTROL & DYNAMICS OPERATIONS TEAM (CDOT) MEMBERS

Team Lead	Joe Williams (United Space Alliance)
TSS DYNAMICS Book Mgr	Sally Davis (NASA/JSC)
Rendezvous GPO	Joe Williams (United Space Alliance) Sally Davis (NASA/JSC) Bill Ober (United Space Alliance)
Tether Procedures Support	Paul Snow (United Space Alliance) Dustin Hamm (NASA/JSC) Randy Moon (United Space Alliance)
Tether Dynamics	Steve Staas (United Space Alliance) Trang Le (NASA/JSC) Doug Hamilton (United Space Alliance)
Profile	Nate Pemberton (Lockheed-Martin) Bill Othon (LinCom)
Tether Dynamics Support	Jay Estes (NASA/JSC) Debra Hurdelbrink-Meyerson (Lockheed-Martin)
Skiprope Observer Support	Haik Biglari (Sverdrup) John Glaese (Control Dynamics) John Tietz (Lockheed-Martin)
	Mike Whitlock (United Space Alliance) Carl Perkins (United Space Alliance)
Tether Consultant	Dave Lang (Lang Associates)
	Don Tomlin (NASA/MSFC) Keith Mowery (NASA/MSFC) Ken Welzyn (NASA/MSFC)
	Bob Mahoney (United Space Alliance) Dave Rose (United Space Alliance)
STS-75 Flight Crew	Jeff Hoffman (NASA/JSC)

ABOUT THE AUTHOR

Mr. Williams served as the lead Rendezvous Guidance and Procedures Officer for STS-75 as the direct representative to the Houston Flight Director of the tether deployment/retrieval and tether dynamics control team in the Flight Control Room of the Mission Control Center in Houston, TX. Mr. Williams was also the team lead of the Tethered Satellite Control & Dynamics Operations Team, consisting of members from flight operations, crew training, the STS-75 flight crew, and tether dynamics experts at the Johnson Space Center and at the Marshall Space Flight Center, which addressed the issues of tether dynamics training and execution by the flight controllers and the crew onboard Space Shuttle Columbia for STS-75.

Page intentionally left blank

THE DYNAMICS OF THE TIPS TETHER EXPERIMENT

John R. Glaese Control Dynamics Division of bd Systems September 9, 1997

Sponsorship

This work was sponsored under contract to the Naval Research Laboratory (NRL) with funding provided by the National Reconnaissance Office.

ABSTRACT

The Tether Physics and Survivability (TiPS) experiment results have been simulated and analyzed. Both the initial tether deployment phase and the long term libration phase have been studied. Available data is sparse except for telemetry from the SEDS deployer during deployment and occasional ground observations via laser and radar to indirectly estimate tether libration angles and orbital properties. These data indicate large initial in plane and out of plane libration angles of 40° and 30° respectively which were quickly damped over the first 2-3 months to values of less than 15-20°. Damping slowed from this point eventually ceasing entirely with residual amplitudes of 5-7°. Simulations of deployment matched well during early and mid deployment after appropriate adjustments were made for tether properties and the spinning of the deployer. Late deployment which included a pause and a restart of deployment did not match the restart time. However later analysis with a smaller initial out of plane attitude angle for the deployer matched much better. Libration simulations showed that internal tether damping could provide sufficient damping to explain libration angle decay rates. A nonlinear libration resonance phenomenon was observed which helped explain damping of out of plane libration. The simulation results adequately duplicate the TiPS behavior, but some discrepancies remain such how to account for observed simultaneous in plane and out of plane damping which probably can't be answered without more precise libration data.

PRESENTATION OUTLINE AND OVERVIEW

- TiPS Deployment Dynamics Study
 - Best estimate of initial conditions for libration
 - Adds to knowledge of behavior of SEDS deployers
 - Spinning deployer effects
 - Initial deployment attitude
 - Tether bowing
 - Estimate of skip rope
- Nonlinear Tension and Friction Model
- TiPS Libration Dynamics Study (Damping)
 - Minimal data available to study dynamics
 - SEDS deployment data (except tension) available
 - Laser and radar ground remote observations used to estimate libration
 - No libration angles known during deployment
 - Large tether bow observed, large skip rope inferred
 - Initial librations 40° and 30° for in plane and out of plane respectively
 - Significant initial libration damping in and out of plane, settles at 5°-7° steady amplitude
- Deployment Revisited
- Conclusions

DEPLOYMENT DYNAMICS STUDY

- Form of Tension Model Given from Previous Work
- TiPS Deployer Spinning at 3 RPM at Time of Deployment Start. Addition to Deployer Model Required to Model this
 - Minimum deployer friction when tether turn rate induced by deployment just counteracts cannister spin (tether direction of wrap must be in same direction as spin so that tether despins as it unwraps -- this is consistent with data)
 - Most deployer parameters retain SEDS-1&2 values
- Initial Deployer Attitude Unknown
 - Varied for best match of deployment ending angles to starting libration Angles (40° and 30° previously noted)
 - Cone angle of deployer spin estimated by NRL to be within 28° of local vertical at deployment start

SEDS DEPLOYER TENSION MODEL

$$T_{dep} = T_{dep\, \mathrm{min}} + I_{\mathit{mult}} \rho (1 - A \frac{L}{L_{\mathrm{max}}})^{-E} \stackrel{?}{L}^2. \label{eq:Tdep}$$

$$T_{dep \, min} = T_{dep \, min \, 0} + (T_{dep \, min \, 1} - T_{dep \, min \, 0})(2\phi - \phi^2)$$
; where $\phi = smaller(1, \frac{L}{L_0})$

Sling-Scrub Tension Modification: Models tether moving relatively freely in the open space between the spool and canister inner surface to rubbing against the spool surface on its way to the exit port at the top of the canister.

$$T_{dep_total} \, = \, T_{dep} \, + S_{Sl_sc} \, T_{dep \, \mathrm{min} \, 1} \, . \label{eq:total_dep}$$

Assumed to occur as the deployed length exceeds a minimum value $f_{tran} = L/L_{max}$ and as the deployment rate drops below the transitional level $V_{mnsl.}$

Spinning Deployer Modification
$$I_{mult} \rho (1 - A \frac{L}{L_{max}})^{-E} (\dot{L} - \dot{L_0})^2$$

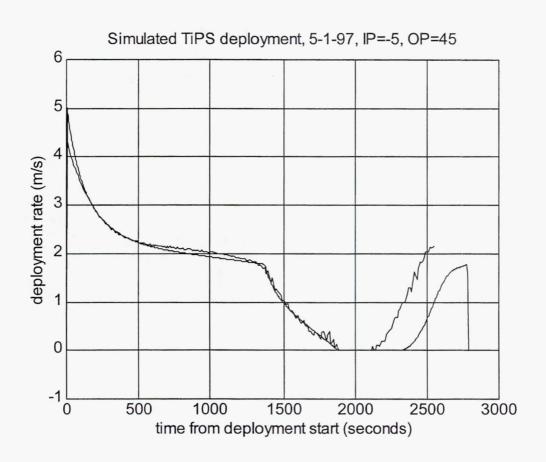
 L_0 is the rate at which tether rotation induced by deployment cancels the tether rotation induced by canister rotation.

The tension model parameters are
$$I_{mult}$$
 = 7.5; ρ = 1.5 gm/m; A = 0.9424; E = 0.6; L_{max} = 4.0 km; $S_{sl\ sc}$ = 3.5;

 $L_0 = 0.8$ m/s. The expected increase in tension due to the T_{depmin} term cannot be observed in the data. Thus, we have taken advantage of this feature of the model to allow us to select a separate value for the scrubbing friction. Accordingly, we have used the values $T_{depmin0} = -0.017$ N and $L_0 = \infty$; $T_{depmin1} = 0.015$ N. The remaining parameters are $f_{tran = 0.8}$ and $V_{mnsl} = 3.2$ m/s.

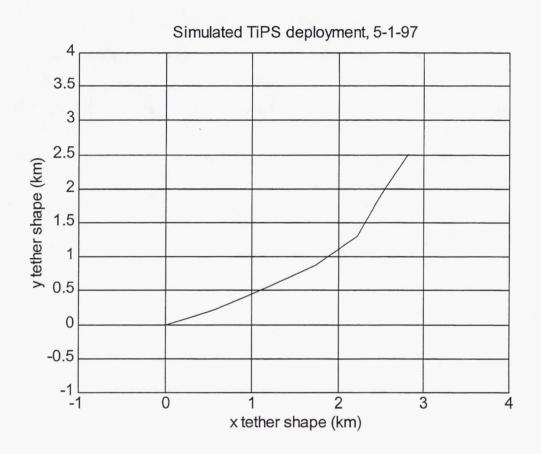
DEPLOYMENT SIMULATION RESULTS

- Summary:
 - Matches well early in deployment
 - Matches deployment pause
 - Restart time is later than flight data. Lower tension or greater deployer friction is probable cause.
 - Significant skip rope oscillations and large tether bow observed in simulation results
- Comparison plot of simulated and actual TiPS deployment rate vs time. TiPS deployment data provided by Chris Rupp/MSFC.



DEPLOYMENT SIMULATION RESULTS (CONTINUED)

• Snapshot of tether shape for TiPS deployment simulation at 5000 seconds after deployment started.



NONLINEAR TENSION AND FRICTION MODELS

The elastic tension in the tether is modeled using a nonlinear relationship developed from previous studies of TSS and SEDS deployment dynamics including both test and flight data.

Ten =
$$AE[(s^n + a^n)^{\frac{1}{n}} - a]$$
; AE=4000N; n=10; a=0.004, .008

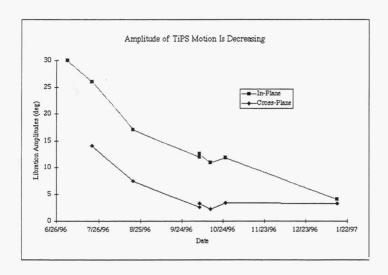
For simulation purposes this equation is modified to eliminate the discontinuity at a strain rate of 0. This modified form is best described as a sliding equilibrium point model in which the sign() function is replaced by a function g(s) which is linear within a small region around an equilibrium value and is limited to lie within the range -1 to +1. The form of this function within its linear range is

$$g(s) = G(s - s_e).$$

Logic is implemented to keep the equilibrium strain s_e sufficiently close to s that the value of this function remains between +1 and -1. The value of G is chosen to avoid small step sizes but be sufficiently large that the linear range remains small compared to the region of motion.

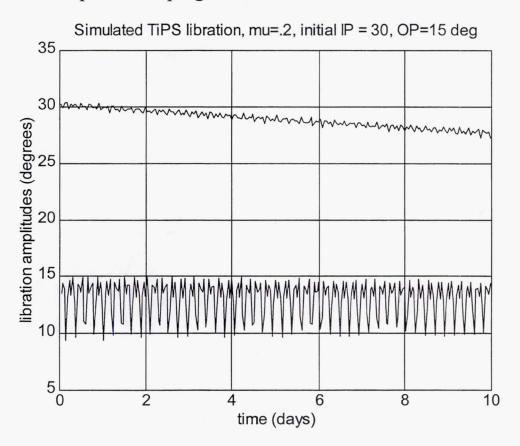
TETHER LIBRATION DYNAMICS STUDY

- Initial Tether Dynamics Damping Considerations
 - In plane and out of plant libration both damped
 - No damping below 5-7 degrees (suggests nonlinear phenomenon (perhaps Coulomb)
 - Large damping rates required (5-20% Coulomb)
- Simulation Studies
 - Effectiveness of Coulomb internal friction model
 - Relative effectiveness of in plane and out of plane damping
- TiPS libration angles vs time obtained from NRL Tips Web Site. These solutions were obtained by NRL with software called GEODYN using scanning laser radar observational data.



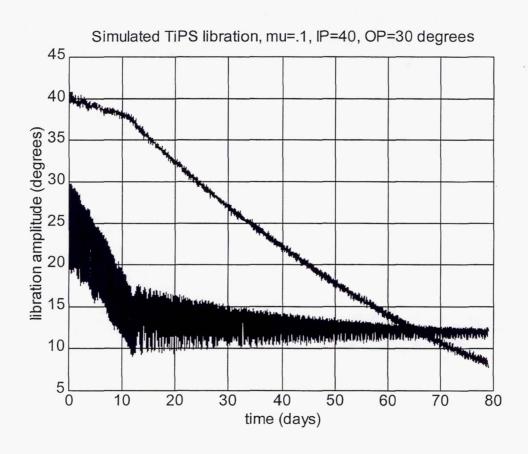
20% DAMPING RESULTS

- Coulomb Damping Level at 20% Results in Sufficient Damping of in Plane Libration
 - 1-2 degrees amplitude loss per week matches flight observations
 - Damping of out of plane component also observed but at much slower rate
- Ten day simulated libration dynamics comparing in plane and out of plane damping effectiveness.



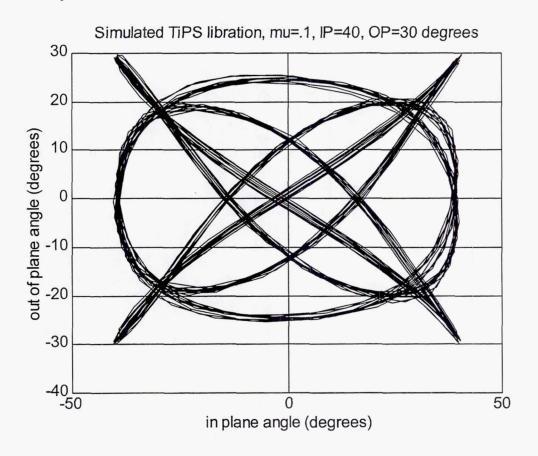
10 % DAMPING RESULTS

- New Phenomenon Observed
 - Fast damping out of plane while slowed damping in plane
 - Abrupt stop to out of plane damping as in plane damping increases
- Multiply Periodic Phenomenon Observed
 - 5 out of plane cycles per 4 in plane cycles
 - Maintained for may days over wide range of amplitudes
- Plot of simulated TiPS libration amplitudes with 10 percent coulomb damping.

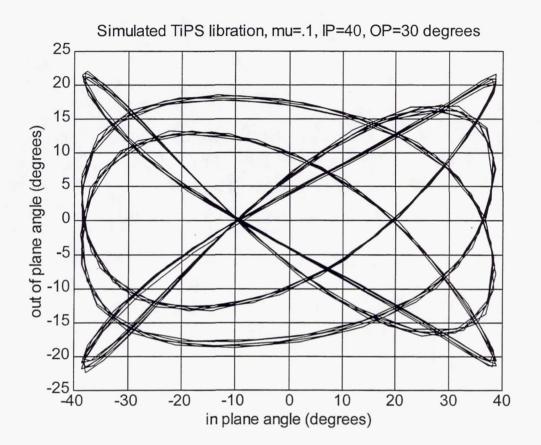


COHERENT LIBRATION MOTION

• Plot of out of plane libration vs in plane libration over the first day of simulated time.

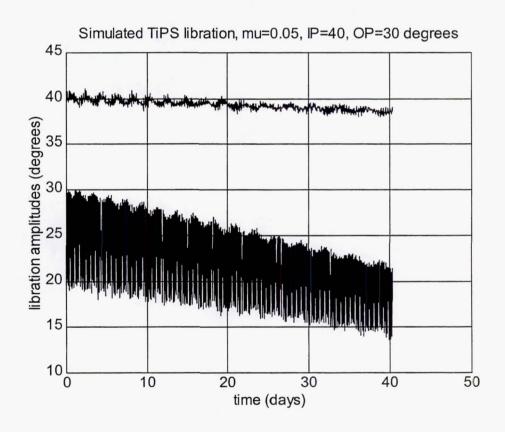


• Out of plane libration versus in plane libration after 7.5 days for 10 percent damping case.

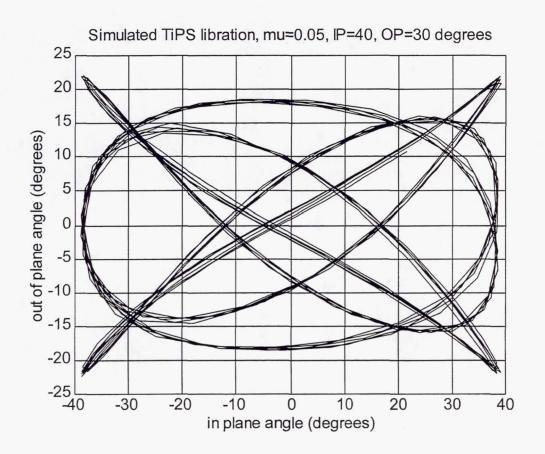


5% DAMPING RESULTS

- Lower Damping Coefficients Extend Period Required to Damp
- Limit Cycle Behavior is Maintained over Many Days and a Large Range of Angles
- Small Amplitude Frequency Ratio, in plane/out of plane is 0.866 versus 0.8 Observed in TiPS Simulations
 - Persists for out of plane as small as 12 degrees
 - Cannot persist significantly smaller than 12 degrees
- TiPS libration amplitudes with 5 percent coulomb damping.

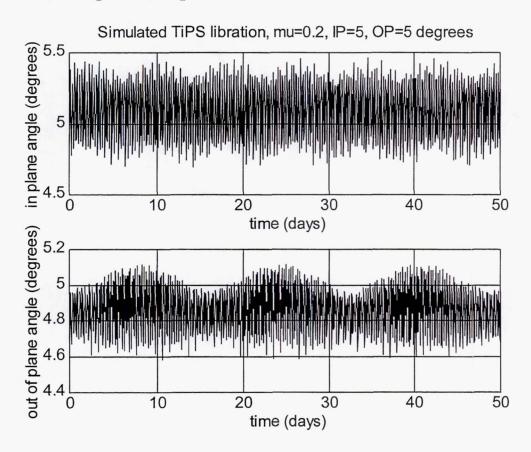


• Out of plane libration versus in plane libration showing the coherence of the oscillation continues to day 40 for the 5 percent damping case.



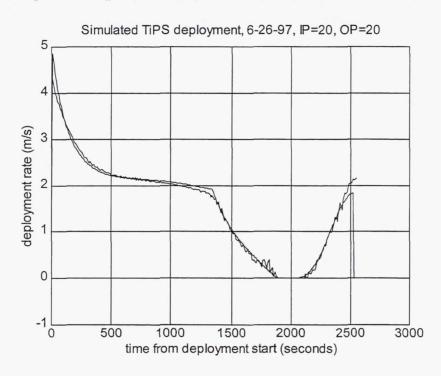
RECENT OBSERVATIONS

- Simulations at Small Amplitudes (~5°) with Coulomb Damping Duplicate Observed no-damping Behavior
- Amplitude Where Damping Stops Depends on Damping Factor (5%, 10%, 20%). Higher Factor Means Larger Steady Amplitude.
- In plane and out of plane libration amplitudes. The angles are
 plotted separately below to make it easier to separate their
 variations. The initial transients result in a slight adjustment in
 their long term amplitudes.



DEPLOYMENT REVISITED

- Let us now take one more look at deployment to see what might happen if we assume that the initial out of plane angle was in actuality much smaller than the observed value. If we set the initial in plane and out of plane angles to be consistent with the 28° half cone angle estimated by NRL and make adjustments to the deployer model parameters, we produce the results shown the the plot below. Some deployer parameters had to be changed from previous: these are L_0 , old value 0.8 m/s, new value 0.7 m/s; $T_{depmin0}$, old value -0.017 N, new value -0.007N, $T_{depmin1}$, old value 0.015 N, new value 0.020 N.
- Comparison of simulated and actual TiPS deployment rate versus time. Note that deployment restart matches quite well now due to greater tether tension. Smaller out of plane attitude angle of deployer at start, only significant change.



CONCLUSIONS

- TiPS Deployment Dynamics Reasonably Well Matched by Simulations
- Tether Internal Dissipation Shown Capable of Damping Librations at Observed Rate
- Nonlinear/Resonant Phenomena Discovered which can Significantly Enhance Damping of out of Plane Libration
- Final Considerations:
 - Best overall deployment match obtained with small out of plane libration
 - Observed simultaneous high damping of in plane and out of plane difficult to reproduce in simulations. Sufficient observational uncertainties exist to suggest that the initial out of plane libration amplitude was in the range of 10-20°
 - Best overall conclusion is that out of plane libration was not quite as large as data suggested and was damped quickly for a few days through resonance effect and then settled into steady amplitude while in plane libration damped.

Session II—Planned Missions

Page intentionally left blank

The BOLAS Mission

By
H. Gordon James
Communications Research Centre
Ottawa, Ontario K2H 8S2, Canada

Abstract

Bistatic Observations using Low Altitude Satellites (BOLAS) is a basic science experiment implemented with a spacecraft comprising two payload packages that are separated by a 100-m tether. The objectives will be to improve the understanding of two classes of ionospheric dynamic processes that redistribute plasma energy in its flow from the sun to the low atmosphere: fluid instabilities near the peak of the ionospheric F region, and microscale instabilities in the collisionless topside plasma. The operation of the double payload will be coordinated with ground radio facilities to probe high-latitude density structures hitherto only observed on the ground. The primary facility for radioscience objectives will be phase-coherent receivers on both ends of the tether that measure the direction of arrival, signal delay and other parameters of transionospheric waves. Particle detectors on both ends of the tether will be associated with the receivers in the study of spontaneous auroral processes whose spatial extent approximates the tether length. Electron density distributions will be measured tomographically using transmissions from the Global Positioning System (GPS) satellites to GPS receivers aboard BOLAS. The mission will be implemented with a low-cost spacecraft consisting of two small and nearly identical subsatellites connected by the nonconducting tether. The current plan is to launch BOLAS into low-earth orbit as a Secondary Payload with RADARSAT II on a Delta II vehicle in the year 2001. The tethered subsatellites will rotate in a cartwheel fashion, approximately in the orbit plane. BOLAS has attracted support from various Canadian and U.S. agencies for its technology research. BOLAS will employ established sounding rocket and tether technology as a base, but also will see new applications, particularly of tethers, microsats and the use of GPS in orbit. Proposed technology demonstrations of the mission have significance to future Canadian microsat and smallsat missions, and to future space station-related and interplanetary missions of NASA.

1. Introduction

The Bistatic Observations using Low Altitude Satellites (BOLAS) experiment exploits a unique set of capabilities in Canada and the U.S.A. for novel space science that benefits from recent advances in tether and microsat technology. A multi-disciplinary Canada-U.S. team with interests in space plasmas and microsats/tethers proposed to the Canadian Space Agency (CSA) a scientific experiment implemented with a low-cost spacecraft comprising two payload packages that are separated by a 100-m tether and in a bolas (cartwheel) rotation in low earth orbit [James, 1997a]. The spacecraft is to be launched using the Secondary Payload resource of the Delta Launch vehicle.

The objectives in basic space science, described in Chapter 2, will be to improve the understanding of two classes of ionospheric dynamic processes that redistribute plasma energy in its flow from the sun to the low atmosphere. Attention is given to the class of the fluid processes around the peak of the ionospheric F region that give rise to density irregularities, such as the gradient-drift instability. Spaceborne BOLAS radio instrumentation will be used to view these irregularities from low-earth orbit (LEO) and hence allow scientists to see the shape of density structures from a new perspective. The other class of processes is in the realm of microscale plasma instabilities. The simultaneous observation of thermal and suprathermal particles and concomitant waves will lead to improved models of the formation of ion conics, cavitons and other phenomena that must be part of the transport phenomena that control energy and mass flux in the collisionless topside auroral ionosphere. As well, the electron density distribution will be measured with tomography using transmissions from the GPS satellites to GPS receivers aboard BOLAS.

The operation of the two-point (bistatic) payload will be coordinated with ground radio-science and other facilities to yield insight into auroral density structures hitherto only observed on the ground. The primary facility for radio-science objectives will be phase-coherent receivers on both ends of the tether for measuring the direction of arrival, signal delay and other parameters of the transionospheric waves. Particle detectors on both ends of the 100-m tether will be associated with the receivers in the study of spontaneous auroral processes whose spatial extent approximates the tether length. The bolas rotational motion of the ensemble will allow the double probe to investigate the dependence of measured parameters on the direction with respect to the local magnetic field **B**.

The BOLAS science experiments will be implemented with a low-cost spacecraft consisting of two small and nearly identical subsatellites connected by a nonconducting tether of about 100 m length. Each subsatellite will carry an HF receiver, a dipole antenna, a GPS receiver and clock, and two instruments to measure electrons and ions in the ambient plasma. The baseline launch service is as a Secondary Payload with RADARSAT II on a Delta II vehicle in the year 2001. The tethered subsatellites will rotate in a cartwheel fashion, approximately in the orbit plane. Over the mission life, this will provide scanning of the ionosphere by dipole HF antennas and the particle

instruments. The required experiment operations involving measurement of direction of arrival of rf transmissions will be carried out when the spacecraft is traversing the auroral region of Canada at an orbital height of 350 - 600 km. RF transmissions will be received from SuperDARN and CADI sites in Canada. The experiments involving reception of signals by the satellite's GPS antenna will be conducted when the line of sight between the BOLAS satellite and a particular GPS satellite passes through the upper atmosphere of the earth.

Chapter 3 deals with the spacecraft and mission design for the above scientific experiments. Section 3.1 contains the experiment requirements. The top-level mission requirements are summarized in 3.2. Then in 3.3, the functional requirements and design of the science instruments are listed. Section 3.4 describes the low-cost spacecraft that will carry the science instruments (i.e., the two subsatellites and the tether subsystems). In 3.5, the proposed arrangements for the launch service and other options are reported. As well, required BOLAS-associated Delta II orbital maneuvers are given. Section 3.6 describes the deployment phase of BOLAS from the Delta II, including the ejection of the first subsatellite and tether deployment to a gravity-gradient stabilized state, ejection of the second subsatellite, and spin-up by partial retrieval of the tether.

Chapter 4 comments on Canadian and U.S. program interests in BOLAS. It has attracted support from various agencies for its technology research; BOLAS space technology demonstrations are outlined in 4.1. BOLAS will employ established sounding rocket and tether technology as a base, but also will see new applications, particularly of tethers, microsats and the use of the Global Positioning System (GPS) in orbit. The CSA Space Technology Program and the NASA Marshall Space Flight Center (MSFC) are contributing partners in the project. These organizations will use and extend expertise in tether technology and in Secondary Payload integration acquired in the U.S. SEDS, PMG and TIPS orbital missions and in the Canadian OEDIPUS suborbital flights. The first-time application of GPS technology to instrument synchronization and to differential determination of the inertial direction of the tether will be new applications of this technology, which also will supply spacecraft ephemeris. Proposed technology demonstrations of the mission have significance to future Canadian microsat and smallsat missions, and to future space station-related and interplanetary missions of NASA. NASA is interested in the BOLAS as a basis of study of the long term orbital stability of large spin stabilized structures and as a scale model of future spacecraft employing spin to produce artificial gravity for interplanetary manned missions. The configuration also is of interest to the NASA science community for its in-situ atmospheric and ionospheric measurements. Section 4.2 discusses how the public will be informed about BOLAS. Finally, in 4.3, the scientific and industrial benefits of the mission are outlined.

The CSA Space Science Program (SSP) approved BOLAS for Phase A study under its Small Payloads Program announced in July 1996. BOLAS is currently the subject of feasibility and conceptual design study, principally at Bristol Aerospace Limited, Winnipeg and NASA/MSFC.

2. BOLAS Science

2.1 Objectives

The BOLAS experiment is a novel approach to improved understanding of the ionosphere. It uses two payloads separated in space by about 100 m to focus on two major areas of current research, firstly density irregularities that affect radio waves and secondly small-scale instabilities. As well, measurements of the density distribution of the ionosphere are made in a novel way. All the areas are linked to the dynamics of the auroral plasma. Although other multiple-satellite missions are being operated or proposed abroad, BOLAS will occupy a special niche by virtue of its small payload separation and its relatively low altitude at and just above the ionosphere-magnetosphere interface.

The scientific objectives of BOLAS are to:

- (1) Investigate ionospheric density irregularities that affect radio wave transmission, using an in-space two-element direction finding array coordinated with ground transmissions from SuperDARN and CADI ground sites.
- (2) Investigate kinetic instabilities of the auroral plasma involving low-energy ions and electrons using field and particle probes separated by about 100 m.
- (3) Measure the two-dimensional electron density distribution in the ionospheric space between a GPS spacecraft and a BOLAS GPS receiver, to provide the basis for improved global density models.

As regards objective (1), arguments in favour of coordinated ground and space observations of the ionosphere-magnetosphere have had currency since spacecraft exploration began. Ground radars operate through finite time intervals to produce integrated images of the spatial distribution of various parameters. Spacecraft move relatively quickly through part of the radar coverage yielding snapshots of the same parameters. Brought together, these two data sets permit data analysts to understand the complete spatial-temporal behaviour of atmospheric dynamics.

Admittedly there are objectives adequately addressed with ground facilities alone. Data from incoherent backscatter, coherent HF backscatter and ground ionosondes when compared yield consistent measurements of certain quantities, for instance the drift velocity of the convecting ionospheric plasma. These parameters tend be of the bulk-parameter or large-scale variety. However, other scientific objectives unavoidably require in-situ, space observations. These include micro-scale observations of plasma processes in general, and, in the context of electromagnetic (EM) wave spectrum, observations of wave parameters which simply are not accessible from the ground. Objectives (1) and (2) exploit the potential of a tethered payload for these two kinds of in-situ observations. Objective (3) is a unique and novel method for tomography of the ionosphere, which will be done with orbiting GPS receivers that are necessary for objectives (1) and (2).

2.2 Investigation of density irregularities using coordinated space and ground measurements

The high-latitude ionosphere can have a dramatic effect on EM waves passing through it. Waves can be refracted, scattered, amplified or damped depending on the local state of the medium. Using coherent backscatter at High Frequency (HF, 3-30 MHz), facilities like the SuperDARN radar [Greenwald et al., 1995] have been designed to provide hemisphere-wide maps of the plasma convection. The interpretation of HF scatter has been based on hypotheses of ray-optics propagation to/from regions of irregularity where aspect-sensitive scatter returns some of the incident wave energy back to the radar. These hypotheses are important in the assumed relation of the characteristics of the scatterers to the overall motion of the medium.

A goal is to investigate wave processes at F-region heights, principally coherent scatter and refraction, happening between ground radars and observing spacecraft. The radar waves probe irregularity structures that result from fluid instabilities of the F-region plasma [Tsunoda, 1988]. The structures are normally assumed to be aligned with B and to extend to altitudes of the BOLAS orbit. HF radar work, and therefore this experiment, are mainly focused on the F region because the cross-section for coherent scatter maximizes there, on account of a combination of plasma-physical and radio-wave propagation factors.

Scattering hypotheses will be tested through coordinated studies of BOLAS and the ground facilities SuperDARN and the Canadian Advanced Digital Ionosondes (CADIs) [MacDougall et al., 1995]. An ionospheric perspective on the details of scattered HF waves is sought. BOLAS synchronized radio receivers will record ground-originating signals, and onboard particle sensors will detect the density structure on the field lines near the apparent scattering source(s). Wave parameters analyzed will include signal amplitude, delay and direction of arrival (DOA). The latter two parameters will be made possible by synchronization of the wave receivers through the GPS [Hoffmann-Wellenhof et al., 1992; Wells et al., 1987].

Figure 2.1 illustrates the relationship of ground facilities, the BOLAS spacecraft and ionospheric targets. A ground HF radar, e.g. SuperDARN, is aimed at the E and F regions of the high-latitude ionosphere. The radar receives backscatter from density irregularities in both the E and F regions. F-region scatter can be detected on direct paths like "b" and from one-hop paths like the dotted line just below the "b" path that involve an oblique F-reflection and a subsequent ground-reflection before backscatter from ionospheric irregularities located beyond the right side of the diagram. GPS-based synchronization permits the data analyst to determine the scattering direction. The intensity of scattered, or of smoothly propagated, radar waves is followed as a function of the position of the orbiting receiver, giving information about the angular distribution of the scatter. Oblique scatter may be detected in both the forward and backward directions, corresponding to paths "f" and "d" in Figure 2.1, respectively.

The limitations of the DOA measurement with two conventional radio receivers

with GPS clocks have been investigated. The inherent accuracy of GPS-based clocks permits phase-difference measurements up to at least High Frequency (3-30 MHz). Direction-finding can be applied confidently to manmade waves from ground transmitters, and possibly to some kinds of spontaneous electromagnetic waves.

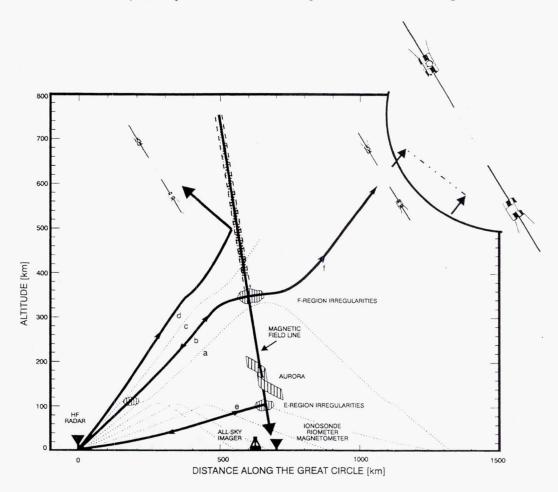


Figure 2.1 The BOLAS double receiver is coordinated with ground radars and ionosondes giving new perspectives on F-region and topside irregularities.

The DOA measurement is based on the two-element interferometer, as follows. Consider independent wave receivers on the two BOLAS endbodies having a separation vector \mathbf{T} . A plane, monochromatic electromagnetic (\mathbf{E} and \mathbf{H} fields perpendicular to its wave vector \mathbf{k}) wave impinges on both spacecraft, as shown in Figure 2.2. The wave front is at angle θ to \mathbf{T} . The two-dimensional geometry of the wave vector \mathbf{k} with respect to \mathbf{T} makes the distance $s = T \sin \theta$, or the total phase path separation of the two observing points

$$\Phi = \mathbf{T}.\mathbf{k} \tag{1}$$

The double receiver configuration can be thought of as a steerable beam or

interferometer. This can be seen by rewriting (1) as

$$\sin\theta = \frac{\Phi}{Tk} = \frac{\lambda}{T}(m + \frac{\phi}{2\pi}) \tag{2}$$

If the refractive index is n, then $\lambda = nc/f$, where c is the speed of light and f is the frequency. Synchronized by GPS, the BOLAS wave receivers measure the residual phase difference $\phi = \Phi$ modulo 2π , but have no way of determining m. Therefore, separation T should be no more than a few wavelengths in order to minimize the m-fold 2π ambiguity. EM waves transmitted by SuperDARN or CADI at frequency f = 10 MHz have a wavelength $\lambda = 30$ m. A BOLAS tether length T of 100 m is called for so as to make m no more than a few. The known locations of the spacecraft and collaborating ground radar and frequency-difference techniques may be used to sort out m. An analysis of the tethered two-element direction finder yields conservative estimates of the error in DOA of about 5% for EM waves at HF [James, 1997b].

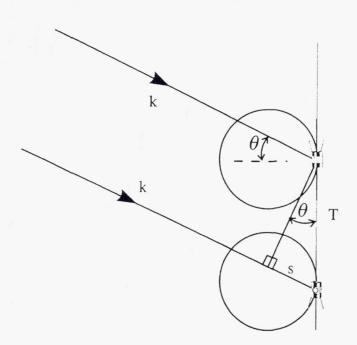


Figure 2.2 Measurement of the direction of arrival of plane waves incident from the upper left on a tethered double receiver. The circles indicate the receiving patterns of the short dipoles.

The interpretation of transionospheric waves at heights up to 600 km altitude will require two-dimensional models of the electron density N_e in the great-circle, vertical plane defined by the spacecraft and the transmitter. If the spacecraft passes near the zenith of ground ionosondes, these supply information about N_e . Indirect information about N_e along smooth propagation paths will also be available from the signal delay and amplitude of the radar waves at BOLAS, and from the GPS occultation analysis.

Signal delay τ_D is the integral of (group velocity)⁻¹ with respect to distance along the ray path. In BOLAS, the transmission of pulse sequences at SuperDARN and CADI and their sampling after reception at BOLAS will be coordinated with reference to GPS-supplied time. Iterative searches will be made for the two-dimensional N_e distribution that makes the theoretical history of τ_D agree with the observed. In addition, the observed history of the signal amplitude during the pass will provide a consistency check on the mode when compared with the results of ray tracing.

Like BOLAS, SuperDARN has an "interferometer" mode, with which it measures the elevation angle of backscattered rays. By identifying the propagation direction, SuperDARN thereby distinguishes among direct, one-hop or two-hop paths to the scattering region. At the BOLAS satellite, a particular mode will be readily identifiable by its elevation angle. Thus a clear picture of propagation paths will emerge from the amalgamated ground and satellite DOA data sets.

Analysis of the DOA of EM waves from ground radars either propagating smoothly over the entire intervening space or scattered by ionospheric irregularities will require some assumptions or preconditions. A two-element array can determine only one DOA angle, θ , so one is limited to two-dimensional analysis. Operators will especially look for satellite passes that stay within one or a few of the sixteen SuperDARN beams, defined by great-circle vertical planes through the radar location. Scattering will be mapped through both the orbital motion, at about 7 km s⁻¹, and possibly by the rotation of the bolas about its center of mass with a period of minutes. This will sweep θ , but the phase of the bolas rotation will not be controlled.

Orbital motion will carry the spacecraft near field lines threading irregularity sources. The thermal particle sensors will measure the absolute background density N_e . Relative density fluctuations from the sensors will characterize the irregularity spectrum responsible for the scatter seen earlier or later during the pass. Evidence like this could help to establish the relevance of the competing theories for scatterers: the gradient-drift instability [Simon, 1963] versus the current convective [Chaturvedi and Ossakow, 1981].

The particle sensors will provide measurements of density gradients when traversing ionospheric structures. The gradient-drift instability is believed to be the principal source of irregularities that are generated preferentially on one side of the density patches during polar cap traversals. A direct measurement of density gradients associated with patches will improve our understanding of the irregularity production.

In general, the patches and the adjacent density depletions are elongated in the east-west direction. Figure 2.3 is an example of a SuperDARN observation of polar patches, in relation to possible northbound and southbound BOLAS passes through the center of the patch region. With BOLAS traversing these ionospheric structures nearly perpendicularly, the geometry is very suitable for the direction finding technique.

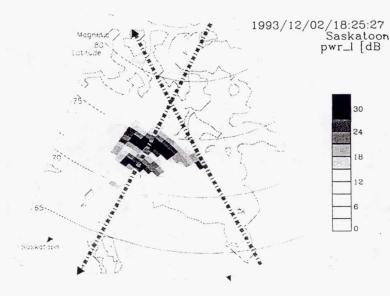


Figure 2.3. Ground tracks of sample BOLAS passes in relation to polar patches detected by the SuperDARN radar at Saskatoon.

Gravity waves are another candidate for coordinated studies [Samson et al., 1989, 1990; Bristow et al., 1994, 1996; Bristow and Greenwald, 1995]. The associated periodic density gradients will produce periodic focusing and defocusing of HF rays at the BOLAS altitude. Yet another phenomenon of current interest in the SuperDARN community is double-peaked Doppler spectra [Schiffler, 1996] produced in regions of intense soft-electron precipitation. It is speculated that these regions are ionization columns containing a radial electric field which therefore induces vortical plasma motion. Such columns may be related to past observations of field-aligned currents [Lee, 1986] and may be further confirmed through the evidences of curl of the convection pattern [Sofko et al., 1995].

Passes of BOLAS will be planned over the CADIs, whose beams are centered on the vertical. This transionospheric radar experiment has the potential for sensitive two-dimensional measurements of two-dimensional F-region ionospheric structures such as troughs, gravity waves, auroral blobs, and polar cap patches [MacDougall et al., 1996]. Orbital motion will allow BOLAS to sweep a range of ray directions and thereby probe the shape of a structure. Figure 2.4 shows the results of a simulation of the raypaths, for a typical high latitude blob [Tsunoda, 1966], from a ground transmitter to the topside ionosphere. The rays are at 1° increments of elevation angle. A number of effects can be seen: focusing of energy (where the raypaths are close together), angular deviation of the rays, group delay effects (the tic marks on the rays show the time elapsed) and multiple raypaths to the satellite height (with different time delays). The raypath picture is found to be sensitive to the relative geometry, probing frequency, and electron densities. Thus, measuring the amplitude, DOA and the time delays of pulses at BOLAS should allow us to deduce a fit to the structure density contours, as for SuperDARN.

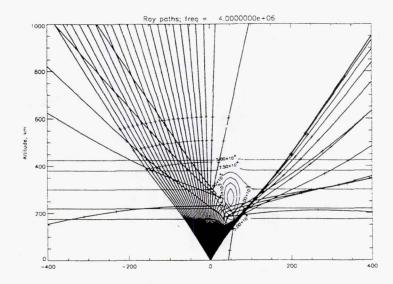


Figure 2.4. Rays traced from a CADI ionosonde through an ionospheric F-layer model in which an auroral blob density enhancement is embedded.

2.3 Auroral wave-particle interactions

The flight of a tethered pair of subsatellites instrumented for field and particle detection presents a unique opportunity for space plasma research when the separation of the two bodies is about 100 m. Spontaneous wave structures are found to have scale sizes of this order of magnitude. The 100-m separated pair will be exploited to compare particle and wave parameters measured simultaneously across this separation. This will lead to improved models of localized plasma instability.

This investigation focuses on thermal and suprathermal energies because recent research has shown their importance in auroral physics. New instrument technologies will explore a spectrum of particle energies - from thermal to 50 eV - in order to characterize both the sources and consequences of low to mid-altitude plasma waves. Particle properties will be compared with wave properties, which, by virtue of the BOLAS 2-point geometry, will include the wave number k-spectrum, a critical but heretofore poorly measured quantity necessary for evaluating theories of wave production.

The two-point BOLAS measurements will provide new information on both wavelength and spatial extent. Localized density cavities are associated with ion heating in the nightside auroral zone. The scale size of these cavities is of the same order as the 100-m BOLAS separation. Identical particle sensors on each of the spacecraft will make novel measurements of the spatial/temporal properties of these cavities, and of the state of the low-energy plasma distribution within them. VLF (3-30 kHz) lower hybrid waves are a good example. They are known to occur as "spikelets" concentrated on scales of

the order of 50 m [LaBelle et al., 1986], and they produce localized ion heating [Kintner et al., 1992; Arnoldy et al., 1992; Vago et al., 1992].

The Freja satellite mission has revealed a pertinent ELF phenomenon (below 3 kHz): Solitary Kinetic Alfvén Waves (SKAW) [Wahlund et al., 1994]. These waves are localized on scales of hundreds of meters. They may also generate localized ion heating [Knudsen and Wahlund, 1997], although this point awaits definitive experimental verification, hopefully by BOLAS. By traversing these localized heating structures with two spatially separated probes, one can learn much about their form and dimensions and as a consequence clarify their normal modes and sources of free energy.

2.4 Ionospheric tomography based on occultation of GPS

Terrestrial GPS receivers currently measure total electron content (TEC) on different horizontal scales [Komjathy and Langley, 1996]. The GPS-derived TEC at the ground stations can be used to build two-dimensional global zenith TEC maps through interpolation with empirical models, such as the International Reference Ionosphere 1995 (IRI95)[Komjathy et al., 1996]. Such descriptions of the ionosphere are limited by the resolution of these maps, which among other factors is a function of the number of ground stations used in the interpolation, by the land-bound nature of these stations, and by the absence of information on vertical electron density distribution.

It is planned to remove these limiting factors, through spaceborne GPS receivers observing the same signals as the terrestrial receivers. By having BOLAS GPS receivers track GPS satellites rising or setting relative to a BOLAS, vertical profiles of electron density can be determined when the line of sight cuts through the ionosphere. The phase and amplitude of the GPS signals are affected in ways that are characteristic of the index of refraction of the ionosphere [Hajj and Romans, 1996]. These effects can be interpreted geometrically as bending of the GPS signals, as illustrated in Figure 2.5.

Current ionospheric occultation methodologies call for the atmosphere to be composed locally of spherical, symmetrical shells, each shell having a uniform index of refraction. The estimate of the bending of the occulting signal is then derived from isolating the excess Doppler shift induced by the atmosphere [Hajj and Romans, 1996]. This excess Doppler shift is the difference between the measured Doppler shift by the BOLAS GPS receiver of an occulted GPS satellite and the computed, theoretical, "occultation-free" Doppler shift that would have been observed at the BOLAS GPS receiver. This latter quantity is derived from a precise orbit determination (POD) of the LEO, utilizing measurements made with the LEO GPS receiver of unocculted GPS satellite L1 and L2 signals. From the BOLAS and GPS POD information, the theoretical Doppler shifts can be derived. An Abel integral transform is used to derive the index of refraction from the bending. The electron density along the ionospheric profile can then be determined from a formula for the index of refraction [Langley, 1996, p.127].

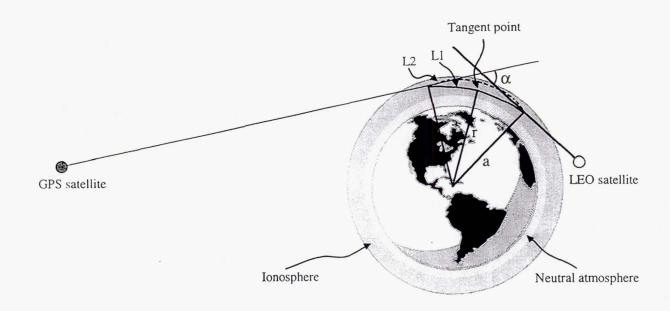


Figure 2.5. The radio occultation geometry. Angle α is the occultation bending angle, a is the impact parameter, and r is the radius to the ray periapsis tangent point. L1 and L2 are the GPS Link 1 and Link 2 frequencies, respectively. In the case of BOLAS-GPS links, this diagram greatly exaggerates the amount of L1 and L2 ray bending: α values of less than 0.01° are expected

The combination of such spaceborne data and terrestrial data will allow for high resolution two- and three-dimensional tomography [Yunck and Melbourne, 1996]. This level of spatial and temporal coverage for the global ionosphere cannot presently be provided by any single technique. It is planned to use terrestrial GPS-based ionospheric profiling in combination with the spaceborne occultation technique to provide three-dimensional ionospheric images.

3. BOLAS Implementation

3.1 BOLAS Experiment Requirements

The primary radio observations will be of waves with signal levels between 1 and at least 1000 mV m⁻¹. The frequency range will be 100 Hz to 20 MHz. Important observables will be amplitude to $\pm 10\%$, signal delay to $\pm 20~\mu s$ and the DOA angle θ to $\pm 5^{\circ}$. The received signals will need to be sampled at the tether extremities with less than 10 ns differential error in the clocking rates.

Electron and ion fluxes will be required at energies between 0.1 and 50 eV. The detectors should give good angular (10° pitch angle by 40° azimuth bins) and energy (10%) resolution at high time resolution, the goal being to measure drift energy, direction, temperature, and density of the core population every 1-10 ms. Both sweptenergy and fixed-energy modes will be required for obtaining the overall energetics and spatial resolution of small structures, respectively. A complete energy-pitch angle distribution should be determined within one second. A mode of operation interleaving fixed- and stepped-energy measurements will be required.

The BOLAS experiments will take place in the auroral oval and its neighbourhood. It is planned to conduct primary BOLAS operations when the spacecraft flies near the center of the overlapped coverage areas of the SuperDARN radars at Kapuskasing and Saskatoon shown in Figure 3.1. The large fan-shaped areas shown in the figure are the coverage of the SuperDARN radars at 350 km altitude where each fan shape is subdivided azimuthally into 16 individual beams. In the overlapping coverage, the ionospheric convection velocity can be determined. At some points during the orbital passes, at least near the beginning and end, the radars will produce area-wide maps of the distribution of back scatter. At other times, the selection of a beam or of several beams could be tailored to the satellite earth track across each wedge. Additionally, primary BOLAS operations will be conducted when flying over the CADI ionosondes. The six medium-sized circles in Figure 3.1 are the coverage areas at 350 km altitude of the CADI ionosondes. Bottomside sounding will be carried out. For both SuperDARN or CADI collaborations, the spacecraft operating mode will be based on knowledge of the orbital path and the state of ionosphere in the sector. The large circle in Figure 3.1 shows the area of coverage of a ground telemetry-command station at Saskatoon.

The ionospheric occultation investigation requires that the GPS receivers process the relative phase of the L1 and L2 frequencies. The GPS units must have software control that allows selection of the relevant spacecraft near the earth horizon.

A summary of the science measurements and specifications is provided below in Table 3.1.

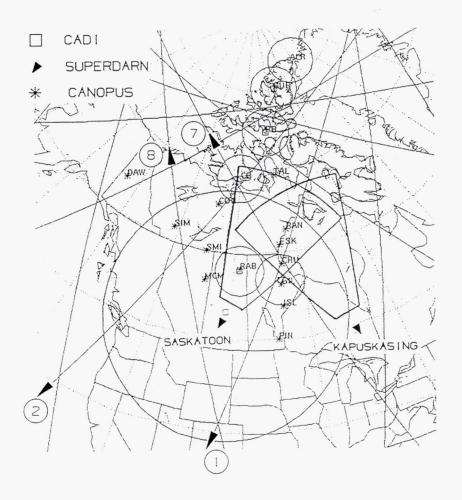


Figure 3.1 Ground tracks of typical ascending-node ("7", "8") and descending-node ("1", "2") BOLAS passes over the center of the region of collaborating ground facilities.

3.2 Orbit, Spacecraft, and Mission Parameters

The requirements of the science experiments outlined Table 3.1 are to be met with two tethered subsatellites in a low-altitude, high-inclination orbit that maintain a fixed separation and that rotate relative to each other in a cartwheel fashion to allow observation of the ionosphere in a variety of inertial orientations. Orbital heights of about 350 km altitude are sought for in-situ probe measurements of density irregularities that scatter observable waves. Pass altitudes above 600 km in the collisionless plasma of the topside ionosphere also are required for the auroral wave-particle investigations. To insure passes through the auroral ionosphere in both cases will require an orbital inclination not less than 65°. A summary of the systems-level spacecraft and mission requirements are given below in Table 3.2.

Table 3.1 Summary of the Science Measurements and Specifications

Measurement Method and Accuracy Planned		Comments		
Radio observations	6 m tip-to-tip dipole antenna on each satellite; 5 m min. Align dipoles along tether direction to ±10°; 1 - 1000 μV/m signals; 100 Hz - 20 MHz; 10 ns synch. of receivers; 5° DOA knowledge	The principal observables include signal level amplitudes to 10% and the signal delay to $\pm 20~\mu s$. The two receivers, one on each subsatellite, will allow for direction of arrival (DOA) measurements of an incoming signal. The dipole antennas on each subsatellite used for the radio observations should be aligned along the tether line.		
	Region of interest over SuperDARN & CADI sites; 2-3 passes per day; Measurements in both dayside and nightside	The primary science will be conducted when passing through the region covered by the SuperDARN radars and the CADI ionosondes shown in Figure 2.1. The CANOPUS network will also provide information on the state of the ionosphere before and during a pass. During interesting ionospheric activity, 2-3 orbital passes will be required per day for a typical duration of 3 days. At other times a lower frequency of passes is possible to allow for other operational modes. Flexibility in the science operations should be		
	auroral ovals are required	maintained to operate in other regions relative to the earth.		
Electron & ion measurements	0.1 - 100 eV 10% energy resolution 10° x 10° angular resolution 1-10 ms sampling time	Goal is to measure drift energy, direction, temperature and density of the core electron and ion population. Both swept-energy modes and fixed-energy modes are required, and a complete energy pitch-angle distribution is required every second. Measurements to be done while radio observations are being made		
Tomography using a GPS receiver	L1 & L2 carrier phase precision of 0.2 mm; selection of GPS satellites	The GPS tomography studies require the use of the L1 and L2 frequencies, and the ability of the GPS receiver to select specific GPS satellites that are near the horizon to get rays that travel horizontally through the ionosphere.		

Table 3.2 Summary of the Systems Level Requirements

System Parameter	Requirement	Comments		
Subsatellite separation (tether length)	50 m - 300 m 100 m (ideal)	The subsatellite separation is the baseline between the two satellites used to calculate the DOA of an incoming wave.		
Rotat. rate of BOLAS config	10-30 times the orbital rate	The BOLAS rotation permits DOA measurements at various orientations		
Orientation of BOLAS config	in-orbit plane (ideal)	A cartwheel rotation is desired but is not mandatory		
2-body attitude determination	±1°	Attitude determination of the two body vector in inertial space		
Orbital altitudes	350 km to at least 600 km	Altitudes near 350 km and above 600 km are of primary interest		
Inclination	above 65°	Measurements are to be made in and near the auroral oval		
Local mean 10:00 - 14:00 (primary) (LMST)		The 10:00-14:00 is the region of most interest. Hence, the orbit plane should remain in the 10:00- 14:00 LMST for as long as possible.		

3.3 Science Instrument Design

The BOLAS broadband HF Receiver measures wave fields from both manmade and spontaneous sources. Basicly it is a preamplifier and an rf signal processor. The preamplifier matches the high impedance of the BOLAS dipoles to the 50-ohm input of the signal processor. The processor consists of two branches. One is for direct amplification at frequencies up to 50 kHz. The other is a double heterodyne for frequencies between 100 kHz and 20 MHz, at 50 kHz steps. The receiver has considerable heritage from the OEDIPUS-C REX [Barnes et al., 1996]. The preliminary specifications for the receiver with the preamplifier are given below:

Mass:

9 kg, plus cables

Power:

10.8 W

Size:

Preamplifier - 127x99x33 mm

Signal processor - 295x257x175 mm (separable into two or more

units)

L'requency range:

50 Hz to 20 MHz, not necessarily continuous

Instant. Bandwidth:

50 kHz

Dynamic range:

-100 to -10 dBm at 50 ohm

Diff. phase acc.:

Resolves direction of arrival to 5 ° after ground processing

Output data:

133333.33 16-bit samples per second

Antenna:

6-m tip-tip dipole, parallel to tether, storable tubular elements

Reference signal:

5 MHz from GPS receiver

Timing information: Nominally ± 10 ns post flight, from GPS receiver

Preamplifier: Voltage gain=1; high impedance input; 50-ohm output

The Thermal Electron Capped Hemispherical Sensor (TECHS) instrument is an azimuthal top-hat electrostatic analyzer. By sweeping the analyzer voltage the instrument measures a count rate that can be directly related to the particle distribution function [Pollock et al., 1996b]. From these measurements, integral moments of the electron distribution function, including density, anisotropic temperature, bulk drift and heat flux may be derived. A version of the instrument flew successfully on the SCIFER sounding rocket [Pollock et al., 1996a, 1996b]. The TECHS sensor mounts on the end of a 1-m boom. The TECHS preliminary specifications are:

Mass: Sensor and boom: 1.5 kg; electronics: 3 kg

Power: 5 W average

FOV: $\pm 4^{\circ} \times 360^{\circ}$ in a plane perpendicular to boom

Boom length: 1 m

Telemetry: 30 bin angles x 1 energy per ms = > 30 kB/s = 240 kb/s Dimensions: Sensor: 2.5 cm dia. x 5 cm long; electronics: 19x18x7.6 cm

Sensor skin bias: ± 1 N Attitude knowledge: $\pm 1^{\circ}$ Angular resolution: 10°

Energy range: 0.3 to 1 eV Energy resolution: dE/E = 8%

The Suprathermal Ion Instrument (SII) images the 2-D ion distribution from 0-50 eV, and provides an integral measure of ion flux at rates sufficient to resolve localized ion heating on spatial scales of tens of meters. The two SII's on BOLAS are identical. Each consists of three parts: 1) a 2.5 cm diameter cylindrical sensor head with a rectangular baseplate housing electronics; 2) a 1-m boom; and 3) a power and control unit housed inside the subsatellite. The SII is based on the design of the Freja Cold Plasma Analyzer [Whalen et al., 1994], with two major modifications: the dimensions will be shrunk by a factor of roughly 3, and the detector design will be based on a charge-coupled device (CCD). A summary of the instrument specifications is as follows:

Mass: Sensor-500 g, Boom-1 kg, PCU-3.5 kg, total-5 kg

Power: 10 W operating, 20 W Peak

Field of view: $\pm 5^{\circ} \times 360^{\circ}$ in a plane perpendicular to the boom

Boom length: 1 m

Telemetry: 50 kbits/image, 5-10 images/s = > 250 kbps

Dimensions: Sensor: 2.5 cm dia, 5 cm long; 10x10x2 cm square baseplate

PCU: 19x18x7.6 cm

Sensor skin bias: $-10 < V_{skin} < 10 V$ (must be isolated from boom)

Attitude knowledge: Sensor rotation about boom axis must be known to within 5°

Angular resolution: 10°

Energy range: 0 eV (with an accelerating sensor skin potential) to 100 eV

 $E_{max}/(E_{min} + qV_{skin}) = 10$

Energy resolution: dE/E = 15%

3.4 Spacecraft Design

The BOLAS spacecraft is shown below in Figure 3.2 in its final deployed configuration. It comprises two nearly identical subsatellites attached by a 100 m non-conductive tether with a pair of 3-m booms on each subsatellite aligned along the tether. The entire configuration is spinning at about 18 times the orbital rate or approximately 0.2 rpm about its center of mass located approximately at the middle of the tether. The spin of the two body system is achieved by deploying the tether to initially about 326 m, and using the gravity-gradient forces to initiate a slow rotation. The tether is then retrieved at a high rate to its final length of 100 m which causes coriolis forces to spin-up the system. To implement this spin-up approach, a tether deployer (the mini-SEDS deployer from NASA/MSFC) is used for the initial deployment and a separate tether retriever (based on OEDIPUS technology [Eliuk et al., 1996]) is used to retract the tether. This approach of using separate systems to deploy and retrieve the tether minimizes hardware complexity and allows for capitalizing on the technology developed for the U.S. tether programs (SEDS, PMG, TiPS, ATeX) and the Canadian OEDIPUS tether missions.





Figure 3.2 BOLAS spacecraft in final deployed configuration, separation not to scale

The main hardware elements of each subsatellite are listed in Table 3.3. The two subsatellites are identical with the exception of the tether deployer and retriever. To reduce development costs, only one subsatellite design will be developed that will be able to accommodate either the tether deployer or retriever.

Table 3.3 BOLAS Spacecraft Mass and Power Summaries

Subsatellite	BOLAS-1		Subsatellite BOLAS-2		
Item	Mass (kg)	Power (W)	Item	Mass (kg)	Power (W)
HF revr with pre-amp	9	10.8	HF rcvr with pre-amp	9	10.8
Booms (2 @ 3 m)	2.7	-	Booms (2 @ 3 m)	2.7	-
TECHS electronics	3	5	TECHS electronics	3	5
TECHS sensor & boom	1	-	TECHS sensor & boom	1	-
SII electronics	3.5	10	SII electronics	3.5	10
SII sensor & boom	1.5	-	SII sensor & boom	1.5	-
Tether deployer	1.5	-	Tether retriever	2.5	6.44
Tether (maximum)	2.7	-			
Transmitter (2W)	0.45	18.2	Transmitter	0.45	18.2
Tx Antenna patch (2)	0.2	-	Tx Antenna patch (2)	0.2	-
Command Receiver (2)	0.72	4.48	Command Receiver (2)	0.72	4.48
Antenna - Rx (2)	0.4	-	Antenna - Rx (2)	0.4	-
On-board Computer	6	2.5	On-board Computer	6	2.5
Solar Arrays	2.1	-	Solar Arrays	2.1	-
Batteries	3.4	-	Batteries	3.4	-
GPS receiver	2.3	6	GPS receiver	2.3	6
Magnetometer	0.2	1.12	Magnetometer	0.2	1.12
Torque coil	0.1	2	Torque coil	0.1	2
Accelerometers (3)	0.45	1.80	Accelerometers (3)	0.45	1.80
Wiring Harness	4.5	-	Wiring Harness	4.5	-
PDU & DC-DC conv	0.3	2.2	PDU & DC-DC conv	0.3	2.2
Structure & thermal	14.1	-	Structure & thermal	14.1	-
Contingency (20%)	12.02	12.82	Contingency (20%)	11.68	14.11
TOTAL	72.1 kg	76.9 W (peak)	TOTAL	70.1 Kg	84.65 W (peak)

The layout of one of the subsatellites is shown in Figure 3.3. The overall configuration is driven by the accommodation requirements for the Delta 2 launch vehicle. The tether from the tether deployer goes through the boom package and out the tip of the boom. This ensures the booms are aligned with the tether and avoids the possibility of the tether getting tangled around the boom. It also helps to stabilize the payload oscillations relative to the tether. The concept uses two individual BI-STEM boom packages, each deploying a single element. The tether is fed through the back of the boom package and out the tip of the boom when stowed and when deployed.

As the payloads will be stabilized by the tether and the BI-STEM booms, subsatellite attitude control about the orthogonal axes to the tether is not required. However, for thermal reasons, a magnetic torque coil is provided to allow for intermittent open loop spin control (via the ground) about the tether axis. Three axis attitude determination will be provided by the magnetometer via processing on the ground. Magnetometer based attitude determination was used for the SEDS tether missions, and NASA Goddard will develop an algorithm based on this technique for

BOLAS. Accelerometers will be used to provide attitude rate information and also to determine the tether tension.

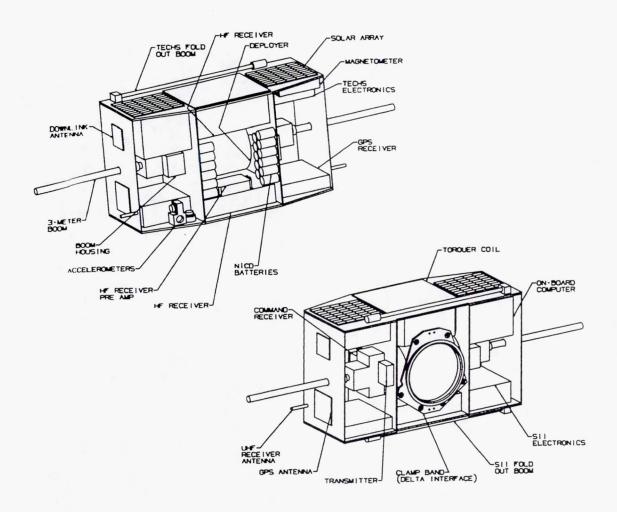


Figure 3.3 BOLAS subsatellite layout

The power system consists of two small solar arrays (each made up of 45 2 x 4 cm Si cells) mounted on each face of the subsatellite (except the ends), a 4.5 A-hr battery made up of commercial NiCd D-cells, and a Power Distribution Unit (PDU) and DC-DC converters used to provide switchable power to the instrument and subsystems. The 28-V solar arrays on each face provide the necessary power for all orientations of the two-body system and at all orbital equator crossing times. Since the current generated from the solar arrays is very low (well below the trickle charge rate), a battery charge regulator and shunt regulator are not needed and the solar arrays are connected directly to the batteries.

The on-board computer (OBC) consists of a processor card, an I/O card, a data handling card, and 4 mass memory cards. It decodes commands from the command

receiver, executes real-time and time-line commands, collects science and housekeeping data, provides 64 Mbytes of on-board storage, and outputs a 2 Mbps serial bit stream to the telemetry transmitter. Low power is a prime requirement and a 80C186 processor has been selected for the baseline concept as it has adequate capability at very low power and has considerable space flight heritage. The OBC will be developed jointly with NASA/MSFC. It will be manufactured from SEL-free, military grade parts, where appropriate. Screened commercial grade parts may be used in non-critical areas to reduce costs without compromising critical functions. Through hole construction will also be employed to reduce cost without greatly affecting size and mass.

The GPS receivers are modified versions of the TurboStar units from Allen Osborne and Associates. These units provide the necessary features including dual frequency capability and sufficient on-board processing to allow selecting up to 8 GPS satellites. The units will require minor modifications to provide a clean 5-MHz reference signal that will be used by the HF receiver for synchronization between the signals received from BOLAS-1 and 2 via ground processing (currently the reference signal is corrected by the GPS clock once every second). The baseline downlink transmitter is an S-Band 2-W RF telemetry transmitter which accepts binary bits and produces a Linear or Binary Phase modulated carrier. Two UHF Command Control receivers are envisaged, each connecting to a small UHF dipole antenna located at each end of the subsatellite. Both receivers will be on continuously (although strobed to minimize power requirements) so that a command can be received in almost any orientation of the twobody system. The GPS and transmitter antennas are microstrip patches that are located on each end of the subsatellite as shown in Figure 3.2. The GPS antennas (L-band) will be designed for this mission to provide a nearly omnidirectional pattern. The two S-band antennas for the transmitter can be switched via timeline commands so that only one is used at a given time when it is oriented towards the ground.

Some optional hardware will be considered if it can be accommodated from a resource and cost point of view. The possible hardware includes a "running line" tensiometer such as that used in the SEDS tether missions which may provide better tether dynamics data. The other possibility is a small digital camera aligned to view the tether and the subsatellite on the other end. The current resources on the subsatellite allow for taking a picture every second for up to approximately 5 minutes and storing on-board or for about 12 min. Once a series of video "still pictures" is obtained on the ground, it can be processed to make a video movie (e.g., an MPEG file) that runs at, say, 30 frames a second. This will be very useful from a dynamics point of view. Additionally, it will be very valuable for public relations. Video clips could be made to show different stages of the mission (deployment phase, spin-up phase) at various times throughout the mission life.

3.5 Launch Vehicle and Related Operations

The BOLAS as a secondary payload will be manifested inside the same fairing envelope as the primary spacecraft on the Delta II vehicle. The accommodation of BOLAS on Delta is depicted in Figure 3.4. The current baseline for launch as a

secondary payload is with the RADARSAT-II mission in the fourth quarter of 2001. The expected mass margin for RADARSAT II, assuming it is identical to RADARSAT I, is 167 kg, which is adequate for BOLAS.

Launch will be from Vandenberg AFB and the ascending node will cross the equator at 1800 hr PST. The inclination will be 98.64 degrees and its orbital period 100.7 minutes. This is a circular orbit at 800 km altitude, and sun-synchronous with dawn-dusk orientation. The BOLAS orbit can be achieved by the Delta second stage after deployment of the RADARSAT-II spacecraft with a two impulse orbit transfer strategy.

Primary science data will be taken when the satellite passes through the auroral oval at low height. Both daylight and darkness passes are required over the course of the mission. The requirements can be satisfied with perigee and apogee of 350 km and 600 km respectively, and a drift over the course of the mission from an initial dawn-dusk local time through and beyond noon-midnight. As well, the perigee should be near the auroral oval during the main period of science measurements. The BOLAS orbital plane will drift by about 120° in 6 months. This requires an orbit inclination of 102.24°. The corresponding drift rate of the perigee will be approximately -3° per day.

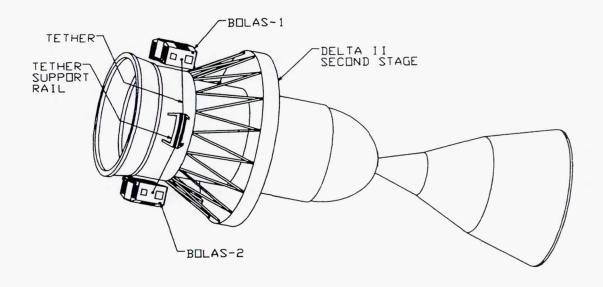


Figure 3.4 BOLAS subsatellites integrated on Delta II Second Stage

3.6 Deployment, Separation and Spin-Up of the Spacecraft

The BOLAS subsatellite separation and spin-up is achieved initially by deploying the tether to a length of 326 m which allows the gravitational forces to initiate a slow rotation of the two-body system. The tether would then retrieved at a relatively high rate to allow the resulting coriolis forces to spin-up the system to the final rate of about 0.2 rpm with the tether about 100 m long. In this gravity-gradient assisted spin-up, only a

relatively simple tether retriever is required. It will be based on already proven technology developed for the OEDIPUS-C tether mission, and will avoid the use of an attitude control system and spin-up thrusters. The deployment, separation and spin-up of the spacecraft is depicted in Fig. 3.5. A timeline study has confirmed that all maneuvers with the Delta can be accomplished within the allowable operational time, i.e., before the Delta batteries run down.

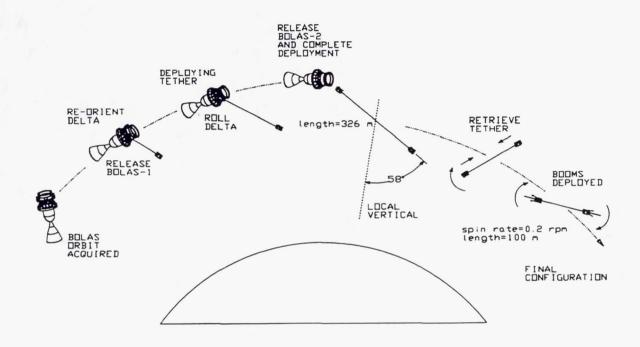


Figure 3.5 BOLAS tether deployment and spin-up scenario

To confirm the feasibility of the gravity-gradient assisted spin-up, deployment simulations were conducted at NASA/MFSC using flight proven tether dynamics software, with a deployer friction model based on test results of SEDS deployer hardware on NRL's TiPS mission. The spin-up dynamics was jointly analyzed by NASA/MSFC and Bristol, using simplified mathematical models that have been verified by comparing independent formulations [Tyc and Pradhan, 1996; Carrington, 1996; Vadali, 1991].

4. Programmatic Aspects of BOLAS

4.1 Tether and Low Cost Spacecraft Demonstration Objectives

The flight demonstration of important space technologies is an integral part of the BOLAS mission. The tether technology, the GPS application, and the low-cost design of the subsatellites are at the forefront of space technology R&D. Elements of BOLAS have potential for future application, to solar-terrestrial space science missions, to International Space Station, to future space stations requiring artificial gravity, and to several missions involving GPS in orbit.

Consequently, the CSA Space Technology Branch, NASA/MSFC, the Defence Research Establishment Ottawa, and Bristol Aerospace Ltd. participate in the mission. The technology demonstrations envisaged are:

- A. The controlled deployment and spin stabilization with a U.S. SEDS deployer of a 400-m tether.
- B. The operation of a Canadian tether retriever, to achieve spin-up.
- C. The short and long-term passive stabilization of BOLAS, in particular stable orientation of the end bodies, non-decaying spin rate, and predictable motion relative to the orbit plane.
- D. The survivability of a non-conducting 2 mm tether of Spectra 1000 material, in the orbital debris and atomic oxygen environment for at least six months.
- E. Determination of orientation and position of the large rotating configuration, using GPS in-orbit receivers and differential GPS ground processing.
- F. Operation of a data processor for this category of low-cost satellite, based on a MSFC design and Bristol implementation.

The BOLAS project will draw on NASA's experience with the successful SEDS-1, SEDS-2, PMG, and TiPS missions [Rupp, 1995]. The missions employed the Small Expendable Deployer System (SEDS), and this design of deployer is being offered as the tether deployer for BOLAS. The two SEDS missions were launched into orbit as Secondary Payloads on the Delta II launch vehicle in 1994 and 1995. The deployer for the TiPS mission was launched by the U.S. Air Force in 1996. The proven tether dynamics modelling software and tether test facilities at MSFC will be used to support design and development of the mission.

Experience gained in the OEDIPUS-A and C suborbital tether missions will be the base for the Canadian part of the tether activity [Jablonski et al., 1996; Tyc et al., 1996; Vigneron et al., 1996]. Canadian team members will have the lead responsibility for the system dynamics and stabilization of BOLAS. They will use and extend modelling and software developed over the past several years at McGill University and the University of British Columbia. The tether retriever for the spin-up maneuver will be developed under sponsorship of the CSA Space Technology Branch. Its design will be

based on the successful tether reel design of the OEDIPUS missions. Ground tests of the retriever and stabilization principles will be performed to qualify the system for in-orbit operation. The CSA-sponsored evaluations and technical work on the use of GPS for satellite applications [Bisnath and Langley, 1996] will serve as a base for the novel uses of the GPS by the BOLAS project.

4.2 Communications Strategy and Public Relations

The BOLAS project clearly has potential for public relations, given the leadingedge nature of its science and technology. The following public relations activities are envisaged.:

- A. Dissemination of information on the mission which emphasizes the following points.
 - Contribution of basic science results to the "space weather" theme, and the associated improvements to applications.
 - The novel in-space interferometry technique and application of GPS, and significance as a possible technique for future communications applications.
 - Significance of the spacecraft in the context of the trend to low-cost applications-focused (faster, cheaper) microsats.
 - Advances in tether technology, and significance to future Canadian applications including space science and return of Canadian microgravity samples from International Space Station.
 - Relevance of the BOLAS configuration to future space stations that require artificial gravity (induced by centrifugal force of rotation), for long duration interplanetary human travel.

Information in the form of brochures and other hand-out materials could be prepared by team members, possibly with support from CSA public relations experts. The material could include VHS videos of computer-generated animation of the tether deployment sequence and rotating BOLAS. The team and/or individual scientists would respond to opportunities for presentation in public and secondary schools, universities, and for press releases.

- B. The BOLAS configuration will be visible in the night-time sky, by naked eye or binoculars, and also with low-power telescopes of amateur astronomers. BOLAS orbit position information could be made available to instructors of science programs in secondary schools and universities, by the CSA. Various groups of students could then use the information to participate in observation and identification of the dynamics of the tether and configuration. This type of public awareness activity was carried out by NASA during the SEDS and TiPS tether missions, and was very successful in motivating interest and participation by students.
- C. An on-board camera will be considered for addition to the plan in Phase A. In-orbit photos of the configuration could be obtained in near-real time. The data could be used

in the context of both items A and B above.

4.3 Potential benefits

A. Mitigation of Undesirable Effects of the Ionosphere

The understanding of the ionosphere is arguably the most significant limiting factor on space communication system performance. In many instances the root of a communication problem can be traced to the densest part of the ionosphere, the F region at around 300 km altitude where inhomogeneity exists through a wide range of scale sizes. Turbulence, manifested as random distributions of density, degrades signals being sent through it, at all frequencies in the radio spectrum. The BOLAS transionospheric radio experiments address the need for better models of the irregularities. Better models of density irregularities could be used to address problems which arise in geosynchronous and low-earth orbit communications at frequencies up to UHF.

UHF communications suffer perturbations during magnetic storms which increase ionospheric irregularity. Communications systems operators would like to be able to predict the occurrence, in time and location, of the perturbing irregularities. This means understanding how irregularities form and, once formed, what structure, or spatial spectrum, they have. The latter is important because it determines whether irregularities are a problem for a specific carrier frequency.

BOLAS will address these problems by measuring irregularity spectra using its particle sensors. At the same time, propagation between the ground and BOLAS will be observed when irregularities are present. The measured irregularity spectra could be used to predict the fluctuations expected. A theory that agrees with observations might become the basis of a code for predicting unwanted effects in communications applications.

BOLAS propagation investigations are carried out at HF where the weaknesses of communications are well documented: the disruptive effects of natural unpredictable events like polar cap absorption and sudden ionospheric disturbances; the difficulty of characterizing manmade interference; and limited bandwidths. The use of HF nevertheless persists in northern Canada and Alaska. Low population densities neither justify nor need the expensive communication infrastructure used at lower latitudes. In the military context, the ionosphere is a robust medium that recovers much quicker than other media from natural and manmade disruptions. BOLAS research will provide new perspectives on point-to-point communications at high latitudes.

As in communications, ionospheric irregularities also limit the GPS. One area of public concern which could benefit from improved performance of GPS is earthquake prediction through the monitoring of the movement of the earth's crust. For example, in the area of the Juan de Fuca plate in British Columbia, the magnitude of errors in GPS positioning techniques imposed by ionospheric irregularities can be larger than the crustal movement. Glaciologists also are interested in using GPS receivers on high-latitude glacier ice to gather information about systematic widespread decreases in glacier thickness indicating global warming. GPS system developers require a methodology for

characterizing ionospheric turbulence and for subtracting its effects on transionospheric GPS propagation. The BOLAS research on irregularity spectrum, transionospheric propagation and ionospheric tomography all will aid the construction of better models.

B. Canadian Industrial Benefits

BOLAS offers the following industrial and technological benefits:

- Flight experience with numerous elements that are integral to CSA's tentative plans in low-cost satellite development. These include the GPS hardware and technique, tether hardware, on-board computer and several other low-cost spacecraft subsystems.
- Cooperation with NASA, and alliances and knowledge transfer in tether expertise, on-board computer technology, and secondary payloads integration.
- Relationships with NASA and U.S. companies that could lead to a role as supplier in future NASA and/or military programs.
- A unique technology solution that provides for science missions that require two separated locations in space.
- A technology base relevant to several future international application areas, for example, sample-return capability from space stations, interferometric synthetic aperture radar, and rotating space stations with artificial gravity for long duration human space presence.

References

- Arnoldy, R.L., K.A. Lynch, P.M. Kintner, J. Vago, S. Chesney, T.E. Moore and C.J. Pollock, Bursts of transverse ion acceleration at rocket altitudes, *Geophys. Res. Lett*, 19, 413, 1992.
- Barnes, G., B. Gordon, H.G. James, and G. Rumbold, Transmitter/receiver for OEDIPUS-C ionospheric wave propagation experiment, *Proc. 9th CASI Conf. on Astronautics*, 209-222, Canadian Astronautics and Space Institute, Ottawa K1P 6E3, 13-15 Nov. 1996.
- Bisnath, S.B. and R.B. Langley, "Assessment of the GPS/MET Turbostar Receiver for Orbit Determination of a Future CSA Micro/Small-Satellite Mission", Final report of study conducted for CSA Space Technology, Geodetic Research Laboratory, University of New Brunswick, 1996.
- Bristow, W.A., R.A. Greenwald, and J.C. Samson, Identification of high latitude acoustic gravity wave sources using the Goose Bay HF radar, *J. Geophys. Res.*, 99, 319-331, 1994.
- Bristow, W.A. and R.A. Greenwald, Estimating gravity wave parameters from oblique high-frequency backscatter: Modeling and analysis, *J. Geophys. Res.*, 100, 3639-3648, 1995.
- Bristow, W.A., R.A. Greenwald and J. P. Villain, On the seasonal dependence of medium-scale atmospheric gravity waves in the upper atmosphere at high latitudes, *J. Geophys. Res.*, 101, 15,685-15,699, 1996.
- Carrington, C.K., BOLAS Deployment Dynamics Feasibility Analysis, *Technical Memorandum*, Program Development, NASA/MSFC Code PD12, November 26, 1996.
- Chaturvedi, P.K. and S. L. Ossakow, The current convective instability as applied to the auroral ionosphere, J. Geophys. Res., 86, 4811, 1981.
- Eliuk, W., I. Walkty, R. Rob, G. Rumbold and H.G. James, OEDIPUS-C tethered suborbital mission description and flight performance, *Proc. 9th CASI Conf. on Astronautics*, 332-341, Canadian Astronautics and Space Institute, Ottawa K1P 6E3, 13-15 Nov. 1996.
- Greenwald, R.A., K.B. Baker, J.R. Dudeney, M. Pinnock, T.B. Jones, E.C. Thomas, J.-P. Villain, J.-C. Cerisier, C. Senior, C. Hanuise, R.D. Hunsucker, G. Sofko, J. Koehler, E. Nielsen, R. Pellinen, A.D.M. Walker, N. Sato and H. Yamagishi,

- DARN/SUPERDARN A global view of the dynamics of high-latitude convection, *Space Science Reviews*, 71, 761-796, 1995.
- Hajj, G and L. Romans, Ionospheric mapping with the GPS/MET, *Proceedings of the 52nd Annual Meeting Navigation Technology For the 3rd Millennium*, The Institute of Navigation, Cambridge, Mass., U.S.A., 19-21, June., pp. 539-545, 1996.
- Hofmann-Wellenhof, B., H. Lichtenegger and J. Collins, *GPS Theory and Practice*, Springer Verlag, Vienna, 1992.
- Jablonski, A.M., F.R. Vigneron, G. Tyc, R.P.S. Han, A.K. Misra, V.J. Modi and R. Chandrashaker, OEDIPUS-C Tether Dynamics Experiment, *Proc. of the 9th CASI Conf. of Astrodynamics*, 12-15 Nov., 1996, Ottawa, Ont., 1996.
- James, H.G., BOLAS Bistatic Obervations with Low Altitude Satellites, A proposal in response to the Small-Payloads Solicitation of July 1996 by the Space Science Program of the Canadian Space Agency, Communications Research Centre, Ottawa K2H 8S2, Canada, 1997a.
- James, H.G., Phase-path measurements in space using receivers with GPS clocks, submitted to AGU Monograph Measurement Techniques for Space Plasmas, 1997b.
- Kintner, P.M., J. Vago, S. Chesney, R.L. Arnoldy, K.A. Lynch, C.J. Pollock and T.E. Moore, Localized lower hybrid acceleration of ionospheric plasma, *Phys Rev. Lett.*, 68, 2448, 1992.
- Knudsen, D.J. and J.-E. Wahlund, Core ion flux bursts within solitary kinetic Alfvén waves, *J. Geophys. Res.*, in press, 1996.
- Komjathy, A. and R.B. Langley, Improvement of a global ionospheric model to provide ionospheric range error corrections for single-frequency GPS users, Proceedings of the 52nd Annual Meeting Navigation Technology For the 3rd Millennium, The Institute of Navigation, Cambridge, Mass., U.S.A., 19-21, June., pp. 557-566, 1996.
- Komjathy, A., Langley, R., and D. Bilitza, Updating the International Reference Ionosphere using a global network of GPS stations: Preliminary results, Presented at the Workshop for *Ionospheric Delay Correction for Single-frequency Radar Altimetry*, Colorado Center for Astrodynamics Research of the University of Colorado, Boulder, Col., U.S.A., 24-25 September 1996.
- LaBelle, J., P.M. Kintner, A.W. Yau and B.A. Whalen, Large amplitude wave packets observed in the ionosphere in association with transverse ion acceleration, J.

- Geophys. Res., 91, 7113, 1986.
- Langley, R.B., Propagation of the GPS signals, in GPS for Geodesy, Lecture Notes in Earth Sciences, 60. (Eds.) A. Kleusberg and P.J.G. Teunissen, Springer-Verlag, Berlin, Germany, 407 pp., 1996.
- Lee, L.-C., Magnetic flux transfer at the earth's magnetopause, in *Proceedings of Chapman Conference on Solar Wind-Magnetosphere Coupling*, edited by Y. Kamide and J. Slavin, p. 297, Terra Scientific, Tokyo, 1986.
- MacDougall, J.W., I.F. Grant and X. Shen, The Canadian Advanced Digital Ionosonde: Design and results, in *Ionosonde Networks and Stations, Rep. UAG-104*, pp21-27, World Data Cent. A for Sol.-Terr. Phys., Boulder, Colo., 1995.
- MacDougall, J.W., I.F. Grant and A. Hamza, Velocity fluctuations associated with polar cap patches, *Radio Science*, 31, 595-605, 1996.
- Pollock, C.J., T.E. Moore, M.L. Adrian, P.M. Kintner, and R.L. Arnoldy, SCIFER Cleft Region Thermal Electron Distribution Functions, *Geophys. Res. Lett.*, 23, 1881, 1996a.
- Pollock, C.J., V.N. Coffey, J.D. England, N.G. Martinez, T.E. Moore and M.L. Adrian, Thermal electron capped hemisphere spectrometer (TECHS) for ionospheric studies, submitted to AGU Monograph Measurement Techniques for Space Plasmas, 1996b.
- Rupp, C.C., Flight Data From the First and Second Flights of the Small Expandable Deployer System (SEDS), *Proc. of the 4th Int. Conf. on Tethers in Space*, Smithsonian Inst., Washington, D.C., 10-14 April, 1995.
- Samson, J.C., R.A. Greenwald, J.M. Ruohoniemi and K.B. Baker, High-frequency radar observations of atmospheric gravity waves in the high-latitude ionosphere, *Geophys. Res. Lett.*, 16, 875-878, 1989.
- Samson, J.C., R.A. Greenwald, J.M. Ruohoniemi, A. Frey, and K.B. Baker, Goose Bay Radar observations of Earth-reflected atmospheric gravity waves in the high-latitude ionosphere, *J. Geophys. Res.*, 95, 7693-7709, 1990
- Schiffler, A., SuperDARN Measurements of Double-Peaked Velocity Spectra, M. Sc. Thesis, University of Saskatchewan, September, 1996.
- Simon, A., Instability of a partially ionized plasma in crossed electric and magnetic fields, *Phys. Fluids*, 6, 382, 1963.

- Sofko, G.J., R.A. Greenwald and W.A. Bristow, Direct determination of large-scale magnetospheric field-aligned currents with SuperDARN, *Geophys. Res. Lett.*, 22, 2041-2044, 1995.
- Tsunoda, R.T., High-latitude *F*-region irregularities: a review and synthesis, *Rev. Geophys.*, 26, 719-760, 1988.
- Tyc, G., F.R. Vigneron, A.M. Jablonski, R.P.S. Han, V.J. Modi and A.K. Misra, Flight Dynamics Results From the OEDIPUS-C Tether Mission, *Proc. of the AIAA/AAS Astrodynamics Conf.*, July 29-31, San Diego, CA, 1996.
- Tyc, G. and S. Pradhan, Dynamics of the BOLAS Tethered Spacecraft Configuration, *Technical Memoranda, Bristol Aerospace Ltd.*, October 21 and November 25, 1996.
- Vadali, S.R., Feedback Tether Deployment and Retrieval, *Journal of Guidance, Control and Dynamics*, 14(2), 469-470, 1991.
- Vago, J., P.M. Kintner, S.M. Chesney, R.L. Arnoldy, K.A. Lynch, T.E. Moore and C.J. Pollock, Transverse ion acceleration by lower hybrid waves in the topside auroral ionosphere, *J. Geophys. Res.*, *97*, 16,395, 1992.
- Vigneron, F.R., R. Chandrashaker, A.M. Jablonski and G. Tyc, Damped Gyroscopic Modes of Spinning Tethered Space Vehicles with Flexible Booms, AAIA 96-3574, *Proc. AIAA/AAS Astrodynamics Conf.*, pp. 51-60, July 29-31, San Diego, CA, 1996 (to appear in *AIAA J. Spacecraft Rockets*, 34, 1997).
- Wahlund, J.-E., P. Louarn, T. Chust, H. de Feraudy, A. Roux, P.-O. Dovner and C. Holmgren, On ion acoustic turbulence and the nonlinear evolution of kinetic Alfvén waves in aurora, *Geophys. Res. Lett.*, 21, 1831, 1994.
- Wells, D.E., N. Beck, D. Delikaraoglu, A. Kleusberg, E.J. Krakiwsky, G. Lachapelle, R. B. Langley, M. Naskiboglu, K. P Schwarz, J.M. Tranquilla and P. Vaníček, *Guide to GPS Positioning*, Canadian GPS Associates, Fredericton, Canada, 1987.
- Whalen, B.A., D.J. Knudsen, A.W. Yau, A.M. Pilon, T.A. Cameron, J.F. Sebesta,
 D.J. McEwen, J.A. Koehler, N.D. Lloyd, G. Pocobelli, J.G. Laframboise, W.
 Li, R. Lundin, L. Eliasson, S. Watanabe and G.S. Campbell, The Freja F3C
 Cold Plasma Analyzer, *Space Sci. Rev.*, 70, 541-561, 1994.
- Yunck, T.P. and W.G. Melbourne, Spaceborne GPS for earth science, in GPS Trends in Precise Terrestrial, Airborne, and Spaceborne Applications, Eds. G. Beutler, G.W. Hein, W.G. Melborne and G. Seeber. International Association of Geodesy Symposium Number 115, Boulder, Col., U.S.A., 3-4 July, 1995, pp.

PROPULSIVE SMALL EXPENDABLE DEPLOYER SYSTEM (ProSEDS) SPACE DEMONSTRATION

By

Les Johnson
National Aeronautics and Space Administration
George C. Marshall Space Flight Center
Mail Code PS02
Huntsville, Alabama 35812

Judy Ballance
National Aeronautics and Space Administration
George C. Marshall Space Flight Center
Mail Code EE61
Huntsville, Alabama 35812

Abstract

The Propulsive Small Expendable Deployer System (ProSEDS) space experiment will demonstrate the use of an electrodynamic tether propulsion system. The flight experiment is a precursor to the more ambitious electrodynamic tether upper stage demonstration mission which will be capable of orbit raising, lowering and inclination changes-all using electrodynamic thrust. ProSEDS, which is planned to fly in 2000, will use the flight proven Small Expendable Deployer System (SEDS) to deploy a tether (5 km bare wire plus 15 km spectra) from a Delta II upper stage to achieve ~0.4N drag thrust, thus deorbiting the stage. The experiment will use a predominantly 'bare' tether for current collection in lieu of the endmass collector and insulated tether approach used on previous missions. ProSEDS will utilize tether-generated current to provide limited spacecraft power. In addition to the use of this technology for orbit transfer and upper stages, it may also be an attractive option for future missions to Jupiter and any other planetary body with a magnetosphere.

Introduction

Since the 1960's there have been at least 16 tether missions. In the 1990's, several important milestones were reached, including the retrieval of a tether in space (TSS-1, 1992), successful deployment of a 20-km-long tether in space (SEDS-1, 1993), and operation of an electrodynamic tether with tether current driven in both directions—power and thrust modes (PMG, 1993)¹. A list of known tether missions is shown in Table 1. The ProSEDS mission, to be flown in 2000, is sponsored by NASA's Advanced Space Transportation Program Office at The George C. Marshall Space Flight Center (MSFC).

NAME	DATE	ORBIT	LENGTH	COMMENTS	
Gemini 11	1967	LEO	30 m	spin stable 0.15 rpm	
Gemini 12	1967	LEO	30 m	local vertical, stable swing	
H-9M-69	1980	suborbital	500 m	partial deployment	
S-520-2	1981	suborbital	500 m	partial deployment	1
Charge-1	1983	suborbital	500 m	full deployment	

Charge-2	1984	suborbital	500 m	full deployment
ECHO-7	1988	suborbital	?	magnetic field aligned
Oedipus-A	1989	suborbital	958 m	spin stable 0.7 rpm
Charge-2B	1992	suborbital	500 m	full deployment
TSS-1	1992	LEO	<1 km	electrodynamic, partial deploy, retrieved
SEDS-1	1993	LEO	20 km	downward deploy, swing & cut
PMG	1993	LEO	500 m	electrodynamic, upward deploy
SEDS-2	1994	LEO	20 km	local vertical stable, downward deploy
Oedipus-C	1995	suborbital	1 km	spin stable 0.7 rpm
TSS-1R	1996	LEO	19.6 km	electrodynamic, severed
TiPS	1996	LEO	4 km	long life tether

Table 1. Known tether flights.

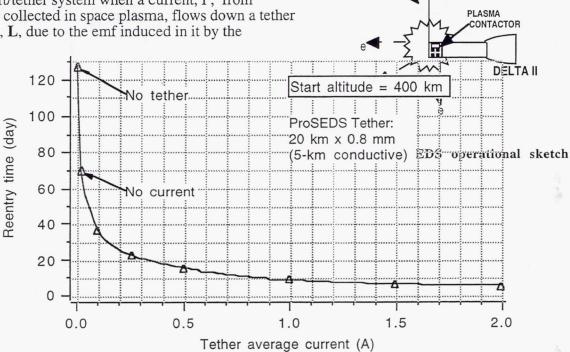
Experiment Overview

The ProSEDS experiment will be placed into a 400 km circular orbit as a secondary payload from a Delta II launch vehicle (Figure 1). Once on orbit, the flight-proven SEDS will deploy 15 km of insulating Spectra tether attached to an endmass, followed by 5km of predominantly bare wire tether (Figure 2). Upward deployment will set the system to operate in the generator mode, thus producing drag thrust and electrical power. The drag thrust provided by the tether, with an average current of 0.5A, will deorbit the Delta II upper stage in approximately 17 days, versus its nominal ≥6 months lifetime in a 400 km circular orbit (Figure 3)². Approximately 100 W electrical power will be extracted from the tether to recharge mission batteries and to allow extended measurements of the system's performance. A plasma contactor will be attached to the Delta II to complete the circuit and emit electrons back into space. Performance and diagnostic instruments mounted on the Delta II will be used to correlate the propulsive forces generated by the electrodynamic tether and the existing plasma conditions. These instrument will measure plasma density, temperature, energy, and potential. ProSEDS will be the first tether mission to produce electrodynamic thrust, use a bare wire tether, and recharge mission batteries using tether-generated power.

Figure 1. Artist concept of ProSEDS on a Delta II upper stage

Electrodynamic Tethers

The ProSEDS flight experiment will demonstrate electrodynamic propulsion (through drag thrust) in space. From theoretical analyses and preliminary plasma chamber tests, bare tethers appear to be very effective anodes for collecting electrons from the ionosphere and, consequently, attaining high currents with relatively short tether lengths. A predominantly uninsulated (bare wire) conducting tether, terminated at one end by a plasma contactor, will be used as an electromagnetic thruster. A propulsive force of $\mathbf{F} = \mathbf{IL} \times \mathbf{B}$ is generated on a spacecraft/tether system when a current, I , from electrons collected in space plasma, flows down a tether of length, L, due to the emf induced in it by the



ProSEDS SKETCH

15 km Spectra

55 LB

Endma

5km Bare Wire

Figure 3. Predicted demonstration of ProSEDS propulsive drag thrust. The upper stage reentry time versus tether average current is shown.²

geomagnetic field, **B**. Preliminary test indicate that a thin uninsulated wire could be 40 times more efficient as a collector than previous systems (Figure 4)³.

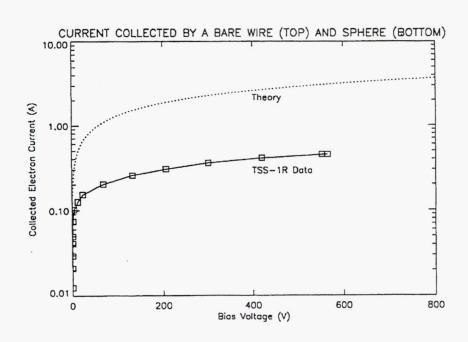


Figure 4. Current collected by a bare wire versus a sphere3.

Potential Applications

The main advantage of electrodynamic tethers is that they can be used as propellantless (no resupply required) space propulsion systems. Tethers take advantage of the natural plasma environment and sunlight to provide thrust and power. For example, if solar arrays and an external power supply are used, an emf can be generated in the tether such that current collected from the ionosphere produces thrust rather than drag. This thrust can then be used to raise the orbit of the system or change its inclination - all without propellant or rocket engines. It is envisioned that this type of propulsion could be used on a reusable upper stage to provide a low cost alternative to chemical stages. The electrodynamic tether upper stage (Figure 5) could be used as an orbital tug to move payloads within low earth orbit (LEO) after insertion. The tug would rendezvous with the payload and launch vehicle, dock/grapple the payload and maneuver it to a new orbital altitude or inclination within LEO without the use of boost propellant. The tug could then lower its orbit to rendezvous with the next payload and repeat the process. Such a system could conceivably perform several orbital maneuvering assignments without resupply, making it low recurring cost space asset. The ProSEDS itself could be used operationally to extend the capability of existing launch systems by providing a propellantless system for deorbiting spent stages. The launch service provider need not carry additional fuel for the soon-tobe-required deorbit maneuver, thus allowing all the onboard fuel to be used for increasing the vehicle's performance. Similarly, satellites thus equipped could safely deorbit at their end of life without using precious onboard propellant. Both of these applications would help reduce the increasing threat posed by orbital debris. An electrodynamic tether system could be used on the International Space Station (ISS) to supply a reboost thrust of 0.5-0.8N, thus saving up to 6000kg of propellant per year (Figure 6). The reduction of propellant needed to reboost the ISS equates to a \$2B savings over it's 10 year lifetime⁴. Other advantages of using the electrodynamic tether on ISS are that the microgravity environment is maintained and external contaminants are reduced. Yet another use for electrodynamic tethers is the exploration of any planet with a magnetosphere, such as Jupiter. Jupiter's rapid rotation produces a condition where a tether can produce power and raise orbit

passively and simultaneously. MSFC is working with the Jet Propulsion Laboratory (JPL) to determine the use of electrodynamic tethers for future Jovian missions such as the Europa Orbiter and Jupiter Polar Orbiter (Figure 7).

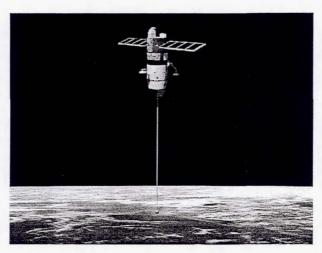
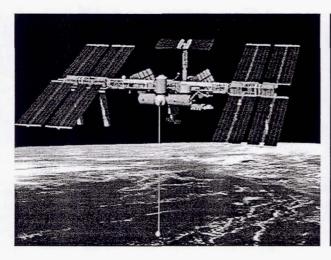


Figure 5. Artist concept of an electrodynamic tether upper stage.



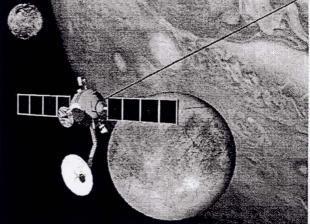


Figure 6. ISS with Electrodynamic for Reboost Tether Concept

Figure 7. Jovian Electrodynamic

Conclusions

Tether technology has advanced significantly since its inception over 30 years ago. The recent successes of the SEDS system show that tethers are ready to move from experiment and demonstration to application. One of the most promising applications for tethers is space propulsion and transportation. The use of electrodynamic tether propulsion for reusable upper stages, planetary missions, space station, and launch vehicle deorbit applications will soon be demonstrated with the ProSEDS mission. The ProSEDS mission will also demonstrate and validate the production of power in space using a bare wire tether which produces drag thrust propulsion.

References

- 1. Johnson, L., Estes, R., and Lorenzini, E., "Space Transportation Systems Using Tethers", 1997.
- 2. Lorenzini, E. C., Unpublished data from ProSEDS Analysis, May 14, 1997.
- 3. Colombo, G., "Study of certain launching techniques using long tethers," NASA-CR-164060, March 1981.
- 4. Unpublished data from the Tethered Satellite System Reflight (TSS-1R), 1996, and Unpublished Plasma Chamber Test Results by Sorensen, Jim, NASA, MSFC, May 1997.
- 5. Johnson, L., Caroll, J., Estes, R., Lorenzini, E., Gilchrist, B., Martinez-Sanchez, M., Sanmartin, J., and Vas, E., "Electrodynamic Tethers for Reboost of the International Space Station and Spacecraft Propulsion", 1997.

The "Terminator Tether" A Near-Term Commercial Application of the NASA/MSFC ProSEDS Experiment

Dr. Robert L. Forward and Dr. Robert P. Hoyt
Tethers Unlimited
8114 Pebble Court, Clinton, WA 98236 USA
Phone/Fax: +1-360-579-1340; Email: TU@tethers.com; Web: www.tethers.com

Chauncey Uphoff
ACTA Consulting Group
7020 Elm Street, Longmont, CO 80503
Phone: 303-652-3591; Fax: -3976; Email: chauncey@oneimage.com

Abstract

The NASA/MSFC ProSEDS Experiment is designed to demonstrate that electrodynamic drag on a conducting tether can rapidly deorbiting a spacecraft. This paper discusses the future commercial application of this technology for mitigating the long-lived orbital debris hazard created by constellation satellites through the use of an electrodynamic drag "Terminator Tether"™ which will remove constellation satellites from orbit after their end-of-life. We show that the electrodynamic drag of a conducting tether is dependent predominantly on the mass, density, and conductivity of the tether, not its length, and we develop analytical tools for predicting the time required for a Terminator Tether to deorbit spacecraft from various orbits. We find that aluminum wire tethers massing just 1 to 5% of the mass of the host spacecraft can deorbit LEO constellation satellites within a few weeks or months, depending upon the initial orbit. Although the tether increases the total collision cross-sectional area of the satellite-plus-tether system during the deorbit phase, we find that the product of the collision cross-sectional area of the satellite-plus-tether times the deorbit time (Area-Time-Product), can be reduced by orders of magnitude by using a Terminator Tether instead of depending upon atmospheric drag alone, greatly reducing the risk of collision with other spacecraft.

I. INTRODUCTION

This paper investigates the use of a highly survivable, conducting electrodynamic tether for use as a "Terminator Tether" for removing unwanted Low-Earth-Orbit (LEO) spacecraft from orbit at the end their useful lives. When a spacecraft fails, or has completed its mission and is no longer wanted, the Terminator Tether, weighing a small fraction of the mass of the host spacecraft, would be deployed. At both ends of the tether, a means of providing electrical contact with the ambient plasma will be provided to enable current to be transmitted to and from the ionospheric plasma. The electrodynamic interaction of the conducting tether moving at orbital speeds across the Earth's magnetic field will induce current flow along the tether. The resulting energy loss from the heat generated by the current flowing through the ohmic resistance in the tether will remove energy from the spacecraft. Consequently, the orbital energy of the spacecraft will decay, causing it to deorbit far more rapidly than it would due to atmospheric drag alone. Whereas a defunct spacecraft left in its orbit can take hundreds or thousands of years to deorbit due to atmospheric drag, a spacecraft with a Terminator Tether can be deorbited in weeks or months. The Terminator Tether thus is a low-mass means of reducing both the risk of spacecraft fratricide and the amount of orbital space debris that must be coped with in the future.

In the first section of this paper, we will begin by discussing the orbital debris problem motivating the development of the Terminator Tether. We will then describe the basic concept of electrodynamic tether drag, and review the results of past experiments related to this concept. In the second section, will develop analytical methods for predicting the effectiveness of Terminator Tether systems for deorbiting spacecraft from various orbits. In the third section, we will describe methods of optimizing the electrodynamic drag on the spacecraft, while concurrently stabilizing the electrodynamic tether libration. In the fourth section, we examine the effectiveness of the Terminator Tether for reducing the Area-Time-Product for orbital decay of LEO spacecraft, and compare it to conventional deorbit methods. Finally, we describe two implementations of the Terminator Tether concept for reducing the LEO debris environment.

I.A. MOTIVATION: ORBITAL DEBRIS IN LEO

Currently, the US Space Command tracks roughly 6,000 objects in LEO. Less than 300 of these objects are operational spacecraft. The rest are spent rockets and derelict spacecraft.³ In addition, there are countless numbers of debris objects too small to be tracked; these objects result from explosions of rocket stages and fragmentation of spacecraft. These objects pose a growing risk to operational spacecraft. Moreover, in the near future, a number of companies will begin deploying telecommunications constellations with tens or even hundreds of satellites. These satellites will have operational lifetimes of approximately 5-10 years. Unless proper measures are taken to remove these satellites from orbit at the end of their lives, the debris population in LEO may grow exponentially, making many orbital slots useless.

NASA Safety Standard

NASA and other agencies have begun to address this problem. The current status of efforts to mitigate the orbital debris population is expressed in the NASA Safety Standard NSS 1740.14 *Guidelines and Assessment Procedures for Limiting Orbital Debris.*⁴ The relevant portion of the Standard starts on page 6-3:

General Policy Objective - Postmission Disposal of Space Structures.

<u>Item 6-1:</u> "Disposal for final mission orbits passing through LEO: A spacecraft or upperstage with perigee altitude below 2000 km in its final orbit will be disposed of by one of three methods."

The method of interest relevant for this paper is the atmospheric reentry option:

Option a: "Leave the structure in an orbit in which, using conservative projections for solar activity, atmospheric drag will limit the lifetime to no longer than 25 years after completion of mission. If drag enhancement devices are to be used to reduce the orbit lifetime, it should be demonstrated that such devices will significantly reduce the area-time product of the system or will not cause the spacecraft or large debris to fragment if a collision occurs while the system is decaying from orbit."

The NASA standard applies only to NASA spacecraft and even then only to completely new spacecraft designs. New versions of existing designs are to make a "best effort" to meet the standard, but will not be required to change their design to do so. The DoD has adopted the NASA standard with the same provisos. An Interagency Group report has recommended that the NASA Safety Standard be taken as a starting point for a national standard. It is NASA's recommendation to the Interagency Group that the safety requirement be phased in only as we reach consensus internationally. This consensus is being sought through the International Debris Coordination Working Group, whose members are Russia, China, Japan, ESA, UK, India, France, Italy, and the US.

Thus, although the NASA Safety Standard in its present form is not a "Law", the existence of the standard means that at some time in the future a similar requirement may be imposed on all spacecraft. In fact, most of the satellite constellation companies have already acknowledged that, even without regulatory requirements, they must take proactive steps to

prevent orbital debris from contaminating their valuable orbital slots. Several, including Teledesic, Iridium, and GlobalStar, have committed to de-orbiting their satellites at the end of their operational lifetimes.^{5,6} For many of the satellite constellations currently under development, the Terminator Tether can provide a low-cost, low-mass, low-Area-Time-Product, reliable, and safe means for deorbiting post-mission satellites and launch/dispenser rocket stages.

I.B. SUMMARY OF CONCEPT

The electrodynamic drag concept for deorbit of LEO spacecraft is illustrated in Figure 1. The idea of using electrodynamic drag to remove unwanted spacecraft from orbit was first discussed by Joseph P. Loftus of NASA Johnson Space Center in June 1996. A first-order analysis published by Robert L. Forward in July 1996 found that a conducting tether with mass m_T orbiting above the magnetic equator through a transverse magnetic field of strength B_T at a velocity with respect to the magnetic field v_M , will generate an electrical power P in the tether given by the equation:

$$P = \frac{m_T \left(v_M B_T \right)^2}{rd} \tag{1}$$

where r is the resistivity and d the density of the conducting tether material. This power is converted into heat by the resistance of the tether and radiated away into space, extracting kinetic energy from the host spacecraft. For a m_T =10 kg tether of aluminum with resistivity of r=27.4 n Ω -m and density d=2700 kg/m³, orbiting over the magnetic equator at an altitude of 1000 km, at a velocity v_M =6814 m/s relative to the Earth's transverse magnetic field B_T =20 μ T, the power dissipated is P=2510 W! This energy loss in the form of heat must necessarily come out of the kinetic energy of the host spacecraft. For a typical example, a 1000 kg spacecraft in a 1000 km high orbit subjected to an energy loss of 2510 J/s from a 10 kg tether (1% the mass of the host spacecraft) will be deorbited in a few weeks. Similar conclusions have been reached by many others, including members of the NASA/MSFC ProSEDS Experiment team. 7,8,9,10

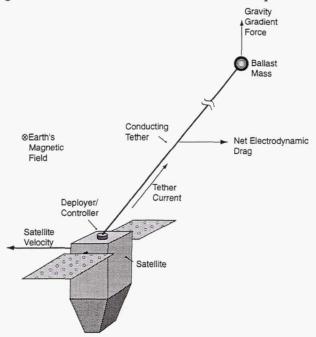


Figure 1. The Terminator Tether™ concept.

Experimental Confirmations of Induced Power Levels

Power levels of the magnitude estimated in the previous paragraph have been measured in a <u>real</u> orbital space experiment, the TSS-1R mission carried out on the Shuttle Orbiter in 1995. In that experiment, a large Italian spacecraft, 1.6 m in diameter, was deployed upward from the Shuttle Orbiter at the end of a conducting copper wire tether covered with electrical insulation. As the tether was slowly deployed upwards, a series of measurements were made of the open circuit voltage induced in the tether by its motion through the Earth's magnetic field. The voltage between the end of the tether and the Orbiter ground varied from zero volts at the start to 3500 V when the amount of tether deployed approached its maximum length of 20 km. Periodically, the end of the tether was connected either to one of two different electron guns, which supplied contact to the surrounding space plasma, or to the Orbiter ground, which proved to be a surprisingly good plasma contactor via a combination of ion collection and secondary electron emission. The current flow through the tether was deliberately limited by control circuits and the current capacity of the electron guns, but power levels of 1800 W were reached.

The tether was intended to have a fully deployed length of 20 km, but at a deployed length of 19.5 km, when about 3500 V was being induced at the end of the tether inside the Orbiter reel mechanism, a flaw in the insulation allowed an electrical spark to jump in an uncontrolled manner from the tether to the Orbiter ground. With no control circuits to keep the current level down, the current flow jumped to 1.1 A and the total power generated was $P=3850\,\mathrm{W}$. Most of this energy went into the electrical arc, which burned through the tether, causing it to break and halting the experiment. This experiment showed that large areas of bare conducting material, such as that provided by the Italian spacecraft and the Orbiter spacecraft, can collect amperes of current, while thousands of volts of potential can be generated by sufficiently long tethers moving at orbital speeds.

Thus, both theory and experimental data indicate that significant amounts of electrodynamic drag force can be obtained from a low mass conducting tether attached to a host spacecraft, <u>provided</u> the ends of the conductor can exchange sufficient numbers of electrons with the surrounding space plasma.

Experimental data from the TSS-1R data also produced the amazing result that the efficiency of a bare metal surface in "contacting" the space plasma is many times better than the standard theory would predict. The 8 square meters of bare surface area of the Italian spacecraft were sufficient to collect the 1.1 A of electron current. This amount of area is easily replicated by a few hundred meters of bare wire, 12 considering that the effective collection diameter around the wire is the Debye length, which is a few centimeters at the typical values for space plasma density and temperature.

Flight Demonstration of Electrodynamic Drag Deorbiting

Because of this result from the TSS-1R experiment, that a bare wire can easily collect electrons, Les Johnson, Nobie Stone, Chris Rupp, and others at NASA Marshall Space Flight Center have formed a team, which includes the present authors, which is embarked on a new flight experiment. The experiment is scheduled for a piggy-back flight on a Delta II launch of an AF Global Positioning Satellite in early 2000. The goal of the experiment is to demonstrate that electrodynamic drag from a wire moving at orbital speeds through the Earth's magnetic field will create a large enough electrodynamic drag force to deorbit the >1000 kg Delta II second stage in a few weeks. This is essentially a demonstration of the Loftus electrodynamic drag deorbit concept and the first step in the development of a Terminator Tether.

The ProSEDS (Propulsion Small Expendable-tether Deployer System) mission is presently baselined to use a 5 km long copper wire massing 18 kg, a 20 km long nonconducting tether, and a 25 kg ballast mass on the end of the tether. The total of 25 km of tether length and the 25 kg ballast mass on the end will provide enough gradient force to keep the tether aligned near the

zenith, so that the direction of the current in the tether is at right angles to both the direction of the spacecraft motion in the nominal EW direction and the Earth's near-equatorial magnetic field in the nominal NS direction.

An important feature of the ProSEDS experiment is that it is designed to be completely self-powered. It uses a battery to initiate deployment and to power up the plasma contactor, but once current is flowing through the tether, some of the power is tapped off and used to recharge the battery. The battery in turn powers the current control electronics, the telemetry system, and the plasma contactor. The ProSEDS mission will not be designed to allow ground control changes in operation, primarily because of the increase in cost associated with that option.

Terminator TetherTM

In this paper we propose a commercialized version of the ProSEDS experiment, which would consist of a small, low-mass deployer/controller package containing a large collecting area, short length, highly-survivable, multiline space tether, such as a Hoytape mesh¹³ made of aluminum wire, as a "Terminator Tether" for upper stages and LEO spacecraft, especially the expected multitude of LEO constellation satellites and their upper stage launcher/dispensers. The Terminator Tether would be deployed when the host vehicle is no longer working or no longer wanted. The electrodynamic drag from the Terminator Tether would rapidly remove the unwanted vehicle from the constellation orbit altitude and a few weeks later complete the deorbit of the host vehicle from space by burnup in the upper atmosphere of the Earth. For a Terminator Tether to be of maximum usefulness for constellation satellites, it would be desirable to minimize the mass and the length of the tether, while at the same time maximizing the electrodynamic drag force. A lower tether mass means more mass for revenue producing transponders, while a shorter tether length means a lower collision cross-section Area-Time-Product during deorbit. Since the proposed Terminator Tether would autonomously maintain contact with ground control during the deorbit phase, and ground control can control its rate of descent, a Terminator Tether can avoid the larger spacecraft with well-known and predictable orbits, thus decreasing the probability of a collision below that predicted using the Area-Time-Product alone.

Electrodynamic Tether Constraints

The electrodynamic tether is assumed to be made of a conducting metal, and have a length L, density d, resistivity r, and cross-sectional area A that is constant along the length of the tether. If the tether is a single round wire of diameter D, then the cross-sectional area is $A=\pi D^2/4$. Because of the micrometeorite and space debris hazard, however, it is likely the tether will be made up of redundantly interconnected multiple lines whose individual cross-sectional areas add up to A. Given these assumptions, the tether mass is then $m_T=dLA$, while the end-to-end tether resistance is $R=rL/A=rdL^2/m_T$.

Specific Conductivity Parameter:

The choice of the metal conductor to be used in a space tether is determined by a combination of low resistivity (high conductivity) and low density, with cost, strength, and melting point as secondary considerations for certain applications. Copper has a resistivity $r=17.0~\rm n\Omega$ -m, a density $d=8933~\rm kg/m^3$, and a "specific conductivity" of $1/rd=6,585~\rm m^2/\Omega$ -kg. Aluminum has a resistivity $r=27.4~\rm n\Omega$ -m, which is significantly greater than that of copper, but it has a much lower density of $d=2700~\rm kg/m^3$. As a result, aluminum's "specific conductivity" of $1/rd=13,500~\rm m^2/\Omega$ -kg is twice the conductivity per unit mass of copper. Silver, because of its higher density and higher cost, is not competitive as an electrodynamic space tether even though its resistivity of $16.1~\rm n\Omega$ -m is slightly less than that of copper. An alternate candidate material would be beryllium, with a resistivity $r=32.5~\rm n\Omega$ -m, density $d=1850~\rm kg/m^3$, and a

specific conductivity of $1/rd=16,630 \text{ m}^2/\Omega\text{kg}$, slightly better than that of the much cheaper aluminum. Beryllium also has a higher melting point at 1551 K than aluminum at 933 K, so some of its alloys may be a preferred material for some electrodynamic applications despite its higher materials cost. Unfortunately, despite decades of metallurgical research by the nuclear power industry, highly ductile alloys of beryllium have not been found, so it is difficult to make it into wire. As a result, because of its high specific conductivity, low cost, and ready availability in ductile wire form, we will assume for this paper that the electrodynamic tether will be made of aluminum wire.

Typical Resistance Values: To be competitive, the mass of the tether needs to be a small fraction of the mass of the host spacecraft it is required to deorbit. Since a typical constellation satellite has a mass of about 1000 kg, a typical Terminator Tether with a mass that is 2% of the host spacecraft mass would consist of a deployer/controller package with a mass $m_D=10$ kg, containing an aluminum tether with a mass $m_T=10$ kg with a volume of $m_T/d=LA=3.70 \times 10^{-3}$ m³. If this 10 kg of aluminum were formed into a tether with a length of L=2 km and a cross-sectional area of A=1.85 mm², then the end-to-end resistance of the tether would be $R=rL/A=rdL^2/m_T=29.6$ Ω. A longer tether would have a proportionately smaller cross-sectional area and a higher resistance; for example, a 5 km long tether with the same mass would have a resistance of 185 Ω.

II. TERMINATOR TETHER ANALYSIS AND OPTIMIZATION

II.A. CHANGING A SPACECRAFT ORBIT USING ELECTRODYNAMIC TETHER PROPULSION

To determine the effectiveness of the Terminator Tether system for de-orbiting a spent spacecraft, we will now develop analytical tools for predicting the time required for a electrodynamic tether to deorbit a spacecraft from a specified altitude h and inclination i.

Assumptions:

Circular Orbit

We will assume that the spacecraft trajectory is a nearly circular spiral which can, for each orbit, be approximated by a circular orbit with radius *r*.

Tether Orientation

We will assume that there is a balance between the electrodynamic drag on the tether and the gradient forces on the tether which causes the tether to hang at an angle α from the local vertical, with the rotation in the direction opposite to the velocity vector. In reality, variations in the electrodynamic forces along the tether length will likely cause the tether to hang in a curved manner, and variations in the drag force during an orbit will cause the tether to librate around some equilibrium point, but for this analysis we will assume that it hangs straight at the specified angle.

The tether length vector can thus be expressed as

$$\mathbf{L} = L \left(\hat{\mathbf{r}} \cos \alpha + \hat{\mathbf{v}} \sin \alpha \right). \tag{2}$$

Current Collection

We will assume that the Terminator Tether system provides sufficient current contact with the ionospheric plasma to transmit the full current possible between the tether and the ambient plasma. Consequently, we will ignore the limitations in the tether current level that may occur due to ionospheric plasma density variations between the day and night sides of the Earth.

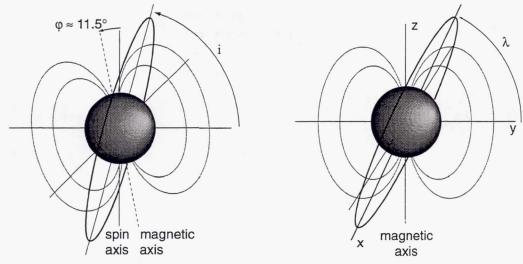


Figure 2. Tilted-dipole approximation to the geomagnetic field.

Figure 3. Spacecraft orbit in the reference frame aligned with the magnetic axis.

Geomagnetic Field Model:

To first order, the Earth's magnetic field can be approximated by a magnetic dipole with the magnetic axis of the dipole tilted off from the spin axis by approximately $\phi{=}11.5^{\circ},$ as illustrated in Figure 2. For this analysis, we will ignore the 436 km offset of the dipole center from the Earth's center. At any given point, the magnetic field can be expressed as consisting of two components, a vertically-oriented component:

$$B_V = \frac{B_E R_E^3}{r^3} \sin \Lambda \tag{3}$$

and a North-South oriented horizontal component:

$$B_H = \frac{B_E R_E^3}{r^3} \cos \Lambda \tag{4}$$

where B_E =31 μ T=0.31 gauss is the strength of the magnetic field on the magnetic equator at the surface of the Earth, R_E =6378 km is the radius of the Earth, r is the radial distance of the point from the center of the Earth, and Λ is the magnetic latitude starting from the magnetic equator.

Reference Frame

In order to make the calculations tractable, we will perform the calculations in a reference frame that is rotated so that it has its z axis aligned with the axis of the Earth's magnetic dipole. The inclination λ of the spacecraft orbit with respect to the geomagnetic frame will vary from $\lambda = i - \phi$ to $\lambda = i + \phi$ once a day as the Earth rotates. For the analysis in this paper we will neglect the slight variation of λ during a single orbit, and average the effects of the rotation over many orbits. For simplicity, we also choose the orientation of the reference frame so that the ascending node of the orbit lies on the x axis.

Expressed in Cartesian coordinates, the geomagnetic field is given by

$$\mathbf{B} = \frac{B_{\rm E} R_{\rm E}^3}{r^3} \begin{bmatrix} 3xz/r^2 \\ 3yz/r^2 \\ 3z^2/r^2 - 1 \end{bmatrix} = \frac{B_{\rm E} R_{\rm E}^3}{r^3} \begin{bmatrix} 3\sin\lambda\sin\theta\cos\theta \\ 3\sin\lambda\cos\lambda\sin^2\theta \\ 3\sin^2\lambda\sin^2\theta - 1 \end{bmatrix},$$
 (5)

In this rotated frame, the circular orbit of the spacecraft can be parameterized in terms of the angle θ around the z axis as

$$\mathbf{r} = \begin{bmatrix} x \\ y \\ z \end{bmatrix} = r \begin{bmatrix} \cos \theta \\ \cos \lambda \sin \theta \\ \sin \lambda \sin \theta \end{bmatrix}, \tag{6}$$

and the velocity as

$$\mathbf{v} = v_o \begin{bmatrix} -\sin\theta \\ \cos\lambda\cos\theta \\ \sin\lambda\cos\theta \end{bmatrix},\tag{7}$$

where the magnitude of the orbital velocity is given by:

$$v_O = \sqrt{\frac{GM_E}{r}},\tag{8}$$

where G=6.67x10 $^{-11}$ m³/kg-s² is Newton's gravitational constant, and M_E=5.976x10 24 kg is the mass of the Earth.

The motion of the tether across the geomagnetic field induces an electric field in the reference frame moving with the tether

$$\mathbf{E} = -\mathbf{v} \times \mathbf{B}.\tag{9}$$

Consequently, in the reference frame of the tether there is a voltage along the tether

$$V = \mathbf{E} \bullet \mathbf{L}.\tag{10}$$

After some trigonometric yoga, Eq. 10 reduces to

$$V = \frac{L B_E R_E^3 v_o}{r^3} \cos \alpha \cos \lambda = L B_T v_o \cos \alpha . \tag{11}$$

where $B_T = B_E R_E^3 v_o \cos \lambda / r^3 = B_H (\Lambda = \lambda)$ is the tangential component of the magnetic field at right angles to both the velocity vector and the tether.[†]

If the Terminator Tether system provides a means for the tether to make electrical contact with the ambient space plasma, such as a hollow cathode plasma contactor, field emission device, or a bare wire anode, this voltage will cause a current to flow through the tether conductor. If the total resistance of the Terminator Tether system, including tether resistance, control circuit resistance, plasma contact resistance, and parasitic resistances, is R , the current in the tether will be

Note that in Eq. 9, the correct velocity vector to use is the relative velocity $v_{\rm M}{=}v_{\rm o}{-}\omega_{\rm E}r\cos\lambda$ between the orbiting spacecraft and the geomagnetic field, since the geomagnetic field rotates with the Earth at the rate of $\omega_{\rm E}{=}2\pi\,{\rm rad/day}$. For an equatorial orbit at an altitude of 1000 km, the velocity of the geomagnetic field is 0.536 km/s or only 7% of the orbital velocity of 7350 m/s. For nonequatorial orbits the difference is even smaller. We will ignore this small difference to keep the equations manageable.

[†] By a geometric coincidence, the transverse magnetic field B_T and therefore voltage V given by Eq. 11 are both essentially constant over the entire orbit, despite the fact that the horizontal magnetic field varies from a maximum at the magnetic equator $B_H(\Lambda=0)$ to a smaller value of $B_H(\Lambda=\lambda)$ at the northernmost portion of an orbit with geomagnetic inclination λ . The variation in horizontal magnetic field strength $B_H(\Lambda)$ with latitude Λ on the Earth and the variation in the angle at which the velocity vector crosses B_N , combine to produce a constant transverse magnetic field $B_T = B_H(\Lambda=\lambda)$ over the entire orbit.

$$\mathbf{I} = \frac{V}{R}\hat{\mathbf{L}}.$$
 (12)

If, as will be the case most of the time, the electron current is leaving the space plasma and entering the tether along an appreciable length of the tether near the end, then Eq. 12 needs to be replaced with an integral of the current along the length of the tether.

The reaction of this current with the geomagnetic field will induce a Lorentz force on the tether. Integrating this force along the length of the tether, the net electrodynamic force F_{E} on the tether system is

$$\mathbf{F}_E = L(\mathbf{I} \times \mathbf{B}) = \frac{V}{R} (\mathbf{L} \times \mathbf{B}) = \frac{-L^2 B_E^2 R_E^6 v_o \cos \alpha \cos^2 \lambda}{R r^6} = \frac{-L^2 B_T^2 v_o \cos \alpha}{R}.$$
 (13)

The drag force F_D on the tether is the component of the electrodynamic force F_E that is parallel to the velocity vector \mathbf{v} ,

$$F_D = \mathbf{F}_E \bullet \hat{\mathbf{v}} = F_E \cos \alpha = \frac{-L^2 B_E^2 R_E^6 v_o \cos^2 \alpha \cos^2 \lambda}{R r^6} = \frac{-L^2 B_T^2 v_o \cos^2 \alpha}{R}.$$
 (14)

Using Lagrange's planetary equations and the assumption that the orbit is nearly circular, the time rate of change of the orbital semi-major axis *a* can be found to be

$$\frac{\partial a}{\partial t} = \frac{-2L^2 B_E^2 R_E^6 \cos^2 \alpha \left\langle \cos^2 \lambda \right\rangle}{M_S R} \left(\frac{1}{a^5}\right),\tag{15}$$

where M_S is the total mass of the spacecraft (including the tether system), and $\langle \cos^2 \lambda \rangle$ is the average of $\cos^2 \lambda$ as λ varies over one day due to the rotation of the Earth:

$$\left\langle \cos^2 \lambda \right\rangle = \frac{1}{16} \left(6 + 2\cos 2i + 3\cos \left[2(i - \varphi) \right] + 2\cos 2\phi + 3\cos \left[2(i + \varphi) \right] \right). \tag{16}$$

Taking the reciprocal of Eq. 15 and integrating from the initial to the final orbit radius, we obtain an estimate of the total time required for a Terminator Tether to deorbit a spacecraft:

$$\Delta t = \frac{M_S R}{12L^2 B_E^2 R_E^6 \cos^2 \alpha \left\langle \cos^2 \lambda \right\rangle} a^6 \Big|_{a \ initial}^{a \ final}. \tag{17}$$

It should be noted that if current can flow in only one direction in the system, then the calculation of $\langle\cos^2\lambda\rangle$ must be handled differently for orbits with inclinations greater than 78.5°. This is due to the fact that for such high inclination orbits, the spin of the Earth will rotate the magnetic dipole so that the spacecraft's orbit will actually move in the retrograde direction relative to the magnetic field during a portion of the day. Consequently, the voltage will reverse direction for a part of the day.

Deorbit Times For Constellation Satellites

To illuminate the utility of using the Terminator Tether system to remove dead and obsolete satellites from useful orbital slots, we have used the equations developed above to estimated the time required for a tether massing only 2.5% of the total satellite mass to deorbit satellites from typical Big- and Little-LEO constellation orbits. In these calculations, we have assumed that the control and parasitic resistances of in the system equal half of the tether resistance. Table 1 compares the predicted time required for a Terminator Tether to deorbit a

Table 1. Deorbit times for example constellation satellites using a Terminator Tether system with an aluminum tether massing 2.5% of the spacecraft mass.

Constellation	Altitude (km)	Inclination (degrees)	Deorbit Time, no TT (Derelict)	Initial Orbit Decay Rate (km/day)	Deorbit Time, with Terminator Tether
Orbcomm 1	775	45	100 years	44	11 days
Orbcomm 2	775	70	100 years	11.6	41 days
LEO One USA	950	50	600 years	32	18 days
GlobalStar	1390	52	9,000 years	22.3	37 days
Skybridge	1475	55	11,000 years	18.5	46 days
FaiSat	1000	66	800 years	13.5	45 days
Iridium	780	86.4	100 years	2.1	7.5 months
Teledesic	1350	89.5	7000 years	1.2	23 months

satellite from the orbits used by several existing or planned constellation systems to the time required for the satellite to deorbit under the influence of atmospheric drag alone. The times for atmospheric decay are rough estimates based upon the assumption of a $10\,\mathrm{m}^2$ satellite cross-sectional area, a drag coefficient of 2.0, and use of the 1977 Jaccia static atmosphere model¹⁴ for the mean exospheric temperatures (see Section III.A). As Table 1 shows, a Terminator Tether massing only a very small percentage of the total system mass can deorbit a satellite within a few weeks to a few months, many orders of magnitude faster than the satellite would deorbit due to atmospheric drag alone.

It should be noted here that true measure of the effectiveness of a deorbit method is not just whether it reduces the orbital lifetime compared to atmospheric drag decay, but whether it reduces the product of the orbital lifetime times the collision cross-sectional area of the spacecraft. This Area-Time-Product provides a measure of the risk of the defunct spacecraft colliding with another spacecraft during its orbital lifetime. In Section III, we will show that the Terminator Tether can significantly reduce the Area-Time-Product for most LEO orbits.

Inclination Change

While Table 1 shows that a Terminator Tether system can rapidly deorbit a spacecraft from orbits with inclinations below about 75°, the rate of altitude drop for a near-polar orbit is low. Because electrodynamic tether propulsion can be used to change the inclination of an orbit, ¹⁵ we explored the possibility of decreasing the deorbit time for a polar satellite by modulating the tether current to reduce the orbit inclination, thus bringing the satellite into an orbit with a more favorable interaction between the velocity and magnetic field vectors. For a nearly polar orbit, however, the rate of inclination change achievable by a passive tether system turns out to be very small. The rate of inclination change is given by the rate of orbit precession caused by the net electrodynamic torque T_T on the orbit in the transverse direction perpendicular to both the line of nodes (the x axis, in this case) and the orbit axis:

$$\frac{\partial i}{\partial t} = \frac{T_T}{\Omega},\tag{18}$$

where $\Omega = \mathbf{r} \times \mathbf{p} = M_S(\mathbf{r} \times \mathbf{v})$ is the angular momentum of the satellite in its orbit. This torque results primarily from the out-of-plane forces on the tether when the satellite is near

^{*} The results for orbits with *i*>78.5 assume that the tether system can carry current in both directions; if the tether system is designed to carry current in one direction only, the deorbit times will be roughly twice as long, due to portions of the day when the orbit is retrograde to the magnetic dipole.

the equator; because the velocity vector for polar orbits is nearly parallel to the magnetic vector when the satellite is at the equator, this force is rather small. Averaging the torque on the orbit due to the electrodynamic force given by Eq. 13 over one orbit, we obtain

$$\frac{\partial i}{\partial t} = \frac{L^2 B_E^2 R_E^6 \cos^2 \alpha \left\langle \sin 2\lambda \right\rangle}{4M_S R} \left(\frac{1}{r^6}\right). \tag{19}$$

If we choose an orbit such as the one used by the Iridium constellation (780 km altitude, 86.4° inclination), the maximum inclination change that a tether massing 2.5% of the spacecraft mass could cause would be only about 0.35° per year. Consequently, modulating the tether current to maximize the inclination change rate will not result in a significant improvement in the overall deorbit rate.

II.B. MAXIMIZING ELECTRODYNAMIC DRAG

Because the electrodynamic forces are perpendicular to the tether, the tether will tend to trail behind the spacecraft. In fact, it is necessary for the tether to hang at an angle behind vertical for the electrodynamic forces to decelerate the spacecraft. The hang angle of the tether will depend upon the balance between the electrodynamic drag force, which tends to pull the tether back, and the gradient force, which tends to restore the tether to a vertical orientation. Because the gradient force decreases as the tether libration increases, if the electrodynamic drag is too large, this balance can become unstable, resulting in loss of control of the tether system. In this section, we analyze the drag torque to gradient torque balance and develop a means of not only optimizing the electrodynamic drag but also stabilizing the tether libration.

Force and Torque Balance Analysis

We will now calculate the forces and torques on the tether and, using the fact that the electrodynamic and gradient torques on the tether must balance each other out to achieve a stable tether orientation angle, calculate some optimum values for some of the Terminator Tether parameters.

Electrodynamic Force and Torque

As discussed in previous sections, both theory and experiment show that: provided the conducting tether is moved rapidly through the Earth's magnetic field in order to generate a voltage across it, and provided good contact is made with the space plasma, we will have a conducting tether that has a current flowing through it. When a wire (moving or not) carrying a current I is embedded in a magnetic field B, there will be an electrodynamic force F_E generated on each element of the wire. The electrodynamic force will be at right angles to both the magnetic field vector and the length vector of the wire, with a magnitude given by Eq. 13:

$$F_E = -\frac{B_T^2 L^2 v_o \cos \alpha}{R}.$$
 (20)

The electrodynamic force is always at right angles to the conductor, and stays at right angles to the conductor as the angle a varies, as shown in Figure 4. Assuming that the electrodynamic drag force is applied uniformly along the length of the tether, we can make the simplifying assumption that the integrated force is effectively applied at right angles to the center of mass of the tether at the point L/2 as shown in Figure 4. The electrodynamic torque on the tether is:

$$T_E = F_E \frac{L}{2} = \frac{B_T^2 L^3 v_o \cos \alpha}{2R}.$$
 (21)

Gradient Forces and Torques

When a tether and its ballast end mass are deployed from a host spacecraft, the gravity gradient force field of the Earth, combined with the orbital centrifugal gradient force field will cause the tether to deploy either up or down from the host spacecraft. The direction desired depends on which end of the tether is connected to the electron emitter. Normally, the electron emitter will be on the end attached to the host spacecraft, in which case the desired direction of deployment will be upward so that the induced voltage in the tether will produce an excess of electrons at the electron emitter end of the tether. The desired upward direction is chosen by having the deployer eject the ballast mass in the upward direction. Once the ballast mass has been started in that direction, the centrifugal force due to the orbital motion of the ballast mass will cause the ballast mass to continue to accelerate in the upward direction until it is brought to a halt by the full deployment of the tether.

If there were no electrodynamic or atmospheric drag, the equilibrium direction of the tether would be exactly along the vertical, since the combined gradient field is a maximum in that direction. Because we expect a significant amount of electromagnetic drag, the actual angle of the tether with respect to the local vertical will be at some angle α , lagging behind the spacecraft motion in the plane of the orbit, as shown in Figure 4. In the following analysis, we will find there is an optimum angle for α that produces the largest electrodynamic drag force on the host spacecraft, hastening its deorbit time.

The combined vertical gravity gradient and centrifugal gradient field 3Γ acting on the ballast mass m_B at the end of the tether of length L will produce a gradient force F_{GB} given by:

$$F_{GB} = 3 \Gamma m_B L \cos \alpha, \tag{22}$$

where the gradient field strength $\Gamma = \omega_o^2 = v_o^2/r^2 = GM_E/r^3$. The strength of the force depends not only on the ballast mass m_B and the strength of the gradient field 3Γ , but also the radial component of the distance of the ballast mass from the center of mass of the spacecraft, which is $L\cos(\alpha)$. As shown in Fig. 4, this force acts in the vertical direction along the radius vector leading from the ballast mass away from the center of the Earth. The component of this gradient force that is at right angles to the tether, given by $F_{GB} \sin \alpha$, will produce a torque T_{GB} on the tether that tends to restore the tether toward the vertical, lessening the angle α .

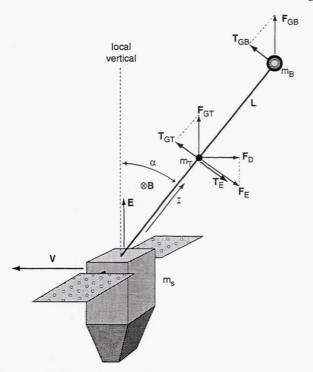


Figure 4. Gradient and electrodynamic forces and torques on the tethered system.

$$T_{GR} = L F_{GR} \sin \alpha = 3 \Gamma m_R L^2 \sin \alpha \cos \alpha$$
 (23)

The tether mass m_T also contributes to the gradient force and torque. If we assume that the tether has a uniform cross section, then we can replace the distributed mass of the tether with an equivalent point mass m_T placed at the center of mass of the tether, which is the point L/2 along the tether, and a distance $L/2\cos\alpha$ in the radial direction. The gradient force due to the tether mass is then:

$$F_{GT} = \frac{3}{2} \Gamma m_T L \cos \alpha \tag{24}$$

While the gradient torque is:

$$T_{GT} = \frac{L}{2} F_{GT} \sin \alpha = \frac{3}{4} \Gamma m_T L^2 \cos \alpha \sin \alpha$$
 (25)

The total gradient torque attempting to restore the tether to its vertical orientation is then:

$$T_G = T_{GB} + T_{GT} = 3 \Gamma \left(m_B + \frac{m_T}{4} \right) L^2 \cos \alpha \sin \alpha$$
 (26)

It is important to notice the variation of the total gradient torque as the tether angle α is varied. Since the gradient force is always in the radial or vertical direction, there is no torque on the tether when the tether is vertical, as would be the case when there are no aerodynamic or electrodynamic drag forces. Once the drag forces become important and start to apply torque to the tether, increasing the tether angle α , those drag torques causing an increase in tether angle α will be opposed by a rising gradient torque which will attempt to decrease the tether angle. The gradient torque reaches its maximum at α =45°, where $\sin\alpha$ =cos α =0.707 and $\sin\alpha$ cos α =0.50. When this angle is reached, we are at a point of catastrophic instability, for if there is a further increase in the electrodynamic drag force due to an increase in magnetic field strength or plasma density, causing a increase in current flow through the tether and causing the angle α to become greater than 45°, the gradient torque, instead of growing stronger to counteract the increased drag torque, will become weaker. The tether will become unstable and the angle α will go rapidly to 90°, where the drag force will also drop to near zero.

To restore control to the tether angle if the instability occurs, it will be necessary to turn off the electrodynamic drag forces by shutting off the current flow through the tether. The α =90° position for the tether and ballast mass is a gravitationally unstable orientation. After a time, slight fluctuations in the gravity field will allow the gradient force to slowly take over and restore the tether to the vertical orientation, which, unless it can be controlled in some way, is equally likely to be up or down. It would therefore be desirable to maintain control of the tether angle so as to avoid the tether angle getting into the region of instability. To avoid this possibility of tether instability, the ProSEDS mission planners are planning on using a large ballast mass and a long non-conducting tether in order to keep the gradient forces high. To keep the electrodynamic forces from getting too large, they are also planning on limiting the current flow through the tether to less than 0.5 A average.

Torque Balance on a Stable Tether

The angle α of a stable tether is determined by the balance between the electrodynamic torque T_E attempting to increase the angle α and the gradient torque T_G attempting to decrease the angle α . Balance is achieved when the two torques are equal:

$$T_E = T_G = T_{GB} + T_{GT} \tag{27}$$

or, using Eq. 21 and Eq. 26:

$$T_E = \frac{B_T^2 L^3 v_o}{2 R} \cos \alpha = 3 \Gamma \left(m_B + \frac{m_T}{4} \right) L^2 \sin \alpha \cos \alpha = T_G$$
 (28)

Simplifying Eq. 28, we obtain a relationship between the electrodynamic and gradient parameters of the tether that must hold if the tether is to be in a stable equilibrium state.

$$\frac{B_T^2 L v_o}{R} = 6 \Gamma \left(m_B + \frac{m_T}{4} \right) \sin \alpha \tag{29}$$

At first glance, it might seem that the optimum angle for the tether would be 45°, since a that angle the gradient torque is largest and therefore can counteract a larger electrodynamic drag force, despite the fact that at 45° the tether is at the onset of instability. The optimum angle, however, is that which maximizes the horizontal or drag component of the electrodynamic force that opposes the host spacecraft motion, not the <u>total</u> electrodynamic force. This horizontal drag force is given by Eq. 14:

$$F_{D} = F_{E} \cos \alpha = -\frac{B_{T}^{2} L^{2} v_{o}}{R} \cos^{2} \alpha = -\frac{B_{T}^{2} L^{2} v_{o}}{R_{C} + rdL^{2} / m_{T}} \cos^{2} \alpha$$
 (30)

This equation gives a maximum drag force for long tether length L, small tether resistance R and small tether angle α . But to maintain α near zero when there is a large drag force on the tether requires a large ballast mass or a very long tether. If a large ballast mass were available, such as might be obtained by cutting off a large portion of the host vehicle (a solar panel, for example), then this is a mode of operation which can allow the maximum electrodynamic force F_E that is available to produce the maximum drag force F_D . If, however, the amount of drag force that can be applied to the tether is limited by tether instability, as it is in the NASA/MSFC ProSEDS mission and the various Terminator Tether applications, then instead of looking at the electrodynamic limits to maximizing the drag force F_D , we want to look at the gradient limits to maximizing the drag force. To do this, we use Eq. 29 in Eq. 30 to obtain:

$$F_D = -6 \Gamma L \left(m_B + \frac{m_T}{4} \right) \sin \alpha \cos^2 \alpha \tag{31}$$

This equation says that for maximum drag force on the host spacecraft, you want long tether length L, as well as massive ballast mass $m_{\rm B}$ and tether mass $m_{\rm T}$. The equation also states that a small tether angle α (tether near vertical) is not optimum. If a very large ballast mass is available then it is possible to operate with α at a small angle and get the maximum drag force available from the maximum electrodynamic force made possible by the available environmental parameters. More realistically, for any given ballast mass, it is better to operate the tether at the angle α that maximizes the drag force. We can determine that optimum angle by setting the partial derivative $\partial F_D/\partial \alpha=0$ and solving the resulting equation. When we do this, we find that the optimum angle for the tether that gives the maximum electrodynamic drag force F_D , while still keeping the tether torques balanced and under control, is $\alpha=\arctan(0.707)=35.26^\circ$. This angle is well below the angle of 45° where tether instability sets in. With this angle selected, we obtain an equation for the maximum stable drag force of:

$$F_D(\max, \alpha = 35.26^\circ) = -6\sin\alpha\cos^2\alpha\Gamma L\left(m_B + \frac{m_T}{4}\right) = -2.31\Gamma L\left(m_B + \frac{m_T}{4}\right)$$
(32)

The tether angle in a Terminator Tether will be controlled by controlling the current through the tether to compensate for variations in magnetic field strength and direction, plasma density (which affects the plasma resistance), and other factors, and thereby maintain the tether at an intermediate angle where both the electrodynamic and gradient forces are at an appreciable level and balance each other. This can be done in a number of ways, either by varying a control resistor or inserting stepped values of ballast resistors in series with the resistance of the tether, or by periodically interrupting the current through the tether to keep the average current at the desired value.

There are many ways to generate the sensing information needed to provide the feedback signals to the tether current controller, but the simplest is to merely measure the drag acceleration on the host spacecraft with a set of accelerometers, and maximize the deceleration force in the direction opposite to the host spacecraft motion. Another method would be to measure the current in the tether, and knowing the tether resistance and the amount of control resistance, calculate the power being extracted and maximize that value. Alternate methods would be to use GPS receivers at both ends of the tether to measure the angle of the tether or an optical position sensor to measure the position of the ballast mass with respect to the host spacecraft. These methods of controlling the drag force or the tether angle should also stabilize the tether oscillations that presently concern the ProSEDS mission planners.

Electrodynamic Drag Force and Power Levels

We will now estimate the magnitude of the electrodynamic drag force and power attainable from a Terminator Tether. If we assume the Terminator Tether is in orbit at an altitude of 1000 km, where the gradient field Γ =0.99x10⁻⁶/s², and the electrodynamic tether has a length of L=5 km, a mass of m_T =10 kg, a ballast mass of m_B =10 kg, and a tether tilt angle α =35.26°. then the gradient-force-limited maximum allowable stable drag force using Eq. 32 is F_D =0.143 N. This is to be compared with the electrodynamic drag force obtainable from the aluminum tether moving at velocity v_M =6814 m/s with respect to the transverse magnetic field B_T =20 μ T. If we assume the control resistor R_C =0 Ω , then the maximum available electrodynamic drag force using Eq. 30 is 0.246 N, which is more than the stable drag force of 143 N. The control resistance must be increased to lower the current flow through the tether and bring the electrodynamic torque down to a level where it will balance the gradient torque and leave the tether at the optimum angle to produce the stable drag force level of 0.143 N.

This maximum stable drag force F_D =0.143 N opposing the motion of the host spacecraft, assumed to be in an equatorial orbit with λ =0 and a velocity with respect to the magnetic field of v_M = v_o - ω_E r cos λ =(7350-536) m/s=6814 m/s, is equivalent to a deceleration power of:

$$P = F_D v_M = 975 \text{ W}$$
 (33)

Since, as pointed out in Eq. 1, the power generation capability of an electrodynamic tether is proportional primarily to its mass, the Terminator Tether will be designed to have a high conductivity tether with enough mass to exceed the design power levels needed for any particular initial orbit and host vehicle. The current through the tether would then be controlled at the gradient-limited maximum stable power level so as to maintain the tether at the optimum angle to give maximum stable drag. For example, the power level P that could be generated and dissipated in an electrodynamic tether can be obtained either by using Eq. 11 for the voltage induced across the tether and dividing the square of the tether voltage V by the tether resistance R, or by using Eq. 14 or 30 for the electrodynamic drag force and multiplying it by the spacecraft velocity V_M with respect to the geomagnetic frame:

$$P = \frac{V^2}{R} = \frac{(B_T L v_M \cos \alpha)^2}{R_c + r d L^2 / m_T} = F_D v_M$$
 (34)

Where R_C is the control resistor, and $R_T=rdL^2/m_T$ is the tether resistance. An aluminum tether of length L=5 km and mass of $m_T=10$ kg has a tether resistance $R_T=185~\Omega$. A spacecraft in orbit at 1000 km altitude over the magnetic equator will have a velocity with respect to the magnetic field of $v_M=6814~\text{m/s}$, and will see a transverse magnetic field of $B_T=20~\mu\text{T}$. Using Eq. 34, we calculate that the above aluminum tether trailing at the optimum drag tether angle of $\alpha=35.26^\circ$ has the ability to generate up to 1670 W of power if the control resistor is set to zero. A control resistor of $R_C=132~\Omega$ will bring the power level down to the desired 975 W. Variations in the control resistor would then be used to keep the tether stabilized at an angle of $\alpha=35.26^\circ$, despite variations in magnetic field strength and plasma density. Since B_T varies as $\cos\lambda$, a 10 kg tether will suffice for orbit inclinations up to $\lambda=40^\circ$. For orbits with higher inclinations and therefore lower horizontal magnetic fields, a tether with a larger mass would be called for. Since the tether mass also determines the maximum gradient-limited drag force, the more massive tether would allow for a higher allowable stable drag force.

III. EFFECTIVENESS OF THE TERMINATOR TETHER FOR DEORBITING SPACECRAFT

III.A. COMPARISON WITH ATMOSPHERIC DRAG DECAY

The most straightforward method of removing a spacecraft from orbit is to simply allow atmospheric drag to decay the orbit. For orbits above about 500 km, however, orbital lifetimes can be tens to thousands of years. The NASA Safety Standard discussed in Section II.A. states that if a drag-enhancement method is used to speed the deorbit of a spacecraft, it must also significantly reduce the total Area-Time-Product of the system. The use of a several-kilometer long tether will increase the cross-sectional area of the spacecraft system. Nonetheless, the effectiveness of electrodynamic drag is so many orders of magnitude greater than atmospheric drag for most LEO orbits that the total Area-Time-Product can be greatly reduced.

For a spacecraft decaying due to atmospheric drag alone in a near-circular spiral trajectory, the Area-Time-Product is given by

$$A_{S} \int dt = -\frac{M_{S}}{C_{D}} \int_{r_{inital}}^{r_{final}} \frac{dr}{\rho(r,t)\sqrt{\mu_{e}r}},$$
(35)

where A_S is the cross sectional area of the spacecraft, r is the average semimajor axis of the orbit, C_D is the coefficient of drag, and $\rho(r,t)$ is the atmospheric density as a function of the semimajor axis and of time (to account for solar variations).

Figure 5 compares the Area-Time-Products for spacecraft with Terminator Tether systems to the Area-Time-Products for spacecraft deorbiting due to atmospheric drag alone. For these calculations we have assumed that the spacecraft mass 1000 kg, are in near-circular equatorial orbits, and have a coefficient of drag of C_D =2.0. In addition, we have used the 1977 Jaccia static atmosphere model for the exospheric temperatures. The figure shows that the use of electrodynamic tether drag can reduce the deorbit Area-Time-Product by several orders of magnitude. As a result, the Terminator Tether system can greatly reduce the risks of a decaying spacecraft colliding with another spacecraft.

As pointed out before, a well-designed Terminator Tether can lower the collision probability even further than the blind chance probability implied by the use of the Area-Time-Product criteria, by using ground control of the rate of descent to avoid collision with the larger objects in space with well-known and predictable orbits.

Note that Figure 5 is conservative in two ways. First, the assumed cross-sectional area of the tether is much larger than its neutral drag cross section (the area presented to the "wind") and, second, the power generated in the tether is assumed to be constant at values that are considerably less than those to be expected in the range of altitudes shown in Figure 5. For example, a 5 km, 10 kg tether whose resistance is 185 ohms, would generate over 4000 watts a t 622 km altitude if it had perfect contact with the plasma and if it were orbiting in the magnetic equator. In these examples, we have assumed that the same tether will generate only 1570 watts throughout its descent from 622 to 250 km altitude, although, in the ideal case, the power would increase with decreasing altitude. These assumptions are based on the power levels observed in the TSS-1R electrodynamic tether experiment. These lower power levels are thought to have resulted from incomplete contact with the plasma. As the technology matures, the higher theoretical values may be possible. The induced power values used in the calculations presented in Figure 5 are the lower values, which we can be confident of, rather than the higher theoretical values.

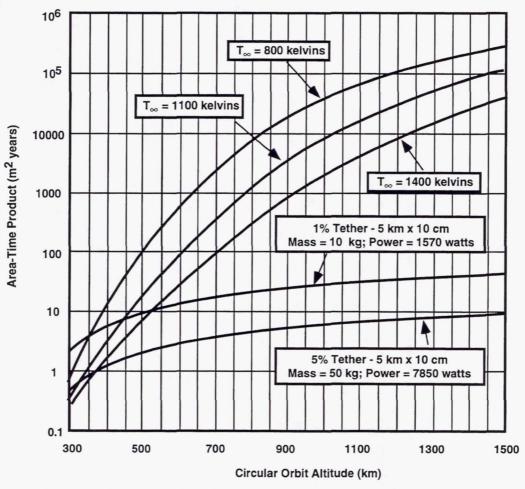


Figure 5. Area-Time-Product vs. Initial Altitude for a 1000 kg Spacecraft. Upper curves show results for atmospheric drag alone at mean and extremes of exospheric temperature. Lower two curves show results for Terminator Tether systems.

III.B. COMPARISON WITH SOLID ROCKET MOTORS

The other conventional method of removing a spacecraft from a LEO orbit is to build into the spacecraft system a rocket mechanism capable of deorbiting the spacecraft. This method, however, requires that a significant fraction of the spacecraft's launch mass be dedicated to the propellant needed for deorbit.

If a spacecraft manufacturer were to use a rocket deorbit system, the design requirements for the system will be more stringent than those for ordinary spacecraft; the system must operate after many years on-orbit and when some or all other components of the spacecraft have failed. Moreover, a rocket deorbit system must be capable of proper operation under many kinds of anomalous situations, such as spacecraft tumbling due to attitude control failure, offset of center of mass, or lack of orbital position knowledge.

Figure 6 shows the percent additional solid-rocket propellant mass required to drop a spacecraft from a circular orbit at the specified altitude to a new orbit with a perigee of 200 km. At this altitude, atmospheric drag will remove a typical spacecraft from orbit in a few revolutions. The contours of constant stage propellant mass fraction range from low values of 0.5 up to the values associated with the best solid motors (\approx 0.93) that can be built without adding

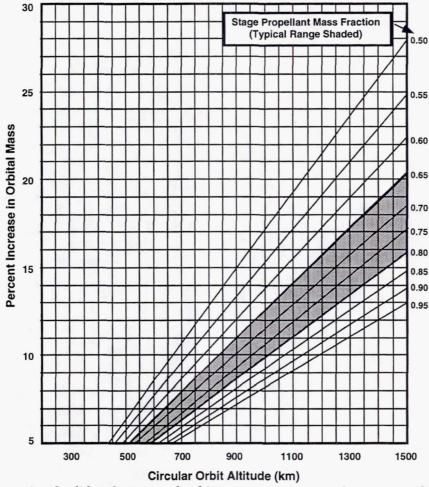


Figure 6. Conventional solid rocket motor deorbit system percent mass increase vs. altitude and stage propellant mass fraction (I_{sp} =288 sec).

any extra hardware to the deorbit stage. An effective, independent stage to provide a retro ΔV of 50-325 m/s will almost certainly have a mass fraction on the order of 0.6 to 0.75. If the deorbit stage is required to perform its own attitude determination, the stage propellant mass fraction may be as low as 0.5.

The figure shows that a solid-rocket deorbit system will require a mass allocation that is a significant fraction of the spacecraft's launch mass. For a spacecraft in a 1000 km orbit, a deorbit rocket system with a reasonable propellant mass fraction of 0.7 will consume nearly 13% of the vehicle's launch mass. A Terminator Tether system, however, can achieve deorbit of the spacecraft while requiring as little as 2 to 5% of the launch mass. The mass savings achieved with the Terminator Tether system can be used for additional revenue-producing transponders, or for more station-keeping fuel to provide longer operational lifetimes.

IV.IMPLEMENTATION

IV.A. The Terminator TetherTM

The basic optimum structure for the electrodynamic tether in a Terminator Tether system would be one of the many types of Hoytethers.¹³ A multiline (2-10 primary line) Hoytape will provide the largest contact area with the plasma, since both sides of the tape would be able to pass current to the plasma. If the spacing between the primary lines is chosen to be larger than twice the expected average Debye length of the plasma, then the effective maximum current collection area per unit length of the Hoytape is proportional to the width of the Hoytape mesh, not the diameter of the wires in the mesh. Thus, a Hoytape not only provides an assured longer life for the Terminator Tether, but very short lengths may also provide a very large current collection areas.

The deployer for the tether can deploy the Terminator Tether either down or up or both. The deployer could stay attached to the spacecraft as was done in the SEDS missions, and as is planned for the ProSEDS mission, which will use a standard SEDS deployer. However, a better alternative would be to have the deployer ejected from the spacecraft, with one end of the tether still attached to the spacecraft, reeling out tether as it leaves. The empty deployer would then act as a ballast mass at the end of the Terminator Tether, improving its performance.

The standard Terminator Tether would be a completely autonomous package with no connections to the host spacecraft except bolt holes. It would contain the electrodynamic tether and its deployer, communication, command, and control circuitry, a battery sufficient to operate the electronics during the deployment period and during portions of the deorbit cycle where the electrodynamic voltages are weak, a small photovoltaic array to supply a trickle charge to the battery during the long waiting period prior to the deorbit command, a more robust battery charging circuit that pulls power off the current running through the tether, one or more methods, such as plasma contactors or field emission devices, to collect and eject electrons from the ends of the tether, one or more methods to control the current through the tether, and one or more methods, such as an accelerometer package, to determine the maximum electrodynamic drag and/or tether tilt angle.

The Terminator Tether package would normally be powered down except for timing circuits, backed up by temperature sensors on the base plate connection to the host spacecraft--a cold host means a dead host, and accelerometer signals--continued acceleration in free fall means a stuck thruster and a spacecraft out of control. Periodically the Terminator Tether electronics package would wake up, go through a self-check, listen for radio signals from the host spacecraft to determine if the host is still functioning, and make a status report to ground control through its telemetry system. If the Terminator Tether fails to report, or reports a

serious malfunction, then ground control still has the option of using the last portion of the stationkeeping propellant on the host spacecraft to deorbit the spacecraft. When the host spacecraft dies, or becomes obsolete, ground control can activate the deorbit sequence the next time the Terminator Tether checks in. There would be suitable safety features to prevent accidental or malicious activation of the deorbit sequence. The most reliable one would be to have the Terminator Tether check for radio transmissions from the host spacecraft. If the host is still transmitting, no deorbit would be performed.

Once the deorbit sequence was initiated, the tether would be deployed with the current control circuit open. Although a voltage will be generated across the tether, and can be measured between the end of the tether and the Terminator Tether ground, with no current flow there will be no drag. If needed, small amounts of current flow can be used to damp out any oscillations resulting from deployment. Once the tether is stabilized, the current control circuit would slowly allow the current to rise. The drag force, as measured by the accelerometers or other means, will start to increase and the tether will start to lag behind. After a few orbits at low drag, to determine the maximum and minimum voltages experienced, and the ease with which electrons are collected and ejected from the ends of the tether, the current flow would be allowed to increase until the maximum deceleration level is reached. The current flow would then be varied as needed to maintain that maximum deceleration level while at the same time using phase-shifted rate feedback to cancel out any induced tether oscillations from the orbit going through regions of high and low plasma density on the dark and light hemispheres, or though regions of low or high magnetic field. As the host spacecraft starts its decent from the constellation, it will likely be necessary to have ground control vary the rate of descent to avoid fratricide with other spacecraft in the constellation. Of course, since ground control has control over the rest of the spacecraft in the constellation, their stationkeeping propellant systems could also be used to avoid the host spacecraft and its tether during the early phases of the deorbit process. After the host spacecraft is clear of the constellation, the deorbit process can proceed with little input from the ground, except for those orbital altitudes known to contain large spacecraft, when again ground control of the rate of descent should be sufficient to avoid collision.

It is not known at this time if the control of the rate of descent is sufficient to insure that the host deorbits into one of the ocean basins. Since the strength of the magnetic field is stronger at lower altitude, there will be more electrodynamic drag force available. Whether that stronger control of the electrodynamic portion of the drag can compensate for the unpredictable portion of the variations in the atmospheric drag at low altitudes is unknown at this time.

IV.B. The "Remora Remover"TM

The Terminator Tether concept, combined with anti-satellite technologies, can also provide a method of safely removing from orbit existing large objects such as derelict, rogue, or hostile spacecraft. This "Remora Remover" spacecraft would consist of a Terminator Tether attached to small seeker missile similar to the small "hit-to-kill" missiles developed by the Space Defense Initiative Office, which has evolved into the Clementine vehicle used for space exploration. Since, in this case, the host vehicle for the tether has operational electronics, the amount of specialized electronics needed to control the current in the tether would be minimal. The Remora Remover missile would hunt down a spacecraft that needs to be removed from space, but instead of hitting the spacecraft, the missile would be programmed to rendezvous with the spacecraft and attach itself to the host spacecraft using a hooked net, harpoon, or adhesive "sucker." The Remora Remover missile would then deploy the Terminator Tether, which would bring down both the derelict spacecraft and the missile.

V. CONCLUSIONS

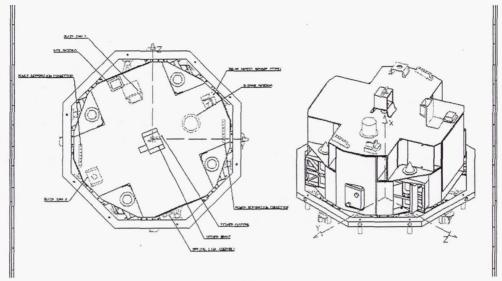
By using electrodynamic drag to greatly increase the orbital decay rate of a spacecraft, a Terminator Tether system can remove unwanted objects from LEO rapidly and safely. Using an analytical approach, we have developed methods for predicting Terminator Tether deorbit times from various orbits. Using these methods, we have shown that tether systems massing just 2 to 5% of the total spacecraft mass can deorbit a typical communication satellite within several weeks or months, depending upon the initial orbit. The low mass requirements of a Terminator Tether system makes it highly advantageous compared to a conventional solid-rocket deorbit stage. Moreover, the drag enhancement provided by the electrodynamic tether technique is so large that the total deorbit Area-Time-Product can be reduced by several orders of magnitude compared to atmospheric drag alone, minimizing the long-lived orbital debris hazard created by a constellation spacecraft after their end-of-life. In addition, we have developed a method of optimizing the electrodynamic drag on the tether system by controlling the tether hang angle. This method also provides a simple method for stabilizing the tether libration.

REFERENCES

- 1. Loftus, J.P., JLoftus@ems.jsc.nasa.gov, personal communication via email Monday 10 June 1996 15:50:10.
- 2. Forward, R.L., "Electrodynamic Drag 'Terminator Tether'", Appendix K, in Final Report on NAS8-40690, 10 July 1996.
- 3. Office of Science and Technology Policy: 1995, Interagency Report on Orbital Debris 1995, The National Science and Technology Council
- 4. NASA Safety Standard: Guidelines and Assessment Procedures for Limiting Orbital Debris. (NSS 1740.14, August 95).
- 5. Space News, March 31-April 6, 1997, p 16.
- 6. Space News, Aug 4-10, 1997, p 30.
- 7. Estes, R., restes@mars.harvard.edu, personal communication via email Friday 31 May 1996 10:39:16.
- 8. Loftus, J.P. JLoftus@ems.jsc.nasa.gov, personal communication via email Wednesday 19 June 1996 08:20:39.
- 9. Lorenzini, E., personal communication, 13 March 1997.
- 10. Johnson, L., "Propulsive Small Expendable Deployer System Mission (ProSEDS)", OAST Advanced Propulsion Workshop, JPL, Pasadena, CA, 20-22 May 1997.
- 11. Gilchrist, B., personal communication, 12 May 1997.
- 12. Sanmartín, J.R., Martínez-Sánchez, M., Ahedo, E., "Bare Wire Anodes for Electrodynamic Tethers," J. Propulsion and Power, 7(3), pp. 353-360, 1993
- 13. Hoyt, R.P., Forward, R.L., "Electrodynamic Hoytethers for ISS and LEO Spacecraft", Appendix E of *High Strength-To-Weight Tapered Hoytether for LEO to GEO Payload Transport*, Final Report on NASA Contract NAS8-40690,10 July 1996.
- 14. Jaccia, L.G., "Thermospheric Temperature, Density, and Composition: New Model," SAO Special Report 375, Mar. 1977.
- 15. Penzo, P.A., and Ammann, P.W., eds., Tethers In Space Handbook, 2nd Edition, NASA/OSF, 1989, p. 168-9.

Page intentionally left blank

The YES satellite: a tethered momentum transfer in the GTO orbit



By
Michiel Kruijff
Delta-Utec
Kamperfoeliestraat 63, 2563 KC Den Haag
Delta-Utec@Delta-Utec.demon.nl

Erik Jan van der Heide Delta-Utec

Abstract

The Young Engineers' Satellite YES is a payload of the Ariane 502 and one of the experiments of the ESA/ESTEC project TEAMSAT. It has been built to perform a tether deployment and tethered momentum transfer in GTO, in order to study the special and unexplored dynamics of a tether in a highly elliptic orbit. To record the dynamics of the system, GPS, cameras, sunsensors and accelerometers are part of the satellite's instrumentation. As a technological demonstration and for clearing of the orbit after the mission, a precise cut would deliver sufficient ΔV to de-orbit a subsatellite called TORI, together with the tether. As a way to mitigate the collision risk for the tether with operational satellites in LEO, a preferred launch time, governed by the effect of solar pressure, has been requested but was not compatible with other requirements that turned up during the launch preparations. Therefore, the ESA Steering Committee has decided that YES will fly, but the tether will be cut as to prohibit deployment, already before the launch.

In this paper the planned mission is described, along with the measures foreseen to minimize orbital lifetime of the tether. A description of the subsystems related to the tether experiment will show that still very interesting science can be performed, that can fulfill the project's secondary objectives. The tether experiment will be operated as a rehearsal for a re-flight on an Ariane 4 in the near future.

I Introduction

Delta-Utec proposed in October 1996 the Young Engineers' Satellite (YES) on the second qualification flight of Ariane 5. Supported by ESTEC, ESA's technical center at Noordwijk, the YES satellite was built and qualified within 8 months.

YES has served an educational purpose by offering to many students and young engineers hands-on experience in an end-to-end project.

The YES satellite contains a 35 km tether and has as its primary objective to investigate tether deployment and dynamics in GTO, for the first time, and demonstrate tethered momentum transfer for future applications, i.e.:

- study of deployment dynamics;
- study of dumb-bell dynamics in an elliptic orbit;
- end mass attitude behavior;
- demonstrate momentum transfer by staging.

Secondary objectives are:

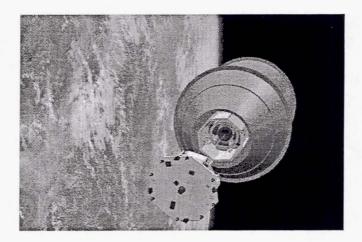
- to demonstrate the use of GPS at high velocity (GTO perigee) and high altitude (GTO apogee);
- to measure ionizing dose in GTO behind thin shielding using the RADFET experiment;
- to measure particle fluxes in GTO with the Scintillating Fibre Detector;
- to demonstrate off-the-shelf and commercial technology for short space missions (PC104).
- to demonstrate the LIGA/Si sensor technology for 3-axis accelerometers in space.

In June 1997, when the satellite was ready for shipment to the launch site in French Guyana, ESA's Steering Committee decided not to allow deployment of the tether, because the imposed launch hour differs too much from the request of the YES group and therefore the tether would pose a risk to operational satellites in LEO. Excluding the tether deployment itself it was decided that the YES satellite would be operated as originally intended to test the hardware and software that was developed.

This paper summarizes the studies performed for the tethered mission. In Chapter II the YES satellite and its subsystems will be introduced. Chapter III will discuss the deployment strategy and the behavior of the tether in an elliptic orbit. In chapter IV the control of the YES dynamics is discussed, focusing on de-tumbling of the YES satellite after an ejection with high tip-off rate. The study on the influence of solar pressure on the orbital lifetime is summarized in chapter V.

To better understand the YES tethered mission first four satellites need to be introduced:

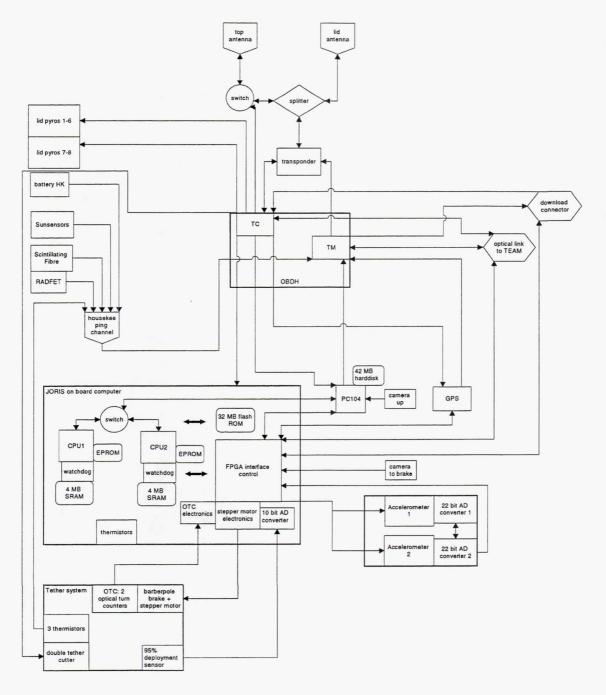
- YES, the Young Engineers' Satellite. This 175 kg satellite is carrying the tether deployer and the main subsystems as described in the next paragraph;
- TORI, Tethered ORbit Insertable. A 12 kg passive tether end-mass;
- TEAM, Technology and Educational payload Added to MaqSath. The TEAM satellite
 contains both the former mentioned satellites and in addition 3 cameras, a star mapper
 and an oxygen measurement unit. Including YES and TORI the weight is 308 kg;
- MagSath. A dummy satellite of ~2100 kg.



Both YES and TORI (red on picture) are stored in the TEAM satellite. For the tether mission, first YES will be ejected followed shortly by TORI.. The TEAM satellite will stay attached to the Magsath satellite.

II YES Subsystems Related to the Tether Experiment

This chapter will summarize the subsystems of the Young Engineers' Satellite that constitute the tether experiment. The satellite is designed for a mission of up to 7 days. Design drivers have been delivery time and cost. YES carries engineering models and flight spares, and re-flies components of earlier ESA missions. Commercially available parts are used for selected functions, with adjustments and testing for sufficient shock, vacuum and outgassing properties. Some instruments involving new technologies were delivered at low or no cost by their developers to have their maiden flight on YES.



Schematics of YES electrical subsystems and interfaces

YES has no customary active attitude control. The Maqsath will spin at 0.5 rpm. Other than that, YES relies on manipulation of the tether tension during deployment.

II.1 The deployer

It was decided to use parts of the SEDS deployer [Car:93] because it could be made available on short term and because earlier studies gave confidence that even with the irregular friction of the barber pole brake, accurate deployment paths can be followed when applying the right feedback [Hei:96].

The canister contains a 35 km double strand tether with the following layout (from TEAM to YES) [Car:97]:

	TEAM/TORI	YES		
	260 m kevlar round 0.7mm 34.8 km 2 stra	her every 180 m	10 m 11x215 Spectra	
	tether design + material	length [m]	break load [N]	Melting point [°C]
•	1 strand 8x400, 0.7 mm Kevlar 2 strands 7x100 Dyneema SK66 1 strand 11x215 Spectra	260 34750/35100* 10	450 275/165** 800	425 150*** 150

the longer strand is slack under normal conditions

The shorter tether will under normal circumstances (<40 N) carry the tension by itself. For elongation larger than 1%, the second strand will contribute in carrying the tension. Under break load (3.6% strain), the shorter tether will carry 60% of the tension, which results in a 275 N break load if both strands are intact and a 165 N final strength is assumed.

The connections at the end and the transitions between the various tether parts have been tested to be at least as strong as the tether itself. The parallel splices in the Dyneema were verified to fail at over half the break load, not harming the individual strands, so as to allow them to take the full tensional load.

The Kevlar is thick and better resistant against the (possible) heat from the aluminum structure of MAQSATH, TEAM or TORI. The Dyneema part consists of a force carrying tether and a slack redundant tether stitched together every 180 m to minimize meteoroid risk (Carroll Caduceus). They are wound tightly in criss-cross shape around a hollow core, in total about 86000 turns, and are tied down by 3 knots located on the outside of the winding, the first of which needs a 30 N tension jerk to break. Upon ejection, the tension peaks will be about 1 second apart and >10 N for roughly 0.01 s.

^{**} value from industry: ~ 240 N per strand. Testing (J. Carroll): 165 N per strand. For a cold tether (minutes after deployment), this value will be at least 20% higher.

^{***} operating temperature recommended below 70 °C

On top of the barber pole brake¹ 2 AirTech [Air:96] tether pyro-cutters designed for parachute industry have been mounted. The control of the barber pole brake as well as the registration of the turn counts with the SEDS optical turn counts (OTC's) have been implemented in the onboard computer Joris!.

II.2 The onboard computer

All experiments are controlled by a newly developed 'rad-smart' powerful on-board computer - Joris! - consisting of:

- 2 highly integrated SH7032 RISC microcontrollers from Hitachi at 32 MHz, with host selector and optional external host;
- 40 MB storage FlashROM & SRAM;
- FPGA & OctoUART + redundant installation from ROM by H/W design;
- latch-up detection & auto reboot;
- regular and programmable automatic warm & cold reboots by H/W & S/W;
- Watchdog circuit;
- redundant S/W loading;
- built-in stepper motor H/W and infra-red sensor electronics (OTC);
- test connector for monitoring and uploading of S/W;
- many data and control interfaces to other subsystems and/or instruments.

The S/W developed for Joris! is written in C and C++ and based on the MicroCOS operating system, featuring DMAC, semaphores and multitasking. It allows for read-out and control of the individual experiments, up to 250 time tagged telecommands, S/W patches uploading, storage of telemetry frames, per application, into circular buffers, historical and real time data, telemetry and telecommand identification and automatic resending of missing telecommands and telemetry packets. The tether task includes nominal profiles that can be updated by telecommand, various feedbacks based on OTC pulses, a warm-up and a test sequence, various motor drive modes and a tension pulse mode.

II.3 TORI, the AUTEC & the absorptive tether

TORI stands for 'Tethered ORbit Insertable'. It is a 30 x 8 cm 10.7 kg Aluminum passive disk that acts as a counter mass to YES and is therefore attached to the other end of

¹ The barber pole is a white pole with a red spiral painted on it. Sticking out of the wall, it serves as a landmark for barber shops all over the world. It is however not commonly known that the barber pole symbolizes the throats of the clients of the London barber Sweeney Todd, after he was finished shaving and killing them by holding tight his knife to their throats while turning the barber chair they were sitting on.

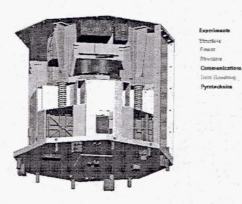
the tether. An excavation on the TEAM facing surface is to store the so-called 'absorptive tether', subject of the next paragraph.

Mounted to TORI is the AUTEC: the AUtonomous Tether Cutter, basically a timer, battery and an AirTech cutter that cuts the tether four days after TORI ejection. This is an addition for extra mission safety reducing the orbital lifetime of the tether in a contingency case.

Upon cutting of two pyro bolts, TORI is ejected shortly after YES with 0.2 m/s from the TEAM structure and out of its box.

After its ejection, TORI is linked to the MAQSATH by a 1.4 m, 0.8 cm diam. so-called absorptive tether [Ock:87]. This tether is a steel cable carrying alternatingly cylindrical and spherical beads. If the cable is tensioned, the beads are pressed together and when bent, a friction force is induced between them, thus absorbing energy. The absorptive tether is used to dampen TORI's ejection velocity so that TORI is stopped just outside the TEAM box. The tether then acts as a rod with some bending stiffness under the low tension applied during the major part of the deployment. When deployment is finished, the absorptive tether is cut by another pyro at the TEAM end and TORI is released. This way a new tethered system is created: TORI-tether-YES.

TEAMSAT Subsystem Classification



II.4 Ejection mechanism

The ejection mechanism consists of 8 pyrobolts and 4 springs. The 8 pyrobolts hold down the YES lid onto the TEAM box. In two sessions the pyros are cut: the first session cuts 6 bolts leaving 2 opposite bolts around the axis of the lid with the highest inertial moment (9 kg.m 2). The stored energy of the springs will give the 175 kg YES satellite a ΔV of 1.7 m/s once the last two pyros are fired and the tether mission starts. The uncertainty in pyro firing time of 1 ms, the CoM offset and the inbalance of the springs can lead to tip-off rates upto 10°/s of the YES satellite. In absence of a high deployment tension stabilizing of YES can be done by special braking as explained in Chapter IV.

II.5 YES GPS

The YES satellite carries a Trimble TANS II GPS receiver LEO configuration. The GPS experiment is threefold [Pol: 97]:

- it will be the first GPS receiver above the GPS satellite constellation. It will be used to collect signals from the side lobs of the GPS satellites when YES is at 20.000 km as well as raw data from the weak signals of the satellites *behind* the Earth when YES is in apogee. Ideally, about 1-4 satellites are expected to be in view in this range of the orbit;
- it will receive at velocities upto ~9.92 km/s in perigee;
- it will give additional data of the tether deployment (length & velocity).

Two antennas are connected to the GPS receiver:

- one is on the outside of the TEAM box and is operational both before and after ejection;
- the other is mounted 'on top of YES', initially inside the TEAM box, and will be used after ejection.

II.6 Solar aspect sensors

There are 7 solar aspect sensors on the TEAM/YES satellites that will be used to determine the direction of the sun vector with an accuracy of 2.5 degrees [Not:97], and therefore will give information about the spacecraft attitude and rotation rates. Using other information like telemetry and GPS S/N ratio and the camera output, it will be possible to determine the attitude history of the satellites.

Each solar aspect sensor consists of two perpendicular slits, each with a photo-sensor, a NPN silicon transistor, and a field of view of about 90 degrees by 3 degrees of width. The timing of the successive pulses yield for the sun vector. To get omni-directional coverage, a rather large number of sensors is installed. Each sensor contains also a small electronic circuit to convert the impedance to a low value and provide RF filtering.

The data of the sensors are on-off time tags on a separate location in the housekeeping channel for each sensor, sampled every 4 s and transmitted in real time.

II.7 Accelerometers

Two newly developed Triad 442T accelerometers [For:97] are installed symmetrically with respect to the YES center of mass and approximately 30 cm away from it.

The accelerometer unit represents 2 LIGA sensors and a single Si sensor. The LIGA sensing element is made of Nickel. It consists of a freely movable seismic mass suspended by springs and deflected by forces of inertia when subjected to accelerations. The same mass acts as the middle electrode of a differential capacitor, which is operated in a force to rebalance mode. The applied electrostatic force can be measured with extremely high precision and equals the force of the inertia to be determined.

Accuracy and resolution are respectively 1 μ g and 1 μ g/ \sqrt{Hz} for the technology as described. The YES will provide the Triads' maiden flight before fine tuning and calibration of the new sensors could be completed. Therefore, for temperature range of -10 to 30 °C, specified for this mission, due to thermal hysteris and thermal drift the guaranteed accuracy is below 0.4 mg. Of course, when temperature turns out to be rather constant, this number would be better.

Order of magnitude of the expected accelerations during the mission are the following:

Ejection: 4 g

First minute of deployment: peaks of 20 mg

Larger part of deployment: 10-60 μg End of deployment: 5 mg

TORI ejection: drop to 0.1 mg

Spinning YES-TORI system: 0.6 mg
Tether cut: drop to 0 g
Spin/tumbling: 25-200 µg

From this it can be seen, that no accurate tether tension level during the larger part of deployment can be determined. However, because of the double measurement, the effect of rotations can be eliminated so it will be possible to focus on the translational accelerations. The frequency of the measured harmonics may tell about the rotational velocity of the space craft.

The main use of the accelerometers is to witness:

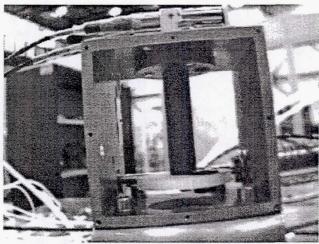
- · ejection,
- breaking of the 3 tie downs,
- · end brake.
- · TORI release,
- tension during the spin phase (YES-TORI),
- · slackness effects and duration.

- · tether jamming,
- and the tether cut.

II.8 Camera

Two QuickCams will be flown to witness the ejections and the deployment of the tether. Both are mounted on the top cover plate of the YES satellite and will therefore be inside the TEAM box until ejection. One, connected to Joris! will be aimed at an open side of the brake assembly. It will witness the way a double strand is wound around and moves along the barber pole and associated with e.g. possible tension spikes. Also the cutters will be in view so the tether cut can be witnessed as well. A second camera is looking straight up, to witness the ejection of YES, but also to see the deploying tether move by as the satellite turns around its axis.

The QuickCam is black and white CCD camera, 320x240 pixels, and has a field of view of 30x 23°.



Picture of barber pole brake and Airtec tether cutters mounted on YES as seen by the YES QuickCam connnected to Joris!

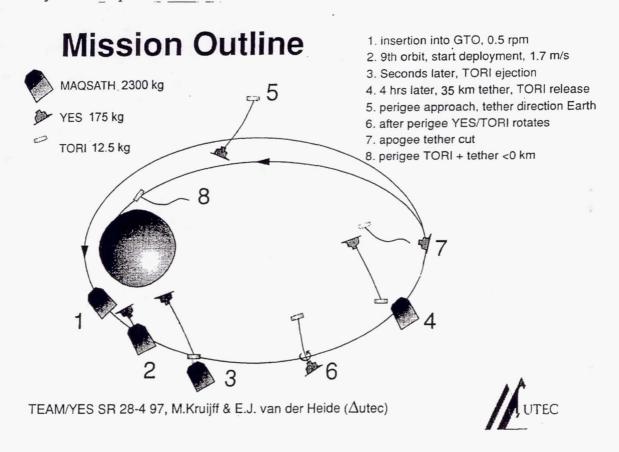
II.9 Commercial computer

A second computer has been added to the satellite. The PC104 will report its health and take images of the deploying tether with one of the QuickCams. The only modification to the PC is coating of the board and gluing of the components to withstand vibration. The processor has a thermally conductive link to the PC's housing. This computer is an experiment itself, but can also be used as a back-up transponder for receiving Joris!' TC.

III YES Deployment Strategy: Tether Behavior in Elliptic Orbits

The vast majority of tether applications consider tethers in circular orbits whereas only a few studies involve the motion of tethers in elliptic orbits [Bel:93, Cre:96, Ock:96]. One aspect of tethers in elliptic orbits is that for eccentricities above 0.45, an initially radially positioned tether will start to rotate. This aspect will be used to obtain the ΔV required for de-orbitation of the TORI satellite.

The tether mission is planned to start at a true anomaly of 90°2 with a backward downward ejection of the YES satellite of 1.7 m/s. Closely after ejection TORI is pushed out of the TEAM box by small springs and will be restrained by the absorptive tether. A deployment of the tether from YES, aided by the gravity gradient forces, will follow at a fairly constant speed of 2.5 m/s.



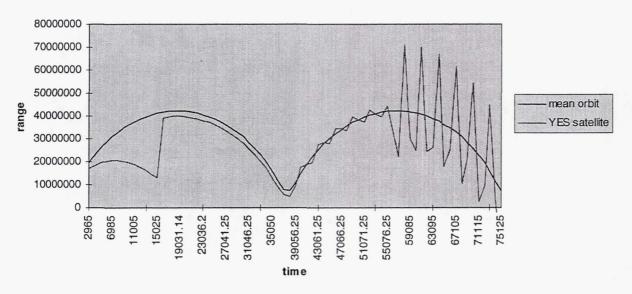
In the first apogee after ejection (15450 s) the deployment will be smoothly stopped by a tension drop caused by the release of TORI (cut of absorptive tether) which minimizes the effect of tether slackness. The new tethered system (YES & TORI) will orbit slightly below that of Maqsath and pick up an in-plane rotation during its pass through perigee (eccentricity of GTO $\sim 0.7 > 0.45$ critical value of 'stability'). The rotations are in the direction of the orbit and take about 50 minutes. Close to the apogee,

² As the gravity gradient in the GTO orbit is very small, technically speaking, a start of deployment before perigee is preferable. However the attitude of MaqSath was imposed on us and dictated a late ejection.

when TORI is swinging backward, the tether will be cut at the YES side. This decision will be based on the most direct data from ranging measurements of the YES satellite.

Ranging

The YES satellite has a coherent transponder. Its ranging capability is foreseen to be used to determine the motion of the YES satellite, from which also the tethered system's center of orbit can be derived. When the tether is deployed, the distance between YES and the center of orbit is ~2 km. As the range accuracy of a transponder is ~20 m the motion of YES with respect to the center of mass can be determined with sufficient accuracy to determine the attitude of the system and thus when to cut the tether.



deployment | YES-TORI approaches perigee | YES-TORI rotates | TORI-tether after cut

Orbit of tethered system's CoM and the motion of YES around it (enhanced for visual effect)

The orbit of the tether system's center of mass can be assumed to coincide, approximately, with the orbit of a point mass. It is possible to reconstitute such an orbit from integration and averaging of the YES motion.

Both anomaly and range of the YES satellite are measured and can be compared with the predicted position of the center of mass to yield the relative position.

This measurement could give us extremely useful information about deployment and dumb-bell dynamics that cannot be required otherwise:

- the accelerometers do not have sufficient resolution to be integrated to yield position;
- GPS cannot be relied upon for decision making as it is an experiment of its own and its results may require non trivial and extensive processing as well;

• sun sensors will only be good to give the direction of the satellite body (not of the tether!) with respect to the sun vector.

For a tether cut using the ranging capability, there are two requirements:

- 1. close to apogee;
- 2. TORI should be at lesser altitude than YES, and less than 45 degrees from the vertical (Earth direction).

This means that the transponder should be a few km higher than the center of mass at tether cut.

On the approach to apogee, the TORI/YES system is expected to rotate in the orbital plane at a rate of 1 rotation per ~ 50 minutes, so the cut has to be performed within one of about three 12 minute windows.

IV Control of YES Dynamics

The Maqsath satellite is inserted into GTO orbit as a spin stabilized platform with 0.5 rpm spin rate. This rate is a compromise between three requirements:

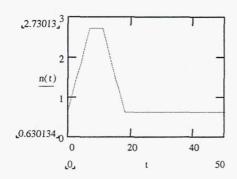
- 1. high spin: no tumbling of Maqsath or YES to be expected;
- 2. low spin: required to turn around YES with the tension in the tether when in the rotational phase;
- 3. low spin: requirement from the TEAM AVS camera experiment.

Tip-off rates of 10° /s can be expected with the design of the YES ejection mechanism. The main contribution to the tumbling is due to the delay between firing of the last two pyros: about 1ms at 1σ .

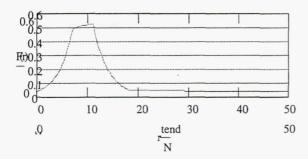
In absence of a reasonable deployment tension in GTO, the deployment would come to a preliminary stop as the tether would wrap around the satellite, in which the deployer is located.

Additional braking profiles were studied to increase the tension and to transform the tumbling into an oscillation.

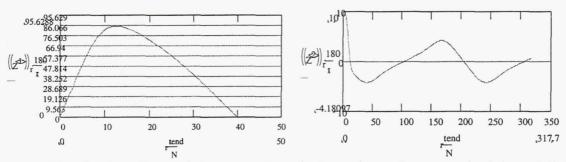
The stepper motor would start turning directly after ejection close to maximum speed, hold for a few seconds and turn back again as shown in the figure below.



The resulting tension in the tether is:



The satellite would react as depicted in the two figures below [respectively the angle and the angular velocity in 2D].

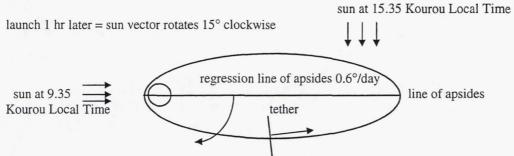


The short, well tuned, but open loop brake pulse reduces any initial tumbling within the expected range to a harmless oscillation of YES. Further optimization is needed but not performed. On-ground tests will be performed early 1998 to show the feasibility of above brake profile as well of the earlier developed Flex End Brake [Kru:97].

V Influences of Solar Pressure

The effect of solar pressure on the nominal tether mission is negligible. The tether would re-enter within a day. However in an off-nominal mission scenario the tether with its 35m² surface could stay in orbit for much longer. In this case, the tether orbital lifetime would be mainly dependent on the effect of solar pressure. The effect is of one

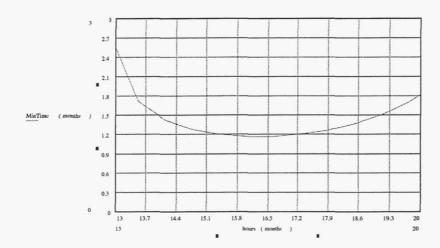
order higher than that of the gravitational effect of the Sun and Moon and the effect of air drag at 600 km.



Angle of line of apsides w.r.t. solar vector at 2 launch hours: 9.35 & 15.35 KLT

The initial angle between the lines of apsides and the solar vector is a function of launch time and is shown in the picture above. Due to the nodal regression (-0.373 $^{\circ}$ /day), the apsidal precession (0.738 $^{\circ}$ /day) and the rotation of the earth around the sun (-0.986 $^{\circ}$ /day), the angle between the line of apsides and solar vector, as depicted above, recedes with -0.621 $^{\circ}$ /day.

The solar pressure is decelerating the tethered system at apogee so that the perigee will drop. The effect is strongest when the solar vector is perpendicular to the line of apsides. Taking into account the regression of the orbit, the integrated effect of solar pressure on the re-entry time of the tether is as shown below.



The graph shows the time needed for the perigee to drop until burn-up against the hour of launch. Launches before 13.00 KLT will not lead to a quick burn-up and life times in the order of (tens of) years can be expected. Launches after 13.00 will leave the tether in orbit for some few months.

The assumptions made for the calculations are:

• reflection coefficient is 0.8, absorption coefficient is 0.2;

- the effective surface is 22.3 m² (rotating tether);
- tether with no endmasses (see AUTEC chapter II.3);
- no air drag above 150 km;
- a critical perigee height of 150 km, below which the air drag will quickly circularize the orbit and re-entry will take place.

The launch window of Ariane 5 was imposed to us in May 1996 being 9-12 AM. This is not compatible with the proposed risk mitigation by solar pressure effects. It was decided unanimously not to deploy the tether for this case.

VI Conclusions

The YES satellite - an *almost* tether mission - was conceived, proposed, designed and built within 8 months time. The 35 km tether would have de-orbited a 12 kg disk, TORI, from the 580 km x 35796 km Ariane 5 GTO orbit, using the characteristic dynamics of highly elliptic orbits. However, the imposed launch time was not compatible with the proposed risk mitigation strategy for contingency cases. The strategy relied upon the effect of solar pressure that can 'blow' down the tethered system's perigee causing reentry within a few months. Although the ESA Steering Committee considered tethers in GTO technically and scientifically interesting it judged the risk of a (partial) tether deployment unacceptable.

The ESA Steering Committee decision makes the primary, tether related objectives of the mission not feasible, however the mission will be a rehearsal for future tethered missions to reach those mission objectives with a higher probability of success. The Steering Committee supports a successor mission 'YES2' to be flown on Ariane 4. Ariane 4 has a much lower perigee (200 km), that ensures a quick re-entry by air drag.

The five secondary mission objectives on the other hand can still be achieved:

- to demonstrate the use of GPS at high velocity (GTO perigee) and high altitude (GTO apogee);
- to measure ionising dose in GTO behind thin shielding using the RADFET experiment;
- to measure particle fluxes in GTO with the Scintillating Fibre Detector;
- to demonstrate off-the-shelf and commercial technology for short space missions (PC104, QuickCam);
- to demonstrate the LIGA/Si sensor technology for 3-axis accelerometers in space.

Despite the short time in which the satellite has been built, some major developments have taken place:

- a highly flexible satellite system design;
- design, simulation and implementation of the first tether experiment in highly elliptic orbit;
- a flexible on-board computer Joris! with integrated SEDS I/F H/W;
- complete on-board and ground segment S/W development;
- an OBDH using asynchronous virtual channel multiplexing, developed at ESTEC.

With an interesting mission still ahead, the main goal of the YES project has already been achieved, namely to provide an opportunity for many students and young engineers to experience an end-to-end and hands-on project.

Acknowledgments

The YES satellite has been a major effort of many young engineers and Delft students supported by ESTEC staff, *Bravo!* to all.

We would like to thank Joe Carroll for his knowledge and enthusiasm with which he supported us in many areas.

The YES satellite has been made possible through funding by the Dutch government and the European Space Agency.

References

Air:96	AirTec GmbH, private communications +49 2953-8010, 1996
Bel:93	Beletski, V.V., Levin, E.M., Dynamics of Space Tether Systems, 1993
Car:93	Carroll, J.A., SEDS Deployer Design and Flight Performance, AIAA 93-
	4764, 19 93
Car:97	Carroll, J.A., private communications, 1997
Cre:96	Crellin, E., Jansens, F., Some properties of the In-Plane motion of a
	dumbbell in elliptic orbit, ESTEC, 19 96
For:97	Forschungszentrum Karlsruhe, private communication, 1997.
Hei:96	Heide, E.J van der, Kruijff, M, StarTrack a swinging tether assisted re-
	entry for the International Space Station, Noordwijk, 1996
Kru:97	Kruijff, M, Heide, E.J. van der, The Flex End Brake, Noordwijk, 1997
Not:97	Noteborn, R.M.H, Small satellites are fun, Delta-Utec, 1997
Ock:87	Ockels, W.J., Absorptive tethers - a first test in space, ESTEC Noordwijk,
	19 87
Ock:96	Ockels, W.J., Biesbroek, R., Verduyn, D., Enhanced Efficiency by using
	the upperstage momentum transferred by tether, IAF-96-A.2.01, China
	19 96
Pol:97	Pol, M. van de, The YES GPS experiment, Delta-Utec, 1997



Delta-Utec 1997

Experiments In Tether Dynamics Planned For ATEx's Flight

 $\mathbf{B} \mathbf{y}$

Michael F. Zedd
Naval Research Laboratory, Code 8233
4555 Overlook Avenue, SW
Washington, DC 20375-5355

ABSTRACT

Following the successful one year operation of the Tether Physics and Survivability (TiPS) satellite, the Naval Research Laboratory (NRL) plans to fly a second tethered satellite system in mid-1998. Advanced Tether Experiment (ATEx) is designed to extend our knowledge of control and survivability of tethered space systems. Experiments in active control will study deployment dynamics via a constant-speed motor and utilization of both in-plane and crossplane thrusters to excite and arrest librations. Additionally, ATEx will investigate the survivability of long-life tether materials. paper will describe the ATEx payload carried by the Technology Experiment (STEX) spacecraft and preview anticipated flight experiments as shown by the results of two tethered system dynamics simulations.

INTRODUCTION

The NRL built the ATEx to ride atop the STEX spacecraft. ATEx was delivered to the STEX contractor as government furnished equipment for integration and test. The launch is planned for February 1998. After approximately ninety days of spacecraft early-orbit checkout and orbit transfer to 425 NM (787.1 km) circular altitude at 85° inclination, the ATEx mission will begin and continue for a maximum experiment duration of ninety days.

ATEx offers a next step in low-cost tether flight experience. Placing the tether's lower end-body atop an active spacecraft permits opportunity to be the first to perform libration control experiments.

To date, no tether mission has demonstrated extended control of system librations. Comfort with the ability to control these motions, along with the remaining objectives, is necessary before continuing to develop more sophisticated tethered space systems. There are three ATEx mission objectives:

- 1. Demonstrate tether system stability and control.
- 2. Demonstrate end-body attitude determination and control.
- 3. Fly a tether designed for survivability.

ATEx consists of five major structural components: an upper end-body (UEB), the tether, a lower end-body (LEB), and the interface deck. A fifth component is the contractor-built STEX spacecraft. When deployed, the UEB is 6.05 km from the LEB. The LEB is attached to the STEX spacecraft for ninety days of active flight experiments. Then it is separated.

This paper presents an overview of the ATEx and STEX The on-board sensor suite provides an indirect configurations. estimate of system libration. Two important considerations of the tether mission are the host spacecraft's attitude control system and the perturbations caused by the solar panel motions. discussion of the tether and spacecraft dynamics simulations is given before showing typical results. The motorized tether deployment profile and the accompanying spacecraft pitch scenario highlighted to demonstrate a controlled deployment momentum-bias attitude control.

The paper includes a derivation of the control equations used to calculate the ΔV supplied by the LEB thrusters to obtain tether system excitation or damping. A listing of the planned libration experiments is given along with some simulated results of libration and sensor output. At the end of the attached phase, ATEx is jettisoned from the STEX spacecraft to become a passive tethered system. A comment is made on material survivability and the desire to keep the tethered system intact until reentry due to drag.

ATEX AND STEX CONFIGURATION

System components, dimensions, and mass properties are shown in Figures 1a and 1b and Tables 1a and 1b. During ATEx operations, the STEX spacecraft's attitude control system will maintain reference to the local-vertical-local-horizontal (LVLH) attitude frame using on-board propagation of the orbit ephemeris. The spacecraft's body-fixed frame has its +X-axis directed toward the velocity vector, the +Y-axis directed toward the orbit normal, and the -Z-axis directed toward nadir. The spacecraft can thrust only along the X and Y axes to affect translation along these axes or rotations about all three axes. The solar panels track the sun by rotating in elevation about the Y-axis and then in azimuth about the new Z-axis.

The origin of the UEB and solar panel frame is at their centroid and the origin of the combined LEB and STEX frame are at their centroid. The respective frames are parallel to the spacecraft body frame shown in Figure 1a.

Upper End-body

The tether system's UEB resembles a pizza box. As shown in Figure 1b, this body connects to the blade-like initial deployment guide (IDG), which in turn connects to the tether, which is anchored through the guide. When deployment begins, the IDG is accelerated from rest deploying both the UEB and tether at a constant feed rate.

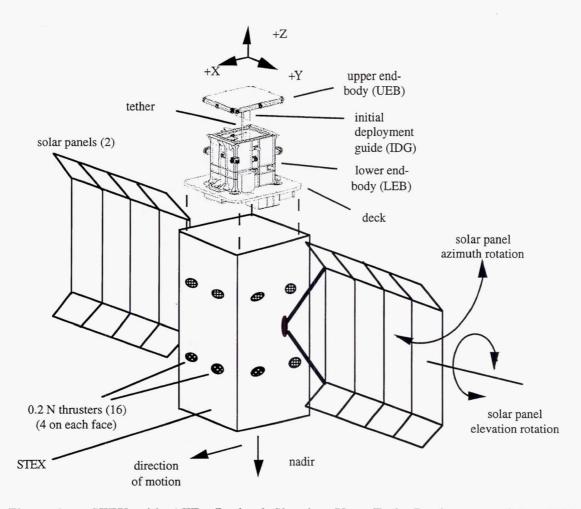


Figure 1a: STEX with ATEx Payload Showing Very Early Deployment of the UEB as the IDG Exits the Motor-Driven Pinch Rollers

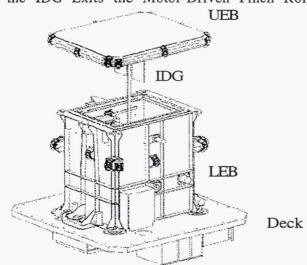


Figure 1b: ATEx Showing UEB and Initial Deployment Guide (IDG) Exiting Pinch Rollers

Table 1a
APPROXIMATE DIMENSIONS AND WEIGHTS OF ATEX AND STEX

		Dimensions	3		
		(in)		Mass	Total Mass
		(m)		(1bm)	(lbm)
Component	X	Y	Z	(kg)	(kg)
UEB	24.3	20.3	2.6	26.1	
0.20	0.62	0.52	0.07	11.8	
Tether	0.005	1.0	242,992	29.6	
(amount carried)	0.0001	0.03	6,172	13.4	
(amount carriou)	0.0001	0.05	0,172	10.1	ATEX
LEB	21.0	17.0	23.5	60.8	116.5
	0.53	0.43	0.60	27.6	52.8
*					
Deck	32.0	32.0	1.25	64.7	
	0.81	0.81	0.03	29.3	
STEX (no deck,	48.3	48.3	80.8	1,080	
no panels)	1.23	1.23	2.05	489.7	
					STEX
Each Solar	20.8	77.1	68.0	22.5	1,189
Panel	0.53	1.96	1.73	10.2	539.4
panel brace	-	21.3	-		
* Control of the Control	-	0.54	-		
					combined
overall	48.3	240.6	106.9		1,306
	1.23	6.11	2.72		592.3

Table 1b APPROXIMATE MOMENTS OF INERTIA OF ATEX AND STEX

Component	Ine	·	
	0.37	0.0	0.0
UEB	0.0	0.55	0.0
	0.0	0.0	0.91
LEB	364.0	0.0	0.0
a n d	0.0	273.0	0.0
STEX	0.0	0.0	182.0
Each	6.5	0.0	0.0
Solar	0.0	2.1	0.0
Panel	0.0	0.0	4.6

Tether

ATEx's tether was specified by the Lockheed Martin Company^{1&2}. This tape-shaped tether is designed to achieve long life by statistically being less susceptible to impact than the small diameter cord of TiPS and to survive the degrading effects of the space environment. ATEx will carry a 6.172 km length of 1 inch wide by 0.005 inch thick low-density-polyethylene tape. This material is similar to the thicker clear plastic used to wrap bulk-food items. The tether density is 0.002173 kg/m. Because the deployed tether's tension is very low, 0.3 N (1.1 oz), the tape will not be pulled taut nor appear as a straight line when viewed on the side. Figure 2 shows both tether sides in front of an inch-graduated scale.

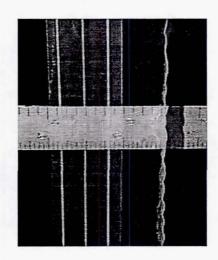


Figure 2: Front and Side Close-up View of Tether Showing Wrinkles and Warping Under Approximately 1 oz of Tension

Presumably, orbit debris would not penetrate the full 1 inch width, rather it would graze or pass through only a portion of the tether. Interior to the polyethylene, there are three strands of 0.003 inch thick Spectra® 1000 uniformly spaced along the tether width. The strands provide rip-stop protection and are not normally expected to take the tension load. We anticipate deploying 6.050 km (3.76 statute miles) of tether.

The tether's material properties such as Young's modulus, E, and axial stiffness, EA, (Young's modulus \times cross-sectional area) have not been estimated for the low tension and space environment. We simply use E = 3.069 E10 N/m² and EA = 495 N (111 lb) as

estimated in laboratory tests at room temperature. Additionally, we cannot state the tether's deployed shape. For example, the tether may slightly twist due to the memory set while stored on the supply reel inside the LEB for at least eighteen months. Perhaps the distance between end-bodies will be 5.9 km, although we deployed 6.05 km.

Lower End-body

ATEx deployment mechanisms and all but one science sensor are located within the LEB. Externally, there are mechanisms to separate the UEB from the LEB and, later, the LEB from the deck. ATEx power and telemetry are provided by STEX. After the ninety-day attached phase is completed, ATEx will be jettisoned, becoming a passive satellite, and beginning the mission's survivability phase. The sensors will be described below.

Inside the LEB is the tether supply reel, tether guides, and two pinch rollers. The tether is supplied by a reel with dimensions of 14.25 inches outside and 6.625 inches inside diameter. The 8 inch wide reel has its axle parallel to the spacecraft Y-axis. A geared stepper motor drives one pinch roller, which pulls the tether from the reel. Reference 3 describes these mechanisms and the associated design, construction, and test processes.

Deck

The deck is the top of STEX and holds most of ATEx's electronics. There are few electronics boxes on ATEx's LEB. When ATEx separates from the spacecraft, all telemetry ceases.

As a point of clarification, the tether system's lower end-body includes ATEx's LEB, the deck, and STEX. When ATEx's LEB separates from the deck and STEX, the tethered system consists of ATEx components only (UEB, tether, LEB).

ATEX INSTRUMENTATION

There are no on-board capabilities to directly measure the libration angles. We can only infer the system librations. First, there are on-board sensors that measure the 3-axis accelerations of the

system at the LEB and the 3-axis tensions at the tether connection point to the LEB. These respond to all motions of the system. Additionally, examination of STEX's pitch and roll attitude data will complement the indirect estimate of libration from the earlier mentioned 3-axis devices. And lastly, we may measure the range to each end-body from the ground via satellite laser ranging or radar techniques.

Figure 3 shows a sketch of the body-fixed axes and defines various angles. The local angles are the angles the tether makes with respect to the +Z-axis at the top of the LEB measured in the X-Z and Y-Z planes. The system libration angles are the angles measured from the nadir vector to the line connecting the mass center (CM) of each end-body. These are commonly known as the in-plane and out-of-plane libration angles.

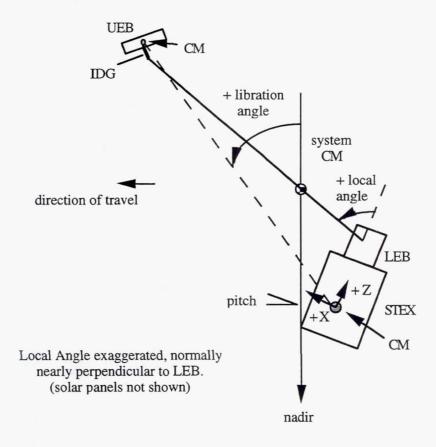


Figure 3: Sketch of Various In-Plane Angle Geometries, While Not Shown, These are Similar For Out-of-Plane Geometries (where "pitch" is replaced by "roll" and "direction of travel" is replaced by "normal to orbit")

Retroreflectors

In anticipation of imitating the same passive SLR techniques from the TiPS experiment, retroreflectors covered both end-bodies⁴. A retroreflector, or corner-cube, reflects received light back to its source. TiPS was to have demonstrated the technique of using ground-based satellite laser ranging to estimate the tether's libration angles and orbit ephemeris⁵. TiPS's upper end-body was covered with 18 infrared-laser-sensitive retroreflectors and the lower end-body was covered with 18 green-laser-sensitive retroreflectors. Each set of retroreflectors provided spherical coverage so that no matter what the orientation of an end-body, the incoming laser beam would be reflected by a retroreflector—as long as the end-body was in line-of-sight of the beam. Other benefits of laser ranging were to specifically identify end-bodies, which end-body was up, and to notice if the tether cartwheeled. There is no indication TiPS cartwheeled.

For ATEx, there are forty-three green-sensitive retroreflectors mounted on all sides of the UEB providing optically spherical coverage. Another forty-three infrared-sensitive retroreflectors are mounted around the four sides of the LEB providing optically spherical coverage. There are six infrared-sensitive retroreflectors mounted on the bottom of STEX providing hemispherical coverage centered about its -Z-axis.

The ATEx program expected successful results from the TiPS mission of using ground-based satellite laser ranging and tether system modeling to predict tether system libration and orbit. Before TiPS's launch and the subsequent success or failure of this ranging technique, the ATEx project had to procure long-lead retroreflectors. The TiPS's mission laser ranging and solution techniques were not sufficient and timely enough to demonstrate a level of success necessary to support ATEx mission operations, some of which are timed to the libration angle cycle. This forces exclusive reliance on the original ancillary accelerometer, tensiometer, and STEX roll and pitch attitude measurements. These are now our primary instruments.

Local Angle Sensor

ATEx is STEX's first experiment and will be jettisoned after the experiment duration. The ATEx must not jeopardize the STEX and a few safeguards are in place to rapidly and autonomously jettison ATEx if any problem indications are detected. The STEX is not in continuous contact with the ground and there is no on-board camera to see what the tether is doing in the vicinity of the STEX. A local angle sensor is the one safeguard that the ATEx provides to detect local angle extremes. See Figure 3 for a sketch of the local angle and body-fixed axes. A rectangular matrix of paired light emitting diodes and detectors sense the tether in the spacecraft's X-Z and Y-Z planes. During deployment these specific local angles, as measured from the +Z-axis, in the X-Z plane are ±3.5°, ±17.1°, ±57.9°, and ±60.0° and in the Y-Z plane are ±3.5°, ±17.1°, ±47.4°, and ±51.0°. If the tether sequentially trips the sensors and then blocks the extreme sensor, on-board logic control signals the jettison of ATEx's LEB.

After deployment, the tether is grabbed by the tensiometer arms 2 inches above the pinch rollers. This changes the tether's attach point and geometry relative to the fixed detector pairs. Thus in the post-deployment, or libration control phase, the local angles become $\pm 8.1^{\circ}$ and $\pm 35.4^{\circ}$ in both the X-Z and Y-Z planes. The other detectors are not used after deployment because they measure angles beyond the 35° safety limit. During the libration control phase, if the tether's local angle trips any of these extreme sensors, the ATEx will be jettisoned. Should the experiment go as planned, ATEx will only trip the $\pm 3.5^{\circ}$ X-Z plane sensor during nominal deployment and trip no sensors during libration control.

Tether Reel Turn Counter

There is a tether supply reel turns counter. As the tether was wound, the turn count vs. tether length was recorded. Additionally, the stepper motor is deploying the tether at a constant 2 cm/s rate for 3.5 days. Therefore, knowledge of deployed tether length at any point should be straightforward. In turn, the tether system's mass center location will be continually recalculated. When fully deployed, the mass center is to be 189 m (620 ft) from the bottom of STEX.

Tensiometer

The ATEx program procured a custom-built tensiometer from NASA Langley⁶. Earlier units were provided to NASA Marshall for use on the Small Expendable Deployer System (SEDS 1 and SEDS 2 tether missions). The tensiometer is a 3-axis strain gauge system to measure component forces. The tensiometer mounts on the frame supporting the ends of the pinch rollers and two 6-inch arms, above the pinch rollers, close around the tether after deployment. They grab the tether 2 inches above the center of the rollers. The associated electronics provide a ±1 N range and 0.5 mN resolution of tension along each axis. Resolution of the tension force along the X-, Y-, and Z-axes yield libration phase and frequency and permit calculation of local angle.

Additionally, the procurement included Langley's low-pass filter and a 12-bit analog-to-digital converter. Tensiometer signals pass through a 0.2 Hz low-pass filter, a cut off specified by tether system frequencies of interest. The sampling rate is 8 Hz, significantly greater than the Nyquist frequency to detect tether system oscillations below 0.1 Hz.

Figures 4a and 4b present isometric drawings looking into the top of the LEB along the +X+Y-axes. In Figure 4a, note the open arms that connect to the tensiometer ready to close upon the tether after deployment. Above the arms are holes for the light emitting diode and detector local angle sensors. The IDG is shown between the pinch rollers. In Figure 4b, the tether is pulled off the supply reel to the left around an unseen horizontal roller, then across to the right around the vertical stationary guide and up through the pinch rollers. The vertical guide maintains the tether's exit point at the center of the pinch rollers. Figure 5 shows a drawing of the tensiometer and sweep area indicative of closing arms. Although not shown, one arm has a pad of pins to pierce the tether as it closes on the other arm. Figure 6 shows the closed arms grabbing the tether 2 inches above the pinch rollers effectively changing the apex of local angle measurements. The tether's vertical guide is shown behind the tensiometer.

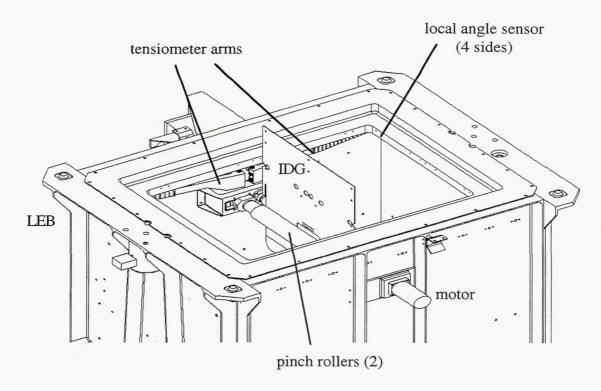


Figure 4a: The UEB is Held by IDG in Pinch Rollers

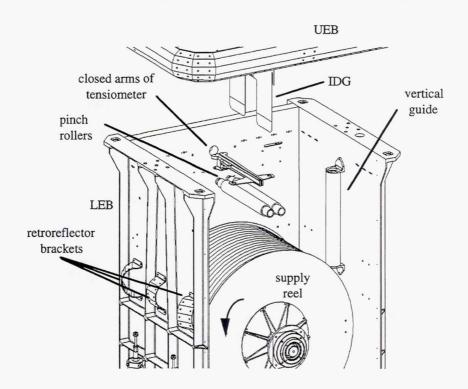


Figure 4b: Cutaway Drawing of LEB Highlighting Internal Deployment Hardware (tether not shown)

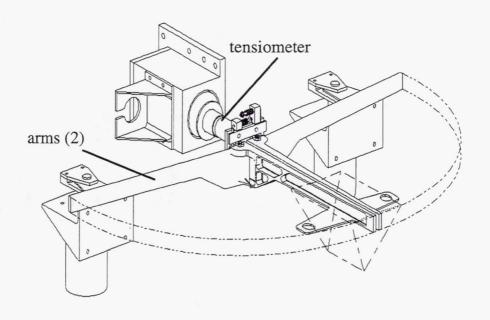


Figure 5: Time-Lapse of Initially Open Arms Closing to Grab Tether (tether not shown)

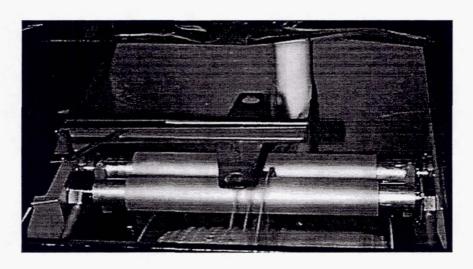


Figure 6: Closed Tensiometer Arms Grab Tether After Deployment

Accelerometers

There are three Allied-Signal QA-3000-010 single-axis accelerometers, aligned along the STEX body axes underneath the ATEx electronics deck to measure accelerations. The associated electronics provide a ± 1 mg range and 0.5 μ g resolution of acceleration along each axis. Signals are filtered and sampled the same as those of the tensiometer.

Transponder on STEX

The Air Force's Satellite Control Network with their Remote Tracking Stations will interrogate STEX's transponder to provide range and range rate observations to the NRL. This data, when coupled with the known tether system mass center location, will assist us with tether orbit and libration estimates via the TiPS techniques⁴. Additionally, the Air Force's orbit analysts will provide an element set for STEX using the same observations. Their orbit analysts currently plan to do orbit determination on the STEX and LEB combination, which will be 189 meters away from the system's mass center and accept the errors introduced by the STEX and LEB not being in a Keplerian orbit. They may use knowledge of the tether system's mass center location by changing the transponder bias to effectively change the range measurement. Practically, they will wait for the flight to further examine their orbit determination process. Naval Space Command will provide their estimate of the tether system's orbit to the ATEx team. We plan to collect and compare the three different element sets.

Radar Tasking and Possible Use SLR and Optical Measurements

There are plans for routine tasking of Air Force phased-array radars to provide near-simultaneous ranging of each end-body. If plentiful and timely electronically transmitted data can be obtained, these data would be fed into the TiPS solution technique for ATEx. There may be very occasional separate tasking of lasers to range each end-body. Additionally, there will likely be optical telescopes trained on the system during portions of deployment and libration control. Video tapes will be sent to the NRL for optical attitude determination.

STEX'S ATTITUDE CONTROL SYSTEM AND SOLAR PANEL MOTIONS

The STEX spacecraft has a 3-axis attitude determination and control system. Attitude data is sampled at a 10 Hz rate.

There are three different STEX attitude control system functions employed during the tether experiment's duration:

Function 1, activated during deployment, is pitch-axis momentum-biased control using a Y-axis aligned momentum wheel typically spinning at 5,000 rpm ±1,000 rpm and moment of inertia of 0.031 kg-m². Analysis showed the wheel would despin in early tether deployment causing STEX to tumble and possibly tangle with the tether. A control system design change to incorporate the use of the existing three single-axis electromagnetic torque rods, in Function 1, to damp rates solved the problem of the despinning wheel. ATEx cannot impart a total angular impulse greater than 1.6 N-m-s on the spacecraft during early deployment because STEX has minimal control authority.

Function 2 is activated after full tether extension and turned off during infrequent thrusting operations. This function uses active yaw attitude control using the X-axis thrusters. Only the X-directed thrusters are used because the solar panels may be at any orientation and harmed by Y-directed thrust plumes. The tether's gravity-gradient tension maintains passive roll and pitch control. Torque rods damp roll, pitch, and yaw rates. The spacecraft behaves as a second pendulum with respect to the tether. This function cannot tolerate slack tether because the gravity-gradient would disappear. The wheel is off.

Function 3, called libration control, uses the $\pm X$ - and $\pm Y$ -directed thrusters to maneuver STEX to provide excitation or damping of system librations. The solar panels are first rotated to the null position, 0° "elevation" and 0° "azimuth", to avoid thrust plumes.

During tether operations, the STEX uses a propagated local reference (based on on-board ephemeris sent by the ground) to maintain LVLH. The spacecraft is powered by double-gimbaled solar

panels. Unfortunately, panel rotations negatively impact ATEx science by rotating at a frequency near orbit and tether system libration rates. The panels point toward the Sun by first moving their "elevation" angles (about the body Y-axis) and then rotating "azimuth" angle (about the new Z-axis) to match the Sun's beta angle. In practice, the "azimuth" angle is set once a day and the "elevation" angle continually changes. During each orbit, the "elevation" angle rotates at orbit rate approximately 270° for 3/4 an orbit and rewinds at three times orbit rate for 1/4 orbit. Mechanical limits are placed on "azimuth" angles to $\pm 50^{\circ}$ such that the ATEx mission is restricted to beta angles within $\pm 50^{\circ}$.

From ATEx's perspective, STEX's operations will handicap ATEx science; that is, STEX was not designed for tether science as its primary objective, but rather modified to accept a government-furnished active payload. STEX's momentum-bias attitude control system is somewhat sensitive to unbalanced disturbances and drove ATEx's deployment to a motorized scheme instead of the higher impulse experience of SEDs and TiPS. As discussed above, the solar panels add unwanted disturbances to the tether system at a frequency near that of libration. Fixed solar panels are preferable. Additionally, the torque rods affect the LEB/STEX pitch and roll free response to libration as they beneficially damp unwanted panel disturbances. In turn, these two attitude channels provide data to infer librations.

TETHER SYSTEM SIMULATIONS

Before continuing to describe the deployment and libration control, let us survey two employed tethered-system dynamics simulations used to predict and study system behavior during various mission phases.

A simplified model of a momentum-bias spacecraft deploying a tethered end-body was developed by the NRL. The model consisted of two end-bodies in orbit connected by a variable length tether. The end-body portraying the STEX consisted of a rigid body carrying an ideal wheel allowing spin about a fixed axis. The body representing the UEB was rigid and passive. The tether was treated as a massless tensile member of variable length, directed along the

straight line connecting the attachment points on the respective end-bodies. Both extensible and inextensible tethers could be considered. The system was subject to the gravitational attraction of an inertially spherical Earth and reaction forces from spacecraft thruster firings. Attitude control models for both the momentum wheel and the thruster system were included. This model captured the fundamental libration and end-body pendular motions as well as the first longitudinal stretch mode (when considered extensible) all under variable tether length conditions.

In order to include the influence of tether transverse deflections, and longitudinal vibration characteristics beyond the fundamental mode, a tether model possessing mass is necessary. To study these effects, as well as the nonspherical gravitational field of the Earth, the program GTOSS (Generalized Tethered Object Simulation System) was used. GTOSS was developed by David Lang Associates for the NASA Johnson Space Center and was used extensively for analyses of the Shuttle-based Tethered Satellite System missions. The program models tether mass as a distribution of equally spaced point masses interconnected by extensible tether segments. A full complement of environmental forces are also offered. GTOSS was modified to allow inclusion of the STEX thruster control system.

We do not have complete simulations of the STEX and tether interactions. For example, we do not model the solar panel motions at the NRL. When we propose a tether operation for the mission, we pass the proposed operation to the attitude engineer at the contractor's facility for checking with their combined tether dynamics and attitude control system. The two groups complement one another. We do detailed analysis to describe a tether maneuver and the contractor furthers success of the maneuver by meeting their control and stability needs.

MOTORIZED TETHER DEPLOYMENT

The goal of controlled UEB deployment, as would be expected for future active end-bodies, is described in this section. A constant-speed motor drives a pair of pinch rollers to accelerate the IDG and UEB combination from rest to the 2 cm/s deployment speed and pull the 6.05 km tether off the supply reel. As the deployment begins,

the tether length increases and the system's pitch rate slows below orbit rate. The system pitches backwards and the STEX spacecraft must begin a pitch rotation profile to maintain the local angle nearly perpendicular to the X-Y spacecraft frame. After two in-plane oscillations, the pitch profile completes because the relatively small librations that occur during remaining 3.5 days of tether deployment will not influence STEX attitude beyond acceptable tolerances.

The spacecraft's attitude control system can tolerate only extremely small Z-axis directed disturbances caused by ATEx's UEB separation. Employing a motor to pull the tether from the supply reel alleviates the quantification of impulse and friction issues associated with a forceful spring separation used by other small tether projects.

Due to the limited instrumentation and lack of on-board processing to maintain tether control during the entire deployment, the deployment will be open loop. A motor will drive pinch rollers to pull the tether from the supply reel at a slow enough rate such that the tether system will not tumble in pitch. This can be shown using the equation for in-plane angular acceleration, copied from Reference 7:

$$\ddot{\theta} = -3\Omega^2 \sin\theta \cos\theta - 2(\dot{\theta} + \Omega) \left(\frac{\dot{L}}{L} + \dot{\phi} \frac{\sin\phi}{\cos\phi} \right) \tag{1}$$

where θ is the in-plane libration angle, ϕ is the out-of-plane libration angle, Ω is the orbit angular speed, and L is the deployed tether length. The dots indicate time derivatives.

Assume that θ and $\dot{\theta}$ are very small and there are no out-ofplane motions such that $\dot{\phi} = \phi = 0$. Then

$$\ddot{\theta} = -3\Omega^2 \theta - 2\Omega \left(\frac{\dot{L}}{L}\right) \tag{2}$$

The second term (Coriolis) is not small relative to the first term (gravity-gradient). If \dot{L} is relatively fast and L small, the tether system will rapidly pitch backward and can tumble.

By deploying slowly, ATEx will pitch backwards, but not tumble. In fact, the stepper motor's gearing and drive electronics were specified for speeds of 1 and 2 cm/s because analysis of faster speeds (10 cm/s and above) indicated that significant slack tether could generate due to perceived motor speed variations. The gravity-gradient tension is very small at tether lengths under 500 m. Only after the Astro Instrument stepper motor and associated drive electronics were tested, did we appreciate the precise speed control, less than 0.3% error, of this motor type. This is a lesson learned as we wished perhaps for a faster deployment of 3 to 4 cm/s.

We demonstrated by analysis and test that even with slight motor speed variations and IDG tip-off, the UEB should safely move away from the LEB.

The Deployment Sequence

- 1. For pre-deployment, the spacecraft's body-axes are aligned with the LVLH frame and the attitude control system is set to Function 1.
- 2. Restraints at the four corners of the UEB release.
- 3. Prior to locking the solar panels for 170 minutes, they rotate to "elevation" and "azimuth" angles applicable at the end of this time. At least for the first two in-plane tether system librations, the spacecraft inertia changes due to panel motion will not be allowed to disturb the tether nor cause roll and yaw motions.
- 4. The motor is turned on and off to permit a 1 inch IDG "kick out". This raises the UEB off the LEB.
- 5. We do not influence the system for ten minutes while oscillations damp.
- 6. The motor again turns on to accelerate the IDG and UEB to 2 cm/s. Deployment continues for 3.5 days.
- 7. After one minute (1.2 m of deployed tether), STEX begins a pre-programmed pitch rotation profile designed to maintain a small local tether angle—approximately 90° to the X-Y plane of the LEB. See Figure 7.

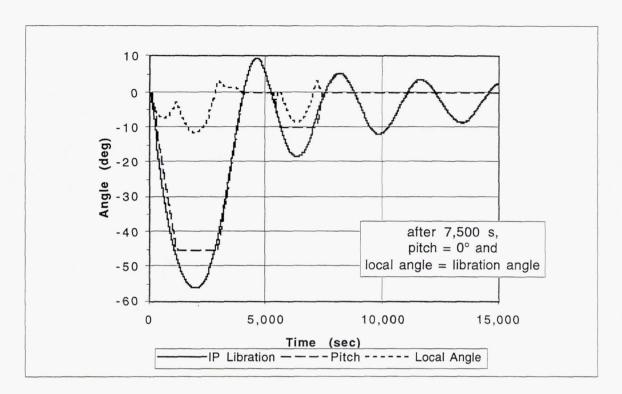


Figure 7: System Libration and STEX's Pre-programmed Pitch Maneuver

- 8. Note the large libration angles especially during the first two inplane librations. Consider that the first maximum libration angle occurs at 42 meters of deployed tether (2,100 seconds) and a -57° libration angle. A mission safety jettison signal is at -60° local angle. To reduce the risk, STEX will pitch -45° yielding a safer -12° local angle. The spacecraft's pitch profile continues for 7,500 seconds, to the end of the second largest in-plane libration. This duration corresponds to 150 m of deployed tether. The attitude control system remains in Function 1. At the discretion of the attitude engineer, a pitch bias not smaller than -1° may to maintain wheel speed during commanded momentum the remainder of the tether's deployment.
- 9. STEX's attitude control analysts estimate that when 2,000 m of tether are deployed, the magnitude of the gravity-gradient tension will be large enough to transition to Function 2. (The analysts may choose to remain in Function 1 for the entire deployment.) Figure 8 shows the in-plane libration angle for the remainder of deployment. The programmed pitch angle is between 0° and -1° . As L increases,

the \dot{L}/L term's effect in the Eq. (2) becomes smaller. Note that as in Figure 7, the libration angle is biased off 0° because \dot{L} is nonzero. In fact the bias changes from about -1.5° to -0.2° as the length increases. Both the libration angle and bias decrease. When deployment is stopped, by turning off the motor, the system oscillates with no bias.

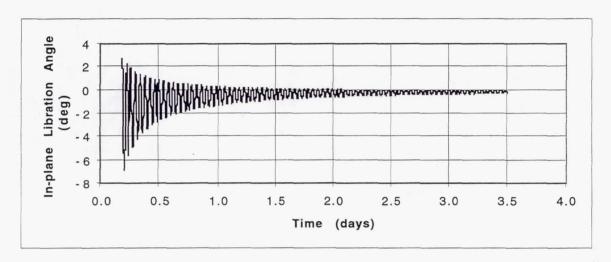
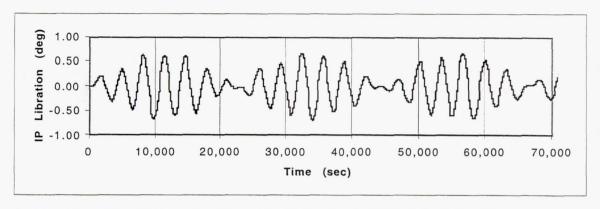


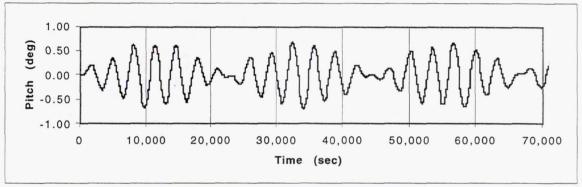
Figure 8: System Libration During Remainder of Deployment

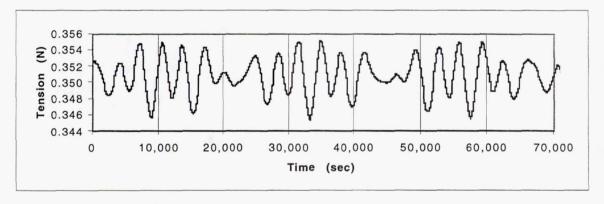
Fully Deployed Tether in Quiescent State

Before moving on to the excitation of tether oscillations, let us examine the simulated quiescent state of the fully extended tether in the nonuniform gravitational environment. This shows a lower bound of libration for an uncontrolled tethered system.

The simulation began with no librations using a nonspherical Earth, J_2 gravity model, end-bodies aligned with the tether local vertical such that the local angles were zero degrees. The system mass center was in circular orbit. There are no perturbations due to solar heating, solar wind, and atmospheric drag in Figures 9. Corresponding plots are given for the pitch attitude and tensiometer output. Let us review what these plots reveal.







Figures 9a, b, c: Quiescent System In-Plane Libration and Corresponding STEX Pitch Attitude and Tension

The in-plane libration plot of Figure 9a covers 20 hours, or 11.9 orbits, showing repetition of the beating between the orbit frequency of 0.000166~Hz~(100.6~min) and the in-plane libration frequency of 0.000281~Hz~(59.3~min). We estimate an in-plane libration of about $\pm 0.75^{\circ}$ for this tether system, which will manifest as "background" libration, an error to precise libration control. That is, the ATEx can probably control in-plane libration to no better than $\pm 1^{\circ}$.

The STEX's attitude control system, during the 87 days of infrequent thrusting, permits pitch and roll to be gravity-gradient stabilized according to Function 2. As shown in Figures 9a and b, pitch follows in-plane libration so closely that the curves plot over one another. Here is an example of pitch attitude data (recorded during non-thrusting operations) providing direct indication of in-plane libration amplitude, frequency, and phase.

The magnitude of the 3-axis tension illustrates that tension tracks the in-plane libration. In Figure 9d, the tension has been rescaled to fit on the same graph as the libration. Note that tension appears at the same frequency and 90° ahead of libration in phase. Both spacecraft pitch and tension plots offer important corroboration of nadir passing of the tether. As the tether moves forward through 0° libration, tension is maximum. At maximum libration (+0.75°), the tension decreases to its mean value of about 0.35 N. As the libration decreases toward vertical, the tension is minimum. The cycle is complete when the libration reaches the minimum (-0.75°) and the tension increases to its mean value.

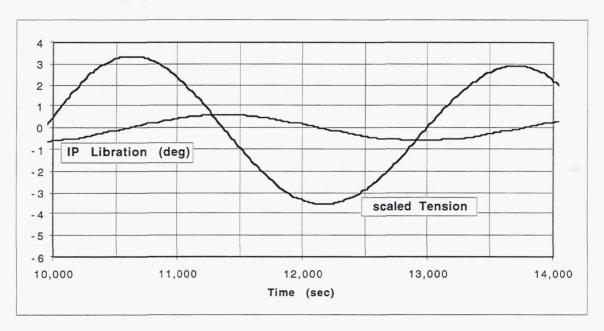


Figure 9d: Over Plot of Quiescent System In-Plane Libration and Tension Highlights Phasing Information from Tensiometer

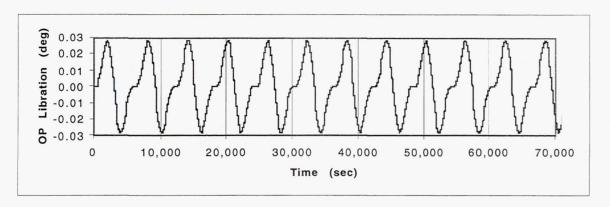


Figure 9e: Quiescent System Out-of-Plane Libration

Figure 9e shows the negligible out-of-plane libration due to the gravitational environment. Although not shown, the plot of roll attitude tracks the out-of-plane libration to indicate out-of-plane amplitude, frequency, and phase. Active thruster control maintains LEB and STEX spacecraft yaw attitude within $\pm 1^{\circ}$.

LIBRATION CONTROL: STARTING AND STOPPING TETHER OSCILLATIONS

The active portion of ATEX's mission, which is the attached phase, offers the world its first controlled long-duration space tether experiment. Below we derive the open loop control equations, list the planned libration experiments, and review in-plane and out-of-plane excitation and damping maneuvers.

Open Loop Control Equations

The goals of the control equations are to specify a ΔV magnitude, direction, and application time of spacecraft thruster force to achieve the desired $\Delta \theta$ or $\Delta \phi$.

Let L_1 and L_2 represent the length of the tether from the system's center-of-mass to each end-mass M_1 and M_2 , respectively. Assuming an inextensible and massless tether

$$L_1 + L_2 = L$$

$$M_1 + M_2 = M$$

$$M_1L_1 = M_2L_2$$

where L is the tether length and M is the system mass. It follows that

$$L_1 = \left(\frac{M_2}{M_1 + M_2}\right) L \tag{3}$$

$$L_2 = \left(\frac{M_1}{M_1 + M_2}\right) L \tag{4}$$

Let δV represent the change in speed of the center-of-mass and ΔV_1 represent the change in speed of end-mass M_1 due to an impulsive thrust. Equating the impulse on M_1 to that on the system $M_1 + M_2$, the change in speed of the system's mass center is given by

$$M_1 \Delta V_1 = M \delta V$$

$$\delta V = \frac{M_1}{M} \Delta V_1$$

The angular momentum H of the system about the center-of-mass is given by

$$H = \left(M_1 L_1^2 + M_2 L_1^2\right) \left(\Omega + \dot{\theta}\right) \tag{5}$$

The angular impulse associated with ΔV_1 is $\Delta H = L_1 M_1 \Delta V_1$. Neglecting the change in the orbit angular speed due to the impulse, the change in the angular rate of the pendulum from Eq. (5) is

$$\dot{\theta} = \frac{H}{\left(M_1 L_1^2 + M_2 L_1^2\right)}$$

$$\Delta \dot{\theta} = \frac{L_1 M_1 \Delta V_1}{\left(M_1 L_1^2 + M_2 L_1^2\right)} = \frac{\Delta V_1}{L} \tag{6}$$

with the simplification provided by use of Eqs. (3) and (4). Eq. (6) provides the relation between the speed change of M_1 and the inplane libration angle.

The familiar linear small-angle equations of tether system motion and their solutions are reviewed here. Further simplify Eq. (2), with \dot{L} equal zero

$$\ddot{\theta} + 3\Omega^2\theta = 0$$

A solution to this is

$$\theta = \theta_{\text{max}} \sin(\sqrt{3}\Omega t)$$

$$\dot{\theta} = \sqrt{3}\Omega\theta_{\text{max}} \cos(\sqrt{3}\Omega t)$$

$$\dot{\theta}_{\text{max}} = \sqrt{3}\Omega\theta_{\text{max}}$$
(7)

where t is time, θ_{max} is the amplitude of the swing, and $\dot{\theta}_{max}$ is the speed when the pendulum passes through nadir.

The out-of-plane equation for tether system motion is copied from Reference 7.

$$\ddot{\phi} = -\sin\phi\cos\phi\left(3\Omega^2\cos^2\theta + \left(\dot{\theta} + \Omega\right)^2\right) - 2\frac{\dot{L}}{L}\dot{\phi} \tag{8}$$

Eq. (8) can be simplified for the fully extended tether with no in-plane motions, $\dot{L} = \theta = \dot{\theta} = 0$, and for small out-of-plane librations, ϕ

$$\ddot{\phi} + 4\Omega^2 \phi = 0$$

A solution to this is

$$\begin{split} \phi &= \phi_{\text{max}} \sin(2\Omega t) \\ \dot{\phi} &= 2\Omega \phi_{\text{max}} \cos(2\Omega t) \\ \dot{\phi}_{\text{max}} &= 2\Omega \phi_{\text{max}} \end{split} \tag{9}$$

where t is time, ϕ_{max} is again the amplitude of the swing, and $\dot{\phi}_{\text{max}}$ is the speed when the pendulum passes through nadir.

Substitute Eq. (6) into Eq. (7) to obtain the following relation between the ΔV magnitude for an impulsive thrust and the desired magnitude of in-plane angle θ_{max} .

$$\Delta V = \Delta \dot{\theta} L = \sqrt{3} \Omega L \Delta \theta_{\text{max}} \tag{10}$$

An impulsive speed change, $\Delta\dot{\theta}$, occurring at the nadir crossing produces a corresponding change in the swing amplitude, $\Delta\theta_{\text{max}}$.

Similarly, one obtains the out-of-plane libration control relationship

$$\Delta V = 2\Omega L \Delta \phi_{\text{max}} \tag{11}$$

The direction of the applied ΔV is that of the desired $\Delta \theta$ or $\Delta \phi$. The application of an impulsive ΔV is at the nadir crossing point in the libration. A finite ΔV duration will be centered about nadir.

Planned Libration Experiments

The Request For Proposal for the STEX was written to require a ΔV budget of 40° for in-plane and 40° for out-of-plane librations. This corresponds to a ΔV_x of 7.6 m/s and ΔV_y of 8.8 m/s, respectively. There is little desire to use the entire budget at once; for example, to excite 20° in-plane, then damp 20° in-plane, and similarly for out-of-plane. We choose to repeat the experiments to demonstrate repeatable results. Note however, the repetition is not exact because we want to confirm that magnitude differences do linearly scale. Table 2 shows the seven experiment sets, which group

similar libration conditions. For example in Set 1, the in-plane excitation is 4° , followed a few days later by the first in-plane damping, which is planned to be 2° to determine how well this libration reduction can be achieved. Perhaps more or less ΔV will be necessary to reduce the remaining libration. In Set 2, the in-plane excitation and damping is essentially the same as Set 1; however, the damping performance may be enhanced by the experience of Set 1. The same ideas are planned in Sets 3 and 4 and Sets 5, 6, and 7. We plan to wait a few days in between each thrust to assess the effects by estimating the current libration and predicting the next thrust duration and command time.

Table 2 LIBRATION EXPERIMENTS PLANNED FOR THE ATEX

Set	Thrust Action			
	In-plane excitation 4°			
1	In-plane damping 2°			
	In-plane damping 2°			
2	In-plane excitation 5°			
	In-plane damping 5°			
	Out-of-plane excitation of 4°			
_	Out-of-plane damping of 2°			
3	Out-of-plane damping of 2°			
	(optional in-plane damping of X° due to coupling caused by out-			
	of-plane librations)			
	Out-of-plane excitation of 6°			
4	Out-of-plane damping of 6°			
4	(optional in-plane damping of X° due to coupling caused by out-			
of-plane librations)				
5	In-plane excitation of 3°			
3	Out-of-plane excitation of 3° Out-of-plane damping of 3°			
	In-plane damping of 3°			
	In-plane damping of 3 In-plane excitation of 4°			
6	Out-of-plane excitation of 3°			
U	Out-of-plane damping of 3°			
	In-plane damping of 4°			
	In-plane excitation of 4°			
7	Out-of-plane excitation of 4°			
,	Out-of-plane damping of 4°			
	In-plane damping of 4°			

There are shortcomings in the control equations: The equations assume small libration angles and impulsive, not finite burns. The ATEx mission will operate under small libration angles primarily due

to propellant limitations. Years ago, when these equations were used to estimate the ΔV budget to be imposed upon STEX, the thruster force was unknown.

An In-Plane Example

By applying a finite thrust of 573 seconds (16% of in-plane libration period) with the four -X-directed thrusters of approximately 0.193 N (0.69 oz) each, an in-plane libration of +4° can be excited. The ΔV equaled 0.76 m/s. The results are shown in the set of Figures 10.

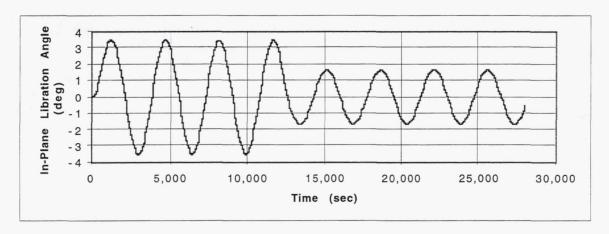


Figure 10a: Excite a 4° In-plane Libration Followed by a Damping of 2°

Because the ΔV was not centered about nadir (the tether here is initially at rest) and the burn is finite, the resulting libration is about 3.5°. Examine that the in-plane damping of 2° effected by applying the 286 second burn, centered about nadir, using the same thrusters produced the desired result. The ΔV equaled 0.38 m/s.

In Figure 10b, the time scale of Figure 10a has been expanded and the pitch angle plotted over the in-plane libration. The eye can smooth the pitch curve to see how well it follows the libration in amplitude, frequency, and phase. The higher frequency pitch motion is the LEB and STEX combination behaving as a second pendulum. Its magnitude is about $\pm 0.5^{\circ}$ centered about the current libration angle.

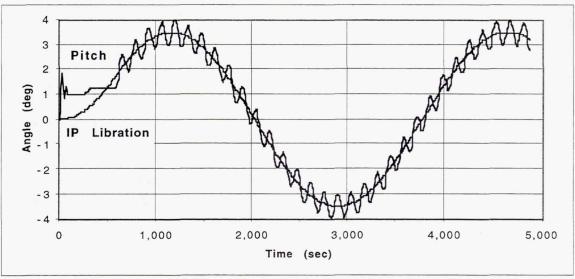
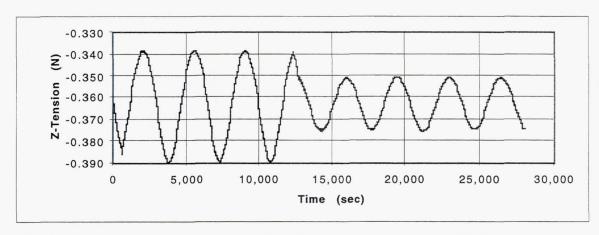
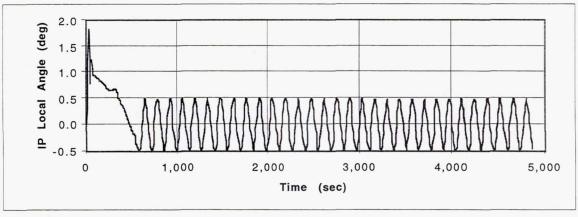


Figure 10b: Expanded Time Scale Showing STEX Pitch Control During Burn and STEX Pitch Angle Showing its Motion as a Second Pendulum





Figures 10c, d: The Z-axis Tension Component Indicates Libration Phase and Frequency. The X and Z Tension Components Form the In-plane Local Angle

Figure 10c shows the scalar tension used to indicate system libration, frequency, and phase. In Figure 10d, the arc tangent of tension components in the X-Z spacecraft frame give the local angle. The amplitude of $\pm 0.5^{\circ}$ and the higher frequency pitch motions correspond to those shown in Figure 10b.

Although not shown here, the magnitudes of the 3-axis tension and 3-axis acceleration also track the system librations. These traces appear at the same frequency with a fixed-offset phase compared to libration. Both STEX pitch and roll attitude plots compared with tension and acceleration plots offer important corroboration of the tether's nadir crossing time.

An Out-of-Plane Example

By applying a thrust of 661 seconds with the four thrusters' forces directed along the -Y-axis, an out-of-plane libration of 4° can be excited. The results are shown in the set of Figures 11. Again, the tether here is initially at rest and the ΔV not centered about nadir.

The roll follows the libration in amplitude, frequency, and phase. The higher frequency pitch motion is the LEB and STEX combination behaving as a second pendulum. Its magnitude is about $\pm 1^{\circ}$ centered about the current libration angle.

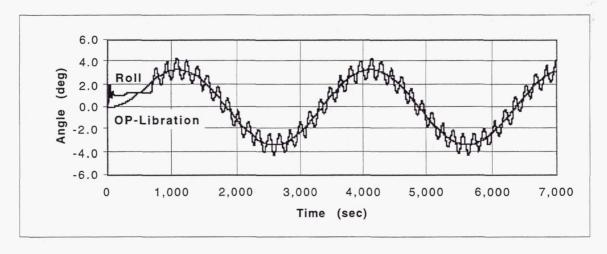


Figure 11a: Excite a 4° Out-of-plane Libration Excitation

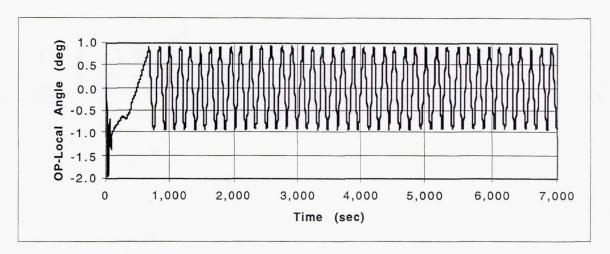


Figure 11b: The Resulting Out-of-plane Local Angle

In Figure 11b, the arc tangent of tension components in the Y-Z spacecraft frame give the local angle. The amplitude of $\pm 1^{\circ}$ corresponds to the higher frequency pitch motions shown in Figure 11a.

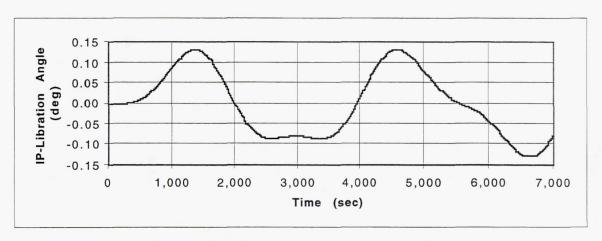


Figure 11c: Exciting a 4° Out-of-plane Libration Excitation Slightly Couples into In-plane Libration and STEX Pitch

Note in Figure 11c, there is a small coupling of out-of-plane libration into in-plane libration. This can be seen by using Eq. (1) for a fully deployed tether $(\dot{L}=0)$. Assuming $\dot{\theta}$ is zero for small angles θ and ϕ , the equation is simplified to

$$\ddot{\theta} + 3\Omega^2\theta = -2\Omega\dot{\phi}\phi$$

The term on the right causes a coupling to in-plane libration. Perhaps this coupling will make damping out-of-plane librations difficult.

DATA PROCESSING/DIGITAL SIGNAL PROCESSING

Timely data processing is vital to the success of the ATEx flight operations. We must estimate tether motions using data from these sensors, perhaps enhanced with radar tracking, and predict the nadir time of the swing. A final command load must be built approximately twelve hours before the thrusters are fired. The sensors do not measure libration directly, although the STEX attitude follows librations in a reliable and similar manner.

We shall use Fast Fourier Transform techniques to observe the system frequencies from our massive GTOSS simulated data and flight data available from the SEDS missions. We plan to investigate results with frequency estimates for tethered systems. Our effort will give us familiarity with expected system frequencies to better identify instrument signals during flight.

Additional work is ongoing toward using an eigensystem realization algorithm⁸ (ERA) for modal parameter identification and model reduction from simulated and test data. The 8-10 Hz mission data will be first filtered and resampled to reduce noise, remove biases, and decrease the number of data points to support analysis of tether system frequencies of interest below 0.1 Hz. The model realized by ERA is used to predict the future of the data channels, such as tension and pitch, to estimate the nadir point of the tether's swing.

MATERIAL SURVIVABILITY

At the end of the attached duration, the LEB will be jettisoned so that the STEX can pursue other mission objectives. Jettison will eliminate all power and telemetry. The ATEx will become a passive tether similar to TiPS. Simulation analyses were used to examine if the STEX could be oriented such that when the 2 ft/s relative ΔV between the STEX and the LEB occurred, the tether would

demonstrate libration conditions not seen the previous ninety days. Within the orientation constraints of the STEX, which are approximately $\pm 8^{\circ}$ in roll or pitch, simulations showed that significant system libration could not be excited by the planned jettison. Simulations showed only very small libration (0.06°) due to the short durations (50 s) of tether slack. A normal jettison from local vertical produces a repeated cycle of slack and retension of the tether; however, the periods of slack are sufficiently short such that the libration never achieves significant magnitude.

In contrast to the planned jettison, an emergency jettison could occur at any operational STEX orientation and rate. These conditions could generate some interesting ATEx motions; however, there was no examination of possible tether motions.

Analysis showed that the ATEx tether system's orbit would decay in 2-3 years. The tether material was specified to survive the space environment until reentry due to drag. After jettison, the ATEx will be tracked via USSPACECOM and NAVSPACECOM. (SLR or radar tasking would be useful in following a nearly vertical tether to observe long-term stability.) Should the tether sever, the NRL would eventually be notified as alarms at the tracking facilities directed attention that the end-bodies are following diverging Keplerian orbits. The cause of the sever, by debris or material failure, cannot be known. However, observations of ATEx after jettison from STEX will contribute useful statistical data to the topic of space tether survivability.

ACKNOWLEDGMENTS

Stephen S. Gates is the lead dynamicist on the ATEx project. He developed the NRL tether code and used it and GTOSS to produce all the graphical results shown in this paper. Additionally, Steve provided many valuable comments to improve this paper.

Dr. K. T. Alfriend provided the libration control laws.

REFERENCES

- 1. Shepard, Donald, Edward Pierson, and Frank Kustas. Simulated Space Environment Exposures and Mechanical Properties Testing For Long-Life Space Tethers. Denver, CO: Lockheed Martin, Sept. 5, 1995.
- 2. Kustas, Frank. Evaluation of the Effects of Vacuum Exposure on Tether Samples For Long-Life Space Tethers. Denver, CO: Lockheed Martin, Sept. 11, 1995.
- 3. Koss, Steve. "Tether Deployment Mechanism for the Advanced Tether Experiment (ATEx).", In 7th European Space Mechanisms & Tribology Symposium, Noorwijk, Netherlands, October 1997.
- 4. Alfriend, Kyle, William Barnds, Shannon Coffey, and Lynda Stuhrenberg. "Attitude and Orbit Determination of a Tethered Satellite System." In *Advances in the Astronautical Sciences*, Vol. 90, Part 1, 1995: 831-848.
- 5. Purdy, William, Shannon Coffey, William Barnds, Bernard Kelm, and Mark Davis. "TiPS: Results of a Tethered Satellite Experiment." In *AAS/AIAA Astrodynamics Conference*, August 4-7, 1997, Sun Valley, ID, 97-600.
- 6. Melfi, Leonard, et al. "Engineering Performance of the SEDS Tethered End Mass Payload." In *AIAA Space Programs and Technologies Conference and Exhibit*, September 21-23, 1993, Huntsville, AL, 93-4769.
- 7. Chapel, Jim, and Howard Flanders. "Tether Dynamics and Control Results for Tethered Satellite System's Initial Flight." In 16th Annual AAS Guidance and Control Conference, February 6-10, 1993, Keystone, CO, 93-042.
- 8. Juang, Jer-Nan, and Richard Pappa. "An Eigensystem Realization Algorithm for Modal Parameter Identification and Model Reduction." In *Journal of Guidance, Control, and Dynamics*, Vol. 8, No. 5, September-October 1985: 620-627.
- * TiPS Web Page http://hyperspace.nrl.navy.mil/TiPS/home.html

Page intentionally left blank

Session III—Future Missions

Page intentionally left blank

A Station Tethered Express Payload System (STEPS)

Joseph A. Carroll Tether Applications Chula Vista, CA 91913 (619) 421-2100, -2111 fax tether@home.com July 6, 1997

Introduction

Most capsules designed to return payloads from earth orbit use rockets for deorbit. They have modest payload mass & volume fractions. Active attitude control raises costs, and the deorbit rocket imposes risks which increase development and operational costs. This note describes an alternative concept now being developed under NASA SBIR Phase II funding. It uses a tether to both deorbit and orient the capsule. This allows simultaneous reduction of capsule complexity, cost, loads, hazards, and reentry errors.

The flight of SEDS-1 in 1993 proved out the basic concepts (ref. 1). A 20 km tether slung a 26 kg payload back to earth from a 740x190 km orbit, accurately enough for a pre-positioned observer to videotape the reentry. As air drag built up just before reentry, the tether was blown back and became a kite-tail, with tension increasing as predicted before flight. The tether was still attached at ~110 km, when telemetry was lost.

For tethered capsule deorbit, the station ejects the capsule downward at 0.6 m/s. This will deploy ~1 km of tether, by which time gravity gradient forces are strong enough to continue deployment. The capsule drifts forward and deployment rates rise to 15 m/s. A capstan-type brake adjusts the deployment tension and brings deployment to a smooth stop. Then the tether and capsule swing back to the vertical and are released. The tether drops the capsule perigee ~13 tether lengths, so deorbit requires a tether length of 8% of perigee altitude. Rate feedback during deployment allows enough control of deployment and swing timing to limit the capsule recovery zone to an acceptable size. As on SEDS-1, the tether serves as a kitetail to orient the capsule just before reentry, and a lossy attachment "whip" damps out oscillations. Spin can be used to null out lift during reentry.

Why STEPS?

Payload return opportunities to earth from the International Space Station are limited to 4-5 shuttles, 2 Soyuz, and 4-5 Progress flights each year (the Progress burns up, but it can deorbit a "Raduga" capsule with ~100 liters of payload). To increase the duration of "microgravity" periods on the station, traffic is being clustered. As a result, payload return opportunities are often 2-3 months apart. This can be a severe constraint, especially on inherently iterative R&D projects. We first proposed STEPS to expedite such R&D, but the list of potential uses is now much longer:

Potential STEPS Payload Categories

- 1. Microgravity materials samples and products
- 2. Station ORUs needing quick repair and return
- 3. CD-ROM disks, film, & other high-density data
- 4. Crew medical samples for research or diagnosis
- 5. Small animals needing prompt return to earth
- 6. Time-critical international payloads
- 7. Inside or outside environmental samples
- 8. Lower-priority items that fit in unused space.

Lifting vs Ballistic Reentry

Lifting entry reduces peak gee-loads on payloads, and can adjust reentry range and crossrange. But a closer look uncovers various problems. Lifting entry makes a capsule heavier, more expensive, and less robust, since more things have to work right. Also, ballistic reentry dispersions are small, and each day there are multiple recovery zones over water but near land. Poor control of a lifting entry can introduce large range and crossrange dispersions. This may force the recovery zone to be moved further out to sea, raising recovery costs and risks. However we do plan to scar STEPS for an optional GN&C & roll-control package, so that when necessary, STEPS can return payloads that cannot tolerate a 7-gee ballistic reentry.

STEPS Shape and Size

Once we decided to use zero or low-lift entries, we studied bucket, sphere, and Apollo-like shapes (see ref. 2). A bucket can right itself from most initial conditions, but it does not stow compactly, and has a far heavier heatshield than do Apollo shapes. Spheres do not allow compact stowage or lifting entry. An Apollo-like shape allows ballistic or lifting entry and a very light heatshield, but it needs a reliable means of orientation for reentry, such as the "kite-tail" effect seen on SEDS-1. The Apollo shape has another benefit: heatloads on the afterbody are only a few % of those on the forebody, so flexible TPS can be used there. This plus a shallow forebody allow compact storage.

After studying sphere-cone, spherical cap, and "Iso-Q" forebody shapes, we chose a spherical cap, because a spherical surface simplifies finishing, inspecting, and fitting. A 30° half-angle gives stagnation-point heating only ~15% higher than that of a properly trimmed iso-Q shape, and if the capsule has a modest CG offset, a spherical cap actually has lower peak heatloads and smaller lift coefficients. The forebody has "near-iso-Q" rim rounding, to reduce local heat loads and make the rim more resistant to handling damage. We now plan to use a ~30° half-angle conical afterbody, truncated to reduce capsule length.

The current baseline design is 78 cm in diameter and 63 cm long. This allows STEPS to fit through the Progress/Mir hatch, to enable early testing from Mir. This size also allows use on the space station without EVA, by using a robotic airlock in the Japanese Experiment Module (JEM).

STEPS Mission Scenario

Fig. 1 shows possible STEPS on-orbit operations. First the forebody mounts in a soft "trampoline." Up to 100 liters of payloads weighing up to 30 kg are attached with Velcro. Making the forebody oscillate axially allows mass and balance checks. CG offsets cause rocking, which can be detected by photopairs straddling the 3 springs. Small dense payloads are attached last, near the rim, to balance the forebody. Then the load is lashed down and the afterbody attached.

The capsule and a new tether mount in a folding Balancer-Ejector-Deployer (BED) assembly. The BED mounts on the JEM airlock's slide table and slides into the airlock. Then the door closes, the airlock is pumped down and vented, the outer door is opened remotely, and the BED and slide table are extended. The JEM "fine arm" near the airlock grabs the BED and moves it to a nearby trunnion pin. The BED holds the pin and uses it to react ejection and tether loads. The arm itself provides power and datalinks to the station.

On command, STEPS is ejected at ~0.6 m/s. The ejector uses a soft onset and long stroke to limit reverse-gee forces on payloads. The ejector also induces a slow capsule spin, to limit range errors. The 32 km tether deploys & swings to the vertical in 2 hours. Differential GPS (dGPS) can be used to compute the best tether release time, and later to vector the recovery helicopter to the capsule. A half hour after release, drag blows the tether back and orients the slowly spinning capsule for reentry. The tether burns off; capsule reenters ballistically; and then it opens a parachute once it reaches ~10 km altitude.

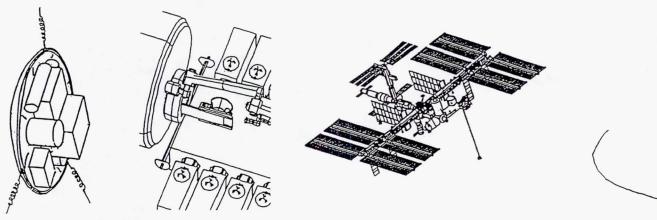


Figure 1. Possible STEPS Operational Scenario

Soft Mid-Air Recovery Technique

We plan to use mid-air recovery because it allows a simpler capsule, low peak gee-loads, good range safety, and many recovery sites. Previous methods required high closure rates & special winches (see ref. 3). Those capabilities have largely been lost, so we are developing the concept shown in Fig. 2. It uses simple recovery hardware which includes a folding hoist. A travelling recovery crew can carry it to a helicopter based near the recovery site, and install it during flight out to the recovery zone.

The crew vectors to the capsule with dGPS or a tracking receiver. After rendezvous, they slow down, open the cargo door, and deploy a folding boom. The boom angles outward so the pilot can see the boom and target throughout approach and capture. Angled slots in the boom snag a capture line on the chute. The ram-air chute's forward speed allows low closing rates and soft captures.

After capture, the helicopter flares into level flight and slows down until its downwash moves forward enough to collapse the chute. Then a weighted inverted funnel is lowered over the boom, chute, lines, & bridle. The funnel deploys a tubular mesh that traps the chute and lines, to allow their safe retrieval. The funnel has a lobster trap arrangement that snags the bridle and lifts STEPS when the funnel is lifted. Then STEPS is hoisted up and swung through the door with the hoist. Then the chute and boom are boarded, and the door closed. Then the helicopter returns to base.

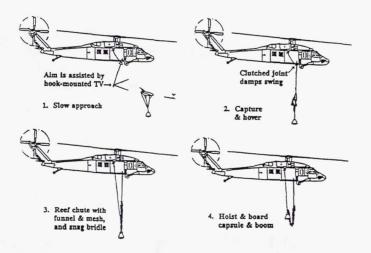


Figure 2. Soft Mid-Air Recovery Technique

Research pilots at NASA Ames say the Blackhawk helicopter is suitable for this operation. They say that flying qualities are adequate under relevant conditions (20-50 knots & 900 fpm descent rate). They say they have no qualms about going 500 km from land in the twin-turbine Blackhawk, if they have over-the-horizon com hardware & redundant inertial navigation. The Blackhawk has > 550 km usable radius with two 220 gallon external tanks. The tanks do not hamper chute or boom visibility, or interfere with use of the standard winch.

STEPS Hardware

The forebody is a graphite/phenolic dish covered with ceramic tile. The afterbody is coated quartz cloth and MLI insulation over graphite/phenolic "tentpoles." Other hardware includes:

Active Capsule Components

- o Ejection spring, pilot chute, and ram-air chute
- o A pressure switch & cutters to deploy chutes
- o A telemetry transmitter or radio beacon
- o Batteries and safe/arm/fire circuits

The Folding "BED" (Balancer/Ejector/Deployer)

- o Springs, sensors, and LEDs for balancing
- o A 3-arm slingshot that also spins the capsule
- o A reloadable mini-SEDS tether deployer
- o A SEDS brake/tensiometer/cutter assembly
- o A JEM arm interface & trunnion pin socket
- o A control computer, GPS, & video cameras

Other Support Requirements

- o A supply of 32 km long tethers (~2 kg each)
- o Launch supports and ~200 liters storage space

Table 1. Tentative STEPS Timeline

Start	Time	
Hr:Mn	Hr:Mn	Activity
0:00	0:10	Set up balancer & mount forebody
0:10	0:20	Velcro payloads in place & balance
0:30	0:10	Cinch payloads & attach afterbody
0:40	0:20	Mount tether & capsule in deployer
1:00	1:00	Mount in airlock, close, pump down
2:00	0:30	Grab assembly, position, and wait
2:30	2:00	Deploy tether, swing, and release
4:30	0:30	Coast until tether burns off
5:00	0:10	Reenter, and open chute at 10 km
5:10	0:20	Descend and get captured at 2 km
5:30	1:00	Helicopter returns & lands at base

Station "Microgee" Constraints on STEPS

The space station program has promised users at least 180 days/year of "microgee" operations, in increments of at least 30 days. The relevant part of the specification here is the "quasi-steady-state" environment, which is for frequencies <0.01 Hz:

- < 1.0 ug acceleration at 1/2 of the user racks
- < 0.2 ug normal to the mean residual acceleration
- < 0.02 ug imposed by any single component

The peak load imposed on the station by a 40 kg capsule is 15 newtons, or 3.7 ug. This is discouraging for the 180 days/year that it applies, particularly since microgee periods are usually followed by down traffic within 1-3 weeks. But some periods are followed by maintenance rather than launches, so STEPS could have unique value then. In addition, shuttle launches are often 1-2 weeks into a non-microgee phase, so STEPS could return components to earth for repair and prompt STEPS also allows payload return independent of shuttle launch slips. This may be critical for some users. Also, the space station may need to relax its microgee spec for other reasons. Finally, station users may find STEPS useful enough to obtain waivers to allow its use.

Other STEPS Constraints and Issues

Station ground tracks and recovery site weather constrain STEPS, but may not be a problem: the US has ~8 off-coast opportunities/day, over ~15 hours, and Russia, Europe, and Japan each have several chances per day. Over 2000 Blackhawks are in use in 16 countries, so this should not constrain recovery much. Restricting recovery to daytime VFR weather reduces the opportunities, but with experience that may not be necessary.

The tether uses two intermittently-bonded strands to reduce the risk of cut by micrometeoroids, and has a safety factor >4, but there is no way to absolutely preclude failure. If it does fail under load, it will recoil and 100-200 m may foul on the station. Any fouled tether will have to be blown away with jets or cut with a laser or a hot wire.

Finally, STEPS will impose torques on the station. Like a dancer who leans back to keep balance while swinging a partner, the station needs to pitch up ~15° during deployment, so the swinging tether will just pull it back to its normal attitude.

SBIR Phase II Effort (Feb 96-Feb 98)

Our SBIR Phase II effort includes these tasks:

- o Develop and test "Mini-SEDS" tether deployer
- o Develop forebody/TPS fabrication techniques
- o Develop and test mid-air recovery technique
- o Develop several other needed components
- o Refine mission scenarios and capsule design
- o Deliver 2 protoflight capsule assemblies

If work during Phase II indicates that Progress-based flight tests are feasible and affordable, then protoflight capsules can be identical to operational ones. Otherwise they will be adapted for other launch vehicles. One possibility is to launch as a Delta secondary payload, mounted much the same way as Losat-X. In this case, the deployer and computer can be mounted inside the capsule, to allow recovery and reuse of those components.

Phase II does not include standard off-the-shelf items, the folding BED assembly, mid-air recovery tests with large helicopters like the Blackhawk, or any formal testing. We plan to propose work on those items as part of a flight experiment, once we are confident of success on the Phase II effort.

Acknowledgements

Most of the work described above is supported by NASA MSFC under SBIR contracts NAS8-40544 and NAS8-40645 and purchase order H-2592D, all with Chris Rupp as contract monitor. Colleagues at Tether Applications and at Performance Designs, Boeing, NASA Marshall, and NASA Ames provided invaluable assistance.

References

- 1. J.A. Carroll, SEDS Deployer Design and Flight Performance, in Proceedings of 4th International Conference on Tethers in Space, April 1995; pub. by Science & Technology Corp., Hampton, VA.
- 2. Maxime A. Faget, Preliminary Studies of Manned Satellites, Wingless Configuration: Nonlifting, NASA TN D-1254, March 1962.
- 3. M.J. Ravnitzky, "Catch a Falling Star: Parachute System Lessons Learned During the USAF Space Capsule Mid-Air Recovery Program, 1959-1985," AIAA paper 93-1243, in Proceedings of the 12th RAeS/AIAA Aerodynamic Decelerator Systems Technology Conference and Seminar, London, England, May 1993.

Multiple Tethered Satellites for Ionospheric Studies (MTSIS)

B. E. Gilchrist

Space Physics Research Laboratory, University of Michigan 2455 Hayward, Ann Arbor, MI 48109-2143

R. A. Heelis

Center for Space Sciences, University of Texas at Dallas Richardson, TX 75080

Abstract

Multiple Tethered Satellites for Ionospheric Studies (MTSIS) is a new mission concept study sponsored by NASA Space Physics intended to place a multiple tethered satellite mission on firm footing as a means to significantly advance our understanding of ionosphere-thermosphere-magnetosphere coupling processes. Many scientific questions concerning the distribution of plasma structures and electromagnetic fields in the ionosphere must separate space and time variations with minimal ambiguity. The controlled vertical separation of measurement platforms offered by a tethered configuration makes resolving vertical gradients along nominally horizontal orbit tracks practical. In this report we illustrate scientific questions which could benefit from such vertical gradient measurements including the study of auroral acceleration regions, equatorial spread-F, and ionospheric layers. A conceptual design is described which is being used to expose critical issues required for a feasible scientific mission. These issues include the selection of appropriate tether geometries and materials to address survivability issues from micrometeoroid and atomic oxygen flux while minimizing atmospheric drag, a sensible methodology and design for tether deployment, mechanisms for satellite attitude control, instrument payload accommodations, and a sensible power and communications design.

1. INTRODUCTION

Recently there has been growing recognition within the space science community of the importance for achieving a better description of the spatial and temporal variations in planetary atmospheres. The task of separating spatial and temporal variations is not straightforward due to the many spatial directions over which temporal variations may take place. Imaging in two horizontal directions with sufficient time resolution provides an important step to describing the spatial and temporal variations, but may not provide unambiguous information about the physical processes at work which are responsible for

the variations. Thus, it is important to consider specialized satellite configurations which may shed light on these processes.

It is well recognized that horizontal separation of observation locations is adequate for defining the horizontal variations of physical phenomena such as large scale convective motions and the global configuration of the aurora. This horizontal separation may be achieved with two-dimensional imaging or by multiple satellites in the same orbit. If the variability of the phenomenon is largely horizontal and exists on time-scales that are larger than the time taken for a satellite to traverse the phenomena, then much of the relevant physics can be exposed by high temporal sampling from a single satellite. This is the premise behind NASA's Fast Auroral Snapshot (FAST) Small Explorer mission. However, if important physics is embedded in horizontal and vertical variations then a single satellite cannot provide the required information. Attempts to provide vertical separations at the right place and time with individual satellites is extremely difficult and cannot be sustained over long periods of time such that statistical uncertainties can be removed. However, if the required vertical separations are of order 10 km or so, then they can be easily retained for extended periods by utilizing a tether to connect two or more observing platforms [Gilchrist, et al., 1997] and this represents the focus of the Multiple Tethered Satellites for Ionospheric Studies (MTSIS) study. As an exampleof multiple tethered satellites, Figure 1 shows the location of a three satellite system at various locations along an elliptical orbit. The satellite configuration is shown with respect to some plasma feature that is limited in latitudinal and altitudinal extent. It can be seen that if the feature is not moving rapidly with respect to the satellite traversal time, then its features are described by deconvolving the temporal signals from the three platforms.

The space tethered satellite concept has been under serious development for more than a decade. To date, four orbital demonstration and science flights have been successfully flown from unmanned launch vehicles and two flights have also been conducted from the space shuttle. In addition, numerous sub-orbital tethered rocket flights have been conducted successfully starting in the early 1980's and continuing to the present [James and Rumbold, 1995]. Thus, recent set-backs in the engineering associated with long conducting tethers from the shuttle should not be applied detrimentally to the notion of tethered satellite systems in general. Specifically, high-voltage electrical arcs which were encountered during the flight of TSS-1R are not of concern for multipoint applications discussed here since current conduction along the tether is not required.

This paper is organized as follows. Section 2 provides some examples of scientific questions which motivate the need for multipoint measurements. Section 3 describes the MTSIS conceptual design while Section 4 provides more detailed description of technological considerations as well as relevant efforts to improve upon tether state-of-the-art. Table 1 identifies the MTSIS PI/Co-I team who, along with engineers from NASA's Marshall Space Flight Center, are conducting the new mission concept study.

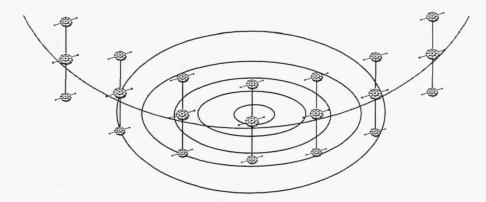


Figure 1. Schematic illustration of a three satellite system executing an elliptical orbit through an ionospheric feature. The same satellite system is shown at various locations along the trajectory.

Table 1- MTSIS PI/Co-I Team

Principal Investigator:

R. Heelis, The University of Texas, Dallas

Co-Investigators:

B. E. Gilchrist, The University of Michigan

W. J. Raitt, Utah State University

L. Johnson, Marshall Space Flight Center

R. Hoyt and R. Forward, Tethers unlimited

2. SCIENCE MOTIVATION

Tethered spacecraft systems can address a number of scientific challenges by advancing our understanding of those physical situations requiring controlled, vertically separated measurements. To illustrate, we briefly discuss below three compelling science examples which require the use of tethered satellite systems to make vertical gradient measurements.

Magnetospheric-Ionospheric Coupling: Auroral Acceleration Region

Extensive investigation of auroral acceleration processes has led to a rather common picture wherein a parallel electric potential is distributed along the magnetic field lines. This potential serves to accelerate the electrons at the top of the ionosphere in accordance with an "Ohm's law" condition (e.g., Lyons [1980]). The way in which the field-aligned potential is distributed along the field line is not well understood. There are suggestions that it may be distributed over large distances with quite small parallel

electric fields involved. Alternatively, the potential may be distributed over quite small distances in a configuration like a double layer. So-called V-shape and S-shape potential distributions have been used to describe such a configuration. Figure 2 shows the potential distribution consistent with narrow spike-like horizontal electric fields observed in the topside ionosphere. Modeling of these double layers suggest that they are not stationary structures but may propagate between the high and low potential ends of the flux tube [Singh and Schunk, 1982] and indeed evidence for potential drops extending down to quite low altitudes has been presented [Heelis, et al., 1984]. Answers to the following questions would aid considerably in our understanding of this phenomena.

- 1) How does the field-aligned potential distribution change as a function of altitude?
- 2) What is the change in electron pitch-angle distribution at different altitudes?
- 3) What is the dependence of these features on horizontal scale-size?

Again we emphasize that these key questions can only be addressed with measurements in which a controlled vertical separation in the observations is achieved.

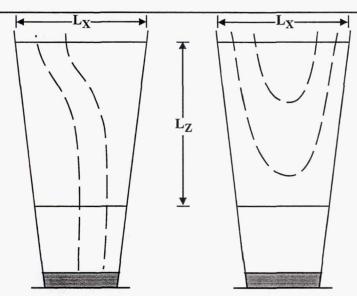


Figure 2. Schematic illustration of the electrostatic potential variation as a function of altitude associated with auroral particle acceleration. (after *Kan and Lee* [1981])

Spread-F

Equatorial ionospheric structure is a pervasive feature of the nighttime ionosphere. The structure is responsible for anomalous reflections of HF radio signals radiated from the ground and for phase and amplitude scintillation of VHF and UHF radio signals propagating through the region. Our understanding of the formation and

evolution of so-called "spread-F" is quite primitive due in part to the interdependence of the small-scale horizontal structure and the underlying vertical gradients in the plasma and neutral constituents [Mendillo, et al., 1992]. Considerable advances in our understanding of the formation of initial polarization fields in spread-F bubbles and the subsequent upward motion of bubble plasma could be achieved by simultaneously measuring the horizontal structure and the vertical variations in the structure. To date we have accumulated statistics on where and when such plasma depletions are observed, but all the data pose the following questions.

- 1) Where is the structure with respect to the F-peak?
- 2) Is the bubble plasma accelerating upward?
- 3) How does the upward motion of the depleted plasma affect the background ionosphere as it moves upward?
- 4) How are the smaller scale features in bubble plasma associated with the larger scale gravity wave disturbances responsible for initial seeding?

These questions do not encompass the full range of scientific inquiry into the topic but they reinforce the realization that with simultaneous measurements in the same plasma depletion, but separated in altitude, answers to key questions concerning the production and evolution of spread-F can be achieved.

Ionospheric Layers.

There have been many observations of plasma layers in the bottom-side of the ionosphere's F-region which are thought to be formed by shears in the meridional and zonal horizontal wind fields of the region. Figure 3 shows an often used example of these layers and it points to several problems. First the composition of the layers is not well understood and second the role of neutral winds depends so greatly on the vertical wavelength and the background density gradients that it is not possible to determine the unique combination that produces any given layer without knowledge of the vertical gradients in the underlying atmosphere.

Bottom-side ionospheric layers may have a significant effect on the flux-tube-integrated conductivity depending on the altitude of their formation. The winds that produce the layers must have relatively small vertical wavelengths and thus drive local current loops in the lower F- and E-regions. Winds with larger vertical wavelengths drive current systems that are dramatically modified by the local conductivity gradients and in turn the large-scale convective motions of the ionospheric plasma is modified. The nature of the modification depends on the latitude and longitude extent of the conductivity modification. Observations of ionospheric concentration from an orbiting spacecraft suffer from an interpretive ambiguity. Variations along the spacecraft track may be signatures of ionospheric layers or simply the passage of the spacecraft through vertical variations in the height of the main F-peak. Such an ambiguity could be removed by simultaneous measurement of the ion concentration from tethered platforms spaced 5

to 20 km apart. Then, measurements of the ion concentration and the neutral and ion drift velocities would completely resolve questions surrounding the dynamics and electrodynamics of the layers.

In order to advance our understanding of these layers and their effects on the global electrodynamics of the region it is necessary to address the following kinds of questions.

- 1) What is the horizontal wind and its vertical gradient over the region of layer formation?
- 2) What role does the electric field play, if any, in the layer formation and evolution?
- 3) Is the layer "sheet-like" with large horizontal dimensions or "blob-like"?

While not inclusive, these questions are designed to emphasize the need for controlled vertical sampling across a layer region.

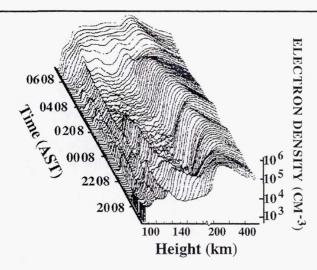


Figure 3. Ionospheric layers in the bottomside of the F-region are frequently seen at midlatitudes. They move slowly to lower altitudes during the night. (after *Shen*, et al. [1976])

3. MTSIS Conceptual Design

We are pursuing an implementation plan which utilizes three satellites tethered with a separation of 10 km for a total tether length of 20 km. Both common and unique requirements for satellite missions represnting the objectives of the three science examples above are being identified and addressed in this study.

We are considering several tethered satellite deployment scenarios for MTSIS. One approach assumes that two satellites are deployed from a central spacecraft up to a distance of 10 km using long-duration tether material. An alternative configuration places a primary spacecraft at the top (or bottom) of the configuration and the two sub-satellites are sequentially deployed downward (or upward), again with up to 10 km of separation between spacecraft. For the first case, the deployment hardware could remain with the primary spacecraft while for the second case deployment hardware would be placed on the sub-satellites. Both design approaches are being considered in light of a typical instrument and spacecraft sub-systems payload and the possible need to re-boost the deployed system at some point in its mission. The deployment system will be derived from the successful Small Expendable Deployer System (SEDS) used previously with detailed configurations to be determined from this study. We anticipate using a long-duration, low-drag, multi-stranded tether configuration, presently under development which is described later in this paper [Forward, 1997] will be used. Figure 4 shows an initial configuration of the multiple satellite system being used for the MTSIS study.

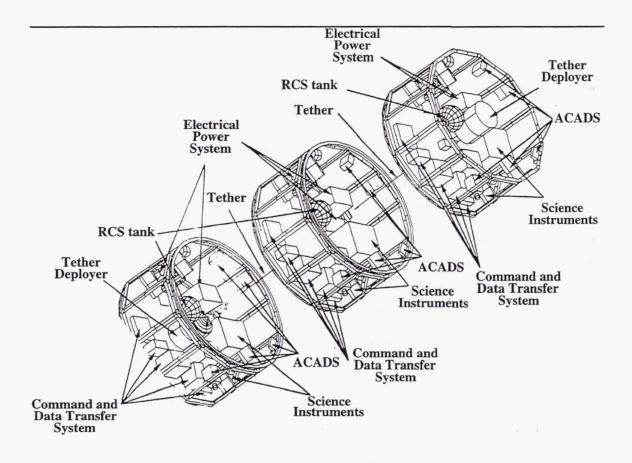


Figure 4. Initial configuration used for MTSIS systems studies.

The SEDS deployment procedure has a demonstrated success and, once deployed, the proposed configuration is stable along the radius vector due to the gravity-gradient force. In an elliptical orbit with perigee near 140 km, the satellite system will experience a significant differential drag that will change the orientation from the nominally radial direction. Preliminary studies show that this deviation will not be large (<10 deg), but detailed orbital analysis will quantify the system's behavior in different orbits.

An extended lifetime following low perigee excursions will require that the system be reboosted. The effects of such a reboost on the system dynamics and stability will need to be carefully studied. We note however that significant studies of auroral acceleration mechanisms and spread-F evolution could be undertaken without the requirement to penetrate low altitudes where atmospheric drag is high. The tethered satellite system would probably employ a "Med-lite" launch vehicle. We are targeting a mission plan which will allow a minimum one-year duration with observations taking place on at least a 75% duty cycle.

4. Technological Considerations

For the MTSIS study we have identified several key issues which need to be addressed in order that a sensible mission could be proposed within known constraints. For example, tether characteristics are important aspects to be considered for operational phases. Its survivability in the space environment and additional drag must be considered as part of mission design. Tether dynamical inputs to sensor platforms must be accounted for in the design of pointing systems. Finally, the requirement for simultaneous telemetry from multiple sensor platforms requires additional sophistication in the data handling system. Below we summarize these issues as discussed in our original proposal and in Gilchrist, et al. [1997].

Orbit Lifetime: Tether and Deployer Design

Long-lifetime tether systems require consideration of four critical issues: (1) survivability in a micrometeoroid and debris environment, (2) atmospheric drag, (3) tether material affects due to atomic oxygen flux, and (4) tensile strength requirements. Micrometeoroid survivability and atmospheric drag impose competing constraints. Atomic oxygen erosion constrains material selection. Both drag and atomic oxygen effects become more severe at lower altitudes.

To date, the predominantly-used non-conductive tether configuration has consisted of a single bundle of closely packed Spectra[™] strands. For such a tether, the minimum tether diameter has been determined by survivability considerations from micrometeoroid damage rather than tensile strength constraints. This has, for example, lead to strength safety margins of 80 or higher even for missions designed to last only a few days [Gilchrist, et al., 1995]. However, as tether diameter increases, atmospheric drag on the system increases. For example, a 20-km tether with only a 1-mm diameter still represents

a total cross-section of 20 m², a significant contributor in assessing overall atmospheric drag effects.

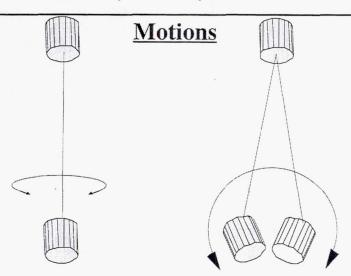
One promising approach that improves upon both tether survivability and atmospheric drag effects is the low-drag, long-life Hoytether [Forward, 1997]. Hoytethers are interconnected, multi-line net structures consisting of a number of primary load-bearing lines running the length of the structure with nearest-neighbor primary lines cross-linked by diagonal secondary lines. With proper design, the secondary lines remain slack when the primary lines are loaded and the structure maintains separation between the lines. Analysis shows that the redundant linkage provided by these structures enables them to achieve lifetimes measured in years to decades while the masses are comparable to single line tethers which have corresponding lifetimes measured only in days or weeks. By careful selection of the of the diameters of the primary load-bearing lines and the secondary "safety" lines, the structure can also be made to have an aerodynamic drag that is comparable to or less than the drag of a single line tether, while at the same time having less volume, less mass, and adequate load-bearing capacity. For example, Forward and Hoyt [1997] are studying one approach for MTSIS which uses two primary lines with 2.5-cm separation, dual cross-linked attachments every 12.5-cm, and tether material for all lines being 75-µm diameter single-fiber S-2 glass (optical fiber). Such a 20-km long tether design would have a survival probability of 98.6% after 2 years, have a total of 6-m² broadside area, and weigh 1 kg. Glass also has the potential for considerable atomic oxygen resistance, though this remains to be fully tested as of this writing.

Thus, the key issue will be a determination of the orbital drag and subsequent lifetime of the system. As mentioned earlier we can confidently consider a mission for which the perigee altitude is sufficiently high. However, we are also addressing the significant challenge of determining a useful methodology by which satellite propulsion can be used to re-obtain an given orbital configuration. In the three satellite MTSIS configuration, the reaction of the entire system to propulsion applied to one of the tethered masses must be determined. Knowledgeable inputs suggest that there are no specific problems attached to this maneuver, but part of our study includes determining the consequences of carrying a diminishing fuel supply and consuming that fuel for restoring a low perigee operations phase of the mission. There will, quite clearly, be trade-offs between accessible altitudes, orbital lifetime, and science payload mass that will need to be understood thoroughly for planning a mission.

Sensor Attitude Pointing

A tethered satellite system possesses unique dynamical responses which need to be considered in any pointing and control system. They are overall libration of the tether (described as an angle from local vertical), tether-satellite pendulous motions, and satellite yawing motions. The latter two are shown schematically in Figure 5. Tether satellite missions to date have shown that all these motions are well behaved and can be rather easily controlled. The SEDS-2 mission had satellite masses separated by 20 km

and displayed overall libration angles of less than 4° [Glaese, 1995]. Initial investigations of three-mass systems also show stable libration characteristics [Niles, 1995]. More detailed analysis of such motions given well-defined tether characteristics and satellite masses are planned for this study but we expect that, even with a low perigee, the libration characteristics will be easily tolerated by the instrumentation.



Satellite Pendulum and Yawing Motion

Figure 5. A space tether can couple its own dynamics into a spacecraft platform including pendulous and yawing motions, but can also act to damp such motions.

Pendulous and yaw motions also tend to be stable and can be dampened with time, but information available at present [Cosmo, et al., 1995] suggests that significantly large angles will require active damping and control. It seems perfectly feasible to employ a simple reaction wheel to control torsional yaw effects. At low and middle latitudes we anticipate that instruments to derive the cross track neutral winds and ion drifts will utilize arrival-angle measurements. It may be possible to use these instrument outputs in a nulling circuit to maintain a satellite look direction along the ram. Of course, more conventional sun and horizon sensors may be employed, but a trade-off between a new approach and the added mass of these systems should be considered.

Further, much of the science exposed in the above sections requires reliable determination of the relative velocities of the ions and neutral particles along the satellite track and between sensors. This determination only requires that the satellite system have very small short-term motions and not that these motions be accurately specified. Thus we point out that very accurate attitude determination may not be a strong requirement in many cases. However, there are certainly science questions that require the accurate specification of the absolute neutral and plasma drifts and thus may require a

specification of attitude to less than 0.1°. Such pointing requirements can be easily achieved using conventional star trackers and may only need be utilized on one of the satellite systems.

Multipoint Telemetry Requirements

Multiple tethered satellites introduce a requirement for simultaneously handling multiple telemetry streams. We are investigating two basic concepts shown in Figure 6. One allows independent command and telemetry traffic between the ground and each satellite. While straightforward, this requires each satellite to have appropriate power, memory storage, and computer "intelligence" for these operations. A second approach transmits telemetry to and from the ground from only one "host" satellite, with the other two satellites handling telemetry between themselves and the host. This requires the management of internal communications protocols and is more sensitive to a single-point failure at the host satellite, but allows much smaller transmitters on two of the satellites with appropriate reduction in the power requirements. At this time, we are only considering independent control from the ground to each satellite. We anticipate that work in this area will benefit from the wide variety of development work being conducted in the use and deployment of satellite constellations.

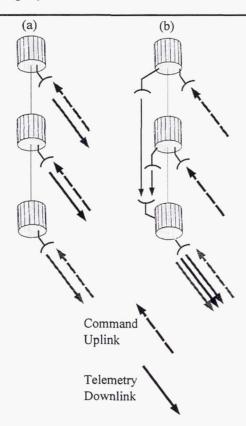


Figure 6. Communication system alternatives showing (a) independent telemetry from and commanding to each spacecraft, and (b) telemetry to a host platform where it is stored and transmitted as a single stream.

5. Conclusion

It is generally recognized that there are many phenomena, often those of greatest interest and controversy, which can not be resolved from the data of a single spacecraft. Multiple tether based sensing platforms "flying" in formation represents a new capability for space research which surpasses single satellite measurements by providing continuous measurement of vertical gradients. Focused campaigns using a multipoint tether system and drawing upon continuous ground based observations and global models offer the best opportunity for addressing complex physical phenomena. Here, we have provided examples of fundamental science questions which can be addressed and presented examples of technological concerns which are being addressed as part of the MTSIS investigation.

References

- Cosmo, M. L., E. C. Lorenzini and G. E. Gullahorn, Acceleration levels and dynamic noise on SEDS end-mass, paper presented at 4th International Conference on Tethers in Space, Washington, D.C., 1995.
- Forward, R., Highly survivable tethers, paper presented at *Tether Technology Interchange Meeting*, Huntsville, AL, 1997.
- Forward, R. and R. Hoyt, MTSIS Glass Fiber approach for low drag and high survivability, Personal Communications, 1997.
- Gilchrist, B. E., R. Heelis and W. J. Raitt, Ionospheric multi-point measurements using tethered satellite sensors, In Press, in *AGU Monograph on In-Situ Space Plasma Measurements*, Sante Fe, 1997.
- Gilchrist, B. E., R. A. Heelis, W. J. Raitt and C. Rupp, 1994 International Summer Workshop on Space Tethers for Ionospheric-Thermospheric-Mesospheric Science, Space Physics Research Laboratory, Ann Arbor, MI, 1995.
- Glaese, J. R., A comparison of SEDS-2 flight and dynamics simulation results, paper presented at 4th International Conference on Tethers in Space, Washington, D.C., 1995.
- Heelis, R. A., J. D. Winningham, M. Sugiura and N. C. Maynard, Particle acceleration parallel and perpendicular to the magnetic field observed by DE-2, *J. Geophys. Res.*, 89, 3893-3902, 1984.
- Hoyt, R. P. and R. L. Forward, Failsafe multistrand tether SEDS technology, paper presented at 4th International Conference on Tethers in Space, Washington, D.C., 1995.
- James, H. G. and J. G. Rumbold, The OEDIPUS-C sounding rocket experiment, paper presented at 4th International Conference on Tethers in Space, Washington, D.C., 1995.
- Kan, J. R. and L. C. Lee, in *Physics of Auroral Arc Formation* S. Akasofu, J. R. Kan, Eds. (AGU Geophys. Monograph, 1981), vol. 25, pp. 206-217.

- Lyons, L. R., Generation of large-scale regions of auroral currents electric potentials and precipitation by the divergence of the convection electric field, *J. Geophys. Res.*, 85, 1980.
- Mendillo, M., J. Baumgardner, P. Xiaoqing, P. J. Sultan and R. Tsunoda, Onset conditions for equatorial spread F, J. Geophys. Res., 97, 13865-13876, 1992.
- Niles, P., B. Gilchrist and J. Estes, Dual tethered satellite systems for space physics research, paper presented at 4th International Conference on Tethers in Space, Smithsonian Institute, Washington, D.C., 1995.
- Shen, J. S., W. E. Swartz and D. T. Farley, Ionization layers in the nighttime E region valley above Arecibo, *J. Geophys. Res.*, 81, 5517-5526, 1976.
- Singh, N. and R. W. Schunk, Dynamical features of moving double layers, *J. Geophys. Res.*, 87, 3561, 1982.

Page intentionally left blank

Tethered Satellite Investigations of the Ionosphere and Lower Thermosphere

By

R.A. Heelis University of Texas at Dallas MS FO 22 PO Box 830688, Richardson Texas 75083-0688

Abstract

The ability to resolve horizontal structures in the state variables of the lower thermosphere would considerably advance our understanding of this critical region of the geospace environment. Such measurements can only be obtained from a tethered satellite, where atmospheric drag on the very long tether is compensated by reboost of the mother vehicle. Such an arrangement could presently be accomplished using the space shuttle. Here we describe the rationale for consideration of such an undertaking and describe the known technologies that are required.

1. INTRODUCTION

The near earth atmosphere serves to absorb most of the harmful photon radiation from the sun, but it is the outer atmosphere, which incorporates a conducting medium, that in conjunction with the Earth's magnetic field acts as a barrier to electromagnetic and energetic particle radiation originating from the solar environment. Just as understanding the lower boundary interactions of the planet surface with the atmosphere is important, so too is our understanding of the interactions at the outer boundary. The outer boundary is extended in altitude, ranging from about 100 km at its lower bound to 10 Earth radii at the sub-solar magnetopause. The processes within this extended boundary are many and varied and range from consideration of collisionless, fully ionized, magnetized plasmas at the outer limits, to collision dominated, partially ionized, non-magnetized plasmas at the inner limit.

At the inner boundary limit lie the mesosphere and lower thermosphere/ionosphere (MLTI) regions where plasma and neutral dynamics are poorly understood due to the inherent complexity and to the difficulty in making required in situ measurements at these altitudes. Yet this is the region that is the sink for much of the energy delivered to the planet from above and generated internally below. It is the region through which all reentering space vehicles must pass. It is the region that is most sensitive to anthropogenic changes. In order to significantly advance our understanding of the behavior of this region we must make detailed in-situ measurements. This can be accomplished using sounding rockets, satellites with highly elliptical orbits, or satellites tethered from a much more massive deployer vehicle like the space shuttle. All these techniques have advantages and draw-backs and all bring a unique capability to the forefront. Over the past several years efforts directed toward the successful deployment of a tethered satellite from the space shuttle have been accompanied by many workshops aimed at advancing the capabilities of tethered satellites and the attendant deployment hardware. Much of the science rationale identified and discussed during these workshops has highlighted the advantages that tethered payloads would offer: prolonged horizontal sampling over small and intermediate scales in regions that are not readily accessible by orbiting vehicles.

2. SCIENTIFIC ISSUES

It is the not the intent to provide here a rationale and approach for the many science questions that require consideration of tethered payloads. Rather we seek to convey the importance of some of the questions, and the complexity involved in addressing them.

2.1 Ion-Neutral Interactions

Ion neutral interactions in the MLTI are complex coupled phenomenon that are illustrated in figure 1. The MLTI is where neutral wind oscillations of lower atmosphere origin (i.e. tides, planetary waves, and gravity waves) are of the same magnitude as those excited in-situ, and where these upward propagating components undergo severe dissipation. Therefore a wide spectrum of horizontal wave motions propagating upward from below are dissipated in this region, giving up their momentum to the mean flow. There are also substantial mutual non-linear interactions between these propagating components. The wind and wave motions are modified by charged particles through ion drag. Modification of the neutral wind is accompanied by modification of the charged particle distributions and thus the electrical conductivity. Electric fields applied from the

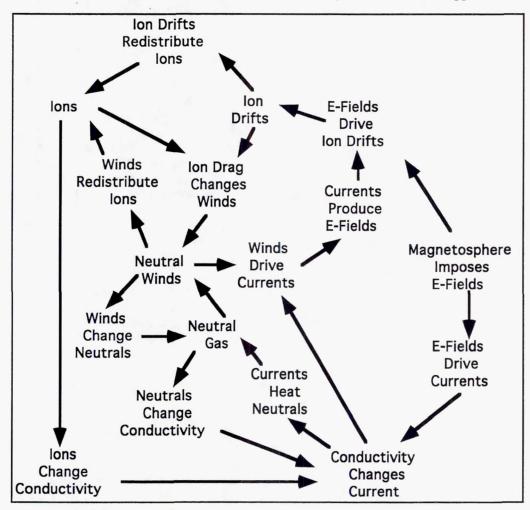


Figure 1. Illustration of ion-neutral coupling processes in the ionosphere-lower thermosphere system

magnetosphere drive convective motions of the charged particles, further modifying the neutral atmosphere dynamics. Through dynamo action, this mutually coupled system of dynamics and electrodynamics also produces electric fields that pervade the entire region by virtue of mapping along the magnetic field. This region also provides closure for the current generated by the global distribution of thunderstorms. The spatial and temporal scales of the electric fields and neutral motions span the range from less than 1 km to order of the planetary circumference and from a few minutes to many hours. By understanding the most important external influences on the region, and by understanding how the region responds to these influences, will be able to answer questions related to atmospheric drag and turbulence, electrical current generation, and the propagation of radio waves.

Two factors directly impact the structure of electrodynamic current closure. These are gradients in the conductivity and spatial variations in the neutral wind. These variations are undoubtedly inter-related since the winds themselves can produce spatial variations in the conductivity. Examples of such variations are dramatically seen in radar observations from Arecibo, Puerto Rico and are illustrated in figure 2. Here ionization layers that may be rather thin in altitude are produced by neutral wind induced ion motions parallel and perpendicular to the magnetic field. These motions result in ionization enhancements and depletions that are separated vertically by distances of 15 km or so. With reasonable assumptions about the nature of the neutral winds responsible for these ionization layers we may anticipate that their horizontal extent is quite large. The layers will appear as thin sheets

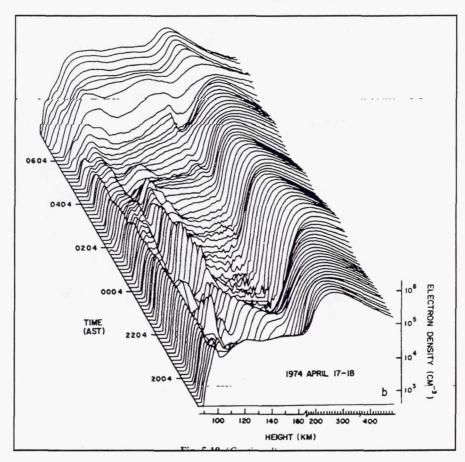


Figure 2. Thin Ionization Layers seen descending from the F-region peak are observed by the Arecibo radar [after *Shen et al.*, 1976]

that trace out the location of the convergent nulls in the neutral wind field. These sheets of enhanced density will provide regions of enhanced conductivity that will effect the current driven by winds. They produce very large altitude gradients in density at which radio signals will be severely distorted and partially reflected. Finally they provide the seat for a multitude of instabilities that may affect the propagation of radio signals from communication and navigation satellites. However, the horizontal spatial extent of the layers is unknown and critical in determining the full range of their effects.

2.2 Winds and Waves

Observations of airglow emissions from the region between 80 km and 100 km altitude show a wide variety of signatures indicative of gravity wave propagating in different directions with horizontal wavelengths near 100 km. This behavior can be contrasted quite dramatically with wave structure observed near 200 km indicating horizontal wavelengths that are larger by a factor of 10. The region between 200 km and 100 km is therefore one of sharply changing conditions with both horizontal and vertical gradient scales of 10's of kilometers. This is illustrated in figure 3 which shows evidence for a two-day wave that is propagating upward into the lower thermosphere. In this region

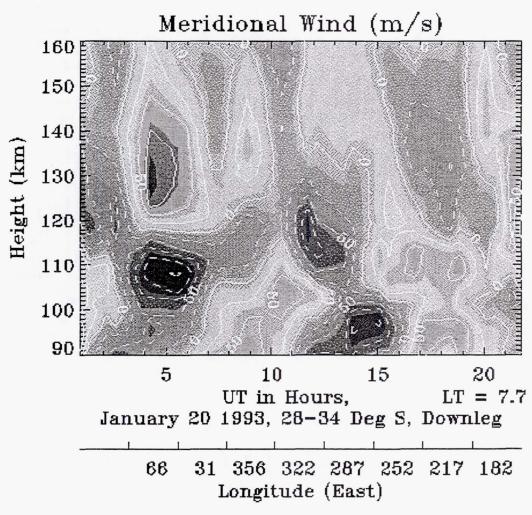


Figure 3. A 2 -day periodic oscillation seen in the meridional winds observed by UARS shows significant effects in the region above 130 km. [after *Ward et al.*, 1996]

the momentum from the wave will be transmitted to the charged particles and the resulting electric fields will be communicated throughout space.

The behavior of winds and waves in the region are closely coupled to perturbations in charged particle and neutral particle composition and density. Perturbations in the ion concentration will affect the currents that are driven by the wind systems and the resulting polarization electric fields that may be produced. They also change the ion drag experienced by the neutral gases and may in turn change the resulting wind system. It is essential to describe the relationships between spatial gradients in the neutral wind and density, and in the currents and the electric fields, in order understand how the wind fields propagate through the region.

A tethered probe can allow the altitude region where the conductivity increases with decreasing altitude to be directly surveyed. Measurements of the ion and neutral composition will allow the conductivity to be derived and spatial variations due primarily to changes in the total ion concentration can be measured with a resolution of 100 m or better. For the first time the local neutral wind can be measured. Changes in the characteristics with altitude will allow wave-wave interactions to be assessed and the mean flow to be determined. A multi-day mid to low latitude tethered satellite deployed from the shuttle could shed considerable light on the differences between, for example, the Andes and open ocean in "seeding" neutral atmospheric structure that eventually may drive instabilities at even F-layer altitudes. The same concept applies to regions of deep convective activity that are now routinely identified using satellite-based cloud brightness temperature measurements. The local wind driven current can be determined and compared to the total current to separate local and remote sources. With measurements of ion drift velocities, electric fields, and neutral winds made at the same rate it is possible to span the regime where electric fields "map" to distant plasma populations along the magnetic field lines and where they drive local current systems.

2.3. Radiative Cooling

In the region between 130 km and 200 km the major thermospheric cooling processes involve the collisional production of vibrationally excited states of CO₂ and NO and the excited fine structure states of atomic oxygen, followed by radiation. Cooling takes place when kinetic energy of the gas is transformed through collisions into internal energy of a molecule or atom which is radiated to space. A detailed understanding of the cooling processes occurring in the lower thermosphere and ionosphere is essential to modeling this region correctly and to providing an in-depth knowledge of the energy balance.

Thermospheric cooling rates due to collisions of NO and CO₂ with atomic oxygen are needed in order to make accurate models which have predictive capabilities. The continuing build-up of "greenhouse" gases such as CO₂ and CH₄ may profoundly increase the amount of cooling taking place in the lower thermosphere, the mesosphere, and even down into the stratosphere. Recent calculations illustrated in figure 4 indicate that the maximum temperature changes may occur in the region between 200 km and 130 km. However, there are considerable uncertainties in the CO₂ cooling rate which cause the predictions of the excess thermospheric cooling resulting from a doubled CO₂ atmosphere to vary from approximately 40° to 75° C. Definitive measurements of thermospheric cooling rates enables us to quantify this critically important upper atmosphere "global change" effect; one which is closely linked to the chemistry and dynamics of the upper atmosphere.

A tethered satellite probe carrying a neutral mass spectrometer measuring densities of O, NO, and CO₂ at altitudes between 130 km and 170 km, coupled with a limb-viewing

infrared spectrometer measuring at 5.3, 15, and 63 microns, would definitively determine the excitation and cooling rates. These measurements could be obtained quite readily in a single satellite mission lasting only several days.

TIGCM NEUTRAL TEMPERATURE (DEG K)

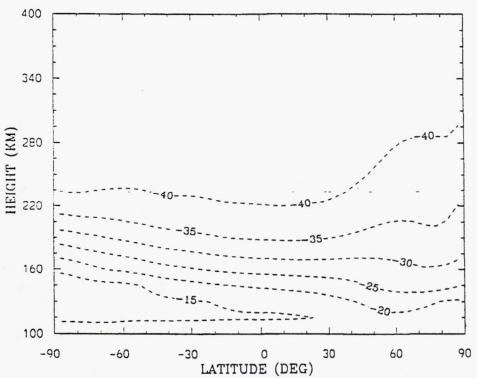


Figure 4. The predicted cooling due to doubling CO₂ and CH₄ is shown at solar minimum to have pronounced effects in the region between 200 km and 130 km [after *Rishbeth and Roble*, 1992]

2.4 Spacecraft and Instrument Interactions with the Environment

A tethered satellite mission to altitudes as low as 130 km provides a unique opportunity to study satellite and instrument interactions in a region where the atmospheric pressure is relatively high and the charged particle population is relatively low. Experience from the Atmosphere Explorer satellites suggests that even at 130 km the supersonic passage of the satellite through the atmosphere will not unduly affect the instrument performance provided that precautions to assure the cleanliness of spacecraft surfaces are taken. Nevertheless, we may expect that a significant ram cloud may develop around the spacecraft at the lowest altitudes encountered and a systematic examination by instruments with sensors inside and outside this cloud would prove extremely useful in understanding the nature of the cloud effects. For example, total ion concentration measurements taken by an e-field-probe, a langmuir probe, and a surface mounted ion trap would allow comparison of the ambient ion currents a different distances for the satellite surface. Ions produced by surface interactions will not possess ram energy, thus allowing for easy discrimination between these ions and those produced in the ambient environment. Interactions in the ram cloud may be more difficult to resolve, but these should produce ion fluxes that increase with decreasing altitude while the opposite dependence will be found in the ambient ion populations. Data taken in this critical atmospheric region will present interesting challenges that should yield information of interest not only to the atmospheric scientist but also to the aeronautical engineer.

3. REQUIRED MEASUREMENTS

The foregoing science discussions clearly illustrate the coupling between horizontal and vertical variations in the charged and neutral species. It is also apparent that the gradient scale lengths of importance may be quite small and not easily elucidated by remote sensing techniques. What is required is a strategic combination of in-situ and remote sensing of the lower thermosphere that will allow more insight into the coupling processes at work.

In-situ measurements from a tethered satellite must include the neutral and charged particle composition and density. These are clearly necessary to evaluate the ionospheric conductivity and the operative atmospheric chemistry critical for determination of the energy balance in the region. A measurement of the ion, electron, or neutral temperature, all of which should be equal in this altitude region, would also be a valuable addition to

specifying the energy state of the region.

In the lower thermosphere the electric field and thermal ion velocity are not the same and are coupled through the ionospheric conductivity and the neutral wind. Measurements of the electric field and the ion and neutral wind velocities are required to describe adequately the electrodynamics of the region and the roles played by local and remote sources of current. Recently algorithms have been developed to derive the horizontal current distribution from local measurements of the magnetic field vector. Thus, measurements of this quantity would be invaluable in describing the current closure

properties of the lower thermosphere.

In addition to coupling electric currents produced locally with those generated at higher altitudes, the lower thermosphere is also the upper layer for the global electric currents driven by the thunderstorm generator. Recent observations of upward lightning strikes to the ionosphere have prompted an investigation of the role of this phenomena in the large scale circuit and the effects on the ionosphere. One product appears to be the energization of charged particles that may subsequently affect the current carrying properties of the region. It therefore may be prudent to make measurements of the energetic particle environment to provide a global description of the average environment and perturbations from this condition in the event that storm systems are encountered. There is a clear advantage to be accrued from remote sensing at the tether satellite. At the tethered satellite a sensor in the far ultra violet may provide a global description of the gravity wave environment at altitudes only a constituent scale-height above the satellite. Monitoring the infra-red emissions in the limb would provide a measure of the atmospheric cooling rate in the region being directly sampled by the satellite borne sensors. Finally, visible monitoring of the Earth from above will provide information on lightning strikes and weather systems that provide perturbations to the region being sampled in-situ.

4. INSTRUMENTATION

The required measurements demand that a rather complete complement of instruments for measuring the particles and fields be considered. There is a very large flight heritage for such instruments although there are particular challenges related to instrument operations at low altitudes. The problems fall largely into three categories. One is associated with instrument operations at large ambient atmospheric pressures that will be even higher on the ram side of the spacecraft. This increase in ram pressure may be used to advantage in closed source spectrometers, but must be relieved with suitable venting to the

wake of the satellite when it jeopardizes the performance of high voltage electronics. Experience from the AE satellites suggests that the enhanced ram pressure does not adversely affect the performance of charged particle spectrometers [Hanson et al, 1981] but the effects are probably a strong function of solar activity and evaluation of these effects will be an intrinsic part of the scientific accomplishments of the mission. A second consideration is the very low charged particle concentrations at night. While large daytime populations can be rather easily measured by direct detection of the ion current to a collector, much lower concentrations at night will require consideration of sensitive electronics and perhaps particle counting techniques. Finally, the ram energy of the ambient neutral gas and the ram flux is sufficient to efficiently eject charged particles form ram surfaces. Experience from AE [Hanson and Heelis, 1975] suggests that the ion flux ejected in this manner may exceed the ambient thermal ion flux. Thus it is necessary to devise ways to suppress the emission and to identify ions liberated from a surface in this manner from the ambient ions possessing the ram energy of the satellite with respect to the sensor. It is evident that these problems can be overcome and we may confidently expect that innovative solutions will result from a flight opportunity. A significant data base will then be accumulated from this mission, describing the nature of spacecraft environment interactions in great detail.

Table 1 provides a list of the instrumentation to provide a first order estimate of the required resources in terms of mass, volume, power, and data rate. These factors will determine the optimal design for the tethered satellite and its subsystems. Most of the instruments require some special accommodation requirements, either to ensure an unrestricted look direction, or to provide deployment to some distance away from the spacecraft body. The list draws upon flight heritage from many previous space missions but it should be emphasized again that the challenges to making reliable measurements at low altitudes will likely be met with innovative new designs.

The Ion Drift Meter, Retarding Potential Analyzer, Ion Mass Spectrometer, Neutral Wind Meter and Neutral Mass Spectrometer all have apertures viewing along the ram direction and require an unrestricted field of view. The energetic particle detector can be body mounted to the side of the spacecraft so that an approximately 11° fan will be unrestricted in the 360° vertical plane parallel to the orbit plane. A simple UV photometer would have a narrow acceptance angle that would require zenith viewing uncontaminated by reflections from the tether itself. All other instruments require probe separation and/or separation from the spacecraft body itself. The magnetometer is a single sensor element that could be sensibly mounted in the wake on a boom of length exceeding 10 m. It is possible that for a satellite employing stabilizing fins in the wake, these fins could provide suitable mounting area for the magnetometer. Electric field double probes may be accommodated in a variety of ways and a detailed satellite design will be required to ensure accommodations that are acceptable to all instrument sensors. We envision three mutually perpendicular double probe pairs mounted so that two pairs are in the orbit plane and at 45° to the horizontal, and the other pair is perpendicular to the orbit plane. An infrared spectrometer utilized to measure radiative emissions from CO₂ and NO could sensibly be mounted on the tethered spacecraft viewing the limb from the wake.

As presented, this list and mission scenario represents the most ambitious undertaking that could be envisioned. It should be emphasized however, that a scientifically viable mission could be undertaken with a small subset of the instrumentation described here. For example, examination of the radiative cooling effects would require only the IR spectrometer and in-situ neutral mass spectrometer. These instruments do not

Table 1: Instrument Accommodation Requirements

Instrument Description	Sensor Dimensions (cm)	Electronics Dimensions (cm)	Sensor Mass (Kg)	E-Box Mass (Kg)	Instrument Power (W)	Telemetry Rate (bps)
Ion Drift Meter	12 dia 7 deep	21x12x16	0.9	2.3	3	2000
Retarding Potential Analyzer	12 dia 7 deep	21x12x16	0.9	2.3	4	1000
Ion Mass Spectrometer	18x12x11	18x12x16	1.8	2.0	6	500
Langmuir Probe	1 dia 15 long boom mount	15x15x10	0.35	3.0	4	5600
Neutral Wind Meter	16 dia 19 deep	18x12x16	2.1	2.2	8	1000
Neutral Mass Spectrometer	18x12x11	18x12x16	2	2.5	10	1000
Energetic Particle Spectrometer	19x15x18	Included in Sensor	2.2	N/A	2	8000
E-Field Double Probes	20 cm dia 6 deep	12x12x8	18 (3x6)	3	10	50K
IR Spectrometer	10x10x21	18x18x13	7	2	13	128K
UV Photometer	10x10x25	Included in Sensor	2.8	N/A	5	320
3-Axis Magnetometer	8x8x21	18x18x13	1	2.5	2	1600
Total Payload			39.05	21.8	67	199.02K

present any extended appendages that might increase the drag and affect the flight dynamics of the satellite. Similarly an investigation of ion-neutral coupling and its effects on winds, waves, and conductivity distributions could be undertaken only with thermal plasma instrumentation and neutral particle detectors. It is important therefore to understand that the payload described here is chosen to provide the maximum possible resource requirement. Failure to meet these requirements, or compromises to mission success produced by over subscribing the payload, will need to be carefully evaluated in order to ensure that a sensible approach is not abandoned prematurely.

5. TETHERED SATELLITE DESIGN

The tethered satellite design must incorporate the requirements placed on it by the science instrumentation, and also be consistent with accommodations requirements on the deployer. The mass, volume, power, and telemetry resource allocations for all the sensors lie comfortably within the resources that could be supplied by a battery powered tethered satellite. Therefore based on the legacy provided by previous tethered satellite missions figure 5 schematically shows a satellite configuration that would satisfy the anticipated needs.

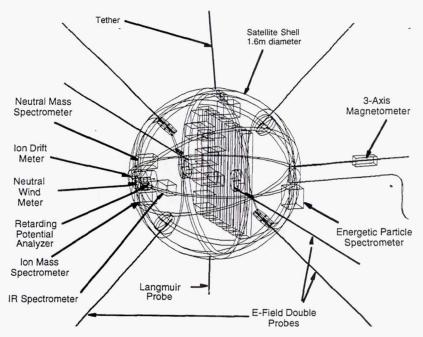


Figure. 5. Tethered satellite configuration showing internal instrument and subsystem locations.

The satellite structure is composed of an equatorial ring with two hemispheres of four flanged quadrants comprising the 1.6 m diameter satellite shell. A smooth surface is desired for aerodynamics and accommodation for deployable antennas will require local stiffening of the structure. Based on preliminary studies the estimated weight of the satellite structure is about 82 Kg.

The mission lifetime of six days requires significant battery power and volume. However, the requirements can be met within the satellite design indicated, with an anticipated battery mass of 105 kg. Ever advancing technology in this area leads us to confidently expect that this required mass is an upper limit, and that a tethered satellite mission would serve as a vehicle for exercising the latest technologies in this area.

Deployment of the satellite to altitudes of 130 km or lower will require serious consideration of frictional heating effects on the tether, the extended booms, and the satellite surfaces. Experience from previous highly elliptical orbiting vehicles is of limited value since the dwell time of such vehicles at low altitudes is relatively small compared to the mission envisioned here. It should be emphasized again, that the mission objectives can be tailored to minimize the hazards in this area. Additionally a deployment scenario can

be constructed for which the hazards from this source increase during the mission while not compromising its initial success. A flowfield temperature analysis performed for an altitude of $130 \, \mathrm{km}$, indicates that temperature variations occur in shock-layers ranging from $800 \, \mathrm{K}$ to $12000 \, \mathrm{K}$. The maximum aero-heating on the tethered satellite surface is about $3 \, \mathrm{kW} \, \mathrm{m}^{-2}$, and a combination of thermal blankets and heaters will adequately protect the satellite sub-systems.

The drag for a spherical shaped satellite of 1.6 m in diameter ranges from 0.92N at 130 km altitude to 0.11N at 170 km altitude. While the drag itself is a minor consideration in determining the orbit lifetime, it remains a consideration given the requirement to control the pointing of the instrumentation in pitch and yaw. A 'tail' assembly may aid in RAM pointing at the lowest mission altitude (~130 km), but active control will be required at all altitudes. A requirement to maintain a spacecraft axis within 5° of the RAM direction, and to provide post flight determination of axis orientation to less than 0.1°, will require a reasonably sophisticated approach. The use of reaction wheels and cold gas thrusters will need further investigation to determine an optimum configuration.

The science instrument data requirement could be quite substantial with options for sustained rates of 250 kbps over a six day mission. This requirement would be most readily met by direct RF communications from the sub-satellite to the deployer. UHF or S-band communications could be used for this task. In this case the data stream would need to be fully integrated with the science and engineering data from the deployer itself. Viewed as a separate high data rate instrument on-board the deployer it is not anticipated that this approach would present any unusual problems. A block diagram of the C&DH system is shown in Figure 6.

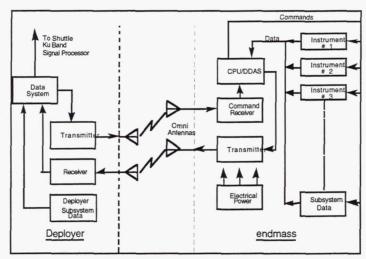


Figure 6. Example communications and data handling system block diagram.

6. TETHER CONSTRUCTION AND DEPLOYMENT

There are significant challenges to accomplishing a tethered satellite mission to the lower atmosphere. However, with the information above, it can be shown that available technologies would allow such a mission to be conducted. In fact considerable experience has been gained from the two tethered satellite missions accomplished from the space

shuttle and from the many tethered satellite missions conducted from rocket borne payloads. These experiences, coupled with on-going developments in tether technologies, allow us to describe a sensible mission, and detail the considerations that would optimize its performance.

In considering appropriate tether materials and construction there are three principal considerations. One is the impact of micro-meteorites and space debris on the tether itself. Another is the sensitivity of the tether material to degradation due to reactions with atomic oxygen. A third is the atmospheric drag experienced by the tethered satellite system, which for long tethers (>40 km) is dominated by the tether and not the orbiting end masses. For a limited duration mission, such as one conducted from the shuttle, the effects of atomic oxygen can largely be neglected. The potential for tether breakage due to micro-meteorites and space debris is significant, but can be overcome with appropriate designs. However, the impact of atmospheric drag on the tether itself is extreme and must be carefully considered in the conduct of the mission. The use of a single-line tether as shown in Figure 7, is a 1.65 mm diameter Kevlar strength member surrounded by a Nomex jacket with a total diameter of 2.16 mm. Such a tether has a break strength of 2892 N and weighs 4.03 kg per km. The tether is non-conducting and could be up to 110 km in length. The probability of tether survival in the micrometeoroid and debris environment of low earth orbit over a six day mission, assuming a critical particle size of 0.3 times the tether diameter, is approximately 0.93. Note that the mission described here does not require a conducting element in the tether. Thus the problems experienced on TSS-1R, associated with accommodating such a requirement, need not be anticipated in this case

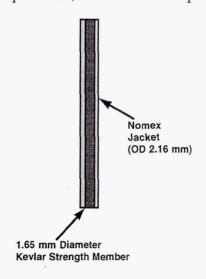


Figure 7. The single-line tether concept.

Alternate highly survivable tether designs could be considered for the mission. When considering comparative lifetimes, a single line tether may be compared to a multi-line design tether shown in Figure 8. This so-called Hoytape tether is made from much smaller individual tether strands widely separated from each other to increase the overall tether's likelihood of surviving a given impact. During such an impact, presumably, one strand would break but several would remain to pick up the load. The survival probability using a particle size of 0.3 of the tether diameter jumps from 91 percent for a single line tether to 99.99 percent for the Hoytape. The effective surface area of the Hoytape can be

made approximately the same as a reasonable thickness single strand tether, and thus the comments concerning atmospheric drag apply to both cases. The probability of survival is of course highly sensitive to critical particle size. Nevertheless Figure 8 indicates that significant improvement in expected lifetime can be achieved by consideration of the new design technologies.

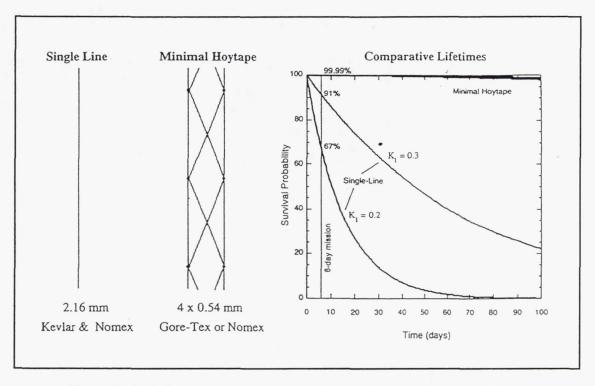


Figure 8. Lifetime comparison of a single strand and multi-strand tethers.

There are two types of deployers that could be considered for a lower atmosphere tethered satellite mission. A modified Tethered Satellite System (TSS) deployer and a modified Small Expendable Deployer System (SEDS). The TSS deployer, shown schematically in figure 9, has flown previously on two shuttle based tether missions. It incorporates hardware to capture and release a substantial satellite end-mass and to control the deployment rate and retrieval rate of the end-mass. The SEDS deployer system, shown in figure 10 has also been successfully used on several secondary payloads attached to the Delta launch vehicle. In the case of a tethered satellite mission conducted from the shuttle, significant re-design of the hardware would be necessary regardless of the chosen deployer system. These re-designs would involve the accommodation of the tethered satellite itself and the safety requirements imposed on the flight program.

The principal difference between these two systems is the ability of the TSS system to retrieve or reduce the effective tether length, whereas the SEDS system can only deploy the tether sequentially. Safety considerations concerning tether dynamics make it most sensible to adopt a mission implementation plan that cuts the tether at the end of the mission. Thus retrieval of the tethered satellite should not be a driver of the mission design. Nevertheless, the ability to increase and decrease the effective tether length is a consideration that requires further examination.

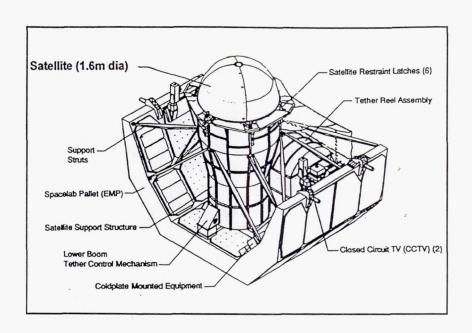


Figure 9. Tethered Satellite System deployer on a Spacelab Pallet.

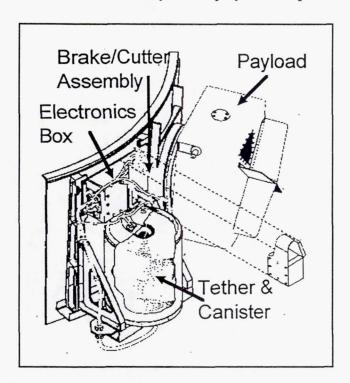


Figure 10. Small Expendable Deployer System shown as it was mounted on the Delta II launch vehicle.

The atmospheric drag on the tether and the satellite will induce libration oscillations of the tether system. This is due to the fact that the atmospheric density is not constant,

thus affecting the in-plane libration of the tether. Figure 11 illustrates the processes at work that may require consideration of mounting hardware for the sub satellite that will allow active control of the tethered satellite pitch in addition to the yaw control required by the instrument payload.

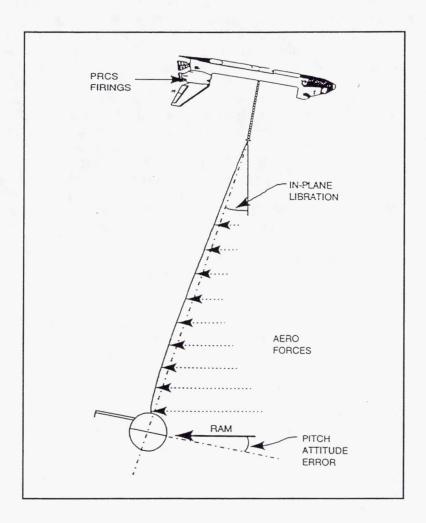


Figure 11. Illustration libration induced by atmospheric drag

MISSION IMPLEMENTATION

There are two essential parts to any mission implementation plan. One is the successful deployment of the payload, operation of the instruments and retrieval of the data. Second is the accomplishment of the science objectives. In the case of a tethered satellite mission, these are not separate considerations but must be carefully planned together to optimize the use of re-boost fuel, maintain the integrity of the tethered satellite system, and obtain the critically needed science data. Consideration of all these factors directs the mission plan toward a 6-day mission with the instrumented satellite deployed at altitudes of 170 km, 150 km and 130 km for each of 2-days.

In a "deploy only " scenario from a nominal 220 km circular orbit the tethered satellite is deployed downward 50 km to 170 km altitude and remains there for two days. On day three, an additional 20 km deployment of the tether lowers the tethered satellite to an altitude of 150 km where it remains for two days. On day five, the tether is deployed a further 20 km lowering the tethered satellite to its final 130 km altitude where it will remain for two days before the tether is cut ensuring re-entry of the sub-satellite. The deployer vehicle altitude will be maintained by use of its Primary Reaction Control System (PRCS). In the case of the space shuttle the estimate of fuel required for this scenario is 1996 kg (4400 lb.) making it a primary driver for the mission.

With a capability to partially or fully retrieve the sub-satellite and alternative implementation scheme could be considered In which the deployer vehicle enters a 280 km circular orbit. The tethered satellite is first deployed downward 110 km to 170 km altitude. As the orbit of the deployer/tether system decays, the tether may be retrieved (~15 km) to maintain the satellite at a constant 170 km altitude. By day three the deployer is at 265 km altitude and an additional 20 km deployment of tether lowers the tethered satellite to an altitude of 150 km. Again, more tether is retrieved (~25 km) to maintain the tethered satellite at 150 km as the system altitude drops over the next two days. On day five, the deployer enters a 240 km orbit and a final 20 km tether deployment lowers the tethered satellite to 130 km altitude where it will remain for two days. The deployer altitude will be maintained by use of its Primary Reaction Control System (PRCS) during the final two days before the tether is cut. In the case of the space shuttle the estimate of fuel required for this scenario is 364 kg (800 lb.).

A tethered satellite mission provides an opportunity for in-situ global diagnosis of a region of our atmosphere that has heretofore been inaccessible except in very limited temporal and spatial domains sampled by sounding rockets and ground-based facilities. The mission should provide a series of horizontal traverses at various altitudes through the upper E region. A high inclination orbit would provide data in the equatorial region, at mid-latitudes, and at the lower edge of the auroral region where electrical coupling to the magnetospheric generator would be strongest. A series of horizontal cuts at 170 km, 150 km, and 130 km (and lower if possible) would allow the transition region to be examined at each latitude and local-time. Note that the high latitude part of the orbit will encompass part of the closure region for field-aligned currents connecting the ionosphere and the magnetosphere. Thus, we can investigate the interactions of all three generators within the global electrodynamic system.

Access to equatorial, mid-latitude, and high-latitude regions, allows the effects of magnetic field geometry to be investigated. At low latitudes the dynamics of the region will be strongly influenced by the equatorial electrojet currents since neutral winds are ineffective in transporting plasma. At middle latitudes, neutral wind transport of plasma along the magnetic field may be extremely important, while at higher latitudes the Pedersen drifts from electric fields may be most important. Satellite passes through different latitudes will enable the neutral wind dynamics to be described in terms of the location of different sources. High latitude particle heating and magnetospheric penetration fields may produce neutral disturbances that propagate from pole to equator. Gravity waves originating from the tropical zone at the Earth's surface will propagate toward the pole. Diagnosis of the spatial spectrum of waves as a function of latitude and local time will allow the influence of these different sources to be assessed.

Such an investigative mission, utilizing the tethered satellite, must be coordinated by the entire community to include strategically chosen sounding rocket flights and

extensive observations from ground based facilities operating both radar and optical equipment. It is a unique opportunity to involve the entire community in an intense effort to further our understanding of the lower thermosphere.

REFERENCES

Hanson, W. B., and R. A. Heelis, Techniques for measuring bulk gas-motions from satellites, *Space Sci. Instrum.*, **1**, 493-524, 1975.

Hanson, W. B., S. Sanatani, and J. H. Hoffman, Ion sputtering from satellite surfaces, *J. Geophys. Res.*, **86**, 11350, 1981.

Rishbeth, H., and R. G. Roble, Cooling of the upper atmosphere by enhanced greenhouse gases-Modeling of thermospheric and ionospheric effects., *Planet. Space Sci.*, **40**, 1011-1026, 1992.

Shen, J. S., W. E. Swartz, D. T. Farley, and R. M. Harper, Ionization layers in the nighttime E region valley above Arecibo, *J. Geophys. Res.*, **81**, 5517-5526, 1976.

Ward, W. E., D. Y. Wang, B. H. Solheim, and G. G. Shepherd, Observations of the two-day wave in the WINDII data during January, 1993., *Geophys. Res. Lett.*, 23, 2923-2926, 1996.

ACKNOWLEDGMENTS

This work is supported in part by NASA grant NAGW-4492 to the University of Texas at Dallas.

This work reflects the efforts of an ad-hoc group of community scientists charged with investigating the benefits of a lower atmosphere tethered satellite mission, and a dedicated team of scientists and engineers at Marshall Space Flight Center who addressed the most critical problems arising during initial investigations of an implementation plan. The authors wishes to thank the following people for their contributions:

The ad-hoc science group

Bob Carovillano Kelly Chance Marlene DenHoutner Greg Earle Cassandra Fesen Jeff Forbes Jeff Hale Brian Gilchrist Fred Herrero Les Johnson Mike Kelley Kate Kirby Craig Kletzing Nelson Maynard Tom Moore Ko-Ichiro Oyama John Raitt Nobie Stone Tom Stuart Jim Vickrey Larry Zanetti

Science and engineering support

NASA MSFC Lockheed Martin

Harold Blevins (C&DH) Howard Flanders (Tether Dynamics, Orbit Analysis)

Holly Chandler (Mass Properties)
Greg Hajos (Configuration)
Kai Hwang (Environments)

Vern Lunsford (Tether Systems)
Lee Marshall (Tether & Deployer)

Lou Maus (Electrical Power) Science & Technology Corporation Steve Pavelitz (Environments)

Robert Shepard (Schedules)

Susan Spencer (Structures)

Viren Dogra (Thermal, Attitude Control)

Leonard Melfi (Aerodynamic Analysis)

Carey Thompson (Cost) George Wood (STC Lead)
Ken Welzyn (Tether Dynamics)

Page intentionally left blank

SPACE TETHERS DESIGN CRITERIA

Donald D. Tomlin, Gwyn C. Faile, Kazuo B. Hayashida, Cynthia L. Frost, Carole Y. Wagner, Michael L. Mitchell, Jason A. Vaughn and Michael J. Galuska

9/10/97

SPACE TETHERS

- The Small Expendable
 Deployable System and Tether
 Satellite System programs did
 not have a uniform written criteria
 for tethers.
- The JSC Safety Panel asked what criteria was used to design the tethers.
- Since none existed, a criteria was written based on past experience for future tether programs.

9/10/97

- Tethers are a single point failure and are susceptible to damage from mishandling.
 - Crimps, pulley pinch, vibration, rubbing,etc
- Testing should include offnominal(tight knots and slice through half the of strength member).
- Proof testing performed end-toend at flight temperatures or load adjusted for being at room temperature.

9/10/97

- To avoid being fragile all tethers should have a minimum ultimate strength of 100 lbs.
- During manufacturing all anomalous conditions should be assessed by engineering.
- Repairs should be qualification and proof tested.

9/10/97

- Tensile strength should be determine based on a minimum of ten samples.
- Breaking strength should be verified using end samples.
- Tethers should be limited to a single mission.
- Reflights should be evaluated on a case by case basis with consideration for strength and performance degradation due to space exposure, loading & anomalous conditions.

9/10/97

- Inspection and reproofing should be performed on all portions of tether exposed to potentially degrading conditions.
 - Qualification testing
 - Factor of safety(ultimate)
 - 5.0 Basic tether, splice and repair methods
 - 2.0 Off-nominal tether conditions
- Flight article is tested at twice the design load from end-to-end.

9/10/97

Meteoroid and Space Debris

- Meteoroids and space debris can sever tethers resulting in the remnants recoiling into the end bodies.
- Probability of tether sever is increased with tether length and time deployed.
- Probability of tether sever can be reduced by tether design and redundancy.

9/10/97

Meteoroid and Space Debris

Probability of tether sever is:

 $e^{-(particle_flux*area*tin)}$ I have $e^{-(particle_flux*area*tin)}$ Manned missions where severed tether could result in an immediate hazard to crew should have a probability of occurrence of less than one chance in a million.

9/10/97

Meteoroid and Space Debris

- Manned missions where severed tether could result in a hazard to crew(but not immediate) should have a probability of occurrence of less than 5 chances in a hundred.
- Loss of mission due to severed tether must be assessed on an individual basis regarding probability of occurrence.
- Hazards should be designed out of missions.

9/10/97

MATERIALS

- Material selections should consider processes, workmanship, radiation, atomic oxygen, storage, hygroscopic characteristic, ionospheric plasma and particulate contamination.
- Tethers containing electrical wires should be concerned with the insulation material (dielectrics, damage due to handling, penetration, and cracking).

9/10/97

MATERIALS

- Electrical tethers should also consider static electricity, corona, arcing, trapped gas and outgassing. A spark test should be the final test.
- Manufacturing and handling should consider processes and environments that are free of particulate contamination, chemicals, adverse storage conditions, and grounding condition which could cause arcing.

9/10/97

DYNAMICS

- The tether acts as a spring between end bodies resulting in oscillations(bobbing).
- Frequency and damping of bobbing depends on tether characteristic which varies with tension, temperature and length.
- Severed tether recoil velocity increase as tension increase.
- Thermal cycling excites bobbing thus low thermal expansion coefficient is desired.

9/10/97

DYNAMICS

- Tether torques are difficult to predict.
 - Ground handling should be careful to not incorporate twist.
 - If deploy adds twist, store twist on spool to nullify effect.
- Pulsating electrical current in tethers will result in skiprope type motion.
 - Proper phasing can damp motion.

9/10/97

SAFETY AND RELIABILITY

- Develop an approved quality plan.
- Have good tracebility records.
- Perform inspections and approval reviews.
- Assess nominal and off-nominal conditions for hazards.
- Design out hazardous conditions, if possible
 - If not, provide adequate crew reaction times

9/10/97

TO OBTAIN A COPY:

HARD COPY:

- Center for Aerospace Information
- Linticum Heights, Md 21090-2934

ELECTRONIC COPY:

- http:\\mtrs.msfc.nasa.gov\mtrs
- Pick 1997 documents
- Doc No. TM108537

9/10/97

Page intentionally left blank

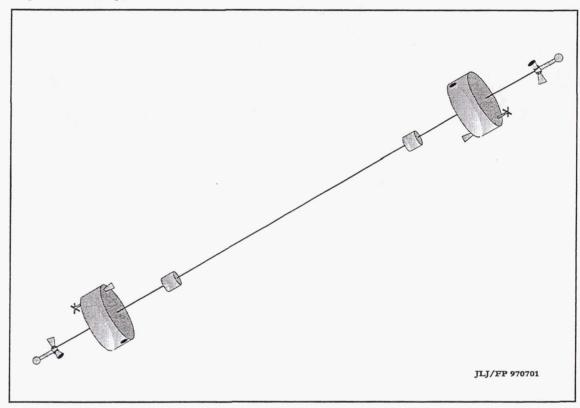
Department of Automation, Technical University of Denmark.

GRADSAT:

A DANISH GEOMAGNETIC GRADIENT MISSION

August 25., 1997/September 1., 1997

Ver. 1.1



In response to:

"Call For Proposals For A Danish Microsatellite Mission," for the "Concepts for Danish Microsatellites,"

A Workshop organized by the Danish Space Research Institute and CRI A/S at DMI on Sept. 4., 1997.

Proposing Consortium:

John L. Jørgensen,
José M.G. Merayo,
Mogens Blanke,
Nils Olsen,
Torben Risbo,
Fritz Primdahl,
Hermann Lühr,
DTU-IAU
DTU-IAU
AU-SATLAB
KU-NBI-GA
KU-NBI-GA
DTU-IAU/DSRI

Scientific Objectives and Basic Payload Concept
1.1 Science Overview
1.2 Satellites
2 Science Case
2.1 Detailed Description of the Project
2.1.1 Internal Fields
2.1.2 External Fields
3 Payload Concept
3.1 Science Payload
3.1.1 CSC Vector Magnetometer
3.1.2 Triple Head Star Imager
3.1.3 Overhauser Effect Trityl Based Scalar Magnetometer
3.1.4 Advanced TurboRouge GPS Receivers
2.1.5 Supporting Magnetoscheric Plants Discounting Lecture 1
3.1.5 Supporting Magnetospheric Plasma Diagnostics Instruments
3.2 Tether and Tether Mechanism
3.3 Spacecraft Total Estimates
4 Science Interest
4.1 Danish Science Community and Opportunities
4.1.1 Danish Solid Earth Research
4.1.2 Danish External Sources Studies
4.2 International Science Interest
5 Mission Requirements
5.1 Orbit Characteristics
5.2 Mission profile and life-time
5.3 Launch Time Requirements
6 Relation to Other Missions
6.1 Ørsted/SUNSAT
6.2 Astrid 2
6.3 SAC-C
6.4 CHAMP
6.5 GRACE
6.6 Overview of Tether Missions
7 Science Operation and Data Archive
7.1 Science Data Analysis
8 Technical Feasibility and Technology Development Requirements
8.1 The Tether Technology
8.2 The "Puppet-on-a-String" concept
8.3 Instrumentation Miniaturization
9 Management and Funding
9.1 Consortium Construction
9.2 Industry Management and Funding
9.3 Science Instrumentation Management and Funding
9.4 Science Data Handling and Science Analysis Management and Funding
10 References
APPENDICES
(A) Overview of Tethered Missions Flown and Flying
(B) Letters of Support
Gilbert W. Ousley BDM FEDERAL, consultant to NASA
Robert A. Langel Retired, NASA-GSFC Patrick T. Taylor NASA-GSFC
Michael Purucker Hughes STX Corp. and NASA-GSFC
William Webster NASA-GSFC
John LaBrecque NASA-JPL
Lars Sejr Kristensen TERMA A/S
(C) The TiPS Mission
(D) Danish Geomagnetic Gradient Mission Overview
(E) Call for the Tether Technology Interchange Meeting, Jim Harrison.

1 Scientific Objectives and Basic Payload Concept

We propose a mission of two identical tethered micro satellites for simultaneous two-point mapping of the Earth's magnetic field and of the first space derivative of the field. Launch in the 2002 time frame into a low altitude near polar and approximately circular orbit, slowly drifting in local time. An approximately 3 month's lifetime in the tether mode (similar to METS), continuing as free flyer(s) for up to 2 years depending on the actual solar cycle atmospheric swelling.

The Danish Ørsted Earth's field mapping mission brought Denmark into the international front in space magnetometry. A Danish Magnetic Gradient Mission will bring Denmark far ahead, and will consolidate our position in space magnetometry and advanced space technology.

The proposed 600-400 km altitude polar orbit and the 20km gravity gradient extended tether are optimized for simultaneous observations of the field signatures and for the separation of the field sources below the orbit, from sources traversed by the satellites and from sources above the orbit.

1.1 Science Overview

The pioneering Earth's field mapping mission, Magsat 1979-80, provided absolute vector field observation on essentially a shell of orbits enclosing the Earth (Fig. 1).

Almost 20 years of still ongoing analysis of the data has yielded a vast body of planetary science results. The limitations of the Magsat data set and of the mathematical analysis tools now begin to show up as a fundamental uncertainty in separating the field sources responsible for the Earth's magnetic signatures. The task is tremendous in discerning between fields originating in the Earth's core or crust, in situ ionospheric currents, and the more distant

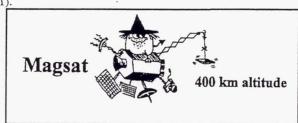


Figure 1 Magsat cartoon. Courtesy: Charlie Barton, Austral. Geol. Survey

magnetospheric currents. Fitting separate models to the sources, some of which are highly time varying, presents a challenge, which is at present met at the level of "a few nT's" residuals [Langel, lecture, 1997]. Contributions to the residual noise are manifold. Inabilities to mathematically extract further information from the data, perhaps owing to mathematical shortcomings or computational problems, but also because of the statistical nature of the phenomena and the inherent instrumental noise, and plausibly from still other as yet unrecognized sources.

Clearly, more information is needed, and the data from the planned Danish Ørsted and the German CHAMP missions are expected to add further high quality data to the Magsat set. Proposed multi-survey missions with several simultaneous mapping satellites in different orbits are highly desirable and will certainly lower the statistical fluctuations. The co-launch of the South African SUNSAT together with Ørsted is a valuable contribution to this.

The proposed Gradient Mission will add a new dimension to Earth's field observations. The vertical gradient of the vector field is measured along the tethered satellites' orbits, and this vector parameter constitutes an entirely new observational input to the mathematical modeling algorithms, in addition to the absolute vector field. This, and the recent progresses in instrument absolute accuracy and resolution, based on the Ørsted, Astrid-2 and CHAMP developments, will dramatically augment the accuracy of source separation discussed above.

The availability of two almost coincident closed shells of vector magnetic data will allow two independent and simultaneous model determinations of the core field, and for the first time provide a test of the validity and power of the mathematical procedures.

The addition of the vertical gradients of the field vector components, reflecting the close sources in the crust, will, for the first time, provide large scale crustal mapping and enable the national and continental magnetic surveys to be joined globally.

The vertical differences of the vector components, and the corresponding time changes along the orbits multiplied into the orbital velocity vectors allow for calculation of the curl of B perpendicular to the tether sweep plane. This curl is a direct measure of the ionospheric and field aligned currents (FAC's) flowing in the plasma between the two tethered satellite orbits, and determination of and correction for these field sources greatly facilitates the separation of external and internal sources. This, together with the gradient supported determination of the crustal fields, will dramatically improve the core field models.

New mathematical algorithms, including the curl-corrected gradients and corrections for the crustal signatures, will be developed for estimating the spherical harmonics coefficients to much higher order and degree than previously possible. This will give a new and much more detailed picture of the otherwise inaccessible Earth's liquid core flow pattern, and it will contribute greatly to the understanding of the physical origins of the Earth's magnetic field.

1.2 Satellites

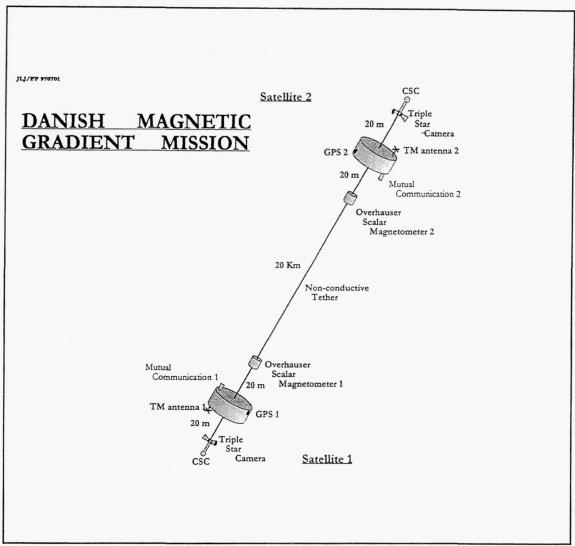


Figure 2 System overview.

Two exactly identical satellites, each carrying a 10 km tether, are joined together and flying with 20 km vertical separation. The "dumbbell" system is kept apart by the tidal forces, and the same gravity gradient effect is tending to align the tether vertically along the gradient. The two subsystems are identical, so that the satellites may interchange positions, and the mission is planned to be designed in a way, so that the system is tolerant to even large oscillations about the vertical equilibrium direction. The tether technology is well proven and operational, as follows from the list of 16 tether missions attached as appendix (A).

The supporting argumentation for a gradient mission is vitally based on the integrity of the tether. However, tethers in space are known to have limited lifetime, either as consequence of a tether disruption, or because of re-entry caused by the considerable air drag on the string. Therefore, we suggest that each satellite carries a cutting mechanism, the plan being to let the satellites cut the string, if the tether is severed by a hitting particle, or when, after some months, the mission is air dragged towards the atmosphere. The mission will continue after cutting the tether, either as two free fliers, or, in the case of an approaching re-entry, the top satellite will be lifted to a slightly higher orbit continuing the mission. The lower spacecraft is proposed cut from the loose end tether some days later bringing this satellite down to perhaps 300-320km for a closer look at the crustal fields. During spiraling towards re-entry, the free-flying lower satellite will provide much needed additional low altitude crustal anomaly data.

The satellites are exactly identical, and the primary science instrumentation on each satellite is proposed to consist of:

- GPS receiver for positioning
- CSC Vector Magnetometer
- Triple Head Star Imager System for absolute attitude

Supporting instrumentation is:

- Scalar Overhauser Magnetometer for CSC calibration
- Optional additional plasma diagnostics experiments.

The CSC magnetometer sensor and the triple head cameras are joined mechanically as a unit and extended 20 m away from the satellite held by the cables oppositely to the tether. This is the previously proposed "Puppet-on-a-String" concept [Jørgensen & al., 1996], which relieves the carrier spacecraft from requirements for strict satellite level magnetic cleanliness and magnetic calibration.

The Overhauser scalar magnetometer sensor is hinged to the tether at a position 20 m away from the spacecraft. (When the tether is cut, this is done at the satellite, and the magnetic sensors are foreseen kept extended on the flexible cable booms by the gravity gradient, or by centrifugal force in case the free flying satellite is spinning).

The satellite bus will carry the following systems:

- Computer
- Ground communication transceiver and antenna
- Low power inter-satellite communication microwave transceiver and antenna
- Electrical power supply systems including solar power panels
- Other satellite systems
- Tether w/mechanical systems including the deployment controls.

2 Science Case

The proposed mission will bring a new dimension into geomagnetic research by measuring the vertical gradient of the magnetic field in addition to the field itself. This is optimal for studying the following tasks:

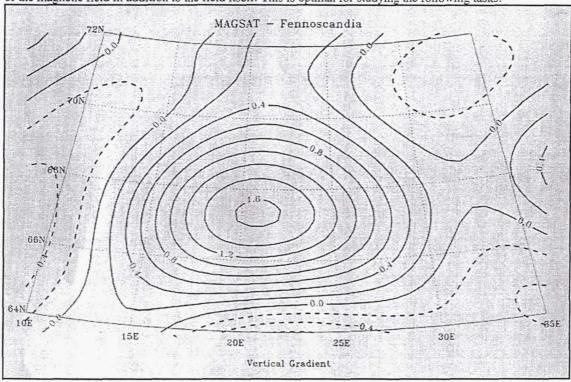


Figure 3 Field gradients in the Fenno-Scandic area, nT/28.5km at 400km. Courtesy Pat Taylor.

- Modeling of the geomagnetic core field and its secular variation.
- Determination of the crustal fields with hitherto unknown accuracy.
- Estimation of the time-space structure of the equatorial and polar electrojets, and analysis of their variability, for example with the solar wind.
- "In situ" measurement of F-region currents with a resolution of 10 nA/m², which is well below
 expected current density of several hundred nA/m² at high latitudes. This enables a monitoring of
 Field-Aligned Currents (FAC) and their variability.
- Detection of plasma waves: The proposed satellite configuration allows for separating temporal variations of the magnetic field from spatial variations and hence is suited as a wave telescope.
- Non-geomagnetic applications with (a) Atmospheric density information from positioning and the large effective drag-affected area; and (b) Profiling of temperature, humidity and other meteorological parameters using GPS tomographic sounding of the troposphere.

The expected launch time in 2002-plus will fill the gap between previous and forthcoming geomagnetic satellite missions and fits the IAGA Resolutions for a "Decade of Geopotentials Research" as well as the "Polar Cap Measurements Effort" project (see references).

The lifetime as a tethered mission will be comparatively short (METS had a projected lifetime of 6 weeks to 3

month) and highly dependent on the solar cycle-governed atmospheric swelling. By monitoring the actual braking of the satellites, the tether may be cut at a predetermined altitude, after which the mission will proceed as two free-flying satellites resulting in an overall mission lifetime of 2 years. The slowly decreasing lower orbit provides for a close look at the crustal anomalies for days to months after the tether is cut.

From a science point of view a tethered gradient mode mission in the order of weeks will give ample data for excellent crustal gradient field decomposition. Science will certainly prefer a shorter mission sooner, compared to a longer lasting mission later. This is because a close look at the crust will immensely improve the interpretation of the Magsat-data, and the expected data from Ørsted and CHAMP. Science is not about getting maximum number of bits per Krone, - but getting the right quality and amount of data, and getting it before everybody else.

2.1 Detailed Description of the Project

Besides measuring the magnetic field itself, the proposed mission brings a new dimension into geomagnetic field research by also observing the magnetic vertical gradient. This considering that the gradient is useful because of three reasons:

- Geomagnetic potential modeling using the gradient in addition to the field itself will drastically enhance the signal-to-noise ratio. This is especially helpful for resolving features of the core and lithosphere fields in the intermediate wavelength range represented by spherical harmonics with degree between 10 and 14, where sources in the core and in the crust contribute with comparable magnitudes, and thus where a separation of the two is particularly difficult.
- Direct measurement of the current density between the two satellites is possible by applying Ampere's law.
- Separation of temporal from spatial variations enables the detection and study of plasma wave phenomena.

The planned launch date and the expected total lifetime of about two years will continue geomagnetic field monitoring in space by missions like Ørsted, SUNSAT, SAC-C, CHAMP and others. Such a continuous magnetic field observation from space is necessary, for example for studying secular variation and the fluid motions dynamo in the Earth's core, and fits the upcoming "Decade of Geopotentials Research" as proposed by the International Association of Geomagnetism and Aeronomy (IAGA) (see the references), and with other international efforts for studying polar cap physics and the solar-terrestrial environment.

2.1.1 Internal Fields

The great advantage of a magnetic gradient mission becomes evident when considering that any magnetic field configuration can be described by a superposition of magnetic dipoles as an alternative to the common expansion in terms of spherical harmonics (see Fig. 4). For the core field these dipoles are located at the core-mantle boundary (at a depth of 3000 km). For crustal contributions they are located few kilometers beneath the Earth's surface, whereas ionospheric contributions are describable by dipoles at a height of 115 km, where the bulk part of the ionospheric currents flow.

Let us assume a dipole source at a distance h below the two satellites, which are separated vertically by Δ =20 km. If this source produces a magnetic field of strength B at satellite height, then the difference in the magnetic field between the two satellites will be δB =3 B Δ /h. Currents in the ionospheric E-layer (about h=300 km, below the proposed lower height of the satellites of 400 km), which produce a magnetic signature of 10 nT at the satellites (corresponding to a rather weak ionospheric field), yield a magnetic gradient of δB =2 nT, well above the resolution of the gradiometer. Crustal features of the same magnetic field strength at satellite height will produce a gradient of 1.5 nT, whereas a dipole at the core-mantle boundary will produce a gradient of only 0.2 nT (see Fig. 3).

Hence the strength of a gradiometer mission lies in its ability to detect and model near sources in the ionosphere and crust. However, the core field study will benefit from a gradient mission too, since any main field model requires a separation of contributions from the crust, the ionosphere and the magnetosphere.

2.1.2 External Fields

The proposed mission will also greatly enhance our knowledge of the external field contributions especially at high latitudes. The space-time structure of polar and equatorial electrojets can be studied more accurately using both the magnetic field and its gradient, and field-aligned currents associated with those jets can be measured directly using the magnetic gradient: A horizontal current density of 10 nA/m² between the two satellites produces a magnetic field difference of 0.2 nT. Typical field-aligned currents at high latitudes have a strength of several hundred nA/m² even during geomagnetic quiet conditions, and hence are well above the expected resolution of the gradiometer of 10 nA/m².

In addition to that, the proposed configuration with two identical sub-satellites in a fixed separation of 20 km allows, for the first time, a separation of temporal and spatially varying phenomena. This enables the detection and study of plasma waves, especially in the frequency range between 0.1 and 10 Hz.

Higher degree and order model coefficients and therefore more accurate models will be derived. This is desired since the current IGRF models only go up to n=10, which in particular is not sufficient for matching regional surveys into a global picture. A global anomaly vector map can therefore be constructed with the purpose of joining all the existing national, regional and continental surveys. This is accomplished without the low pass filtering along the orbit of the measurements traditionally carried out in earlier missions, such as Magsat, thus enhancing the resolution of the north component of the crustal features, the direction in which the filtering takes place.

Accurate global gradient mapping of the crustal anomalies will allow patching of regional crustal maps made from aeromagnetic surveys (horizontal), it will permit downward and upward continuation of aeromagnetic data (vertical), and allow studies of crustal long wavelength features.

The field differences measured at the ends of the tether are strictly proportional to the distance between the magnetometers. A 20 km tether offers a maximum signal-to-noise ratio of 300 as discussed above, and an observational quality of this order of magnitude is necessary for reliably mapping the Lithosphere. From a science standpoint the availability of tethers of this size is very fortunate, because clearly the observations will drown in noise with a 200 m tether, and be compromised and unreliable even at 2 km.

The sub-satellites will enclose a surface in which the vertical vector and scalar gradients are directly measured as well as the along-track gradients from the directional time derivatives of the field vector at each sub-satellite. This constitutes a "closed loop" through which the current density can be sensed with a resolution of 10nA/m².

A 20 km tether separation between the magnetometer sensors is extremely well suited for crustal and external fields description. For shorter tethers the signals will be quenched in noise, and longer tethers will demand higher altitudes, again reducing the crustal and ionospheric signals. A 20 km tether is technically highly feasible, where longer tethers will give mechanical and dynamic problems, and require a higher altitude to keep the mission lifetime in the range of two years.

400 km altitude
gradiometer

40 km
magnetic
crust

Figure 4 GRADSAT cartoon. Courtesy: Charlie Barton.

The differential magnetometer measurement approach will provide an excellent opportunity to

get the longitudinal extent of the electrojets. The North-South crossings will give a good view of the length of the currents, and how they close in the magnetosphere.

The space- and time-structure of the FAC's can be monitored owing to their geometry (they are tilted 10-12 degrees with respect to the vertical in the Auroral Zones). With the very simple assumption that the Field Aligned Currents flow exactly along the main magnetic field, then the full curl of B and the FAC density can be evaluated. The time variation offers the opportunity for studying wave phenomena in connection with solar influx and magnetospheric reconnection. The wave telescope aspect of multiple probe magnetic measurements is an important part of the Cluster Mission science, and analysis of the AMPTE observations has confirmed the feasibility of a two-probe approach combined with plane of minimum variance techniques for determining the wave propagation vector [Helbert, 1997].

An important addition to the science payloads, particularly for interpreting the physics of the currents flowing in the Earth's Ionosphere/magnetosphere is the inclusion of E-field experiments allowing for more reliable studies of the plasma electrodynamics. Double probe experiments or Ion Drift Meters would offer very attractive science additions to the instrumentation complex.

3 Payload Concept

The primary science payload consists of the basic instruments needed for a high precision mapping mission:

Star Imager attitude system 0.5 arcseconds

Vector magnetometer
 0.1 nT abs. 10 pT resolution

Scalar magnetometer 0.1 nT abs.

• GPS receiver system < 10 cm abs.

The basic vector rate is 100 samples/sec with an upper 3 dB frequency of 33 Hz.

3.1 Science Payload

Recent developments in magnetometry and in instrumentation for stellar navigation (Instrumentation for Ørsted, ASTRID-2, Sporadic-E suborbital, CHAMP) have demonstrated and verified the reality of the advanced resolution levels, as also analyzed in the GSO-Study for ESA [Primdahl, 1996]. One important difference in measurement technique from the previous magnetic missions, is the relief from magnetic contamination fields from the carrier platforms. The combination of an attitude unit and a vector magnetometer frees the probes from orientation constraints, and particularly allows the use of the proposed 20m flexible cable booms thus bringing the magnetic sensor outside the range of spacecraft generated local fields. And in addition to this, no spacecraft

245

magnetic calibration nor strict cleanliness programs are needed.

Detailed science instruments descriptions may be found in Primdahl [1996, 1997], and in the previously submitted proposal in Jørgensen et al. [1996].

3.1.1 CSC Vector Magnetometer

The third generation mapping quality magnetometer will have a resolution of 10 pT rms in the frequency range from 50 mHz to 12 Hz, and an absolute accuracy of 0.1 nT. The vector sampling rate is proposed to be 100 Hz with an upper frequency response 3 dB limit at about 33 Hz. The instrument will (at variance with the Ørsted magnetometer) include a CPU for timing, instrument mode control, communication with the satellite computer, etc. The total weight will be less than 1500 g and power consumption less than 2.7 W including the CPU.

3.1.2 Triple Head Star Imager

The proposed triple head Star Imager consists of a camera platform accommodating three independent camera heads with high performance optics and stray light baffles. The three cameras are connected to a computer performing all necessary tasks, including search engine, attitude fine tuning and attitude merging into a single high precision attitude quaternion output. As the system only needs a valid output from two cameras per attitude estimate, the system is exceedingly robust towards occultation, bright objects and motion smear. The instrument has an absolute accuracy of 0.5 arcsecond and a noise equivalent angle of 0.2 arcsecond. This accuracy is 1σ values for pitch, yaw and roll. The update rate may be from 0.125Hz to 2 Hz with virtually no impact on the noise performance. The mass of the computer unit is 600g and of the triple camera head 700g. The power consumption of the system is <7W unregulated.

3.1.3 Overhauser Effect Trityl Based Scalar Magnetometer

The proposed absolute scalar magnetometer for in flight calibration and stability monitoring of the vector magnetometer is a new Trityl based Overhauser effect instrument developed at the DTU-IAU [Primdahl, 1996, 1997]. The instrument will fly on the NASA Sporadic-E suborbital sounding rocket in the beginning of 1998, and it was part of the METS proposal for a tether experiment to NASA. The following data are from the METS proposal. The absolute accuracy is $0.1~\rm nT$, and the rate is three 20 bit samples per second. Each field value is derived from an about $0.1~\rm second$ duration free proton precession signal. The measurement range is from < 16 000 nT to 70 000 nT. The weight is 1800 g for the tether attached sensor and 900 g for the electronics box. The instrument includes a CPU for signal processing and for communication with the satellite computer. The power consumption is about 2 W during continuous sampling.

3.1.4 Advanced TurboRouge GPS Receivers (TRSR II)

The GRADSAT will each carry the advanced TurboRouge dual frequency GPS receivers. This is a next generation design from that carried by the Ørsted spacecraft and an improvement over the CHAMP and SAC-C receivers. The receiver will feature advanced tracking loops to improve performance during ionosphere scintillation expected in the auroral regions and will provide Total Electron Content (TEN) measurements of the ionosphere and atmospheric temperature during the entire orbit. In conjunction with other orbiting and ground based GPS networks and the magnetic and particle detection instruments aboard GRADSAT, the measurements should provide significant information on the activity of the ionosphere and upper atmosphere in response to solar activity and magnetic storms. This is very important in better understanding the solar-terrestrial interactions and their role in climatic variability. Precision orbit determination should be accurate to better than 10 cm and relative positioning to the two spacecraft should be at the millimeter scale. The TRSR II will have multiple antenna inputs to allow for spacecraft rotation and the TRSR II mass will be below 5 kg and power consumption will be below 5 W.

3.1.5 Supporting Magnetospheric Plasma Diagnostics Instruments

E-field probes and/or Ion Drift Meters are proposed included by the Alfvénlaboratory, RIT, Stockholm. Estimated power is 3 W and the weight is 2 kg. In case of the probe instrument, the need for tether supported or wire boom supported spherical plasma probes must be considered in the early phase A study. The accuracy is in the sub-mV-range, with reservations for the DC-offset, and the system is ideally suited for high frequency wave studies. For this reason the data rate may expand to what is available in the TM.

In case of the Ion Drift Meter the demand for resources is much less, and the instruments just need to be mounted flush with the surface in the ram direction, and the DC-response is excellent. The drawbacks are the poor frequency response and the sensitivity only to fields perpendicular to the main magnetic field.

3.2 Tether and Tether Mechanism

A long life tether experiment is flying on TiPS (appendix C). Deployment and dynamics were demonstrated during the SEDS program [Rupp, 1994; Wallace, 1994]. We strongly recommend sending a representative to

the Huntsville Tether Technology Interchange Meeting (TIM) September 9. -10., 1997 to learn about the technique and for establishing a contact network to the tether community (appendix E).

SATLAB at Ålborg University proposes to study the tether deployment and flight dynamics [M. Blanke, private communication], and they will study the inclusion of tether strain gauges and active dynamic oscillations damping. The measurement of tether dynamic behavior and static strain is also proposed as a study subject for gravity field observation purposes.

The mass and volume of a 10 km tether (as foreseen on each of the satellites), and of the deployment mechanism and controls are typically of the order of 14 kg for the tether [TiPS, appendix C], and 5 to 10 kg for the mechanism and controls. The volume is of the order of 10 liters. The 20 km FIPEX tether for TEAMSAT to be deployed from Ariane 502 weighs 21 kg for string, mechanism and all included [Wubbo Ockles, T.U. Delft, The Netherlands, private communication]. The dimensions of this unit are 25.4 cm in diameter and 35 cm high, including a conical top, or about 16 liters.

A phase A study will show the realistic numbers for a tether adapted to the dual satellite deployment for this proposed mission. However, the result will not deviate much from the estimates given above.

3.3 Spacecraft Total Estimates

Each basic S/C is estimated to weigh about half of the Ørsted satellite, plus an estimated added weight of 17kg for half the tether system, i.e. weighing about 47kg. Sufficient solar power should be insured by a minimum solar power panels output of about 50W. The mass will fit inside an envelope, 60cm diagonal and 35cm high. To this has to be added separation mechanisms, etc.

4 Science Interest

We do claim that this Magnetic Earth's Field Gradient Mission has the potential of attracting at least as much international scientific attention as did, very successfully, the science of the Danish Ørsted Mapping Mission. The new advanced technology and the step forward in science will once again bring Denmark ahead in international space research.

4.1 Danish Science Community and Opportunities

Danish planetary science includes strong groups studying Earth's potential fields, gravitational and magnetic, which together with seismological studies are the only ways to gain knowledge of the otherwise inaccessible Earth's interior. The Ørsted mission has strengthened this research, particularly in magnetics, but also in gravity and other planetary science. The science involvement in the Ørsted project has greatly stimulated student interest in the area, and has resulted in an increasing number of Ph.d. projects for education of future Danish Earth scientists.

4.1.1 Danish Solid Earth Research

A long tradition of Earth's core magnetic studies exists at the Geophysical Department of the Niels Bohr Institute at Copenhagen University. Gravity and Geodesy is also strong at the NBI, as is Seismology. At present, no specific studies of the Earth's Crust is ongoing, but this field is attracting the interest of students, particularly in view of the wide international emphasis on the area.

4.1.2 Danish External Sources Studies

Studies of the Ionospheric, Magnetospheric and Solar Wind sources of the near Earth's magnetic field mainly goes on at the Danish Meteorological Institute, but also at the Niels Bohr Institute and at the Danish Space Research Institute, as evidenced by the publications. Related areas are the atmospheric and ionospheric tomography studies by GPS satellite occultation at the Meteorological Institute [Per Høeg, private communication]. Again, these Danish research fields are filling their proper place with essential international science contributions.

4.2 International Science Interest

Despite the relatively short time for responding, several letters of support have been received expressing interest in a Danish Gradient Mission, in particular from the groups at the Geodynamics Branch, NASA-GSFC involved in the METS (Magnetic Earth Tethered Satellite) proposal, unfortunately not supported by NASA. (See Appendix B). Dr. Will Webster, GSFC offered several suggestions, which have been incorporated into this proposal. With the SEDS mission he suggested flying a pair of tethered magnetometers, and a dual tethered satellite magnetic gradient mission is very much in line with their future intentions.

Dr. John LaBrecque, NASA-JPL, JPL Program scientist for Geodynamics and NASA mission scientist for SAC-C, also stated his interest in the gradient science (see Appendix B), and he indicates the realistic possibilities for JPL contributing the Advanced TurboRouge GPS receivers to the mission.

247

Gilbert Ousley (Appendix B) discussed the idea of a magnetic gradient mission with Dr. Mario H. Acuña, NASA-GSFC. Acuña expressed his personal interest and is willing to provide advice and support to our activities.

One of us (J.M.G.M.) presented the proposal for a Magnetic Gradient Mission at the IAGA-meeting in Uppsala 4.-15. Aug., 1997 (Div. 5, WG on Geomagnetic Measurements, chaired by Fred Quinn, US Geological Survey). Many people at IAGA were attracted to the proposal, and it received very positive responses.

Dr. Hermann Lühr, GFZ, Germany was very interested, he offered many suggestions for external fields science applications, and responded positively to an invitation to participate.

Dr. Göran Marklund, the Alfvénlaboratory, RIT, Stockholm also expressed interest in the science, and suggested the addition of E-field experiments supplied by the RIT plasma group.

5 Mission Requirements

The following suggested parameters are weighed estimates considering that the 2002-plus launch time frame is approaching Solar minimum, that the lifetime of a tether, despite multiple strand design, might be limited because of the statistics of micro particles hitting the string, this against the desires to have a mission long enough to ensure a world class science data set. Built in options to cut the tether at both spacecraft, and let the satellites continue the mission as free flyers in two different orbits, will save part of the science, even if early bad luck breaks the string, - or when the tether air drag threatens to bring the system into destruction in the denser atmosphere. At tether disruption, one satellite will go into a higher altitude orbit, and the other will be lowered. As free flyers, then at least one of the satellites will provide additional mission life time continuing part of the science.

5.1 Orbit Characteristics

A 600-400 km near polar and approximately circular orbit is proposed. This is slightly higher than Magsat at 350 km with < 1 year life time, and it aims at 2 years or more for the total mission. Still 400 km is sufficiently close to the Earth's surface, so that the gradient measurement combined with the increased resolution of the instruments will scale the crustal anomalies. In case of an unlikely (but possible) early disruption of the tether, the two free fliers will last for at least the planned mission lifetime, and in the case of on command cutting of the string, just before reentry becomes imminent at a low air dragged altitude, then one of the satellites will offer additional mission time, while the other will provide some additional low altitude data.

An off-sun-synchronous orbit is proposed in order to allow the satellites to sweep over all local times in a time span of the order of 6 months to one year.

5.2 Mission Profile and Life-time

The proposed GRADSAT mission profile is divided into three sub-missions. The first and most important part is the tethered phase (see Figure 5) for collecting a magnetic field gradient science data set for modelling the important crustal anomalies signatures and for in situ studies of the curl of B (from currents flowing between the GRADSAT orbits). Additionally, this phase offers a wave telescope facility.

The second phase starts by cutting the upper satellite loose from the tether thus ending the gradient mission. This is proposed done by carefully monitoring the altitude versus time of the tethered system, and balancing the science request for a high

quality gradient data set at a low altitude ensuring good signal-to-noise, and for a time, sufficiently long, to give full global covering. Against this weighs the desire to release the upper satellite flyer continuing the mission as a low altitude Earth's field magnetic mapper for "as long as possible". This can be qualified by saying that the minimum need is a good quiet time global data set, estimated to take of the order of a month, and the optimum situation would be a continued free flyer mission for the total of two years.

The third phase, embedded into phase two, starts by letting the single-end attached tether drag the lower satellite down to

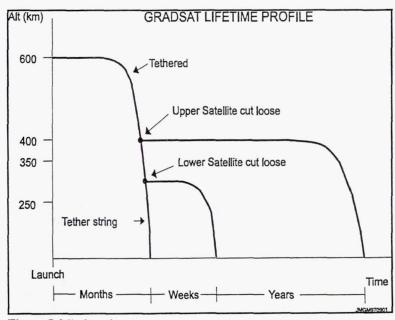


Figure 5, Mission phases.

an altitude of suitably increased air-drag, and then cutting the lower end of the tether. The string will then go down rapidly, and the lower free-flyer will in the matter of days or weeks spiral into burn-up in the atmosphere. During this short time a very valuable additional data set for crustal anomalies modelling and ionospheric currents observations will be collected.

Depending on the solar cycle-controlled atmospheric swelling, and on the weights placed on the science importance of the different phases, then the total mission life time will vary. Careful kinematic modelling of the mission scenario is proposed to be held up against continuous precise monitoring of the actual dynamics behaviour, as the best basis for deciding precisely when the phase changes should be initiated.

The important gradient science mission can be completed in the matter of weeks, and the close look at the crustal anomalies by the rapidly decaying lower satellite is done over days. As stated above, the science tasks do not demand a long duration mission, but it is important to be the first or among the first groups collecting this kind of data.

The 20 km tether is optically a large target, and it can be observed from the ground. First following the deployment, then the two cutting events, and eventually the decay of the string into the atmosphere.

5.3 Launch Time Requirements

At the present, no specific launch time requirements are foreseen. The mission may be flown anytime. But of course, the influences from the solar activity during the operational phase will set the life time for the suggested 600-400 km orbit.

At solar minimum, the life time is optimum at these low altitudes, thus offering good gradient resolution of the crustal anomalies observations. The presently proposed instrumentation will produce the desired scientific results even at slightly higher altitudes.

Herman Lühr made the very interesting suggestion that the Danish Geomagnetic Gradient experiment be launched together with GRACE planned for the 2001-plus time frame. This will exploit the extra lift capability on the planned Russian launcher. The combination of GRACE, a dual CHAMP gravity mission with 10 times improved resolution, and the Danish GRADSAT provides a very attractive Earth's fields potentials system, and points forward towards new era possibilities and results in Earth's and planetary science.

6 Relation to Other Missions

Recommendations at the second Ørsted International Science Team Meeting (OIST) and at the 8'th IAGA Scientific Assembly Uppsala, 1997 for the International Geopotentials Study Decade strongly underline the international support for and interest in geomagnetic and gravitational fields satellite missions. Below, some important missions in the this field are listed and commented.

6.1 Ørsted/SUNSAT

Ørsted is the much needed re-fly of the geomagnetic mapping Magsat mission, planned for launch in May 1998. Under extraordinary international science interest the science team has been formed of more than 40 institutions world wide, and substantial mission support comes from the US NASA/DOD (launch), the French CNES (scalar magnetometer) and the German DARA (calibration).

Similarly supported by NASA is the South African, State University of Natal Earth's Observation Satellite SUNSAT, also carrying a vector magnetometer and being on the same NASA/DOD launch with Ørsted. The high absolute accuracy of Ørsted is used to cross-calibrate SUNSAT in orbit, thereby performing independent two-point geomagnetic satellite measurements. The Ørsted/SUNSAT missions have design lives of 1 year.

6.2 Astrid 2

The Swedish Space Corporation's 28kg micro-satellite ASTRID-2 carries an ionospheric research science payload, including the next generation stellar navigation camera and vector magnetometer after Ørsted. Launch is planned to the last quarter of this year (1997) on a Russian COSMOS vehicle into a 1000 km circular 80° inclination orbit. The star camera is a new lightweight, low power single head version, and the magnetometer has single axes' compensation in a light weight vector sensor, supported by a new development of a fully digital synchronous detection, integration and feedback loop, and offering 24 bits resolution in the full 50 000 nT Earth's field. Both these instruments are supplied by DTU-IAU, the magnetometer in collaboration with RIT, Stockholm, and supported by STVF.

6.3 SAC-C

The Earth observation satellite SAC-C is a collaboration between the Argentine CONAE and NASA. The launch on a Delta 2 is planned to mid 1999, and the Danish Ørsted consortium has been invited to participate with the Ørsted type magnetic experiment complex consisting of the boom, power supply, computer and the Ørsted gondola equipped with a Danish star camera and CSC vector magnetometer. The funding is planned to come from Danish government sources and from industry. The boom tip scalar magnetometer is a metastable

249

He⁴ optically pumped instrument delivered by NASA-JPL, who also delivers the next generation TurboRouge GPS receiver after Ørsted with advanced tracking on all 16 channels while Oersted has advanced tracking on two of its 8 channels. SAC-C will include the GOLPE experiment to track the entire GPS ray path environment to test applications in ionospheric, atmospheric mospheric as well as

reflected signal science including altimetry and scatterometry. The instrumentation performance requirements will be as specified for Ørsted, and the science purpose is the very important continuation of the space based geomagnetic survey, re-initiated after Magsat by Ørsted. The orbit is 704km sun synchronous with the descending node at 10.15 am, and the satellite is Earth oriented. The design life time is planned to be 4 years.

6.4 CHAMP

CHAMP is the German geopotentials satellite equipped with accelerometers and with two dual camera head Star Imagers and two CSC vector feedback mapping magnetometers representing the third generation instruments after Ørsted. The project is funded by the German DARA under management of GeoForshungsZentrum (GFZ), and the cameras and magnetometers are delivered by DTU-IAU under contract to GFZ. The launch is planned to mid 1999 on a Russian COSMOS vehicle into a 470 km altitude and 83° inclination circular orbit. The mission design lifetime is 5 years. The magnetic part of the CHAMP mission will give a closed shell single point mapping of the Earth's geomagnetic potential with a quality designed to be a factor of 4 better than Ørsted.

6.5 GRACE

The DARA-NASA dual satellites 'coordinated flying' GRACE mission (Gravity Recovery and Climate Experiment) is planned for launch in the 2001-plus time frame on a Russian COSMOS launcher into a similar orbit as that of the CHAMP mission. The science is, briefly stated, "10 times the gravity part of CHAMP", but without magnetometry [H. Lühr, private communication]. The mission is a highly advanced Earth's gravitational potential mission, and Hermann Lühr points out that launching GRADSAT on the same vehicle would permit the two missions to complement each other, supplying the combined Earth's gravity and magnetic potentials. The complementarity of GRADSAT to GRACE is very important, because the second half of the geopotential decade is currently without a quality magnetometer mission.

6.6 Overview of Tether Missions

Appendix A presents an overview of all the 16 flown and flying tether missions to date [courtesy Gil Ousley]. The tether technology is now highly operational and should be considered a tool for obtaining hitherto inaccessible science results. As stated in the US letters of support, the technology is available to interested partners on a collaborative basis. A highly effective entrance into the space tether community would be to participate in the NASA sponsored Tether Technology Interchange Meeting (TIM) Sept. 9-10, 1997 in Huntsville, Alabama, chaired by Jim Harrison, Marshall Space Flight Center (see appendix E). TiPS (appendix C) is MSFC's tether long life and dynamics experiment in space, which has a demonstrated survival for more than one year, and still in one piece. The 20 km SEDS (Small Expendable Deployer System) experiments are described in Rupp (1994) and Wallace (1994). SEDS-1 and -2 are experiments performed from the second stage of a Delta vehicle, where end masses of 25 kg constituting complete self-contained sub-satellites were deployed on a 20 km tether. Michael L. Exner, UCAR GPS/MET Program, Boulder CO, gave a seminar in Copenhagen in September, 1996, and during the following discussions at the DTU we became convinced about the success of the technique, and were made aware of the interest of UCAR in seing tethers exploited in worlds class space science missions.

7 Science Operation and Data Archive

The Ørsted Operation Center and routine data handling procedures will be well suited for expansions to a capacity for handling the foreseen larger and longer duration data stream from GRADSAT.

7.1 Science Data Analysis

The International Ørsted Science Team organization for ensuring maximum science output from Ørsted under Danish leadership is seen as excellently designed for the responsibility of steering and controlling the international access to and full exploitation of the larger GRADSAT data set.

The fact that the leadership responsibility rests with a Danish organization will surely stimulate Danish Ph.d. students and researchers to participate in all the fields related to geomagnetism and geopotentials.

8 Technical Feasibility and Technology Development Requirements

The Danish industrial community involved in Ørsted has clearly demonstrated their space technology capabilities. The basic technologies are well established. Where required, new capabilities are available, and the organizations have demonstrated that they are highly qualified for the transfer of new know-how.

The tether deployment technology is certainly a challenge, but as discussed above, collaboration is being offered from the international centers of excellence. An offer that should not be refused.

The augmentations of the science instrumentation over the Ørsted performance have been well demonstrated in the laboratory and at test facilities, and will be confirmed in space flights in the near future for all the proposed experiments. In short, all the principles and capabilities have been verified, and the instruments are ready for the mission specific adaptations and developments common to all space programs.

8.1 The Tether Technology

The tether technology already exists, and the best way to start in this area is to participate in the MSFC Tether Technology Interchange Meeting, Sept. 9-10, in Huntsville, Alabama. Contacts with interested suppliers and collaborators can definitely be established here.

8.2 The "Puppet-on-a-String" concept

The "Puppet-on-a-String" proposed at the December 1996 Workshop is very much feasible for the proposed mission. A triple camera head for the Advanced Stellar Navigation System mounted on a carbon fibre tubular optical bench with the Ørsted type CSC (Compact Spherical Coil) vector feedback sensor mounted at the other end [Jørgensen et al., 1996]. The unit is proposed separated 20 m from the spacecraft by using the (probably reinforced) cabling as a flexible wire boom. The triple camera head and the mechanically fixed orientation relative to the CSC sensor will render the absolute orientation uncritical. The long wire boom will make the magnetic signature of the carrier spacecraft negligible, and consequently free the spacecraft from any strict magnetic cleanliness program and magnetic calibrations. The puppet is proposed deployed after the 20 km tether has been fully extended, and in a situation where a maximum gravity gradient tidal force acts on the unit pulling it away from the tether side.

The Institute of Control and Engineering Design at the DTU has experience in releasing long cabling in space. They designed the mechanism for successfully deploying the 10 m diameter optical fiber ring from the NASA suborbital sounding rocket Auroral Turbulence 1 launched in March 1994, and they built the spinning machine for weaving the textile cover on the 21 turn optical fibre ring. A similar technique is proposed for the deployment of the Puppet unit.

8.3 Instrumentation Miniaturization

Science instrumentation miniaturization and resources consumption reduction has been an ongoing effort for the generations of instruments after Ørsted. This is much facilitated by the very fast development and marketing of new electronics components. Tasks we did not dream of doing on Ørsted, are possible to day, and nothing seems to stop this trend.

9 Management and Funding

Management functions must be separate from and independent of subcontracting functions. E.g. the CHAMP industry and science management and the funding control are trusted to GeoForschungsZentrum (GFZ), an independent German governmental research institution.

Because of the very high international science return expected from this mission, bi- or multinational funding constellations might prove viable. We strongly recommend that this approach be explored with our traditional collaborative foreign institutions.

9.1 Consortium Construction

Headed by the Danish lead governmental institution a consortium of Danish aerospace industry companies and Danish university and other research institutions shall be formed with the purpose of procuring and/or building the satellites and the science instrumentation. International relations for procuring the launch and for exploiting the science results will be the responsibility of the Danish lead government institution.

9.2 Industry Management and Funding

Under responsibility to the lead governmental institution the industry will do their own management and they will be responsible for the part of the funding coming from industry or from industry related government sources. The industry funding from the other government sources will be managed by the Danish lead governmental institution. The CHAMP project industrial contracts may serve as an example of a government/industry collaboration relation.

9.3 Science Instrumentation Management and Funding

The science instruments and related activities will be procured from Danish and foreign institutions under contract with the lead institution for the equipment funded by the Danish government. Other contributions will

251

be delivered according to bilateral agreements with the Danish lead institution. The CHAMP contract with DTU-IAU may serve as a paradigm.

9.4 Science Data Handling and Science Analysis Management and Funding

Funding for the full Danish exploitation of the science data set must be part of the total project funding plan. This, unfortunately, has often been lacking in other projects, leaving the science data analysis and interpretation dependent on uncertain and time consuming fund-raising late in the mission. In retrospect, a very large part of the nationally prestigious mission results is the science output. This has certainly been true for the Magsat mission. Science management shall rest with the institutions receiving the funding, under ultimate responsibility to the funding authorities.

10 References

- Langel, R.A., Latest Magsat Results, Lecture at the Danish Geophysical Society Meeting at the Niels Bohr Institute, Copenhagen University, May 13., 1997.
- Rupp, Charles C., Flight Data from the First and Second Flights of the Small Expendable Deployer System (SEDS), NASA Marshall Space Flight Center, PS04, Huntsville AL 35812, USA, 1994.
- Wallace, Bruce K., SEDS Tether Deployment Ground Tests, NASA Marshall Space Flight Center, EL64, Huntsville AL 35812, USA, 1994.
- Jørgensen, John L., F. Primdahl and Chr. Boe, "Puppet-on-a-String", in: Proposals for New Danish Space Missions, Mission Concepts Presented at a Workshop at the Danish Meteorological Institute, Dec., 12., 1996.
- IAGA '97 Resolution: Recommendation for establishing an "International Decade of Geopotentials Research", IAGA 8' Scientific Assembly, Uppsala, Sweden, Aug. 4.-15., 1997.
- IAGA '97 Resolution: Recommendation for carefully considering how the regions close to the poles may become covered by magnetic measurements, IAGA 8' Scientific Assembly, Uppsala, Sweden, Aug. 4.-15., 1997.
- Primdahl, F., Payload Definition Document, Study on SGO Mission Architecture WP 2000, DMI/GSO/RPT/002, Danish Meteorological Institute, ESA Contract Number 11334/95/NL/CN, 1996.
- Primdahl, F., Scalar Magnetometers for Space Applications (Review), in: AGU Geophysical Monograph Series Volume on "Measurement Techniques in Space Plasmas", edited by Joseph E. Borowsky, Robert Pfaff and David Young, in print, 1997.
- Helbert, Jörn, The Wave Analyzer: A high resolution spatial spectral analysis method for multi-spacecraft missions, Diploma Thesis, Institute for Geophysics and Meteorology, Technical University of Braunschweig, Braunschweig, Germany, July 1997.

Session IV—Transportation

Page intentionally left blank

Tether Transport System Study Summary Performed under contract to Marshall Space Flight Center under NAS8-39400

Prepared by

Boeing Contributors Smithsonian Astrophysical Observatory (SAO)

Dan Vonderwell Enrico Lorenzini Mike Bangham Mario L. Cosmo Heather Dionne Markus Kaiser

Beth Fleming

Bill Klus Marshall Space Flight Center

Karmel Herring Linda Vestal
Elton Suggs Les Johnson
Larry Walker Connie Carrington

The Boeing Company 689 Discovery Drive Huntsville, AL 35806

Abstract

This is a summary of the Final Report, "Tether Transport System Study", prepared under NAS8-39400. The main rationale for this study is to reduce the mission cost of transporting payloads to GEO. A two stage tether transport system was proposed for boosting payloads from LEO to GTO/GEO. The feasibility of the concept is addressed from the point of view of orbital mechanics and other principles of physics. The report presents the results of an engineering analysis that defines the system, major elements and subsystems, and assesses the feasibility (i.e., the technology readiness level) of designing and developing the system. Results indicate that significant cost savings can be realized over traditional upper stages within a few launches. Certain key technical issues, such as payload rendezvous and capture, need to be addressed in future studies. Advancements in certain technology areas, such as power generation and highly efficient propulsion systems, will have significant effects on the overall system design.

Introduction

This study is the first detailed analysis of a two-stage tether system to transfer payloads (9,000 lb or less) from low earth orbit (LEO) to geosynchronous earth orbit (GEO), including the implementation of the operational system. The main rationale for this study is to reduce the mission cost of transporting payloads to GEO. The cost of placing a payload in LEO is expected to drop due to the introduction of the Reusable Launch Vehicle (RLV). The use of tethers has been identified as a means of reducing cost of going from LEO to GEO by eliminating the requirement for traditional chemical upper stages, reducing the launch mass and cost. Tethers are capable of providing very large ΔV 's to the payload with minimal propellant consumption.

The feasibility of the concept is addressed from the point of view of orbital mechanics and other principles of physics. The report presents the results of an

engineering analysis to define the system, major elements and subsystems, and to assess the feasibility (i.e., the readiness of technology) of designing and developing the system. The report then presents an assessment of the tether system performance and an estimate of the cost of the system. While the main focus of this report is on the transport of payloads from LEO to GEO, lunar or inter-planetary missions are not excluded.

Concept Overview

On-orbit facilities will transfer payloads to GEO-transfer orbit (GTO) and/or GEO via momentum exchange. Spinning tethers are used to impart the desired ΔV (or ΔV 's) to the payload to be transferred. Each spinning facility has a counter platform on the opposite side of the tether. The spinning facility acts as a giant momentum wheel, i.e., for each ΔV imparted to the payload there is a ΔV , proportional to the payload/platform mass ratio, imparted to the platform. After release, the payload is injected into a higher orbit and the platform drops to a lower orbit, determined by the payload/platform mass ratio. In order to avoid placing design restrictions/requirements on the payload, it is assumed that all systems required by a payload to interface with a tether facility are provided in the form of a Payload Adapter Vehicle (PAV).

This can be provided by a single-stage tether system or through two smaller ΔV 's provided by a two-stage tether system. A two-stage tether system involves two facilities permanently in orbit: a spinning facility in LEO and another one in medium Earth orbit (MEO) with a perigee close to the LEO facility. This latter configuration is preferable with current tether-material technology (as explained below). The payload is first boosted to MEO by the LEO facility; subsequently, it is captured (with zero relative velocity) at perigee by the MEO facility and later injected into GTO. In this study, the circularization ΔV from GTO to GEO will be provided by an element of the overall tether transportation system attached to the payload.

After payload delivery the two orbital platforms are reboosted. The masses of the payloads to be handled by the tether transportation system are assumed in the range 907 kg - 4082 kg (2000 lb - 9000 lb). According to present projections, this will constitute almost 80% of the traffic to GEO in the future (2010). A platform reboosting time of 30 days is assumed. This corresponds to 12 payloads boosted per year. The payload maximum mass and rate of deployment were derived from the Commercial Spacecraft Mission Model Update, dated 25 July 1996 (P.N. Fuller)

Tether Types

Tethers can have a constant cross section (cylindrical tethers) or a varying cross section (tapered tethers). The maximum velocity that a cylindrical spinning tether can sustain (the critical velocity), without any payload attached to its end, is limited by its material properties and can be written as:

$$Vc = \sqrt{\frac{2\sigma}{\rho}}$$
 (1)

where σ is the ultimate strength of the tether material and ρ is its mass density. A more realistic approach is to adopt a ratio $\sigma^* = \sigma$ /f where f > 1 is the stress safety factor. The ΔV that a cylindrical tether can provide, therefore, is bounded. For example, Spectra 2000 has a Vc = 2.6 km/s ($\sigma = 3.25 \times 109$ N/m², $\rho = 970$ kg/m³) for f = 1.0 (no safety margin) and Vc = 1.96 km/s for f = 1.75.

Since the maximum stress is at the hub of a spinning tether, the tether can be tapered thus saving tether mass and removing the limitation on the maximum sustainable ΔV . The mass of an optimally (i.e., with a constant stress distribution) tapered tether can be written as a function of the tip mass (payload) M_{PL} follows:

$$M_{tether} = M_{PL} \sqrt{\pi} \frac{V}{V_c} \exp\left(\frac{V^2}{V_c^2}\right) erf\left(\frac{V}{V_c}\right)$$
 (2)

where V is the tip velocity and erf() is the error (E.C. Lorenzini). Figure 1 shows the tether/payload mass ratio for a cylindrical and a tapered tether of the same material (Spectra 2000) and a safety factor equal to 1.75. As can be seen here, a tapered tether is lighter than a cylindrical tether especially for $\Delta V > 1$ km/s. It is also important to note that the ΔV that a tapered tether can impart is not bounded by the strength to density ratio of the material.

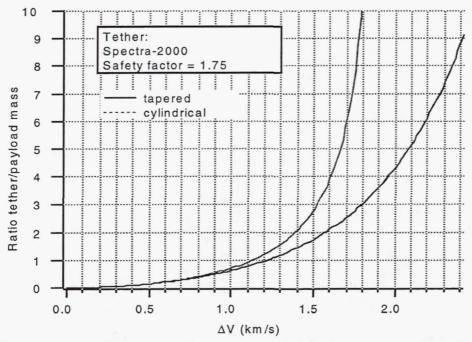


Figure 1: Tether/payload mass ratio for cylindrical and tapered tethers.

Tether Materials and Future Trends

The tether critical velocity depends on the material strength to density ratio. Figure 2 shows that the strength to density ratio of tether materials had two distinct eras

during this century. The metal era before 1960 had a very slow increase of the strength to weight ratio, while the carbon fiber era showed a dramatic increase of the ratio after 1960. If we believe in the linear regression analysis shown in Figure 2, the strength to density ratio should be expected to increase by about 70% in the year 2010 (with respect to the present value of Spectra 2000). Conversely, the tether critical velocity should increase by about 30% in the year 2010 with respect to the present value of Spectra 2000. Consequently, the tether in the year 2010 could be 3 times lighter than at present for a single stage tether system from LEO to GTO.

These improvements might seem dramatic but they could be completely eclipsed if experimental materials like Fullerenes come on line for the construction of long tethers. Fullerenes have demonstrated, in the laboratory, a strength to density ratio almost two orders of magnitude higher than Spectra 2000. At present, the samples being produced are only a few microns long (B.I. Yakobson) but several attempts are underway at making this new material suitable for forming tethers.

One other area of concern is the risk of orbital debris impacts resulting in a severed tether. To address the issue of tether survivability it is proposed to use Hoyt tethers (Hoyt & Forward). Redundant end masses can also be included in the system design to increase the survivability of the tether facilities.

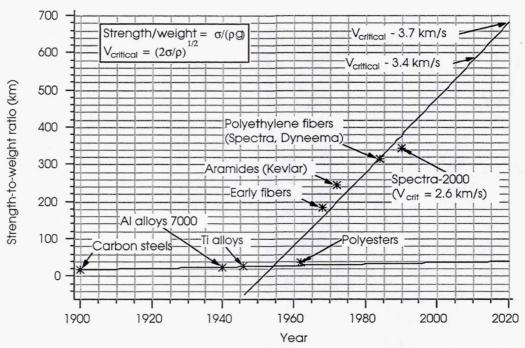


Figure 2: Strength to density ratio of tether materials (with extrapolation)

Mission Sequence

As stated above, due to limitations on current materials technology, a two-stage tether system is preferred over a single stage. Figure 3 presents a simplified sketch of the orbits for the two-stage tether system. After receiving the payload from the RLV, the first stage

spinning in LEO injects the payload into a higher orbit where it is captured by the second stage spinning in MEO. After the capture, the payload is released at a perigee passage into GTO. The first stage provides a velocity increase $\Delta V_1 = V_{\text{TIP-1}}$ where the latter is the tip velocity of the first stage. The second stage captures the payload at the bottom of the spin, during its retrograde rotation, and releases it at the top of the spin, during its posigrade rotation. Consequently, it accelerates the payload (with respect to the speed of its CM) from $-V_{\text{TIP-2}}$ to $+V_{\text{TIP-2}}$ thereby providing a velocity increase of $\Delta V_2 = 2V_{\text{TIP-2}}$. Therefore, the total velocity imparted to the payload by the two-stage tether system is $\Delta V_1 + \Delta V_2 = V_{\text{TIP-1}} + 2V_{\text{TIP-2}}$. A more detailed mission analysis is presented in "Mission Analysis of a Tethered System for LEO to GEO Orbital Transfers." (E.C. Lorenzini)

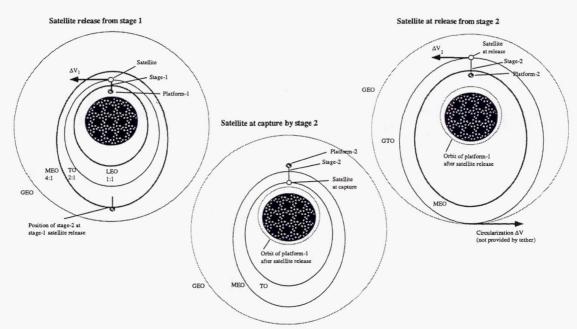


Figure 3: Mission Sequence

System Architecture

Figure 4 is a top-level system architecture block diagram of the tether system. As explained in the previous section, the system consists of two tether facilities, one in LEO, the second in MEO. The facilities are in a common orbital plane. The LEO facility captures and deploys the payload toward MEO for rendezvous with and capture by the MEO facility. The MEO facility subsequently deploys the payload into GTO. Each facility consists of a base facility (from which the tether is deployed and spun up) and a Payload Capture and Release Assembly (PLCRA) at the deployed end of the tether.

System Configuration Overview

For Case 6d presented in the Special Report by E. Lorenzini, et al, the flight segment of the Tether Transfer System consists of the LEO facility with 60 km tether, the MEO facility with 80 km tether, and the PAV. Two general LEO/MEO facility configurations are shown in Figure 5. Both the LEO and MEO facilities consist of one or

more tethers, a Payload Capture and Release System, and a platform with power generation and storage, tether control subsystems, and reboost propulsion. The platform can be mounted on the end or at the center of mass (CM) of the facility. The PAV provides an interface between payloads and the Payload Capture and Release System and provides final circularization ΔV to the payload. Each facility captures the payload, releases it at the appropriate point, and then reboosts itself to its nominal operational orbit for the next mission. Due to its unique functions, the PAV stays with each payload; therefore, a new PAV is required for each mission. See sections 4.2 through 4.7 of "Tether Transport System Study Final Report" (Vonderwell, et al.) for a detailed analysis of each subsystem.

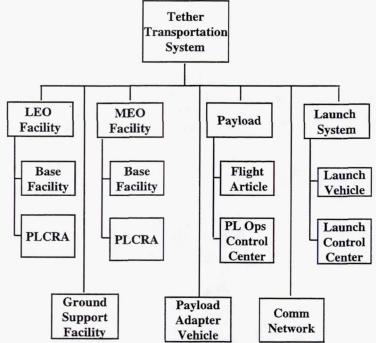


Figure 4: System Architecture Block Diagram

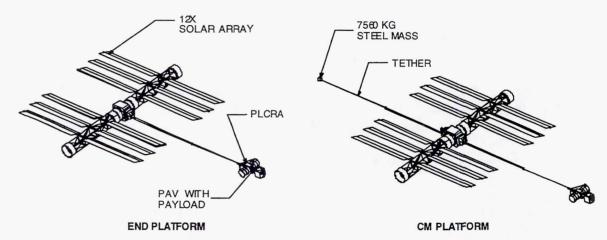


Figure 5: Tether Transport System Configurations

Payload Capture

The requirements that drove the design of the Payload Adapter Vehicle (PAV) included the following:

- Launch vehicle/payload interface
- · Payload/facility interface
- Payload maneuverability
- Final circularization ΔV

The payload needs to interface with the launch vehicle and the LEO/MEO facilities' Payload Capture and Release Systems. The payload should have its own subsystems to maneuver itself and aid payload capture. The payload also requires propulsion, guidance/navigation, power storage, and communication subsystems to provide the final circularization ΔV needed to go from GTO to GEO after being boosted from the MEO facility.

The PAV, shown in Figure 6, provides the interfaces between both the launch vehicle and the tether facilities. The PAV will mimic the interfaces of current upper stages to both the payload and the launch vehicles in order to be transparent to the users of the system. The PAV will also provide the final circularization ΔV for the payload and therefore will have the fuel load, thrusters, guidance and control, and other subsystems of an autonomous spacecraft. This will enable the PAV to perform much of the terminal maneuvering leading up to capture.

The PAV is envisioned to consist of a structural ring connecting the launch vehicle to the payload. This structural ring will contain deployable grapple systems for capture by the tether facilities, fuel tank and propulsion components, reaction wheels, primary batteries, and the computer and communication system. Rendezvous beacons and antennae would be mounted to the outside of the cylinder and attitude control thrusters would penetrate the cylinder. Additional aft-facing thrusters would be provided for the circularization burn.

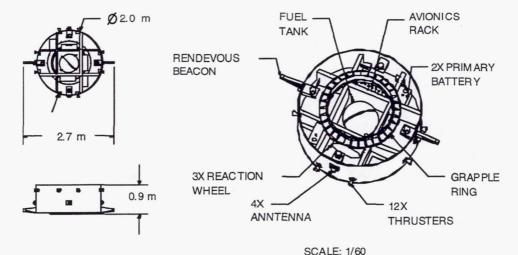


Figure 6: Payload Adapter Vehicle

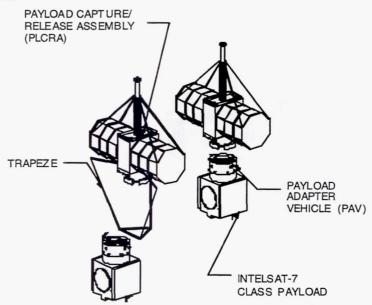
Payload Capture/Release Assembly

The requirements that drove the design of the Payload Capture/Release Assembly (PLCRA) included:

- Facility rotation
- Payload capture transient loads
- PAV capture scenarios
- · Payload mass

The constant rotation of the facility drives the design due to the constant load and the continuously changing sun angle on the solar arrays. Transient loads at capture and release and during acceleration of the payload to the facility spin rate are also significant design conditions.

The capture and release method for the PAV is another major design driver. Two extreme scenarios are shown in Figure 7. The one scenario of flying the payload directly to a hard dock is mechanically simpler but levies very tight requirements on rate and attitude control, as well as position and velocity control (measured in centimeters). The other scenario would deploy a trapeze (larger than the PAV's uncertainty box) and guides. The trapeze and the PAV work together to accomplish a soft dock followed by reeling in the trapeze to a hard grapple. The final design approach selected will likely be between these extremes.



TRAPEZE CAPTURE DIRECT RENDEVOUS
Figure 7: Capture Methods

A PLCRA will be located at one end of each tether facility. It will consist of a capture and grapple mechanism, a structural tether interface, a communication and tracking subsystem (for PAV rendezvous and capture), attitude control sufficient to

maintain alignment for capture, and power generation and storage to accomplish these functions. The PLCRA communication and tracking subsystem will work with the incoming PAV during rendezvous and capture. It will contain attitude control sufficient to maintain alignment for capture and power generation and storage to accomplish these functions. Interfaces to the platform would be limited to communications and the tether itself.

The PLCRA configuration, shown in Figure 8, consists of a conical structure which flares from the tether attachment to the Marmann-clamp style grapple ring. Shelves surrounding the central cone provide mounting for subsystem equipment and the barrel-style solar arrays. A deployable boom extends from the top of the cone to inhibit wrapping of the tether around the PLCRA. The boom also serves as a kingpost to brace the solar arrays against the transient loads resulting from payload capture. The functional and load requirements on the PLCRA identified thus far for the LEO and MEO facilities are similar enough that the same design would suffice for both. The barrel configuration for the PLCRA solar arrays was selected for simplicity and rigidity. The arrays are small enough that the added area would not be prohibitively heavy or expensive. This is particularly true when compared to the cost of constantly rotating planar arrays robust enough to withstand capture and release transient loads. The steady state load due to rotation is a function of desired ΔV and tether length. Early in the study, a 20 km tether was assumed, which resulted in steady state loads of the order of 9 G. The current configuration, however, provides a more benign 1.26 G for LEO and 0.8 G for MEO. Further studies should address overall natural frequency requirements to ensure that the PLCRA does not interact with any tether modes.

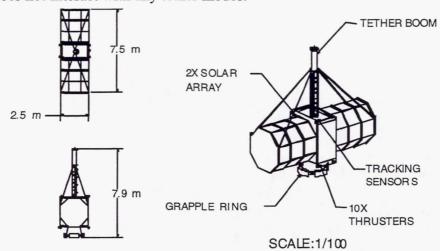


Figure 8: Payload Capture/Release System

Major Design Issues

Part of this study involved defining the major design drivers/issues pertaining to the overall feasibility of the system, as well as identifying areas where future investment is required to develop enabling or enhancing technologies. The most significant issue identified for the two-stage system is the Rendezvous and Capture (R&C) activities. The

most sensitive phase is between release from the first stage and transition and capture by the second stage. This capture is not perform in the fashion that R&C activities have been performed at present with manned spacecraft such as the Shuttle or the Russian Mir re-supply missions. The tether system R&C has high approach velocities and very short capture periods. The previous sections describe the R&C approach that is very rapid when compared to the automated R&C now being explored by NASA or is being used by the Russians. In those activities the vehicles fly in formation for a long period of time and close the gap in a slow system approach that may take several hours to complete that last 10 meters for the Shuttle activities. The recent Mir accident clearly demonstrated the risk of an accident during even these slower docking activities.

The analysis discussed earlier does demonstrate that zero differential velocities and accelerations are possible with properly designed orbits. Essential aspects for this system to be successful require high precession of the knowledge and control of the payload and the rotating tether system. Position / state data accuracy not verified but expected to be on the order of tenths of meters. In order to enable this approach, knowledge of the orbital positions and orientation will be required for the entire orbit. At present the only mechanism to obtain this position accuracy and orientation information is from optical sensors located on the ground. With the advent of a space based differential GPS or space and ground automated optical system this accuracy could be obtained. Future GPS constellations are being considered with modifications to improve space based navigation and attitude control. This combined with positioning beacons on the PAV and the PLCRA would provide sufficient information to determine and control the positions to within 10's of cm or better. A detailed sensitivity analysis is required to determine the required precision and accuracy but has not been performed to date. Future studies should address this to ensure that the capture and release process is practical.

Another issue is the post capture dynamics, loads and tether management. The tether system will experience significant loading following the capture event. The tether was designed to account for the shock loads but these will be mitigated by managing the tether length just after capture very similar to what occurs after capturing a fish with rod and reel. This reeling out and then back in operation is described very well in "Preliminary Design of a 1 km/sec Tether Transport Facility" (J.A. Carroll). These dynamics where not simulated in this study but are acknowledged to be an issue that needs to be addressed in subsequent studies. The motion of the payload and the tether system will damp out rapidly after capture. The combination of reeling in and out can be used to ensure that the damping occurs in a reasonable period. A single orbit is planned before the second release event but additional orbits can be used. The single orbit was chosen to minimize the total transfer time. The use of additional orbits to damp the perturbations introduced is not expected but penalizes only the total transfer time.

The power system for reboost and tether management is large when compared to the current generation of spacecraft but it is comparable to the ISS power system. The total power requirements are 93 to 151 kW for this study. There are indications that this could be reduced by as much as 50% with new technologies.

The issue of collision avoidance is brought up consistently but has a low probability of occurrence even with the entire tether fully extended. The cross sectional area exposed to collision varies with rotation about the center of mass and the planned operational orbit is in an area that is not being used by most satellites of commercial or national interest. The zero degree inclination is not a prime orbit for communication satellites and the limited ground area coverage places constraints on earth resource missions. Because of the low thrust levels and the rigidity of the rotating masses, it is not practical to provide for sudden orbit changes (to accommodate collision avoidance maneuvers) by propulsive means. Orbit tracking of other material in the appropriate orbits will be performed to ensure that sufficient time exists to maneuver and avoid potential collisions.

System Performance

A two-stage tethered system of reasonable size and relatively small mass can be designed for transferring satellites with a mass up to 9,000 lb from LEO to GEO (with the circularization ΔV provided by the PAV or an apogee kick motor on the satellite). The transfer times from LEO to GEO for the two-stage systems examined here are between 16:23 hr:min and 16:50 hr:min which is competitive with the 5:30 hr:min from LEO to GEO of a conventional upper stage. The best estimate of the end-of-life system mass is about 16,500 kg for the two stages without propellant. Assuming the system will be reused 24 times over 2 years to launch 9,000 lb satellites, about 8,000 kg of propellant must be added to the end-of-life system mass (see BIG TETHER REPORT section 4.6). This gives a total mass of 24,500 kg for 24 missions at maximum payload capacity. The tether system therefore would become competitive with respect to a present upper stage (e.g., IUS) on a mass basis after only two launches.

The orbital mechanics of the system are designed with resonant orbits so that there are frequent conjunctions (or visits) between the 1st and 2nd stage. This allows multiple opportunities for re-capture of the satellite in case of a missed capture by the 2nd stage. The revisit time ranges between 7:18 hr:min and 8:10 hr:min for the cases analyzed for this study (E.C. Lorenzini, et al.)

The tether system combines the efficiency of electrical propulsion (high specific impulse) and the delivery speed to GEO of a chemical system. The system is flexible and can be adjusted to limit payload accelerations and to accept for a range of payload masses. The total power/energy requirements are manageable and are comparable to ISS levels. The power and propulsion system is one of the pacing technology areas for this tether system to be successful. The study here addressed using existing technologies, but with advancements now being developed in both the power and electrical propulsion arenas the solutions will be less demanding then assumed here. A single stage tether system from LEO to GEO would be >3 times more massive than a two stage system with present day tether technology. However, an increase of the strength-to-weight ratio of 70% (which is conceivable over the next 15 years from the current trend) would reduce the tether mass by a factor of three and consequently make the single stage tether system much more attractive than at present. As a final comment, the tethered system can not only be used to deliver payloads to GEO but also to return satellites from GEO to LEO.

In a future scenario, not analyzed in this report, the return traffic could be used to offset a large portion of the propellant used for reboosting the stages.

Recommendations / Flight Experiments

This report addresses the system level assessments of a single and two stage tether momentum transfer system. While conclusive evidence of the success of such of a system can not be ascertained, the study did indicate that the approach has significant merit. This tether system is worthy of further detailed analyses including:

- Verifying the influence of environmental perturbations over time and the necessary adjustments to the orbital design
- Developing an approach for the guidance and control during rendezvous and docking
- Assessing the flow of angular momentum and the use of return traffic to restore the momentum
- Determine the feasibility of using the spinning tethers for storing electrical energy, which would reduce the requirement for batteries
- Perform an investigation of alternative orbital scenarios which enable the second stage to provide the circularization ΔV at apogee
- Perform a detailed analysis of the system architecture and the identification of the most favorable configuration
- Determine concepts or issues for ground testing & flight testing

Obviously, an excellent first step would be to demonstrate some of these concepts with a flight experiment. While several flight concepts were discussed, we elected to divide the need for flight experiments and flight demonstrations into two categories. The first category is the subsystem enhancements that include systems such as the power generation and storage, and electrical propulsion. These systems are common with most of the spacecraft being developed and extensive development work is on going in both commercial and the government arenas. These areas are not being suggested as flight experiments due to the development work already underway and the fact that most of these technologies are considered enhancing and not enabling.

The second category is the tether-related efforts. These areas are receiving limited attention in projects being developed by the Naval Research Laboratory. The Canadian Space Agency is proposing a mission called BOLAS which will support some of the orbital motions and dynamics issues but we see the need for an additional flight which would demonstrate many if the issues identified here. The experiment is called Spinning Tether Orbit Transfer System (STOTS) and would demonstrate the spinning tether technologies for LEO to GEO payload transfers. The experiment could be flown as a Delta secondary payload using an MSFC developed deployer and the Canadian reel system from BOLAS. The mission would be six months long with a launch date in 2000. Figure 9 presents the Delta deployment sequence for this mission. The initial cost estimate for this mission is less than \$5 million.

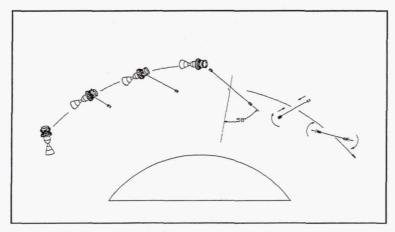


Figure 9: Delta deployment sequence for STOTS

Summary and Conclusions

The results of this study indicate it is possible to obtain the transfer times of chemical upper stages with the efficiencies of electrical propulsion systems by using the momentum transfer between either a single or two stage tether transfer system. A single stage is practical with advances in tether materials and may be achievable within the next ten years. The single stage is preferable over a two stage system due to the complexity of the capture and release events between the first and second stage transfers of the two stage system. The costs are very competitive with existing systems even when the tether system is required to incorporate the development costs.

It is clear that the market is going to continue to expand over the next 10 years with a projected increase in traffic to GEO locations. Sizes of the payloads are increasing due to the desire to extend lifetimes and functionality and due to the very large cost of the slots that are now being auctioned. From the mission analysis results obtained in "Tether Transport System Study Final Report" (Vonderwell, et al.), the tether system from LEO to GEO appears to be highly competitive from a mass standpoint vs. the present chemical upper stages. Additional studies are required, however, to examine the sensitivities of orbit perturbations and to validate the R&C events for a two stage system. While there are clear disadvantages in the complexity of the Rendezvous & Capture (R&C) events, there are potential workarounds and engineering solutions to manage this complexity. A single stage system reduces the complexity of the R&C events considerably and is the preferred solution.

The majority of the required system hardware and software is available with today's technology. The propulsion system design analysis was performed using thrust levels, specific impulse, and power consumption values that exist in commercial off-the-shelf (COTS) hardware from a number of vendors. Lifetime (or number of cycles) of the ion thrusters is the main area where advances (or just demonstrations) in performance need to occur. Table 1 presents the technology readiness levels of the critical technology areas. The technology readiness levels used to assess the technology maturity are similar to those standards being used throughout the industry with a range of 1 to 9. The lower

the Technology Readiness level indicates a lower readiness level. Technology Readiness TR levels of 4 and 5 indicate that the technology is being demonstrated in laboratory environments but not in actual flight applications. A TR of 6 indicates that similar applications have been developed and demonstrated in appropriate environments. TR's of 7 indicate that the technology is currently in use on spacecraft with similar applications. Higher TR's are not presented since they indicate a robust production line with numerous applications in similar environments.

From the engineering analysis results, tether facility rendezvous, and capture of the payload is complex, requiring extrapolations from present technologies for the Attitude Determination and Control System. Additional studies are required to examine the sensor accuracy requirements. The next generation of tether material will likely enable a single-stage system, which, though larger, allows much simpler operations.

Table 1: Technology Readiness levels for critical hardware (excluding tethers)

- OV		Comment
Technology Area	Technology	Comment
	Readiness Level	
Propulsion - Electrical	6	Scale factors for larger systems require additional
		development as well as demonstrating the life times /
		number of cycles.
Power - Storage	7	Technologies exist today with considerable development
		effort underway to improve the systems
Power - Generation	7/4	If current technology is used the costs will be as estimated
		but new technologies such as AMTEC show a great deal of
		promise to reduce size and provide some portion of the
		energy storage needs. These systems have only been
		demonstrated in the laboratory
Space Differential GPS	5	Technology is matured for application on the earth surface
-		in aircraft but applications to space have not been
		demonstrated
ADCS - tether system	5	Only limited demonstrations of a tether system have been
		conducted. Additional data is required to validate the
		control and attitude determination approach.
Automated Rendezvous	5	Similar technologies are being developed but not for the
and Capture		approach velocities required here. Additional development
(AR&C)		is required to support the approach velocities

References

- J.A. Carroll, "Preliminary Design of a 1 km/sec Tether Transport Facility." Final Report to NASA Headquarters, prepared under NASW-4461, March 1991.
- P.N. Fuller, "Commercial Spacecraft Mission Model Update." Report of the COMSTAC Technology & Innovation Working Group, US Department of Transportation, July 1995.
- R.P. Hoyt and R.L. Forward, "LEO-Lunar Tether Transport System Study." Final Report to Smithsonian Astrophysical Observatory, April 1997.
- E.C. Lorenzini, M.L. Cosmo and M. Kaiser, "Mission Analysis of a Tethered System for LEO to GEO Orbital Transfers." Special Report to NASA Marshall Space Flight Center, prepared under NAG8-1303, September 1997.
- D.J. Vonderwell, et al., "Tether Transport System Study." MDC97W5162, Final Report to NASA Marshall Space Flight Center, prepared under NAS8-39400, December 1997.
- B.I. Yakobson and R.E. Smalley, "Fullerene Nanotubes: $C_{1,000,000}$ and Beyond." American Scientist, Vol. 85, 324-337, July-August 1997.

Page intentionally left blank

TETHER SYSTEM FOR EXCHANGING PAYLOADS BETWEEN THE INTERNATIONAL SPACE STATION

AND THE LUNAR SURFACE

Robert P. Hoyt
Tethers Unlimited
8114 Pebble Ct., Clinton WA 98236
www.tethers.com

Abstract

Systems composed of several rotating and/or hanging tethers may provide a means of exchanging supplies between low Earth orbit facilities and lunar bases without requiring the use of propellant. This work develops methods for designing a tether system capable of repeatedly exchanging payloads between a LEO facility such as the International Space Station or a Space Business Park and a base on the lunar surface. In this system, a hanging tether extended upwards from the LEO facility places a payload into a slightly elliptical orbit, where it is caught by a rotating tether in a higher elliptical orbit: This rotating tether then tosses the payload to the moon. At the moon, a long rotating "Lunavator" tether catches the payload and deposits it on the surface of the moon. By transporting an equal mass of lunar materials such as oxygen back down to the LEO facility through the tether transport system, the momentum and energy of the system is conserved, allowing frequent traffic between LEO and the lunar surface with minimal propellant requirements.

Nomenclature

a semimajor axise ellipse eccentricity

E orbital energy

L tether arm length

r radius

 r_p perigee radius V velocity

V velocityγ phase angle

φ flight path angle

 μ_e Earth gravitational parameter = GM_e

 μ_m Luna gravitational parameter = GM_m

subscripts:

apogee
 perigee
 perigee
 apogee
 perigee
 apogee
 perigee
 apogee
 apogee

TLA's:

SSO Space Station Orbit

LEO Low-Earth Orbit

EEO Elliptical Earth Orbit

PEO Payload Elliptical Orbit

LLO Low-Lunar Orbit LTO Lunar Transfer Orbit

ISS International Space Station

SOI Gravitational Sphere of Influence

TTF Tether Transport Facility

Introduction

In his paper "Tether Transport from LEO to the Lunar Surface," Forward showed that it is conceptually possible to construct a system of rotating tethers in Low-Earth Orbit (LEO), Elliptical Earth Orbit (EEO), and Low-Lunar Orbit (LLO) which can lift payloads from LEO to the lunar surface while simultaneously dropping lunar resources down to LEO, without requiring any propellant.¹

In reality, such a LEO-Lunar transport system will require some propellant for orbital maintenance of the tether facilities and for performing modifications to payload orbital-trajectories. In this section, we discuss the design of such a tether transport system and develop a method for planning orbital parameters for the system that will minimize the propellant mass required for payload propulsion.

In designing a tether transport system, minimizing the total mass of the system is a primary design driver. The two largest contributions to the total mass of the system are the tether mass required to support the loads on the rotating tethers and the facility ballast mass necessary to prevent de-orbit of the tether after a payload boost operation. The tether mass can be minimized by staging the lunar transfer orbit insertion into two or more ΔV operations. The necessary facility mass can be minimized by using the mass of a LEO space station, such as the International Space Station (ISS), as ballast mass for one stage of the system, and by proper choice of orbital parameters of the system.

LEO-EEO Tether Staging

While it is possible to design a single tether in LEO to throw payloads to the moon, the large ΔV requirements make a single tether very massive. However, the scaling of tether mass with ΔV makes it possible to greatly reduce the necessary tether mass by splitting the ΔV operations up between two or more tethers.

The mass of a <u>tapered</u> rotating tether with tip speed V_t depends upon ratio of the tip speed to the maximum tip speed V_t of an <u>untapered</u> tether constructed with the same material:

$$V_c = \sqrt{\frac{2T}{Fd}},\tag{1}$$

where T is the tensile strength of the material, F is the design safety factor, and d is the material density. For Spectra 2000, the best fiber presently available, T = 3.25 GPa, d = 0.97 g/cc, and thus $V_c = 1.83$ km/s for a safety factor of F = 2. Moravec found that a tapered tether capable of giving a payload with mass M_v a velocity increment ΔV has a mass M_T given by

$$M_T = M_p \sqrt{\pi} \frac{\Delta V}{V_c} e^{\frac{\Delta V^2}{V_c^2}} erf\left\{\frac{\Delta V}{V_c}\right\}, \tag{2}$$

where $erf\{x\}$ is the error function of x. The mass of the tether thus depends upon the exponential of the square of the ratio $\Delta V/V_c$.

A spacecraft in LEO orbit requires an injection speed of approximately 11 km/s to reach the moon. For a tether in a circular orbit at 300 km altitude, a tip speed of approximately 3.3 km/s is required to throw a payload into a lunar transfer orbit (LTO). To accomplish this ΔV with Spectra 2000 at a safety factor of 2 would require a tether massing approximately 80 times the payload mass. If, however, this ΔV operation is instead accomplished using two rotating tethers, the total tether mass required can be greatly reduced. For instance, a tether in 300 km circular orbit could be used to impart a 1.1 km/s boost to a payload, throwing it into a temporary elliptical orbit. The payload could then be caught and boosted by a second rotating tether facility. If that facility is moving 1.1 km/s faster than the payload, then if its tether has a tip speed of 1.1 km/s it could capture the payload with zero relative velocity on its downward swing and throw the payload on its upward swing, providing it a total ΔV of 2.2 km/s for that second stage. The total ΔV would be the required 3.3 km/s, and the two-stage tether system would require a total tether mass of only 2 times the payload mass. Consequently, until advances in the state of the art of high-strength fibers increases the strength-per-weight of tethers substantially, a multi-stage tether system will have great advantages for reducing the required tether mass.

Design of the Tether Transport Facility Orbits

In this work we develop methods for designing a staged tether system for exchanging payloads between a LEO space station and a lunar base. While staging the tether transport system can significantly reduce the tether mass required, it adds the complication of the necessity to carefully select the tether lengths, rotation rates, and orbital parameters to enable

payloads to be passed from one tether to the next and tossed into a LTO that will intercept the upper tip of a tether orbiting the moon.

In his paper, Forward¹ suggested staging the tether transport system by combining the LEO tether transport facility proposed by Carroll,³ illustrated in Figure 1, with the Elliptical Earth Orbit tether facility proposed by the California Space Institute,⁴ illustrated in Figure 2, to toss payloads into a lunar transfer orbit where they would be caught by a Moravec lunar rotovator ("Lunavator"),⁵ illustrated in Figure 3, which would transfer them to the lunar surface. An idealized schematic of the Forward LEO-Lunar Tether Transport System is shown in Figure 4.

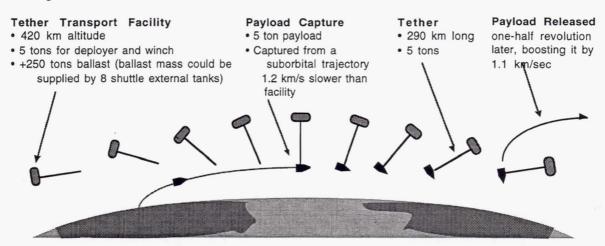


Figure 1. Schematic of the Carroll Tether Transfer Facility design.

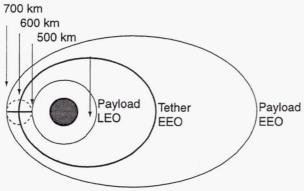


Figure 2. Schematic of the tether in Elliptical Earth Orbit (EEO) proposed by the UCSD Space Institute.

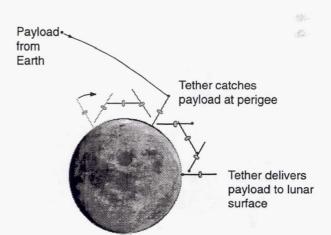


Figure 3. Illustration of a two-arm Moravec Lunavator capturing a payload from Earth and depositing it on the lunar surface.

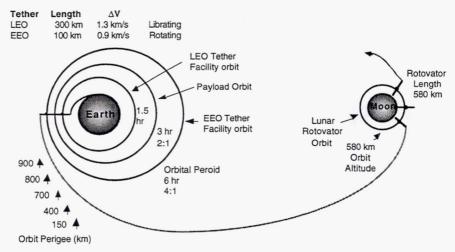


Figure 4. Idealized schematic of the orbital configuration of the Forward LEO-Lunar Tether Transport System where the payload begins in a suborbital trajectory. (Not to scale)

LEO Station to Lunar Surface Transport System

In previous papers, we have presented designs of tether systems for transporting payloads to the lunar surface beginning from sub-Earth orbit (SEO) trajectories⁶ and from low Earth orbit (LEO). However, the largest potential market for a LEO⇔Lunar tether transport system will likely be in exchanging supplies and materials between LEO facilities and lunar bases. It may, therefore, be possible to simplify the LEO-to-Lunar tether transport system by eliminating one of the two Earth-orbit rotating tether facilities used in the SEO-Lunar and LEO-Lunar designs and replacing it with a hanging tether extended upwards from an existing LEO space station. Such an approach will place a larger ΔV requirement on the rotating tether, thus necessitating a higher mass for the rotating tether. However, this system will utilize the existing mass of the space station as ballast mass for one of the tethers, thereby keeping the total mass required by the tether transport system low. A schematic of a tether system for LEO station to lunar surface transport is shown in Figure 5. A payload is assembled onboard the station and then deployed at the end of a long upward-hanging tether. When the tether is fully deployed, the payload is released, injecting it into perigee of an elliptical orbit (PEO). Half an orbit later, when it is at apogee, it is caught by a rotating tether in elliptical earth orbit (EEO), which carries it around one orbit and then throws it into a lunar transfer orbit (LTO). At the moon, a Lunavator catches the payload and swings it down to a base on the lunar surface.

Alternatively, the first stage of this system could be a hanging tether extended upwards from a reusable launch vehicle in LEO in a manner similar to that proposed by Bekey.⁸,9

Because the laws of conservation must be obeyed, the energy and momentum gained by the payload on the way to the moon must come out of the orbital energy and momentum of the tether facilities in Earth orbit. If the tether system is also used to pick payloads up from the lunar surface and drop them down to LEO, and if the return payload mass is equal to the outbound payload mass, the energy and momentum of the payloads falling down into Earth's gravity well can restore the orbital energy of the tether facilities. These return payloads could be oxygen, aluminum, or other products of lunar factories— or they could just be bags of lunar dirt. The total energy required to transport payloads to the moon can thus be reduced to the energy required to launch them into a suborbital Earth trajectory.

During periods when there is not return traffic to balance the upward mass flow, the orbital momentum and energy of the system can be replenished using high specific impulse propulsion such as ion or Hall thrusters. The propellant savings payoff will not be as high as when there

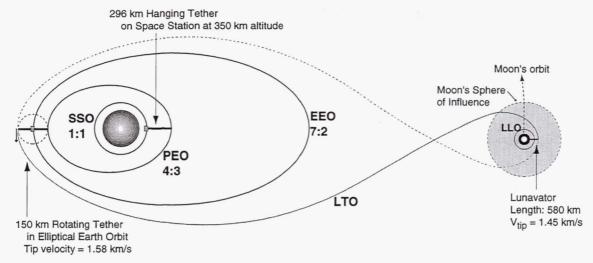


Figure 5. Schematic of a Tether Transport System composed of one hanging tether on a LEO space station, one rotating tether in elliptical Earth orbit, and one Lunavator. (Not to scale).

is return traffic, but the tether system will enable payloads to be transferred to the moon with the fuel economy of electric propulsion without requiring the multi-month transfer times usually associated with high-Isp propulsion.

Orbital Design

The purpose of this analysis is to determine the feasibility of designing a staged tether system to transport payloads between LEO and the Lunar Surface, and to develop a method of planning the scheduling of payload transfers. Accordingly, these initial analyses will not pursue a full-up orbital mechanics calculation including all of the possible perturbative effects. Rather, the analysis will use several simplifying assumptions described below; if the results of this initial analysis indicate that this design is worthy of further development, improved designs of the orbital parameters for the tether transport system can be developed using the same methodology but using improved models for the orbital mechanics.

Simplifying Assumptions

- 1. Elliptical Low-Earth Orbits. We ignore the perturbative effects of the sun, the moon, and other bodies on the orbits of the LEO and EEO tethers, and assume that their orbits are described by Keplerian orbital mechanics (i.e.- their orbits are ellipses).
- 2. Ignore Nodal Regression. The oblateness of the Earth causes nodal regression (rotation of the orbital plane) of satellites in non-equatorial orbits. The regression rate depends upon the inclination and altitude of the orbit, and thus will be different for the LEO and EEO tether facilities (and, to a much smaller extent, the moon). For this first analysis we will assume that the LEO station and EEO tether orbit in the Earth's equatorial plane and thus do not suffer nodal regression.
- 3. Co-Planar, Circular Lunar Orbit. An additional and very significant complication is that the orbit of the moon is inclined by an average of 5°8′ to the ecliptic, while the Earth's axis of rotation is inclined to the ecliptic by 23°27′. Thus even an equatorial tether transport system will require either careful scheduling or some propulsion capability on the payload to permit intercept with the moon. For these preliminary analyses, the tether facilities and the moon were assumed to be in co-planar equatorial orbits. We also ignored the slight eccentricity of the lunar orbit ($e_m \approx 0.0549$), and assumed that the moon travels in a circle with radius of 384,400 km with a velocity of 1.018 km/sec.

- 4. Large Tether Facility Ballast Mass. The transfer of momentum from the tether transfer terminal to a payload will significantly alter the orbit of the tether terminal. For this analysis, we assume that the payload mass is small compared to the terminal ballast mass so that changes in the terminal orbit will be negligible.
- 5. Use Patched Conic Approximation for LTO. We will utilize the methods of 2-body orbital mechanics by assuming that a payload in a Lunar Transfer Orbit moves under the influence of Earth's gravity alone until it enters the gravitational "sphere of influence" (SOI) of the Moon. Thus, the payload trajectory from LEO to the SOI is described by a conic section. Inside the lunar SOI, the gravitational effects of the Earth are assumed to affect the payload and Moon orbits equally, and so the payload is assumed to move relative to the moon under the influence of only the gravitational field of the Moon; the payload trajectory in the Moon's reference frame is thus hyperbolic. In addition, we assume that the lunar sphere of influence is perfectly spherical with a radius of 66,300 km.

Orbital Mechanics of a Staged ISS to Lunar Tether Transport System

The LEO space station has a circular orbit with radius r_{SSO} . The hanging tether extended upwards from the station has a length of $L_{\rm I}$. In an inertial frame of reference, the tether rotates once per orbit with an angular velocity of $\omega_{\rm I} = 2\pi/P_{SSO}$. The EEO tether facility has an armlength of L_{EEO} , rotates with angular velocity ω_{EEO} , and orbits in an elliptical trajectory with semimajor axis a_{EEO} and perigee altitude $r_{p,EEO}$.

The station tether will release the payload into an intermediate elliptical orbit (PEO-payload elliptical orbit). Later, the EEO tether will capture the payload at the apogee of its orbit and toss it into a lunar transfer orbit

We will use the following relationships between the orbital parameters of the space station, payload, and EEO tether:

• Space Station orbital velocity:
$$V_{SSO} = \sqrt{\frac{\mu_e}{r_{SSO}}}$$
, (3)

• Space Station orbital period:
$$P_{SSO} = 2\pi \sqrt{\frac{r_{SSO}^3}{\mu_e}},$$
 (4)

• PEO orbital period:
$$P_{PEO} = 2\pi \sqrt{\frac{a_{PEO}^3}{\mu_e}},$$
 (5)

• PEO Facility Perigee:
$$r_{D,PEO} = a_{PEO}(1 - e_{PEO})$$
 (6)

• PEO Facility Apogee
$$r_{a,PEO} = a_{PEO}(1 + e_{PEO}),$$
 (7)

• PEO orbital energy:
$$E_{PEO} = \frac{V_{p,PEO}^2}{2} - \frac{\mu_e}{r_{p,PEO}} = -\frac{\mu_e}{2a_{PEO}},$$
 (8)

• EEO Facility orbital period:
$$P_{EEO} = 2\pi \sqrt{\frac{a_{EEO}^3}{\mu_e}}$$
, (9)

• EEO Facility Perigee:
$$r_{p,EEO} = a_{EEO}(1 - e_{EEO}),$$
 (10)

• EEO Facility perigee velocity:
$$V_{p,EEO} = \sqrt{\mu \left(\frac{2}{r_{p,EEO}} - \frac{1}{a_{EEO}}\right)} = \sqrt{\frac{\mu_e}{a_{EEO}} \left(\frac{1 + e_{EEO}}{1 - e_{EEO}}\right)},$$
 (11)

where $\mu_e = GM_e$ is the Earth's gravitational parameter.

We desire that the space station and the EEO facility have orbits which are resonant so that transfers opportunities occur periodically. Additionally, we desire that the payload orbit be resonant with these orbits so that if a payload is released by the space station tether and is not successfully caught by the EEO tether, the EEO tether will have additional opportunities to rendezvous with the payload several orbits later. Consequently, we specify that the orbital period of the payload in PEO is M times that of the station orbit, and the orbit of the EEO facility is N times that of the station:

$$P_{PEO} = M P_{SSO} \tag{13a}$$

$$P_{FFO} = N P_{SSO} \tag{13b}$$

Note that *M* and *N* need not be round integers, but should be rational numbers, preferably with small numerators and denominators to permit frequent rendezvous.

From Eqns. (13) and Eqns. (4,5,&9):

$$a_{EEO} = N^{2/3} r_{SSO}. \tag{14a}$$

$$a_{PEO} = M^{2/3} r_{SSO}. {14b}$$

If the space station is in a circular orbit with radius r_{SSO} and the hanging tether has a length L_1 , the initial payload orbit will have a semimajor axis and eccentricity of

$$a_{PEO} = \frac{R_{SSO}^{3} (R_{SSO} + L_{1})}{2R^{3} - (R_{SSO} + L_{1})^{3}}$$
(15)

$$e_1 = \frac{\left(R_{SSO} + L_1\right)^3 - R_{SSO}^3}{R_{SSO}^3} \tag{16}$$

The resonance ratios M and N specify the semimajor axes of the PEO and EEO orbits via Eqns. (14). Using (5) and (15), we find that for a desired resonance ratio M, the hanging tether length L_1 must be

$$L_{1} = \frac{\left[9M^{2}R_{SSO}^{3} + \sqrt{3M^{2}(1 + 27M^{2})R_{SSO}^{6}}\right]^{1/3}}{\left[3M\right]^{2/3}} - R_{SSO} - \frac{R_{SSO}^{2}}{\left[9M^{2}R_{SSO}^{3} + \sqrt{3M^{2}(1 + 27M^{2})R_{SSO}^{6}}\right]^{1/3}}$$
(17)

We can then specify the EEO tether length as L_{EEO} and find the eccentricity of the EEO from

$$e_2 = 1 - \frac{r_{a,PEO} + L_{EEO}}{a_{EEO}},\tag{18}$$

where the PEO apogee is given by

$$r_{a,PEO} = a_{PEO}(1 + e_{PEO}).$$
 (19)

We then obtain the angular velocity of the EEO tether necessary for zero relative velocity at payload capture by calculating the PEO apogee velocity and the EEO perigee velocity and using

$$\omega_{EEO} = \frac{v_{p,EEO} - v_{a,PEO}}{L_{EEO}}.$$
(20)

We can then calculate the perigee velocity and radius at injection into the lunar transfer orbit.

Lunar Transfer Orbit

After the payload is captured by the EEO tether, the tether length can be adjusted to change the tether rotation rate (via conservation of angular momentum) so that the payload will be at the top of the tether when the tether returns to perigee. The payload is then injected into a lunar transfer orbit (LTO) by releasing it from the end of the EEO tether at this time. Thus, the LTO perigee condition for the payload are:

$$V_{p,LTO} = V_{p,EEO} + V_{tip,EEO} = \sqrt{\mu_e \left(\frac{2}{r_{p,EEO}} - \frac{1}{a_{EEO}}\right)} + \omega_{EEO} L_{EEO}$$
 (18)

$$r_{p,LTO} = r_{LEO} + L_{LEO} + 2L_{PEO}.$$
 (19)

The lunar transfer trajectory is illustrated in Figure 6. With the perigee velocity and radius obtained from our original specification of r_{LEO} , L_{LEO} , L_{EEO} , N, and M, we can then calculate patched-conic orbits by specifying two additional parameters: the injection flight path angle ϕ_o and the angle λ_1 , which specifies the point where the spacecraft enters the lunar sphere of influence. If the tether is released exactly at EEO tether perigee and with the tether exactly vertical, then the flight path angle at injection is $\phi_o = 0$.

We calculate the patched-conic LTO following the procedure of Bate, ¹⁰ and find the perilune radius and velocity that will be obtained with the specified parameters. Using an iterative process, we have found a solution which matches the perilune radius and velocity with the radius and velocity of the upper tip of a Moravec Lunavator. This LEO Station to Lunar Surface Tether Transport System will move payloads to and from the moon in the following stages:

Space Station

First, a payload would be assembled onboard a LEO space station such as the ISS. In this analysis, the station is assumed to have a circular orbit with an altitude of 350 km and an orbital period of 91.5 minutes. The payload is then deployed at the end of a 296.4 km long tether and deployed upwards from the station. Because the load on the tether is quite small, the tether mass required is very low, approximately 1/200 times the payload mass.

Payload Elliptical Orbit

The hanging tether releases the payload, injecting it into the perigee of an elliptical orbit with a semimajor axis of 8151 km and an eccentricity of 0.138. This orbit has a period of 122 minutes, 4/3 times the period of the space station; thus the station could retrieve the payload 3 orbits later if necessary.

EEO Tether

Half an orbit later, when the payload is at apogee with an of altitude 2,897 km and a velocity of 6.09 km/s, the payload will be caught by a 150 km long rotating tether in elliptical Earth orbit. The tether facility will be in an elliptical orbit with a semimajor axis of 15511 km and an eccentricity 0.39. This orbit has a period of 320.25 minutes, 7/2 times the period of the space station, so there are frequent opportunities for transfer of the payload from the station to the EEO tether. The facility's orbit will be timed so that, when the payload is at apogee, the facility is at perigee with a velocity of 7.67 km/s. Thus if the tether rotates prograde to its orbit with a tip velocity of 1.58 km/s, the tether tip can rendezvous with the payload with zero relative velocity. Once the tether has caught the payload, the payload will experience a centripetal force of 1.7 g. The EEO facility carries the payload for one orbit. When it returns to perigee, it throws the payload into a lunar transfer trajectory.

Tether Mass: This system places a larger ΔV requirement on the EEO tether than the SEO-Lunar design, and, as a consequence, the EEO tether must be more massive. Using Spectra 2000 fiber with a design safety factor of 2.4, the required tether mass is approximately 3.3 times the

tip mass. With a tip vehicle massing 0.2 times the payload mass, the required tether mass is (1+0.2)x3.3 = 4 times the payload mass.

Facility Mass: Because the facility is in a highly elliptic orbit, the facility mass can be as small as two times the payload mass and the facility will not de-orbit after a boost operation. It may be possible to initiate the system with a small ballast mass and build the ballast up over time using lunar material sent down to LEO as return traffic.

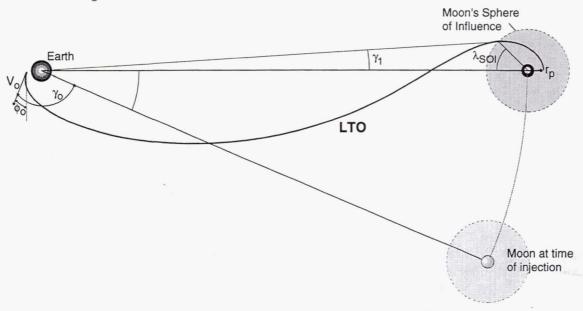


Figure 6. Schematic of the lunar transfer orbit (LTO).

Lunar Transfer Orbit

The EEO tether injects the payload into a lunar transfer trajectory with a perigee altitude of 3197 km and a velocity of 9.26 km/s. The lunar transfer orbit is illustrated in Figure 6. As with the SEO-Lunar system, the transfer trajectory is hyperbolic, with a time-of flight from perigee to the lunar sphere of influence of only 31 hours. The transfer trajectory has a semimajor axis of -158,708 km, and an eccentricity of 1.06. If the insertion into the transfer trajectory is timed so that the angle between the perigee and the moon, γ_o , is 131.4 degrees, the payload reaches the moon's gravitational sphere of influence with a velocity of 2.23 km/s relative to the moon at an approach angle λ_s of 82.9 degrees.

Lunavator

Once inside the lunar sphere of influence, the payload travels in a hyperbolic orbit under the influence of the moon's gravity. It reaches perilune at a radius of 2898 km with a velocity of 2.9 km/s relative to the moon. When it reaches perilune, it can be caught by the tip of a 580 km long Moravec "Lunavator" tether in orbit around the moon. The Lunavator facility would orbit around the moon at an altitude of 580 km. The Lunavator tether would rotate prograde to its orbit with a tip speed of 1.45 km/s, equal to the orbital velocity of the facility. Thus, at the top of its swing it could rendezvous with the payload with zero relative velocity between the tether tip and the payload, and at the bottom of its swing it can deliver the payload to a lunar base with zero velocity relative to the moon's surface.

It should be noted that because the trajectory of the payload in both the Earth and Lunar frame is hyperbolic, if the payload and Lunavator do not successfully rendezvous, the payload will be left in a trajectory that has sufficient energy to leave the Earth-Moon system. The

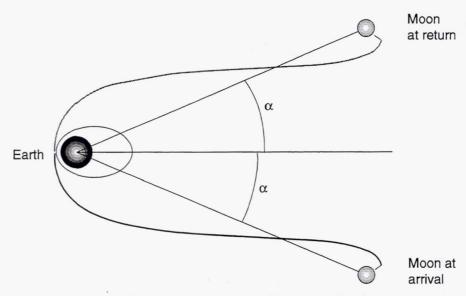


Figure 7. Schematic of outbound and inbound trajectories (not to scale).

payload, therefore, should have some propulsion capability to change its trajectory into one that will return to either the Earth or the Moon.

Lunavator Tether Mass: Since Moravec performed his analysis of the Lunavator concept, available material strengths have improved significantly, greatly reducing the tether mass required. Moreover, although Moravec envisioned a two-arm tether that would touch down on the lunar surface six times per orbit, only one arm is really necessary. Using Spectra 2000 fiber at a safety factor of 2.4, the Lunavator tether mass required would be 2.5 times the tip mass. If the Lunavator has a tether tip vehicle 0.2 times as massive as the payload, the required tether mass is approximately 2.9 times the payload mass.

Return Traffic

Using this system for outbound traffic only would save propellant and time over other methods by allowing high-Isp propulsion to be used to boost payloads to the moon without requiring the long transfer times normally associated with electric propulsion. However, the key to making this SEO-Lunar transport system worthwhile is to have return traffic to balance the flow of orbital momentum and energy in the system. By balancing outbound and inbound mass flow, the system can reduce the amount of propellant required to move mass between Earth and the Moon to the small amounts required for trajectory corrections. By properly scheduling payload departures and returns, the lunar transfer trajectories can be selected to allow rendezvous with the tether facilities in Earth orbit.

The outbound and inbound payload trajectories are illustrated in Figure 7. At the time of arrival of the payload at the upper tip of the Lunavator, the angle between the Earth-Moon radius vector and the centerline of the LTO hyperbola is $\alpha = 23.43^{\circ}$. After depositing the payload on the surface of the moon and picking up a return payload, the orbit and rotation rate of the Lunavator are adjusted slightly so that 3 days, 13 hours, and 43 minutes later, when the moon is at an angle α above the hyperbola centerline, the Lunavator is in position to throw the return payload back down to Earth in a transfer trajectory that is essentially the mirror image of the outbound trajectory. The perigee of the transfer trajectory will thus be at the same point as the perigee of the outbound trajectory, enabling the return payload to rendezvous with the EEO tether.

Opportunities for these ideal trajectories will occur once every 27.3 days. It should be possible to exchange payloads at other times by throwing and catching payloads at positions

other than perigee, and by using propulsion onboard the payload to alter the transfer trajectory. However, unless the tether facilities are very massive, the alterations to the facility orbits caused by non-perigee maneuvers will make trajectory planning quite complicated. For the near future, the 13+ opportunities per year to exchange payload between Earth and the lunar surface that can be provided by perigee-only maneuvers would seem to be more than sufficient.

Facility Mass

In previous studies of tether transfer facilities, 1,3 the LEO facility orbit was chosen to be circular. As mentioned above, in this sub-LEO to Lunar surface transport system design the LEO facility orbit was chosen to be elliptical rather than circular. This choice was driven by the desire to minimize the facility mass required to keep the tether facility in orbit after a boost operation. The LEO tether boosts the payload by a total $\Delta V_{\rm payload} = 2V_{tip}$ Because total momentum must be conserved, the LEO facility will be decelerated by approximately

$$\Delta V \cong 2V_{tip} \frac{1}{\chi_{LEO}},\tag{20}$$

where χ_{LEO} is the ratio of LEO facility mass to payload mass and V_{tiv} is the tether tip velocity. Therefore, if the LEO facility began in a circular orbit, immediately after the LEO facility releases the payload the facility would be placed into a new orbit with an apogee roughly equal to its original circular orbit radius and a perigee that depends upon the mass ratio. For an orbit altitude of 400 km and a tip speed of 1 km/s, a mass ratio of $\chi_{LEO} > 75$ is required to keep the facility perigee above 300 km of altitude, and the tether must be retracted rapidly to prevent it from burning up in the atmosphere. While it may be feasible to use on-orbit waste (spent booster rockets, main shuttle tanks, ISS waste materials) to provide this ballast mass, this large mass requirement appears to make a circular orbit impractical for the LEO facility. However, if the LEO orbit is chosen to have a significant eccentricity, its perigee velocity will be significantly above the circular orbit velocity at that altitude. Thus, with a sufficient mass ratio χ_{LEO} , the post-boost facility orbit will have essentially the same perigee altitude, and will not be de-orbited. For the design given above, a facility mass of 5 times the payload mass would be adequate to keep the reduction in facility perigee to less than 30 km. Thus, by choosing an elliptical initial orbit, the required facility ballast mass can be reduced by over an order of magnitude compared to previous designs.

Because the EEO tether facility is in a highly elliptical orbit, its total mass can also be low while still maintaining the perigee altitude. In fact, a EEO facility mass of approximately 2 times the payload mass would have an interesting benefit in that after the boost operation, the facility would be placed into an orbit nearly the same as the payload orbit (PEO), where it could periodically rendezvous with the tip of the LEO tether. The EEO tether could therefore be captured, serviced, or refueled by the LEO tether facility.

Note, however, that with such low mass ratios, Eqns. (3)-(19) must be modified to account for the finite mass ratio effects.

The mass ratio required for the Lunavator facility is higher, but still within the limits of reason. The required facility mass is driven not so much by the need to keep the facility from deorbiting into the moon, but rather to keep the payload from pulling the facility too far away from the moon after capture. The Lunavator rotates in the same direction as it orbits the moon; consequently, when it captures the payload sent from the Earth-orbit tethers, the payload is traveling faster than the Lunavator center of mass. After payload capture the facility and payload center of mass will be in an elliptical orbit with radius always equal to or greater than the facility's initial orbit radius. A facility mass of 20 times the payload mass will keep the post-capture orbit eccentricity below 0.1. The orbit will also be altered when a payload is deposited on the surface of the moon. Because the tether decreases the orbital momentum of the

payload when it deposits it on the surface, the orbital momentum of the facility will again be increased. Alterations to the orbit can most effectively be minimized or eliminated by picking up a return payload at the same time a payload is delivered to the surface.

As with the LEO and EEO tether facilities, it may be most economical to build a relatively low mass Lunavator facility to begin with and build its mass up over time using material lifted from the lunar surface. Oldson and Carroll have found that, with proper timing, a slowly spinning tether can pick up a payload and release it into an orbit that will rendezvous with the tether facility with a low relative velocity. Thus a Lunavator could possibly build up its ballast mass by picking up bags of lunar dirt and tossing the bags to itself like an elephant tossing peanuts into its mouth.

Numerical Simulation

In order to refine the preliminary design of this system by removing the assumptions of coplanar orbits, patched-conic trajectories, and including the effects of finite ballast mass, we have developed a software tool for numerical simulation of staged tether systems in the Earth-Moon system. This program, called "OrbitSim," models the 3-D orbital dynamics of rotating tethers, payloads, and other satellites. We are currently using this program to improve the designs of the ISS-Lunar and other tether transport systems. Animations of simulations conducted with this program are available on the web at www.tethers.com.

Tether Rendezvous

When considering tether transport systems, the most significant issue that must be addressed is how to accomplish rendezvous between the payload and a spinning tether. The payload-tether rendezvous is fundamentally different from the rendezvous maneuvers usually performed in orbit, such as between the shuttle and the Hubble telescope. In those maneuvers, rendezvous is accomplished by gradually matching the orbits of the two spacecraft. Because the spacecraft co-orbit, the matching of positions and velocities can be accomplished over a relatively long period. In a tether transport system, however, the payload and tether tip do not move in the same orbit; the payload orbit must osculate the trajectory of the tether tip, and both the positions and velocities must be matched at a specific time. To determine just how time-sensitive this rendezvous problem is, we have used the OrbitSim program to examine the rendezvous between the payload at the apogee of the PEO trajectory and the tip of the tether attached to the EEO facility. The relative separation between the payload and tether tip is plotted for the ten seconds before rendezvous in Figure 8. Figure 9 shows that the relative velocity drops essentially linearly until the velocities are matched at t=0; the relative acceleration is approximately 1.6 g. The relative vertical and horizontal separation between the payload and tether tip is shown plotted once a second for the ten seconds before rendezvous in Figure 10. The relative motion is almost entirely in the vertical direction; the rendezvous maneuver is thus conceptually similar to standing on a second story fire escape and catching a coke can that someone standing on the sidewalk below has tossed up to you. The rendezvous maneuver thus is time-critical, but if the tether grapple vehicle has the capability to reel in or out a short length of tether, or if the payload has maneuvering thrusters with a several m/s2 acceleration capability, a capture window of at least several seconds is possible.

Conclusions

By properly choosing the orbital design, a staged tether system for frequent round-trip traffic between a station in low Earth orbit and lunar bases can be developed with very reasonable total mass requirements. Using several simplifying assumptions, including that of coplanar orbits, circular lunar orbit, neglecting nodal regression, and the patched-conic approximation for the lunar transfer orbit, we have developed a preliminary design for a tether transport systems that can throw payloads from a LEO space station and transfer them to the lunar surface. By returning an equal mass of lunar material to the station through the same transportation system, the orbital energy and momentum of the system can be conserved,

allowing payloads to be transported to and from the moon using little or no propellant. By leveraging the system upon the mass of an existing space station, the required mass for the system can be minimized. Using currently available high-strength tether materials, such a system could be built with a total tether mass of less than ten times the payload mass, and a total system mass of less than thirty times the payload mass.

Acknowledgments

This research was supported by a subcontract on the NASA Grant P3776-5-96 to the Smithsonian Astrophysical Observatory, entitled "In-Space Transportation with Tethers." The author would like to acknowledge Bob Forward of Tethers Unlimited, Enrico Lorenzini of SAO, and Joe Carroll of Tether Applications for useful discussions.

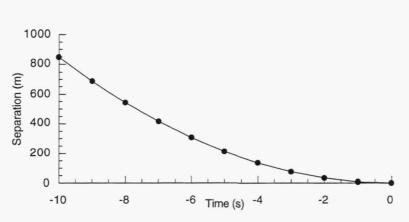


Figure 8. Relative separation between payload and tether tip.

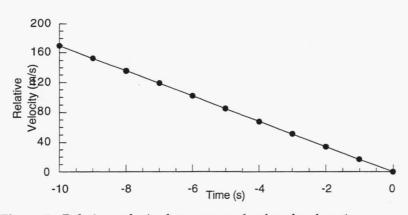


Figure 9. Relative velocity between payload and tether tip.

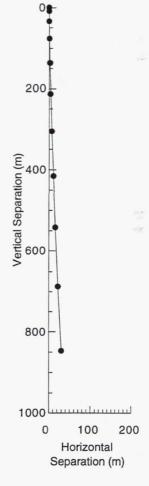


Figure 10. Relative position.

References

- 1. Forward, R.L., "Tether Transport from LEO to the Lunar Surface," AIAA paper 91-2322, 27th JPC, July 1991.
- 2. Moravec, H, "Free Space Skyhooks," unpublished notes dated November 1978.
- 3. Carroll, J.A, Preliminary Design of a 1 km/sec Tether Transport Facility, March 1991, Tether Applications Final Report on NASA Contract NASW-4461 with NASA/HQ.
- Stern, M.O., Advanced Propulsion for LEO-Moon Transport, NASA CR-172084, June 1988, California Space Institute Progress Report on NASA Grant NAG 9-186 with NASA/JSC.
- 5. Moravec, H., "A Non-Synchronous Orbital Skyhook," J. Astronautical Sci., 25(4), Oct-Dec 1977, pp. 307-322.
- 6. Hoyt, R.P., Forward, R.L., "Tether Transport from Sub-Earth-Orbit to the Moon And Back!", invited paper, 16th International Space Development Conference, Orlando, Fl, May 1997.
- Hoyt, R.P., "Tether System for Exchanging Payloads between Low Earth Orbit and the Lunar Surface," AIAA Paper 97-2794, 33rd Joint Propulsion Conference, Seattle WA, July 1997.
- 8. Bekey, I., "Decreasing the Cost/Pound and Increasing the Performance of the Reusable Launch Vehicle by Using Tethered Payload Deployment," NASA/HQ white paper, March 25, 1996.
- 9. Bekey, I., "Tethering: a new technique for payload deployment," Aerospace America, March 1977, pp. 36-40.
- 10. Bate, R.R., Mueller, D.D., White, J.E., Fundamentals of Astrodynamics, Dover, 1971, pp. 333-344.
- 11. Oldson, J, Carroll, J.A., "Potential Launch Cost Savings of a Tether Transport Facility, " AIAA paper 95-2895, 31st Joint Propulsion Conference, July 1995.

Orbiter-Towed Reboost for ISS

By Connie Carrington NASA MSFC Program Development Mail Stop PD12 MSFC, AL 35812

Vernon Keller NASA MSFC Program Development Mail Stop PS02 MSFC, AL 35812

Abstract

Orbiter towing provides a backup reboost capability for the International Space Station (ISS). Results from recent studies are presented, showing performance, system configuration, mission operations, and programmatics. A proposed flight demonstration to mitigate risks is also discussed.

Introduction

Recent events on Mir have highlighted the need to plan for continued maintenance of orbital space stations. Russian innovation in the ongoing solution of spaceflight crises is impressive, but has prompted new questions about ISS's long term plans to handle contingencies. Discussions of Mir lifetime and reboost have focused new attention on ISS plans for long-term reboost capability. Backup and contingency plans include attached Orbiter reboost for early-build ISS, and propellant transfer or tradeout of propulsion modules for long-term options. Another option being considered is an innovative, extremely low-cost alternative, in which the Orbiter uses its own, already-proven propellant systems to tow ISS to a higher orbit. This paper addresses Orbiter towing capability for ISS, as well as an optional demonstration mission to develop and prove this concept.

ISS Towed Reboost

Introduction

Orbiter towing makes use of a Small Expendable Deployer System (SEDS) and a non-conducting, expendable tether, as shown in Fig. 1. The tether is a compliant coupler between the reboosting vehicle and the Station, isolating the Station from hammering and contamination of propulsion systems. Towing also accommodates ISS configuration changes without hardware modifications, since the towing angle can be adjusted so that

reboost loads will pass through the Station center of mass. The SEDS deployer has already been successfully demonstrated in spaceflight on expendable launch vehicle missions: SEDS-1 in 1993, SEDS-2 in 1994 and the Plasma Motor Generator (PMG) in 1993.(4,18,30,33,46) Although the two SEDS missions deployed small payloads on 0.75 mm thin, 20 km tethers, SEDS can readily accommodate much larger payloads and thicker tethers.(3) In June 1996, as part of the Naval Research Lab's Tether Physics and Survivability Experiment (TiPS),(47) SEDS deployed a 2 mm thick, 4 km long tether, similar to the ISS towing tether proposed here. SEDS deployers are *much* simpler, smaller, lighter and less expensive than the powered reel-type retrievable deployer of the Tethered Satellite System (TSS), flown on STS-46 in 1992 and STS-75 in 1996.

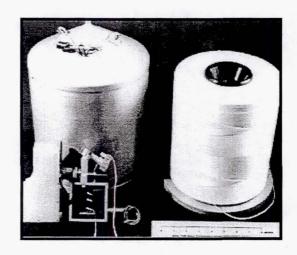


Figure 1. SEDS Deployer, Brake Assembly, and 20 km of Tether (As Used for SEDS-1 and SEDS-2)

Study Guidelines and Trades

Recent studies have determined feasibility and performance of towing the ISS to a higher orbit, using Orbiter Maneuvering System (OMS) and aft Reaction Control System (RCS) propellant on the Orbiter.(15,20) Towing would occur late in the mission, and any propellant reserved but not used for phasing and docking could be used for towing. Additional OMS "top-off" propellant could be flown on missions having launch performance margins that permit it, providing more propellant for towing. Recent JSC studies of attached Orbiter reboost for ISS have estimated that 1000-1500 lb. of OMS and aft RCS propellant may be available for towing, immediately before Orbiter departure.(7,17) These estimates are consistent with OMS and aft RCS propellant levels allocated for dispersions and contingencies in rendezvous and docking on the STS-79 mission to Mir, which had no margins for additional "top-off" propellant.(14)

Top level trades in the ISS tether studies included expendable versus reusable tethers, and vehicle-based versus station-based deployers. Guidelines to minimize the

impacts to Station operations, configuration, schedule and cost, as well as to utilize existing Station hardware and facilities, led to the selection of expendable tethers in vehicle-based deployers. Reloading the tether and relaunching the deployer was found to be more cost effective than developing a TSS-type deployer for reusable, retrievable tethers. The TSS-type deployer design requires a permanent tether location on ISS, rewinding the tether each mission after the Orbiter leaves, and doing the necessary on-orbit maintenance of a reusable-tether deployer.

Study trades also examined the affects of varying tether length. The tether should be long enough to minimize exhaust contaminants near ISS during reboost, and longer tethers provide more Station altitude increase from momentum exchange during deployment. But longer tethers increase tether tension during towing, which increases the loads on Station. Longer tethers also increase the probability of sever due to micrometeroid or debris impact, as well as increase packaging size and system weight. These considerations led to the selection of a 3 km length. With a nominal 2.2 mm width, the current SEDS canister will not need to be resized for this application.

The studies also investigated options for tether attachment to ISS. Power Data Grapple Fixtures (PDGFs) on Station could provide utilities for health monitoring and tether cut commands, to simplify tether handle functions and design. Examination of PDGF interface requirements, such as those for the Space Station Remote Manipulator System (SSRMS) Latching End-Effector (LEE), gave an estimate of the size, weight, complexity, and cost for this attachment option. The study also found that PDGFs were unsuitable due to the small number of sites that could satisfy towing angle requirements, with adequate clearance between the tether and Station components, and that would produce minimal yaw torques on the Station during towing. Other tether attachment options included module trunnions designed for Orbiter transport of modules, and Flight Releasable Grapple Fixtures (FRGFs) and Rigidize Sensing Grapple Fixtures (RSGFs) used by the Shuttle Remote Manipulator System (SRMS) and SSRMS during ISS assembly. A quick assessment of trunnions determined that they would need endcaps and other modifications to ensure that the tether would remain safely and reliably attached during deployment and towing at a variety of loads and angles. FRGFs or RSGFs are present on every Station module, are capable of withstanding the towing loads of an assembly-complete Station in both shear and tension, and provide a small, simple interface that is compatible with robotic manipulator designs. Suitable FRGFs have been selected for towing ISS 4A, assembly-complete, and several other configurations during build.

Performance

The studies used Station propellant savings and lifetime increases as metrics for towing performance. Assembly-complete Station altitude increases, propellant savings, and lifetime as a function of Orbiter OMS propellant are shown in Table 1 and Fig. 2. Propellant savings are estimated by comparing ISS propellant for circular-to-circular reboost, versus Orbiter propellant for towing and ISS propellant for circularization.

Table 1. Assembly-Complete Station Propellant Savings From Orbiter Towing

Orbiter OMS Propellant (lb.)	Station Prop Savings (lb.)	Station Altitude Increase (nm)
0	288	1.6
1000	1065	5.9
2000	1878	8.3
3000	2669	8.6
4000	3843	14.8
5000	4648	16.8
6000	5445	17.5

Orbiter thrust is along the local horizontal, and the towing angle between the Orbiter and the Station is 45° from the local vertical. For 1500 lb. of OMS propellant (which is the current estimate of propellant that may be regularly available for towing), 1470 lb. of Station propellant is saved, even with orbit circularization. The Station altitude is increased 7 nm, and the Station lifetime increases from 215 days to approximately 330 days (if reboost occurs at 221 nm, and the altitude decays to 190 nm). Note that a 1.6 nm altitude increase occurs even for no Orbiter propellant usage, due to momentum transfer during tether deployment. Tether deployment and release puts the Station on a higher elliptical orbit, and the Orbiter on a lower one. Although the Orbiter rises with the Station during towing, the momentum transfer during release saves deorbit propellant on the Shuttle, and nearly offsets the extra propellant needed for deorbit. The additional propellant for Orbiter return to its initial altitude is less than 10 percent of the total used for towing, as shown in Fig. 3.

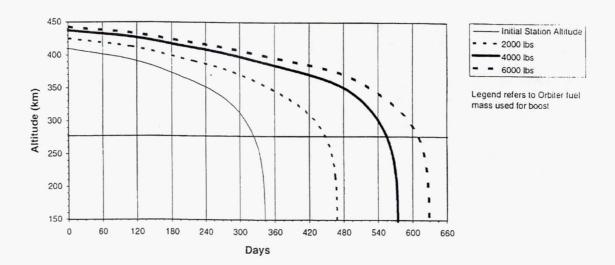


Figure 2. Potential Orbit Lifetime Increase for Assembly-Complete ISS from Orbiter Towing

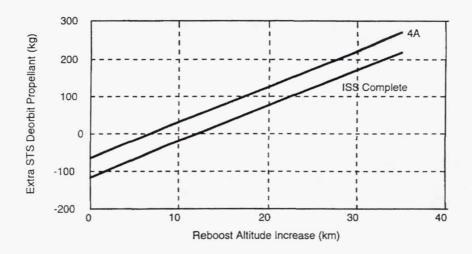


Figure 3. Additional STS Propellant for Deorbit After Towing of ISS

Hardware

Hardware components for Orbiter towing include the SEDS tether deployer system, an Orbiter sill-mounted carrier, and a tether handle to attach the free end of the tether to a Station FRGF. The system mass without the carrier is estimated at 155 lb., with a volume of 2.5 ft³ for the handle and its cradle, and 3.7 ft³ for the deployer and supporting subsystems. Total power requirements are less than 50 W, and a nominal data rate of 5 KBPS is estimated. The SEDS tether canister, brake, cutter, and electronics box together weigh under 30 pounds, can fit in a space of 26 x 10 x 10 inches, and require under 30 W of power. Twenty-five lb. have been allocated for carrier-mounted power and electrical distribution boxes, and for pyrotechnic initiator assemblies (PICs). The tether handle and its cradle/grapple fixture mount weigh approximately 100 lb.

Some modifications to SEDS exit guides and the brake are necessary to accommodate the thicker, 3 km long tether and higher tensions. A modified brake concept has been proposed that will also provide both coarse and fine control.(36) The single anvil-blade tether cutter flown in previous missions will be replaced by two cutters in series to address Orbiter safety requirements.(10,13,24,28)

The tether handle, used as an Orbital Replacement Unit (ORU) on Station, will be grappled by the SRMS to attach the free end of tether to a Station grapple fixture. Earlier operational plans, as shown in Fig. 4, assumed the tether handle would be compatible with both the SRMS and the SSRMS, but voltage incompatibilities between these two systems complicate the handle design. Current plans assume that the handle will be only SRMS-compatible. Spar Aerospace Ltd. has several workable handle concepts under consideration, using existing snare mechanism designs that mate with FRGFs.(42) The SRMS performs all tether attachment operations without EVA, while the Orbiter is docked to the Station. The handle will remain on ISS after towing and tether cut, and will be retrieved on a subsequent mission by the SRMS for return and refurbishment. Hence

the internal, FRGF-compatible mechanisms, as well as the external SRMS-compatible interface, must be functional during handle removal after a cold-soak of perhaps several months. Two options for internal drive mechanisms were considered: a brushless motor, actuator-driven system, or a completely mechanical snare based on the Hand-Operated End-Effector (HOEE), which would be driven by an actuated tool on the SRMS.

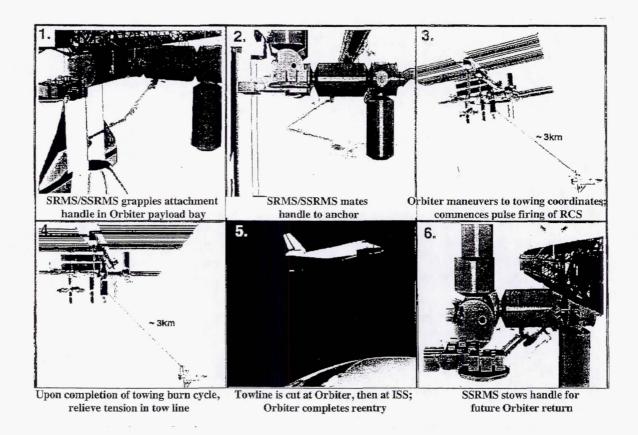


Figure 4. Possible Mission Scenario for Station Reboost From Orbiter Towing (Current baseline for handle is only SRMS-compatable)

The handle also has an external SRMS grapple fixture and target for handle attachment and retrieval on ISS. A concept drawing by Spar is shown in Fig. 5, with a preliminary weight estimate of 70 lb.(43) The baseline design at this time is a completely mechanical, lead-screw driven snare mechanism, based on the HOEE design, with mechanical, electrical, and communications interfaces through the handle grapple fixture. The handle will be controlled by the SRMS end-effector. The handle also includes a transponder/receiver system and antennas compatible with the Orbiter Payload Interrogator (PI), batteries and a power regulation system, a data management system for health and safety monitoring, two tether cutters with safety inhibits, signal conditioning, heaters, cables, and bracketry.(44,45)

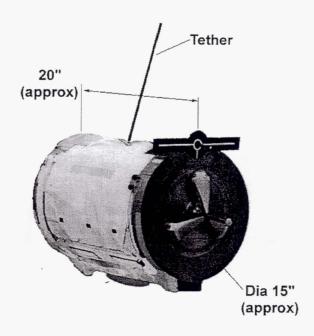


Figure 5. Concept for SRMS-compatible, Reusable Tether Handle

The handle cradle on the carrier will consist of a grapple fixture, and a belt and suspenders for support. To meet redundancy requirements on handle containment within the payload bay, a handle-mounted latch mechanism will interface with the APS, and would be deactivated by the SRMS end-effector for handle release from the cradle, at the same time the internal snare mechanism releases the grapple fixture. The handle is dormant until connected to the SRMS, and all health monitoring, mechanical and avionics system warmups, and battery charging functions will be managed through the SRMS Special Purpose Electrical End-effector (SPEE) connection. This simplifies the Orbiter interfaces for the handle APS. The same SRMS end-effector tool will send commands to warm up the mechanisms for "used" handle removal on subsequent Orbiter missions to the Station. Handle avionics and batteries will not be active for handle removal, and do not have to be functional after being left on the ISS grapple fixture for several months.(45) Handle costs could be reduced by EVA retrieval at the Station immediately after use, to eliminate requirements for long-term cold exposure.

Towing the assembly-complete Station with a 3 km tether produces a tension of less than 1100 N (250 lb). The tether and all hardware must accommodate these loads (and loads during off-nominal conditions) with suitable factors of safety for their components. A variation of the outer sheath for the NRL TiPS tether was selected as a first-cut for the towing tether. This tether is 16 x 650 braided Spectra 1000, with a mass estimate of 1.16 g/m. It is about 2.2 mm in diameter when unstretched, and produces a flat braid when wound. Preliminary tests were conducted to estimate an effective spring

coefficient, the product of Young's Modulus with the cross-sectional area (EA).(27) Vertical "bob-tests" were performed using a 30 m length of tether, in a highbay at MSFC in ambient humidity and at about 75° F, with various weights that provided loads between 1 N up to 1100 N.(38) A top-level assessment of static displacement and period-of-oscillation estimates indicated EA values ranging between 200 and 350 kN.(27) These values are significantly higher than the NRL TiPS EA estimates, but the towing tether has 4 more braided strands, does not have the acrylic core of TiPS, and was subjected to much larger loads. No estimates of damping characteristics have been done at this time, although damping was clearly evident in test plots.(5) Tensile testing has not provided breaking strength estimates at this time. Preliminary worst-case estimates of sever due to micrometeroid or debris impact, while towing with 3 km of this tether at 350 km altitudes for 6 hours, indicates that the probability of remaining intact varies between 0.9989 to 0.99994, for particles ranging between one-fifth to one-half the tether diameter.(25) The towing tether has been selected according to design criteria specified in NASA TM 108537.(37)

Table 2. Orbiter Small Payload Accommodation Carriers

Carrier	Load Capability (lb.)	Beam & Attach HW Wt. (lb.)
APC	90-300	25
EAPC	750-1000	60, 68 or 76 (bay dep.)
MEAPC	300-1000	187-248
SPA GAS Adapter	700	170

Several existing and planned small payload carriers that side-mount on the Orbiter cargo bay may be suitable for integration.(35) These include an Adaptive Payload Carrier (APC), an Extended Adaptive Payload Carrier (EAPC), a Modified Extended Adaptive Payload Carrier (MEAPC), and a Small Payload Accommodation (SPA) Get-Away Special (GAS) adapter beam.(29) Table 2 contains load capabilities and beam weights for these carrier options. These carriers have approximately the same mounting surface area, 20 in by 40 in, although the EAPC and MEAPC are capable of slightly larger mounting surfaces. Carrier selection depends on several considerations: accommodation of primary payloads for STS missions to ISS, dynamic loads applied to the Orbiter sidewall during deployment and towing, and tether exit guide location with respect to the Orbiter center-of-mass. Preliminary estimates locate the exit guide 6 to 9 inches behind the Orbiter center-of-mass, so that tether tensions on the Orbiter balance thruster firings and reduce attitude control propellant requirements. In many cases, the Orbiter center-of-mass is located at the forward edge of bay 9,(26) which places the tether exit guide in bay 9. Maximum towing loads are estimated at 250 lb., and with the hardware weight estimate at 155 lb., one APC may accommodate the entire towing system, depending on dynamic loads analysis. A possible layout of the towing hardware is shown in Fig. 6, using a GAS adapter beam for sizing purposes. This configuration shows the tether handle extending above the sill, which may not be suitable for access to primary payloads in the cargo bay. Hence two APCs may be necessary, in which the deployer and electronics are mounted on one APC at the aft end of the cargo bay, and the handle, its cradle, and the tension-bearing exit guide are mounted on a second APC in bay 9. Both APCs will be mounted on the same side of the cargo bay, with conduit to carry and protect the tether between the two APCs. A preliminary cargo bay layout for accommodation of the towing hardware on STS-91 indicated that either port or starboard locations are feasible, and that the towing hardware and carriers would not impact the primary Orbiter payloads.(19) The carriers will provide health-monitoring capability for the deployer, and will support loads of all components during launch and towing. For two APCs with mounting brackets, cabling, and a lightweight active latch for the tether handle-cradle, the total carrier weight is estimated at 130 lb. The total towing system weight on the Orbiter is 293 lb. (132 kg).

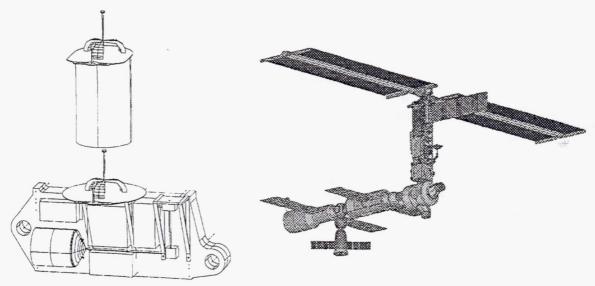


Figure 6. Hardware Layout on One Sidewall Carrier (Baseline is two APCs)

Figure 7. ISS 4A Configuration

Operations

An ISS 4A towing mission was assessed, in which LaRC provided ISS configurations and mass properties (6), MSFC analyzed tether dynamics and control, JSC provided top-level ISS structural loads impacts, and LaRC analyzed Station attitude control during deployment and towing.(16) The 4A configuration consisted of the FGB, the Service Module, the Soyuz, and the Z1-truss with a solar array assembly, as shown in Fig. 7.(6) The ISS mass is 82,500 kg, and the assumed Orbiter mass is 100,000 kg. While the Orbiter is still berthed to ISS, the SRMS end-effector connects to the tether handle and begins warmup and checkout functions. The SRMS then removes the handle from its cradle and attaches it to grapple fixture 2 on PMA3, and the arm is stowed. Deployment is begun by the Orbiter departing PMA3 vertically downward at Lowz

separation burn rates, similar to the current Orbiter Rbar separation sequence from At 600 ft separation, the Orbiter yaws 180° if it is in the tail forward configuration, and then initiates a ΔV of 0.1 ft/s to start natural tether deployment, at an initial tension of 0.75 N. The Orbiter will move forward and down from the Station due to Coriolis effects, and the brake is lightly engaged at ~1.8 km tether length to slow the deployment rate and increase the tension. Due to the sill location of the tether exit guide. the Orbiter slowly rolls to ~60° as the tension increases, providing additional tether clearance with the Orbiter tail and wing. The Orbiter uses its RCS thrusters to slowly pitch up, maintaining a near perpendicular orientation with respect to the tether. Braking increases when ~2.6 km of tether is deployed, and then increases again at 2.9 km to bring deployment to a gentle stop. The tether is now at an 81° libration angle with respect to vertical, and the Orbiter will begin its pendulum swing downward. At a 63° libration angle the Orbiter fires both +X PRCS thrusters for 35 seconds to stop the swing at the 62° towing angle, using 99 kg of OMS prop. The Orbiter then slowly pitches down to local horizontal to begin pulse firing for towing. This scenario is depicted in Fig. 8. Length rates are low during deployment, with a maximum of less than 0.5 m/s. Tether tension is also low, with a maximum of 165 N. The maximum power for braking is 40 W. The Station LVLH attitude is held during deployment by the Service Module RCS thrusters, using 4.5 kg of propellant. Deployment and swing takes approximately 2.75 hours.

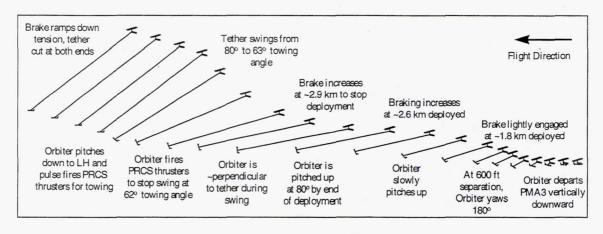


Figure 8. Tether Deployment for Orbiter Towed Reboost of ISS 4A

The 62° in-plane towing angle aligns the tether tension through the Station's center-of-mass. A slight transverse offset between GF2 on PMA3 and the Station center-of-mass will produce a yaw torque. ISS's attitude control system is put into free-drift during towing, which uses no Station propellant. The Station's attitude response remains close to LVLH and is well-behaved, since the tether provides a torque to counteract the gravity-gradient and aerodynamic torques. Very small oscillations occur about the steady-state yaw angle of -3° and roll angle of 5°, and pitch oscillations are ±7° about LVLH.(16) The towing angle is maintained by pulse firing two +X PRCS thrusters at a duty cycle that on the average will counteract the gravity-gradient forces which produce pendulum motion. For ISS 4A and the Orbiter, the duty cycle is approximately 1 second

on for 9 seconds off. The PRCS engines each provide 870 lb. of thrust, and can operate in pulse mode with a minimum impulse of 0.08 seconds.(32) Recently approved Orbiter software modifications will be implemented to automate RCS pulsing for Orbiterattached ISS reboost.(7) These modifications will also provide RCS pulsing simultaneously with RCS attitude control, which will accommodate Orbiter towing. The average tension for towing 4A is 550N, which is well within the ISS structural safety margins. Using the higher estimate of EA at 350 kN, the longitudinal frequency of vibration is 0.008 Hz, very much lower than the Station's lowest frequency at 0.1 Hz, so that there is negligible excitation of the Station's structure from towing. After the OMS propellant allocated for towing is exhausted, the tether brake is eased to unload the tether tension on both the Station and the Orbiter, and the tether is cut at both ends, on command from the Orbiter. For 2000 lb. of Orbiter propellant usage (swing attenuation and towing), the Station's orbit is raised from 380 km circular to 423 x 390 km after tether release. Using an efficiency metric of Orbiter propellant per equivalent ΔV , towing efficiency is estimated at 43 lb. per ft/s. This estimate includes an additional 10 per cent of Orbiter RCS propellant usage for maneuvers and attitude control. The efficiency for towing can be compared to the reboost efficiency of 48-75 lb. per ft/s for Orbiter attached reboost, which was determined for Flights 3A, 5A, and 7A.(17) The Orbiter is put on a 416 x 385 km orbit after release, and the tether on a 419.5 x 387 km The tether without endmasses has an orbit life of between 3 and 13 days, depending on solar activity, after which it reenters and burns up.

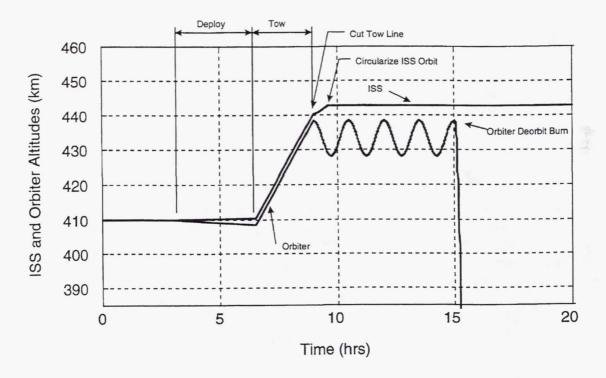


Figure 9. Timeline for Orbiter Towed Reboost of Assembly-Compete ISS, 6000 lb. Propellant Usage

A top-level assessment of towing the assembly-complete Station was also performed. A towing angle of ~41° was maintained, with a thruster duty cycle of 0.95 seconds on for 9 seconds off. Tether tension was less than 1100 N during towing, and for 6000 lb. of Orbiter propellant, a 17.5 nm altitude increase is achieved. A timeline for this mission is shown in Fig. 9.(41)

Technical Risk Assessment and Abatement Plans

The SEDS/SEDSAT SEDS-3 mission was demanifested from its Orbiter flight primarily due to concerns about safety issues.(21,22,23) Although Orbiter towing has a very different mission profile from the deployment and swinging release of a payload, there is much to be learned and applied from the SEDS-3 experience. For the towing mission, deployment rates are much lower and can be controlled more readily by the Orbiter due to higher tensions. A short mission length as well as tether size and construction significantly reduces risks due to micrometeoroid cut and subsequent tether snapback issues. The second towing study team, which initiated work in July 1996, consisted of the SEDS/SEDSAT engineering, operations, safety, and management team, and provided lessons learned and continuing design experience from SEDS-3. (10,12,13,24,28,34,37,40)

Several technical risks were identified in the second towing study, and plans to address those risks were proposed. The implementation of two-fault tolerance was identified as an issue that must be solved early in the program schedule. A preliminary failure mode analysis study was recommended, as well as a Phase 0 safety TIM with joint Shuttle and ISS safety review panels, and an implementation plan for the safety review panel recommendations. Concerns about tether deployment and system dynamics for the towing operation will be addressed by a preliminary dynamics analysis and assessment, as well as winding/deployment tests, and brake and fast cutter tests. Results would be reviewed with JSC Mission Operations Directorate and the ISS Project Office. MSFC currently has a small activity to characterize towing tether properties, and to perform winding and deployments. The tether handle provides new technical and schedule risks not present in the SEDS-3 mission. Abatement plans include an emphasis on the development of requirements and hardware design early in future activities, and pursuit of parallel attachment concepts until Preliminary Requirements Review (PRR). Tether sever and snapback risks are partially addressed by very low probabilities of occurrence with micrometeoroid impact, as well as promising new test results of snapback attenuation with mass discontinuities in the tether.(31) Towed reboost depends on Orbiter PRCS pulse firing, and software modifications to automate this process. Recently approved Orbiter software modifications appear to adequately satisfy these needs, and the development of more detailed requirements for towing implementation will address these concerns. In addition to the risk abatement tasks identified above, future work also includes project planning, systems requirements development and documentation, brake and fast cutter assessment, design modifications and testing, a preliminary loads and thermal analysis, and Orbiter sill carrier integration analysis.

Benefits From Towing

The Station propellant savings from Orbiter towing are significant for even nominal amounts of OMS propellant, and the Orbiter has the capability to provide reboost throughout the lifetime of ISS. Towed reboost requires little or no physical modifications to either the Orbiter or the Station, using proven Orbiter propulsion systems and avoiding the cost, complexity, and safety risks of on-orbit fluid transfer from the Shuttle. Orbiter thruster firings far from ISS minimize contamination and risks of damage, and tethers provide a soft coupling between the Orbiter and Station that readily accommodates Station configuration growth. A schedule that minimizes initial program costs would still provide hardware ready for STS integration after 24 months. At costs that have been estimated at an order of magnitude lower than on-orbit propellant transfer or propulsion module options, Orbiter towed reboost provides an extremely low-cost option for supplementing ISS onboard propulsion systems.

Progress Demonstration Mission—Raduga Deboost By Progress-M Towing

Introduction

A towing demonstration mission is proposed, in which the 350 kg Raduga (VBK) reentry capsule is deployed and towed on the 3 km tether downward by the Russian Progress-M. Flight objectives are to develop hardware and operational procedures, provide confidence in tethered towing, and demonstrate altitude-change performance. Mission phases to be demonstrated are deployment, braking, swing and pulsed towing, tension reduction, simultaneous tether cut, and release of the two vehicles and the tether into their respective orbits. Hardware to be demonstrated includes the thick 3 km towing tether, the handle avionics and tether cutters, the deployer, brake, fast cutters, deployer electronics, and GPS receivers on both endmasses.

Deployment will be monitored and recorded visually from Mir or ISS by Inspector, the small freeflying robotic facility to be flight-tested this December.(11) GPS data from the two endmasses will provide orbit verification, and if deployment and towing are phased properly, optics from Hawaii will be able to visually record the tether cut and track the tether trajectory with respect to the two vehicles. The thermal protection system on Raduga will have been removed, so that it will burn up rather than survive reentry as usual.

Operations

All system components are to be integrated into Raduga and Progress-M at Baikonur, with tether connection to Raduga being made either at the launch site, or onorbit by the Mir/ISS cosmonauts. The SEDS deployer and Raduga mounted in its standard carrier bracket in the Progress-M cargo hold are shown on the left of Fig. 10, with the docking module in its docking position. After regular Progress-M operations at

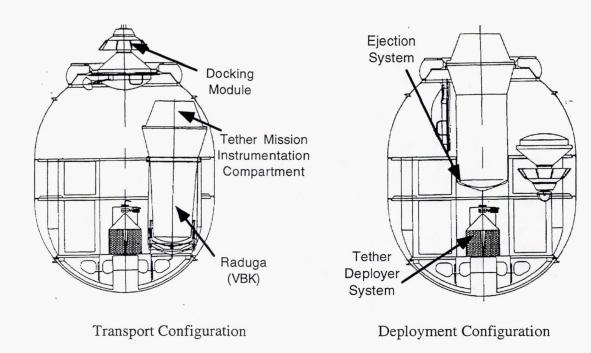


Figure 10. Raduga in Progress-M Cargo Bay (2,39)

the Station, the cosmonauts will install Raduga into its ejection system, as shown on the right of Fig. 10, one day prior to Progress-M departure. The Progress-M departs to a safe distance from the Station, but still within sight of Inspector's cameras. The Station's cosmonauts will teleoperate Progress-M maneuvers, power on the systems, and initiate the experiment. The cargo opening of Progress-M is pitched backward 15° from nadir, and the Raduga is ejected at approximately 1 m/s. After release, the tether and capsule swing down and forward, as shown in Fig. 11. Data from both the Raduga and Progress-M will be transmitted to the ground at TsUP. Braking is initiated at 2.75 km of deployed tether, and increases in increments as the tether deploys to its 3 km length. Maximum braking power is 21 W. At full deployment, the tension is 14.5 N and the tether is at a 51° libration angle from nadir. The tether swings to the towing angle, which has been selected at 45° for simulation purposes. Progress-M and Raduga documentation indicate center-of-mass locations along the vehicle centerlines, so towing angles are not constrained as in Orbiter/ISS towing. In later analyses, towing angles may be selected to minimize propellant usage by balancing Progress-M tension and RCS torques. The Progress-M performs a series of small pulses to slow and stop libration, and at the same time pitches slowly up into a local-horizontal attitude for downward towing. Towing requires a pulse of 1.2 seconds on for Progress-M's 417 kg main engine, with 10 seconds off between pulses. Deployment and swing take approximately 52 minutes, and for 33 minutes of towing, the Progress/Raduga system is lowered by about 4 km. At the end of towing, tension will be reduced to a predetermined value by unwinding the brake, which will lower the recoil velocities back toward each vehicle if cutting is not simultaneous. One cut command will be transmitted from the ground to both vehicles, which will sever the tether at both ends. From an initial 300 km circular orbit, Progress-M is released into

a 293 x 245 km orbit, Raduga will go into a 289 x 237 km orbit, and the tether trajectory will follow 291 x 241 km. Progress-M will then be commanded by the ground to reenter and burn at an appropriate point in its orbit. Raduga without its thermal protection system may last from 13 to 24 days before reentry and burn, and the tether will burn up after 1 to 3 days.

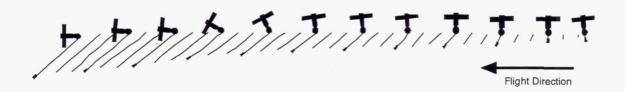


Figure 11. Raduga Deployment From Progress-M

Hardware

Table 2 lists towing system components and their mass, size, and power estimates for both Progress-M and Raduga. The SEDS canister has not been resized from the SEDS-1 and 2 missions, although the brake and cutters are newer variations of those designs. The running tensiometer is similar to that of the SEDS missions, but the computer is a new design currently being developed at MSFC. The ejection system, designed by RSC Energia, is an explosive bolt that activates a cascaded spring system.(2,39) Power will be provided by Progress-M for components in its cargo bay.

Raduga's components consist of the Alenia Aerospazio transponder/receiver system that flew on TSS-1.(1) It was selected since it is already compatible with the Orbiter Payload Interrogator, and will be suitable for the ISS towing tether handle. Only one tether cutter is being integrated into the Raduga, and since it is inboard of the 3-axis Langley endmass tensiometer, it will need to be modified to provide clearance so that tether motion will not interfere with tensiometer readings. The accelerometer package consists of 3 QA-2000 accelerometers, and the battery is the 28 V Eagle Pitcher silverzinc one that provided 11 hours of on-orbit power to the SEDS endmass.

Benefits of the Towing Demonstration Experiment

Many of the technical risks of Orbiter-towed reboost of ISS can be minimized by on-orbit demonstration with unmanned vehicles. The SEDS deployer with the thick 3 km towing tether will be demonstrated in space, and much of the handle avionics will be proven. The mission will determine in the proper space environment such tether characteristics as deployment friction and stiffness, damping, and longitudinal motion during pulsed towing. All mission phases will be demonstrated, including controlled deployment, towing performance, synchronized cut at both ends of the tether, and release of the vehicles and tether into separate and safe trajectories. Instrumentation includes

tension, accelerometer, and GPS data from both vehicles, as well as visual data from Inspector at the Station for deployment and transition to towing, and visual monitoring of tether cut from Hawaii.

Table 3. Progress-M Towing Demonstration Hardware

	Mass (kg)	Dimensions (mm)	Power (W)
Progress-M		No.	
Canister/spool	10	354 x 253 diam	
Tether	3.5	3 km x 2.2 mm	
Brake	0.5	152 x 76 x 66	5
Cutters (2)	1	152 x 76 x 66	10 (instant)
Tensiometer	0.5	25 x 25 x 66	1
Computer	3	152 x 152 x 101	8
GPS receiver	2	250 x 220 x 143	5
Signal conditioning	1.2	76x 176 x 152	1
Power conditioning	3	152 x 152 x 101	2
Ejection system	10		?
Brackets	5	1	,
Cables	4		
Progress-M Total	45		32 +
Raduga	-		
Transponder	3.6	250 x 220 x 143	12.7 @ 2W Rf
Receiver	4.5	152 x 152 x 101	8
Antennas (2)	0.5	37.5 x 150 diam	
Computer	3	152 x 152 x 101	8
3-axis accelerometer package	0.7	59 x 59 x 59	5
SEDS EM tensiometer	0.6	126 x 76 x 51	1
Signal conditioning	1.2	76 x 176 x 152	1
Cutter	0.5	76 x 76 x 66	5 (instant)
Power conditioning	3	152 x 152 x 101	2
Battery	4.4	177 x 177 x 152	
GPS receiver	2	250 x 220 x 143	5
Brackets & mounts	4	1	
Cables	2		
Raduga Total	39		48
System Total	84		

Discussions with Energia indicate that nothing less than a 24 month schedule is reasonable for the Progress-M/Raduga demonstration. Costs of this mission have not yet been estimated, but since the Raduga towing hardware does not require the tether handle's snare mechanisms, the redundant systems requirements, survivability requirements for

release and return from ISS, or power, data, and mechanical interfaces with the SRMS, towing hardware costs are expected to be less than those for ISS towing. The cost of Russian vehicle use has not been estimated. The sill carriers and Orbiter integration costs are also not incurred, although the experiment will need Progress-M power and data interfaces, and integration by Energia.

Summary

Orbiter towing is a low-cost backup option for ISS reboost, in synch with backup plans for attached-Orbiter reboost of early-build Station. It provides a flexible, light-weight Orbiter-based system that does not impact already manifested primary payloads, and takes advantage of propellant not used for rendezvous and docking. Propellant utilization is comparable with Orbiter-attached reboost, but towing can be put to use throughout Station life. To prove out towing operations and allay safety concerns, an unmanned demonstration mission has been proposed. Validation of the tether towing process by this risk-mitigation experiment enhances capability to perform towing of ISS during late-assembly and operational stages.

Acknowledgments

The authors need to recognize the early work of Joe Carroll of Tether Applications, and Gordon Woodcock, Irwin Vas, and Jeffery Johnson of Boeing Huntsville, in identifying the feasibility of Orbiter towing for ISS reboost. The MSFC SEDS-3 tether team made major contributions to the ISS towing mission discussed in this paper, as well as James Dagen, Bill Jordon, and the ISS Program Office at JSC. The authors would also like to thank A. Kuznetsov of Energia for his recommendations on the Progress-M/Raduga demonstration.

References

- 1. Allasio, A., "TSS Communications System," Faxes, May 1997.
- 2. Alenia Spazio S.p.A., RSC Energia, and Daimier-Benz Aerospace, "TATS, Tether Assisted Transportation System Execute Summary," ESTEC Contract No. 11439/95/NL/VK, Jan. 1996.
- 3. Carroll, J., "SEDS Characteristics and Capabilities," *Fourth International Conference on Tethers in Space*, Washington D.C., April 1995, pp. 1079-1090.
- 4. Carroll, J., "SEDS Deployer Design and Flight Performance," *Fourth International Conference on Tethers in Space*, Washington D.C., April 1995, pp. 593-600.
- 5. Coleman, A., "Orbital Tether Towing Development Test Measurements," TCP# PTT-DEV-ED97-085, Aug. 1997.
- 6. Cruz, J., "ISS 4A Configurations," Fax, Dec. 1996.
- 7. Dagen, J., personal communication, May 1997.
- 8. Evans, S., "Preferred Orientation for Orbiter Tether Towing Risk Mitigation Experiment," memo, July 1996.
- 9. Evans, S., "Tether Motion With Respect to Progress M," memo, Aug. 1996.

- 10. Galuska, M., "Orbiter Tether Towing (OTT) Flight Demonstration, Safety and Unique Hazards Control," Jan. 1997.
- 11. Harwood, W., "NASA to Test Robotic Camera," *Space News*, Vol. 8, No. 31, Aug. 4-10, 1997, p. 24.
- 12. House, K., "Fast Cutter Designs," July 1996.
- 13. Jackson, R., "ISS towing Mission Flight Demonstration/Operational Hardware Top Level Requirements," July 1996.
- 14. JSC Flight Design and Dynamics Division, "STS-79 Flight Requirements Document, Level A Groundrules and Assumptions," Appendix A, Flight Cycle (FLT) Profile, Jan. 1996.
- 15. Keller, V., et. al., "Space Station Reboost Via Orbiter Towing," AIAA Space Programs and Technologies Conference, Huntsville, AL, Sept. 1996, Paper No. AIAA 96-4252.
- 16. Kumar, R., "Space Station Stage 6 Flight 4A Attitude Control Analysis," Jan. 1997.
- 17. Martin, M., "Orbiter Translation of ISS Stack for 3A-7A, Rigid Body Analysis," Dec. 1996.
- 18. McCoy, J., et. al, "Plasma Motor-Generator (PMG) Flight Experiment Results," *Fourth International Conference on Tethers in Space*, Washington D.C., April 1995, pp. 57-84.
- 19. Melkerson, Y., "JSC SRMS Mission Design," May 1996.
- 20. MSFC, Boeing Defense and Space Group, and Tether Applications, "Downmass Deployment/Disposal From International Space Station Using Tethered Systems," Contract NAS8-50000, Schedule F, TOF-007, Final Report, Jan. 1996.
- 21. NASA JSC Payload Safety Review Panel, "SEDS/SEDSAT Phase 0/1 Flight Safety Review, Summary of Action Items," Jan. 1996.
- 22. NASA JSC Payload Safety Review Panel, "SEDS/SEDSAT Phase 0/1 Flight Safety Review, Payload Hazard Report," May 1996.
- 23. NASA JSC Payload Safety Review Panel, "SEDS/SEDSAT Safety Technical Interchange Meeting, Summary of Action Items," May 1996.
- 24. Parker, J., "Orbiter Tether Towing (OTT) Flight Demonstration, Functional Mission Concept(s) and Architecture," Jan. 1997.
- 25. Pavelitz, S., "Tether Survivability Results for the Tether Towing Study," Sverdrup Technology Memo, Aug. 1996.
- 26. Ponce, W., private communication, Oct. 1996.
- 27. Powers, J., "Tether Towing Material Loads vs. Strain," private communication and analysis results, Aug. 1997.
- 28. Ray, D., "Orbiter Tether Towing (OTT) Pre-Phase 0 Flight Safety Compliance Data Package and Hazard Analysis," Jan. 1997.
- 29. Rockwell International Space Operations/Integration & Satellite Systems Division, "Adaptive Payload Carriers," Fax from W. Jordon, JSC Small Payloads Integration Office, June 1997.
- 30. Rupp, C., "Flight Data from the First and Second Flights of the Small Expendable Deployer System (SEDS)," Fourth International Conference on Tethers in Space, Washington D.C., April 1995, pp. 133-148.

- 31. Santangelo, A., "AIRSEDS-S Recoil Effects," Faxes, Aug. 1977.
- 32. Shuttle Project Office, "Orbiter Reaction Control System," 1994.
- 33. Smith, H.F., "The First and Second Flights of the Small Expendable Deployer System (SEDS)," Fourth International Conference on Tethers in Space, Washington D.C., April 1995, pp. 43-56.
- 34. Smith, H.F., "SEDS/SEDSAT Lessons Learned," July 1996.
- 35. Space Shuttle Project Office, "Small Payload Accommodations," Appendix 4, Revision K, of NSTS 21000-IDD-SML, Feb. 1994.
- 36. Tomlin, D., "Brake Concepts Friction Comparisons for the Towing Mission," memo, Sept. 1996.
- 37. Tomlin, D., et. al., "Space Tethers: Design Criteria," NASA TM 108537, July 1997.
- 38. Verhage, M., "Tether Test Plans," June 1997.
- 39. Vsokanov, V. et. al., "Readiness of Tether Technologies for Use at the Orbital Station," *International Round Table on Tethers in Space*, Noordwijk, The Netherlands, Sept. 1994, pp. 309-348.
- 40. Wallace, B., "SEDS/SEDSAT Safety Issues Applicable to OTT," Nov. 1996.
- 41. Welzyn, K., "Orbiter Towed Reboost Dynamics for Assembly-Complete ISS," April 1997.
- 42. Willson, C., "OTT Handle," Fax, Jan. 1997.
- 43. Willson, C., "Tether Handle Mass," Fax, Oct. 1996.
- 44. Willson, C., "Tether Handle ROM," Fax, Feb. 1997.
- 45. Willson, C., "Tether Handle Summary," email memo, Dec. 1996.
- 46. Wood, G., et. al., "The Small Expendable Deployer System (SEDS) End Mass Experiments," *International Round Table on Tethers in Space*, Noordwijk, The Netherlands, Sept. 1994, pp. 126-145.
- 47. Zedd, M., "TiPS," Tether Technology Interchange Meeting, Huntsville, AL, Sept. 1997.

Page intentionally left blank

Application of an Electrodynamic Tether System to Reboost the International Space Station

Irwin E. Vas, * Thomas J. Kelly, * and Ethan Scarl*

ABSTRACT

The results of a study on the application of an electrodynamic tether system to reboost the International Space Station are presented. A new and novel method is recommended using a partially bare tether. Locations are suggested as to where the tether system is to be attached at the Space Station. The effects of the tether system on the microgravity environment have been characterized and actually may be beneficial in that the system could be operated during the quiescent period. Alternative approaches to tether deployment and retrieval are discussed. It is shown that a relatively short tether system, 7 km long, operating at a power level of 5 kw could provide a cumulative savings of over a billion dollars during a ten-year period ending 2012. This savings is a direct result from a reduction in the number of flights normally required to deliver propellant for reboost.

*The Boeing Company Information, Space and Defense Systems Group 499 Boeing Blvd. Huntsville, AL 35824-6402

NOMENCLATURE

a	semi-major axis
\boldsymbol{A}	wetted surface area
C_d	drag coefficient
D	atmospheric drag force
F_{t}	tether force
'n	orbital altitude
I_{sp}	specific impulse
m	ISS mass
m_r	reboost mass
n	mean motion
T	tangential perturbation acceleration
t	tether thickness
w	tether width
μ	mass parameter $(398600.5 \text{ km}^3/\text{sec}^2)$
ρ	atmospheric density
ν	orbital velocity
R_e	Earth radius

INTRODUCTION

There has been a renewed focus on reboost of the International Space Station (ISS) due in part to a delay in the delivery of the Russian Service Module and the use of the Progress spacecraft. A major means to provide reboost to the ISS would be by regular flights of the Russian Progress M. Several other reboost propellant carriers/reboost vehicles have been proposed such as the Progress M2, Propulsion Control Module, Interim Control Module, and a variation of the Inertial Upper Stage. The Progress M is the only existing vehicle that performs this task. All other vehicles have either to be designed and built or be modified. A different approach presented in this paper is to provide reboost by a propellantless method.

There has been extensive work carried out with tethers in space. Most of this work has been documented in conference proceedings up to 1995. The first demonstration of a non-conducting tether took place in 1967 with Gemini II in low Earth orbit illustrating spin stabilization. Most of the flight demonstrations, however, have taken place in this decade for both non-conducting and conducting tethers. Electrodynamic tethers have been demonstrated in space on a number of missions. The Tethered Satellite System (TSS) was an Orbiter-based system which deployed to a length of 19 km and generated approximately 2 kw of electrical power. The Plasma Motor Generator (PMG) was flown as a secondary payload on a Delta II which deployed to a length of 0.5 km and successfully demonstrated the principles of electrodynamic tether reboost. The Small Expendable Deployer System (SEDS) flew twice as a secondary payload on Delta II launches which demonstrated hollow cathode current collection limits from 200-900 km. In addition, an electrodynamic tether propulsion for upper stage applications is planned for development as part of the Advanced Space Transportation Program.

The low-Earth orbit of the ISS will be optimized for economical reachability which will subject it to such high levels of aerodynamic drag that the orbit will be vulnerable to collapse if not reboosted at intervals of a few months. An electrodynamic tether is the only reboost method capable of using solar energy while consuming no propellant. It takes advantage of the fact that the near-Earth environment provides a magnetic field as well as aerodynamic drag. This environment also supplies a thin environmental plasma that is capable of closing a tether circuit without transmitting the resulting deceleration to the tether or its attached platform. The conductivity of the environment requires that the tether be insulated along any portion which is to generate voltage or thrust, keeping the surrounding plasma from shorting out its circuit.

Because it is easier to collect electrons at the far end of a tether, and easier to reemit them from an electron gun (plasma contactor) on the platform, electrodynamic tethers are usually operated with their negative end at the platform, directed nadir for reboost or zenith for power generation. This mechanism is fortuitous, but limits the allowable current to the excess capacity of the Station's existing plasma contactor, assumed to be about 5 amperes. Thus, to power the tether with 5 to 10 kW, approximately 1 to 2 kilovolts are required. This is about the limit of what was assumed to be an acceptable voltage, even if insulated, at the Station surface. To achieve this voltage the tether length would need to be between 5 and 15 km long.

ISS DRAG AND REBOOST PROPELLANT NEEDS

The results presented in this paper are derived from a study (References 1 and 2) conducted in 1996 which assumed that the first element of the ISS would be in orbit in late 1997. Even though there is a delay in the flight assembly sequence, the trends illustrated herein remain valid. With the proposed initial flight taking place in 1997, ISS would be totally assembled by 2003.

This study used the results from the Design and Analysis Cycle 4 (DAC #4) as a baseline for the altitude profile and reboost propellant needs of the ISS. (Reference 3) During the build-up phase and subsequent years of operation, the planned altitude of the ISS is shown in *Figure* 1. The altitude profile of the ISS is subjected to a number of competing performance requirements such as quasi-steady microgravity, resupply vehicle limitations, and 180-day minimum orbit lifetime. Satisfying these requirements is made more difficult by the variations in atmospheric density which exhibits daytime highs and nighttime lows, as well as variations commensurate with the 11-year solar cycle. In *Figure* 1, the negative slopes are the result of orbital decay due to aerodynamic drag, whereas, the sharply positive slopes are the result of orbit raising propellant reboost maneuvers. Note, these reboost maneuvers do not occur during the

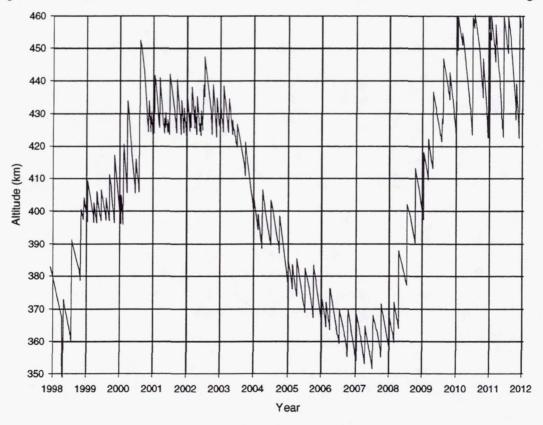


Figure 1 Recommended Space Station Altitude

quiescent microgravity periods. The propellant required to keep the Station in its planned orbit is approximately 135 mt over the assembly phase 1998 - 2002, and the ten year operational phase from 2003 to 2012. The distribution of propellant over this period of time is shown in *Figure* 2. An agreement made between the U.S. and Russia in June 1996 stated that the U.S. was responsible for 71 percent of the total propellant demand. In addition to maintaining orbit altitude, propellant is required by the Reaction Control System (RCS) to periodically off-load the momentum accumulated in the attitude control system prior to its saturation.

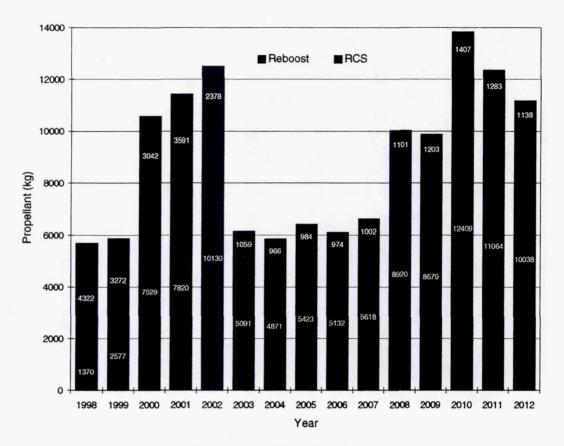


Figure 2 ISS Annual Propellant Requirement

The aerodynamic drag force D, exerted on the ISS is directed opposite its orbital velocity vector according to the familiar relationship

$$D = 1/2\rho v^2 C_d A. \tag{1}$$

For the range of altitudes in *Figure* 1 atmospheric density varies between 10^{-13} and 10^{-11} kg/m³. The circular orbit velocity of the ISS is described by

$$V = \sqrt{\mu / \left(R_e + h\right)} \,. \tag{2}$$

Its wetted surface area was computed from the relationship

$$A = m / \beta C_d \tag{3}$$

using the DAC #4 data for ballistic coefficient β and mass. The drag coefficient was set to $C_d = 2.35$ which corresponds to a worst-case value for an object in low-density free molecular flow. Note, following assembly complete changes in A are small. This results in the orbit-averaged aerodynamic drag profile illustrated in *Figure* 3.

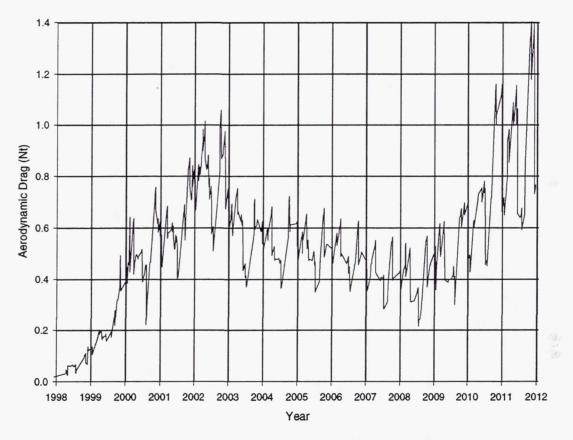


Figure 3 Space Station Orbit - Averaged Aerodynamic Drag

TETHER ENVIRONMENT AND ELECTRON COLLECTION

Tether Thrust

The thrust produced by a conducting tether when driven with a certain power level depends upon the magnetic field, the orbital velocity, and the tether current. While velocity is predictable and constant for a circular orbit, the Earth's magnetic field can vary by a factor of two. Furthermore, the current depends upon the combination of driving voltage and plasma electron density, the latter affecting the conductivity of the current's return path. The local electron density depends upon the effects of solar radiation; it therefore depends upon the phase of the solar cycle and whether the orbital segment is in sunlight, and can easily change by an order of magnitude over a single orbit, Figure 4. The strongest fluctuations are caused by variations in exposure to sunlight and the solar wind, with other periodicities due to the changing regions of the magnetosphere intercepted by the orbit. The voltage induced by the orbital motion, which affects the voltage which a power supply must impose upon the tether to achieve a given current, follows a similar curve, Figure 5, and reflects variations in the field magnitude and the angle between field and orbit plane. These factors cause variations in tether efficiency, effective tether length (with a bare tether electron collector), and the driving voltage required to compensate changes in induced voltage and plasma conductivity. Under reasonable assumptions, the resulting orbital variations in tether thrust are shown in Figure 6 for a 7 km tether driven with 5 kw, and are seen to vary between 0.22 and 0.53 Newton.

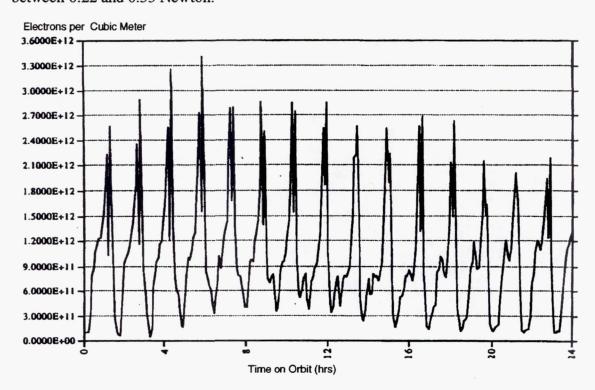


Figure 4 Electron Density Variations

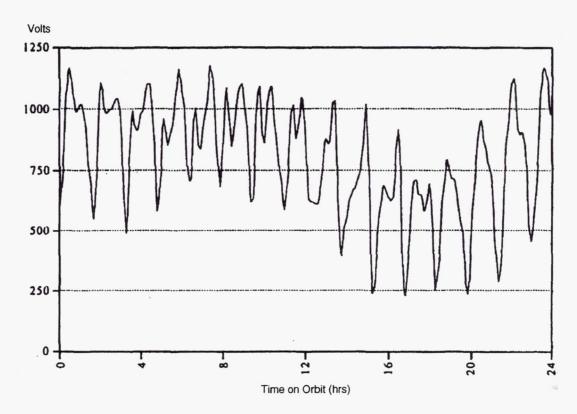


Figure 5 Motional Voltage Variations

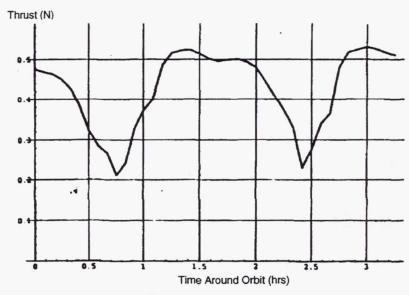


Figure 6 Thrust for the 7 km Long Tether at 5 kw

Electrodynamic Tether Drag

Determination of the tether aerodynamic drag force differs from the ISS drag force calculation only in that the values used for the wetted surface area and drag coefficient are different. The projected area of the nadir directed tether will vary as it rotates and/or twists. For a ribbon tether of thickness, t = 0.6 mm, and width, w = 1.1 cm, the wetted surface area per km was at most

$$1000 (w+t) 2 / \pi \approx 6.8 \text{ m}^2 / \text{km}.$$

A tether drag coefficient of 2.2 was used which is a nominal value for a platelike object in low-density free molecular flow. As illustrated in *Figure* 7, the total tether drag force was found to be approximately 6 percent of the ISS drag force value.

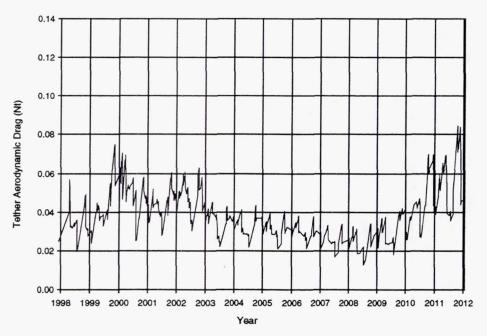


Figure 7 Ribbon Tether Aerodynamic

Bare Tether for Electron Collection

Any metallic surface at the end of the tether will serve to collect electrons. It has been determined that a long thin collector, such as an uninsulated extension of the insulated conducting tether, is a more efficient at electron collection than a sphere of the same surface area. This bare tether collector has the interesting property that its actively collecting length naturally varies to compensate the significant changes in plasma electron density which occur as the platform moves through different regions of the

magnetosphere, especially between the day and night sides of the Earth. This process is illustrated schematically in Figure 8, in which the continuous behavior of the tether is approximated by a series of discrete incremental segments of length ΔL . Each ΔL has resistance ΔR . Most of these lie in the insulated portion L, from which current cannot leak. Diodes are shown on the leakage paths from the uninsulated tether to indicate that current can leave but not enter the tether (i.e., electrons can be captured but not emitted), and the forward conductivity of a diode corresponds to its connection to the plasma. If this conductivity is sufficiently great in the first segment ΔL of uninsulated tether (the first diode path I_i), the full current I follows this path, $I = I_i$, and the remaining currents (I_n, for n>1) are all zero. If the plasma conductivity of the first uninsulated segment is less than perfect, however, the next ΔL will have some voltage drop ΔV across it and part of the remaining tether current (I - I₁) will flow as I₂. At night time, or under other conditions of lowered free electron density in the plasma, these diode conductivities will be lower so that more of them will be involved in conducting the full current I, and the positive voltage will extend further along the bare Thus, the bare tether must be long enough to accommodate the lowest anticipated electron densities, but only as much of it as needed will actually be conducting.

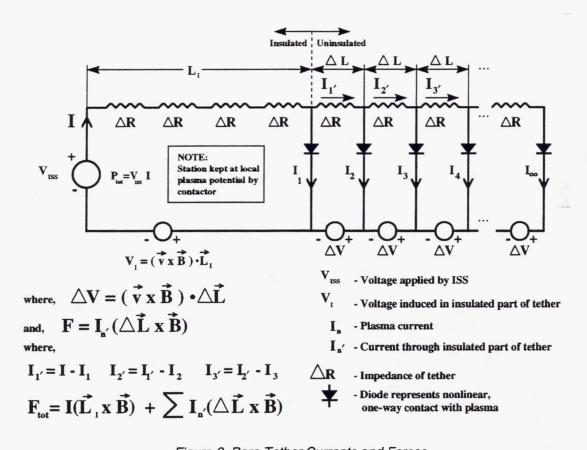


Figure 8 Bare Tether Currents and Forces

TETHER DEPLOYMENT

Deployer Strategies

We have considered alternatives in deployer design, grouped into three general areas:

- Expendable
- Payout & Retrieve
- Up & Down

Expendable

Expendable tether systems, in which the tether is simply cut after use and allowed to naturally drift away from the platform to eventually fall and burn in the upper atmosphere, are generally simpler, lighter, and cheaper to build. The obvious downside of expendable tethers is that they are good for a single use, and must be discarded and replaced in cases where damage or environmental factors (like the arrival of a spacecraft) may only temporarily require its removal.

Retrievable Deployment

The principal example of a deployer designed to retrieve a tether, as well as paying it out, is the design by the Martin Company for the TSS1 and TSS-1R tethered satellite experiments. (Reference 4) This was a heavy deployer (2000 kg) with a large deployment boom. Part of the reason for this weight was undoubtedly the intended generality of its application, being built to accommodate tethers up to 100 km long, with end weights of up to 500 kg mass. This deployer was flown twice and suffered from problems of tether snagging and breakage. Payout is similar for both approaches to deployability, but retrieval leads to potentially severe problems of control. amplification of lateral motions, due to the conservation of angular momentum as the tether's moment arm is shortened, leads to instabilities which require active control strategies. These difficulties are most acute in the late stages of retrieval, where each meter of length reduction leads to an increasingly large fractional reduction in the tether's moment arm. Nevertheless, solving these retrieval problems will be necessary in maintaining a significant permanent presence in the magnetosphere over extended periods. This is clearly true when the tether itself is a heavy and expensive instrument intended for use over periods much longer than a deployment cycle, as might be expected in the case of a tether intended for use over the life of the Space Station approached by many service vehicles per year.

"Up-Down", or "Pass-Through" Re-Deployment

The worst retrieval problems are likely to occur in the later stages of rewinding. These and other considerations led us to consider the merits of a rather different approach to retrieval: rather than winding the tether back on its spool, *let it pass straight on through* the deployer, to effectively "re-deploy" on the opposite, *Figure 9*.

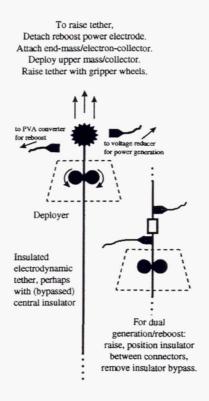


Figure 9 Bi-Directional Electrodynamic Tether

Bi-directional tethers have been previously considered, which allow easy switching between power generation and reboost functions (functional reversal) and which have minimal effect on the full platform's center of mass (CM) and orbit. It can be used to provide either reboost or power. The suggestion here is that power generation could be a secondary function, available to supplement solar power in unusual or emergency circumstances.

The obvious advantages of pass-through deployment and retrieval are:

- possible functional reversal
- snag-free redeployment.

The general requirements for pass-through tether retrieval are:

- electrical disconnection from platform power sources or loads
- the attachment of an alternative endmass for stability/control or an electron collector for functional reversal in place of these power sources or loads.
- a mechanical means of gripping and moving the tether at any point along its length
- a path through the platform to the other side, with sufficient angular clearance for both deployment and retrieval

Other specific advantages and disadvantages depend upon whether the intent is to fully re-deploy the tether on the opposite side of the platform, or to stop midway at a "balanced" configuration. This choice depends upon the motivation for retrieval.

Full Pass-Through

If the motivation is to remove the tether from potential interference with a service vehicle approaching from beneath, if there is a need to shift the platform's center of mass (CM), or if there is need to repair damage at or near the tether's outer end, then a non-rewinding retrieval must pass the full tether length through or past the deployer and its platform. The process is illustrated in *Figure 10*.

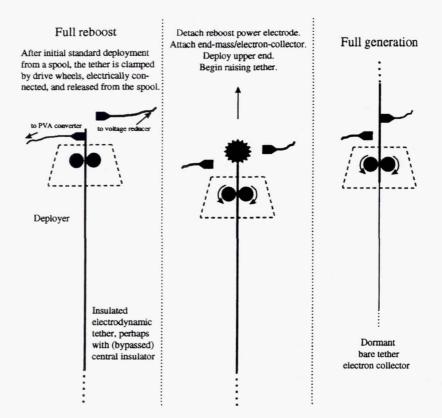


Figure 10 Bi-Directional Tether Concept

This has the following advantages:

- torque equilibrium angle (TEA) control by rotating tether boom about y-axis
- · freedom from conflict with approaching vehicles on the original side
- ability to access a damaged region anywhere along its length
- · full functionality for both power generation and reboost
- electrical reconnection at original site of the electron collector
- if configuration acceptable, bare tether original electron collector can remain unretrieved without electrical hazard
- · fine-tuning of platform CM and TEA

The disadvantages include:

- · full retrieval tether instability
- disconnection of original electron collector
- if bare tether originally used for electron collection, then rewinding or separate retrieval needed to resolve vehicular conflict
- · CM and TEA shift possibly significant
- electrodynamic functional suspension likely if adjustment of CM or TEA is motivation (since connection points may not be near platform).

ALTERNATIVE POWER SOURCES AND LOCATIONS

The current design of the ISS was used to determine suitable locations for the physical and electrical attachment of a deployer and its power supplies. The full-up Station carries four pairs of photovoltaic arrays capable of generating 20 kilowatts each. Of this 80 kW, 54 kW are intended for housekeeping functions. It is not expected that the 5 kW planned for reboost would overburden the remaining user allocation. The Station's batteries will support the same power availability as sunlight operation.

The tether current is limited by the excess electron rejection capacity of the currently designed plasma contactor. This contactor has a nominal design rating of 10 A, with normal operation requiring 2-3 A to maintain Station to within 40 volts of ambient plasma potential. This should readily permit a 5 A default allocation to tether reboost power. Modest short term overcurrent demands are not harmful, other than somewhat increasing the normal depletion of the hollow cathode's xenon supply. Nevertheless, if a stronger tether thrust is to be used, to totally compensate drag with a shorter duty cycle, or even gain altitude, this contactor should be replaced by one with larger design capacity.

Tether reboost operation can be treated as a low-priority resource demand, so long as long-term planned duty cycle requirements are met. Thus, tether power can be cut to accommodate peak user demand times with no effect other than a change in net aerodynamic drag forces. The acceleration induced by tether thrust is approximately $0.4N / 400,000 \text{ kg} = 10^{-6} \text{ m/s}^2 \approx 0.1 \text{ µg}$, which is low for even the Station's best µ-gravity environments. Normally, tether thrust will improve the µ-gravity environment by canceling the comparable deceleration from aerodynamic drag, but it is possible that extremely sensitive payloads might be affected by rapid changes in this range.

Likely physical attachment locations for a tether deployer are on the S0 truss, the Z1 truss, or a direct mounting on Node 1. Node 1 is considered a good choice as it is close to the Station's center of mass, although a truss location may be preferable if any of the pass-through deployment options presented in this paper are adopted. To avoid mechanical interference, the tether must honor an envelope to assure clearance of all ISS hardware under normal, abnormal, and abort conditions. A 10° cone of operational clearance should suffice, since tether libration would be controlled to less than that value. In principle, one may attach a small truss at any convenient location, as long as it extends to a position below Station where the deployer will give a tether alignment that exerts the desired torque levels (or lack thereof) on the Station. For the most flexible control of the tether's applied torque, and its consequent effect on the Station's torque equilibrium angle, the tether's force vector should pass reasonably near the center of mass, but guided by a boom with freedom of rotation about a y-axis, Figure 11.

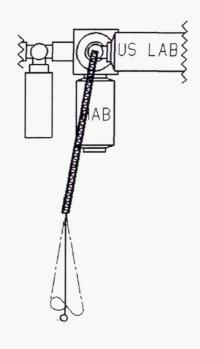


Figure 11 Tether Attachment

Electrical power can be obtained by connection to the Station's Main Bus Switching Unit where power has been conditioned to 160 VDC, Figure 12. The tether's own power supply will raise this 160 VDC to the 1500 volts DC required to overcome the tether's motion-induced voltage and impress as much as 5 A of downward current. This power supply includes an inverter, transformer, rectifier, filter, and regulator as shown in Figure 13. Because of its high voltage output, the power supply should be located close to the deployer rather than to its power source.

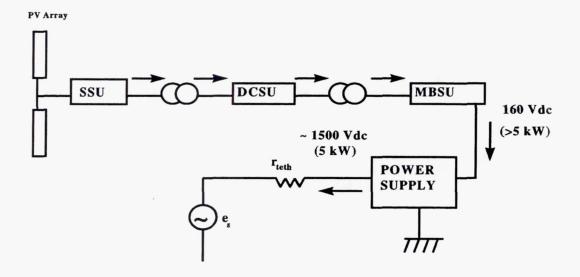


Figure 12 Tether Power Connection

Assumptions

- Tether requires 5 kW from ISS
- Tether requires 1500 Vdc
- ISS provides 160 Vdc

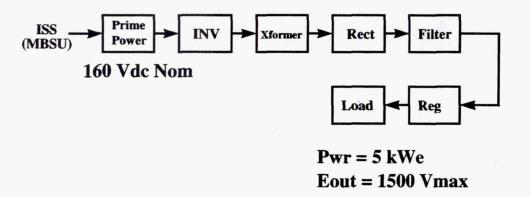


Figure 13 Power Supply for Tether

REBOOST OPTIONS

The primary benefits of the electrodynamic tether system is savings to the ISS in the form of reduced propellant mass requirements and extending the time between planned propellant reboosts. To characterize these savings, the altitude profile for approximately three one-year periods following assembly complete were analyzed assuming an operational electrodynamic tether system. The time-periods chosen were 2003, 2006, and 2009 which, from *Figure 1*, are representative of the ISS orbital decay profile. The electrodynamic tether force ranged from 0.43 - 0.7 N with a 25% - 50% duty cycle range.

Gauss's form of Lagrange's variational equations can be used to describe the orbital decay of the ISS orbit. (Reference 5) For a circular orbit the mean angular motion is given as

$$n = \sqrt{\mu/a^3} \,\,\,(4)$$

The time rate of change in the semi-major axis a, is described by

$$\dot{a} = 2T/n. \tag{5}$$

The tangential perturbation acceleration T possesses two components

$$T = -\frac{1}{2}\rho v^2 C_d A / m + F_t / m, \tag{6}$$

the first due to aerodynamic drag as previously described and the second due to electrodynamic tether thrust with the ISS mass.

Equation (5) is separable and can be integrated in closed-form by assuming constant values for the slowly varying parameters. This restricts the validity of the solution to small time intervals or equivalently small altitude changes. An integrated form is

$$\log \left[\frac{(\pm \sqrt{a_f} - \sqrt{\alpha})^2}{\mp \alpha \pm a_f} \right] - \log \left[\frac{(\pm \sqrt{a_i} - \sqrt{\alpha})^2}{\mp \alpha \pm a_i} \right] = \pm \frac{2F_t}{m} \sqrt{\frac{\alpha}{\mu}} (t_f - t_i), \tag{7}$$

where

$$\alpha \equiv \frac{\rho C_d A \mu}{2F_t} \,, \tag{8}$$

with the upper sign used when $a > \alpha$ and the lower sign for $a < \alpha$ over the interval of integration. The subscript i denotes the value at time t_i and subscript f denotes the value at time t_f where $t_f > t_i$. This can be rewritten as a quadratic in $\sqrt{a_f}$

$$a_f (1 \mp \gamma) \mp (2\sqrt{\alpha}) \sqrt{a_f} + \alpha (1 \pm \gamma) = 0, \qquad (9)$$

with

$$\gamma = \exp\left\{\log\left[\frac{(\pm\sqrt{a_i} - \sqrt{\alpha})^2}{\pm a_i \mp \alpha}\right] \pm \frac{2F_t}{m} \sqrt{\frac{\alpha}{\mu}} (t_f - t_i)\right\}.$$
 (10)

Solving for a_t gives the two solutions

$$a_{f_1} = \begin{cases} \alpha \left(\frac{1+\gamma}{1-\gamma} \right)^2 & \text{for } a > \alpha \\ \alpha \left(\frac{1-\gamma}{1+\gamma} \right)^2 & \text{for } a < \alpha \end{cases}$$
(11)

$$a_{f_2} = \alpha. \tag{12}$$

As mentioned earlier, this solution becomes less accurate for large altitude changes which necessitates a composite approach to its evaluation. By evaluating this expression for small time intervals, the variation in those parameters held constant during the analytic developments can be accommodated by specifying an updated constant value for each subsequent evaluation period.

This approach was used to construct a modified reboost profile for the time periods mentioned earlier, Figure 14. The electrodynamic tether system was assumed operating at 5 kw which provides a propulsive force of 0.43 N which is slightly less than the aerodynamic drag force illustrated in Figure 3. Both tether reboost, free decay, and propellant reboost are seen to occur with corresponding changes in slope between successive events. The elapsed time between the start of tether reboost and the end of free decay was iteratively determined such that the propellant reboost maneuver occurred on the lower boundary of the altitude band (as described by Figure 1) subject to the constraint that tether reboost occurs during 25% of this interval (i.e., 25% duty cycle). The propellant reboost maneuver was assumed to occur instantaneously.

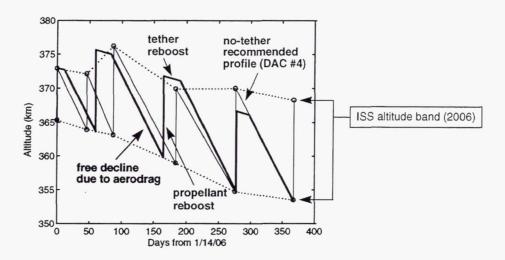


Figure 14 Tether Reboost Profile - 5 kw

Altitude change due to propellant reboost was determined using the familiar rocket equation and Hohmann transfer relationships. At the end of the free decay, the semi-major axis a_1 , and the circular orbital velocity $v_1 = \sqrt{\mu/a_1}$, are known. Two impulsive maneuvers are then assumed to occur instantaneously. The first maneuver raises apogee while the second maneuver circularizes the orbit by raising perigee an equivalent distance. Theoretically, the minimum elapsed time between these two maneuvers is one-half the orbital period which was assumed negligible for purposes of this analysis. The total velocity increment Δv , impulsively delivered by the $\Delta m = 1,000$ kg of propellant supplied by the Progress M was determined from the rocket equation as

$$\Delta v = -g_0 I_{sp} \log \left(1 - \Delta m / m_r\right), \tag{13}$$

using gravitational acceleration $g_0 = 9.81$ m/sec², specific impulse $I_{sp} = 300$ sec, and reboost mass m_r , which exceeds m by the mass of the resupply vehicle. Denoting the velocity on the raised circular orbit by v_2 the velocity ratio $\sigma = v_2 / v_1$ can be determined from the Hohmann transfer relationships as

$$\Delta v / v_1 + (1 - \sigma) \left[1 - (1 - \sigma) \sqrt{2/(1 + \sigma^2)} \right] = 0.$$
 (14)

Solving numerically for σ , the velocity on the raised circular orbit is then determined from $v_2 = \sigma v_1$ with corresponding semi-major axis $a_2 = \mu/v_2^2$, and hence, altitude $h_2 = a_2 - R_e$.

The effects of a higher power electrodynamic tether on the reboost profile can be seen in *Figure 15*. This figure illustrates the savings of two propellant reboost flights (or equivalently 2,000 kg of propellant) to the ISS for the year 2006. The electrodynamic tether system was assumed operating at 10 kw which provides a propulsive force of 0.7 N which is somewhat greater than the aerodynamic drag force illustrated in *Figure* 3. The duty cycle for the tether reboost was again 25%.

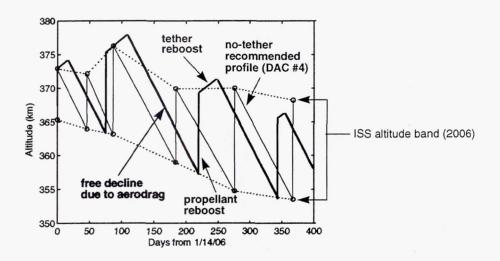


Figure 15 Tether Reboost Profile - 10 kw

Similar analysis was performed for the years 2003 and 2009. Figure 16 summarizes these results by illustrating the annual propellant savings accrued from the electrodynamic tether reboost system. It is seen that for the range of parameters considered herein the tether reboost system can reduce the number of propellant reboost flights from between one to four annually.

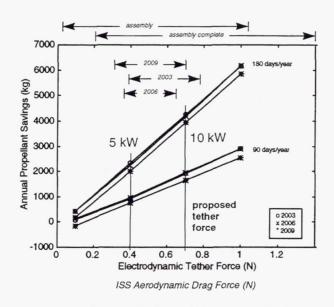


Figure 16 Annual Propellant Savings

IMPACTS TO ISS

The utilization of an electrodynamic tether to provide reboost to the Space Station raises several issues. Some of these issues are addressed in the section that follows.

Effects on Center-of-Mass and μ-Gravity

The proposed tether does have a significant impact on the Z component of the Station's center of mass. The tether itself would have the most impact due to its long moment arm, as shown in Figure 17. The proposed 7 km tether with a 200 kg endmass would lower the Station's CM by about 4.5 m. This would effectively lower the projected μ -gravity contours from those currently planned without a tether to those with a tether system, Figure 18. This shows that the region of best μ -gravity has been shifted from the top of the US Lab to the bottom, with a similar shift - and possibly even an improvement - for the European and Japanese labs. This shift could be reduced by maneuvering the tether boom shown in Figure 11 to adjust the Station's tongue equilibrium attitude so as to raise its leading edge.

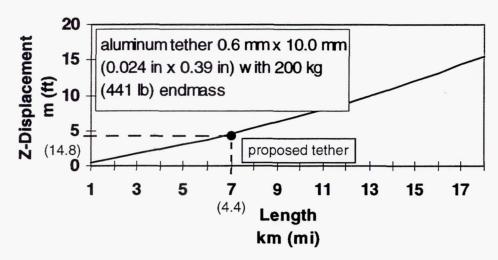
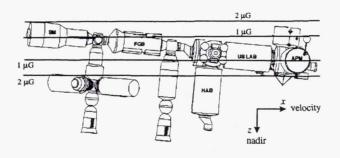


Figure 17 Displacement of ISS Center of Mass by Tether



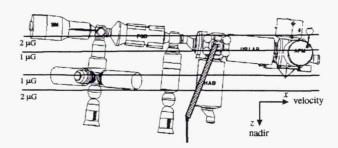


Figure 18 Microgravity Environment: Top Without Tether, Botton With Tether

The effect of the tether's deployer on the X component of the Station's CM is negligible, since even a 500 kg deployer located 20 m forward of the CM would displace the CM forward by only 2.5 cm. X-axis displacements are of less concern than vertical (z-axis) displacements.

Power Demands Upon ISS

The tether requirement for 5 kw (or 10 kw) of power from the 80 kw available from the generating sources does not appear excessive during the "day light" hours. Extracting this level of power from the batteries during "night" operation may not be satisfied at all times. Under these conditions, the tether power would be reduced and the reboost thrust accordingly.

Retrieval or Jettison of Tether - Normal Conditions

The tether system for reboost would be utilized during quiescent periods as it would tend to nullify the station drag. At times when visiting spacecrafts come to the ISS, the extended tether might interfere with their docking procedure. Under these circumstances, the tether would need to be cut and discarded or be retrieved prior to the spacecrafts visit. As it is expected that spacecraft will be visiting on a fairly regular basis—six flights at least for Orbiter, four to six flights for Progress M, flights by other

spacecraft - the cut and discard of the tether may become a cost issue. Retrieval of the tether appears a candidate solution but raises technical issues particularly when the tether length is short (less than approximately 1 km). Retrieval systems inherently are more costly than expendable systems. Further analysis and design would be needed to address these issues.

Maneuverable Boom to Guide Tether

It was mentioned previously that a boom be utilized in deploying the tether. The feature of the boom is to move the tether away from elements of the ISS and also to place one component of the tether center of gravity in proximity with the center of gravity of the Station. Additionally, the tether boom may be used to complement the actions of the Control Moment Gyros.

Other Issues

There are many other issues that concern utilization of the tether system at the Station. Specific placement of the tether system on the Station would have mechanical and electrical impacts. Safety and reliability issues need also to be addressed. The current study did not delve into these details.

COST SAVINGS TO ISS

Over the past several years the Russian resupply vehicle Progress M has proven itself to be a highly reliable means of delivering life support materials and reboost capability to low Earth orbit. Of the propellant reboost options considered for the ISS, only the Progress M is operational. The Soyuz launch vehicle is used to insert Progress M into low-Earth orbit at a cost of approximately \$15-25M. (Reference 6) The propellant cost is an additional \$20M for a total cost of between \$35-45M. Commercial sources indicate that this value may be as high as \$65M. The \$35-45 k/kg estimate of Progress M propellant launch cost (i.e., the lower cost number) is used in this paper.

Propellant savings provided to the ISS as illustrated in *Figure* 16 can be converted to dollar savings using this launch cost of propellant estimate. *Figure* 19 illustrates the results of this conversion expressed as a cumulative cost savings to the ISS obtained over the ten-year operational period. The two regions shown correspond to 25 percent and 50 percent duty cycles of tether reboost operation for a tether force of 0.43N (5kw). The widening of these regions with time results from the differences in the computed annual propellant savings between the three one-year periods considered. At the higher duty cycle it is seen that a savings in excess of one billion dollars over the operational life of the ISS is possible. At the higher reboost value of 0.7N (10 kw), the savings are approximately twice as much.

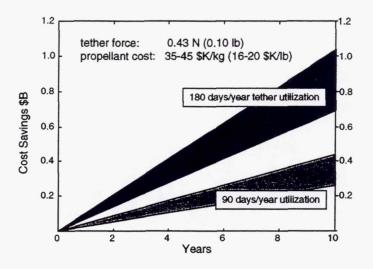


Figure 19 Cumulative Cost Savings

CONCLUSIONS

Multiple benefits are accrued by the use of a propellantless system to reboost the ISS. As the ISS will stay in orbit for over ten years as a research and test facility, means of providing reboost is an important factor. The electrodynamic reboost system could satisfy some of the total reboost needs of the ISS resulting in a reduction in flights that deliver propellant. The higher the usage of the electrodynamic tether, the larger the cost savings resulting from fewer propellant re-supply flights. Use of this method of reboost would provide for additional quiescent days as the system would have no major impact on the microgravity environment and under certain conditions could improve the microgravity environment. In addition, a maneuverable boom could provide some variation/control in the ISS torque equilibrium attitude.

ACKNOWLEDGMENTS

We wish to thank Dr. Robert Estes and Dr. Enrico Lorenzini of the Smithsonian Astrophysical Observatory, Cambridge, MA for providing the computation of plasma parameters and their effect on tether voltage, tether efficiency, and effective tether length. We also wish to thank Kai Shen Hwang of CSC, Huntsville, AL for information regarding the capabilities and limitations of the Space Station's plasma contactor. The study participants from the Boeing Company, Huntsville included Thomas R. (Buddy) Akins for his work on tether attachment location and power demands, and Ron Lajoie for his adaptations of the ISS altitude and drag projections.

Finally we wish to acknowledge the direction provided by the COTR, Mr. Les Johnson, NASA Marshall Space Flight Center. His support and that of numerous technical personnel at MSFC were instrumental in the overall study effort. The Boeing study was conducted under NAS8-50000, TOF018.

REFERENCES

- "Electrodynamic Tether Reboost, International Space Station Application," NASA, Marshall Space Flight Center, April 1997.
- ²"Electrodynamic Tether System for Power and Reboost, International Space Station Application," The Boeing Company, Document Number D567-70008, July, 1997.
- ³"Design and Analysis Cycle 4 (DAC #4) Assessment, TDS 4.1-2: ISS Altitude Profile," McDonnell Douglas and NASA JSC (EA 44) Presentation to NASA SSPO, September 6, 1996.
- ⁴Ryan, R.S., Mowery, D.K., and Tomlin, D.D., "The Dynamic Phenomenon of a Tethered Satellite," NASA TP 3347, May 1993.
- ⁵Batin, R.H., An Introduction to the Mathematics and Methods of Astrodynamics, AIAA Education Series, 1987.
- ⁶Tsakowitz, S.J., International Reference Guide to Space Launch Systems, AIAA, 1991.

An Overview of Electrodynamic Tether Performance in the Jovian System

D. L. Gallagher NASA Marshall Space Flight Center, Huntsville, Alabama

F. Bagenal
Department of Astrophysical, Planetary, and Atmospheric Sciences, University of Colorado,
Boulder, Colorado

J. Moore SRS Technologies, Huntsville, Alabama

L. Johnson NASA Marshall Space Flight Center, Huntsville, Alabama

Abstract

The Jovian magnetosphere with its strong magnetic field and the rapid rotation of the planet present new opportunities and challenges for the use of electrodynamic tethers. An overview of the basic plasma physics properties of an electrodynamic tether moving through the Jovian magnetosphere is examined. Tether use for both propulsion and power generation are considered. Close to the planet, tether propulsive forces are found to be as high as 50 Newtons and power levels as high as 1 million Watts.

Introduction

In recent years, tethers have come to offer significant opportunities in many low Earth orbit applications. Conducting and non-conducting tethers are being considered for electrical power and propulsion systems [Johnson et al., 1996]. Conducting or electrodynamic tethers derive their properties as a result of the current flowing through a moving wire in a magnetic field and in the presence of a plasma or conducting medium. Tethers may be useful in any planetary system where there exists a magnetic field and a plasma through which current closure can occur.

But why Jupiter? The first inducement is the large Jovian magnetic field, much larger than that at the Earth. The real motivation, however, is the need for alternative power generation and propulsion techniques for future missions to Jupiter. Due to low solar luminosity, radioactive thermoelectric generators (RTG) have been used for electrical power in all past deep space missions. The finite risk of releasing plutonium into the terrestrial environment may rule out RTGs on future missions. The possibility of using solar panels for electrical power generation has improved in recent years. Even with improvements in this technology, however, extended exposure to high levels of radiation in the Jovian system are expected to rapidly degrade the effectiveness of solar arrays. Extended operations in the Jovian system, or around any planet, also typically require use of an expendable propellant for orbital maneuvering. This may lead to high "wet" spacecraft mass at launch and/or limited lifetime on orbit. It is for these reasons and because of the strong magnetic field and rapid planetary rotation that electromagnetic tethers are being considered for use in the Jovian magnetosphere. The purpose of this report is to determine whether electrodynamic tether usage is feasible from a plasma physics point of view. The engineering feasibility will be addressed elsewhere.

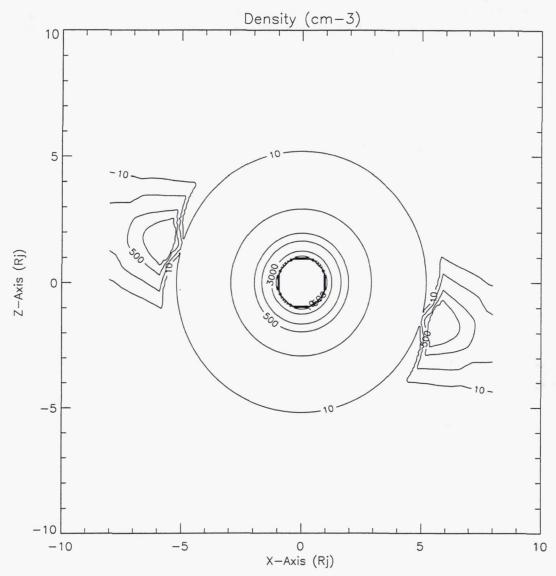
Tether Physics at Jupiter

This report discusses the initial results of analyzing the performance of an electrodynamic tether in the Jovian planetary system. Tether modeling is based on results from the TSS-1R mission and the theories of Parker and Murphy [1967] and Sanmartin et al. [1993]. The computed tether performance represent maximum limiting current and resulting power estimates. The Jovian magnetic field model is obtained from Khurana [1997], consisting of the GSFC O_6 internal field model and an

Euler potential formulation for the external field. The plasma density model is a simplified version of that presented by Bagenal et al. [1994] and consists of a spherically symmetric distribution, plus an Io torus. The results also depend on several assumptions. The first is for the electron temperature, which is used to estimate the thermal current to the tether. The electron temperature is taken to be a fixed 10eV. Inside of 5Rj the electron temperature is only a few eV. Outside of this distance it is 10-50eV. That means the estimated current will be somewhat high inside this distance and low, outside this distance. Tether current varies with the square root of the thermal electron temperature, so is not tremendously sensitive to it. A tether length of 10km has been assumed, along with a cylindrical tether of 1mm diameter.

The analysis of electrodynamic tether performance is accomplished in two coordinate systems. One is the System III (1965) coordinate system, which rotates with the Jovian magnetic. Both the magnetic field and density models are defined in this coordinate system. The second is an inertial coordinate system, where the z-axis is along the planetary spin axis. Due to the preliminary nature of this study, no effort has been made to orient the x-axis of this inertial coordinate system toward the first point of Aries or any other inertial reference point. All results are shown graphically in the x-z plane of this work's inertial coordinate system. Each of the displays extend $\pm 8~{\rm R}_{\rm p}$ along the x and z axes and show constant level contours of various quantities.

The first plot is for total electron density, with constant density contours at 10, 100, 500, 1000, 3000, and 6000 cm⁻³. It is made up of three components: inside the Io torus, the Io torus, and outside the torus. Inside and outside the torus the density falls of exponentially. Inside the torus, the density is derived from linear interpolations of a measured radial profile. The torus falls off exponentially away from the magnetic equator.



Induced tether current will depend upon the speed with which the tether moves through the Jovian magnetic field. That speed will depend on spacecraft motion around the planet (\vec{v}_{sc}) and planetary rotation (\vec{v}_{J}). For the purpose of initially exploring tether behavior, the spacecraft motion is assumed to result from a circular orbit at each radial distance and latitude where the calculations are made:

$$\vec{v}_{sc} = \left(\frac{GM_J}{r}\right)^{\frac{1}{2}} \left(-\sin(\theta)\hat{\theta} + \cos(\theta)\hat{\phi}\right)$$
 (1)

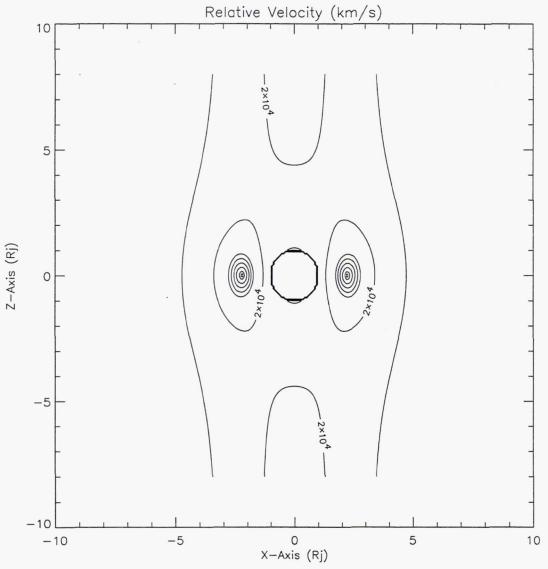
where θ is the latitude and ϕ is the longitude. This velocity is added to the velocity of a stationary location relative to planetary rotation, given by

$$\vec{v}_I = -1.7585 \cdot 10^{-4} \cdot r \cos(\theta) \hat{\phi} . \tag{2}$$

Jupiter is assumed to rotate with a period of 9 hours 55 minutes 29.70333 seconds. The resulting speed of the spacecraft relative to the planetary magnetic field (\vec{v}_{rel}) is plotted next. Constant velocity contours are shown for 1, 2, 4, 6, 8, 10, 20, and 40km/s.

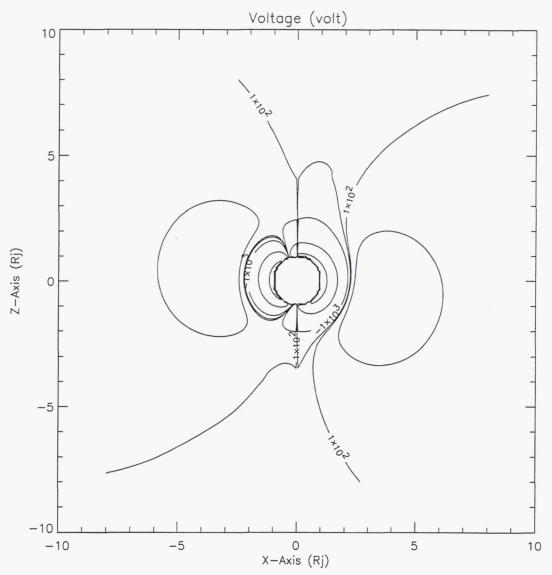
$$\vec{v}_{rel} = \vec{v}_{sc} + \vec{v}_J \quad (3)$$

You can see that for most locations, the planetary rotation dominates the plotted speed, i.e. it increases with increasing distance. Close to the planet, the orbital spacecraft speed begins to dominate over the planetary rotation. At 90 degrees, the planetary motion is not a factor, leaving only the orbital motion to contribute to induced EMF in the tether.



The next plot is for induced EMF in the 10km tether. Contours are shown for -50, -10, -1, -0.1, 0.1, 1, and 10kV values. Induced voltage depends upon the tether length (\vec{l}), the velocity relative to the magnetic field (\vec{v}_{rel}), and the vector magnetic field (\vec{B}).

 $V = \vec{l} \bullet \vec{v}_{rel} \times \vec{B} \tag{4}$



Tether current is plotted in next. Here, contours are shown for 0.1, 0.5, 1, 5, 10, and 20 amperes. Based on Parker and Murphy [1967], current into a conductor in a magnetic field is equal to the thermal current (I_o) times a factor. The factor is a function of induced voltage (V), the area of the conducting surface (a), and the magnetic field strength (B). The thermal current is a function of the cross-sectional area of the conducting surface and the component of the thermal current density along the magnetic field. Thermal current density (j_o) is a function of the density and the mean thermal electron velocity.

$$j_o = \frac{en_e v_{T_e}}{4} \tag{5}$$

The component of that along the magnetic field is obtained by taking ¼ of the total thermal current density. The area of the conducting surface is taken to be the area of the tether projected onto a plane transverse to the magnetic field.

$$a = d \cdot l \cdot \sin(\alpha) \,, \tag{6}$$

where d is the diameter of the tether (0.001m), l is the tether length (10⁴m), and α is the angle between the radial tether and the vector magnetic field. This angle is obtained from

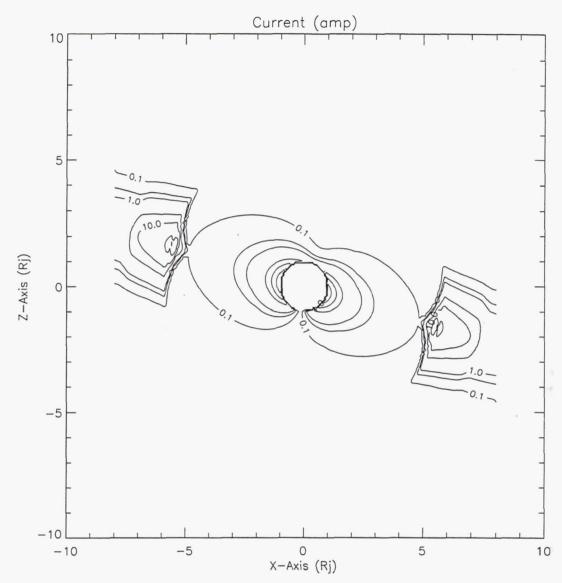
$$\alpha = \cos^{-1}\left(\frac{B_r}{B}\right),\tag{7}$$

where B_r is the radial component of the Jovian magnetic field. The thermal current is multiplied by a factor of 2 to take into account the collection of current from both the parallel and anti-parallel directions along the magnetic field.

$$I_{o} = 2 \cdot a \cdot j_{o} \tag{8}$$

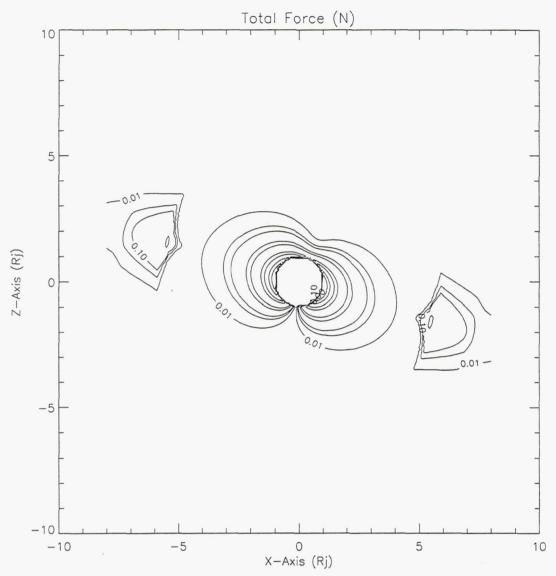
Finally, the current determined following Parker and Murphy [1967] is multiplied by factors of 2.5 and 30. The limiting current into a tether was found to be a factor of 2-3 times greater than Parker and Murphy [1967] in the TSS and TSS-1R missions, which is the source of the first factor. The second results from the analysis of bare tether performance, which is thought to enhance the current collection by a factor of at least 30 over the spherical end-collector used in the TSS and TSS-1R missions (Sanmartin et al., 1993; Shiah et al., 1997).

$$I = 75I_o \left(1 + \left[4.56x10^{-3} \frac{V(volts)}{a^2 (meters) B^2 (gauss)} \right]^{\frac{1}{2}} \right)$$
 (9)



Next, the force (\vec{F}) a current carrying tether would experience is plotted, with contours at 0.01, 0.05, 0.1, 0.5, 1, 5, 10, 25, and 50 Newton. The force is obtained from the tether length (l), current (\bar{I}), and the magnetic field (\bar{B}).

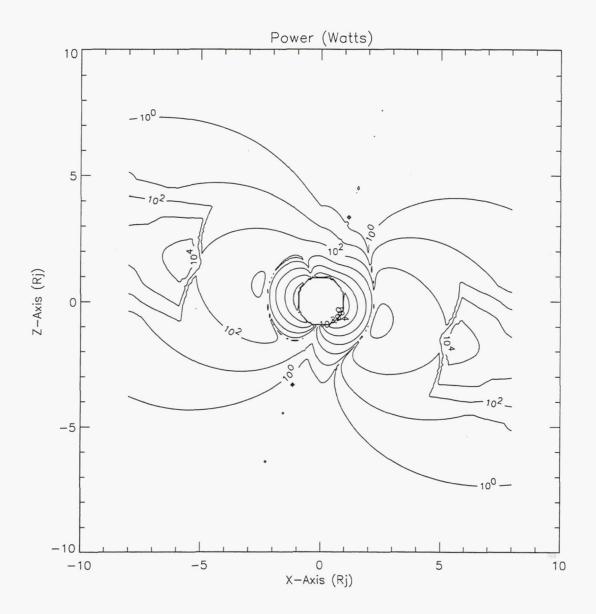
$$\vec{F} = l\vec{I} \times \vec{B} \tag{10}$$



Finally, the power represented in a current carrying tether is shown. Contours are drawn for even decades from 1 W to 10 MW. Power is simply obtained from the product of the induced EMF and the current.

$$P = V \cdot I \tag{11}$$

It can be noted that Europa is at a distance of $9.4\mathrm{Rj}$ and has an orbital period of 3.551 days. That puts Europa beyond these plots, but clearly at low tether functionality, without mitigation by the availability of enhanced ionization (Ip , 1996).



Clearly, use of electrodynamic tethers in the Jovian system presents entirely new challenges and opportunities. Near the planet, it appears that induced tether voltages can reach as high as 50,000 volts, currents can become greater than 20 amperes, power levels can reach over a million Watts, and propulsive forces can reach higher than 50 Newton. The answer to our original question is yes. Electrodynamic tethers appear, on the basis of plasma physics, to be feasible for use in the Jovian magnetosphere. They also appear to present significant engineering challenges. High levels of tether current mean that managing a spacecraft system's thermal budget is not simple. The complex geometry of forces that a tether would experience around Jupiter means that sophisticated control of tether current will be required in order to achieve specific mission orbital characteristics. Continued analysis of the use of tethers at Jupiter will require use of a more realistic plasma density model than that used here. A model for electron temperature is also needed. More representative modeling of the Jovian plasma system can then be used in engineering studies to explore development of practical spacecraft systems for use at Jupiter.

References:

- Bagenal, F., Empirical model of the Io plasma torus: Voyager measurements, JGR, 99, 11043-11062, 1994.
- Johnson, Les, et al., Electrodynamic Tethers for Reboost of the International Space Station and Spacecraft Propulsion, AIAA 96-4250, 1996 AIAA Space Program and Technologies Conference, September 24-26, 1996, Huntsville, Alabama.
- Khurana, Krishan K., Euler potential models of Jupiter's magnetospheric field, J. Geophys. Res., 102, 11,295-11,306, 1997.
- Sanmartin, J. R., M. Martinez-Sanchez, and E. Ahedo, Bare wire anodes for electrodynamic tethers, J. Propulsion and Power, 9, 353-360, 1993.
- Shiah, A., K. S. Hwang, S. T. Wu, and N. H. Stone, Three-dimensional simulation of current collection in space, Planet. Space Sci., 45, 475-482, 1997.

Session V—Advanced Tether Technology

Page intentionally left blank

OEDIPUS-C MISSION TETHER DYNAMICS RESULTS

Alexander M. Jablonski and Frank R. Vigneron Canadian Space Agency, Saint-Hubert, Quebec J3Y 8Y9, Canada

George Tyc
Bristol Aerospace Limited, Winnipeg, Manitoba R3C 2S4, Canada

H. Gordon James Communications Research Center, Ottawa, K2H 8S2, Canada

ABSTRACT

The OEDIPUS-C Sounding Rocket Mission was successfully launched on November 6, 1995. The spinning two payloads had two large pairs of booms and were connnected by a tether which reached 1174 m in full deployment. It had scientific objectives to address natural and artificial waves in the ionospheric plasma in series of experiments. A comprehensive Tether Dynamics Experiment was also included to investigate complex dynamics of the configuration. At first this paper describes scientific objectives of the OEDIPUS-C mission. A short description of two subpayloads (aft and forward) follows. Then dynamics states of the flight are described and some examples of the flight dynamics data are presented. The paper also includes the overall status of the tether technology developed in association with this mission. This tethered mission was filmed by the camera situated at the aft subpayload and a short description of the video is also included. Present status of the post-flight analysis is presented.

INTRODUCTION

OEDIPUS acronym stands for Observations of Electric Field Distribution in the Ionospheric Plasma - a Unique Strategy. Two missions have been accomplished: OEDIPUS A in January 1989 (Andøya, Norway) [James et al., 1995a] and OEDIPUS C in November 1995 (Poker Flat, Alaska) [James et al., 1995b]. The OEDIPUS-C mission was successfully launched using the Black Brant XII sounding rocket, on November 6, 1995 into a suborbital trajectory from the Poker Flat Research Rocket Range, near Fairbanks, Alaska. The OEDIPUS-C suborbital mission was a joint Canadian Space Agency (CSA) and NASA program to investigate ionospheric plasma physics with the tether and booms used as probes/antennas to support both passive and active space science experiments. The OEDIPUS-C trajectory had a greater range in plasma density than OEDIPUS A trajectory and provided an extended perspective on plane and sheath waves and their interaction with space plasma. To understand the importance of the conducting tether for the propagation of rf waves between the subpayloads, the tether was

cut from both ends on the down leg part of the flight. The science experiments were also designed to help to understand how charged particles associated with aurora affect the satellite transmissions. There were 13 experiments (three instruments from the Canadian Space Agency, seven from the National Research Council of Canada, and three others from the University of Saskatchewan and the US Air Force Phillips Laboratory). The OEDIPUS-C payload was provided by the Canadian Space Agency and the payload contractor was Bristol Aerospace Ltd. One of the main investigations on OEDIPUS C was the project on the controlled radio-wave experiments funded by the CSA Space Science Program. The radio instruments (HEX and REX) were built by CAL Corp. and Routes Inc., both from Ottawa, Ontario, and the PI was Dr. Gordon James, Communications Research Center, in Ottawa, Canada [Jablonski et al., 1996; Eliuk et al., 1996].

This category of space science experiments requires two payloads in space that transmit and receive rf energy. Separation distance must be of order of 1 km and known accurately for post-flight data processing. The orientation of the separation vector relative to the geo-magnetic field is an important parameter that must be conveniently established in flight. Tether technology is ideally suited to meet the needs of this category of science missions.

In the OEDIPUS-A mission, the aft payload exhibited a rapidly diverging coning angle that reached a 35 degrees (half angle) by the end of the flight [Tyc et al., 1995b]. The developed dynamic models did not predict nor explain this phenomenon. Therefore, the Tether Dynamics Experiment (TDE), was established by the Space Technology branch of the CSA. The TDE requirements included: development of a comprehensive understanding of the OEDIPUS class spinning tethered system, and development of an attitude stabilization method for the mission. During the OEDIPUS-C mission the altitude at apogee reached 824 km and a 1174 m tether was successfully deployed. All on-board instruments and subsystems on both forward and aft subpayloads operated as expected. The TFS instrument was flown as a primary flight instrument that was developed as a part of the Tether Dynamics Experiment (TDE). The TDE includes mathematical modeling of dynamics of the OEDIPUS-like configurations [Tyc et al., 1994; Tyc et al., 1995b; Vigneron et al., 1994, Vigneron et al., 1997b], ground testing [Jablonski et al., 1995; Modi et al., 1995; Tyc et al., 1994; Vigneron et al., 1997a], development of the stabilization technique for the OEDIPUS-C [Tyc, 1994], the development of the Tether Force Sensor (TFS) situated at the aft payload to measure components of the tether force vector [Tyc et al., 1995a; Jablonski et al., 1997]. This paper presents an overview of the OEDIPUS-C mission with description of the flight video, and characterizes the present status of related dynamics studies [Jablonski et al., 1996]. A review of the advances of the OEDIPUS related tether technology is also presented along with representative OEDIPUS-C flight dynamics data examples based on the recent status of the postflight analysis [Tyc et al., 1996; Jablonski et al., 1996].

OEDIPUS-C MISSION OBJECTIVES

OEDIPUS-C scientific team attempted to exploit the scientific and technological momentum achieved with OEDIPUS A, using a large double probe similar to A's. A central theme for plasma physics was bistatic propagation using a synchronized transmitter HEX and receiver REX. The HEX and REX were operated synchronously in the frequency range 0.1-8 MHz over the entire flight of OEDIPUS C. The OEDIPUS-C flight scenario called for a launch on a four-stage Black-Brant XII (BB XII) rocket to an altitude of 800 km over an active aurora. The goal was to investigate dc and ac electric fields in the more tenuous plasma existing at altitudes attainable with the BB XII. The output power of the scientific transmitter HEX had been increased over OEDIPUS A and the associated dipoles lengthened from 5 to 18 m tip-to-tip. To give better understanding of the differences between plane-wave and sheath-wave excitation, the tether was cut on the downleg and the transmitter connected exclusively to the dipoles. Detectors of thermal and energetic particles provided needed information on the particle interaction with waves and with the subpayloads. Flux-gate magnetometers and plasma probes monitored the state of the auroral ionosphere in vicinity of the OEDIPUS-C configuration. In addition collaborative experiments were planned using radio equipment on the ground to observe the payload transmissions and natural emissions triggered by auroral particles. The above scientific objectives were grouped into the following classes of experiments: active bistatic experiments sheath waves (using a transmitter-receiver pair HEX and REX) on tether-guided waves and plane waves (to study wave-particle interactions (WPI) between HEX-excited waves and natural electron beams); passive observations of space plasma in the auroral zone, including analysis of the dc electric field E. In the latter case, the Tether Current Monitor (TCM) measured the E component along the tether direction and a set of flush-mounted sensors detected a motion at right angles to the payload, whence the total E could be determined. The Thermal Ion Detector established the potentials of each subpayload with respect to its ambient plasma and the Plasma Probes measured ambient temperature, ambient density and floating potential [James et al., 1995b].

In addition these plasma physics experiments the Tether Dynamics Experiment (TDE) was proposed and it had the following objectives:

- derive of theory and develop simulation and animation software for analyses of multibody dynamics and control of the spinning tethered two-body configuration;
- provide dynamics and control expertise, for the tethered configuration and science investigations, develop an attitude stabilization scheme for the payloads and support OEDIPUS C payload development;
- acquire dynamics data during flight, and compare with pre-flight simulations to demonstrate that the design technology is valid.

The Tether Force Sensor (TFS) was developed to measure three components of the tether force sensor at the aft subpayload [Jablonski et al., 1997]. It was a prime flight instrument for the TDE. The summary of the scientific instruments is presented in the Table 1.

Table 1 Summary of OEDIPUS-C Scientific Instruments

Name (Location)	Measures	Range, Sensitivity	Investigator
High-Frequency	-	RF power: 0 - 10 W	H. G. James
Exciter (HEX) (F)		Freq.: 0.025 - 8 MHz	CRC
Receiver for	Amplitude and	-100 to -10 dBm	H. G. James
Exciter (REX) (A)	delay of EM waves	Freq.: 100 Hz - 8 MHz	CRC
Energetic Particle	Dist. func. of electrons;	10 eV - 20 keV; eight	D. A. Hardy
Instrument (F,A)	wave correlation	17.5° X 8° accept. fans	USAF Phillips Lab.
Thermal Ion Detector	Dist. func. of thermal	Ions: 0 - 20 eV;	D. J. Knudsen
(F,A)	ions and electrons	Electrons: 0.02 - 20 keV	NRCC/HIA
Triaxial Fluxgate	3 compon. of earth's	$\pm 0.9 \text{ nT}$, at 800 s ⁻¹ (dc)	D. D. Wallis
Magnetometer (F,A)	mag. field; ion waves	± 25 pT,10-400 Hz (wave)	NRCC/HIA
Plasma Probe (F,A)	Electron and ion	n_e : 10 ³ - 10 ⁶ cm ⁻³	D. D. Wallis
	density,	T _e : 200 -1000 K	NRCC/HIA
	electron temperature		
Ram Sensor (A)	Ambient density, float.	n_e : 10 ³ - 10 ⁶ cm ⁻³	J. A. Koehler
	potential, currents	Pot.: -9 to +9 V	U. of Saskatchewan
Tether Current	Induced voltage and	Volt.:± 100 V at 1600 s ⁻¹	D. D. Wallis
Monitor (A)	current along tether	Current: ± 150 µA	NRCC/HIA
Tether Force	Magnitude and	Ranges: $\pm 0.45 \text{ N}$ (z axis),	A. M. Jablonski
Sensor (A)	direction	$\pm 2.4 \text{ N} (y,z \text{ axes})$	CSA
	of tether tension		

A - aft subpayload

F - forward subpayload

OEDIPUS-C PAYLOAD DESCRIPTION

A schematic view of the OEDIPUS-C configuration is presented in Fig. 1. The OEDIPUS-C payload had a total mass of approximately 209 kg and was comprised of two spinning subpayloads with radial booms and a nominally 1 km conductive tether. The key OEDIPUS-C parameters are presented in Table 2. The forward and aft subpayloads had 13 different scientific instruments (5 on the forward and 8 and aft subpayload), and all required support subsystems (i.e. power, telemetry, instrument control, booms, ACS) as well as the tether deployer and tether cutters (at both ends), cold gas separation subsystem and other subsystems (like magnetometers and Tether Force Sensor (TFS)) to measure the flight dynamics quantities.

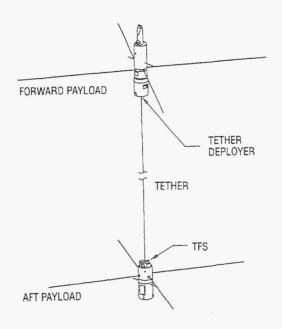


Figure 1 OEDIPUS-C Payload Configuration

Table 2 OEDIPUS-C Parameters

Parameter	Forward	Aft
	Payload	Payload
subpayload		
mass (kg)	115.44	92.99
length (m)	2.313	1.29
diameter (m)	0.438	0.438
MOI with booms stowed		
A_o (kg-m ²)	40.26	13.42
B_0 (kg-m ²)	40.26	13.42
C_0 (kg-m ²)	2.262	2.186
MOI with booms		
deployed	113.43	36.97
A $(kg-m^2)$	113.43	36.97
B $(kg-m^2)$	148.59	49.06
C $(kg-m^2)$		
boom properties		
length (m)	9.5	6.5
mass rate (kg/m)	0.128	0.128
EI $(N-m^2)$	116.2	116.2
tether properties		
final length (m)	1174	
mass rate (kg/m)	0.003	
EA (N)	40	68

The subpayload configurations are presented in Figs 2 and 3, respectively. The description of the tether technology components developed for the OEDIPUS-C are discussed below. The addition of a wide-file-of-view CCD star camera on each subpayload allowed to obtain an information not only for post-flight 3-axis attitude determination and, for the first time, a video filmed in space of the spinning tethered system of this class. For a more detailed description of the payload refer to Eliuk et al. [Eliuk et al., 1995].

OEDIPUS C MISSION AND ITS DYNAMICS STATES

The OEDIPUS-C flight sequence is presented in Figure 5 and a pictorial view of the suborbital flight trajectory is shown in Figure 4. Initially, the payload is injected into a suborbital trajectory by a Black Brant XII, four-stage sounding rocket. Figure 5 illustrates subsequent firing of the stages. The vehicle was spun-up by canting the fins during the ascent through the atmosphere to spin-stabilize the fourth stage motor burn (which was at this point out of the Earth's atmosphere) [Tyc et al., 1996]. An exo-atmospheric burn consisted of the fairing the nose and then the fourth stage motor was fired. The initial payload spin rate after separating from the last stage motor was 3.75 cps. Then the ACS system was activated and to align the spinning payload to within 5 degrees of the Earth's magnetic field. It was required by the science requirements to deploy the tether along the Earth's magnetic field line.

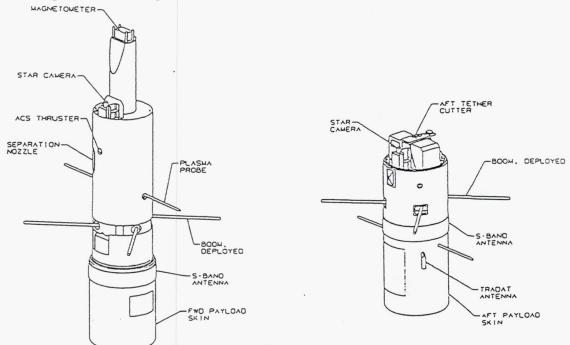


Fig. 2 Forward Subpayload Configuration

Fig. 3 Aft Subpayload Configuration

A crucial maneuver was deployment of the two pairs of the long booms associated with each subpayload before actual separation of them. There were simultaneously deployed to their full length: 19 m tip-to-tip for the forward subpayload and 13 m tip-to-tip for the aft subpayload respectively, at T+129-154 s after the launch. This brought the payload spin rate from 3.75 cps down to 0.084 cps due to conservation of the angular momentum law. The booms acted as antennas for the active space plasma experiments and also as stabilization factor for the attitude dynamics of the both subpayloads. Tether deployment was initiated soon after at +T174 s . The mechanical initiation by the set of springs was followed by the cold gas thrusters to provide approximately 60 N of sustained separation force until the relative separation velocity reached $\sim 7 \text{m/s}$. Then the deployment continued in the passive mode.

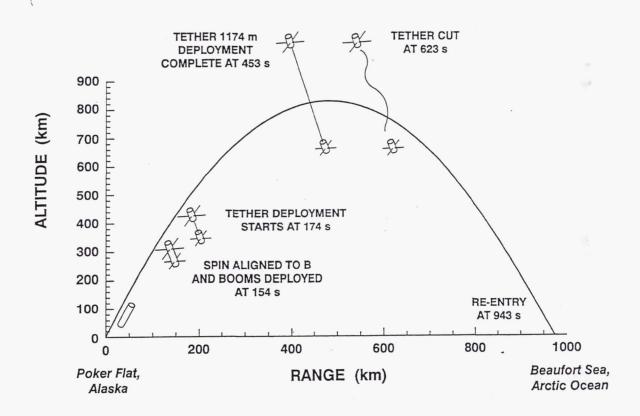


Figure 4 Pictorial View of the OEDIPUS-C Mission Trajectory

The tether deployment was decelerated by applying a constant braking torque to the deployment spool using a magnetic hysteresis brake. The magnetic brake was preset to achieve a nominal 1 km deployment. Full tether deployment of 1174 m was achieved before apogee was reached at T+453 s. OEDIPUS C continued its flight with the fully deployed tether for about 170 s. At T+623 the tether was cut from both ends. Then two subpayloads re-entered the atmosphere at T+943-957 s and burned over Beaufort Sea North from Alaska [Eliuk et al., 1996].

The video from the Attitude Video Camera (AVC) located on the aft payload provided a unique and excellent qualitative flight dynamics data. One example of the frozen image from the video is presented in Fig. 6. The actual capturing time for the AVC was ~13 min. Due to full Moon conditions the tether and the forward subpayload were clearly visible for most of the flight.

The video starts with startling moment of the movement of the forward subpayload into slowly rotating starry background. The rotating background was due to that the AVC was in the rotational movement w.r.t. the longitudinal axis of the aft subpayload. The interested observed phenomenon of the slow rotation of the forward subpayload can be explained that the subpayloads spin rate had differ slightly (which was confirmed by the other measurements). The forward subpayload is seen together with four antenna booms (fully deployed) and with visible small eccentricity during the initial portion of the video. The video also confirmed that the chosen stabilization method (two pairs of the almost radial booms) worked well and from the captured video images the forward subpayload is remarkably stable. Its location remains almost, to the moment of the tether cut, always near the geometrical center of the rotating background.

The video also provides more insight to the dynamics of this complex configuration. The tether oscillations remained relatively small and bounded and the tether was generally straight, especially during deployment. The booms also showed very stable behavior without any large in-plane deformations or oscillations. After completion of the deployment the tether had formed a big bow due to near zero value tether tension (slack situation was very well recorded by the Tether Force Sensor (TFS)).

The recoil of the payloads was clearly visible as the moment of restoration of the small tension in the tether and again with repetition of the tether slack with a big bow effect. After the tether was cut simultaneously from the both ends, it very clearly coiled up and was bunched by the gravity forces towards the middle between the subpayloads.

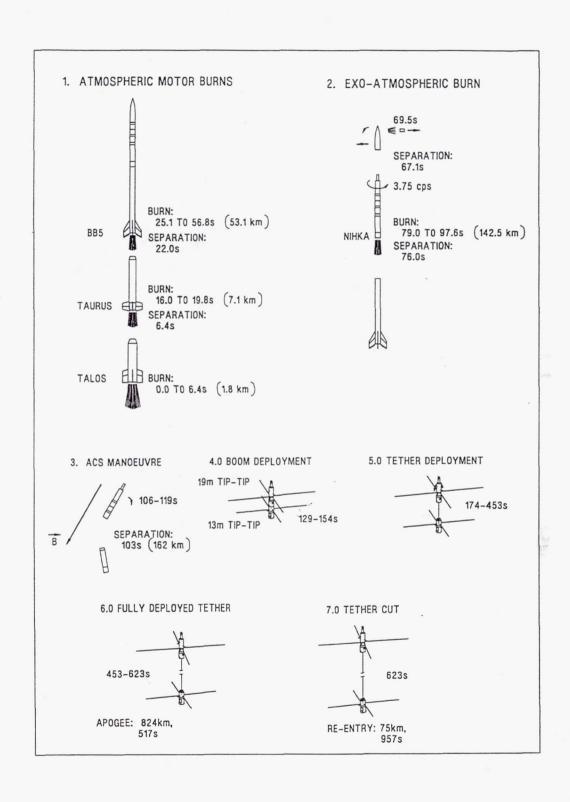


Figure 5 OEDIPUS-C Flight Sequence

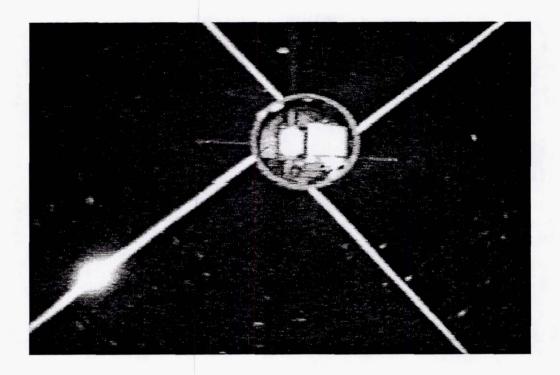


Figure 6 The Video Captured View of the Forward Payload and the Tether

Figure 6 shows a view of the forward subpayload as captured by the AVC from the aft payload. The the tether deployer spool is clearly seen. The offset of the radial booms is also evident. During the first 12 seconds while argon gas thrusters were on, the concurrent operation of the HEX transmitter produced a strong luminous rf discharge around the bases of the boom antennas. The video verified that the stabilization modeling efforts of the TDE team was generally sound and worked during the actual mission.

ADVANCES IN TETHER TECHNOLOGY

The planning for the OEDIPUS-C Tether Dynamics Experiment was initiated in 1992, and culminated with the successful flight on November 6, 1995. Elaborating more on the TDE objectives presented in Introduction, they can be grouped into three groups:

- derive of theory and develop of simulation and animation software for analyses of multi-body dynamics and control of the spinning tethered two-body configuration;
- provide dynamics & control expertise, for the tethered configuration and science investigations, develop an attitude stabilization scheme for the payload and support OEDIPUS C payload development;
- acquire dynamics data during flight, and compare with pre-flight simulations to demonstrate that the design technology is valid.

Thus, the OEDIPUS-C mission supported development of tether technology required for this class of missions and contributed significantly to advances of various elements of this technology. Theses elements are presented below and they consisted of tether related hardware components (tether, tether deployer, TFS and booms), dynamics and stabilization technology, and ground testing technology. The components of the tether technology required for the mission were designed and manufactured by the payload contractor in close collaboration and constant interaction with the Tether Dynamics Experiment team.

Tether Related Hardware Components

Tether

The choice of the tether for this mission was based on the previous experience and performance of the tether during the OEDIPUS-A mission. The same tether was chosen: 24 gauge wire per MIL-22759/32 which has a 19 strand, tin coated copper conductor with white teflon insulation (radiation cross-linked, modified ETFE) rated at 600 V. The deployer accommodated 1300 m of the tether. Tether mechanical properties were assessed during tests at UBC, Bristol and CSA. The tether was a composite type of material and its properties differ depending on loading rate and environmental conditions. The tether survived the flight which lasted about 8 minutes and 20 seconds (time between initiation of deployment and cutting of the tether from both ends). Tether deployment tests were also performed.

Tether Deployer

The tether deployer for the OEDIPUS-C mission was similar to the deployer used for the OEDIPUS-A flight with some modifications (addition of high resolution shaft encoder and additional isolation precautions). The tether deployer is a spool assembly (see Fig. 7). The assembly comprises of the spool (or reel), supporting structure, a magnetic hysteresis brake, a slip ring, high and low resolution shaft encoders, a wire-guard/snare-retainer and the forward tether cutter assembly. The spool was locked prior to separation and released. The spool inertia caused an initial spike in the tether tension as the spool spun up. Then, the magnetic hysteresis brake applied a torque to the shaft to control the tension in the tether. Angular position and velocity was monitored by low and high resolution shaft encoders. The TDE team was consulted during the development of the tether deployer. A simplified mock-up of the spool was developed for the TEther LABoratory Demonstration System as well to perform dynamics tests. Tether deployer was also tested on the ground by its developer - Bristol Aerospace Ltd.

Tether Force Sensor - TFS

The development of the TFS was one of the responsibilities of the TDE team and was sponsored by the Directorate of Space Mechanics, Space Technology, Canadian Space Agency. The main contractor was Bristol Aerospace Ltd. The TFS design was derived from the tethered satellite force transducer developed by NASA Langley

Research Center for the Small Expandable Deployer System (SEDS) designed for the Delta II - based secondary payload to deploy an end-mass. The SEDS sensor was designed to measure tensions in the tether up to 4.50 lb in each direction and resolve tensions as low as 0.0004 lb. The TFS had more stringent requirements and was designed to measure lower tensions in the 0-1 lb range, and with a resolution of 0.000045 lb. It measured 3-axis tension vector components at the tether attachment point to the aft payload. The TFS was a strain-gauge based instrument and it used two independent sets of gauges: foil (F) gauges and piezoresistive (PR) gauges. Design requirements and design overview was presented by [*Tyc et al.*, 1995b] and pre-flight testing and flight performance by [*Jablonski et al.*, 1997]. Calibration background was based on the NASA LRC experience but the TFS was calibrated jointly by NASA and CSA personnel. A software for TFS post-flight data processing was also developed. The TFS flexure with installed two sets of gauges is presented in Figure 8. The flexure was manufactured by Modern Machine & Tool Co., Newport News, VA, using the Wire Electrical Discharge Machine System (EDM) from a single piece of the 7075-T6 aluminum alloy.

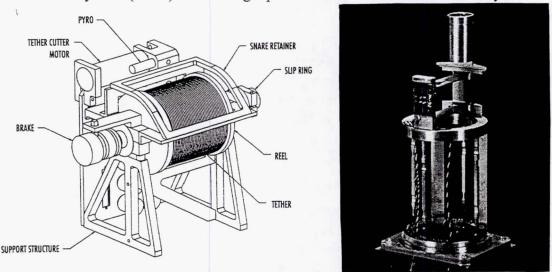


Fig. 7 OEDIPUS-C Tether Deployer Fig. 8 TFS Flexure with Foil and PR Gauges

Description of Booms

Based of the flight requirements booms were developed by Astro Aerospace Corp., CA. The basic boom element was a derivative of the STEM (Storable Tubular Extendible Member). Two sets of booms were installed one at each payload. They served two functions. On the forward payload they provided antennas for the HEX instrument and also served to stabilize the forward payload. Similarly on the aft payload they provided antennas for the REX instrument and also stabilized it. Each package had 4 booms, spaced in four quadrants. The forward booms were 19 m tip-to-tip, and the aft payload booms were 13 m tip-to-tip. Each package used four 0.86 inch diameter Be-Cu BI-STEM boom elements nested in a single spool. The deployment was driven from the single central storage spool element by the boom strain energy and assisted at the end by specially added DC motor. The boom lengths were derived from the stability criteria for

both payloads. A simplified mathematical model was also derived to assess the impact of the deployment on the payload itself. The specific problem of the radial offset of the boom element was found to be of secondary nature. Some stability aspects are also addressed in the section on Dynamics and Stabilization Technology.

Dynamics and Stabilization Technology

System Category

The OEDIPUS class payload is very complex from the dynamics point of view. The understanding of this type configuration requires investigations of the interrelationships between dynamics stability and the various parameters of the payload. The main parameters of this configuration are listed in Table 1. The subpayloads of the OEDIPUS-C configuration are minor axis spinner (cylindrical rigid bodies), but their final configurations are major axis spinners by virtue of the four flexible booms. The derivation of the mathematical models and associated stability criteria for this complex configuration was part of pre-flight dynamics studies.

Modeling Overview

The concentrated effort was the development of two parallel mathematical models: quasi-nonlinear model and linear model as described in the earlier publications [Tyc et al., 1994a and b; Tyc et al., 1995a; Vigneron et al., 1995a; Vigneron et al., 1997a; Vigneron et al., 1997b]. In general, the following aspects were covered by mathematical modeling: dynamics simulation and modal analysis, subpayload attitude stability analysis, tether deployment simulation, subpayload longitudinal dynamics simplified analysis [Tyc et al., 1996]. The main objectives of the modeling efforts were to understand the nutational and flexural dynamics of the subpayloads and coupled lateral vibrations of the tether. The longitudinal vibrations as uncoupled from the end-body nutation were not included in the linear model. The linear model includes one spinning rigid end-body with flexible appendages (booms) connected by the spinning tether modeled as an elastic string. This model was developed initially for the ground test configuration (TE-LAB) and used also for assessment of the flight configuration using quasi-dynamic approach. The motion of the system can be approximated by a weighted sum of two types of damped gyroscopic modes, the first derived from the tethered forward end-body, and the second from the tethered aft end-body [Vigneron et al., 1997b].

Stability Criteria

Closed-form stability criteria were developed for the spinning tether linear model that include one mode of vibration for the flexible radial booms and an arbitrary number of modes for the flexible tether [*Tyc et al.*, 1995a; *Vigneron et al.*, 1995b; *Vigneron et al.*, 1997b]. They were based on the stiffness matrix of the linear model. The simplified versions of the stability criteria for the OEDIPUS-C flight configuration are presented below.

$$T \ge \frac{\rho l^2 S}{n^2 \pi^2}$$
 (1)
 $n = 1, 2, ..., N$

where T is tension in tether, ρ is mass density of the tether, 1 is tether length, S is spin rate, n is number of assumed tether modes (this formulae assumes 3 tether nodes and can be expanded to any number of modes).

$$C_0 = A_0 \ge \frac{1}{3} \rho l b^2 + \frac{1}{S^2} \sum_{n=1}^{n=3} \frac{k_n^2}{\lambda_n} - \frac{bT}{S^2} \left(1 + \frac{b}{l} \right) (2)$$

where C_o , and A_o are moments of inertia (as listed in Table 1), b is the distance from COG of the payload to the tether attachment point, and k_n , λ_n are recursive formulae [Vigneron et al., 1995a]

Equation (1) represents tether-associated criteria and expresses the relationship between the stabilizing tension force and the destabilizing spin-dependent centrifugal forces. The effect of gravity forces is not included.

Equation (2) represents a well-known maximum-moment-of-inertia criterion for stability of the gyroscopic payload (end-body), with extensions to include the stabilizing effect of the tether tension and the destabilizing effect of the tether spin. Again the effect of the gravity forces might be included for the laboratory configuration (TE-LAB).

The above presented criteria were used to derive sufficient length of the booms for both payloads. Their modified versions were used to validate theoretical models with experimental results obtained using TE-LAB ground-test facility. The above studies had helped to understand the complex situation of the OEDIPUS-A instability.

Modes and animation

An important task was analysis of the damped gyroscopic modes of the OEDIPUS-like system as a means of understanding of these very complex configurations [Vigneron et al., 1997a; Vigneron et al., 1997b]. Based on the mathematical model which was derived using the Lagrangian approach, an associated eigen-value problem was derived and subsequently solved. Computer software was developed to solve this problem to yield modal frequencies, modal convergence/divergence ratios, and time varying mode shapes, for given input parameters (inertias of the end-bodies, spin rate, mass, stiffness damping, length of the booms, and mass, damping tension and length of the tether) [Vigneron et al., 1995b]. In general, the solution of this type of the eigenvalue problem leads to complex conjugate pairs of eigenvalues with complex eigenvectors. Through this analysis it was shown that the OEDIPUS-C configuration nutational modes were stable for the nominal parameters of the mission. However, the configuration is susceptible to boom-associated structural instability at spin rates above

0.26 Hz. The actual spin rate during the mission was 0.084 well below the above value. This analysis showed that the damped gyroscopic natural modes could be a very useful tool for understanding spinning flexible configurations. A knowledge of natural modal properties of the system is very useful in the post-flight data analysis.

The animation of the dynamics equations of the system and separately of the damped gyroscopic modes was also performed. The observation of the animation of the dynamic system behavior and its modes was helped to categorize them (nutational like modes, boom-like modes and tether-like system modes) [Chandrashaker et al., 1995; Vigneron et al., 1997b].

Stabilization Technology

Based on the above mentioned analyses a feasibility study was carried out to assess a number of the possible stabilization approaches for the OEDIPUS-C mission: OEDIPUS-A configuration with modified parameters; de-spun tether option; spin-axis aligned momentum wheel; and boom system to achieve favorable moments of inertia. The investigation identified two viable stabilization approaches, one using a momentum wheel, and another using a set of four radial boom on each subpayload. These were recommended by the TDE team to the payload design team at Bristol Aerospace. The implementation of the boom option was chosen as a cost-effective and assuring mass and space efficiency in the both subpayloads. The boom system was described earlier in this paper and additional information can be found in [Tyc et al., 1994b; Eliuk et al., 1995].

Ground Tests

Three general types of ground tests were undertaken as a part of the TDE. The first series of tests obtained qualitative information on a spinning tethered body. These tests, referred as the "Hanging Spin Tests", were conducted at the University of British Columbia [Modi et al., 1995] . The second series of tests were aimed at obtaining detailed quantitative measurements of the dynamic properties of the system and it involved a more complex set-up referred to as the "TEther LABoratory Demonstration System - TE-LAB" (developed by Directorate of Space Mechanics, Space Technology, CSA in collaboration with Carleton University) [Vigneron et al., 1994] The third series of tests involved determination of the tether material properties such as the effective Young's modulus and the damping coefficient and were conducted later at the University of British Columbia. The Hanging Spin Test is a simple configuration where an end-body with the desired mass properties is hung by a tether and spun in a controlled manner. A detailed description of this test facility and the test results are given by [Tyc et al., 1994a; Modi et al., 1995]. The TE-LAB facility consists of four main elements: an end-body attached to a set of gimbals which are driven by a lower rotating system; an upper rotating table with spool assembly; a constant length tether wire (exactly the same type as used during the actual mission), and a computer based data acquisition system and control systems (the major portion of them is called PODS (Payload Orientation Determination System) with a CCD camera). The PODS tracks two light sources on the

top of the end-body with CCD camera and uses their positions in the field of view to compute the three Euler angles describing the end-body's attitude. The TE-LAB tests played a major role in the validation of the mathematical model, provided good insight to understand interaction between spinning end-body and spinning tether, and their interaction, and served as an experimental tool in deriving the stability criteria for the system [Vigneron et al., 1995a; Vigneron et al., 1997a; Jablonski et al., 1995]. Figure 9 shows a photo of the TE-LAB facility at the David Florida Laboratory in Ottawa that investigated two end-body configurations: a minor axis spinner and a major axis spinner.

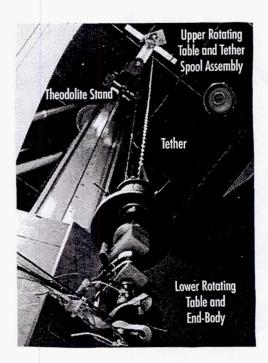


Figure 9 TE-LAB facility (seen from below)

EXAMPLES OF OEDIPUS-C FLIGHT DYNAMICS DATA

Flight dynamics data along with a "Quick Look" analysis was presented by [Tyc et al., 1996]. In this section some of the OEDIPUS-C flight dynamics data are presented based on the above reference and additional findings. The flight data analysis is still continuing. The post-flight analysis includes aspects of the subpayload attitude, subpayload trajectory and tether deployment, and reconciliation of flight data from the Tether Force Sensor (TFS), magnetometer data, and the flight video. The flight dynamics data comprises the TFS instrument data and other data obtained from the engineering support instruments. Some examples are presented below.

Coning angles of the subpayloads

Based on the attitude solution (in terms of the right ascension (RA or α), declination (DE or δ), and roll angles) angular velocities of the subpayloads were

calculated and from them the motion of the angular momentum vector (H-vector) was determined for both subpayloads. The amount of movement of the H-vector for the forward subpayload was found to be higher than the one for the aft subpayload. The processed coning angles are small for both subpayloads (see Fig.10). They confirm that both subpayloads were stable during the flight.

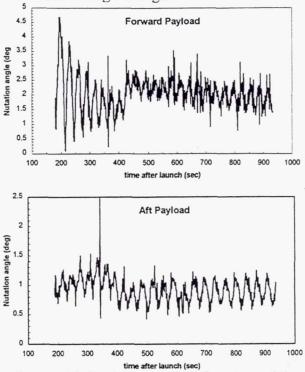


Figure 10 Coning angles as function of time

Subpayload trajectory and tether deployment

Full information about the aft subpayload trajectory was obtained from the TRADAT tracking data downlinked during the mission. The trajectory of the aft payload is showed in Fig. 12. Bristol Areospace Ltd. had processed attitude data obtained from star flight cameras (Attitude Video Cameras - AVC). They served to calculate the magnitude of the separation vector z as a function of time (see Fig. 13). The trajectory of the flight in the declination (DE or δ) as a function of the right ascension (RA or α) is presented in Fig. 14.

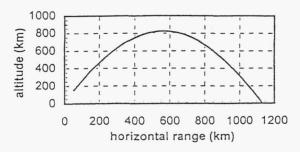


Figure 12 Aft Payload Flight Trajectory

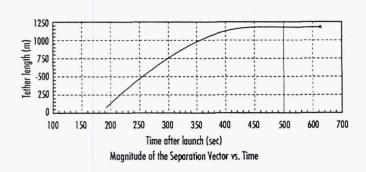


Fig. 13 Tether Seperation Vector

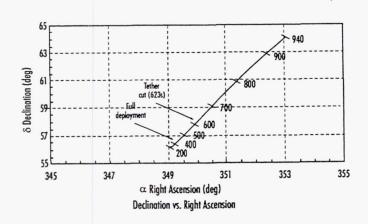


Fig. 14 OEDIPUS-C Trajectory in Terms of Right Ascension and Declination

Trajectory studies involved development of the flight model with two masses connected by an inextensible tether are being performed now. The trajectory model involves a spool model.

Tether Force Sensor (TFS) Flight Data

The TFS flight data was pre-processed and the both sets of strain gauges, foil gauges and PR gauges, provided excellent information on all three components of the tether force vector. Description how the calibration constants were applied to the raw data to determine the actual loads in each axis was presented by [Jablonski et al., 1997]. The total tether force was calculated based on the magnitudes of the three components and is showed in Figure 15 (zero corresponds to the launch).

The TFS data is being now studied and some results were presented earlier [Tyc et al., 1996; Jablonski et al., 1997]. The tension recoil effect also captured by the flight video is clearly evidenced at about 560 seconds after the launch. Some preliminary FFT

analyses of the TFS data indicates that it has a very rich spectral content especially in the longitudinal direction (Z direction). Lateral direction effects are considerable smaller. Based on the initial review of the data obtained from the magnetometers, there are no tether related frequencies present. Thus, magnetometers related data will help identify better boom and payload related dynamic frequencies.

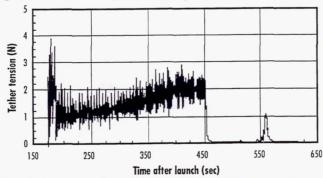


Figure 15 Total Tether Force Based on the TFS Data From the Foil Gauges

Furthermore, the TFS data can be also interpreted for the tether related frequencies in the longitudinal and lateral directions. The examples of the FFT results from the TFS lateral axis data are presented in Fig.16.

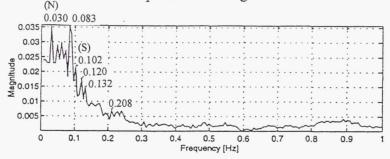


Figure 16 FFT Results for the TFS Lateral Output

There are number of peaks in Figure 16 and two of them 0.03 Hz and 0.083 Hz can be clearly identified. The frequency 0.03 Hz represents the aft payload nutational frequency (one based on the rigid body model of the payload was found to be 0.028 Hz) and the frequency 0.083 Hz represents spin rate of the payload (measured value was 0.084 Hz). The pre-flight modal analysis found that the tether and flexible booms had relatively little effect on the nutational frequency of the payload which also proven by the above results [*Tyc et al.*, 1996]. Initially longitudinal vibrations were not fully explained and would require more investigations as the longitudinal tether vibrations are not presently included in the mathematical model.

The last phase of the post-flight analysis is presently underway. It includes completion of the flight model of the configuration with longitudinal effects and the comparison studies of the flight data with pre-flight simulations. The OEDIPUS-C model might serve as a generic model to study future tether missions. A correlation of spectral

analysis is of the special importance and it will further our understanding of the system dynamics.

CONCLUSIONS

- 1. The OEDIPUS-C tethered payload flight was successful and has provided an excellent flight dynamics data. The TDE team is continuing the post-flight analysis in the light of the future space tether applications.
- 2. Having two successful flights (OEDIPUS A and C) Canada has a proven tether technology platform for the ionospheric and other space science experiments using sub-orbital sounding rockets.
- 3. The effect of the spinning tether on the rotating spinning spacecraft with flexible appendages (booms) was explained in the comprehensive manner including its validation using a unique ground-test facility (TE-LAB). Further studies beyond present linear type of model are required to explain non-linear effects.
- 4. The tethered spinning configuration was filmed in the space resulting in a unique video which shows all dynamics states of the forward payload and the tether after separation, during deployment and after cutting of the tether.
- 5. The advances in the tether technology in the OEDIPUS program have created a base for a future Canadian tether orbital mission.

ACKNOWLEDGMENT

The authors wish to acknowledge the Space Science and Space Technology Branches of the Canadian Space Agency for the support of the Tether Dynamics Experiment (TDE) project and the OEDIPUS-C mission. Contributions and dedication of other members of the TDE team including PDF's, contractors, and students are also acknowledged. Many thanks are also due to all members of the Space Science team including the Space Science Program Office, CSA for cooperation and constant help during this project.

REFERENCES

Chandrashaker, R., F. R. Vigneron, A. M. Jablonski, N. Roberton, B. Brown, G. Tyc, "Computer Oriented 2-D Animation of the Tether Dynamics Model", *Proc. of the* 15th Canadian Congress of Applied Mechanics (CANCAM 95), University of Victoria, B.C., Canada, May 28- June 2, 1995.

- Eliuk, W., R. Rob, G. Tyc, I. Walkty, G. Rumbold, H. G. James, "Design of the OEDIPUS-C Suborbital Tethered Payload", *Proc. of the 4th Int. Conf. on Tethers in Space*, Washington, D. C., 10-14 April **1995**.
- Eliuk, W., I. Walkty, R. Rob, J. G. Rumbold, H. G. James, "OEDIPUS-C Tethered Suborbital Mission Description and Flight Performance", *Proc. of the 9th CASI Conf. on Astronuatics*, Ottawa, Ont., Canada, 12-15 Nov., **1996**.
- Jablonski, A. M., F. R. Vigneron, G. Tyc, R. P. S. Han, A. K. Misra, V. J. Modi, R. Chandrashaker, "The OEDIPUS-C Tether Dynamics Experiment", Proc. of the 9th CASI Conf. on Astronuatics, Ottawa, Ont., Canada, 12-15 Nov., 1996.
- Jablonski, A. M., F. R. Vigneron, R. Chandrashaker, J. Bergmans, B. McClure, D. A. Staley, G. Tyc, "Tether LABoratory Demonstration System (TE-LAB)" A Ground Test Facility for the OEDIPUS Tether Missions", Proc. of the 4th Int. Conf. on Tethers in Space, Washington, D.C., 10-14 April 1995.
- Jablonski, A. M., F. R. Vigneron, R. D. Rhew, J. L. Bergmans, W. R. Whitehead, G. Tyc, "Preflight Testing and Flight Performance of the OEDIPUS-C Tether Force Sensor", AIAA J. of Spacecraft and Rockets, Vol. 34, No. 4, July-August 1997, pp. 533-541.
- James, H. G. and G. Tyc, "Flight Results from the OEDIPUS-A Tether Experiment", Proc. of the 4th Int. Conf. on Tethers in Space, Washington, D.C., 10-14 April, 1995a.
- James, H. G., J. G. Rumbold, "The OEDIPUS-C Sounding Rocket Experiment", *Proc. of the 4th Int. Conf. on Tethers in Space*, Washington, D.C., 10-14 April, **1995b**.
- Misra, A. K., M. Keshmiri, V. J. Modi, S. Pradhan, G. Tyc, R. P. S. Han, F. R. Vigneron, A. M. Jablonski, "Dynamics of Low-Tension Spinning Tethers", *Proc. of the 4th Conf. on Tethers in Space*, Washington, D.C., 10-14 April **1995**.
- Modi, V. J., S. Pradhan, M. Chu, G. Tyc, A. K. Misra, "Experimental Investigation of the Dynamics of a Spinning Tethered Rigid Body", *Proc. of the 4th Int. Conf. on Tethers in Space*, Washington, D.C., 10-14 April **1995**.
- Tyc, G., R. P. S. Han, R. F. Vigneron, A. M. Jablonski, V. J. Modi, A. K. Misra, "Dynamics and Stability of a Spinning Tethered Spacecraft with Flexible Appendages", *Advances in the Astronautical Sciences, Astronautics* 1993, Vol. 85, AAS 93-776, Univelt Inc., San Diego, 1994a.

- Tyc, G., F. R. Vigneron, A. M. Jablonski, R. Chandrashaker, R. P. S. Han, "Design of a Attitude Stabilization System for the OEDIPUS-C Tethered Rocket Payload", *Proc. of the 8th CASI Conf. on Astronautics*, Canadian Astronautics and Space Institute, Ottawa, Ontario, Canada, 7-10 November **1994b**.
- Tyc, G., R. P. S. Han, "Attitude Dynamics Investigation of the OEDIPUS-A Tethered Rocket Payload", AIAA J. of Spacecraft and Rockets, Vol. 37, No. 1, Jan.-Feb. 1995a, pp. 133-141.
- Tyc, G., W. R. Whitehead, J. L. Phillips, J. G. Pierson, A. M. Jablonski, F. R. Vigneron, "Design, Qualification and Calibration of the Tether Force Sensor (TFS) for the OEDIPUS-C Mission", *Proc. of the 4th Int. Conf. on Tethers in Space*, Washington, D.C., 10-14 April **1995b**.
- Tyc, G. F. R. Vigneron, A. M. Jablonski, R. P. S. Han, V. J. Modi, A. K. Misra, "Flight Dynamics Results from the OEDIPUS-C Tether Mission", *Proc. of the AIAA/AAS Astrodynamics Conf.*, Paper AIAA-96-3573, 29-31 July **1996**, San Diego, CA.
- Vigneron, F. R., A. M. Jablonski, R. Chandrashaker, "Tether Dynamics Model for the TEther LABoratory Demonstration System (TE-LAB)", *Canadian Space Agency, CSA Technical Report OED-TR-93-05, Revision 1, Saint-Hubert, Quebec, Canada, November* **1994**.
- Vigneron, F. R., A. M. Jablonski, R. Chandrashaker, "Stability Criteria and Eigenvalue Problem for the TEther LABoratory Demonstration System", *Canadian Space Agency, CSA Technical Report OED-TR-95-01*, Saint-Hubert, Quebec, Canada, January 1995a.
- Vigneron, F. R., A. M. Jablonski, R. Chandrashaker, J. Bergmans, B. McClure, D. A. Staley, G. Tyc, "Validation of Analytical Modeling of OEDIPUS Tethers Using Experimental Results from TE-LAB", *Proc. of the 4th Int. Conf. on Tethers in Space*, Washington, D. C., 10-14 April **1995b**.
- Vigneron, F. R., A. M. Jablonski, R. Chandrashaker, B. McClure, J. Bergmans, G. Tyc, "Comparison of Analytical Modeling of OEDIPUS Tethers with Laboratory Data from Tether Laboratory", *AIAA J. of Guidance, Control and Dynamics*, Vol. 20, No. 3, May-June **1997a**, pp. 471-478.
- Vigneron, F. R., R. Chandrashaker, A. M. Jablonski, G. Tyc, "Damped Gyroscopic Modes of Spinning Tethered Space Vehicles with Flexible Booms", To be published in the AIAA J. of Spacecraft and Rockets, Vol. 34, No. 5, Sept.- Oct. 1997b.

THE HOYTETHER: A FAILSAFE MULTILINE SPACE TETHER STRUCTURE

Robert P. Hoyt, Robert L. Forward Tethers Unlimited

8114 Pebble Court, Clinton, WA 98236 USA Phone/Fax: (206) 306-0400; Email: TU@tethers.com; Web: www.tethers.com

Abstract

The Hoytether is a failsafe, multiline space tether structure for long-duration and high-value tether missions. The Hoytether structure is an open net which provides redundant linkage in such a way as to maintain spatial separation between the individual lines composing the structure as the structure is degraded by orbital debris and meteoroid impactors. The spatial separation between lines prevents one small impactor from severing the entire Hoytether as can happen with a single-line tether. The Hoytether structure thus can suffer many cuts by small impactors while maintaining the design load. Analytical modeling of tether lifetimes in the space debris environment indicate that the redundancy of the Hoytether enables it to provide >99% survival probabilities for periods of months to years. Using numerical modeling, we have developed designs for Hoytether structures capable of operating at very high stress levels while maintaining high reliability for long lifetimes.

Introduction

The successes of the two Small Expendable-tether Deployment System (SEDS) and the Plasma Motor Generator (PMG) experiment have demonstrated the feasibility and reliability of small, inexpensive self-deploying tether systems.¹ Tethers are now being considered for a variety of applications such as studies of the upper atmosphere,² facilities for orbital transfer of payloads,^{3,4} electrodynamic power and propulsion systems for the International Space Station and other satellites,⁵ synthetic aperture radar systems, and rapid de-orbiting of post-operational LEO satellites.⁶ For tethers to be viable candidates for many of these applications, they must be designed to survive the flux of orbital debris and meteoroids for periods of many years and/or operate with high safety factors.

The need for a space tether structure with redundant linkage was illustrated by the results of the SEDS-2 mission flown in 1994¹ and the recent TSS-1R mission.⁷ The second SEDS mission used a tether consisting of a single cylindrical braided line with a diameter of 0.8 mm and a length of 20 km. This tether was cut by a debris or meteoroid impactor roughly 4 days after deployment. In the TSS-2 mission, the conducting-core tether was severed by a high-voltage arc caused by a defect in the electrical insulation, resulting in loss of the tether and the Italian satellite. Clearly, for a tethered system to complete a many-year mission, or for a crewed tether experiment to operate with an acceptable safety factor, a tether structure with built-in redundancy is required.

A tether structure capable of achieving the multi-year lifetimes and high safety factors required for many applications is illustrated in Figure 1.8 This design was invented in 1991 by Robert Hoyt and subsequently named the "Hoytether" by Dr. Robert L. Forward. The "Hoytether" is a tri-axial net consisting of a number of primary load-bearing lines running the length of the structure. These "primary" lines are periodically interconnected by diagonal secondary lines. A section of a tubular Hoytether is illustrated in Figure 1a. Where the secondary lines intersect the primary lines they are firmly connected so that one line does not slip relative to the other. The secondary lines are only put under load if a section of primary

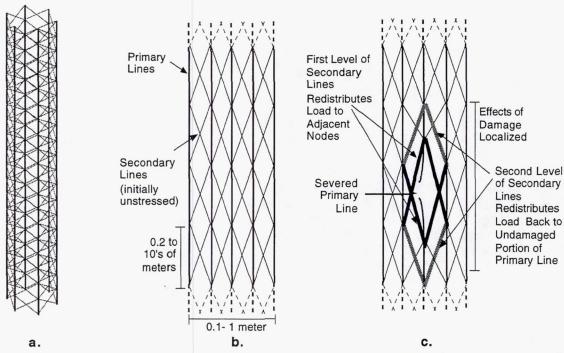


Figure 1. a) Section of a tubular Hoytether ("Hoytube"). b) Schematic of undisturbed tape Hoytether ("Hoytape"). c) Secondary lines redistribute load around a failed primary line without collapsing structure. *Note*: the horizontal scale is expanded relative to the vertical scale; in reality the secondary lines are nearly parallel to the primary lines.

line is cut by space debris. At either end of the structure, a support ring enforces the cylindrical spacing between the primary lines. Because the secondary lines are not initially loaded, they do not cause the structure to neck down, and thus no solid spacers are required along the length of the tether. In this cylindrical configuration, the Hoytether structure is also called a "Hoytube."

The principle of the Hoytether is illustrated in Figures 1b and 1c. The secondary lines are almost parallel to the primary lines and thus are ready to pick up the load if a primary line fails. When a section of primary line is cut by debris, the secondary lines assume the load and redistribute the stresses in such a way that the effects of the damage are localized to a region near the failure. Because the secondary lines are nearly parallel to the primary lines, and because they are initially slack, the structure necks down only slightly. Thus such a tether can suffer many cuts without catastrophic failure. Moreover, the structure degrades gracefully, maintaining separation between the individual lines to minimize the chances that a single object could cut more than one line.

In experimental and numerical investigations during early 1992 under SBIR contract NAS8-39318,9 this design was found to:

- 1. Withstand multiple cuts of individual line segments while retaining structural integrity and degrading gracefully.
- Have lifetimes several orders of magnitude longer than comparable-mass single-line tethers.
- 3. Redistribute loads around a cut primary line in such a way that the distortion due to a line segment failure was localized to within a few sections on either side of the cut. This

localization of the effects of a cut keeps the structure from "pinching" severely, even after many cuts.

4. Maintain separation between the strands without the need for solid bracing structures.

The availability of a multistrand tether system with such failsafe attributes will enable NASA and other organizations to pursue the many advanced propulsion applications of tethers, particularly the many missions in which long-life and safety are important considerations.

Tether Survival Probabilities

A tether deployed in space will be subjected to impacts by both meteorites and man-made orbital debris. For a conventional single-line tether, one strike by an impactor with sufficient energy will cut the tether and cause failure of the mission. A Hoytether, however, has many redundant links, and thus can suffer many cuts to individual lines while continuing to support its design load.

Survival Probability of a Single Line

Currently, experimental data on the rate of failure of a tether line is limited to the results of the SEDS-2 experiment and the ongoing TiPS experiment. Consequently, the most appropriate method of estimating the lifetimes of space tether lines currently available is to utilize models of the flux of debris and meteoroid particles such as that given by Kessler. This data is typically given as the cumulative flux of particles larger than a specified diameter. This particle flux, $F(d_{particle})$, is converted to a flux of lethal impactors by assuming that a tether line will be cut by particles with diameters equal to or greater than a specified fraction k_L of the tether diameter, $f(d_{line}) = F(k_L d_{line})$. This fraction is called the "lethality coefficient." For the analyses in this work, a lethality coefficient of 0.3 is assumed based upon the results of the SEDS-2 experiment. This value of k_L is in the middle of the range of values (0.2-0.5) that are commonly used.

For a single line tether of diameter d and length L, the probability of survival of the tether for a duration T is obtained by first multiplying the flux of lethal impactors by the surface area of the tether line to obtain a rate of cuts c,

$$c_{I} = \pi dL F(k_{L} d), \qquad (1)$$

and multiplying this rate by the lifetime to obtain the expected number of cuts in the time T,

$$N = c_1 T. (2)$$

The survival probability is then obtained using Poisson statistics to determine the probability that the line suffers no cuts during the period T,

$$P(T) = P_N(0) = \frac{N^0}{0!} e^{-N} = e^{-c_I T}.$$
 (3)

The 1/e lifetime of a single line tether is thus $\tau_1 = 1/c_1$.

Survival Probability of Hoytethers

Hoytether Parameters and Cut Ratesi

In a generic Hoytether, there are n primary lines and m secondary lines. The lines are divided up into h segments or tether "levels," determined by the interconnection points of the pri-

For a detailed derivation of the survival probability analysis, please refer to AIAA paper 95-2890, "Failsafe Multiline Hoytether Lifetimes," R.L. Forward and R.P. Hoyt, or to Appendix E, "Small Impactor Survival Probabilities of Hoytethers," in Failsafe Multistrand Tether SEDS Technology Demonstration, Tethers Unlimited Final Report on NASA contract NAS8-40545, June 1995.

mary lines with the secondary lines. For a Hoytether of length L, the length of the individual primary line segments is $l_p = L/h$, and there are a total of nh of these segments.

The primary lines are separated by a distance a, and are connected by diagonal secondary lines which are deliberately made slightly longer than the distance between interconnection points by a "slack coefficient," k_s , which is typically around 1.005.

The survival probability of the individual primary and secondary line segments is found in a manner equivalent to the estimation of single line tether survival in Eqns. (1)-(3):

$$P_p(T) = P_{N_p}(0) = e^{-N_p}$$
 (4)

$$P_{s}(T) = P_{N_{s}}(0) = e^{-N_{s}}$$
 (5)

The probability of at least one cut on a given line segment is given by

$$P_N(>0) = 1 - P_N(0) = 1 - e^{-N}.$$
 (6)

Because the Hoytether design provides redundant paths for bearing the tether load, the loss of a single primary or secondary line segment does not lead to failure of the tether as a whole. In a low load case, where any one of the primary or secondary lines can carry the full load, then all of the primary and all of the secondary lines would have to be cut at the same level before the Hoytether as a whole will be severed. When the tether is under more substantial loading, the tether will survive until the number of uncut primary lines plus the number of uncut secondary lines is insufficient to bear the tether load. Predicting the survival probabilities in this case can be done using Monte Carlo simulation of tether structures subjected to random fluxes of impactors. Alternatively, this problem can be approached analytically by calculating the survival probabilities of the primary lines and the secondary lines separately and then combining them.

The number of primary line segments that must be cut before failure, x, is approximately proportional to the ratio of the applied load W_a compared to the maximum load capacity W_p of all the n primary lines in the uncut Hoytether. Similarly, the number of secondary line segments that must be cut before failure, y, is approximately proportional to the ratio of the applied load W_a compared to the maximum load capacity W_s of all the m secondary lines in the uncut Hoytether:

$$x \ge (1 - \frac{Wa}{Wp}) n \qquad y \ge (1 - \frac{Wa}{Ws}) m \tag{7}$$

Survival Probability of Hoytether Structure

If N_p and N_s are small, then the probability of survival of any one level is very high. However, there are many levels, and failure of any one of them causes failure of the whole tether. The probability of survival of the entire Hoytether is thus the product of the survival of all the h primary line levels in the tether:

$$S_T = S_L{}^h = [1 - (1 - e^{-N}p)^x (1 - e^{-N}s)^y]^h$$

$$S_T(t) = [1 - (1 - e^{-c}p^t)^x (1 - e^{-c}s^t)^y]^h.$$
(8)

Tether Lifetime

When the Hoytether structure is fabricated with many levels (large h), analysis of Eqn. (8) results in an effective tether "lifetime" of

$$\tau = \frac{1}{c_p \left(\frac{x}{x+y}\right) c_s \left(\frac{y}{x+y}\right) h^{\left(\frac{1}{x+y}\right)}}$$
(9)

Although the lifetime given by Eqn. (9) is a "1/e lifetime," in that the probability of survival of the Hoytether at time $t=\tau$ is $S_T=1/e=0.368$, the probability of survival with mission duration does not have the standard "1/e curve" decay with time. Although the individual line segments will have lifetimes described by the traditional exponential decay, the probability of failure of all of the line segments on a particular level is the product of those lifetimes. This "sharpens" the drop time, so that the Hoytether maintains a high probability of survival for periods shorter than the tether lifetime, and has a low probability of surviving after that lifetime is exceeded.

Lifetimes: Hoytethers vs. Single-Line Tethers

A single-line tether with diameter D_I and length L_I has a 1/e lifetime of $\tau_I = 1/c_I = 1/S_I F_I$, where $S_I = \pi D_I L_I$ is the total surface area of the tether and F_I is the flux of space impactors capable of severing the tether. The single-line tether's probability of survival decays exponentially as described by Eqn. (3).

The effectiveness of the Hoytether design can be examined by replacing this single-line tether with a failsafe multiline tether having the same mass as the single-line tether. The Hoytether has n primary lines and m=2n secondary lines. The secondary lines will have half the cross-sectional area of the primary lines, so the secondary lines will have the same total mass as the primary lines. Using these rates in Eqn. (12), the Hoytether lifetime is found to be proportional to the single-line tether lifetime $\tau_1=1/C_1$ by the factors:

$$t = \frac{1}{c_p \left(\frac{x}{x+y}\right) c_s \left(\frac{y}{x+y}\right) h^{\left(\frac{1}{x+y}\right)}} \approx \frac{h^{\left(1-\frac{1}{x+y}\right)}}{2^{\left(\frac{0.75y}{x+y}\right)} (2n)^{0.75}}.$$
 (10)

Inspection of this equation reveals that the lifetime of a Hoytether is greater than the lifetime of an equal mass single-line tether roughly by a factor of the number of interconnection levels h divided by the number of primary lines n.

The analytical relationship for the survival probability as a function of time, expressed in Eqn. (8), shows that the survival probability of the tether does not drop as a simple 1/e decay but rather maintains a high survival probability until the Hoytether lifetime is reached. This means that the Hoytether can achieve very high (>99%) survival probabilities for long periods of time.

Figure 2 shows a comparison between the survival probabilities of a single-line tether and an equal-mass Hoytether designed for a low-load mission such as a gravity-gradient stabilized synthetic aperture radar satellite system.¹⁵ Both tethers are 10 km long and mass 25.5 kg. The Hoytether would be a tubular structure with 6 primary lines connected by secondary lines every 0.2 m. While the single-line tether has a survival probability that drops exponentially with time, the Hoytether can have a >99% survival probability for many decades. [Note: decadelong lifetimes will likely require system capability to avoid large (>1 m) objects, such as derelict satellites.]

High-Strength Survivable Tethers

Motivation

Tethers have the potential to significantly reduce the cost of in-space transportation by providing a means of transferring payloads from one orbit to another without the use of fuel.^{3,4} Systems composed of rotating tethers attached to orbiting facilities could be used to boost payloads from low Earth orbit or even suborbital trajectories to higher orbits by transferring orbital momentum and energy from the tether facility to the payload; the orbit of the facility could be restored by "recycling" orbital momentum from return traffic.

Such tether transport systems will require tethers capable of operating at very high stress levels. In addition, for a tether transport system to be economically advantageous, it must be capable of handling frequent traffic for a periods of at least several years. Consequently, a tether transport system will require the use of tethers designed to remain fully functional at high stress levels for many years despite degradation due to impacts by meteorites and space debris. An additional requirement for this system is that the tether mass be minimized to reduce the cost of fabricating and launching the tethers. These two requirements present conflicting demands upon the tether design that make conventional single-line tethers impractical for this application. For a single-line tether to achieve a high probability of survival for many years, it would have to be very thick and massive. Fortunately the

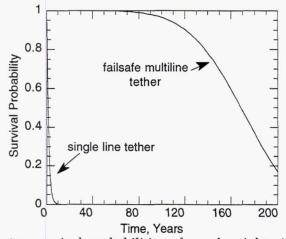


Figure 2. Small-impactor survival probabilities of equal-weight single-line and failsafe multiline tethers for a low-load mission.

Hoytether design can balance the requirements of low weight and long life, enabling tether transport facilities to become feasible. The redundant linkage in the Hoytether enables the structure to redistribute loads around primary links that fail due to meteorite strikes or material failure. Consequently, the Hoytether structure can be loaded at high stress levels yet still achieve a high margin of safety for long periods of time.

Because minimizing the tether mass is critical to the viability of tether systems for inspace propulsion, we have sought to optimize the design of the Hoytether structure so as to maximize the strength-to-weight ratio of the tether while achieving high probability of survival for periods of years.

Minimizing the "Safety Factor" While Maintaining Reliability

When a tension member is developed, it is normally designed to operate at a load level somewhat lower than the maximum it could support without breaking. This derating provides margin of error in case of imperfections in the material or the construction. Typically, a tether is designed to carry a maximum load that is 50% of its breaking limit; this tether would have a "design safety factor" of F = 1/50% = 2.0.

Because a high-speed rotating tether must support its own weight in addition to the weight of its payload, the required mass for a rotating tether increases exponentially as the design safety factor is increased. For rotating tether systems, therefore, it is necessary to operate at the minimum acceptable safety factor so as keep the required tether mass within economically feasible levels. For conventional single-line tethers, however, reducing the safety factor causes a corresponding increase in the likelihood of failure.

For the Hoytether, we define the safety factor as the ratio of the maximum load capacity of both primary and secondary lines to the design load. The safety factor thus provides the same measure of the strength-to-weight ratio of the Hoytether structure as it does for a single-line tether. However, this definition of the safety factor does not accurately represent the true margin of safety for the Hoytether. Because the Hoytether has redundant links that can reroute loads around parts of the tether that have failed, it is possible to load the Hoytether at a large fraction of the capacity of the primary lines (ie.- small "safety factor") and still have a large margin of safety. Consequently, using the Hoytether structure allows us to design the tether with a low "safety factor" to minimize the tether mass and yet still have a very reliable structure. In this effort we have sought to optimize the Hoytether by finding a design that minimizes the safety factor and thus minimizes the required mass while still providing the ability to withstand many cuts due to meteorite strikes.

It should be noted that the manner in which we calculate the Hoytether safety factor below is not obvious. Typically, we refer to Hoytether designs by the level of stress on the *primary lines*. Thus, if each secondary can support 1/2 as much tension as a single primary line can support (i.e.- each secondary has half the cross-sectional area of a primary line), and if it is loaded at 50% of the capacity of the primary lines, it will be loaded at a design safety factor of

$$F = \frac{\left[(\text{\# of primaries})(\text{primary line area}) + (\text{\# of secondaries})(\text{secondary line area}) \right]}{(\text{\# of primaries})(\text{primary line area})} \frac{1}{(\text{primary stress level})}$$
(11)

F = [1+2(1/2)]/50% = 4.

Method: Simulation with the SpaceNet Program

To study the optimization of the Hoytether structure for high-load applications, we performed a series of simulations of variations of the structure using the SpaceNet program. The SpaceNet program uses a combination of finite-element methods with a structural relaxation scheme to calculate the effects of damage to complex 3-D net structures such as the Hoytether.

Results

We began by studying multi-line Hoytethers with secondary lines having 1/4 the cross-sectional area of the primary lines; the secondary lines thus have a total mass of 1/2 of the mass of the primary lines (there are two secondary lines per primary line). In addition, the secondary line length was chosen so that they would be slack under design load. We found that if this tether is loaded at 90% of capacity of the primary lines, giving it a design safety factor of F=1.67, it can survive a cut to one of the primary lines. Moreover, the tether can survive an additional cut on the same level. However, if the second cut is on a primary line immediately adjacent to the first cut, the structure will fail. While the probability of two adjacent primary lines being cut by two separate meteoroid impacts is very small, it is possible that two lines could be cut by one impactor if it is large enough. Consequently, it is necessary to design the tether to withstand several localized cuts. Therefore, a larger safety factor is required.

The results of our subsequent analyses indicate that the design of an optimal Hoytether depends upon how much of its mission duration will be spent under high load. Consequently, there are two classes of Hoytether designs, one for tethers that are always under high load, and one for tethers that are heavily loaded for brief periods only.

Continuous-High Load Tether

If the tether will be under high load for most of its mission, then it should be designed with secondary lines slack at the expected load level. This will enable the tether lines to remain spread apart at all times, minimizing the chances of a single impactor cutting several lines. For this case, a near-optimal tether design would be a cylindrical Hoytether with a large number of primary lines (\sim 20) stressed at 75% of their maximum load and with initially-slack secondary lines that each have a cross-sectional area 0.4 times that of a primary line. Splitting the tether up into a large number of primary lines is necessary. From Eqn. (11), such a tether will have a design safety factor of F=2.4. However, the redundant nature of the structure will make the Hoytether far more reliable than a single line tether with the same safety factor. Simulations with the SpaceNet program have shown that this tether design can withstand multiple cuts on a single level. In fact, even if all of the primary lines on one level are cut, the secondary lines will support the load.

Intermittent High-Load Tether

A tether on a transfer facility, however, would likely be loaded at high levels for only a few hours every month. Therefore, it is possible to reduce the tether weight by designing it to have slack secondaries at the load level experienced during its long "off-duty" periods, but to have the secondaries bear a significant portion of the load during a brief high-stress operation such as a payload catch-and-throw operation. During the high-stress period, the loading of the secondaries will cause the structure to collapse to a cylindrical tube. Once a payload is released and the stress is reduced, however, the tether lines will drift back apart. If this high-load period is brief, it will only slightly increase the chances of tether failure due to impact by a large object. Because the secondaries bear a significant fraction of the stress at high load levels, the tether can safely be loaded to higher levels. Simulations indicate that a 20-primary line Hoytether with secondary lines having cross-sectional area 1/4 of that of the primary line area can be loaded to more than 100% of the primary line capacity and still survive cuts to two adjacent primary line segments. A reliable design for this class of tether would be a cylindrical Hoytether with primary lines sized so that they will be loaded at 85% of their capacity during peak stress operations, and secondary lines with cross-sectional areas 1/4 of the primary lines. The secondary line lengths would be chosen so that they would be slightly slack during off-duty periods. Eqn. (11) above gives the design safety factor of this tether as F=1.75.

Conclusions

Tether applications in which the tether must survive the space environment for long periods will require tether structures capable of surviving multiple impacts by debris and micrometorites. The Hoytether open-net structure provides multiply redundant linkage, enabling the tether to withstand many cuts yet still provide reliable load-bearing capabilities. While the survival probability of a standard single-line tether decreases exponentially with time, the Hoytether structure has a survival probability that remains very high for a long period of time, dropping only when its "lifetime" is reached. We have investigated the design of Hoytethers for demanding applications such as tether transport systems and found that the redundant linkage of the structure enables the Hoytether to operate reliably at very high stress levels; this design thus can minimize the tether mass required for tether transport systems.

References

- 1. Carroll, J.A., "SEDS Deployer Design and Flight Performance," paper WSEDSA-1 at 4th International Conference on Tethers in Space, Washington DC, 1995.
- 2. Heelis, R.A., "Tethered Satellite Investigation of The Ionosphere and Lower Thermosphere", *Proceedings of the Tether Technology Interchange Meeting*, Huntsville, AL (9-10 September 1997).
- 3. Carroll, J.A., *Preliminary Design of a 1 km/sec Tether Transport Facility*, Tether Applications Final report on NASA contract NASW-4461, March 1991.
- 4. Hoyt, R.P., Forward, R.L., "Tether System for Exchanging Payloads between Low Earth Orbit and the Lunar Surface," AIAA Paper 97-2794, 33rd Joint Propulsion Conference, Seattle WA, July 1997.
- 5. Johnson, L., "Propulsive Small Expendable Deployer System Mission (ProSEDS)", OAST Advanced Propulsion Workshop, JPL, Pasadena, CA, 20-22 May 1997.
- 6. Forward, R.L., Hoyt, R.P., Uphoff, C., "The 'Terminator Tether'™: A Near-Term Commercial Application of the NASA/MSFC ProSEDS Experiment", Proceedings of the Tether Technology Interchange Meeting, Huntsville, AL (9-10 September 1997).
- 7. NASA Press Release, Tuesday June 4, 1996, email from NASANews@hq.nasa.gov 14:32:22
- 8. Forward, R.L., "Failsafe Multistrand Tether Structures for Space Propulsion," Final Report on NAS8-39318 with NASA/MSFC, AL 35812. See also AIAA preprint 92-3214,28th Joint Propulsion Conference, Nashville, TN, 1992.
- 9. Forward, R.L., Failsafe Multistrand Tethers for Space Propulsion, Forward Unlimited Final Report on NASA SBIR Phase I Rearch Contract NAS8-39318, 1992.
- 10. Barnes, J, "TiPS: Results Of A Tethered Satellite Experiment", Proceedings of the Tether Technology Interchange Meeting, Huntsville, AL (9-10 September 1997).
- 11. B. Jeffrey Anderson, Editor and Robert E. Smith, Compiler, Natural Orbital Environment Guidelines for Use in Aerospace Vehicle Development, Section 7 "Meteoroids and Orbital Debris", Don Kessler and Herb Zook, NASA TM-4527, June 1994.
- 12. D.J. Kessler, et al., A Computer Based Orbital Debris Environment Model for Spacecraft Design and Observations in Low Earth Orbit, NASA TM (to be released). [Beta test copies of the program can be obtained by contacting Christine O'Neill at JSC at 713-483-5057 or oneill@snmail.jsc.nasa.gov]
- 13. Hoyt, R.P., Forward, R.L, "Failsafe Multi-strand Tether SEDS Technology," Fourth International Conference on Tethers in Space, Washington, DC, April 1995.
- 14. private communication from F. Jarrossy of Martin Marietta Corp.

- 15. R.L. Forward and R.P. Hoyt, "Failsafe Multiline Hoytether Lifetimes,", AIAA paper 95-2890, presented at the 31st Joint Propulsion Conference, July 1995.
- 16. Hoyt, R.P., "Tether System for Exchanging Payloads between the International Space Station and the Lunar Surface," *Proceedings of the Tether Technology Interchange Meeting*, Huntsville, AL (9-10 September 1997).
- 17. "Simulation of Complex Multiline Space Tether Structures: SpaceNet" Appendix N in Failsafe Multistrand Hoytether SEDS Technology Demonstration, Tethers Unlimited Final Report on NASA SBIR contract NAS8-40545, June 1995.

Technology of Bare Tether Current Collection

By Robert D. Estes Smithsonian Astrophysical Observatory 60 Garden St., Cambridge, MA 02138

Juan R. Sanmartín Universidad Politécnica de Madrid Madrid, Spain

Manuel Martínez-Sánchez Massachusetts Institute of Technology Cambridge, MA 02139

Abstract

The outstanding problem for useful applications of electrodynamic tethers is obtaining sufficient electron current from the ionospheric plasma. Bare tether collectors, in which the conducting tether itself, left uninsulated over kilometers of its length, acts as the collecting anode, promise to attain currents of 10 A or more from reasonably sized systems. Current collection by a bare tether is also relatively insensitive to drops in electron density, which are regularly encountered on each revolution of an orbit. This makes nighttime operation feasible.

We show how the bare tether's high efficiency of current collection and ability to adjust to density variations follow from the orbital motion limited collection law of thin cylinders. We consider both upwardly deployed (power generation mode) and downwardly deployed (reboost mode) tethers, and present results that indicate how bare tether systems would perform as their magnetic and plasma environment varies in low earth orbit.

INTRODUCTION

Electrodynamic tethers (EDT), have been demonstrated to work in space, most notably by the TSS-1/R missions [8] and the Plasma Motor/Generator (PMG) experiment [3]. In each case, a long conductive tether, covered by an insulating sheath, served as a conductive path for electrons at one end of the system to a higher electrical potential at the other end. Charge exchange with the ionosphere occurred at the ends of the system. The positively biased subsatellite served as the electron collector for TSS-1/R. At the Shuttle end, electrons were ejected by electron guns, and positive ions were collected by metallic surfaces. PMG used hollow cathodes for charge exchange at each end of the system, which operated in both the motionally biased (generator) mode and in a battery-imposed reversed bias (motor) mode. The generally accepted explanation for TSS-1R's 1 A tether current

flow after the tether break is that rapidly expelled air, which had been held within the tether before the break, ionized sufficiently to serve as a plasma contactor to expel electrons into the ionosphere.

While these experiments demonstrate that the basic concept of electrodynamic tethers is sound, they do not in themselves provide much encouragement for applications such as power generation or reboost for the International Space Station (ISS), which would require high currents on the order of 10 A. PMG attained 0.3 A, but failed to demonstrate efficient electron collection by a hollow cathode in space, particularly under low density conditions. TSS-1R generally exceeded predictions of electron current collection based on the static Parker-Murphy [5] limit by a factor of two or more, but still showed the expected square root dependence on bias voltage [8]. Thus the 1 A current collected by TSS-1R at a bias of around 1.5 kV implies that a 10 A current would require 150 kV, corresponding to a tether length of 850 km!

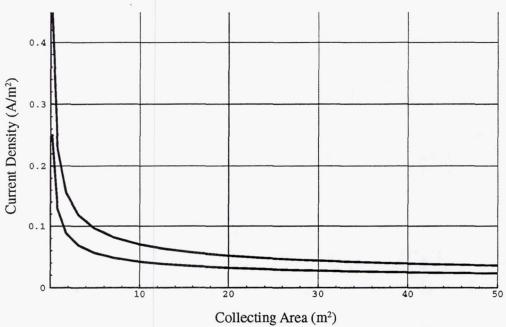


Figure 1. Current density versus collecting area for a passive sphere in typical daytime ionosphere. Upper curve for 1000 V bias, lower curve 300 V. $B_{\text{earth}} = 0.3 \text{ G}$.

Of course, a larger sphere could be used to collect higher currents; but a natural law of diminishing returns quickly sets in, as Figure 1 shows. This is based on a current collection twice the Parker-Murphy limit, which implies lower and lower collection efficiency as the collecting area increases, due to the predominance of magnetic effects (binding of electrons to field lines). An electron density of $0.75 \times 10^{12} / \text{m}^3$ and an electron temperature of 0.15 eV have been assumed. TSS-1R should make us somewhat cautious in drawing firm conclusions based on magnetic limitations, but it does not provide a reason to ignore them.

Small probes (spherical or cylindrical) with dimensions less than the Debye length

and gyroradius (both on the order of a centimeter in the ionosphere) are many times more efficient at collecting current (per surface area) than large balls such as the TSS collector. They avoid the effects of space charge shielding and magnetic guiding. A sphere of such dimensions is much too small to get multiamp currents with a reasonable bias voltage, however. Its area is determined by its radius, and cannot be made large without entering the region of rapidly diminishing returns.

A thin cylinder (wire), however, is still a thin cylinder, no matter how long it is. The current collection problem for a wire is basically two dimensional. Why not just use a long thin wire to collect current from the ionosphere? Collection should be very efficient, and the collecting area can be made large by the length (kilometers). That, in essence, is the bare tether idea developed by Sanmartín, Martínez-Sánchez, and Ahedo [6]. Here, in order to derive the general behavior of the bare tether system under variations of plasma density and motional electric field, we make the simplifying assumption of negligible tether resistance. The analysis shows that, due to the variable collecting area of a bare tether, current collection is much less sensitive to variations in plasma density than passive collection by a large sphere. We will demonstrate how this comes about for both the power generator and thruster modes of EDT operation. We also show that the efficiency of energy conversion is relatively steady under variations in motional electric field in both modes, but with different consequences for steadiness of the desired product in the two cases, since the motional *E* field is the energy source for the EDT generator. In all of the following analysis we assume an eastward moving tethered system in low earth orbit.

POWER GENERATOR MODE

By power generator mode, we mean an upwardly deployed tether, collecting electrons at the upper end of the system by virtue of the motional EMF, whether or not the tether current is being utilized. This is illustrated in Figure 2. At the upper end of the system, the tether itself, which has been left exposed to the ionosphere, serves as the electron collector. Electrons are expelled back into the ionosphere at the lower end by a plasma contactor, which maintains the deployment platform at a low bias with respect to the ambient plasma.

This is the configuration for the ProSEDS mission [2], which is scheduled for a flight in early 2000 as a Delta-II secondary payload to provide the first test in space of the bare tether concept. ProSEDS will in fact utilize electrical power from the tether to recharge its batteries and keep instruments, transmitters, and hollow cathode all working for the duration of the experiment, extending the useful lifetime of the system by days or weeks. Power generation is, however, only a secondary objective of the mission. The primary objectives relate to the magnetic force exerted on an EDT. In the power generator mode, the force is a drag force, which is a drawback if power generation is the goal. However, this drag can be a good thing, if accelerated re-entry is the goal. The force of the magnetic field on the current-carrying tether will also demonstrate the potential for a tether thruster in which the current flows in the opposite direction.

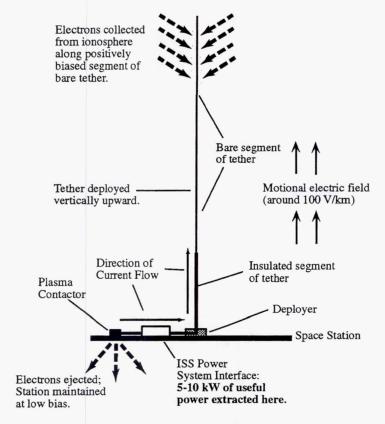


Figure 2. Schematic diagram of a possible EDT power generator for the ISS.

The basic operation of a bare tether power generator can be deduced from the voltage diagram in Figure 3. The vertical axis displays voltages, and the horizontal axis represents distance along the upwardly deployed tether. At the lower end of the tether (far right) a hollow cathode maintains the deployment platform (Station) at the local plasma potential.

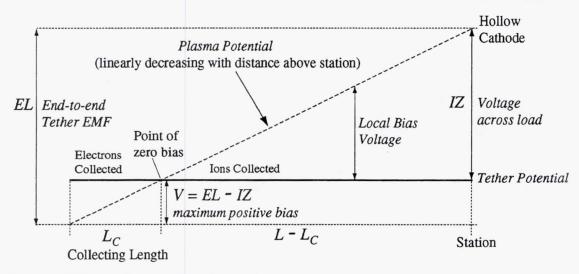


Figure 3. Voltage diagram for a bare tether power generator.

The plasma potential decreases linearly with distance up the tether (moving to left in the figure), reaching a maximum negative value of EL at the upper tip of the tether, where $E = \mathbf{v} \times \mathbf{B} \cdot \ell$ is the component of the motional electric field parallel to the tether, with \mathbf{v} the orbital velocity, \mathbf{B} the local geomagnetic field, ℓ a unit vector pointing up the tether, and L the tether length.

We ignore the ohmic voltage drop in the tether, since it is not the essential feature, and would be a secondary effect for an efficiently designed system. The tether is at a potential ${\it -IZ}$ with respect to the Station, with ${\it Z}$ the load impedance and ${\it I}$ the current delivered by the tether to the Station. Thus the tether is negatively biased with respect to the local plasma as we move up the tether until we reach a point of zero bias. From there on out to the upper tip, the tether is positively biased. It is along this segment, designated ${\it L}_{\it C}$ in Figure 3, that the electron collection occurs. A much smaller ion current, which slightly reduces the current to the useful load, is collected along the negatively biased portion. We neglect this.

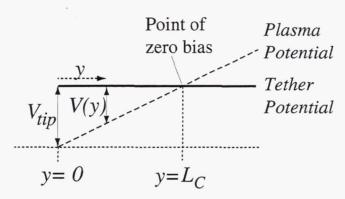


Figure 4. Voltage diagram in region of positive tether bias.

We now concentrate on the positively biased segment, in order to calculate the current collected by the wire. This is shown in Figure 4, where the local bias of the tether with respect to the plasma is indicated by V(y). The maximum bias, which occurs at the tip, is given by $V_{tip} = EL - IZ$. We assume the cross-sectional dimensions of the tether are sufficiently small that electrons are collected in the orbital-motion-limited (OML) regime [4], where both space charge and magnetic effects are unimportant. Generally speaking this means, for a tether of circular cross section, a radius smaller than both the Debye length and the electron gyroradius. In the daytime ionosphere encountered in low earth orbit, these characteristic lengths are of the order of a centimeter. In a companion paper, Sanmartín and Estes [7] examine the limits of OML collection in more detail.

The fundamental equation for current collection by a wire along which the bias varies may be written as

$$\frac{dI(y)}{dy} = C'n\sqrt{V(y)},\tag{1}$$

where n is the unperturbed electron density and the constant C' depends on the dimensions of the tether and the electron mass and charge [6]. Integrating (1) to get the total electron current collected, we obtain

$$I = \int_{0}^{L_{c}} \frac{dI}{dy} dy = \frac{2}{3} \frac{C'}{E} n V_{tip}^{\frac{3}{2}} = \frac{2}{3} C' n \sqrt{E} L_{C}^{\frac{3}{2}}.$$
 (2)

Thus the current collected is proportional to the 3/2 power of the tip bias, or equivalently, the 3/2 power of the collecting length. This 3/2 power dependence has important consequences and gives the bare tether a significant edge over passive spherical collectors, in terms of dependence on plasma density, as we shall see. The primary advantage comes from the size of the factor C', however. This can be seen dramatically by comparing a bare tether collector to two spherical collectors, which we can term equivalent to it by different criteria. We ignore the tether resistance in considering these ideal systems.

For the bare tether system, we take a 10 km-long wire with circular cross section and radius of 3.6 mm (well within the OML collecting regime). It generates 15 kw of power for the reference point plasma density of $7.5 \, 10^{11}/m^3$ and motional electric field of $0.18 \, \text{V/m}$. This is $10 \, \text{A}$ into a $150 \, \text{ohm}$ impedance. The wire collects electrons over $1.7 \, \text{km}$ for the reference point conditions; this corresponds to a collecting area of $39 \, \text{m}^2$. The magnetic drag is around $2.25 \, \text{N}$.

Taking passive sphere electron collection to be twice the Parker-Murphy limit, we can define an equivalent ball system 1, such that it also generates 15 kw of power with a 10 km tether at the reference point conditions (assuming in addition an electron thermal energy of 0.15 ev and a magnetic field of 0.3 G). Such a ball turns out to be enormous. Its radius is 8.3 m, so that it is roughly the size of a five-storey building. Its area is 872 m² (over 20 times greater than the wire's collecting area at the reference point). The mass, drag, and the operational difficulties that deploying and maintaining such a large system would entail make it an implausible equivalent in reality.

Another approach would be to take an equal-area sphere. The wire will collect electrons along 6.1 km of its length when the plasma density decreases by a factor of ten. Equivalent ball system 2 will be defined to have the same collecting area as 6.1 km length of tether. The ball radius is then 3.4 meters. The tether has to be 89 km long to achieve 15 kw under the reference point conditions, and the corresponding magnetic drag is around 20 N!

When we look at what happens as the system passes into darkness, where plasma densities drop by a factor of ten or more, we find the bare tether further demonstrates its superiority to the "standard" passive ball collector.

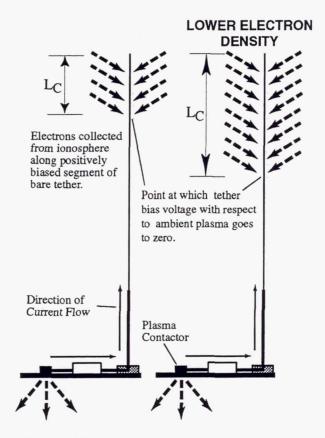


Figure 5. The bare tether power generator automatically adjusts to a density decrease.

At first glance equation (2) might appear to be saying that the current is linear in the electron density n. However, this impression is seen to be false when we write

$$I = C\frac{n}{E}(EL - IZ)^{\frac{3}{2}}.$$
(3)

The current will clearly have to decrease if the electron density decreases. But a decrease in current I implies both an increase in the tip voltage and the collecting length. The zero bias point moves down the tether. This is illustrated in Figure 5.

This corresponds to an increase in the factor in (3) with the 3/2 power. If IZ is comparable to EL (high efficiency case), this factor can largely offset the decrease in density. We consider the case where the efficiency

$$\varepsilon \approx \frac{IZ}{EL}$$

is near unity.

From (3) we obtain the derivative of the current with respect to the density n as

$$\frac{dI}{dn}\left(1 + \frac{3}{2}\frac{IZ}{EL - IZ}\right) = \frac{I}{n}.$$
(4)

Applying the high efficiency condition, we obtain

$$\frac{d(EL-IZ)}{dn} \approx -\frac{2}{3} \frac{(EL-IZ)}{n}.$$
 (5)

This yields an approximate solution good so long as n doesn't take us out of the regime of high efficiency:

$$I = \frac{EL}{Z} \left(1 - \left(\frac{n_0}{n} \right)^{\frac{2}{3}} \frac{L_C^0}{L} \right), \tag{6}$$

where n_0 and L_C^0 are the initial plasma density and collecting length, respectively. Due to the 2/3 power variation in the density ratio, the condition of high efficiency can still be maintained for a relatively large drop in plasma density.

When we carry through the same analysis for a spherical collector, assuming a $V^{1/2}$ law for collection, we arrive at

$$I = \frac{EL}{Z} \left(1 - \left(\frac{n_0}{n} \right)^2 (1 - \varepsilon) \right), \tag{7}$$

where ε is the initial efficiency of energy conversion. This shows that the variation with n is much stronger in the case of the sphere. Expression (7) will clearly run out of the high efficiency regime with relatively small decreases in n.

Figures 6 and 7 compare the performance of the 10-km bare tether system and the equivalent ball system 1 previously considered under plasma density variations of the sort that can be encountered in a single revolution in low earth orbit. The motional EMF is held constant. The power generated, which is proportional to the square of the current, is shown in Figure 6, and the efficiency of energy conversion, which is nearly proportional to the current, is shown in Figure 7.

The motional electric field component $E = \mathbf{v} \times \mathbf{B} \cdot \hat{\ell}$, which provides the voltage that collects the current, also varies around an orbit. We now consider how variations in E affect the current collection. As before, we assume we are in the high efficiency regime to

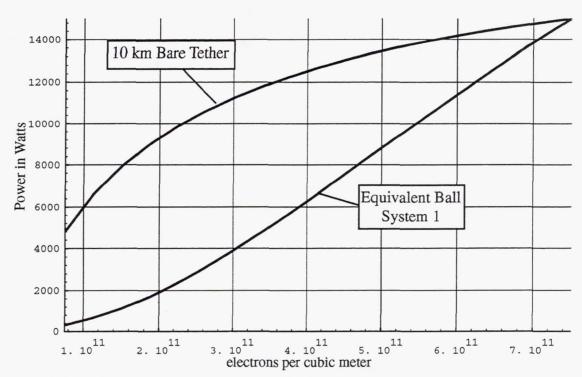


Figure 6. Power variations with electron density for ideal 10-km bare wire and equivalent ball system 1 (equal tether length). Both generate 15 kw at the reference point.

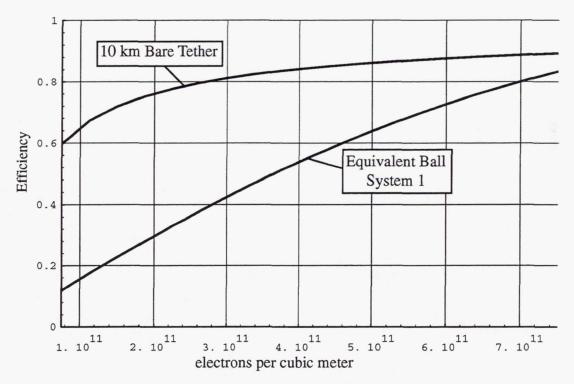


Figure 7. Efficiency of orbital to electrical energy conversion for ideal 10-km bare tether and equivalent ball system 1 (equal tether length) over a range of plasma densities.

start, i.e., plasma density is sufficient. Then the derivative of the current with respect to E can be found from

$$\frac{dI}{dE}\left(1 + \frac{3}{2}\frac{IZ}{EL - IZ}\right) = I\frac{\left(EL - IZ\right) + \frac{3}{2}EL}{E\left(EL - IZ\right)},\tag{8}$$

which simplifies to

$$\frac{dI}{dE} \approx \frac{L}{Z}$$

so long as the efficiency is near unity. Then we have $\frac{I}{E} \approx \frac{I_o}{E_o}$, so long as $E >> (1 - \varepsilon_o)E_0$,

where E_o and \mathcal{E}_o are the original electric field and efficiency, respectively.

The good news out of this result is that, if we are converting orbital energy to electrical at high efficiency, we can maintain good efficiency even with large decreases in the motional electric field (say by a factor of 3 for $\varepsilon_o = .9$).

However, the power will decrease roughly with the square of the motional electric field. There is no 'cure' for this problem, since the electric field is our energy source. The bare tether is no different from a passive sphere tethered system in this respect. We can boost the power, at the expense of efficiency, by decreasing the load impedance. Thus a variable impedance system is required to maximize orbital average power and to minimize power variations. The tradeoff is average power versus efficiency, so system design must take into account which is more important, keeping in mind that lower efficiency means higher magnetic drag, which must be compensated for to avoid orbital decay.

Figure 8 shows an example of how the combined effects of plasma density and motional EMF variations would affect a real bare tether generator. These calculations have been made using the full equations of reference [6], with tether resistance included. The tether considered is made of aluminum and is 18 km long. The tether geometry is that of a tape 0.7 mm by 11 mm. The impedance is varied to keep the maximum instantaneous power below 12 kw, though higher powers (at lower efficiency) could be reached, assuming plasma contactors could handle the higher currents that would be collected. The impedance is lowered to achieve maximum power when troughs in motional *E* field are encountered.

In line with our approximate calculations, the electric field is seen largely to determine performance. This is a near worse case example, with troughs in motional E field and density overlapping, but density variations are clearly a secondary effect.

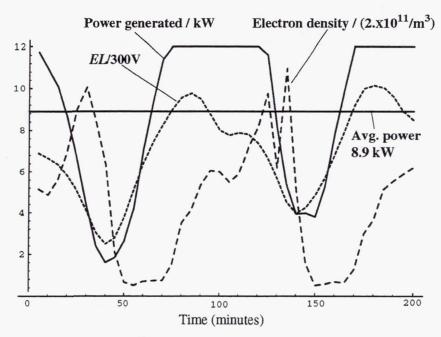


Figure 8. Power generated by a 'realistic' bare tether generator as it encounters varying motional E field and electron density around an ISS-type orbit.

THRUSTER MODE

The potential application of EDT that has drawn the most interest recently is their use for propellantless reboost of the International Space Station [1] or for orbit modification. In either case, the (partially) bare tether is deployed downward and biased positively with respect to the plasma by means of a power supply. Thus a tether based system is a type of electrical propulsion system. Electrons are collected along a portion of the exposed metallic wire. In contrast to the case of the power generator, the maximum bias voltage occurs at the end of the insulation and decreases as we move downward toward the tip of the tether. Despite this difference, the analysis of the system yields results that are analogous to those we have already obtained for the power generator. The thrust comes from the action of the magnetic field on the current in the wire. The general setup is illustrated in Figure 9.

The voltage diagram in Figure 10 contains the basic physics of the bare tether thruster operation. The vertical axis displays voltages, and the horizontal axis represents distance along the downwardly deployed tether. At the upper end of the tether (far left) a hollow cathode maintains the deployment platform (Station) at the local plasma potential. The plasma potential increases linearly with distance down the tether (moving to the right in Figure 10), reaching a maximum positive value of EL at the lower tip of the tether, where L is the tether length and E is the component of motional electric field along the tether, as defined for the corresponding discussion of Figure 3 in the preceding section.

A comparison of the voltage diagram in Figure 10 with the corresponding Figure 3 for the power generator reveals how the two modes of operation differ. The main difference

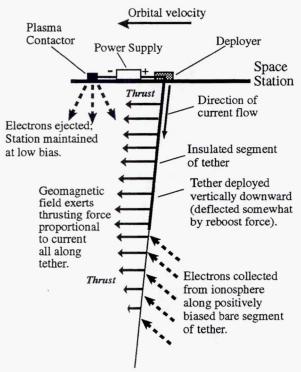


Figure 9. Schematic diagram of a possible bare tether thruster for the ISS.

is that the motionally induced voltage must be overcome by a supplied voltage at the platform in order to drive a current in a direction opposite to the "natural" one.

As before, we ignore the ohmic voltage drop in the tether. We assume a constant input power P to drive the tether current. The tether is at a positive potential P/I with respect

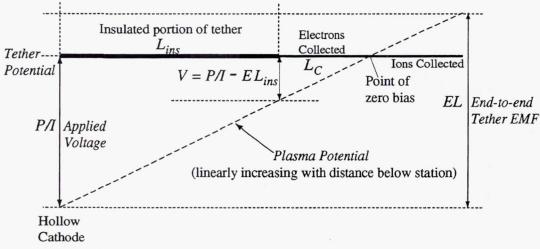


Figure 10. Voltage diagram for a bare tether thruster.

to the Station, with I the current delivered by the tether to the Station. Thus the tether is positively biased with respect to the local plasma as we move down the tether until we reach a point of zero bias. For reasons that will be discussed later, the tether needs to be insulated for a certain length L_{ins} of the upper (attached) portion. In order to collect a current, the supplied voltage must be greater than EL_{ins} . It is along the bare segment of positive tether bias, designated L_c in Figure 10, that electrons are collected. From there on out to the lower tip, the tether is negatively biased. An obvious difference from the case of the power generator is that here the maximum bias voltage occurs at the electron-collecting point on the tether closest to the attachment point.

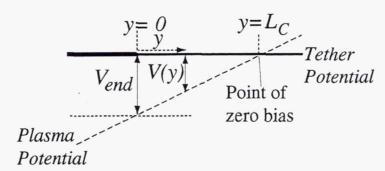


Figure 11. Voltage diagram in region of positive tether bias.

In order to obtain the total electron current collected by the tether we apply the basic equation (1) of OML collection to the situation illustrated in Figure 11. Despite the different source of the bias voltage in the two generator and thruster cases, the integrals for the current in the two cases are completely analogous with the V_{tip} of the generator replaced by the bias voltage at the end of the insulation $V_{end} = P/I - EL_{ins}$. This is clear when Figure 11 is compared with Figure 4.

Integrating over the collecting length, as in the case of the generator, we obtain for the current in the insulated part of the tether

$$I = C \frac{n}{E} V_{end}^{\frac{3}{2}}.$$
 (9)

For zero tether resistance, the efficiency of energy conversion may be written as

$$\varepsilon = \frac{3}{5} + \frac{2}{5} \frac{I}{P} E L_{ins} , \qquad (10)$$

so that the high efficiency condition is

$$EL_{ins} \approx \frac{P}{I}$$
.

The magnetic thrust force on the tether is proportional to the integral of the current along the tether. Lengthening the insulated section forces current to flow over a longer portion of the tether. Although the current reaching the upper platform (for constant input power) decreases as the insulated length increases, the integral of the current along the tether (and thus the force) increases. Thus the efficiency of electrical to mechanical energy conversion increases with the insulated tether length. This is illustrated in Figure 12. The design of a tether thruster has to balance the need to keep tether mass low, the increased efficiency that comes with greater insulated length, and the necessity for having sufficient bare tether available to collect current under conditions of reduced plasma density.

As in the case of the generator, provided the system has been designed with a bare portion that is sufficiently long, the bare tether reboost system can offset to a degree the effect of lower plasma densities, by automatically extending the portion of the bare wire on which electrons are collected.

The bias voltage at the end of the insulated portion of the tether (and the collecting length) increase as the current drops. Again the factor raised to the 3/2 power in the current equation increases:

$$I = C \frac{n}{E} \left(P/I - EL_{ins} \right)^{\frac{3}{2}}. \tag{11}$$

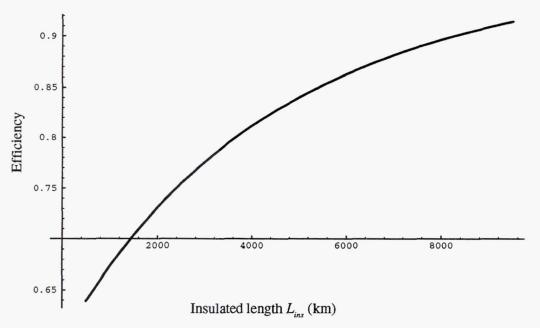


Figure 12. Electrical to orbital energy conversion as a function of insulated tether length.

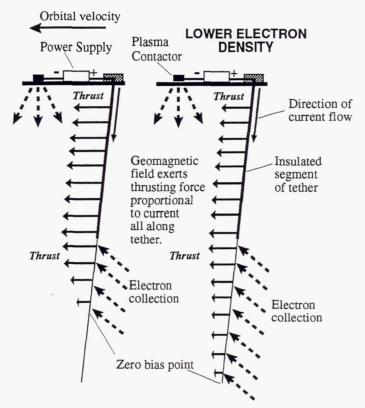


Figure 13. The bare tether thruster automatically adjusts to a drop in plasma density.

It is more convenient to work with the input voltage V = P/I, which satisfies

$$V = \frac{PE}{Cn} (V - EL_{ins})^{-\frac{3}{2}} . {12}$$

Proceeding as before, in the high efficiency regime, we get

$$\frac{d(V - EL_{ins})}{dn} \approx -\frac{2}{3} \frac{(V - EL_{ins})}{n}.$$
 (13)

This has the approximate solution

$$V = EL_{ins} + V_{end}^0 \left(\frac{n_0}{n}\right)^{\frac{2}{3}}$$
 (14)

in the high efficiency region, which can be written as

$$I \approx \frac{P}{EL_{ins}} \left(1 - \left(\frac{n_0}{n} \right)^{\frac{2}{3}} \frac{L_C^0}{L_{ins}} \right), \tag{15}$$

which, not surprisingly, is very similar to the result found for the generator, since the energy source is constant in each case and the current collection equations are the same.

If we carry out the same analysis for a ball collector at the end of an insulated tether of length L, we obtain

$$I \approx \frac{P}{EL} \left(1 - \frac{V_0}{EL} \left(\frac{n_0}{n} \right)^2 \right), \tag{16}$$

where V_o is the original bias voltage of the sphere. This will quickly violate the condition of the approximation as n decreases.

Now we consider variations in the electric field component E. The situation is different from that of the generator mode, where E drives the current. Here, E works against the current, and a lower E means a higher current for constant input power, as there is a lower voltage to overcome.

The derivative of the input voltage V with respect to the motional field component along the tether E is, in the high efficiency region, given by

$$\frac{dV}{dE} \approx L_{ins}.$$
 (17)

This implies $I_0 E_0 \approx IE$, so long as the efficiency $\varepsilon \approx 1 - \frac{3}{5} \frac{V_{end}^0}{EL_{ins}}$ is not far from unity.

The efficiency (and thrust) decrease with decreasing E, but slowly. We also found a steady efficiency under E variations in the power generator case, but the consequences were quite different there, as E was the energy source.

A bare tether thruster, designed for high efficiency, has been shown to generate a steady thrust under variations in motional E field and plasma density, so long as the deviations are not too large. What about a "real world" system? Figures 14(a)-(f) illustrate the operation of a system that might provide reboost for the ISS, utilizing only 5 kw of the Station's solar power. Except for the length, the tether is similar to the one whose perfomance was displayed in Figure 8 in the power generator case. The system does not truly operate at high efficiency (average efficiency is around 0.66) as assumed in our calculations, since the

desire to minimize perturbations to the station led to the choice of a tether only 7 km long. The insulated portion of the tether is 5 km long. Nonetheless, the thrust is seen to vary only by a factor of 2.5, while the density varies by a factor of 15 and the E field by a factor of four.

By comparing Figures 14(b) and 14(c), one sees that when operating at its highest efficiency (around 0.8), the system rides smoothly over fluctuations in motional electric field. The adustment of the system to nighttime density conditions can be seen in Figures 14(a), 14(d), and 14(f). The bias voltage at the end of the insulation shown if Figure 14(d) peaks during the nighttime density troughs of Figure 14(a), while the collecting length extends to the very tip of the tether in Figure 14(f).

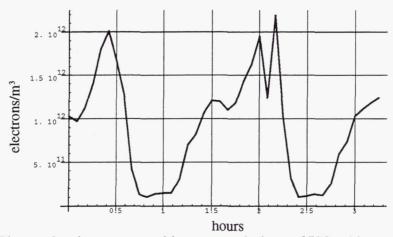


Figure 14(a). Plasma density encontered in two revolutions of ISS orbit.

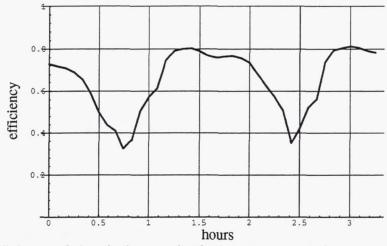


Figure 14(b). Efficiency of electrical to mechanical energy conversion.

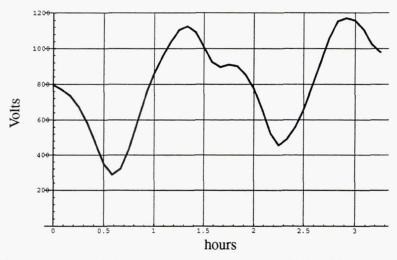
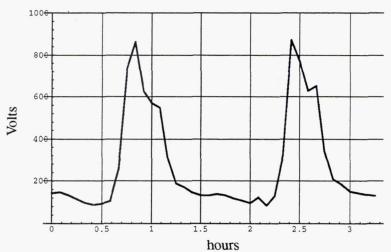


Figure 14(c). EL (motional EMF) around two revolutions of ISS orbit.



hours Figure 14(d). Bias voltage at end of insulation ($V_{\it end}$) in two revolutions of ISS orbit.

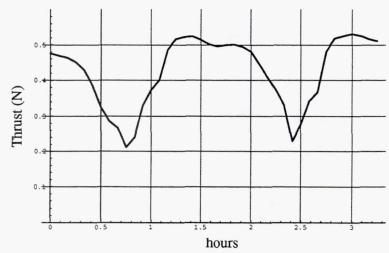


Figure 14(e). Thrust generated around two revolutions of ISS orbit. .

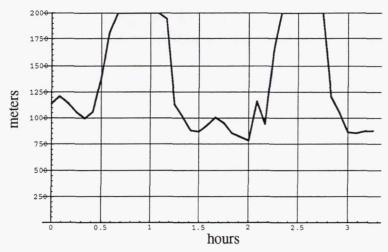


Figure 14(f). Collecting length L_c around two revolutions of ISS orbit.

As might be expected, the thrust generated is roughly proportional to the input power. The signifiance of this is that a single bare tether system could generate more thrust depending upon need and available power. It would be quite flexible in that regard. This is shown for a 10 km system in Figure 15.

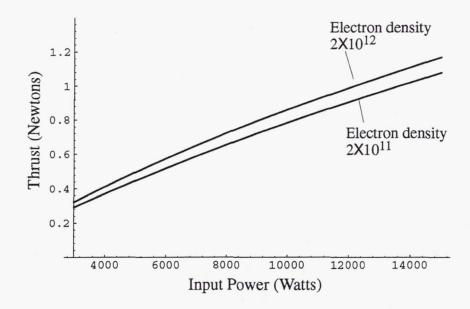


Figure 15. Thrust generated as a function of input power for two plasma densities.

CONCLUSIONS

Bare tethers promise to collect currents in the 10 A range with reasonably sized, simple systems. In addition to efficient current collection, both power generator and reboost systems based on bare tethers should be able to operate night and day, because of the self-

adjusting collecting area inherent in the system. The strength of the magnetic field and its orientation with respect to the system's velocity vector (which determine the component of motional electric field along the tether) mainly determine power variations for any EDT power generator, though high efficiency operation can be maintained if variations in power are acceptable. A bare tether operating as a thruster at constant input power with high efficiency should maintain a fairly steady thrust even with wide variations in motional electric field and plasma density.

ACKNOWLEDGMENTS

The work of R. Estes was supported by NASA Grant NAG8-1303.

REFERENCES

- 1. Johnson, L., Carroll, J., Estes, R., Gilchrist, B., Lorenzini, E., Martinez-Sanchez, M., Sanmartín, J. S., and Vas, I., "Electrodynamic Tethers for Reboost of the International Space Station and Spacecraft Propulsion," *AIAA Space Programs and Technologies Conf. and Exhibit: Strategies for Affordability*, Huntsville, Ala., Sept. 24-26, 1996
- 2. Johnson, L., "The Propulsive Small Expendable Deployer System (ProSEDS) Experiment," *Tether Technology Interchange Meeting*, Huntsville, Ala., Sept. 1997
- 3. McCoy, J., O'Neill, C., Stanley, J., Settecerri, T., Grossi, M.D., Estes, R.D., Dobrowolny, M., Vannaroni, G., Melchioni, E., Bonifazi, C., Cosmovici, C., Iess, L., Jost, R.J., Olsen, R.C., Ferguson, D.C., Tolbert, R., Rau, D., Katz, I., Lilley, J., Carroll, J.A., Tacconi, G., Mina, L., and Goree, W., "Plasma Motor-Generator (PMG) Flight Experiment Results," *Proc. Fourth International Conf. on Tethers in Space*, Smithsonian Institution, Washington DC, April 10-14, 1995, 57-82
- 4. Mott-Smith, H. and Langmuir, I., "The theory of collectors in gaseous discharges," *Phys. Rev.*, **28**, 1926, 727-763
- 5. Parker, L.W. and Murphy, B.L., "Potential Buildup on an Electron-Emitting Ionospheric Satellite" *J. Geophys. Res.*, 72,1967, 1631-1636
- 6. Sanmartín, J.R., Martinez-Sanchez, M., and Ahedo, E., "Bare wire anodes for electrodynamic tethers," *J. Prop. Power*, **9**, 1993, 353-360
- 7. Sanmartín, J.R. and Estes, R.D., "Validity of the orbital-motion-limited regime of cylindrical probes," *Proc. Tether Technology Interchange Meeting*, Huntsville, Ala., Sept. 1997
- 8. Thompson, D.C., Bonifazi, C., Gilchrist, B.G., Williams, S.D., Raitt, W.J., Lebreton, J.-P., Burke, W.J., Stone, N.H., and Wright, Jr., K.H., "The Current-Voltage Characteristics of a Large Probe in Low Earth Orbit: TSS-1R Results," *Geophys. Res. Letters*, 1997 (in press)

Validity of the orbital-motion-limited regime of cylindrical probes

J. R. Sanmartín, ETSI Aeronáuticos, Universidad Politécnica de Madrid 28040, Madrid, Spain

R. D. Estes, Harvard-Smithsonian Center of Astrophysics 60 Garden St., Cambridge, MA 02138

Abstract

An asymptotic analysis of electron collection at high bias Φ_p serves to determine the domain of validity of the OML regime of cylindrical Langmuir probes, which is basic for the workings of conductive bare tethers. The breakdown of the regime is found to occur far from the probe, at energies comparable to the ion temperature T_i . The radius of a wire collecting OML current in an unmagnetized plasma at rest cannot exceed a value, R_{max} , that increases with T_i , and exhibits a minimum as a function of Φ_p ; at Φ_p values of interest R_{max} is already increasing and is larger than the Debye length λ_{De} . It is also found that 1) the maximum width of a thin tape is $4R_{max}$; 2) the electron thermal gyroradius must be large compared with both R and λ_{De} for magnetic effects to be negligible; and 3) an ion ram energy large compared with kT_i but small compared with $e\Phi_p$ would have a complex but weak effect on R_{max} .

1. Introduction

Each point of an electrodynamic bare tether collects current as if it were part of a cylinder uniformly polarized at the local tether bias (9). This is because of the enormous disparity between tether thickness and collecting length, which lie in the millimeter and kilometer ranges respectively. Bare tether applications rest on the assumption that electron collection occurs in the (optimal) orbital-motion-limited regime of cylindrical probes. It is thus important to determine the parametric domain of orbital-motion-limited (OML) validity.

Since OML current is proportional to the perimeter of the cross section, a large tether current may require a large perimeter. If the crosswise dimension is too large, however, the current will not reach the OML value because of electrical screening effects related to a short plasma Debye length λ_{De} . Here we determine the maximum radius of a cylinder collecting OML current in an unmagnetized plasma at rest, and how it depends on the ion temperatue T_i and the bias Φ_p . Values of the ratio $e\Phi_p/kT_e$ of interest for tethers ($T_e \sim 0.15$ eV, $\Phi_p \sim 400$ V) are 10^2 times larger than values previously explored numerically. We also consider the maximum width of a thin tape.

Again, if the crosswise dimension is too large, the current will not reach the OML value because of magnetic guiding effects due to a short thermal electron gyroradius l_e . We consider how large has l_e to be for magnetic effects to be negligible. Finally, we also

study the effects of an ion ram energy large compared with thermal energies but small compared with $e\Phi_p$.

2. Circular cylinder at rest in an unmagnetized plasma

The electron current I to a sufficiently long cylinder in a Maxwellian plasma of density N_{∞} and temperatures T_e and T_i , may be written in dimensionless form as

$$\frac{I}{I_{th}}$$
 = function of $\frac{R}{\lambda_{De}}$, $\frac{e\Phi_p}{kT_e}$, $\frac{T_i}{T_e}$. (1)

Here, I_{th} is the thermal or random current

$$I_{th} = 2\pi RL \times \frac{1}{4} \sqrt{\frac{8kT_e}{\pi m_e}} eN_{\infty}$$
 (2)

where R and L are probe radius and length, and λ_{De} is $\sqrt{kT_e/4\pi e^2}N_{\infty}$. In general, the determination of electron trajectories to obtain the current requires solving Poisson's equation for the potential $\Phi(r)$,

$$\frac{\lambda_{Di}^{2}}{r}\frac{d}{dr}r\frac{d}{dr}\left(\frac{e\Phi}{kT_{i}}\right) = \frac{N_{e}}{N_{e}} - \frac{N_{i}}{N_{e}}, \qquad (\lambda_{Di} = \lambda_{De}\sqrt{T_{i}/T_{e}})$$
(3)

with boundary conditions

$$\Phi = \Phi_p > 0$$
 at $r = R$, $\Phi \to 0$ as $r \to \infty$. (4)

Both the electric field $-\nabla\Phi$ and the probe acting as a sink of particles affect the densities N_e and N_i , and thus $\Phi(r)$ itself. The basic problem in probe theory usually lies in the attracted-particle density N_e . Actually, for the very large $e\Phi_p/kT_e$ values of interest, the repelled-particle density N_i is accurately given by the simple Boltzmann law,

$$N_i \approx N_\infty \exp(-e\Phi/kT_i),$$
 (5)

except near the probe where, anyway, N_i is exponentially small (as the ion current itself). Because of Eq.(5), it proves convenient to normalize potential and radius with the ion parameters, T_i and λ_{Di} , although final results may be given in terms of T_e and λ_{De} .

For the highly symmetrical case of this section, the axial velocity v_z (Fig.1) and the transverse angular momentum and energy,

$$J \equiv m_e r v_{\rm A}$$
,

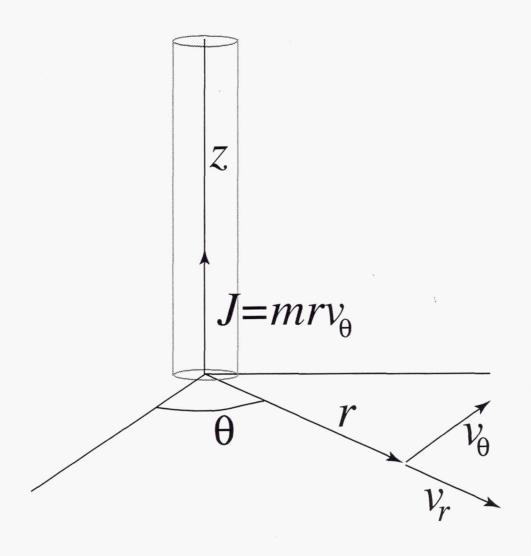


FIGURE 1

$$E = \frac{m_e}{2} v_r^2 + \frac{J^2}{2m_e r^2} - e\Phi(r) , \qquad (v_r < 0, v_r > 0)$$
 (6)

are conserved along electron orbits. The density N_e at each radius r may then be expressed as an integral of the undisturbed Maxwellian distribution function over appropriate ranges of those 3 constants of the motion (1). After a trivial v_z integration one has

$$N_e = N_\infty \frac{m_e}{2\pi k T_e} \iint \frac{\exp(-E/kT_e)dEdJ}{m_e \sqrt{J_r^2(E) - J^2}}$$
 (7)

where we defined

$$J_r^2(E) \equiv 2m_e r^2 [E + e\Phi(r)]$$
 (8)

The E-integral, which only covers positive values (all electrons start at infinity), must be carried out once for $v_r < 0$ (incoming electrons) and again for $v_r > 0$ (electrons that have turned outwards at a radius between r and R); the J-integral can be made to cover just positive values by writing $dJ \rightarrow 2dJ$. The E-J domain of integration in Eq.(7) is r-dependent because of both the electric field and the sink effect of the probe:

i) For an incoming electron of energy E > 0 to actually reach r, v_r^2 must have been positive throughout the entire range $r < r' < \infty$. Using (8) in Eq.(6) for E,

$$m_e^2 r^{,2} v_{r'}^2 = J_{r'}^2(E) - J^2,$$

the *J*-range of integration at that energy will clearly be

$$0 < J < J_r^*(E) \equiv minimum \{ J_r(E) ; r < r' < \infty \} ;$$
 (9)

in general, the minimum occurs at a different r' for a different energy E. If $J_r^*(E)$ differs from $J_r(E)$, those electrons in the range $J_r^*(E) < J < J_r(E)$, for which v_r^2 would be positive, never actually reach r and are thus excluded from the integral in (7); we say that there is an effective potential barrier for r, at energy E.

ii) For an E-electron outgoing at r the J-range of integration will be

$$J_R^*(E) < J < J_r^*(E),$$

electrons with $J < J_R^*(E)$ having disappeared in the probe.

Equation (7) may now be written as

$$N_{e} = N_{\infty} \int_{0}^{\infty} \frac{dE}{kT_{e}} \frac{\exp(-E/kT_{e})}{\pi} \left[2\sin^{-1} \frac{J_{r}^{*}(E)}{J_{r}(E)} - \sin^{-1} \frac{J_{R}^{*}(E)}{J_{r}(E)} \right], \tag{10}$$

half the first term in the bracket being the $v_r < 0$ contribution. The current itself can be easily found to be

$$I = 2LN_{\infty} \frac{e}{m_e} \int_0^{\infty} \frac{dE}{kT_e} \exp(-\frac{E}{kT_e}) J_R^*(E) . \tag{11}$$

We note at this point that, through its dependence on $J_r^*(E)$ [and $J_R^*(E)$], the density N_e is a functional of $\Phi(r)$ and thus cannot be known [for use in solving Eq.(3) for $\Phi(r)$] before the potential itself is found; this results in a complex, iterative numerical solution of Poisson's equation (3). A hypothetical potential with no barriers at all $[J_r^*(E) = J_r(E)$ for $R \le r < \infty$, $0 \le E < \infty$] would simplify N_e in (10) to a function of both r and the local value $\Phi(r)$,

$$N_{e} = N_{\infty} \left[1 - \int_{0}^{\infty} \frac{dE}{kT_{e}} \frac{\exp(-E/kT_{e})}{\pi} \sin^{-1} \sqrt{\frac{R^{2}(E + e\Phi_{p})}{r^{2}(E + e\Phi(r))}} \right], \tag{12}$$

and would allow a ready solution of Eq.(3), but has no real interest.

The case of interest here is that corresponding to the maximum possible current in Eq.(11). Since we have $J_R^*(E) \leq J_R(E)$, from the definition of $J_r^*(E)$ in (9), current is maximum under condition $J_R^*(E) = J_R(E)$, for $0 < E < \infty$ (no potential barrier for just radius R). This is the orbital-motion-limited (OML) current,

$$I_{OML} = 2LN_{\infty} \frac{e}{m_e} \int_{0}^{\infty} \frac{dE}{kT_e} \exp\left(-\frac{E}{kT_e}\right) \sqrt{2m_e R^2 \left(E + e\Phi_p\right)}$$

$$\rightarrow 2RLN_{\infty} e^{\sqrt{2}} e\Phi_p / m_e, \quad \text{for } e\Phi_p >> kT_e.$$
(13)

With the current known, there would now be no need for solving Eq.(3), except for the very purpose of the present work: determining the parametric domain for the OML regime to hold. For $e\Phi_p >> kT_e$, this problem comes out to be reasonably simple.

The OML condition, $J_R^*(E) = J_R(E)$ for $0 < E < \infty$, which does reduce the <u>second</u> term in the bracket of (10) to a function of both r and the local value $\Phi(r)$, is readily shown to be equivalent to condition

$$r^2 \Phi(r) \ge R^2 \Phi_p \qquad (R < r < \infty) \tag{14}$$

on the potential. Condition (14) can be conveniently illustrated by displaying $\Psi = e\Phi/kT_i$ versus $\Psi_p R^2/r^2$ for potential profiles (Fig.2); (14) shows that the profile for $R = R_{max}$

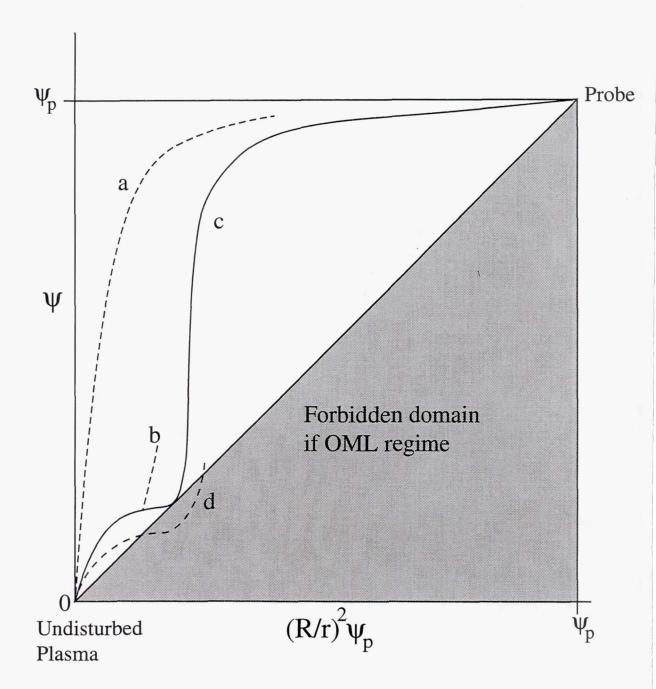


FIGURE 2

(maximum radius for the OML regime to hold, with other parameters fixed) would just touch the diagonal in the figure, as in the case of profile c. Profiles a and b would lie in the OML regime, whereas d would not.

Next, note that the extreme condition $J_r^*(E) = J_r(E)$ for $R \le r < \infty$, $0 < E < \infty$, which led to Eq.(12), would require the potential to satisfy the condition

$$d(r^2\Phi)/dr \ge 0 , \qquad (R < r < \infty)$$
 (15)

which is, of course, more restrictive than (14). In Fig.2 only the hypothetical profile a satisfies (15). Note, however, that if $d(r^2\Phi)/dr$ is positive just beyond some radius r_0 , then we do have

$$J_r^*(E) = J_r(E)$$
 for $r_0 < r < \infty$, $0 < E < \infty$ (16)

and Eq.(10) reduces to (12) for $r > r_0$; cases b-d present this property (0 is the profile point where the tangent goes through the origin).

Figure 3 shows again the qualitative profile c of Fig.2, which we find corresponds to the actual profile for $R=R_{max}$ at large $\Psi_p\equiv e\Phi_p/kT_i$; this may be taken as an ansatz that is used in solving Poisson's equation and verified at the end. Below, we sketch our asymptotic analysis of Eq.(3) for $\Psi_p>>1$, following closely a classical study (5), which assumed, however, a monoenergetic attracted-particle distribution function, and was developed for the non-OML, small λ_{Di}/R , regime:

- i) Both the quasineutral approximation, $N_e \approx N_i$, and the no barrier condition, $J_r^*(E) = J_r(E)$, hold below point 0. Use of Eqs.(5) and (12) determines point 0 exactly.
- ii) The quasineutral approximation remains valid up to a point 1 where $d\Phi/dr \rightarrow \infty$. This property of point 1, and the proximity of values r_0 and r_l , make possible to get an accurate approximation to the potential barrier (and the density N_e) for points in the vicinity of 1, which can then be determined. The same barrier applies to points above 1, i.e., for $r < r_l$ we have $J_r^*(E) = J_{r_l}^*(E) \equiv minimum [J_r(E), r_l < r' < r_0, 0 < E < \infty]$.
- iii) Above point 1 there are two thin, non-quasineutral layers that take the solution to a radius r_2 a bit closer to the probe, and to values Φ satisfying $\Phi_1 \ll \Phi \ll \Phi_p$.
- iv) Finally, a solution to Poisson's equation (with N_i negligible) that matches the inner thin layer at r_2 and satisfies condition $\Phi = \Phi_p$ at r = R, yields a relation between parameters, i.e. determines R_{max} .

Note that both Ψ_0 and Ψ_I are of order unity whereas Ψ_p is very large ($\sim 10^3, 10^4$). Hence, if Fig. 3 were drawn on scale, the near-vertical potential drop in the two thin layers, down to point 1, would occur very close to the Ψ -axis, and point 0 would lie very close to the origin. With $e\Phi_0$, $e\Phi_I \sim kT_i$, the ion temperature should critically affect OML validity.

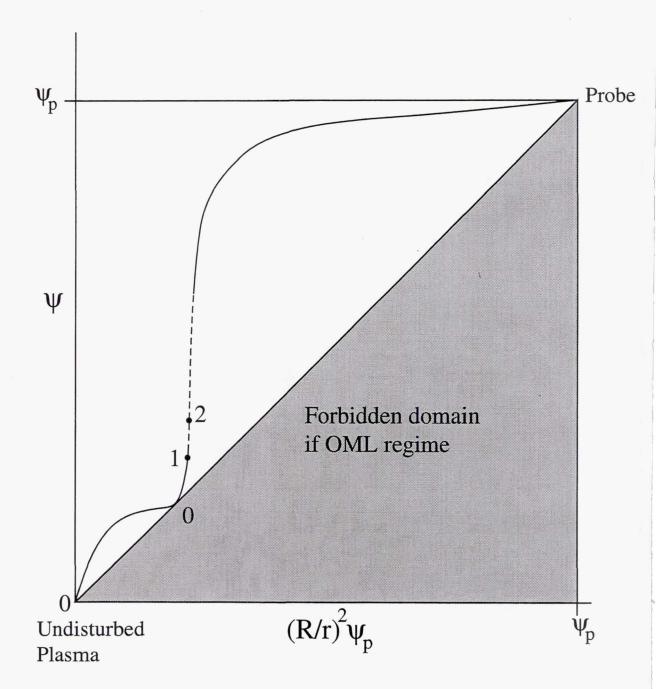


FIGURE 3

Note also that the high probe bias $(\Psi_p >>1)$ makes space-charge effects negligible within some neighborhood of the probe (even if R is not small compared with Debye lengths). Within that neighborhood, and ignoring $N_e - N_i$ in Eq.(3), $\Phi(r)$ behaves as a (logarithmic) solution to the 2D Laplace-equation,

$$\Phi = \Phi_p[1-\alpha \ln (r/R)], \qquad (17)$$

 α being a moderately small constant (of order $1/\ln \Psi_p$).

Figure 4 shows R_{max}/λ_{De} versus $e\Phi_p/kT_e$ for the ionospheric case, $T_i/T_e \approx 1$; R_{max} goes through a minimum as the bias Φ_p increases and, at high enough Φ_p , exceeds λ_{De} . Numerical results for the range $e\Phi_p/kT_i < 25$ had shown R_{max} decreasing monotonically with the bias (3). Figure 5 shows that R_{max} does increase sensibly with T_i .

3. Thin tape at rest in an unmagnetized plasma

In the OML regime, the current to a cylindrical probe is independent of the shape of the cross section; it just depends on its perimeter (4). The limits of OML validity, however, must be determined anew for every cross section. Since angular momentum J is not conserved here, there is no close-form expression such as (10) for N_e . Nonetheless, we find that the high bias condition $(\Psi_p >> 1)$ makes possible to approximately reduce this problem to the case of the circular cylinder.

We use here elliptical coordinates v and w (see Fig.6, where we set a = 1),

$$x = a \cos v \cosh w$$
, $y = a \sin v \sinh w$,
 $(0 \le v < 2\pi)$, $0 \le w < \infty$,

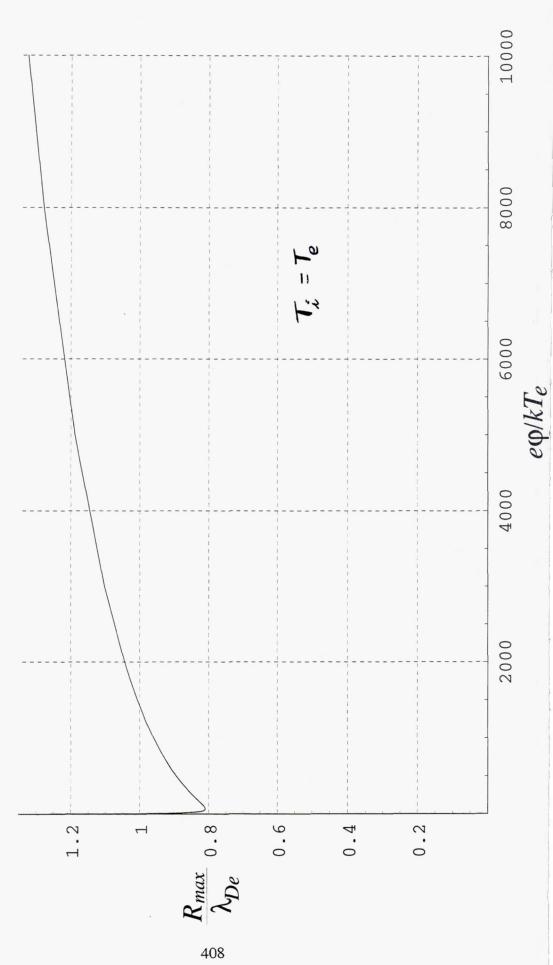
Poisson's equation then reading

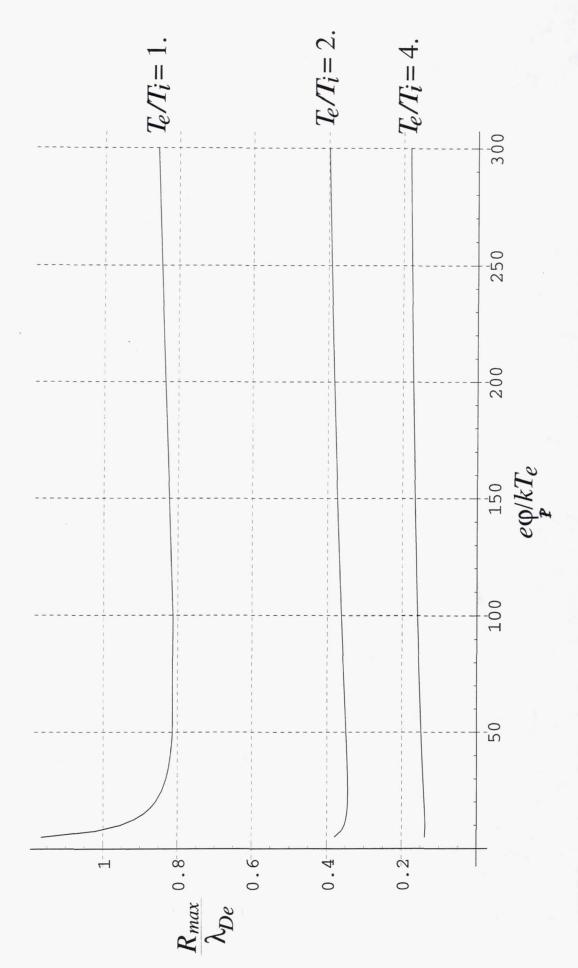
$$\frac{\lambda_{Di}^{2}}{a^{2}\left(\sinh^{2}w + \sin^{2}v\right)} \left(\frac{\partial^{2}\Psi}{\partial w^{2}} + \frac{\partial^{2}\Psi}{\partial v^{2}}\right) = \frac{N_{e}}{N_{\infty}} - \exp(-\Psi). \tag{18}$$

The ellipses w(x,y) = constant approach circles as w increases; at large radial distances one has

$$w = \ln \frac{r}{a} + \ln 2 - \frac{x^2 - y^2}{4r^2} \frac{a^2}{r^2} + \dots$$
 (19)

We may reasonably use the approximation $w = \ln(2r/a)$ for $w > w^*$, with $w^* = 1.25$ or 1.5, say. Note also that the limit ellipse w = 0 is the segment y = 0, -a < x < a, which may represent the cross section of a tape of width 2a and negligible thickness.





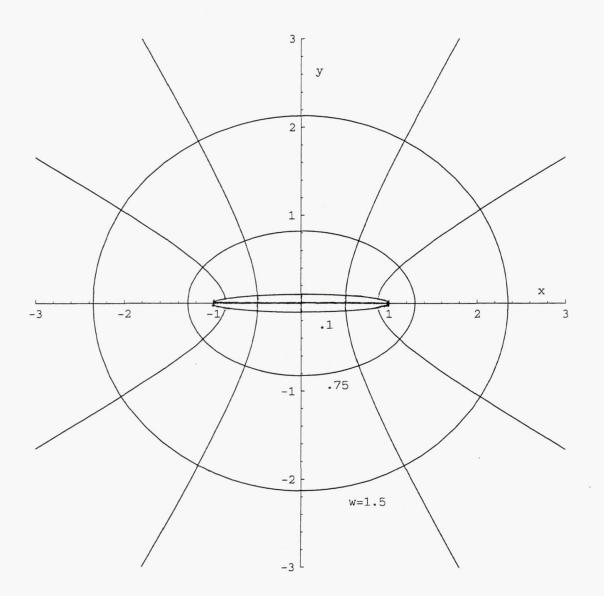


FIGURE 6

As in the previous section, the space-charge may be ignored in some neighborhood of the probe, which, for Ψ_p large enough, extends into the region where wellipses are near-circles, that is, beyond $w = w^*$. We may then argue that the potential Ψ will be nearly independent of v everywhere, i.e. $\Psi(w, v) \approx \Psi(w)$ (and the electric field at $w > w^*$ will be radial) in the following way:

- i) The electron density for $w > w^*$ would then be a function of just w, $N_e = N_e(w)$. This is because, at a point in that region, incoming electrons, and outgoing electrons that did not reach values $w < w^*$, find a radial field throughout their motion and conserve the angular momentum J; their contribution to N_e will be a function of r, and thus, of w. Those outgoing electrons that had reached values $w < w^*$ and missed the probe, have J changed by a quantity ΔJ that is small $(\Delta J \sim J/\ln \Psi_p)$ as a result of the shallow (logarithmic) character of the potential in the vicinity of the probe, where the field is not radial; their contribution to N_e will be weakly dependent on v. On the whole we would have $N_e \approx N_e(w)$.
 - ii) Poisson's equation reads

$$\frac{\partial^{2}\Psi}{\partial^{2}w} + \frac{\partial^{2}\Psi}{\partial^{2}v} \approx 0 \tag{20a}$$

for $w < w^*$, and

$$\frac{\lambda_{Di}^{2}}{a^{2} \sinh^{2} w} \left(\frac{\partial^{2} \Psi}{\partial^{2} w} + \frac{\partial^{2} \Psi}{\partial^{2} v} \right) \approx \frac{N_{e}}{N_{\infty}} - \exp(-\Psi)$$
 (20b)

for $w > w^*$, with some overlapping range of validity. In neither (20a) nor (20b) does v show up explicitly.

iii) Finally, boundary conditions refer to just w,

$$\Psi = \Psi_p$$
 at $w = 0$, $\Psi \to 0$ as $w \to \infty$.

With $\Psi = \Psi(w)$, and $w = \ln(2r/a)$ for $w > w^*$, we now have :

1) Equation (20a) and the probe boundary condition yield

$$\Psi = \Psi_p[1 - \beta w] \tag{21}$$

$$\rightarrow \Psi = \Psi_p \left[1 - \beta \ln \left(\frac{r}{a/2} \right) \right] \quad \text{for } w > w^*.$$
 (22)

2) Equation (20b) for $w > w^*$ recovers (3), whose solution, as in Fig.3 of section 2, will show an outer quasineutral region, thin layers, and a broad, ion-free, inner region. This solution, rather than satisfying the boundary condition at the probe, must match smoothly the behavior given in (22), within the overlapping range of validity. Comparing

Eqs.(17) and (22) shows that, beyond w^* , the solution behaves as in the case of a circular cylinder with an effective radius R = a/2 (the coefficients β and α being equal).

This suggests that, with all other parameters given, the maximum width of a thin tape in the OML regime relates quite simply to the maximum radius of a circular cylinder,

$$2a_{max} = 4R_{max}. (23)$$

Note that, since OML current is proportional to the perimeter, use of a tape would only increase the maximum current by a factor $4/\pi$, or 27 %. A tape might be actually preferable for other reasons: a cylinder with R_{max} might be too heavy and rigid (7); a tape may lead to a shorter tether (2). The main interest of the result is then that the maximum half-width of a tape is twice R_{max} as given in Figs. 4 and 5.

One must still take into account the fact that the Laplace potential (21), for the region $w < w^*$, is quite different from the potential (17). It then comes out that a tape, contrary to a circular cylinder, never collects the full OML current, although this has no practical consequences. There are potential barriers in the vicinity of any flat collecting surface, the effects being weak, however, in the case of a shallow 2D Laplace potential (4). Using (21) we find that potential barriers around the tape lie in a thin region of thickness $\sim a/\ln \Psi_p$, and that current reduction below the OML value is of order $(1/\ln \Psi_p)^2$, or about 1 %. Equation (23) should then properly read that current to a tape keeps very close to the OML value for $a \le 2R_{max}$.

4. Circular cylinder at rest in a magnetized plasma

As in the previous section, there is no closed-form expression for N_e in the presence of an uniform magnetic field \mathbf{B} , which allows for only two constants of the motion, energy and canonical angular momentum. Overall use of these two constants leads to the Parker-Murphy current law, which takes the character of an upper bound at the high bias of interest (6). For $e\Phi_p >> kT_e$ and cylindrical geometry one has

$$I_{PM} \approx I_{OML} \sqrt{\pi/2} \times l_e / R$$
, (24)

where l_e is the electron thermal gyroradius

$$l_e \equiv v_{th}/\Omega_e \ \propto \ 1/B \qquad (v_{th} \equiv \sqrt{k} T_e/m_e, \quad \ \Omega_e \equiv eB/m_e). \label{eq:vth}$$

Equation (24) suggests that if R/l_e is small, I_{OML} then lying well below the I_{PM} bound, the OML current will hardly be affected by magnetic effects.

To get more definite results, we consider the exact equations for electron motion in the presence of the electric field due to probe and plasma, $-\nabla\Phi(x, y)$ [probe and z axes

coincide], and an uniform magnetic field B perpendicular to the probe, say along the y-axis:

$$\frac{d^2 v_x}{dt^2} + \Omega_e^2 \left[1 - l_e^2 \frac{\partial^2}{\partial x^2} \left(\frac{e\Phi}{kT_e} \right) \right] v_x = v_{th}^2 v_y \frac{\partial^2}{\partial x \partial y} \left(\frac{e\Phi}{kT_e} \right) , \qquad (25a)$$

$$\frac{dv_{y}}{dt} = v_{th}^{2} \frac{\partial}{\partial y} \left(\frac{e\Phi}{kT_{e}} \right), \tag{25b}$$

$$\frac{d^2 v_z}{dt^2} + \Omega_e^2 v_z = -v_{th}^2 \Omega_e \frac{\partial}{\partial x} \left(\frac{e\Phi}{kT_e} \right). \tag{25c}$$

Equations (25a and c) were obtained by deriving the respective equations of motion and using the derivative along the electron orbit (10),

$$\frac{dE_x}{dt} = \frac{\partial E_x}{\partial x} v_x + \frac{\partial E_x}{\partial v} v_y,$$

The last two terms of (25c) would give the usual E/B drift; the first two terms represent gyromotion. The important equation is (25a), which should describe the approach to the probe across field lines.

The left-hand side of (25a) would again represent gyromotion if the second term in the bracket were small, that is for B large enough (l_e small enough). Assuming, on the contrary, that l_e is sufficiently large, we neglect the first (gyromotion) term and use the B = 0 solution of section 2 to determine how small must be the magnetic field for the second term in the bracket to be indeed large. In the broad region between probe and thin layers of Fig.3, the resulting condition is, basically, that the R/l_e ratio of the Parker-Murphy law (24) be small; in particular, near the probe, where both Eq.(17) and the approximation

$$\frac{d^2\Phi}{dr^2} \approx -\frac{1}{r} \frac{d\Phi}{dr}$$

hold, the left-hand-side of Eq.(25a) takes the simple form

$$\frac{d^{2}v_{x}}{dt^{2}} + \Omega_{e}^{2} \left[1 - \frac{l_{e}^{2}}{R^{2}} \left(\frac{R^{2}}{r^{2}} \frac{x^{2} - y^{2}}{r^{2}} \alpha \frac{e\Phi_{p}}{kT_{e}} \right) \right] v_{x}$$

with the first 3 factors in the parenthesis moderately small, and the last factor large. In the quasineutral region of Fig.3, the second term in the bracket is never large for $T_i \approx T_e$, but

the electrons are then hardly affected by the potential before they reach r_0 ($e\Phi_0 \approx 0.194$ kT_e). Finally, in the two thin layers, where we have $N_e - N_i \sim N_\infty$ and

$$\frac{d^2\Phi}{dr^2} << \frac{-1}{r} \frac{d\Phi}{dr},$$

the left-hand-side becomes

$$\frac{d^{2}v_{x}}{dt^{2}} + \Omega_{e}^{2} \left[1 - \frac{l_{e}^{2}}{\lambda_{De}^{2}} \frac{x^{2}}{r^{2}} \frac{N_{e} - N_{i}}{N_{\infty}} \right] v_{x}$$

This means that for *B*-effects to be negligible, both R/l_e and λ_{De}^2/l_e^2 must be small.

At the relatively high densities of the F-layer, $\lambda_{De}^2/l_e^2 \propto B^2/N_\infty$ is indeed small (about 10^{-2} and 10^{-1} for $N_\infty = 10^{12}$ and 10^{11} m⁻³, respectively), but it reaches above unity at extreme altitudes. Experiments on board an elliptical-orbit satellite (8) and a rocket (11) did show a current dependent on the angle between B and a cylindrical probe (B-effects) when N_∞ dropped low enough, at very low and high altitudes. In all cases probe bias was only moderately high.

5. Circular cylinder moving through an unmagnetized plasma

The case of interest is that of a large ion ram energy,

$$\frac{1}{2} m_i U^2 >> kT_i$$

where U is the plasma velocity past the probe; for a tether orbiting in the F layer (oxygen ions, orbiting velocity) we have indeed $\frac{1}{2}m_iU^2\approx 4.5$ eV $>> kT_i\sim 0.15$ eV. The unperturbed ion distribution function is now non isotropic and the electric field non radial, but the OML current law, which is independent of both ion distribution and cross section shape, is still valid. The high-bias limit law (13) is particularly robust: it is also independent of the unperturbed electron distribution function as long as it is isotropic, which is the case here ($\frac{1}{2}m_eU^2 << kT_e$).

The ion ram energy could affect, however, the domain of validity of the OML law. For the case of interest, $\frac{1}{2}m_iU^2 << e\Phi_p$, ions would be kept far away from the probe for all directions, with an (angle dependent) potential structure similar to that shown in Fig.3. For all other parameters fixed, the distance r_1 (or r_2) in Fig.3 is directly related to the characteristic ion energy. In a plasma with $T_i = T_e$, a crude model suggests the distances would correspond to an effective ion temperature $kT_i(eff) = \frac{1}{2}m_iU^2$ on the windward side, and $T_i(eff) = T_e$ on the lateral sides; when particularised for a small ratio T_i/T_e , the analysis sketched in section 2 would roughly give $T_i(eff) \sim T_e \times \sqrt{kT_e/(\frac{1}{2}m_iU^2)}$ for the lee side. Since R_{max} increases with T_i/T_e (Fig.5), a wire with $R = R_{max}(U = 0, I_e)$

 $T_i/T_e = 1$) would collect current in agreement with the OML law at the lateral sides and at the front, and below the OML level at the lee side; a preliminary analysis of how the current lags behind the OML value as R increases beyond R_{max} shows, however, that I/I_{OML} keeps closer to 1 the lower the ratio T_i/T_e . A wire with $R = R_{max}(U = 0, T_i/T_e = 1)$ should then collect current very close to the law (13).

We note finally that conditions in laboratory plasmas may substantially differ from those applying in the tether case. The ratio T_i/T_e is usually small and, as a consequence of Fig.5, cylindrical probes will collect current below the OML value unless R is well below λ_{De} . Also, in flowing laboratory plasmas the ion ram energy may be comparable to the bias applied at the probe, $\frac{1}{2}m_iU^2\sim e\Phi_p$; again, unless R is much less than λ_{De} , the potential would be non monotonic, with an overshoot at the front and a trough on the lee side, and the prediction of current would be difficult.

6. Conclusions

Bare tether applications are based on the assumption that the tether collects electrons in the OML regime of cylindrical Langmuir probes. The definite and simple OML current law, which allows for detailed design considerations, has opened the way to a technology of electrodynamic tethers (2). Here, we have determined the domain of OML validity in parameter space; we studied the surface bounding that domain as a relation among the dimensionless numbers

$$R/\lambda_{De}$$
, $e\Phi_{p}/kT_{e}$, T_{i}/T_{e} , $l/2m_{i}U^{2}/kT_{i}$, and λ_{De}/l_{e} ,

for the very large $e\Phi_p/kT_e$ values of interest. (The mass ratio m_e/m_i enters through the irrelevant numbers $\frac{1}{2}m_eU^2/kT_e$ and λ_{De}/l_i .)

We found that the ratio λ_{De}/l_e (actually, λ_{De}^2/l_e^2) must be small for magnetic effects -which would break the OML law otherwise- to be ignorable. This ratio is a property of the plasma rather than a free design parameter. In the Earth's ionosphere λ_{De}^2/l_e^2 is small for N_{∞} clearly above 10^{10} m⁻³; this breaks down at low, and sufficiently high, altitudes.

For λ_{De}^2/l_e^2 small, and first taking $1/2m_iU^2/kT_i\sim 0$, we determined the maximum radius for the OML regime to hold, giving

$$R_{max}/\lambda_{De}$$
 versus $e\Phi_p/kT_e$ and T_i/T_e .

 R_{max} exibits a minimum as a function of Φ_p but, at the bias of interest, is slowly increasing, and above λ_{De} in the ionospheric case $(T_i/T_e \sim 1)$. For λ_{De}^2/I_e^2 small and $R \sim \lambda_{De}$, we have R^2/I_e^2 small too, a second condition we found required for magnetic effects to be weak. We also found R_{max}/λ_{De} increasing with T_i/T_e .

We finally found that if

$$\frac{1}{2}m_iU^2/kT_i \times T_i/T_e \times kT_e/e\Phi_p = \frac{1}{2}m_iU^2/e\Phi_p$$

is small, as in the tether case, the ion ram energy $\frac{1}{2}m_iU^2$ will only affect the potential structure far away from the probe. This structure reaches a distance that depends on the ion characteristic energy, the ram energy making that distance angle-dependent. Both the increase of R_{max} with T_i/T_e (for vanishing U), and the fact that, at low T_i/T_e , the current hardly lags behind the OML value as R exceeds R_{max} , indicate that a wire with $R \le R_{max}(U=0, T_i/T_e=1)$ would collect current very close to the OML value.

If a thin tape is used instead of a wire (with all others parameters equal), the maximum valid width is found to be $4R_{max}$.

Acknowledgments

The work of J.R.Sanmartín was supported by DGYCIT (Spain) under grant PB94-0417-C03-01.

References

- 1. Bernstein, I.B. and Rabinowitz, I.N., Theory of electrostatic probes in a low-density plasma, *Phys. Fluids* 2, 1959, 112-121.
- 2. Johnson, L., Carroll, J., Estes, R., Gilchrist, B., Lorenzini, E., Martínez-Sanchez, M., Sanmartín, J.R., and Vas, I., Electrodynamic tethers for reboost of the international space station and spacecraft propulsion, paper presented at the *AIAA Space Programs and Technologies Conference*, Am. Inst. of Aeronautics and Astronautics, Huntsville, Ala., Sept. 1996.
- 3. Laframboise, J.G., Theory of spherical and cylindrical Langmuir probes in a collisionless, Maxwellian plasma at rest, University of Toronto Institute of Aerospace Studies Report No.100, June 1966.
- 4. Laframboise, J.G. and Parker, L.W., Probe design for orbit-limited current collection, *Phys. Fluids* 16, 1973, 629-636.
- 5. Lam, S.H., Unified theory for the Langmuir probe in a collisionless plasma, *Phys. Fluids* 8, 1965, 73-87.
- 6. Parker, L.W. and Murphy, B.L., Potential buildup on an electron-emitting ionospheric satellite, *J. Geophys. Res.* 72, 1967, 1631-1636.
- 7. Martínez-Sanchez, M. and Sanmartín, J.R., Artificial auroral effects from a bare conducting tether, *J. Geophys. Res.* 102, 1997 (in press).
- 8. Miller, N.J., Some implications of satellite spin effects in cylindrical probe measurements, *J. Geophys. Res.* <u>77</u>, 1972, 2851-2861.

- 9. Sanmartín, J.R., Martínez-Sanchez, M., and Ahedo, E., Bare wire anodes for electrodynamic tethers, J. Propul. Power 9, 1973, 353-360.
- 10. Singh, N. and Chaganti, V.S., Electron collection by a highly positive satellite in the ionosphere: Test particle simulation, *J. Geophys. Res.* <u>99</u>, 1994, 469-478.
- 11. Szuszczewicz, E.P. and Takacs, P.Z., Magnetosheath effects on cylindrical Langmuir probes, *Phys. Fluids* 22, 1979, 2424-2429.

Page intentionally left blank

Poster Session

Page intentionally left blank

Response of Electrodynamic Tethers in Ionospheric Plasma Due to Step Changes in Voltage

Sven G. Bilén and Brian E. Gilchrist Space Physics Research Laboratory, University of Michigan 2455 Hayward St., Ann Arbor, MI, 48109-2143

Abstract

Understanding the transient behavior of an electrodynamic tether system is of special importance to systems detecting natural electric field transient signatures and those utilizing tether current pulses or modulation, such as for low frequency wave generation. Our research is aimed at understanding the nonlinear propagation characteristics of electromagnetic pulses along electrodynamic tethers in the ionosphere. Such a pulse can occur as a tether/plasma system transitions from open—to closed—circuit states, i.e., no current to current flowing states or vise versa. This perturbation takes a finite amount of time to propagate along the tether and affects the surrounding ionospheric plasma as it does so. This interaction in turn affects the tether's transmission line characteristics. One of the important items we examine is the dynamic evolution of the sheath as the pulse front travels past a given section of the tether and disturbs the steady—state sheath.

1 Introduction

Many of the first flights of tethered systems have principally emphasized electrodynamic applications using tethers with conducting wires (Dobrowolny and Melchioni, 1993; Dobrowolny et al., 1994; Godard et al., 1991; James, 1991; Kawashima et al., 1988; McCoy et al., 1993; Sasaki, 1988). Motion of the conducting tether relative to the ambient magnetized plasma of the near Earth environment generates substantial $(\mathbf{v}_s \times \mathbf{B}) \cdot \mathbf{l}$ potentials, where \mathbf{v}_s is the tether motion through the local plasma, \mathbf{B} is the Earth's magnetic field, and \mathbf{l} is the vector end-to-end length of the tether (Banks et al., 1981; Banks, 1989; Dobrowolny, 1987). This electromotive force can be made to drive current through the tether if adequate electrical contact is made with the surrounding plasma (Agüero et al., 1994; Arnold and Dobrowolny, 1980; Banks et al., 1981; Banks, 1989; Martínez-Sánchez and Hastings, 1987).

In order to fully exploit that capabilities of electrodynamic tether (ET) systems, we must first understand both their steady-state and transient electrical responses.

For example, we need to know the steady-state response when examining the dc current collection along a tether as well as at its endpoints. However, this steady-state response is not applicable in the transient case which would occur during pulsed current operations or when used as a transmitting antenna.

In this paper, we report on work in progress aimed at developing an understanding of the transient response of ET systems in the ionosphere. We begin with a description of pulse propagation along ET transmission lines (TL's) including a description of boundary conditions (steady-states) and timescales. We then provide a qualitative description of the transient sheath response due to stepped high-voltage. We use this description to show that our TL is a dynamic system and show the methodology behind determining TL characteristics for the ET. We conclude by providing a summary of results to date and directions for future research.

2 Electrodynamic Tethers as Transmission Lines

Pulse propagation along a tether cannot be analyzed in the same manner as it is along other TL's, such as along coaxial cables or parallel wire lines. This is due primarily to the fact that, unlike these other TL's, the geometry of the plasma/conductor system is not rigid because the plasma forms the outer conductor of the TL. James et al. (1995) state that the tether, sheath, and surrounding plasma can form an approximation to a coaxial RF TL to the degree that the surrounding plasma can be regarded as the outer conductor. This situation is shown in Figure 1. Other researchers have used similar rigid models of electrodynamic tether systems in the ionosphere (Arnold and Dobrowolny, 1980; Banks et al., 1981; Banks, 1989; Dobrowolny, 1987; Greene at al., 1989). In the transient case of a pulse or step propagating along the tether, however, the coaxial approximation breaks down since the surrounding plasma is not a rigid metal sheathing but responds to the voltage perturbation. Thus, a new TL model is needed which takes into account the time-varying, voltage dependent sheath as shown in Figure 2.

2.1 Potential Structures Along the Tether

In an electrodynamic tether system there are two dc steady-states: an open-circuited state called the *voltage mode* where no current flows and a closed-circuited state called the *current mode* where current flows along the tether from one end to the other. These two steady-states, or modes, cause two different potential structures to exist along the tether. The two states represent the initial and final conditions, *i.e.*, the boundary conditions, of the transient case which occurs when a load impedance is connected or disconnected from the system. In this section,

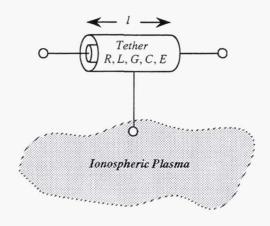


Figure 1: Present electrodynamic tether transmission line model.

the potential structures of the two states will be examined for the case of an insulated tether. Potential structures for uninsulated tethers can be similarly examined, but for that tether, current is collected along the tether length and not just at the endpoints.

The first potential structure occurs when the tether system is in the voltage mode. In this configuration a high impedance load is connected between the tether and the orbiter end of the system, as shown in Figure 3(a). (It should be noted that the load occupies only a negligible amount of length in the overall system, but has been enlarged in the figure for clarity.) Figure 3(b) is a diagram—similar to that found in Martinez-Sánchez and Hastings (1987)—showing the magnitude of the potentials with respect to the overall tether emf. Figure 3(c) is a diagram of the polarity with respect to the plasma potential and is similar to that found in Savich (1988). The diagrams in Figure 3(b) and (c) complement each other. That is, the magnitude diagram shows that with no current flowing, there is no potential drop along the tether. The polarity diagram shows that, with respect to the plasma, the tether is biased more and more negatively along its length as one moves from the satellite to the Orbiter. (The tether potential is negative with respect to the the plasma because the load is at the orbiter end of the system. If the load were at the satellite, the reverse would be true; that is, the tether potential would be positive with respect to the plasma.)

In the voltage mode, the tether emf is divided among the various sections of the system: load, tether, plasma, satellite, and orbiter. Almost the entire voltage drop in the system occurs across the high impedance load since negligible current flows along the tether. Indeed, this is how an accurate measurement of φ_{tether} is

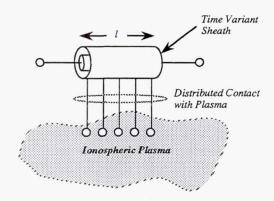


Figure 2: Improved electrodynamic tether transmission line model.

made, since the high impedance load is simply the internal resistance of the voltage monitors. As mentioned above, little voltage drop occurs along the tether. At the satellite and orbiter ends of the tether, there is some potential drop with respect to the local plasma, labeled φ_{sat} and φ_{orb} respectively. These drops are due to the spacecraft charging negative in the absence of current collection such that nearly zero current is collected at their surfaces. (The ionospheric voltage drop, $I_{\text{tether}}Z_{\text{iono}}$, is not included in the figure since its effect is negligible.)

The second potential structure occurs when the tether system is in the current mode. In this mode, a low impedance load is placed between the tether end and the orbiter as shown in Figure 4, and measurable current flows. No longer does nearly the entire voltage drop occur across the load impedance, but a significant fraction of the drop occurs across the tether due to the tether's internal resistance R_{tether} . With the current flowing in the tether, the upper part of the tether is positively biased with respect to the plasma, whereas the lower part is negatively biased. In addition, φ_{sat} and φ_{orb} are established to collect electron and ion currents, respectively. Thus, the satellite tends to be positively biased, whereas the orbiter is negatively biased. The absolute maximum possible tether current is simply $I_{\text{tether}} = \varphi_{\text{tether}}/(R_{\text{tether}} + R_{\text{load}})$, and if this maximum level is achieved, then I_{tether} is said to be tether impedance limited. If the ionospheric plasma cannot provide this level of current—which is often the case, especially in lower density regions— I_{tether} is said to be ionospheric limited (Thompson et al., 1993).

Another way of interpreting Figures 3 and 4 is through the concept of reference frame. For example, the solid black line in Figure 3(b) represents the tether voltage in the reference frame of the tether itself. Thus, it is seen that as one travels down the tether, there is no voltage drop along its length. However, in the reference frame

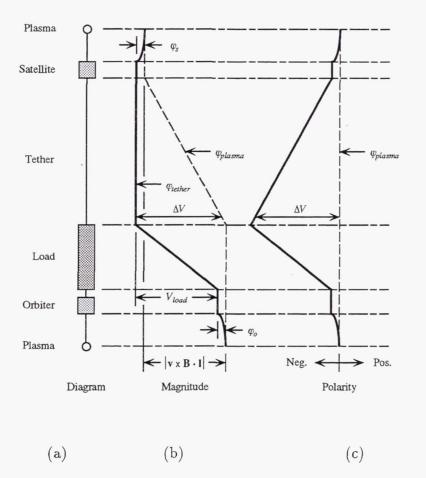


Figure 3: Potential diagram for tether system with high impedance load (voltage measuring mode): (a) placement of system components, (b) magnitude of system potentials, (c) polarity of system potentials. Note: the load occupies only a negligible amount of length in the overall system, but has been enlarged in the figure for clarity.

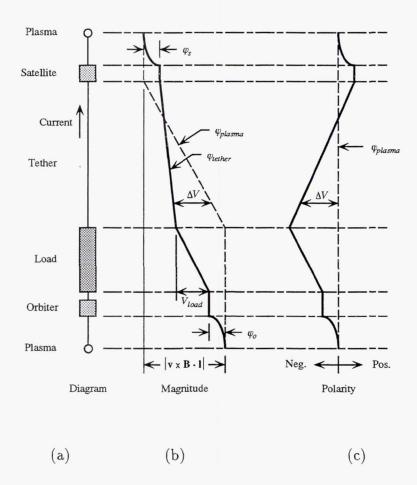


Figure 4: Potential diagram for tether system with low impedance load (current measuring mode): (a) placement of system components, (b) magnitude of system potentials, (c) polarity of system potentials. Note: the load occupies only a negligible amount of length in the overall system, but has been enlarged in the figure for clarity.

of the plasma, *i.e.*, Figure 3(c), the tether is biased more and more negative as one travels down its length. Similar reference frame interpretations can be made for the current mode diagrams of Figure 4.

2.2 Propagation Timescales

There are four timescales to consider when examining the propagation of the pulse past a given section of tether. Each of these four timescales is linked to the timescale of the interaction of the surrounding plasma with the tether section during the voltage change.

- The first timescale is linked to the initial electrical disturbance of the tether's potential as the pulse front moves past a section of tether. Since this timescale is on the order of a fraction of the speed of light, the plasma is not able to respond on this timescale and the sheath remains fairly static.
- The second timescale is linked to the electron response, which is on the order of the electron plasma period ($\tau_{pe} = 1/\omega_{pe}$). Because of their low mass, the electrons are quickly repelled away from the tether surface as the negative voltage is progressively established along the tether, and the tether section becomes biased negatively due to the pulse front having moved past the section of tether. After the electrons have been expelled from the region surrounding the conductor, an "ion-matrix" sheath forms. It should be mentioned that the electrons will tend to oscillate as they are expelled before they settle beyond the ion-matrix sheath distance.
- The third timescale is linked to the ion response time and is on the order of the ion plasma period $(\tau_{pi} = 1/\omega_{pi})$. On this timescale, the ions begin to respond to the voltage disturbance along the tether and are collected to the tether surface.
- The fourth timescale is the time it takes to establish the steady-state sheath structure around the tether. For an insulated tether this timescale depends on the time required for sheath collapse after charging of the insulation and for the bare tether, depends on the time required to establish an orbital-motion-limited (OML) sheath.

3 Transient Sheath Response

When an isolated object is placed into a plasma, a steady-state sheath forms around the object in order to establish a zero net current condition to the object. The sheath also serves to shield the object's electric potential from the bulk of the plasma. Across the sheath region, there is a voltage drop in which the electric potential of the object transitions to the undisturbed plasma potential. When the potential of the object changes, a finite amount of time is required for the sheath to react. Thus, in the transient case, the sheath thickness and ion/electron composition can be dramatically altered. In the case of an ET system, a steady state sheath exists around the tether just before and again some time after application of a voltage step. Between these two times, the sheath structure is altered dramatically and this affects the TL characteristics of the tether/plasma system.

In the case of the ET, the pulse is generally a large value and is applied quickly. This can be seen by examining a single section of tether in Figures 3 and 4 and noting how, as the ET system changes from closed—to open—circuit states, the voltage on the tether section is biased more negative with respect to the plasma potential. There is a fair amount of work in the literature dealing with high negative potentials being suddenly applied to planar, cylindrical, and spherical conductors (for example, Ma and Shunk, 1992; Laframboise and Sonmor, 1993; Collins and Tendys, 1994). Plasma source ion implantation (PSII) is a very active research area which involves high negative potentials being applied to conductors in plasmas (Lieberman, 1989). However, PSII generally involves planar geometries and, as such, the sheaths are generally described by the Child-Langmuir (CL) relation.

3.1 Ion-matrix Sheath

When the high negative voltage is first applied to a conductor (insulated or not), the electrons are expelled from the surrounding region, leaving behind a uniform density "ion-matrix" sheath. The derivation of the ion-matrix sheath thickness begins with Poisson's equation which defines the potential structure surrounding the cylindrical conductor:

$$\frac{d^2V}{dr^2} + \frac{1}{r}\frac{dV}{dr} = -\frac{q}{\varepsilon_0}(n_i - n_e),\tag{1}$$

where V is the potential, n_i and n_e are the ion and electron plasma densities, and the spatial variable r is measured from the center of the conductor. The plasma is assumed to have uniform density initially, i.e., $n_0 = n_i = n_e$, before voltage is applied to the conductor. The solution of Poisson's equation given here relies on the following assumptions and boundary conditions:

- During the ion-matrix phase of sheath evolution, the electron density in the sheath is zero (i.e., $n_e = 0$) and the ion density remains unchanged from before the voltage was applied and uniform (i.e., $n_i = n_0$),
- the potential at the conductor V must equal the applied potential V_0 ,

• the electric field must vanish at the ion-matrix sheath edge position r_{s0} .

The solution of Equation (1) under the above conditions yields the ion-matrix sheath position, r_{s0} , for cylindrical geometry as

$$r_{s0} \simeq \sqrt{2} \left(\frac{V_0 \varepsilon_0}{q n_0}\right)^{5/12} r_a^{1/6} \text{ for } r_{s0} \gg r_a,$$
 (2)

where ε_0 is the permittivity of free space, q is elementary charge magnitude, and r_a is the wire radius. The derivation of this result is very similar to that followed by Conrad (1987), and relies on knowledge of the solutions for the planar and spherical cases, as the cylindrical case is the geometric mean of those two. All three solutions are plotted as a function of applied voltage in Figure 5.

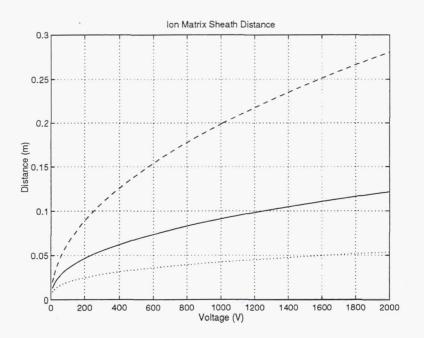


Figure 5: Ion-matrix sheath distances as a function of applied voltage for the following conditions: $r_a = 1.3 \text{ mm}$, $n_0 = 2.8 \times 10^{12} \text{ m}^3$ (solid line: cylindrical, dashed line: planar, dotted line: spherical).

3.2 Sheath Evolution

An OML sheath will evolve around the conductor for the case of a thin cylindrical tether in the ionosphere such that the condition $r_a \ll \lambda_D$ holds $(r_a \lesssim \lambda_D \text{ may also})$

hold as well for large applied voltages), where λ_D is the Debye length and is defined as $\lambda_D = \sqrt{\frac{\varepsilon_0 k T_e}{q^2 n_e}}$. Unlike the C-L sheath which holds in the regime $r_a \gg \lambda_D$, not all particles which enter the OML sheath are collected, only those with trajectories that be bent while still conserving angular momentum. This situation is shown in Figure 6. The current collection density in the OML case is given by the following equation

$$j_{\text{OML}} = 2r_a n_e q v_{\text{th}} \sqrt{\frac{qV}{kT_i}}$$
(3)

where the thermal velocity $v_{\rm th} = \sqrt{\frac{2kT}{m_i}}$, T_i is the ion temperature, k is Boltzmann's constant, and m_i is the ion mass. It is interesting to note that the sheath radius, r_s does not enter into this equation for high applied voltages.

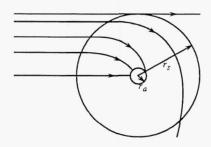


Figure 6: Orbital-motion-limited sheath.

3.3 Sheath Collapse

For the case of the insulated tether, the applied voltage will become shielded from the plasma as ions are collected on the surface of the tether, and the sheath will begin to collapse. The time required for sheath collapse depends on the current density flowing to the tether and can be on the order of several milliseconds for typical tether geometries and plasma densities. For the case of a bare tether, the sheath does not collapse, but rather evolves to the OML sheath. The reason for this is that the applied voltage is not shielded by the collected charges since they move along the tether as a current.

3.4 Sheath Capacitance

When the tether/plasma system is viewed as a capacitor—the tether conductor is one plate and the plasma sheath boundary is the other—then it is easily seen

that its capacitance is a function of voltage and time. The sheath capacitance is a nonlinear function of voltage since the sheath size increases at a diminishing rate as larger voltages are applied. The sheath capacitance is also a function of time since the sheath size does not respond instantaneously to voltage changes, but rather there can be considerable lag times to reach steady-state. For cylindrical (coaxial) geometries, capacitance per unit length is defined as

$$C = \frac{2\pi\epsilon_r\epsilon_0}{\ln(\frac{r_s}{r_s})}.$$

So, in our case, since r_s is a function of voltage and time, so must also the capacitance be, i.e.,

$$C(v,t) = \frac{2\pi\epsilon_r\epsilon_0}{\ln(\frac{r_s(v,t)}{r_s})}.$$
 (4)

4 Transmission Line Lumped Model

We wish to outline here how an analysis of the propagation characteristics of a tether TL which has a capacitance dependent on time and voltage. We begin by assuming the line is of infinite length and that capacitance as defined in Eqn. 4. In should be noted that at time t=0, $C(v,t)=C_{closed-ckt}$ and at time $t=\infty$, $C(v,t)=C_{open-ckt}$. We have defined the remainder of our TL in the usual manner with static resistance and inductance per unit length, R and L, and the emf generated per unit length, E. A typical section of the TL is shown in Figure 7.

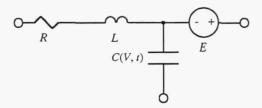


Figure 7: Transmission line section with per–unit–length time and voltage dependent capacitance C(v,t), the usual R and L, and E for the emf.

We can show the voltage and time dependences along the TL length through Kirchhoff's voltage and current laws for a dz-segment of the TL, which are written as:

$$\frac{\partial}{\partial z}v(z,t) = -Ri(z,t) - L\frac{\partial}{\partial t}i(z,t) + E(z), \tag{5}$$

$$\frac{\partial}{\partial z}i(z,t) = -\frac{\partial}{\partial t}[C(v,t)v(z,t)]. \tag{6}$$

The solution of the scalar wave equation given the above coupled equations is non-trivial and is the subject of ongoing research. Their solution should yield interesting results on the TL characteristics of ET's.

5 Conclusion

Pulse propagation along a ET's cannot be analyzed in the same manner as along static TL's because the geometry of the plasma/conductor system is not rigid. Since the plasma responds to the voltage perturbation along the tether, ET's can be considered as dynamic TL's. The two dc steady-states for the ET's are an open-circuited state called the voltage mode where no current flows and a closed-circuited state called the current mode where current flows along the tether from one end to the other. These steady-state sheaths exist around the tether just before and again some time after application of a negative voltage step. Between these two times, the sheath structure is altered dramatically and this affects the TL characteristics of the tether/plasma system. When the tether/plasma system is viewed as a capacitor, then it is easily seen that its capacitance is a function of voltage and time. We can then develop an equivalent lumped TL with per-unit-length time and voltage dependent capacitance C(v,t), the usual R and L, and E for the emf.

Future work is directed toward finding a solution of the wave equation given the dynamic ET TL. We are also interested in determining how the addition of ionospheric effects such as flowing plasma and ambient magnetic field would affect the lumped TL model. Simulations of pulse propagation along the tether as well as sinusoidal excitation of the tether should provide useful data for upcoming and future tethered mission.

References

Agüero, V., P. M. Banks, B. Gilchrist, I. Linscott, W. J. Raitt, D. Thompson, V. Tolat, A. B. White, S. Williams, and P. R. Williamson, The Shuttle Electrodynamic Tether System (SETS) on TSS-1, Nuovo Cimento Soc. Ital. Fiso., 17C(1), 49-65, 1994.

- 2. Arnold, D. A., and M. Dobrowolny, Transmission line model of the interaction of a long metal wire with the ionosphere, *Radio Sci.*, 15(6), 1149–1161, 1980.
- 3. Banks, P. M., Review of electrodynamic tethers for space plasma science, J. Spacecr. Rockets, 26(4), 234–239, 1989.
- 4. Banks, P. M., P. R. Williamson, and K.-I. Oyama, Electrical behavior of a shuttle electrodynamic tether system (SETS), *Planet. Space Sci.*, (Gb), 29(2), 139–47, 1981.
- 5. Collins, G. A., and J. Tendys, Sheath development around a high-voltage cathode, *Plasma Sources, Science and Technology*, 3(1), 10–18, 1994.
- 6. Conrad, J.R., Sheath thickness and potential profiles of ion-matrix sheaths for cylindrical and spherical electrodes, J. of Applied Phys., 62(3), 777-779, 1987.
- 7. Dobrowolny, M., et al., The RETE experiment for the TSS-1 mission, Nuovo Cimento Soc. Ital. Fiso., 17C(1), 101-121, 1994.
- 8. Dobrowolny, M., and N. H. Stone, A technical overview of TSS-1: The first Tethered Satellite System mission, *Nuovo Cimento Soc. Ital. Fiso.*, 17C(1), 1-12, 1994.
- 9. Dobrowolny, M., and E. Melchioni, Electrodynamic aspects of the first Tethered Satellite System, J. Geophys. Res., 98(A8), 13,761-13,778, 1993.
- 10. Dobrowolny, M., The TSS project: Electrodynamics of long metallic tethers in the ionosphere, Riv. Nuovo Cimento, 10(3), 1-83, 1987.
- Godard, R., H. G. James, J. G. Laframboise, B. Macintosh, A. G. McNamara,
 S. Wantanabe, and B. A. Whalen, The OEDIPUS experiment: Analysis of the current/voltage data, J. Geophys. Res., 96(A10), 17,879-17,890, 1991.
- 12. Greene, M., D. Wheelock, and M. Baginski, Electrodynamics of the getaway tether experiment, J. Spacecr. Rockets, 26(6), 452–459, 1989.
- 13. James, H. G., K. G. Balmain, C. C. Bantin, and G. W. Hulbert, Sheath waves observed on OEDIPUS A, Radio Sci., 30(1), 57-73, 1995.
- 14. James, H. G., and B. A. Whalen, OEDIPUS-A: Space research with a new tether, EOS Trans. AGU, 72(12), 137, 139, 140, 144, 1991.
- 15. Kawashima, N., S. Sasaki, K.-I. Oyama, K. Hirao, T. Obayashi, W. J. Raitt, A. B. White, P. R. Williamson, P. M. Banks, and W. F. Sharp, Results from a tethered rocket experiment (CHARGE-2), Adv. Space Res., 8(1), 197-201, 1988.
- 16. Laframboise, J. G., and L. J. Sonmor, Current collection by probes and electrodes in space magnetoplasmas: A review, J. Geophys. Res., 98(A1), 337-357, 1993.
- 17. Lieberman, M. A., Model of plasma immersion ion implantation, J. of Applied Phys., 66(7), 2926–2929, 1989.
- 18. Ma, T.-Z., and R. W. Schunk, High negative voltage spheres in an unmagnetized plasma: Fluid simulations, *Plasma Phys. Controlled Fusion*, 34(5), 783-799, 1992.
- 19. Martínez-Sánchez, M., and D. E. Hastings, A systems study of a 100 kW electrodynamic tether, J. Astronaut. Sci., 35(1), 75-96, 1987.
- 20. McCoy, J. E., I. Katz, J. R. Lilley, A. Greb, V. A. Davis, and D. C. Ferguson, Physics of current flow between the ionosphere and the Plasma Motor Generator (PMG) plasma contactors (abstract), EOS Trans. AGU, 74(43), Fall Meeting

- suppl., 466, 1993.
- 21. Sasaki, S., et al., Tethered rocket experiment (CHARGE-2): Initial results on electrodynamics, Radio Sci., 23(6), 975-988, 1988.
- 22. Savich, N. A., Problems and prospects of fundamental studies of electrodynamic properties of tethered satellite systems, Report, Academy of Sciences of the USSR Institute of Radio Engineering and Electronics, 1988.
- 23. Thompson, D. C., W. J. Raitt, C. Bonifazi, S. D. Williams, V. M. Agüero, B. E. Gilchrist, and P. M. Banks, TSS-1: Orbiter current and voltage experiments, paper presented at 31st Aerospace Sciences Meeting, Am. Inst. of Aeronaut. and Astronaut., Reno, Nev., Jan. 11-14, 1993.

FERROMAGNETICALLY SCREENED REVERSE CONDUCTOR (FSRC) - TETHER: A NEW TETHER PRINCIPLE

Gerhard Liebscher

Electronic Components Consultants Germany

NOTICE:

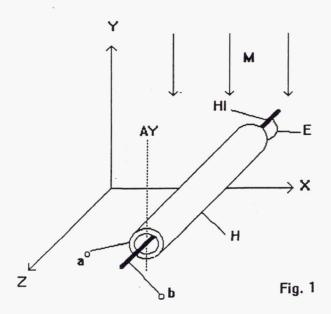
The following paper is included for completeness and as an attempt to allow for free and innovative scientific expression, however, serious doubts have been raised by some reviewers about the technical feasibility of the concept presented.

Page intentionally left blank

FSRC-Tether A New Tether Principle
Ferromagnetically screened reverse conductor (FSRC)

Summary

The new tether principle is based on a direct current generator or a direct current motor with a ferromagnetically screened reverse-conductor (Fig. 1) The principle part consists of an outer hollow conductor (H) made of ferromagnetic material and an inner or reverse conductor (HI) which lies within the outer hollow conductor but is galvanically separated from it. The outer hollow conductor and the inner conductor are connected electrically together at one end (E), while an electric voltage can be extracted at the other end (a and b) by motion of this device in a magnetic field. By forcing an electrical current at one end of the device the principle is made to operate in reverse and so cause the device to move in the magnetic field. Applications are: so called 'tethers' for electrical power generation for satellites in space or satellite motion in space, unipolar electric generators or unipolar motors without sliding contacts, magnetic field sondes or other magnetic field configurations generated by the device while the current will be supplied at one end.



The basis of the FSRC is the fact that the inner conductor is in a zone free of any magnetic field, which is formed by the outer case and which acts as a complete screen against any magnetic field (Fig. 2). The basic construction is similar to that of a coaxial cable. For a very good screening a material with a high permeability is needed.

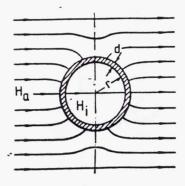
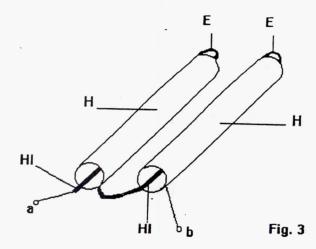


Fig. 2

The FSRC-Tether do not need free electrons for power generation or propulsion thrust. If the screening of the magnetic free zone is 100%, the operation of the FSRC-Tether can easily calculated, because it only depends on:

- 1. the alteration of the magnetic field of the earth
- 2. the speed of the satellite
- 3. the length of the tether
- 4. the specific resistance of the outer und inner conductor
- 5. the inclination and the vector of the tether compared with the earth magnetic field, and the propulsion thrust depends on
- 6. the current which is fed into the tether.

In order to reduce the length of a tether, the FSRC-Tether can be connected in series (Fig.3) or in parallel. So e.g. a 1 km length of the tether can be reduced to 20 m by splitting it into 50 pieces of 20 m.



If two FSRC-Tether are placed closely together but galvanically separated from one another, and a constant current is fed in at the connections a and b, then a circular magnetic field is created around the two tethers, which has approximately twice the strength of that around a single FSRC-Tether.

In order to increase the propulsion thrust this series or parallel connection can be multiplied.

If three multiple FSRC-Tether are fixed perpendicularly to each other at the satellite, then the satellite can be repositioned and realigned by forcing the appropriate direct electric currents through each of the three assemblies.

If, as proposed in the handbook "Tether in Space", the Multiple-FSRC-Tether is cooled down to achieve superconduction temperatures, which should be relatively easy, then such FSRC-Tethers could be used for the propulsion thrust of interplanetary travel by using the week magnetic field of the solar wind.

PAST, PRESENT AND FUTURE ACTIVITY ON TETHERED SYSTEMS

F. Angrilli, R. Basso, G. Bianchini, S. Bortolami, R. DaForno, S. Debei, G. Fanti, F. Reccanello, B. Saggin, A. Zago

Center of Studies and Activities for Space (C.I.S.A.S.) "G. COLOMBO" Department of Mechanical Engineering, University of Padua-Italy

INDEX

1. PAST STUDIES

1.1) Identification of the thermo-mechanical properties of the TSS-1	
SEDS tethers and TSS-2 candidate tether.	pag. 2
1.2) Experimental evaluation of the tether life after progressive damage	pag. 3
1.3) New non-linear model of tethered satellite systems	pag. 4
1.4) Experimental and numerical analysis of tethered stabilized platform	pag. 5
1.5) Monitoring analysis of tethered satellite system	pag. 6
1.6) Analysis of passive methods to damp out the tether flexural motion	
394	1.0.
2. PRESENT STUDIES	
Z. TREBERT STOPIES	
2.1) Analysis of recoil velocity after the cut in the SEDS mission	pag. 8
2.2) <u>Design of new failsafe multifunctional tethers</u>	
2.3) Thermo-mechanical characterization of new tethers	pag. 9
2.5) Thermo-mechanical characterization of new terners	pag. 10
2 NEW PROPOSALS	
3. NEW PROPOSALS	
3.1) Analysis of the Tether Life Due to the Dust Impact	pag. 11
3.2) Studies for a multifunctional experiment.	pag. 12
3.3) Extremely flexible links robots (tethered robots)	pag. 13
REFERENCES	pag. 14

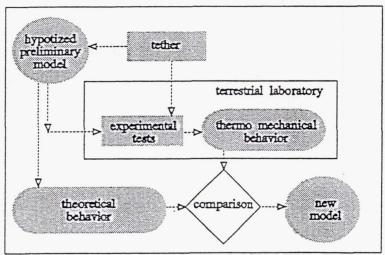
1.1) <u>Identification of the thermo-mechanical properties of the TSS-1 and SEDS</u> tether s and TSS-2 candidate tether.

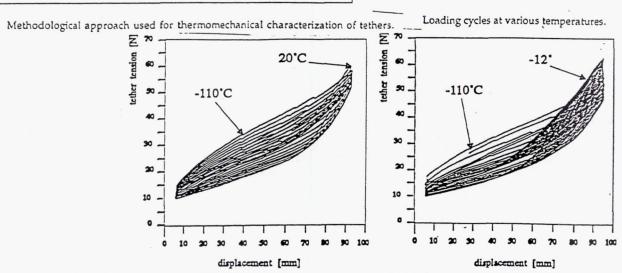
An extensive and fruitful field of research has been since 1987, the experimental identification of the thermo-mechanic properties of the tether used in TSS-1 and SEDS mission and the candidate to TSS-2 mission^{[1][2][3]}. In particular the authors evidenced the highly non-linear and history dependent behaviour of elastic response, of the damping factor both at room and criogenic temperatures, by using a self-designed and realized facility also to simulate the sun-dark transition in orbit.

The investigation has been performed by analytical modelling as well as applying experimental techniques in order to understand and interpret the various ways the energy dissipation takes place in a multifunctional multistrand wires during longitudinal and skip rope vibrations.

The main mechanism of the damping (of the order of 5%)^[13] is due to a sliding between fibres or adjacent layers in torsio-flexural deformation.

The longitudinal motions induced by sudden thermic variations, due to transition in the Earth shadow (variations of the order of 100-200 °K), have been investigated^[4]. Different non-linear mechanisms of stress redistribution among the different tether layers has been detected.





PAST, PRESENT AND FUTURE ACTIVITY ON TETHERED SYSTEMS, F. Angrilli et al, C.I.S.A.S. "G. COLOMBO", University of Padua-Italy, Jan-96

1.2) Experimental evaluation of the tether life after progressive damage

Another field of interest for the authors has been the experimental evaluation of the tether life after progressive damage due to particle impact^[15].

From the experience of SEDS Missions, some relevant problem about the future development of tethered are to be solved:

- the estimation of the working life without damage (of the order of months) of long tethers in spatial environment.

- how to check the integrity of tethers in space and their eventual substitution.

A new generation of tethers, having optimized geometry for micrometeoroid impacts, is being developed and investigated. Their multistrand structure will maintain the bearing function even if multiple impacts of space debris will cut some strand.

The first step consist in studying the mechanical behaviour of these new tethers and to test their effective capabilities after cutting some strand.

Various samples of tethers, some meters long, having different structure, are considered and compared. Braided and multistrand cables are compared with more complex structures such as that of Hoytether.

The experimental set-up allows the measurement of the stress redistribution and the total strain after one or more cuts of some strands and the measurement of the dynamic effects propagating along the length of samples some meters long. The stress-strain relations may be determined by utilizing a vision system with four cameras capable of monitoring the displacements of as many sections relative to the multistrand tether.

The behaviour of these tether is then extrapolated to lengths of the order of some km to predict the dynamic behaviour of the whole tethered system.

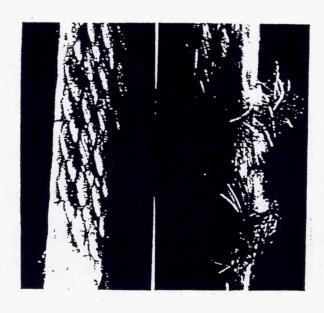
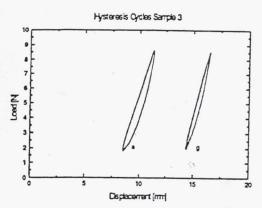


Figure Sample 3 before and after damaging



Hysteresis cycles for sample 3

1.3) New non-linear models of tethered satellite systems

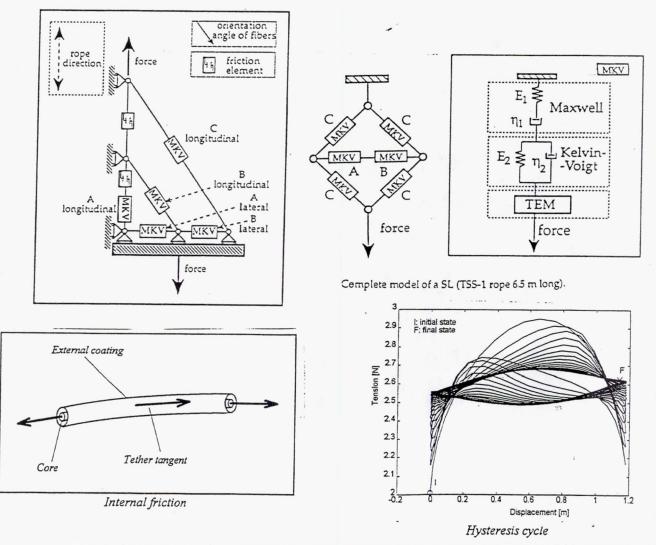
On the basis of the highly non-linear experimental results^[14] the authors developed mathematical models with non-linear behaviour of the tether connecting the Shuttle to the subsatellite.

Based on the characteristics method, it is innovative with respect to present approaches, particularly in respect of full non-linear models in three-dimensional space. By using the theory of quasilinear partial differential equation of hyperbolic type the problem is transferred to the characteristics plane in terms of total differential instead of partial differentials^[16].

The dynamics of end-masse is introduced as boundary conditions, so that the system obtained may be considered as the coupling between a set of partial differential equations and a set of ordinary differential equations.

The principal advantage of the proposed model is the full non-linear three dimensional description of the tethered systems, in particular concerning the non linearity of geometrical type (large deformations).

External friction (Coulombian friction and proportional to the square of the tangent velocity) was introduced along the instantaneous tangent to the tether to give a hysteresis cycle. This allow to model the non-linear interaction between the external laver and the tether core.



PAST, PRESENT AND FUTURE ACTIVITY ON TETHERED SYSTEMS, F. Angrilli et al, C.I.S.A.S. "G. COLOMBO", University of Padua-Italy, Jan-96

1.4) Experimental and numerical analysis of tethered stabilized platform

Starting from the following concepts:

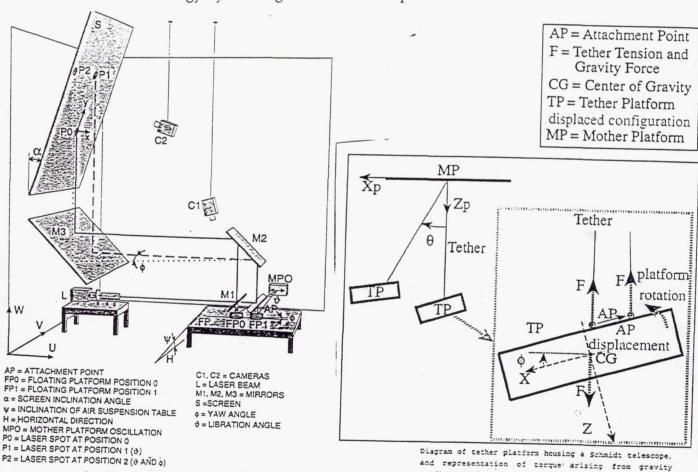
- that the tether may insulate scientific apparatus from the dynamic noise produced by the Space Station,
- that the effects of tether tension on platform attitude are more important than environmental ones and
- that control strategy based on the displacement of attachment point may require less energy than the classical methods,

the idea of controlling the platform attitude by moving the tether attachment point arose.

The control strategy[8][12] is analysed and synthesized through a threedimensional linear model and tested by direct integration of non-linear equations of motion, discretizing the tether by lumped masses, in order to analyse the influence of the tether dynamics on the control strategy.

The control strategy is based on a PID-like control with feedback on platform attitude motion.

The experimental set-up, based on a multilever laser vision system, enables the simulation of the microgravity condition and the physical implementation of control strategy by moving the attachment point.



PAST, PRESENT AND FUTURE ACTIVITY ON TETHERED SYSTEMS, F. Angrilli et al, C.I.S.A.S. "G. COLOMBO", University of Padua-Italy, Jan-96

gradient used to control telescope attitude by moving

tether attachment point.

Experimental apparatus for simulation of floating

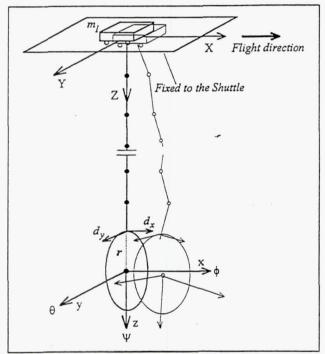
platform.

1.5) Monitoring analysis of tethered satellite system

The problem of monitoring the tether dynamic shape can be successfully solved by the analysis of the observability of the system by using the information of the sensors located at the tether ends.

The method used^{[8][9]} is based on the concept of observability of a dynamic system, in this way it is possible to select a proper set of sensors located at the tether ends in order to estimate the shape of the tether during motion, without its direct measurement.

The simple method allows the enhancement of the estimation accuracy by using the Kalman filter approach.



Lumped model of tethered satellite system

1.6) Analysis of passive methods to damp out the tether flexural motion

The devices to obtain the passive damping of the tether flexural motion can be grouped into two main types^{[6][13]}: tether end dampers and damping rings.

A tether end damper is based on the concept of the reflection factor.

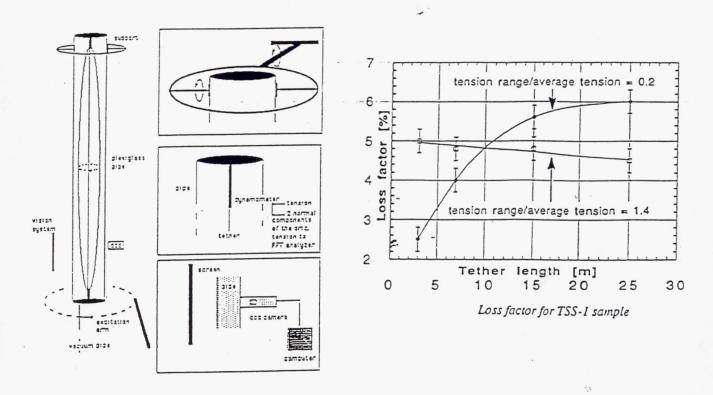
Dissipation is achieved by imposing a zero reflection factor of the incident wave at the end-point. The reflection factor is defined as the ratio between the amplitudes of the reflected and incident waves.

In order to obtain a low reflection factor, it is necessary to reduce reactance. Physically, this may be accomplished by applying the concept of impedance control by modulating the impedance of the mechanical system by a suitable control law using a DC motors.

This method is frequency-dependent. In particular actuator impedance must be tuned in order to dissipate the energy of some desired modes.

Although this dissipation is obtained by external control action, due to dissipation itself, this method is considered passive. For impedance control, the measured quantities are the speed and acceleration of the DC motor.

Damping rings may be viewed as alternatives method to dissipate the energy of the skiprope mode. In this case, a ring located on the boom end dissipates energy, thanks to dry friction.



Flexural damping measurement: experimental set-up

2. PRESENT STUDIES

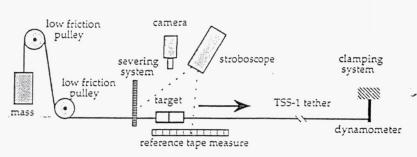
2.1 Analysis of recoil velocity after the cut in the SEDS mission

The authors developed^[17] a numerical and experimental analysis of the tether motion after cutting TSS-1 and SEDS missions sample rope.

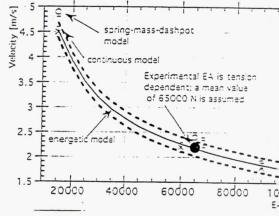
Two different numerical models allow the simulation of a mass-spring-dashpot tether system and the distribution of the recoil speed along the tether immediately after the cut.

The experimental set-up based on a stroboscopic system and an high speed camera, enables the measurement of the recoil velocity.

A simplified mathematical model fully confirms both experimental and numerical results.



Scheme of the experimental apparatus



comparison of experimental and theoretical results as a function of tether stiffness for a sample 14 m long.

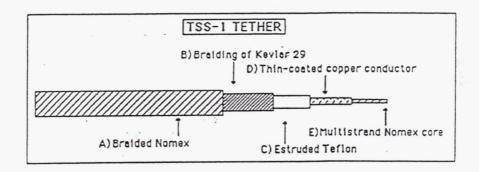
2.2) Design of new failsafe multifunctional tethers

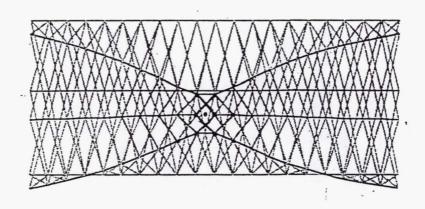
From the experience of SEDS mission, the necessity to design tethers capable of resists to multiple debris impacts results^{[15][19]}.

It has numerically shown that structures such as Hoytether better resisist to debris impacts.

The authors are now studying the possibility to design a tether that combines a structure similar to Hoytether to the multifunctionality of TSS-1 tether.

Preliminary contacts of some authors with Alenia Spazio confirmed the possibility to design and build new multifunctional-failsafe tethers.





Scheme of a old-type multifuctional tether (TSS-1) and representation of a failsafe tether (Hoytether [19])

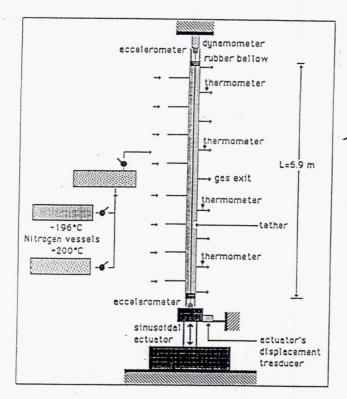
2.3) Thermo-mechanical characterization of new tethers

New failsafe multifunctional tethers will probably have a structure more complex than the composite multilayer structure of TSS-1.

All these new tethers then require a detailed thermo-structural analysis in order to make accurate numerical models of the whole dynamic system.

The characterization also requires the analysis of partially damaged tethers[14][17].

An experimental setup and numerical models are to be developed by the authors.



Experimental apparatus used for testing samples of tethers 6.90 m long, at different temperatures; it consists of a thermal pipe containing the tether, one dynamometer placed at the upper end of the tether, two motion transducers locate at each end, a sinusoidal motion actuator with variable amplitude and frequency and a data acquisition and recording system. The thermal pipe consists of an inner Comflex layer (Ø100 mm) stiffened externally by a PVC pipe, 2 mm thick.

3). NEW PROPOSALS

3.1 Analysis of the Tether Life Due to Dust Impact

In cooperation with S.A.O is being presented a research involving the life determination of tether sample exposed to high velocity (8-10 Km/s) dust impact.

At the actual stage, the pre-scheduled activity phases are:

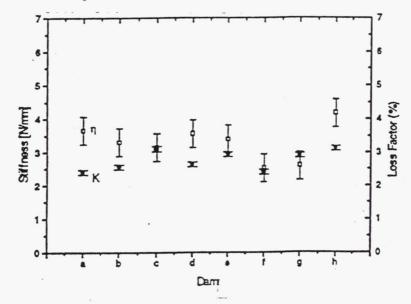
- a) Mission planning,
- b) Laboratory experiment by gas-gun to test the impact strength of the tether on ground,
- c) Design and costruction of an orbiting facility to expose tether samples to dust or debris in orbit.

Phase (b) requires the planning of the experiment on Earth. In particular the definition of:

- -b.1) the mathematical model to analyse the impact against the tether with high velocity travelling mass. The investigation will be accomplished by multiple simulations, varying the impact velocity in order to define the relation velocity-peak stress in the cable cross section at the impact point;
- -b.2) the environmental conditions (sun-dark effect, longitudinal tension, impact direction, impacting mass, impact velocity;
- -b.3) the type of tether in terms of geometry and layers. The geometry plays a key role on the tether life exposed to dust impacts;
- -b.4) the gas-gun facility to obtain particle velocity of the order of 10 km/s, in terms of design and realization.

Phase (c) requires the design and realization of:

- -c.1) the facility on which are mounted the tether samples to be exposed to the dust in the space environment;
- -c.2) the device to manipulate the samples-holder facility (point c.1), in order to obtain the desired exposure orientation.



Tensile stiffness and loss factor of a sample at different degrees of damage.

3.2 Studies for a multifunctional experiment.

From the experience of TSS-1_Reflight it will be known if the tether damping, evaluated by the authors of the order of 5%, will be sufficent to damp out all the vibrations modes dangerous for the tether dynamics. In any case other future applications will probably require an active damping.

In addition to the damping mechanisms presented by the authors, an active

system may consist in a box running along the tether.

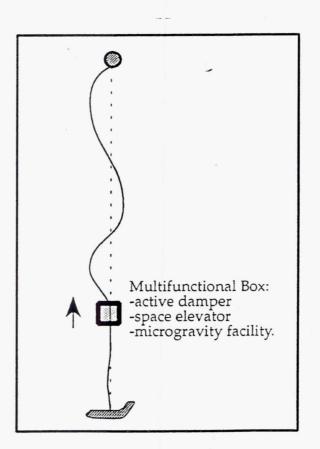
If in a future mission such a box will be present, the following applications may be verified:

-a) both flexo-torsional and longitudinal vibration may be damped out if the box houses a motor that clutches the tether and lets the box to go up and down;

-b) the concept of space elevators may be verified; without using the internal motor, the box may transport a load from the orbiter to the subsatellite;

-c) the box may contain a gravimeter capable to verify the microgravity levels theoretically foreseen and the possible field disturbances; some simple microgravity

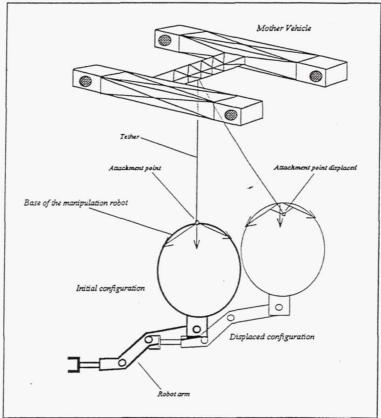
experiment may be allowed.



3.3) Extremely flexible links robots (tethered robots)

The aim of this research is the development of a non-conventional control strategy to stabilize the robot base roto-translational motion, by moving the tether attachment point.

The cable thus can be considered as a very flexible link. The encouraging results of the preliminary analysis indicate this strategy as very interesting for further applications. Examples are tele-robotic assisted by helicopter or space station.



Task scenario

REFERENCES

- 1) F. Angrilli, G. Bianchini, M. Da Lio, G. Fanti: Modelling The Mechanical Properties Of Tethers For The Tss-1 And Tss-2 Missions, ESA Journal 1988, vol.12.
- F. Angrilli, G. Bianchini, M. Da Lio, G. Fanti: Mechanical And Thermal Properties For Evaluation Of Tss-1 Tether Dynamic Behavior, 3rd Int. Conference on Tethers in Space, San Francisco U.S.A. May 17-19 1989.
- G. Fanti, F. Angrilli, P. Baglioni, G. Bianchini: Mechanical Testing On A Composite Flexible Structure, Proc. of the Conference "Spacecraft Structures and Mechanical Testing", ESTEC, Noordwijk, The Netherlands, 24-26 April 1991.
- 4) G. Fanti: Stress Distribution Measurement In Composite Space Ropes, Proc. of the Fourth Int. Conf. on Tethers in Space, Washington 1995.
- 5) F. Angrilli, G. Bianchini, G. Fanti: Private comunication about SEDS Mission to Joe Carroll, 1989.
- 6) G. Fanti, F. Angrilli, G. Bianchini, F. Patanè: Experimental Determination Of The Flexural Damping On The Tss-1: Tecn. Meeting, NASA, MSFC April, 1991.
- S.B. Bortolami, E. lorenzini, C.C. Rupp, F. Angrilli: "Control law for the Deployment of SEDS-2" Advance in Astronuatical Science Series, 1993
- 8) R. Da Forno, B. Saggin. "Analysis of Sensor and Actuator Dynamics in Cable-Like Structures Energy Dissibation: Full Non-Linear Investigation", 1St World Conference on Structural Control, Los Angeles, Ca, USA, 3-5 Aug. 1994.
- R. Da Forno, B. Saggin, F. Angrilli, "Uncertainty Propagation in Manipulation Using Stereo Vision", ISATA International Dedicated Conference on Robotics; Motion and Machine Vision, Aachen, Germany, Oct. 31-Nov. 4, 1994.
- 10) R. Da Forno, B. Saggin, F. Angrilli, "Sistemi di Visione Stereo per il Tracking di Traiettorie 3D: Un Metodo per la Calibrazione del Sistema", Atti della Giornata di Studio MIS-MAC III, Cagliari, 7 Ott. 1994.
- 11) R. Da Forno, B. Saggin, "Uncertainty in End-Point Tension Measurement in Wires Subject to High-Velocity Impact", accettato per la pubblicazione su International Jou. of Mesurement Confederation, 1995.
- 12)F. Angrilli, R. Da Forno, G. Bianchini, G. Fanti and B. Saggin: "Tether Stabilized Platforms Attitude Control by Moving the Attachment Point Influence of Transverse Vibration" Fourth International Conference on Tethers in Space, Smithsonian Institution, Washington D.C., 10-14 April 1995.
- 13)F. Angrilli, G. Bianchini, R. Da Forno, G. Fanti "Active and Passive Damping of Tethered Systems" Fourth International Conference on Tethers in Space, Smithsonian Institution, Washington D.C., 10-14 April 1995.
- 14) F. Angrilli, G. Bianchini, S. Debei and G. Fanti "A Review of TSS Thermomechanical Properties in the Light of First Experimental Results" Fourth International Conference on Tethers in Space, Smithsonian Institution, Washington D.C., 10-14 April 1995.
- 15) F. Angrilli, G. Bianchini, S. Debei, G. Fanti and B. Saggin" Effect of Debris Damage on New Long-Life Tethers" Fourth International Conference on Tethers in Space, Smithsonian Institution, Washington D.C., 10-14 April 1995.
- 16) F. Angrilli, R. Da Forno, B. Saggin, "A New Full Non-Linear Model of the Tethered Satellite System Based on the Characteristics Method", 4th International Conference on Tethers in Space, Washington, D.C., 10-14 Apr. 1995.
- 17) F. Angrilli,, R. DaForno, G. Fanti, F. Reccanello, A. Zago: "Effects of Severed Tethers in Space" presented to the Journal of Spacecraft and Rockets.
- 18) S.B.Bortolami, F.Angrilli, C.Jekeli, M.D. Grossi "Analysis of a Dumbell sensor for Space Gradiometry" 4th International Conference on Tethers in Space, Washington, D.C., 10-14 Apr. 1995.
- 19) R. L. Forward: "Failsafe Multistrand Tether Structures for Space Propulsions", AIAA/SAE/ASME/ASEE 28th Joint Propulsion Conference July 6-8/1992 Nashville, TN, USA.

REPORT DOCUMENTATION PAGE

plasma physics, ionospheric physics, space power generation,

OF THIS PAGE

18. SECURITY CLASSIFICATION

Unclassified

Form Approved OMB No. 0704-0188

Public reporting burden for this collection of information is estimated to average 1 hour per response, including the time for reviewing instructions, searching existing data sources, gathering and maintaining the data needed, and completing and reviewing the collection of information. Send comments regarding this burden estimate or any other aspect of this collection of information, including suggestions for reducing this burden, to Washington Headquarters Services, Directorate for Information Operation and Reports, 1215 Jefferson Davis Highway, Suite 1204, Arlington, VA 22202-4302, and to the Office of Management and Budget, Paperwork Reduction Project (0704-0188), Washington, DC 2050-

AGENCY USE ONLY (Leave Blank)	2. REPORT DATE	3. REPORT TYPE	AND DATES COVERED	
	January 1998	Conterence	e Publications	
4. TITLE AND SUBTITLE			5. FUNDING NUMBERS	
Tether Technology Interchai	nge Meeting			
6. AUTHORS				
James K. Harrison, Compile	:I			
7. PERFORMING ORGANIZATION NAMES(S) AND ADDRESS(ES)		8. PERFORMING ORGANIZATION REPORT NUMBER	
George C. Marshall Space Flight Center		NEFORT NOMBER		
Marshall Space Flight Center, AL 35812		M-847		
9. SPONSORING/MONITORING AGENCY NA	ME(S) AND ADDRESS(ES)		10. SPONSORING/MONITORING	
National Aeronautics and Space Administration		AGENCY REPORT NUMBER		
Washington, DC 20546-000			NASA/CP-1998-206900	
11. SUPPLEMENTARY NOTES				
Prepared by Program Deve	lopment Directorate			
12a. DISTRIBUTION/AVAILABILITY STATEM	IENT		12b. DISTRIBUTION CODE	
Unclassified-Unlimited				
Subject Category 12				
Standard Distribution				
13. ABSTRACT (Maximum 200 words)				
This is a compilation of 25 papers presented at a tether technical interchange meeting in Huntsville, AL, on September 9–10, 1997. After each presentation, a technical discussion was held to clarify and expand the salient points. A wide range of subjects was covered including tether dynamics, electrodynamics, space power generation, plasma physics, ionospheric physics, towing tethers, tethered reentry schemes, and future tether missions.				
14. SUBJECT TERMS tether, tether of	lynamics, tether design,	electrodynamics	15. NUMBER OF PAGES	

OF REPORT

future tether missions

Unclassified

17. SECURITY CLASSIFICATION

462

A20

20. LIMITATION OF ABSTRACT

16. PRICE CODE

19. SECURITY CLASSIFICATION

Unclassified

OF ABSTRACT